ELECTRIC ENERGY SYSTEMS THEORY

AN INTRODUCTION

Olle I. Elgerd

FAC. DE CIENCIAS EXACTAS Y TECNOLOGIA
BIBLIOTECA
Nº R. 2423
S. T. 621.315
E 41e2
Ej 2

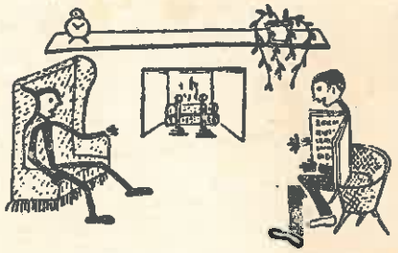

Este libro llega a su casa como un amigo.

No lo detenga mucho. Permita que como Ud. otros puedan gozar de su compañía.

Devuélvalo a la Biblioteca lo antes posible

Muchas Gracias

ELECTRIC ENERGY SYSTEMS THEORY

An Introduction

McGraw-Hill Series in Electrical Engineering

Consulting Editor
Stephen W. Director, *Carnegie-Mellon University*

Networks and Systems
Communications and Information Theory
Control Theory
Electronics and Electronic Circuits
Power and Energy
Electromagnetics
Computer Engineering and Switching Theory
Introductory and Survey
Radio, Television, Radar, and Antennas

Previous Consulting Editors

Ronald M. Bracewell, Colin Cherry, James F. Gibbons, Willis W. Harman, Hubert Heffner, Edward W. Herold, John G. Linvill, Simon Ramo, Ronald A. Rohrer, Anthony E. Siegman, Charles Susskind, Frederick E. Terman, John G. Truxal, Ernst Weber, and John R. Whinnery

POWER AND ENERGY

Consulting Editor
Stephen W. Director, *Carnegie-Mellon University*

Elgerd: ELECTRIC ENERGY SYSTEMS THEORY: An Introduction
Fitzgerald, Kingsley, and Kusko: ELECTRIC MACHINERY
Meisel: PRINCIPLES OF ELECTROMECHANICAL-ENERGY CONVERSION
Odum and Odum: ENERGY BASIS FOR MAN AND NATURE
Stagg and El Abiad: ADVANCED COMPUTER METHODS IN POWER SYSTEM ANALYSIS
Stevenson: ELEMENTS OF POWER SYSTEM ANALYSIS
Sullivan: POWER SYSTEM PLANNING

ELECTRIC ENERGY SYSTEMS THEORY

An Introduction

Second Edition

Olle I. Elgerd

Professor of Electrical Engineering
University of Florida

McGraw-Hill Book Company

New York St. Louis San Francisco Auckland Bogotá Hamburg
Johannesburg London Madrid Mexico Montreal New Delhi
Panama Paris São Paulo Singapore Sydney Tokyo Toronto

This book was set in Times Roman.
The editor was T. Michael Slaughter;
the cover was designed by Charles A. Carson;
the production supervisor was Leroy A. Young.
R. R. Donnelley & Sons Company was printer and binder.

ELECTRIC ENERGY SYSTEMS THEORY
An Introduction

Copyright © 1982, 1971 by McGraw-Hill, Inc. All rights reserved.
Printed in the United States of America. Except as permitted under the United States Copyright Act of 1976, no part of this publication may be reproduced or distributed in any form or by any means, or stored in a data base or retrieval system, without the prior written permission of the publisher.

1234567890 DODO 8987654321

ISBN 0-07-019230-8

Library of Congress Cataloging in Publication Data

Elgerd, Olle Ingemar, date
Electric energy systems theory.
(McGraw-Hill series in electrical engineering. Power and energy)
Includes bibliographical references and index.
1. Electric engineering. 2. Electric power systems.
I. Title. II. Series.
TK145.E487 1982 621.3 81-17194
ISBN 0-07-019230-8 AACR2
ISBN 0-07-019231-6 (solutions manual)

TO
University of Florida

CONTENTS

Preface xvii

Chapter 1 Introduction 1

1-1 Historical Development of the Electric Power Industry 1
1-2 Structure of the US Electric Utility Industry 3
1-3 Voltage Structure of the Electric Energy System 5
1-3-1 Distribution Level 6
1-3-2 Subtransmission Level 7
1-3-3 Transmission Level 7
1-4 The Future 8
1-4-1 Present Generation Mix 9
1-4-2 Need for Planning and Research 9
1-4-3 New Prime Energy Resources 9
1-4-4 Future Generating Equipment 10
1-4-5 New Transmission Methods 10
1-4-6 Electric Storage, Facilities 11
1-4-7 Energy Conservation 11
Summary 12
Problems 12
References 13

Chapter 2 Fundamental Concepts of Electric Energy Systems Engineering 14

2-1 The Fundamental Power Formula—Electromagnetic Energy 15
2-2 Additional Forms of Electric Energy 17
2-2-1 Electric Field Energy w_{ef} 17
2-2-2 Magnetic Field Energy w_{mf} 18
2-2-3 Ohmic, or Dissipative, Energy w_{Ω} 19

2-3 DC Versus AC Power—Concepts of Real and Reactive Powers 19
2-3-1 DC Transmission 20
2-3-2 Single-Phase Transmission 20
2-3-3 Real and Reactive Power 22
2-3-4 Apparent Power 23
2-4 Concept of Complex Power 26
2-5 Per-Unit Representation of Impedances, Currents, Voltages, and Powers 29
2-5-1 Definitions 30
2-5-2 Power and Circuit Formulas in Per-Unit Values 31
Summary 32
Problems 33

Chapter 3 The Symmetrical Three-Phase System 35
3-1 The Symmetrical Three-Phase Transmission System 35
3-1-1 Evolution of the Three-Phase System 36
3-1-2 Voltage Relationships 38
3-1-3 Current Relationships 39
3-1-4 Power Relationships 40
3-1-5 Delta-Connected Loads 42
3-1-6 The Three-Phase Generator as Part of a Power Grid 43
3-1-7 Phase Symmetry 44
3-1-8 "Per-Phase" Analysis 44
3-1-9 Per-Unit Values in Symmetrical Three-Phase Systems 47
3-2 The Unsymmetrical Three-Phase Case 50
3-2-1 Balancing an Unsymmetrical Resistive Load 50
3-3 Load Characteristics 52
3-3-1 Voltage and Frequency Load Dependency 54
3-3-2 Load Management 57
3-4 Transmission Capacity 58
3-4-1 Thermal Capacity Limits 58
3-4-2 Static "Stability" Limits 59
Summary 65
Problems 65
References 67

Chapter 4 The Three-Phase Synchronous Generator 68
4-1 Introduction 68
4-2 Basic Design Features 69
4-3 Induction of Stator EMFs—Flux and EMF Waves 71
4-4 Speed Voltage 73
4-5 The Current-Loaded Machine—The "I Wave" 75
4-6 Armature Reaction 75
4-7 The Terminal Voltage 77
4-8 Magnetic Saliency Effects—Two-Reaction Theory 79
4-9 Power and Torque Creation 81

4-10 Power Formulas 82
4-11 Control of Synchronous Machines Operated Singly 85
4-12 Generator Operated as Part of Large Power Grid 87
4-12-1 Synchronization 87
4-12-2 Modified Power Formulas 88
4-12-3 Real Power Control 90
4-12-4 A Mechanical Analog 91
4-12-5 Electrical Stiffness 91
4-12-6 Pullout Power 92
4-12-7 Control of the Reactive Generator Power 93
4-12-8 A Summary of Operating Cases 95
4-12-9 Machine Operating Limits 98
4-13 Transient Machine Behavior 99
4-13-1 Transients in Magnetically Coupled Circuits 100
4-13-2 Magnetic Inertia 101
4-13-3 Transients along d Axis 103
4-13-4 Transients along q Axis 104
4-13-5 Transient Reactance X'_d 105
4-13-6 Transient Decay Rates 106
4-13-7 Transient Phasor Diagram 107
4-13-8 The EMF behind the Transient Reactance 109
4-13-9 Transient Power Formulas 110
4-13-10 Additional Transient Phenomena 112
Summary 114
Problems 114
References 116

Chapter 5 The Power Transformer 117
5-1 Introduction 117
5-2 Design Features 119
5-3 The n-Winding "Ideal Transformer" 120
5-3-1 IT Voltage Relations 121
5-3-2 Core Flux and "VPT" 122
5-3-3 IT Current and Power Relations 123
5-3-4 Equivalent IT Circuit 126
5-3-5 Impedance Transformations in IT's 128
5-4 The Physical Power Transformer 129
5-4-1 Accounting for Magnetizing Current and Core Losses 130
5-4-2 Accounting for Winding Resistances and Leakage Fluxes 131
5-4-3 Transformer Rating 135
5-5 Per-Unit Analysis 135
5-5-1 Transformer Variables in Per Unit of Ratings 135
5-5-2 Transformer Impedance in Per Units 136
5-6 Three-Phase Transformers 138
5-6-1 Single-Phase versus Three-Phase Cores 138
5-6-2 General Three-Phase Transformer Relationships 139
5-6-3 Y-Connected Transformers 140

5-6-4 Δ-Connected Transformers 145
5-6-5 Analysis of Δ-Y Transformers under Balanced Loading 147
5-6-6 Three-Phase Multiwinding Transformers 148
5-7 Autotransformers 150
5-8 The Transformer as a Control Device 153
5-8-1 TCUL Transformers 153
5-8-2 Regulating Transformers 154
5-8-3 Regulating Transformer for Voltage Magnitude Control 155
5-8-4 Regulating Transformer for Voltage Phase Angle Control 156
5-8-5 Examples on Power Flow Control 156
5-9 Summary 163
Problems 163
Reference 167

Chapter 6 The Power Transmission Line 168

6-1 Introduction 168
6-2 Design Considerations 170
6-3 Line Resistance and Shunt Conductance 172
6-4 Line Inductance 173
6-4-1 The Single-Phase Line 174
6-4-2 Inside Inductance L_i 175
6-4-3 Outside Inductance L_o 176
6-4-4 Total Inductance L 177
6-4-5 Concept of "Apparent" Inductance 178
6-4-6 Extension to the n-Conductor Case 180
6-4-7 Inductance Calculations for Three-Phase Single-Conductor Lines 182
6-4-8 Inductance Calculations for Bundled Three-Phase Lines 186
6-5 Line Capacitance 188
6-5-1 Capacitance of Single-Phase Line 188
6-5-2 Influence of Earth 192
6-5-3 Capacitance of Multiple Conductor Lines 194
6-5-4 Capacitance of Three-Phase, Single-Conductor Lines 196
6-5-5 Capacitance of Bundled Three-Phase Line 197
6-6 Long-Line Theory 199
6-6-1 Long-Line Equations in the Sinusoidal Case 201
6-6-2 Solution of Differential Equations 202
6-6-3 Equivalent Circuit of Long Line 204
6-6-4 Computational Considerations 205
6-6-5 Surge Impedance Loading 207
6-6-6 Lossless Line; Concept of Wavelength 209
6-6-7 Electrically "Short" and "Long" Lines 210
6-6-8 Line Compensation 212
6-7 Summary 214
Problems 214

Chapter 7 The Energy System in Its Normal State—System Modelling and Power-Flow Analysis 219

7-1 Operating States 219
7-2 Megawatt-Frequency ($P-f$) Interaction 221
7-2-1 Load-Frequency Mechanism 222
7-2-2 Load-Frequency Control, LFC 224
7-3 Megavar-Voltage ($Q-|V|$) Interaction 224
7-3-1 Cross-Coupling Between $P-f$ and $Q-|V|$ Control Channels 225
7-4 The Power-Flow Problem 225
7-5 A Two-Bus Demonstration Example 227
7-5-1 System Model—The Power-Flow Equations (PFE) 228
7-5-2 Writing the PFE's in Real Form 231
7-5-3 Important Characteristics of PFE 232
7-5-4 Classification of System Variables 233
7-5-5 Solution of PFE—A Basic Dilemma 234
7-5-6 Modified Specifications—Solution of Our Dilemma 234
7-5-7 Bus Classification on the Basis of Specification 237
7-6 Generalization to n-Bus System 237
7-6-1 General Form of the PFE 238
7-7 Computational Aspects of the Power-Flow Problem 241
7-7-1 Iterative Computation of the PFE 242
7-7-2 Computational Procedure Depends upon Bus Type 243
7-8 Gauss-Seidel (G-S) Iterative Technique 245
7-8-1 The G-S Algorithm 245
7-8-2 The G-S Method Applied to the PFE's 247
7-8-3 A Two-Bus Test System 248
7-8-4 The G-S Method Applied to "Load" Buses 248
7-8-5 The G-S Method Applied to "Voltage Control" Buses 250
7-8-6 Convergence Improvements of the G-S Algorithm 252
7-8-7 Computational Flow Chart 253
7-9 The Newton-Raphson (N-R) Method 255
7-9-1 The N-R Algorithm in Scalar Case 255
7-9-2 The N-R Algorithm in n-Dimensional Case 256
7-9-3 The N-R Algorithm Applied to the PFE 257
7-9-4 Accounting for Voltage Controlled Buses 260
7-10 Computational Aspects of Large-Scale Systems 262
7-10-1 Effects of System Size upon Convergence Characteristics 263
7-10-2 Sparsity of Jacobian Matrix 263
7-10-3 Sparsity-oriented Computer Programming 263
7-10-4 Reducing Storage Requirements 264
7-10-5 Gaussian Elimination and Optimal Ordering 265
7-10-6 "Decoupled" Power-Flow Algorithms 266
7-10-7 Variants of the N-R Method 268
7-11 Control of the Power Flow 268
7-11-1 Power-Flow Control by Source Adjustment 268
7-11-2 Power-Flow Control by Transformer Regulation 269

Summary 270
Problems 271
References 273

Chapter 8 Optimum Operating Strategies 274

8-1 Generation Mix 274
8-2 Optimum Dispatch—Problem Formulation 276
8-3 Optimum Economic Dispatch—The Lossless Case 277
8-3-1 Cost Function 277
8-3-2 Constraint Relations 277
8-3-3 Incremental Generation Costs 279
8-3-4 Optimum Dispatch Equations 280
8-3-5 Optimum Dispatch Formula—Inequality Constraints Considered 283
8-3-6 Computational Considerations 283
8-4 Optimum Generator Allocation—Transmission Losses Considered 284
8-4-1 Analysis of Two-Bus System 285
8-4-2 Analysis of the N-Generator Case 288
8-4-3 Incremental Transmission Loss, ITL 288
8-4-4 Finding the ITL's in the Two-Bus Case 289
8-4-5 Finding the ITL's in General Case 290
8-4-6 Computational Procedure 292
Summary 293
Problems 296
References 298

Chapter 9 The Energy System in Steady State—The Control Problem 299

9-1 Basic Generator Control Loops 299
9-1-1 Cross-Coupling between Control Loops 301
9-1-2 Small-Signal Analysis 301
9-2 The Automatic Voltage Regulator (AVR) 302
9-2-1 Exciter Types 302
9-2-2 Exciter Modeling 303
9-2-3 Generator Modeling 304
9-2-4 Static Performance of the AVR Loop 306
9-2-5 Dynamic Response of the AVR Loop 306
9-2-6 AVR Root Loci 307
9-2-7 Stability Compensation 308
9-2-8 Effects of Generator Loading 309
9-3 Automatic Load-Frequency Control of Single-Area Systems 310
9-3-1 Speed-Governing System 310
9-3-2 Hydraulic Valve Actuator 312
9-3-3 Turbine-Generator Response 313
9-3-4 Static Performance of Speed Governer 314
9-3-5 Closing the ALFC Loop 316
9-3-6 Concept of "Control Area" 319

9-3-7 Static Response of Primary ALFC Loop 319
9-3-8 Dynamic Response of ALFC Loop 321
9-3-9 Physical Interpretation of Results 322
9-3-10 The Secondary ("Reset") ALFC Loop 323
9-3-11 Economic Dispatch Control 328
9-4 ALFC of Multi-Control-Area Systems (Pool Operation) 329
9-4-1 The Two-Area System 330
9-4-2 Modeling the Tie-Line 330
9-4-3 Block Diagram Representation of Two-Area System 331
9-4-4 Mechanical Analog of Two-Area System 333
9-4-5 Static Response of Two-Area System 333
9-4-6 Dynamic Response of Two-Area System 336
9-4-7 Tie-Line Bias Control 337
9-4-8 Tie-Line Bias Control of Two-Area System 338
9-4-9 Static System Response 338
9-4-10 Tie-Line Bias Control of Multiarea Systems 339
9-5 "Steady-State" Instabilities 340
9-5-1 Natural Torsional Oscillatory Modes in a Power System 341
9-5-2 Natural Mode of a Single Generator Operating onto Infinite Bus 343
9-5-3 Effect of Damper Winding 345
9-5-4 Extension to Large-Scale System 346
9-5-5 Negative Damping 347
9-5-6 Effect of Changing E' 347
9-5-7 Factors Causing Changes in E' 348
9-5-8 Inclusion of the AVR Loop 348
9-5-9 Discussion of Results 349
9-6 AGC Design Using Kalman Methods 350
9-6-1 Putting the Dynamic Model in State Variable Form 351
9-6-2 Optimum Control Index I 353
9-6-3 State Space and State Trajectories 354
9-6-4 Optimally Controlled Trajectories 356
9-6-5 OLR Structure—The Riccati Equation 356
9-6-6 Concluding Comments 358
Summary 358
Problems 359
References 361

Chapter 10 Energy System Transients—Surge Phenomena and Symmetrical Fault Analysis 363

10-1 Classification of System Transients 363
10-1-1 Class A. Ultrafast Transients—Surge Phenomena 364
10-1-2 Class B. Medium-Fast Transients—Short-Circuit Phenomena 364
10-1-3 Class C. Slow Transients—"Transient Stability" 365
10-2 Transmission Line Transients 366
10-2-1 The Wave Equation and Its Solution 367

10-2-2 Physical Interpretation of Results 368
10-2-3 Wave Reflections 369
10-2-4 Parameter Lumping 372
10-2-5 Overvoltages and Insulation Levels 373
10-2-6 Circuit Interrupt Devices 373
10-2-7 Switching Transients 375
10-3 Symmetrical Short Circuits 376
10-3-1 Thévenin's Theorem 377
10-3-2 SC Analysis of the Two-Bus System 378
10-3-3 Discussion of Results 382
10-3-4 Short-Circuit Capacity, SCC 383
10-4 Systematic Short-Circuit Computations 384
10-4-1 Network Model 384
10-4-2 $\mathbf{z}_{bus}$ Network Representation 386
10-4-3 Solution of Vector Equation 387
10-5 $\mathbf{z}_{bus}$ Building Algorithms 390
10-5-1 Interpretation of the $\mathbf{z}_{bus}$ Matrix 390
10-5-2 Step-by-Step $\mathbf{z}_{bus}$ Assembly 391
10-5-3 Comments on Results 395
10-6 Summary 396
Problems 396
References 398

Chapter 11 Unbalanced System Analysis 399

11-1 Neutral Currents and Voltages 399
11-2 Symmetrical Components 400
11-2-1 Definitions 400
11-2-2 The Symmetrical Component Transformation (SCT) 402
11-2-3 Decoupling Property between Sequence Currents 405
11-3 SCT of the Generator Performance Equations 406
11-3-1 Performance Equations for Unsymmetrically Loaded Machine 407
11-3-2 Sequence Network Representation of Generators 408
11-3-3 Determination of Generator Sequence Impedances 411
11-4 Sequence Impedances of Transmission Lines 413
11-4-1 Effect of Neutral Current upon Line Equations 414
11-4-2 Sequence Line Impedances 415
11-5 Sequence Impedance of Transformers 416
11-5-1 Positive- and Negative-Sequence Impedances 416
11-5-2 Phaseshift Dependency on Sequence Type 417
11-5-3 Zero-Sequence Impedance 419
11-6 Short-Circuit Analysis of Unbalanced Low-Order Systems 423
11-6-1 The Two-Bus System—Problem Statement 424
11-6-2 Sequence Network Assembly and Reduction 424
11-6-3 Single-Line-to-Ground Fault 425
11-6-4 Line-to-Line Fault 429
11-7 Short-Circuit Analysis of Unbalanced Large-Scale Systems 431
11-7-1 Problem Statement 431

11-7-2 Network Modeling by Means of Sequence Bus Impedance Matrices 432
11-7-3 SC Bus Voltage and Current Vectors 434
11-7-4 The Fault Matrices $\mathbf{Z}_s^f$ and $\mathbf{Y}_s^f$ 435
11-7-5 Short-Circuit Formulas 438
11-8 Summary 444
Problems 444
References 446

Chapter 12 Emergency Control 447

12-1 Concepts of Reliability, Security, and Transient Stability 448
12-2 Preventive and Emergency Control 448
12-3 Protective Relaying 449
12-3-1 "Instrument" Transformers 449
12-3-2 Relays 450
12-3-3 Unit Protection 450
12-3-4 Backup Protection 451
12-3-5 Sequence Filters 452
12-3-6 Line Reclosure 454
12-4 Transient Stability Analysis 456
12-4-1 Mechanical Analog 456
12-4-2 Basic Model Assumptions 458
12-4-3 The Single-Generator Case 458
12-4-4 The "Equal Area" Stability Criterion 461
12-4-5 Coherent Area Dynamics 464
12-4-6 Stability Enhancement Methods 467
12-5 Transient Analysis of Large-Scale Systems 470
12-5-1 Constructing the Dynamic Generator Model 472
12-5-2 Numerical Integration 474
12-6 Long-Term Frequency Dynamics 486
12-6-1 Two Examples 486
12-6-2 Average System Frequency 487
12-6-3 Center of Inertia 489
12-6-4 General Comments 491
Summary 492
Problems 493
References 495

Appendixes

A Elements of Vector and Matrix Algebra 497
A-1 Vectors 497
A-1-1 Special Vectors 497
A-1-2 Elementary Vector Operations 498
A-1-3 The Inner Vector Product 498
A-2 Matrices 501
A-2-1 Elementary Matrix Operations 501
A-2-2 Special Matrices 504
A-2-3 Determinants and Adjugate (Adjoint) Matrices 505

A-2-4 The Matrix Inverse 507
References 508
B Traveling Current Wave in Symmetrically Loaded Synchronous Machine 509
B-1 Standing and Traveling Waves 509
B-2 Application to Current-Loaded Armature Winding 510
B-3 Contribution from All Three Phases 512
B-4 Total Effect—A Traveling Wave 513
B-5 Harmonics Effects 513
C Optimum Search Methods 515
C-1 The Unconstrained Case 515
C-1-1 Geometrical Interpretation 515
C-1-2 Identification of Optimum 516
C-2 The Constrained Case 517
C-2-1 Geometrical Interpretation in Two-Dimensional Case 518
C-2-2 Finding the Constrained Optimum 518
C-2-3 Lagrange Cost Function 519
C-2-4 Several Constraint Equations 519
C-3 Gradient Search 520
C-3-1 Definition of Gradient Vector ∇C 521
C-3-2 Search Algorithm 521
D Turbine Modeling 523
D-1 Steam Turbines 523
D-1-1 Nonreheat Turbine 524
D-1-2 Reheat Type Turbine 524
D-2 Hydroturbines 525
References 526

Index 527

PREFACE

The first edition of this textbook was published in 1971. The intervening decade has witnessed major upheavals in the global energy picture. Most nations have been forced critically to reassess their energy technologies. The United States entered the seventies deeply committed to a petroleum-dominated energy base. Ten years later we see an accelerated shift towards coal, synfuels and other alternate energy resources.

Some of the latter, like solar and wind, make possible an energy supply of the de-centralized variety. Others, like coal, can be utilized only after their energy content has been transformed into electric form. Since these transformations can be economically achieved only in largescale central power stations our society will continue to find itself, in decades to come, increasingly dependent upon conventional-type electric supply systems.

The objective of the present second edition—like the first one—is to serve as an elementary and intermediate level course text for engineering students who pursue a career in design, planning or operation of electric power systems or related technologies. In order to meet the changing needs of the electric utility industry and also to match the evolving curriculum of the typical US university the revision job has been a thorough and major one. The result is a new text version that can be used in systems courses in departments which lack a special machinery program.

The material has been organized into four major parts as follows:

Part I. Introduction, background and fundamental concepts. (Chaps. 1, 2 and 3).

Many users of the first edition have recommended a more thorough coverage of three-phase theory. A whole new chapter has been devoted to this topic.

Part II. Basic components, design, theory and modeling. (Chaps. 4, 5, and 6).

The synchronous machine occupies a central role in power systems. Its steady-state and transient operational features have been allotted extra space in this edition. The mathematics-oriented Park-Blondel transform analysis method has been replaced with the more physical approach using rotating wave concepts. Transformer and transmission line coverages has also been expanded.

Part III. The energy system in its normal state, power flow, optimal dispatch and control. (Chaps. 7, 8, and 9).

More emphasis has been placed on the Newton-Raphson powerflow algorithm. Sparsity-oriented programming is being discussed. The treatment of optimal economic dispatch has been reorganized with the necessary mathematical methods summarized in a special appendix.

The chapter on automatic generation control was well received in the original edition. It has been better organized and considerably expanded in the new version. A special appendix has been added containing the response characteristics for the most commonly used turbine types.

Part IV. The system operating in emergency and extremis states, symmetrical and unbalanced faults, transient analysis. (Chaps. 10, 11, and 12).

The added emphasis on system reliability has necessitated a very thorough reworking of this part. Many new and simple examples have been added on fault analysis. The $\mathbf{Z}_{bus}$ building algorithm is treated in detail. Relay protection is being discussed. Longterm frequency dynamics has been added.

Many people both in industry and on campus have been contributing to this project and I am extending my thanks to them all. My students at University of Florida have shown great patience in the tryout process.

I stand in great debt to professors Paul M. Anderson (Arizona), Leo Grigsby (Virginia) and Bill Kersting (New Mexico) for having taken interest in and added many valuable suggestions to the manuscript.

A sabbatical spent with Florida Power Corporation in St. Petersburg and Florida Power and Light Co. in Miami provided many opportunities for invaluable exchange with engineers in those organizations.

Writing a textbook is an iterative process with often slow convergence. My wife, Margaret, with accuracy and patience provided the necessary and all-important typing service.

Olle I. Elgerd

ELECTRIC ENERGY SYSTEMS THEORY

An Introduction

CHAPTER

ONE

INTRODUCTION

Scenario The crew on the intergalactic explorer ship grew excited about the planet when it still appeared as only a speck on their telescope. Electromagnetic signals picked up by their high-gain antennas revealed an unmistakably intelligent coding pattern.

At closer range the cloudy haze on the illuminated side of the "blue planet" hides any clues as to possible habitation. As the ship passes in over the dark side, the contours of a vast continent become discernible in the weak lunar light. And now a familiar panorama spreads out: blotches of light in all sizes and shapes—the universal markings of electrically illuminated concentrations of intelligent planetary life.

1-1 HISTORICAL DEVELOPMENT OF THE ELECTRIC POWER INDUSTRY

Early Years

The basic human need for safe, efficient, and affordable light became the driving force which led to the development of today's continent-spanning electric energy or power systems. In the mid-nineteenth century gaslight was the predominant—but not very safe and practical—means of illumination.

The inventive genius of Edison brought forth the electric incandescent light bulb—and in the process created the need for an electricity supply system. The first electric "illuminating companies" came into being around 1880. The Pearl

Street system in New York, built by Edison, became the most famous. It supplied electric dc power for lighting of lower Manhattan. The power was generated in steam-engine-driven dc "dynamos" and distributed in underground cables. It is interesting to note that the system in its first eight years of operation had only one three-hour outage, thus setting a standard for reliability that has remained with the electric utility industry throughout its history.

Local electric illuminating companies grew rapidly throughout Europe and America in the first decade of the "electric age." Then came, in the last decade of the century, the invention of the ac induction motor. Power for the growing industry had earlier been limited to the steam engine and to mechanical linkage systems powered by waterwheels. This tended to concentrate a maze of polluting industry around waterfalls. Things grew particularly bad around the famous Niagara Falls starting what was probably the first major environmental movement. "Free Niagara" became the slogan of the day. The idea was born of harnessing the power and somehow sending it off to distant industrial centers, thus freeing the river banks from development.

Niagara became the turning point where the future shape of the electric power systems was to be hammered out. European and American companies competed for the conceptual design. Of the final proposals for power generation and transmission systems seven were for electric, four for pneumatic, two for hydraulic, and one for wire-rope design. When finally, in 1896, the first two generators and the transmission line to Buffalo, N.Y., were put into service, a 25-Hz three-phase electric system had been chosen the winning design.

Later developments

The electric induction motor developed into the dominating industrial powering device—later to be installed in most powered home appliances. Lights and motors were followed in decades to come by a myriad of other electric-use objects which today collectively make up the "loads" in our power systems. In many industrial countries, the available hydro-power could not meet the constantly increasing demand for electricity, and new generating methods were sought. Steam-generated power became the most popular alternative after Parson had introduced his revolutionary steam turbine design. This machine made possible the utilization of the energy contents of the vast deposits of fossil fuels. In 1982, about three quarters of the United States' electric power is derived from fossil fuels.

The introduction of the high-speed steam turbine made it necessary to increase the frequency, and 50–60 Hz are today commonly used. Rural electrification brought electricity to the farm country. As the local power systems thus expanded from cities outward they finally "grew together," and by interconnection we finally created a nation-wide system.

The growth of the U.S. electric utility industry during the first seven decades of the present century (Fig. 1-1) was essentially an exponential one—with an average doubling time of about ten years. The growth rate slowed markedly in

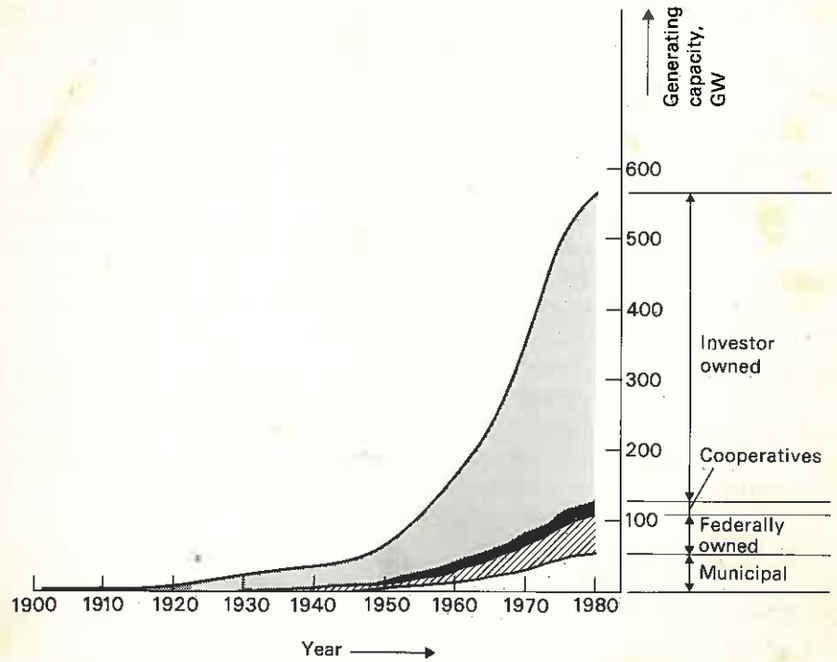

Figure 1-1 The growth of the U.S. electric generating capacity in the twentieth century.

the seventies. The total U.S. installed electric generating capacity, in 1982, is nearly 600 GW which averages out to about 2.5 kW per person. A strong individual can exert on a sustained basis about 100 watts of muscle power. Thus, each American has available about 25 "electric slaves" who in a multitude of ways help make life easier. We have in fact become, for better or worse, so dependent upon this convenient energy form that society during rare local "blackouts" develops a case of paralysis.†

1-2 STRUCTURE OF THE U.S. ELECTRIC UTILITY INDUSTRY

As noted from Fig. 1-1 the U.S. electric energy or power industry, more commonly known as the *electric utility industry*, is made up of four ownership segments, representing more than 3000 separate subsystems, which vary greatly

† It was proposed that President Hoover proclaim a national one-minute "blackout" in tribute to Edison at his funeral in October 1931. It was not accepted due to the risks involved.

in size. The private sector is the dominant one. The total cost of construction, operation, and maintenance is of such magnitudes that duplication cannot be afforded. The industry is thus in a sense a monopoly which, however, is closely regulated by federal and state agencies.

The electric power systems of other nations have organizational and ownership structures that match their different political and economic systems.

For economical and technological reasons, to be discussed in more detail in later chapters, most of the systems are electrically interconnected into vast *power grids* which are subdivided into regional operating groups called *power pools*. Each individual power system within such a pool operates technically and economically independently, but is contractually tied to the other pool members in respect to certain generation and scheduling features.

It is obvious that the best geographical location of the generating plants would be close to the electrical *load centers*, i.e., the regions where the major energy demand exists. However, the locations of the primary conventional energy sources do not necessarily coincide with the nation's population centers. We are therefore faced with the following choice:

1. Build the power plants close to the energy sources and then transport the electric energy to the load centers.
2. Build the power plants close to the load centers and transport the fuel from the source locality.

The electric power grid makes the first alternative technically feasible. However, in reality, the actual choice will be based upon a combination of technical, economical, and environmental factors. As we will see later, the voltage level of a transmission line determines its energy transmission capacity. By constantly increasing the voltage level and physical length of our transmission grid, we are developing a "superhighway system" for large blocks of electric energy that continuously widens our choice in this respect.

We summarize the advantages offered by pool operation:

1. It permits the construction of larger and more economical generating units and the transmission of large blocks of energy from the generating sources to major load centers.
2. It permits reduced reserve requirements by sharing of capacity between areas and sectors.
3. It provides capacity savings by seasonal exchange of capacity between areas which have opposing winter and summer needs.
4. It permits capacity savings from time zone and random diversity. (The peak load in California occurs three hours later than in New York.)
5. It facilitates transmission of off-peak energy.
6. It provides the flexibility to meet unforeseen emergency demands.

1-3 VOLTAGE STRUCTURE OF THE ELECTRIC ENERGY SYSTEM

An electric power system, even the smallest one, constitutes an electric network of vast complexity. The one factor that determines the system structure more than any others is system *size*. We shall not here enter into a discussion of the reasons of economical, political, historical, and technological nature that lie behind the present size distribution. By pointing out the great diversity in system magnitude, we wish to make it clear that there are no general rules regarding system structure that apply to *all* systems. It is possible, however, to discern certain similarities characterizing the majority of the systems.

As we shall see later, power transmittability increases and transmission losses decrease with increasing voltage level. The larger the blocks of power to be transmitted and the greater the distance over which they must be wheeled, the higher must be the operating voltage chosen. The U.S. standard operating voltages are given in Table 1-1.

Table 1-1

Voltage class	Nominal line voltage
Low	120/240 V (single phase)
	208 V
	240 V
	480 V
	600 V
Medium	2.4 kV
	4.16 kV
	4.8 kV
	6.9 kV
	12.47 kV
	13.2 kV
	13.8 kV
	23.0 kV
	24.94 kV
	34.5 kV
	46.0 kV
	69.0 kV
High	115 kV
	138 kV
	161 kV
	230 kV
Extra high	345 kV
	500 kV
	765 kV

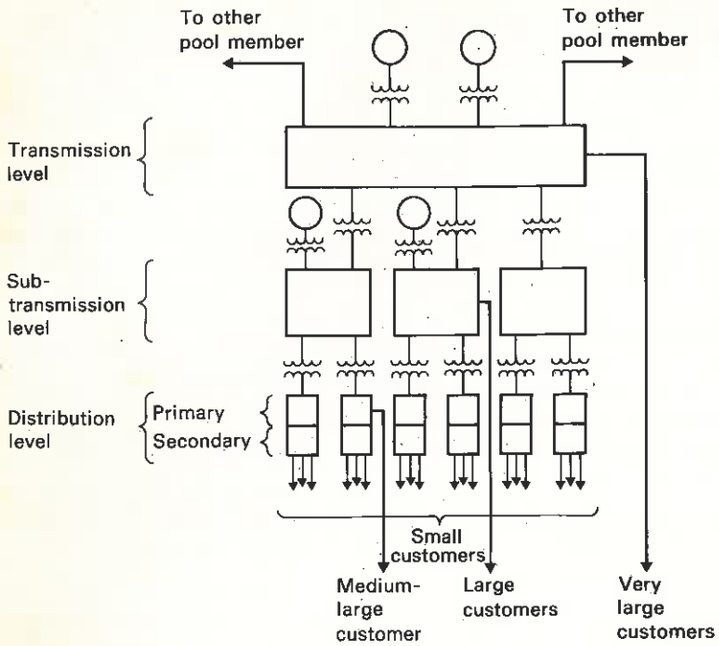

Figure 1-2 Power system structure.

Starting with the lowest voltage class we can distinguish the following transmission levels:

1. Distribution level (secondary and primary)
2. Subtransmission level
3. Transmission and pool level

Figure 1-2 shows schematically how a typical system is structured from a voltage-level point of view.

1-3-1 Distribution Level

The distribution circuits constitute the finest meshes in the overall network. Usually, two distribution voltage levels are used:

1. The *primary* or *feeder* voltage (for instance 23 kV)
2. The *secondary* or *consumer* voltage (for instance 120/240 V)

The distribution circuits, fed from the *distribution substations* (transformer stations), supply energy to the small (domestic) or medium-sized (small industrial and commercial) customers. Distribution engineering is in itself a subtechnology of considerable importance and variety, covering the problems of overhead or underground service, metering, switching, and protection.

1-3-2 Subtransmission Level

The subtransmission circuit distributes energy to a number of distribution substations in a certain geographical area at a voltage level that typically varies between 23 and 138 kV. It receives the energy directly from the generator bus in a generator station or via *bulk power substations*. Large customers are served directly from those stations.

The role of a subtransmission system is mainly the same as that of a distribution system, except that it serves a larger geographical area and distributes energy in larger blocks at higher voltage levels. It should be pointed out that in many systems there are no clear demarcation lines between subtransmission and transmission circuits. Increased load density makes it necessary and economical to superimpose a new and higher voltage grid on the existing one. In this way yesterday's transmission network becomes part of tomorrow's subtransmission network.

1-3-3 Transmission Level

The transmission system is distinctly different, in both its operation and characteristics, from the distribution and subtransmission systems. Whereas the latter two in most cases draw energy from a single source and transmit it to individual loads, the function of the transmission system is quite different. Not only does it handle the largest blocks of power, it also interconnects all the generator stations and all the major loading points in the system. The energy can be routed, generally, in any desired direction on the various links of the transmission system in a way that corresponds to best overall operating economy or best serves a technical objective. Via *interties*, transport of energy can take place to or from other power systems belonging to the same *power pool*.

The fundamental difference in the purpose of the transmission system as compared with the subtransmission and distribution systems shows up in the network structure. Whereas the latter two generally (but not always) are of *radial* structure (Fig. 1-3), the former tends to obtain a *loop* structure, as

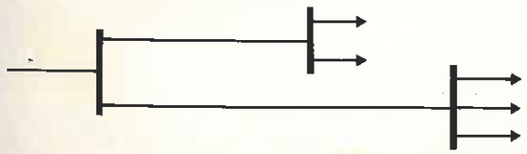

Figure 1-3 Radial network structure.

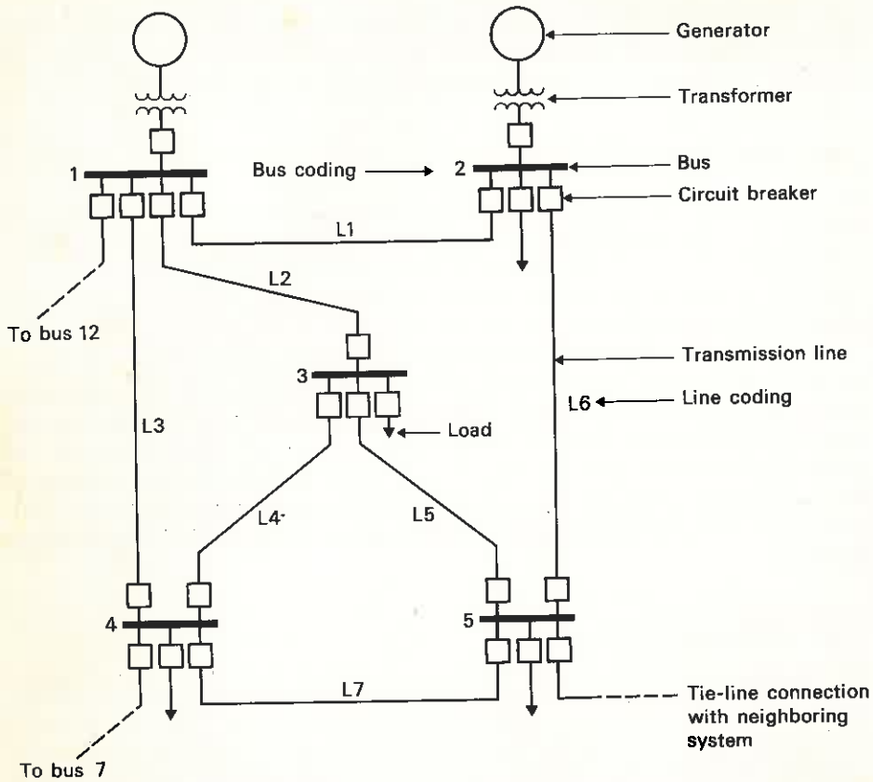

Figure 1-4 One-line diagram of power system.

exemplified in Fig. 1-4.† A radial-type network is the obvious solution where the energy flow has a predominant direction. The loop structure evidently gives more path combinations, and therefore better suits the purpose of the transmission level.

1-4 THE FUTURE

As this is being written the whole energy field is so clouded in uncertainties that it would be foolish to attempt any quantitative predictions for the future. However, certain trends are discernible that will control the developments of the electric utility industry in the decades ahead.

† Figure 1-4 represents a so-called "one-line" diagram of a transmission system. The symbols for generators, transformers, buses, lines, and loads that we shall use throughout the book are introduced in this figure. A nodal point of a transmission network is referred to as a "bus."

1-4-1 Present Generation Mix

No single factor is more important for the future course than the availability of prime energy resources. In 1982, the United States derives its electricity from the following sources:

Coal, gas, oil	72 percent
Hydropower	15 percent
Nuclear	13 percent

There is little doubt that petroleum and natural gas will grow increasingly scarce. Most hydropower in the contiguous states is already developed. Future emphasis will thus inexorably shift toward coal and nuclear resources of which the United States has relatively plentiful supplies. Each of these fuels represents both environmental and health perils. It must be realized, however, that no energy form is entirely risk free. Use of energy brought us out of the caves and made possible our present life styles. In the process, the perils of saber-toothed tigers and rickety dugout canoes were replaced by frontal crashes, oil spills, black lungs and radiation leaks. Our technology is not perfect, but it is the engineer's job to make it better.

1-4-2 Need for Planning and Research

The first century of the development of the electric utility industry took place in an atmosphere of limitless horizons and assumed resource abundance. Environmental and resource constraints are forcing us to approach the future with better planned and researched blueprints. Worldwide, energy research is assuming top priority.

A special cabinet-level energy office, Department of Energy, DOE, was created in the United States in 1977 in recognition of the special attention that energy matters deserve in the nation's future. A major private utility sponsored energy research organization, Electric Power Research Institute (EPRI), has been in existence since 1972. In addition, the largest utility companies have impressive research programs of their own.

The major goals for the future are to develop new primary resources, find better means of generation and transmission, and emphasize better and less wasteful use of electricity. Development of electric storage facilities is also high on the priority list. Let us look briefly at each of these areas:

1-4-3 New Prime Energy Resources

Several possible energy candidates have been identified, of which the more important are:

Solar power *Direct conversion* of solar radiation into electricity can be performed in "solar cells" which output low-voltage dc power. In 1982 such cells

are very expensive and inefficient and it is reasonable to assume that they will have little impact in the near future on electric bulk power generation.

Indirect conversion can conceptually be performed by letting concentrated solar radiation first generate steam which then will power conventional turbines. Small pilot plants will be in operation in the early eighties to test feasibility.

Any form of solar power is hampered by its cyclical availability and sensitivity to atmospheric conditions. Solar energy definitely offers the best potential future uses in *nonelectrical* form, thus helping preserve electric power for uses where no other energy form would do.

Wind, wave, geothermal, and tidal powers All of these have been tested. Some have been found to have limited geographical usefulness. Others, like wave generators, require very expensive and awkward generator designs. In all cases, the energy availability is of either cyclic or random character. Except for use in remote or very specific areas it is doubtful that any of these generation methods will have any greater impact.

Nuclear fusion "Taming of the hydrogen bomb" is a dream that is energetically tackled in many laboratories but where final success, realistically assessed, lies some time into the future. When this generation method succeeds it would start a new energy era, because of the plentiful fuel resources and its expected low environmental impact. In the fusion, like in the present fission process, the atomic energy is released in the form of high-grade heat. Thus transformation into electricity would be the only practical way of utilizing this energy.

1-4-4 Future Generating Equipment

Essentially one hundred percent of today's electric energy is generated in rotating synchronous generators (Chap. 4). There seems to exist no better alternative on the horizon, so our efforts will probably be centered on making this machine still better. Today's maximum generator unit size is exceeding 1 GW, and is limited by the allowable current densities used in rotor and stator windings.

Major efforts are under way to develop *superconducting* machines where the winding temperatures are kept close to absolute zero. The enormous current and flux densities achievable in such machines could possibly increase unit sizes to 5–6 GW. This would mean better generating economy.

1-4-5 New Transmission Methods

Edison's Pearl Street system operated with direct current. Since the early Niagara project, the industry has almost exclusively used ac transmission. In the nineteen-sixties and -seventies many high-voltage dc (HVDC) systems have been taken in use around the world. HVDC has advantages to offer particularly on very long lines (see Chap. 6) and we can expect a partial return to direct current in decades to come.

As the population densities increase we may see a trend to go toward underground transmission. Present-day cables are expensive and in addition have high capacitive leakage currents, prohibiting their use in ac systems for other than short transmission distances. HVDC has no such limitation. A recent HVDC underwater line operating at ± 250 kV transmits power between Norway and Denmark, a distance of about 150 km.

In the overhead ac field testing is ongoing and the present maximum voltage of 765 kV will probably be increased beyond 1200 kV.

1-4-6 Electric Storage Facilities

With the exception of low-power dc storage batteries, present technology possesses no high-energy electric storage devices. This has many drawbacks. All generating facilities must be dimensioned to handle the peak load, which often is twice the daily average load. As a result, the generating facilities are run, on the average, only partially loaded. When solar-electric power arrives on the scene, we would need storage facilities to tide us over rainy days.

Pumped hydropower and compressed gas represent hybrid electric-mechanical storage facilities.[6] Conceptually, superconducting magnetic coils represent a possible solution for "pure" electric storage. Here one would use enormous current densities to achieve very high magnetic-field energy levels, according to the formula

$$w_{mf} = \tfrac{1}{2}Li^2$$

Compare Sec. 2-2-2.

1-4-7 Energy Conservation

The first century of the "electric age" saw little need for emphasizing elimination of wasteful electricity uses. On the contrary, rate structures were often designed so as to encourage wasteful energy consumption. During the nineteen-seventies, as the world painfully became aware of the realities of the global energy shortages, it also became clear that conservation methods constitute our most effective means for bringing fast balance between demand and supply. Electricity is undoubtedly our most high-grade form of energy and it is prudent, therefore, in an age of shortage to pay particular attention to the optimization of its use.

First, we ought to gradually "unload" our electric supply systems of "low-grade" uses that may be equally or even better served by other means. Solar home heating is a good example. In the overall energy picture, it makes little sense to first burn natural gas in an electric power plant, losing in the process about two-thirds of its energy in the form of unwanted "thermal pollution," and then use the electricity to heat homes.

Second, we can achieve considerable electric power savings by reducing unnecessarily high lighting levels, oversized motors, and the like.

Third, the average electricity user can learn, by proper education, how

changed use habits can reduce consumption levels without any essential lowering of comfort. Rate restructuring can add incentives in this process.

Fourth, by various "load management" schemes it is possible to shift demand away from peak hours, thus reducing the capacity need for the power supply companies. More will be said about this in Chap. 3.

These and other conservation measures constitute collectively a "hidden source" of electric power of which we have only scratched the surface.

SUMMARY

We have briefly followed the development of the electric utility industry through its first century.

The United States like many other nations is faced with the necessity of gradually shifting its energy base from relatively scarce petroleum and natural gas to coal and nuclear fission energy. Over a longer time span more exotic energy resources like nuclear fusion, solar, wind, and others will undoubtedly enter the scene. In the vast majority of these cases, the released or captured energy will reach the consumer in electric form.

Electric energy, or power, technology concerns itself with the problems of generation, transmission, and distribution of electricity. In this introductory chapter we have given a sketchy picture of the electric utility industry. Historically the industry has been characterized by a steady growth. We surmise that future changes will be of evolutionary rather than revolutionary character. Economic, environmental, and resource availability factors are bound to exert mounting pressures for technology changes that will create a multitude of engineering challenges for tomorrow's electric power engineer.

PROBLEMS

1-1 Make a study of the ownership structure of the electric utility industry in your home state or region. Summarize your findings in a brief report.

1-2 Make a study of the electric energy consumption growth in the region served by your local electric utility during the last decades. How has the rate structure changed in the same period? Write a brief report.

1-3 Solar energy is characterized by both cyclic and random availability. By means of a so-called pumped hydrostorage facility (Ref. 6) the electric energy generated in a future solar-electric plant could be stored over days and maybe weeks. Discuss in a report how conceptually such a joint generation-storage facility could be incorporated into an existing power grid.

1-4 Solar power satellites, deep geothermal wells, and ocean thermal gradients are but a few "exotic" electric power sources proposed for the future. Choose one of these proposed concepts, research its conceptual viability, and write a brief report of your findings.

REFERENCES

1. EPRI Journal. (This is a monthly journal published by the Electric Power Research Institute. The journal contains timely and relevant articles and can be obtained from: EPRI, 3412 Hillview Avenue, Palo Alto, CA, 94304.)
2. *Structural Reform in the Electric Power Industry*, Federal Energy Administration Report PB-264 589, February 1977.
3. *Technical Reports of the Federal Energy Administration*, NTISUB/C/221-402, April 1977.
4. *Power System Planning and Operations: Future Problems and Research Needs*, EPRI EL-377-SR, February 1977.
5. R. L. Sullivan: *Power Systems Planning*, McGraw-Hill Book Company, New York, 1977.
6. Olle I. Elgerd: *Basic Electric Power Engineering*, Addison-Wesley Publishing Company, Boston, 1977.

CHAPTER

TWO

FUNDAMENTAL CONCEPTS OF ELECTRIC ENERGY SYSTEMS ENGINEERING

The reader is most certainly already well acquainted with the elementary aspects of electric energy, its various forms, the factors affecting its magnitude, etc. Since it will be subject to our continued attention throughout the book, it may be appropriate to review, at this time, some of its basic characteristics.

First, we point out that we shall find it convenient on most occasions to turn our attention not to the energy w itself, but to its *time rate*, or *power* p. By definition we have

$$p \triangleq \frac{dw}{dt} \quad \text{W} \tag{2-1}$$

A few words must be said about our choice of notation. We use lowercase symbols throughout† to indicate time functions or instantaneous values.

The units for electric energy and electric power in the *SI unit system*‡ (which is adhered to throughout the book) are *joule* (J) and *watt* (W), respectively. As one joule equals the energy corresponding to the power of one watt acting for one second it is often referred to as *wattsecond* (Ws).

These units are very small, and the more practical power units *kilowatt* (kW), *megawatt* (MW), and *gigawatt* (GW) are preferred. The conversion constants are as follows:

$$1 \text{ GW} = 10^3 \text{ MW} = 10^6 \text{ kW} = 10^9 \text{ W}$$

† Except for symbols representing electric and magnetic field vectors, in which instances it would be impractical to differ from the well-established practice of using capital-letter symbols.

‡ International System of Units, often referred to as the "metric" system.

The larger energy units *kilowatthour* (kWh), *megawatthour* (MWh), *gigawatthour* (GWh) and *terawatthour* (TWh) are often used. Their conversion constants are

$$1 \text{ TWh} = 10^3 \text{ GWh} = 10^6 \text{ MWh} = 10^9 \text{ kWh} = 3.6 \times 10^{15} \text{ J}$$

2-1 THE FUNDAMENTAL POWER FORMULA—ELECTROMAGNETIC ENERGY

The entire electric power technology is based upon the physical reality that it is possible to transform the "raw" energy forms available in nature into electric form, transmit this electric form of energy to the potential user, and then finally transform it back into useful energy forms of various types. These energy transformations take place often in a rather roundabout fashion.

In this section we shall discuss the characteristics of the energy once it has reached the electric form. However, it is unimportant *how* it reached there. Our starting assumption is therefore the availability of a device, referred to as a *generator*, having a minimum of two output terminals, from which we are able to draw a *sustained* current i at a *sustained* terminal voltage v. We shall make the additional assumption that v and i are *quasi-static*; i.e., their variations are relatively slow, which in practice means that they should not contain frequency components in excess of a few kilohertz.

The *fundamental power formula* now states that the generator supplies energy at the rate

$$p = vi \quad \text{W} \tag{2-2}$$

If the generator is connected to a *load*, as shown in Fig. 2-1, then we have, in fact, the simplest prototype of an electric power *transmission system*.

Although Eq. (2-2) places the emphasis on the *current* which no doubt is localized inside the conductors, the modern physical view tends to place the energy flow *outside* the conductors in the electromagnetic field that surrounds them (Fig. 2-2). Supporters of this view delegate to the conductors the role of

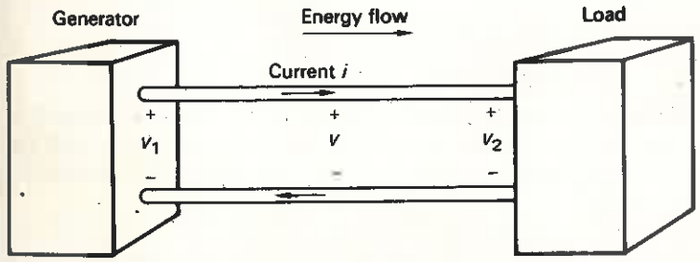

Figure 2-1 Simple electric transmission system.

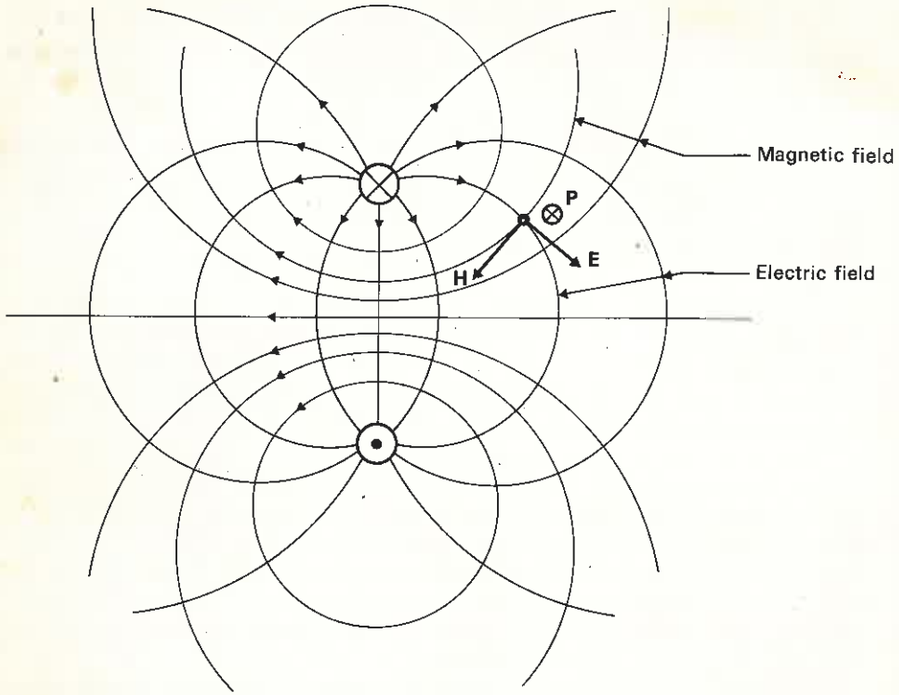

Figure 2-2 Electric and magnetic fields around single-phase transmission line.

waveguides. If we accept this interpretation, we designate the transmitted energy as *electromagnetic* energy w_{em}. We would not, of course, expect to find the energy uniformly distributed in the outside space, but rather having a *volume density* that would increase in some proportion to the intensity of the field vectors. The phenomenon is compactly described by the *Poynting vector* **P**,

$$\mathbf{P} = \mathbf{E} \times \mathbf{H} \qquad \text{W/m}^2 \tag{2-3}$$

In this formula the vector symbols represent

$$\mathbf{E} = \text{electric field strength, V/m}$$

$$\mathbf{H} = \text{magnetic field strength, A/m}$$

The vector **P** defined by Eq. (2-3) and depicted in Fig. 2-2 has a direction perpendicular to the plane containing **E** and **H** and a magnitude $|\mathbf{P}|$ equaling $|\mathbf{E}||\mathbf{H}| \sin \alpha$, where α is the angle between vectors **E** and **H**. It has the dimension of watts per meter squared.

The interpretation of Eq. (2-3) is as follows:

The electromagnetic energy *travels*, or *radiates*, in a direction coinciding with the direction of **P**. The amount of energy that penetrates a unit area is

rapidly diminishing with the distance from the conductors. Note that if the conductors are perfect, the electric field **E** will be zero inside the conductors, and thus no energy travels inside the conductors.

We shall, finally, discuss one additional and important aspect of the electromagnetic energy, its speed of travel, i.e., the speed with which a voltage (or current) perturbation propagates along the line. This velocity varies somewhat with the line parameters, but is always slightly less than the velocity of light.† We can therefore conclude that, for all practical purposes, the energy transmission takes place instantaneously. This fact has important practical consequences. For example, the power called for by the "load" must be delivered by the "generator" at the same instant of time.

2-2 ADDITIONAL FORMS OF ELECTRIC ENERGY

In addition to electromagnetic energy, we shall be concerned with the additional forms of electric energy:

1. Electric field energy w_{ef}
2. Magnetic field energy w_{mf}
3. Ohmic, or dissipative, energy w_{Ω}

2-2-1 Electric Field Energy w_{ef}

This form of energy exists wherever in space there is present an electric field, for instance, between the plates of a plate capacitor or surrounding the conductors of a transmission line. It is *stored* in the field in the amount

$$w_{ef} = \tfrac{1}{2}Cv^2 \qquad \text{J} \tag{2-4}$$

where C is the circuit capacitance, and v the potential difference between conductors.

Example 2-1 A typical power capacitor has a capacitance of 26.5 μF and a voltage rating of 100 kV. It is charged to a dc potential of 100 kV. How much energy is stored in the device?

SOLUTION From Eq. (2-4) we have

$$w_{ef} = \tfrac{1}{2} \times 26.5 \times 10^{-6} \times (100 \times 10^3)^2 = 132{,}500 \text{ J}$$

This energy (0.037 kWh) is not of very impressive magnitude to a power engineer. The example demonstrates that capacitors offer only poor energy storage potential.

Example 2-2 An ac voltage

$$v = v_{\max} \sin \omega t \tag{2-5}$$

† Compare the discussion on wave propagation in Chap. 10.

is applied to the capacitor in Example 2-1. Find the stored electric field energy w_{ef} and the associated power p.

SOLUTION We have first for the *energy*

$$w_{ef} = \tfrac{1}{2}Cv^2 = \tfrac{1}{2}Cv_{\max}^2 \sin^2 \omega t \tag{2-6}$$

For the *power* we get

$$p = \frac{dw_{ef}}{dt} = \tfrac{1}{2}\omega C v_{\max}^2 \sin 2\omega t = p_{\max} \sin 2\omega t \qquad \text{W} \tag{2-7}$$

It is noted that the power varies at a rate of *twice* that of the voltage and is having a *zero average* value.

Assuming a 60-Hz, 100-kV rms voltage (i.e., $v_{\max} = 141.4$ kV) the *peak* value of the power equals

$$p_{\max} = \tfrac{1}{2} \times 377 \times 26.5 \times 10^{-6} \times (141.4 \times 10^3)^2 = 99.9 \qquad \text{MW}$$

This *reactive capacitive* power is of considerable magnitude and is, as we shall see, of great practical significance in power-system operation.

Although stored electric field *energies* are of relatively small magnitudes, the associated *powers* become of important magnitudes at typical power frequencies.

2-2-2 Magnetic Field Energy w_{mf}

Magnetic field energy w_{mf} is stored everywhere in space where there is a magnetic field present. Its magnitude is computed from

$$w_{mf} = \tfrac{1}{2}Li^2 \qquad \text{J} \tag{2-8}$$

where L is the circuit inductance, and i the current.

Example 2-3 Apply the ac voltage (Eq. (2-5)) to a coil of inductance L. Find the stored magnetic field energy and the associated power.

SOLUTION The current will lag the voltage by 90° and equal

$$i = \frac{v_{\max}}{\omega L} \sin(\omega t - 90°) = -\frac{v_{\max}}{\omega L} \cos \omega t$$

From Eq. (2-8) we thus get

$$w_{mf} = \frac{1}{2} L \frac{v_{\max}^2}{\omega^2 L^2} \cos^2 \omega t \qquad \text{J} \tag{2-9}$$

and

$$p = \frac{dw_{mf}}{dt} = -\frac{1}{2}\frac{v_{\max}^2}{\omega L} \sin 2\omega t \qquad \text{W} \tag{2-10}$$

Again we find that the power rate is twice the voltage rate and the average power is zero. In comparing formulas (2-7) and (2-10) we note the 180° phase shifts between inductive and capacitive charging powers.

2-2-3 Ohmic, or Dissipative, Energy w_Ω

Electric energy is dissipated into heat whenever a current i flows in a resistive medium.

The heat dissipation rate, or *ohmic power*, equals

$$p = \frac{dw_\Omega}{dt} = Ri^2 \qquad \text{W} \tag{2-11}$$

where R is the resistance.

In many instances this heat dissipation represents a *useful* energy form as, for example, in an electrically heated oven. In most instances, however, the ohmic energy must be considered a *loss* energy. This is particularly true in a transmission system.

Example 2-4 Assume that we wish to transmit a given amount of power p_{tr} in the system in Fig. 2-1. Due to line resistance R, this transmission will be associated with an unavoidable ohmic power loss

$$p_{\text{loss}} = Ri^2 \qquad \text{W}$$

By using Eq. (2-2) we can express the loss power in the form

$$p_{\text{loss}} = R\left(\frac{p_{tr}}{v}\right)^2 \qquad \text{W}$$

By putting the power loss in relation to transmitted power, we get

$$\frac{p_{\text{loss}}}{p_{tr}} = R\frac{p_{tr}}{v^2} \tag{2-12}$$

This formula teaches us an important lesson: *The relative loss of power is inversely proportional to the square of the transmission voltage.*

The last example brings into focus the need for high transmission voltages. As an extra bonus, a high transmission voltage also results in increased "transmission capacity," a concept we shall explain in Chap. 3.

2-3 DC VERSUS AC POWER—CONCEPTS OF REAL AND REACTIVE POWERS

Direct current has some inherent advantages that make it the ideal transmission medium in certain instances. Alternating current, on the other hand, can be easily generated and conveniently transformed to high-voltage levels, and since cheap and effective ac motors can be built, this has naturally become our most common form of electric energy.

2-3-1 DC Transmission

If the voltages and current in Fig. 2-1 are of the dc type then we have for the sending-end and receiving-end powers, respectively:

$$p_1 = v_1 i = v_1 \frac{v_1 - v_2}{R} = \frac{v_1^2 - v_1 v_2}{R}$$
$$p_2 = v_2 i = v_2 \frac{v_1 - v_2}{R} = \frac{v_1 v_2 - v_2^2}{R} \tag{2-13}$$

R is the total resistance of *both* conductors. Typically $p_1 \approx p_2$ and we define an average transmitted power

$$p \triangleq \frac{p_1 + p_2}{2} = \frac{v_1^2 - v_2^2}{2R} \tag{2-14}$$

Note that this power has a *constant* magnitude. Its direction depends upon the voltage levels at the ends. If we wish the power to flow in the direction $1 \to 2$ we must maintain $v_1 > v_2$. Reversal of the power flow can be achieved only by controlling the voltage levels so that $v_2 > v_1$.

2-3-2 Single-Phase Transmission

We shall proceed to present some of the fundamental characteristics of ac power. We shall start with single-phase and demonstrate in the next chapter the advantages of the three-phase technique.

Consider, therefore, the case where the voltage and current in the system depicted in Fig. 2-1 are of the sinusoidal form

$$v = v_{\max} \sin \omega t$$
$$i = i_{\max} \sin (\omega t - \phi) \tag{2-15}$$

where the radian frequency ω is related to the frequency f by the formula

$$\omega = 2\pi f \qquad \text{rad/s} \tag{2-16}$$

Note, in formula (2-15), *that the phase angle ϕ is defined positive when voltage leads current.*

By using Eq. (2-2) we thus obtain the following expression for the transmitted power:

$$p = vi = v_{\max} i_{\max} \sin \omega t \sin (\omega t - \phi)$$

or, by using well-known trigonometric identities,

$$p = \frac{v_{\max} i_{\max}}{2} [\cos \phi - \cos (2\omega t - \phi)] \tag{2-17}$$

We introduce at this juncture† the *effective*, or *rms*, values of current and voltage

$$|V| \triangleq \frac{1}{\sqrt{2}} v_{\max} \qquad \text{V}$$
$$|I| \triangleq \frac{1}{\sqrt{2}} i_{\max} \qquad \text{A} \tag{2-18}$$

and can then write Eq. (2-17) as follows:

$$p = |V|\,|I| \cos \phi - |V|\,|I| \cos (2\omega t - \phi) \tag{2-19}$$

The transmitted power evidently *pulsates* (Fig. 2-3*a*) around an *average power* ($|V|\,|I|$) cos ϕ) at *double* radian frequency 2ω. During certain periods the power actually may become *negative*, indicating that the energy flow during these intervals is from the load to the generator.

† It is assumed that the reader is familiar with basic ac theory and concepts. To remove any symbol confusion we give this brief review:

Consider the sinusoidal voltage time function

$$v = v_{\max} \sin (\omega t + \alpha)$$

Euler's formula states:

$$e^{j(\omega t + \alpha)} = \cos (\omega t + \alpha) + j \sin (\omega t + \alpha)$$

If by the symbol Im $\{\ldots\}$ we mean "the imaginary part of" we can thus write for the voltage time function

$$v = \text{Im}\,\{v_{\max} e^{j(\omega t + \alpha)}\} = \sqrt{2}\,\text{Im}\left\{\frac{v_{\max}}{\sqrt{2}} e^{j\alpha} e^{j\omega t}\right\}$$

We now *define* the voltage phasor V as the complex number

$$V \triangleq \frac{v_{\max}}{\sqrt{2}} e^{j\alpha}$$

In abbreviated form the phasor is often written

$$V = \frac{v_{\max}}{\sqrt{2}} \underline{/\alpha}$$

The phasor V has a *magnitude*, *rms*, or *effective value*

$$|V| = \frac{v_{\max}}{\sqrt{2}} \qquad \text{V}$$

and a *phase*

$$\underline{/V} = \alpha \qquad \text{rad}$$

In terms of the voltage phasor the voltage time function can be written

$$v = \sqrt{2}\,\text{Im}\,\{V e^{j\omega t}\}$$

Note that phasors are always symbolized by capital letters.

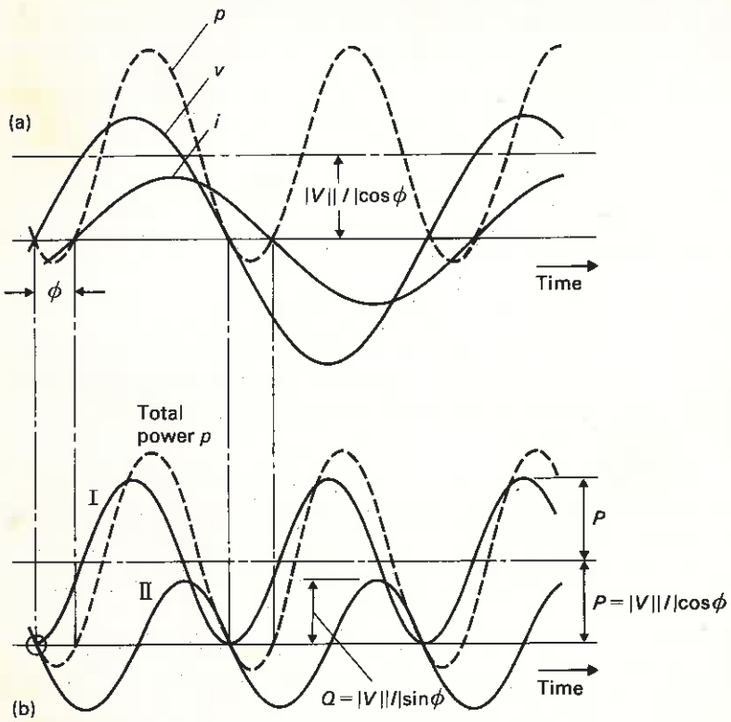

Figure 2-3 Voltage, current, and power in single-phase ac circuit.

2-3-3 Real and Reactive Power

Equation (2-19) can be written

$$p = |V|\,|I| \cos\phi - |V|\,|I|(\cos 2\omega t \cos\phi + \sin 2\omega t \sin\phi)$$

$$= \underbrace{|V|\,|I| \cos\phi(1 - \cos 2\omega t)}_{\text{I}} - \underbrace{|V|\,|I| \sin\phi \sin 2\omega t}_{\text{II}} \qquad (2\text{-}20)$$

We have actually decomposed the power into two components (marked I and II in Fig. 2-3*b*): the first pulsates around the same average value as before *but never goes negative*, and the second has a zero average value.

We introduce here the following two quantities:

$$P \triangleq |V|\,|I| \cos\phi \qquad \textit{real}, \text{ or } \textit{active}, \text{ power}$$
$$Q \triangleq |V|\,|I| \sin\phi \qquad \textit{reactive} \text{ power} \qquad (2\text{-}21)$$

and can then write Eq. (2-20) more compactly

$$p = P(1 - \cos 2\omega t) - Q \sin 2\omega t \qquad (2\text{-}22)$$

These newly defined concepts are of such fundamental importance that we find it appropriate to say a few words about their meaning:

1. The real power P is *defined* as the average value of p and therefore, physically, means the *useful* power being transmitted. Its magnitude depends very strongly on the *power factor* $\cos\phi$.
2. The reactive power Q is *by definition* equal to the *peak* value of that power component that travels back and forth on the line, resulting in zero average, and therefore capable of no useful work.

P and Q both have the physical dimension watts, but to emphasize the fact that the latter represents a "nonactive," or "reactive," power, it is measured in *voltamperes reactive*. The unit is symbolized var. Larger and more practical units are kilovars and megavars, related as follows to the basic unit:

$$1 \text{ Mvar} = 10^3 \text{ kvar} = 10^6 \text{ var}$$

Table 2-1 summarizes the real and reactive powers for the most commonly encountered load types. Note, in particular, that an inductive load absorbs positive Q. In power lingo, we say that an inductor *consumes* reactive power. A capacitive load, on the other hand, absorbs negative Q. We say that a capacitor *generates* reactive power.

Note also that we have included in Table 2-1 only *impedance* loads. Many important practical load types do not fall in this category. More will be said about this in Chap. 3 (Sect. 3-3).

Example 2-5 Compare the earlier derived Eqs. (2-7) and (2-10) with the more general power formula (2-22) and find the reactive powers absorbed by a capacitor and coil.

SOLUTION As both Eqs. (2-7) and (2-10) contain only the second component of Eq. (2-22) we conclude that $P = 0$ in both cases. For the *capacitive* circuit we obviously have

$$Q = -\tfrac{1}{2}\omega C v_{\max}^2 = -\omega C |V|^2$$

For the *inductive* circuit we get

$$Q = \frac{1}{2}\frac{v_{\max}^2}{\omega L} = \frac{1}{\omega L}|V|^2$$

The fact that a capacitor absorbs *negative* reactive power explains why a capacitor is considered a "Q-generator."

2-3-4 Apparent Power

Presently we introduce an additional very important power concept, the so-called *voltamps* (VA) or *apparent power*. As we shall see in later chapters this power concept is most useful as a rating unit. It is defined as the product of the rms voltage across and rms current through a circuit, i.e.,

$$\text{Voltamp} \triangleq |V|\,|I| \qquad (2\text{-}23)$$

Table 2-1

	Load type	Phasor relation	Phase angle	Power absorbed by load P	Power absorbed by load Q
1	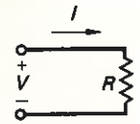		$\phi = 0$	$P > 0$	$Q = 0$
2	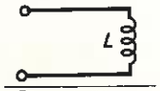	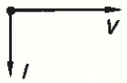	$\phi = +90°$	$P = 0$	$Q > 0$
3			$\phi = -90°$	$P = 0$	$Q < 0$
4	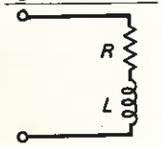	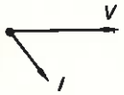	$0 < \phi < +90°$	$P > 0$	$Q > 0$
5	or 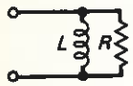				
6	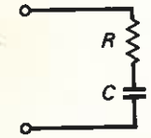	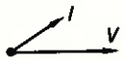	$-90 < \phi < 0$	$P > 0$	$Q < 0$
7	or 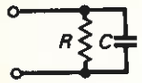				

As Eqs. (2-21) yield

$$\sqrt{P^2 + Q^2} = \sqrt{|V|^2|I|^2\cos^2\phi + |V|^2|I|^2\sin^2\phi} = |V||I|$$

we have proved the important formula

$$\text{Voltamp} = \sqrt{P^2 + Q^2} \tag{2-24}$$

Megavoltamps (MVA) and kilovoltamps (kVA) are more practical units for apparent power. They are related to the basic unit as follows

$$1 \text{ MVA} = 10^3 \text{ kVA} = 10^6 \text{ VA}$$

Example 2-6 Consider the ac load shown in Fig. 2-4*a*. It is fed from a 600-volt source. Compute the various powers absorbed in the two load branches.

SOLUTION As the voltage phasor V is common for both branches we choose it as our reference phasor in our analysis. We obtain for the branch currents

$$I_1 = \frac{V}{10} = \frac{600}{10} = 60.0\underline{/0°} \text{ A}$$

$$I_2 = \frac{600}{5 + j3} = 102.9\underline{/-31.0°} \text{ A}$$

The resistive load branch thus absorbs

$$P_1 = 600 \times 60 \times \cos 0° = 36.0 \text{ kW}$$

$$Q_1 = 600 \times 60 \times \sin 0° = 0 \text{ kvar}$$

The inductive load branch absorbs

$$P_2 = 600 \times 102.9 \times \cos 31.0° = 52.9 \text{ kW}$$

$$Q_2 = 600 \times 102.9 \times \sin 31.0° = 31.8 \text{ kvar}$$

Were we only interested in the *total* powers absorbed by *both* load branches we could have first replaced the actual circuit by its equivalent impedance Z shown in Fig. 2-4*b*:

$$Z = \frac{10(5 + j3)}{10 + 5 + j3} = 3.590 + j1.282\ \Omega$$

For the total current we then have

$$I_{tot} = \frac{600}{3.590 + j1.282} = 157.4\underline{/-19.7°} \text{ A}$$

The *total* powers will thus be

$$P_{tot} = 600 \times 157.4 \times \cos 19.7° = 88.9 \text{ kW}$$

$$Q_{tot} = 600 \times 157.4 \times \sin 19.7° = 31.8 \text{ kvar}$$

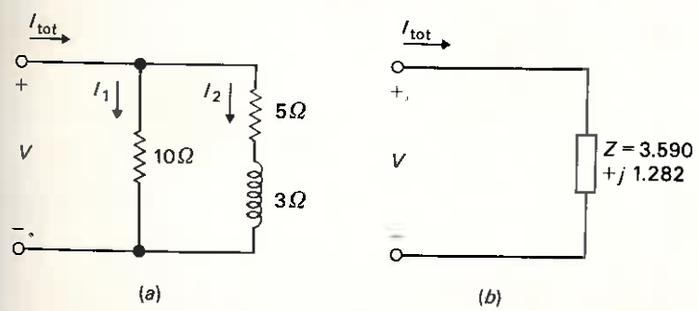

Figure 2-4 Example circuit.

Nº Reg. 2423

FAC. DE CIENCIAS EXACTAS Y TECNOLOGIA
BIBLIOTECA

Note that

$$P_{tot} = P_1 + P_2$$

$$Q_{tot} = Q_1 + Q_2$$

i.e., the total real and reactive powers can be obtained as the algebraic sums of the individual branch powers.

The apparent powers in the two load branches are, respectively,

$$\text{kVA}_1 = 0.6 \times 60 = 36 \text{ kVA}$$

$$\text{kVA}_2 = 0.6 \times 102.9 = 61.7 \text{ kVA}$$

The total apparent power equals

$$\text{kVA}_{tot} = 0.6 \times 157.4 = 94.4 \text{ kVA}$$

Note that

$$\text{kVA}_{tot} < \text{kVA}_1 + \text{kVA}_2$$

The reader should contemplate why the algebraic summation rule does *not* apply in the latter case. (Compare also Eq. (2-32).)

2-4 CONCEPT OF COMPLEX POWER

In power-system studies the so-called *complex power* constitutes a very valuable computational aid. In presenting this concept we consider the single-phase circuit shown in Fig. 2-5. For the voltage and current phasors we write

$$V = |V| e^{j\angle V}$$

$$I = |I| e^{j\angle I}$$

We introduce now the *conjugate* current defined by

$$I^* \triangleq |I| e^{-j\angle I} \tag{2-25}$$

The *complex power* is now defined as the product

$$S \triangleq VI^* \tag{2-26}$$

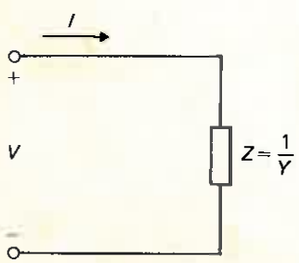

Figure 2-5 Single-phase circuit.

S possesses a very useful property, which we may confirm by substituting I^* into Eq. (2-26).

We get

$$S \triangleq VI^* = |V| e^{j\angle V} |I| e^{-j\angle I} = |V| |I| e^{j(\angle V - \angle I)}$$

The phase angle $\angle V - \angle I$ is the earlier introduced ϕ angle and we thus get

$$S = |V| |I| e^{j\phi} = |V| |I| \cos\phi + j|V| |I| \sin\phi = P + jQ \tag{2-27}$$

The last step follows directly from the definition of P and Q. We can write Eq. (2-26) in two alternative forms by using the relationships

$$V = ZI \quad \text{and} \quad I = YV$$

We obtain

$$S = VY^*V^* = Y^*|V|^2$$

or

$$S = ZII^* = Z|I|^2$$

By summarizing, we thus have the three alternative power expressions

$$S = P + jQ = VI^* = Z|I|^2 = Y^*|V|^2 \tag{2-28}$$

Upon computing S from either of the three alternative expressions (2-28) *we obtain P and Q simply as the real and imaginary parts of S, respectively.*

The magnitude $|S|$ of the complex power S can be expressed in any one of several ways:

$$|S| = |VI^*| = |V| |I| = \sqrt{P^2 + Q^2} \tag{2-29}$$

By comparison with Eq. (2-24) we thus recognize $|S|$ as our earlier defined "apparent" power.

Being a complex number S can be depicted in a complex number plane as shown in Fig. 2-6. The real, reactive, and apparent powers are equal in magnitude to the three sides of the right triangle, sometimes referred to as a *power triangle.*

Very often we find it convenient to use the *summation rule for complex powers.* Consider the two cases shown in Fig. 2-7. In the series circuit the individual impedances absorb, according to Eq. (2-28), the complex powers

$$S_i = |I|^2 Z_i \quad \text{for} \quad i = 1, \ldots, n$$

The *total* power equals

$$S_{tot} = VI^*$$

Since we have

$$V = IZ_1 + IZ_2 + \cdots + IZ_n$$

we can write the total power as

$$S_{tot} = (IZ_1 + IZ_2 + \cdots + IZ_n)I^* = |I|^2 Z_1 + |I|^2 Z_2 + \cdots + |I|^2 Z_n$$

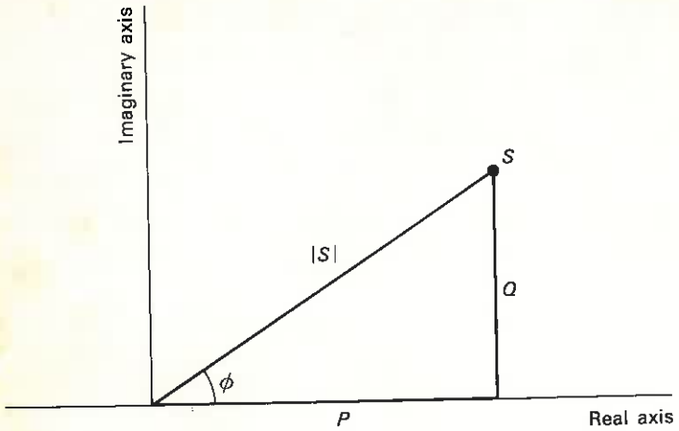

Figure 2-6 The power triangle.

We therefore obtain the summation rule

$$S_{tot} = \sum_{i=1}^{n} S_i \tag{2-30}$$

Similarly, in the parallel circuit in Fig. 2-7*b* the individual admittances absorb the complex powers

$$S_i = |V|^2 Y_i^* \qquad \text{for} \qquad i = 1, \ldots, n$$

By noting that

$$I = VY_1 + VY_2 + \cdots + VY_n$$

we readily prove that formula (2-30) again applies.

For the total *apparent* power in Fig. 2-7*a* we have

$$\begin{aligned} |S_{tot}| &= |V|\,|I| = |IZ_1 + IZ_2 + \cdots + IZ_n|\,|I| \\ &= |I|^2 |Z_1 + Z_2 + \cdots + Z_n| \end{aligned} \tag{2-31}$$

As

$$|Z_1 + Z_2 + \cdots + Z_n| \le |Z_1| + |Z_2| + \cdots + |Z_n|$$

we obtain

$$|S_{tot}| \le \sum_{i=1}^{n} |S_i| \tag{2-32}$$

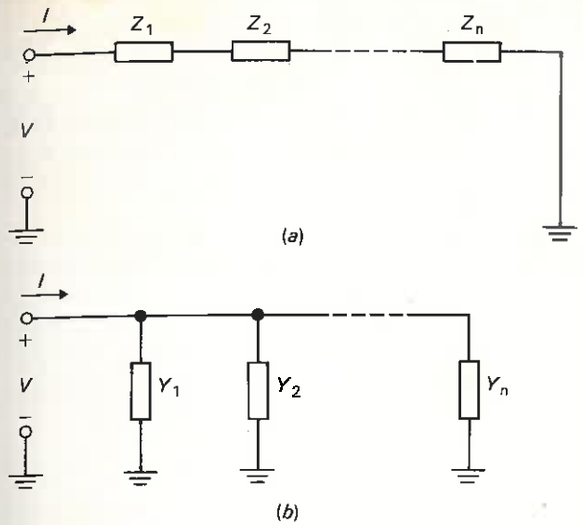

Figure 2-7 Multiload cases.

Example 2-7 Work Example 2-6 using the concept of complex powers.

SOLUTION As the voltage across the load branches is given we use the last form of Eq. (2-28). For the resistive load branch we have

$$S_1 = P_1 + jQ_1 = (\tfrac{1}{10})^* \times 600^2 = 360{,}000 + j0$$

$$\therefore \quad P_1 = 36 \text{ kW}$$

$$Q_1 = 0 \text{ kvar}$$

For the inductive load branch we obtain

$$S_2 = P_2 + jQ_2 = \left(\frac{1}{5 + j3}\right)^* \times 600^2 = \frac{1}{5 - j3} \times 600^2 = 52{,}900 + j31{,}800$$

$$\therefore \quad P_2 = 52.9 \text{ kW}$$

$$Q_2 = 31.8 \text{ kvar}$$

By use of the equation (2-30) and the inequality (2-32) we then confirm the results already obtained in Example 2-6.

2-5 PER-UNIT REPRESENTATION OF IMPEDANCES, CURRENTS, VOLTAGES, AND POWERS

The electric power engineer often prefers to express impedances, currents, voltages, and powers in per-unit (pu) values rather than in ohms, amperes, kilovolts, and megavars or megawatts. Several advantages can be gained by this practice:

1. Per-unit data representation yields valuable *relative* magnitude information.
2. Circuit analysis of systems containing transformers of various transformation ratios is greatly simplified.
3. Circuit parameters tend to fall in relatively narrow numerical ranges making erroneous data easy to spot.

2-5-1 Definitions

These advantages will be demonstrated throughout the text. Here we will present the basic features of the per-unit method. Consider a system link transmitting the complex power S. The voltage and current are represented by the phasors V and I respectively. Arbitrarily we now *define* two *base* values $|V_b|$ and $|I_b|$ expressed in rms voltage and current respectively. Per-unit voltage and current phasors are then defined by the *dimensionless* and *complex* ratios

$$V_{pu} \triangleq \frac{V}{|V_b|} = \frac{|V|}{|V_b|}\underline{/V} \qquad \text{pu volts}$$
$$I_{pu} \triangleq \frac{I}{|I_b|} = \frac{|I|}{|I_b|}\underline{/I} \qquad \text{pu amps} \tag{2-33}$$

For example, if the standard voltage 138 kV is chosen as the base voltage, then the voltage phasor

$$V = 151\underline{/20^\circ}\ \text{kV}$$

would assume the per-unit value

$$1.094\underline{/20^\circ} \qquad \text{pu kV}$$

This per-unit value thus immediately tells us that the actual voltage exceeds the standard level by 9.4 percent.

Next, we define base values of power and impedance in terms of *already chosen* voltage and current bases:

$$|S_b| \triangleq |V_b|\,|I_b| \qquad \text{VA}$$
$$|Z_b| \triangleq \frac{|V_b|}{|I_b|} \qquad \Omega \tag{2-34}$$

A complex power S and an impedance Z can then be expressed in *dimensionless* per-unit values, according to

$$S_{pu} \triangleq \frac{S}{|S_b|} = \frac{P+jQ}{|S_b|} = \frac{P}{|S_b|} + j\frac{Q}{|S_b|} = P_{pu} + jQ_{pu}$$
$$Z_{pu} \triangleq \frac{Z}{|Z_b|} = \frac{R+jX}{|Z_b|} = \frac{R}{|Z_b|} + j\frac{X}{|Z_b|} = R_{pu} + jX_{pu} \tag{2-35}$$

2-5-2 Power and Circuit Formulas in Per-Unit Values

It is important to realize that the general power formula (2-26) holds true if all quantities are expressed in per-unit values. This we prove as follows.

By dividing Eq. (2-26) by $|S_b|$ and making use of the first of Eqs. (2-34) we have

$$S_{pu} = \frac{S}{|S_b|} = \frac{VI^*}{|S_b|} = \frac{V}{|V_b|}\frac{I^*}{|I_b|} = V_{pu}I^*_{pu} \tag{2-36}$$

Of equal importance is the fact that per-unit values still satisfy the general Ohm's law. We prove this as follows:

$$V_{pu} = \frac{V}{|V_b|} = \frac{ZI}{|V_b|} = \frac{Z}{|V_b|/|I_b|}\frac{I}{|I_b|} = Z_{pu}I_{pu} \tag{2-37}$$

Of the four base values $|V_b|$, $|I_b|$, $|S_b|$, and $|Z_b|$ only two can be arbitrarily chosen. In practice, it is most common to choose the pair $|V_b|$ and $|S_b|$. The remaining two are then computed from

$$|I_b| = \frac{|S_b|}{|V_b|} \tag{2-38}$$

and

$$|Z_b| = \frac{|V_b|}{|I_b|} = \frac{|V_b|^2}{|I_b|\,|V_b|} = \frac{|V_b|^2}{|S_b|} \tag{2-39}$$

Example 2-8 Work Example 2-6 expressing all quantities in per unit. Use the following base values:

$$|V_b| = 600\ \text{V}$$
$$|S_b| = 100\ \text{kVA}$$

SOLUTION Using formula (2-39) we first compute the base impedance

$$|Z_b| = \frac{600^2}{100{,}000} = 3.600\ \Omega$$

For the base current we get

$$|I_b| = \frac{100{,}000}{600} = 166.7\ \text{A}$$

In terms of the above base voltage and base impedance we then obtain the per-unit circuit diagram shown in Fig. 2-8. From this diagram we first determine the per-unit currents in the two load branches

$$I_1 = \frac{1.00}{2.778} = 0.360\underline{/0^\circ}\ \text{pu}$$

$$I_2 = \frac{1.00}{1.389 + j0.833} = 0.529 - j0.318 = 0.617\underline{/-31.0^\circ}\ \text{pu}$$

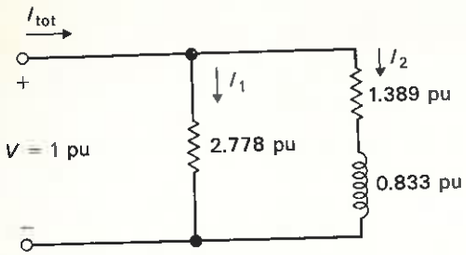

Figure 2-8 Circuit data in Fig. 2-4 expressed in per unit.

For the load powers we have

$$P_1 + jQ_1 = VI_1^* = 1.00(0.360 + j0) = 0.360 + j0 \text{ pu}$$

$$P_2 + jQ_2 = VI_2^* = 1.00(0.529 + j0.318) = 0.529 + j0.318 \text{ pu}$$

As a check we then compute the following actual current and power values, which were earlier computed in Example 2-6:

$$|I_1| = 0.360 \times 166.7 = 60.0 \text{ A}$$

$$|I_2| = 0.617 \times 166.7 = 102.9 \text{ A}$$

$$P_1 = 0.360 \times 100 = 36.0 \text{ kW}$$

$$Q_1 = 0 \text{ kvar}$$

$$P_2 = 0.529 \times 100 = 52.9 \text{ kW}$$

$$Q_2 = 0.318 \times 100 = 31.8 \text{ kvar}$$

SUMMARY

In this chapter we have first reviewed some of the basic energy and power concepts which form the foundation for electric power technology. The fundamental power formula identifies the electric current and voltage along a line as the "carriers" of the electric energy, but the modern physical view places it rather in the electromagnetic field surrounding the line conductors.

Energy can be stored in electric and magnetic fields but not in any appreciable quantities to make capacitors and coils suitable as "bulk storage facilities" for electric energy. These circuit elements do play an important role for temporary energy storage over short periods of time (less than a cycle) and we have shown how this short-time energy storage ties in with the reactive power flow in an ac circuit.

Real, reactive, apparent, and complex powers have been defined and will play an important role in our continuing story. Although SI units are used throughout we have also introduced the "per-unit" system which in all probability will continue to play an important role among electric power engineers.

PROBLEMS

Throughout the book the end-of-chapter Problems marked by a star (*) are considered relatively easy and are intended as "drill" problems.

***2-1** For the capacitive and inductive circuits discussed in Examples 2-2 and 2-3 plot versus time the stored field energies and associated powers.

***2-2** Connect a coil and capacitor in parallel across an ac voltage source of radian frequency $\omega = 2\pi f$. Choose L and C so that they satisfy the "resonance" relationship

$$LC = \frac{1}{\omega^2}$$

Show that the coil and the capacitor alternately will be charged with energy and that this energy will oscillate between the two elements with no energy exchange taking place with the source. (Compare Example 2-5.)

***2-3** For each one of the seven circuits in Table 2-1 find the actual values for P and Q. Your answers should be expressed in terms of $|V|$ (that is, the rms value of the terminal voltage), the radian frequency ω, and the circuit parameters R, L, and C.

***2-4** A 25-μF capacitor is connected to a 100-kV ac source. How many megavars of reactive power does the capacitor generate? The frequency is 60 Hz.

2-5 The generator in Fig. 2-1 generates single-phase ac power at a transmission voltage level of $|V_{tr}|$ volts rms. We neglect the relatively small voltage drop along the line and assume thus that the voltage is the same along the line.

The line impedance can be represented by a resistance R_l in series with an inductive reactance X_l ohms. In a certain loading situation a power $S_{tr} = P_{tr} + jQ_{tr}$ is being transmitted on the line. The resistance R_l will consume a real-loss power of P_{loss} W and the reactance X_l likewise a reactive-loss power Q_{loss} vars. These loss powers are assumed to be relatively small compared with the transmitted powers.

Prove that the transmission losses may be computed from the approximate formulas

$$P_{loss} \approx R_l \frac{P_{tr}^2 + Q_{tr}^2}{|V_{tr}|^2} \quad \text{W} \tag{2-40}$$

$$Q_{loss} \approx X_l \frac{P_{tr}^2 + Q_{tr}^2}{|V_{tr}|^2} \quad \text{var} \tag{2-41}$$

***2-6** Consider the transmission system in Fig. 2-1 again. The load can be represented by an impedance

$$Z_L = 100 + j30 \ \Omega$$

The line impedance equals

$$Z_l = 1 + j4 \ \Omega$$

The voltage V_1 at the generating end—the "sending-end" voltage—equals 100 kV rms. Compute

(*a*) Line current
(*b*) Voltage across load V_2 ("receiving-end" voltage)
(*c*) Voltage drop along line
(*d*) Megawatts and megavars consumed by "load"
(*e*) Megawatts and megavars supplied by "generator"
(*f*) Megawatts and megavars lost on line

Note that "voltage drop" can be interpreted as either $|V_1 - V_2|$ or $|V_1| - |V_2|$. What is the difference?

***2-7** In the previous problem, compute average values for $|V_{tr}|$, P_{tr}, and Q_{tr} based upon sending- and receiving-end values. Then, substitute these values into formulas (2-40) and (2-41) and compute loss powers. How do these *approximate* values compare with *exact* ones you computed in Prob. 2-6*f*?

2-8 Connect now the capacitor you studied in Prob. 2-4 across the load impedance in Prob. 2-6. Then rework Prob. 2-6. You should find now that the reactive power supplied by the generator decreases drastically because the reactive power consumed by the load will be mainly supplied by the capacitor. As a result the megawatts lost in the line will decrease.

You will also find that the load voltage will increase. (In later chapters we shall see that adding shunt capacitors is an important means for boosting voltage levels in a power system.)

***2-9** In the formula (2-32) when does the equals sign apply?

***2-10** A resistor, inductor, and capacitor have the impedances 5, 10, and 15 ohms respectively. They are connected in one case in series, in another case in parallel to form a load fed by a 1.10-kV ac source.

Determine the total real and reactive powers consumed by the loads in each case. Work the problem in per units using the following base values:

$$|V_b| = 1.00 \text{ kV}$$

$$|S_b| = 1.00 \text{ MVA}$$

2-11 In a base system $|S_b'|$ and $|V_b'|$, a certain impedance has the per-unit value Z_{pu}'. If we need to find the per-unit value Z_{pu}'' of the same impedance in the base system $|S_b''|$ and $|V_b''|$ we can use the formula

$$Z_{pu}'' = Z_{pu}' \frac{|S_b''||V_b'|^2}{|S_b'||V_b''|^2} \tag{2-42}$$

Prove this statement.

2-12 Consider the voltage drop in the line discussed in Prob. 2-6, defined by

$$|\Delta V| \triangleq |V_1| - |V_2|$$

In a practical case one typically has

$$|\Delta V| \ll |V_1| \approx |V_{tr}|$$

Prove that the relative voltage drop, or *regulation* defined as $|\Delta V|/|V_{tr}|$, can be computed from

$$\frac{|\Delta V|}{|V_{tr}|} \approx R_l \frac{P_{tr}}{|V_{tr}|^2} + X_l \frac{Q_{tr}}{|V_{tr}|^2} \quad \text{pu} \tag{2-43}$$

CHAPTER

THREE

THE SYMMETRICAL THREE-PHASE SYSTEM

A distinct drawback of the single-phase transmission system discussed in the previous chapter is the pulsating character of the power. In some load objects like heaters, radios, and television apparatus this is of little concern. In others, like incandescent lighting, the light intensity will flicker, but this effect is usually negligible at normal power frequencies.

Electric motors constitute the most important group of load objects and here the pulsating power translates into a pulsating torque. Small "fractional horsepower" ac motors are nevertheless designed single-phase because of lower cost. The undesirable effects of the pulsating torque of such motors can be minimized by elastic mounts. However, in large induction motors—the electric "workhorse" of our industrial society—the torque pulsations are completely unacceptable.

The pulsating torque likewise would reach completely nonpermissible proportions in single-phase ac generators which for economical and other reasons must be designed with ratings in the multimegawatt range. Three-phase ac eliminates these power and torque pulsations and has in fact become our dominant electric transmission medium. This chapter presents the basic theory and features of three-phase power.

3-1 THE SYMMETRICAL THREE-PHASE TRANSMISSION SYSTEM

Consider for a moment the "single-phase" hydraulic generator in Fig. 3-1 which is clearly characterized by a pulsating torque. Considerable torque smoothing can be achieved by an arrangement of the type shown in Fig. 3-2, consisting of three parallel-operating single-phase hydraulic pistons.

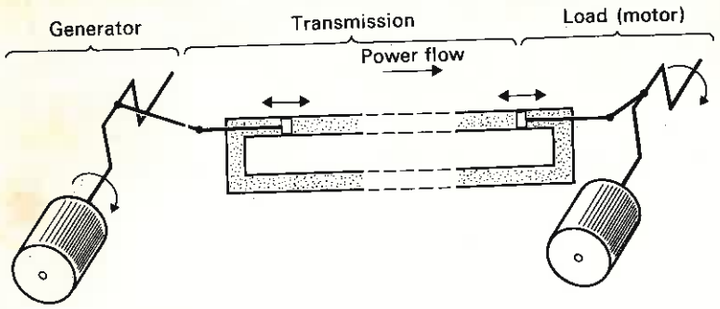

Figure 3-1 "Single-phase" hydraulic transmission system.

3-1-1 Evolution of the Three-Phase System

By taking a cue from the above hydraulic analog we create now the symmetrical electric three-phase transmission system depicted in Fig. 3-3. We start with the three *phases* shown in Fig. 3-3*a*. The phases are identical in all respects except one—the generated emf's e_a, e_b, and e_c have identical rms values but their phase angles are respectively displaced 120 and 240° from each other, in such a way that they reach their peak values in the sequential order *a*, *b*, *c*, *a*, . . . as shown in Fig. 3-4. We say that the emf's have the *phase sequence abca* . . . . How in practice such a set of emf's is actually generated will be discussed in the next chapter.

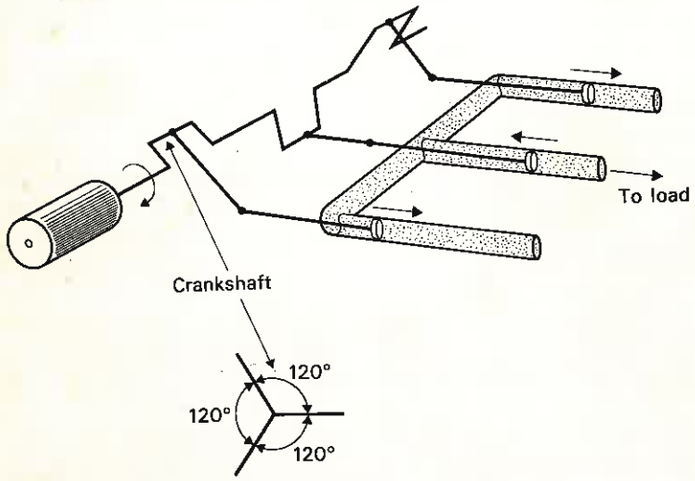

Figure 3-2 "Three-phase" hydraulic generator.

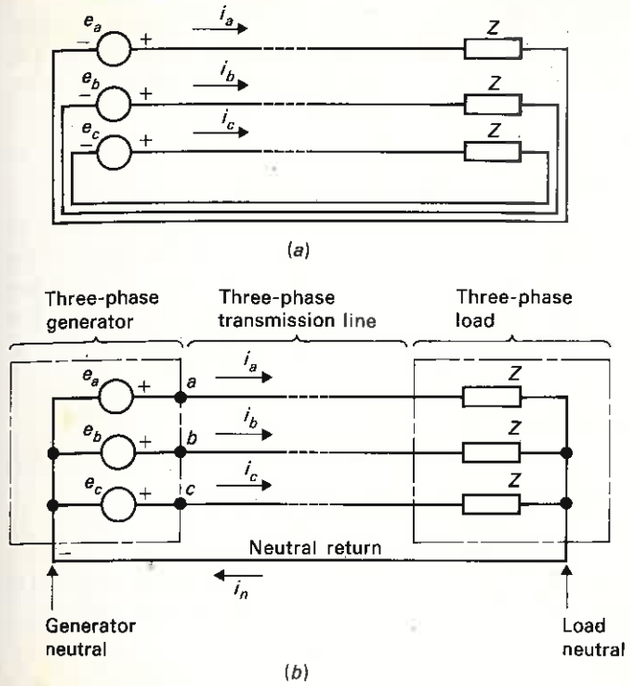

Figure 3-3 Formation of electric three-phase system.

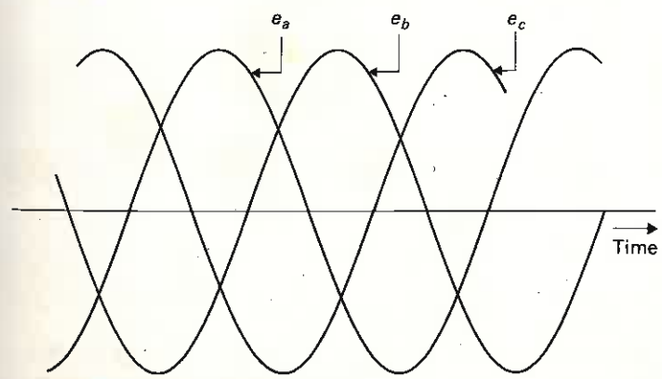

Figure 3-4 Time variation of emf's in previous figure.

Instead of having three separate return lines as shown in Fig. 3-3*a* we interconnect the three phases into a *neutral return* as depicted in Fig. 3-3*b*. The system thus obtained represents the basic form of an electric three-phase transmission system.

3-1-2 Voltage Relationships

The electric potentials of the three generator terminals (marked *a*, *b*, and *c* in Fig. 3-3) relative to the *generator neutral* will not, in general, be equal to the induced emf's because of the internal voltage drops in each generator phase. Because of the symmetry they will, however, like the emf's, have a relative time phase of the type shown in Fig. 3-4 and we can thus write for these *phase*, or *phase-to-neutral*, voltages

$$\begin{aligned} v_a &= \sqrt{2}\,|V_p| \sin \omega t \\ v_b &= \sqrt{2}\,|V_p| \sin (\omega t - 120°) \\ v_c &= \sqrt{2}\,|V_p| \sin (\omega t - 240°) \end{aligned} \tag{3-1}$$

where $|V_p|$ is the phase voltage measured in root mean square.

Visualized as phasors the phase voltages take on the appearance depicted in Fig. 3-5. If V_a is chosen as reference phase voltage we obviously can write

$$\begin{aligned} V_a &= |V_p| \underline{/0°} \\ V_b &= |V_p| \underline{/-120°} \\ V_c &= |V_p| \underline{/-240°} \end{aligned} \tag{3-2}$$

A set of three phasors which are all of equal magnitude but displaced timewise by 120 and 240° respectively *are said to possess three-phase symmetry.*

The *line*, or *phase-to-phase*, voltages are those voltages which we can measure between the phases. They are symbolized by V_{ab}, V_{bc}, and V_{ca} in Fig. 3-5. The line voltages are related to the phase voltages by the equations

$$\begin{aligned} V_{ab} &= V_a - V_b \\ V_{bc} &= V_b - V_c \\ V_{ca} &= V_c - V_a \end{aligned} \tag{3-3}$$

We note directly from Fig. 3-5 that the magnitudes of the three line voltages are equal and of rms value

$$|V_{ab}| = |V_{bc}| = |V_{ca}| = 2|V_a| \cos 30° = \sqrt{3}|V_p| \tag{3-4}$$

or in words: *In a symmetrical three-phase system the line-voltage magnitude is $\sqrt{3} = 1.732$ times the phase-voltage magnitude.*

Power engineers, when referring to the voltage ratings of a three-phase device, always mean the line voltage. For example, a 230-kV transmission line thus has a 230-kV line voltage and a 133-kV phase voltage.

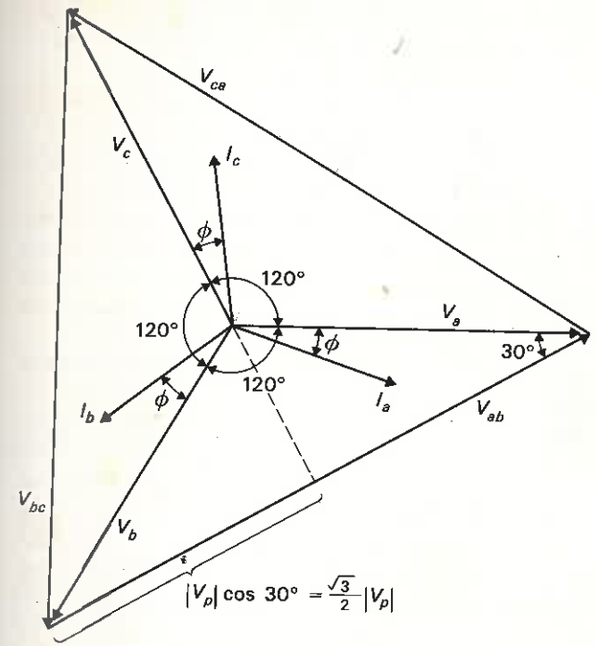

Figure 3-5 Voltage and current phasors in symmetrical three-phase system.

3-1-3 Current Relationships

If the load is assumed *balanced*, or *symmetrical*, the three *phase currents* in Fig. 3-3 will also possess three-phase symmetry:

$$\begin{aligned} i_a &= \sqrt{2}\,|I_p| \sin (\omega t - \phi) \\ i_b &= \sqrt{2}\,|I_p| \sin (\omega t - 120° - \phi) \\ i_c &= \sqrt{2}\,|I_p| \sin (\omega t - 240° - \phi) \end{aligned} \tag{3-5}$$

The phase angle ϕ depends upon the load impedance Z.

With the voltage V_a already chosen as our reference phasor we have for the current phasors

$$\begin{aligned} I_a &= |I_p| \underline{/-\phi} \\ I_b &= |I_p| \underline{/-(\phi + 120°)} \\ I_c &= |I_p| \underline{/-(\phi + 240°)} \end{aligned} \tag{3-6}$$

The current phasors are shown in Fig. 3-5.

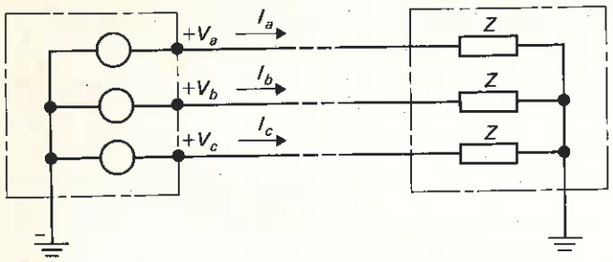

Figure 3-6 No neutral conductor needed in symmetrical three-phase system.

The return current I_n in the neutral is the sum of the three-phase currents. As the vectorial sum of the current phasors equals zero, i.e.,

$$I_n = I_a + I_b + I_c = 0 \tag{3-7}$$

we conclude that *no return current exists in a symmetrical three-phase system and no return lead is therefore needed.* We thus arrive at the typical three-phase system configuration shown in Fig. 3-6. (We hasten to add that in no way is the figure complete. For example, in a practical situation we would, typically, find step-up and step-down transformers at each end of the transmission line.)

The generator and load "neutrals" have been "grounded" in order to fix their potentials. Should we have complete symmetry between the phases and a resulting zero current in the neutral leads then there would obviously exist zero voltage drop between the generator and load neutrals. *All phase voltages in a symmetrically operated three-phase system can therefore be measured relative to a "system ground" which has the same potential (zero) throughout the whole system.*

3-1-4 Power Relationships

The total† transmitted instantaneous three-phase power equals the sum of the individual phase powers, i.e.,

$$p_{3\phi} = v_a i_a + v_b i_b + v_c i_c \qquad \text{W} \tag{3-8}$$

By substitution of expressions (3-1) and (3-5) into Eq. (3-8) and by making use of the trigonometric identities

$$\sin\alpha \sin\beta = \tfrac{1}{2}[\cos(\alpha-\beta) - \cos(\alpha+\beta)]$$

and

$$\cos\alpha + \cos(\alpha - 120°) + \cos(\alpha - 240°) = 0 \tag{3-9}$$

we arrive at the important formula

$$p_{3\phi} = 3|V_p||I_p| \cos\phi = 3P_{1\phi} \qquad \text{W} \tag{3-10}$$

† The subscripts 1ϕ and 3ϕ refer to "single-phase" and "total three-phase" respectively.

In words: *In a symmetrical three-phase system the total instantaneous three-phase power is nonpulsating and equal to three times the real power in each phase. Whenever we refer to the magnitude of the real power in a three-phase system we invariably mean the total three-phase power (3-10).*

It is indeed this constancy of three-phase power that is the primary advantage of three-phase over single-phase. Its most important manifestation is the constancy of torque that characterizes both three-phase generators and motors. Since the instantaneous three-phase power is constant, we are tempted to assume that the reactive power is of no importance in a three-phase system. This is not the case. *Note that the power in each phase still is of pulsating "single-phase type," as described in Eq. (2-22).*

Compare: The three phase currents add up to zero at each instant of time, but they are still very much in evidence in each phase.

Equation (3-10) tells us that the three-phase real power equals three times the single-phase real power $P_{1\phi}$. We are led to ask whether a similar formula, i.e.,

$$Q_{3\phi} \triangleq 3Q_{1\phi} = 3|V_p||I_p| \sin\phi \qquad \text{var} \tag{3-11}$$

is applicable for the reactive power.

We realize immediately that the concept of "three-phase reactive power" $Q_{3\phi}$ makes as little physical sense as would the concept of a "three-phase current" $I_{3\phi} \triangleq 3I_p$. Nevertheless, when we refer to reactive power in a three-phase system, we always express it as a "three-phase power" in accordance with Eq. (3-11). The only reason for so doing is to obtain formula symmetry between real and reactive powers.

Similarly, we talk about a "three-phase VA" which we define as three times the VA per phase, that is,

$$|S_{3\phi}| \triangleq 3|S_{1\phi}| = 3|V_p||I_p| \qquad \text{VA} \tag{3-12}$$

Example 3-1 The equivalent induction motor load on a section of a 138-kV transmission network can be represented by three equal impedances of

$$Z = 80 + j30\ \Omega/\text{phase}$$

as shown in Fig. 3-7. (See also discussion of load representation in Sec. 3-3.)

Find phase currents and real and reactive power consumed by this load.

SOLUTION The phase voltage magnitude is

$$|V_a| = |V_p| = \frac{138}{\sqrt{3}} = 79.67 \text{ kV/phase}$$

The phase current has an rms value of

$$|I_p| = \frac{79.67}{\sqrt{80^2 + 30^2}} = 0.932 \text{ kA/phase}$$

Each phase current lags its phase voltage by an angle

$$\phi = \tan^{-1}\left(\tfrac{30}{80}\right) = 20.56°$$

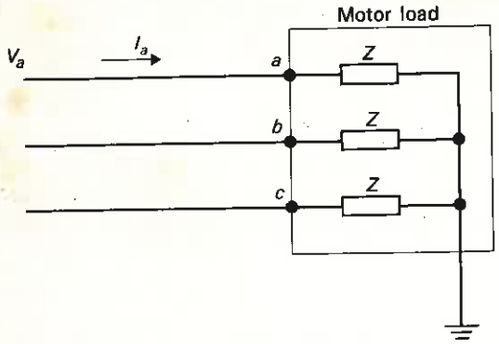

Figure 3-7 Equivalent impedance representation of three-phase induction motor.

We therefore get

$$P_{1\phi} = 79.67 \times 0.932 \times \cos 20.56° = 69.5 \text{ MW/phase}$$

$$Q_{1\phi} = 79.67 \times 0.932 \times \sin 20.56° = 26.1 \text{ Mvar/phase}$$

and

$$P_{3\phi} = 3 \times 69.5 = 208.5 \text{ MW (total 3-phase)}$$

$$Q_{3\phi} = 3 \times 26.1 = 78.3 \text{ Mvar (total 3-phase)}$$

$$|S_{3\phi}| = 3 \times 79.67 \times 0.932 = 222.8 \text{ MVA (total 3-phase)}$$

3-1-5 Delta-Connected Loads

The three-phase load as arranged in Figs. 3-3*b* and 3-7 is referred to as "star" or "Y"-connected. Often a three-phase load is of the "delta"-connected type shown in Fig. 3-8*a*. As each load impedance Z is now connected across the full line voltage it will draw a $\sqrt{3}$ times larger current than in Fig. 3-3*b*. As its voltage is also $\sqrt{3}$ times larger, each load impedance will thus draw three times more power than if Y-connected.

Example 3-2 Assume that the three load impedances in Example 3-1 were connected Δ. Find the current in each load impedance and also the line currents.

SOLUTION The load current has been found to be 0.932 kA in Example 3-1 when the impedance Z was connected across the phase-voltage 79.7 kV. When now connected across 138 kV the *load* or *delta currents* will be

$$|I_{ab}| = |I_{bc}| = |I_{ca}| = \sqrt{3} \times 0.932 = 1.615 \text{ kA}$$

The current I_{ab} will lag the voltage V_{ab} by $\phi = 20.56°$ as shown in Fig. 3-8*b*. Currents I_{bc} and I_{ca} will lag I_{ab} by 120 and 240° respectively. As we note from Fig. 3.8*a* that

$$I_a = I_{ab} - I_{ca}$$

the phase current I_a is simply obtained as the vectorial sum of I_{ab} and $(-I_{ca})$. This vectorial addition is performed in Fig. 3-8*b*. Since $-I_{ca}$ lags I_{ab} by 60° we have

$$|I_a| = 2|I_{ab}| \cos 30° = \sqrt{3}|I_{ab}| = 2.797 \text{ kA}$$

Note also that I_a has the same phase relative to V_a as in Fig. 3.5.

Summary results: Changing the load from Y to Δ has tripled the phase current and all powers. The phase-angle relationship between V_a and I_a is unchanged.

3-1-6 The Three-Phase Generator as Part of a Power Grid

So far we have discussed the simple case of a three-phase generator feeding a separate three-phase load. In reality this is not the normal mode of operation. Typically, the generator would be "synchronized" onto a large interconnected

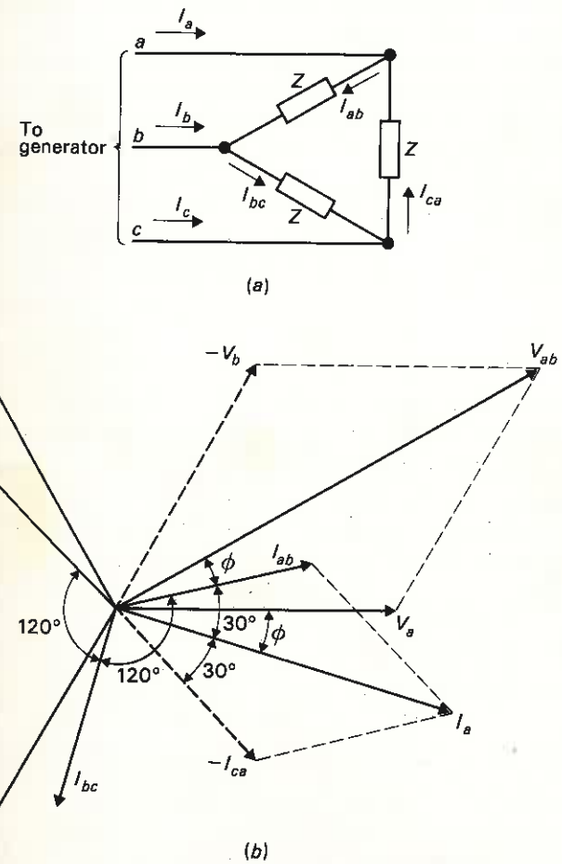

Figure 3-8 Δ-connected load and phasor picture.

grid thus operating in unison or in parallel with all other generators of the overall system supplying energy to all the loads connected to it.

We shall discuss the operating characteristics of a three-phase generator under such conditions in Chap. 4. It suffices at this time to conclude that the generator will supply to the network a symmetrical set of currents of the type shown in Fig. 3-5. The power formulas (3-10), (3-11), and (3-12) will thus apply even in this case.

3-1-7 Phase Symmetry

From a circuits analysis viewpoint a three-phase system represents in general more complexity and difficulty than does a single-phase system. However, in most normal operating cases the various components of the three-phase system are characterized by complete *phase symmetry*, and if such symmetry is assured then the analysis will be particularly simple.

In the case of three-phase generators (Chap. 4), motors, and transformers (Chap. 5), *phase symmetry is assured by design*, and these devices leave the factory with this built-in feature. In the case of single-phase load objects phase symmetry is achieved by balanced distribution between the three phases (Sec. 3-3).

Transmission lines are made phase-symmetric by two alternative methods. Either one can place the identical phase conductors in a symmetric geometrical configuration as demonstrated in Fig. 3-9*a* or one can *transpose* the conductors as shown in Fig. 3-9*b*. (Chap. 6.)

3-1-8 "Per-phase" Analysis

If phase symmetry is assured *throughout* the power system it is possible to simplify the analytical efforts to a great extent by use of so-called "per-phase analysis." We demonstrate this concept by considering the transmission line shown in Fig. 3-9. Due to the design symmetry the line resistances and self- and mutual inductances are equal (Chap. 6) in the three phases, i.e.,

$$R_a = R_b = R_c = R \qquad \Omega \tag{3-13}$$

$$L_a = L_b = L_c = L \qquad \text{H} \tag{3-14}$$

$$M_{ab} = M_{bc} = M_{ca} = M \qquad \text{H} \tag{3-15}$$

For the voltage drops along the three phases we thus have, respectively,

$$\begin{aligned} \Delta V_a &= I_a R + j\omega L I_a + j\omega M I_b + j\omega M I_c \\ \Delta V_b &= I_b R + j\omega L I_b + j\omega M I_a + j\omega M I_c \\ \Delta V_c &= I_c R + j\omega L I_c + j\omega M I_a + j\omega M I_b \end{aligned} \tag{3-16}$$

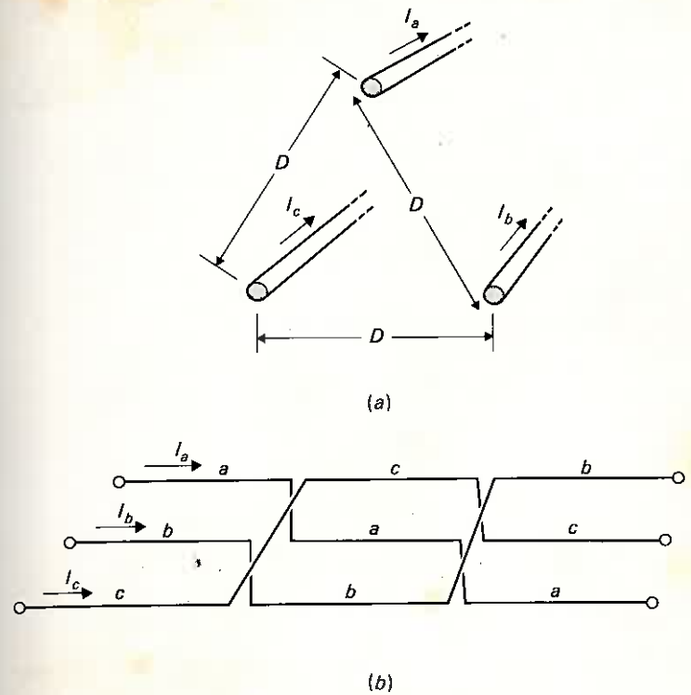

Figure 3-9 Phase-symmetric transmission lines.

If we now make use of Eq. (3-7)† the last equations take on the simple form

$$\begin{aligned} \Delta V_a &= I_a[R + j\omega(L - M)] = I_a Z_p \\ \Delta V_b &= I_b[R + j\omega(L - M)] = I_b Z_p \\ \Delta V_c &= I_c[R + j\omega(L - M)] = I_c Z_p \end{aligned} \tag{3-17}$$

where for brevity we have introduced the *phase impedance*

$$Z_p \triangleq R + j\omega(L - M) \triangleq R + jX \tag{3-18}$$

If we write Eqs. (3-17) in vector-matrix form they become

$$\begin{bmatrix} \Delta V_a \\ \Delta V_b \\ \Delta V_c \end{bmatrix} = \begin{bmatrix} Z_p & 0 & 0 \\ 0 & Z_p & 0 \\ 0 & 0 & Z_p \end{bmatrix} \begin{bmatrix} I_a \\ I_b \\ I_c \end{bmatrix} \tag{3-19}$$

† This equation *only* stipulates zero neutral current. It is *not* necessary at this point to assume that the currents possess three-phase symmetry.

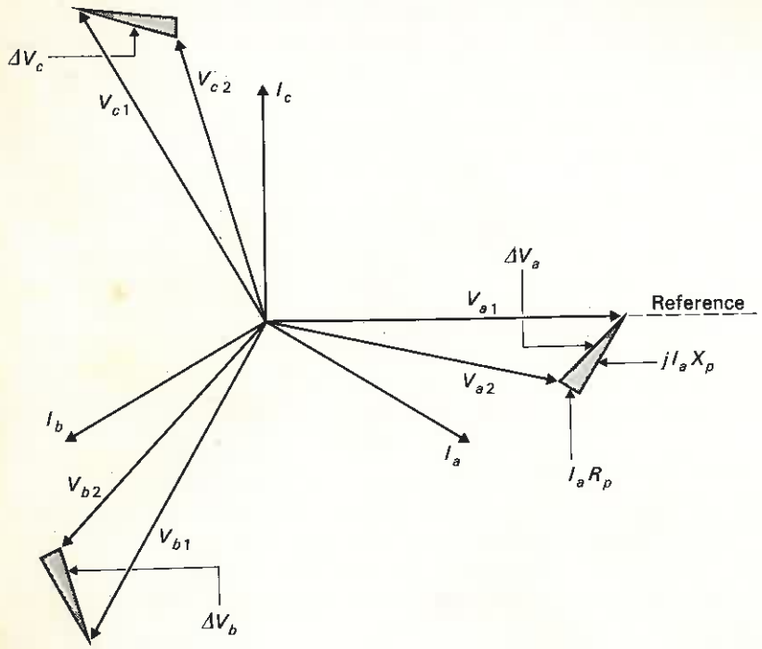

Figure 3-10 Phasor diagram in phase-symmetric system, with currents possessing 3-phase symmetry.

or, in compact notation,

$$\Delta \mathbf{V}_p = \mathbf{Z}_p \mathbf{I}_p \tag{3-20}$$

We note that the *phase impedance matrix* $\mathbf{Z}_p$ is *diagonal* (i.e., all its off-diagonal elements are zeros) and in addition its diagonal elements are all equal. These last two observations have two very important practical consequences:

1. There is complete† "decoupling" between the three phases. This means, as far as phase a is concerned, that the voltage drop ΔV_a depends upon the current I_a only, with no coupling terms from I_b and I_c. *This feature is a result of the assumption of zero neutral return current.*
2. If we make the additional assumption that the currents possess three-phase symmetry then so will the voltage drops. This case is shown in Fig. 3-10.

The phasor diagram in Fig. 3-10 is instructive. Subscripts 1 and 2 refer to "sending" and "receiving" ends of the transmission line respectively. V_{a1} and V_{a2} thus represent the phase voltages of phase a in the respective line ends. The

† In Chap. 6 we shall learn that even if the transmission line is not perfectly phase-symmetric these decoupling features are still *approximately* true.

shaded triangles represent the three voltage drops ΔV_a, ΔV_b, and ΔV_c respectively. *As corresponding phasors will be equal (except for the 120 and 240° phase shifts) in all three phases we can obviously limit our analysis to one phase only.* This is referred to as "per-phase" analysis.

Example 3-3 A three-phase transmission line can be represented by a phase impedance of $Z_p = 5 + j60\ \Omega$/phase. The line power is 210 MW and 30 Mvar as measured at the sending end, where the voltage is kept at 220 kV. Find the power and voltage at the receiving end.

SOLUTION We perform our analysis for phase a and choose the sending-end phase voltage as our reference phasor, i.e.,

$$V_{a1} = \frac{220}{\sqrt{3}} = 127.0\angle 0^\circ \quad \text{kV}$$

The power per phase in the sending end is

$$S_1 = \tfrac{210}{3} + j\tfrac{30}{3} = 70 + j10 \quad \text{MW and Mvar/phase}$$

From Eq. (2-26) we get for the current

$$127.0 I_a^* = 70 + j10 \tag{3-21}$$

which yields

$$I_a = 0.551 - j0.079 \quad \text{kA/phase}$$

The voltage in the receiving end equals V_{a1} minus the drop ΔV_a,

$$V_{a2} = V_{a1} - I_a Z_p = 127.0 - (0.551 - j0.079)(5 + j60)$$
$$= 119.5 - j32.7 = 123.9\angle -15.3^\circ \quad \text{kV/phase} \tag{3-22}$$

The rms value of the line voltage in the receiving end is thus

$$123.9 \times \sqrt{3} = 214.6 \quad \text{kV}$$

The power measured at the receiving end equals

$$S_2 = V_{a2} I_a^* = (119.5 - j32.7)(0.551 + j0.079)$$
$$= 68.43 - j8.58 \text{ MW and Mvar/phase} \tag{3-23}$$

or 205.3 MW and −25.7 Mvar total three-phase.

Clearly, we have lost 210 − 205.3 = 4.7 MW in transmission, the power having been dissipated in the 5-Ω line resistance.

The reactive power loss is larger. 30 Mvar is fed into the line at the sending end, and 25.7 Mvar at the receiving end (note the minus sign) for a total line loss of 55.7 Mvar. (What loss values would formulas (2-40) and (2-41) yield?)

3-1-9 Per-Unit Values in Symmetrical Three-Phase Systems

In working with per-unit values in three-phase system analysis we must exercise some care in distinguishing between line and phase voltages and between single-phase and three-phase values for power. We have established that the "per-phase" method is the obvious choice in work with symmetrical three-phase systems. It is therefore natural that our use of "per units" will be tuned to this method.

Assume that a systems analyst is working with a 345-kV system and that he would like to refer all powers to the maximum transmission capacity, 900 MW, of an important line in the system. He would then choose $345/\sqrt{3} = 199.2$ kV as the "per-phase" voltage base $|V_b|$, and $900/3 = 300$ MVA as the "per-phase" power base $|S_b|$. The base current and impedance would then be computed respectively:

$$|I_b| \triangleq \frac{300}{199.2} = 1.506 \qquad \text{kA/phase}$$

$$|Z_b| \triangleq \frac{199.2}{1.506} = 132 \qquad \Omega\text{/phase}$$

For example, if his analysis would yield a per-unit voltage of 0.9 pu then he would know that this would correspond to

$$0.9 \times 199.2 = 179.3 \text{ kV, phase-to-neutral}$$

or

$$0.9 \times 345 = 310.5 \text{ kV, line}$$

A power of 0.65 pu MW would mean

$$0.65 \times 300 = 195 \text{ MW/phase}$$

or

$$0.65 \times 900 = 585 \text{ MW total 3-phase}$$

As he normally is interested in *line* voltages and *total* three-phase powers, the experienced analyst often practices a "loose" usage of base values. He might then prefer to consider 345 kV and 900 MVA as his "real" base values. However, for the novice this could invite errors. For instance, in the above example we had concluded that the base current equals 1.5 kA.

The inexperienced analyst could use the "base values" 345 kV and 900 MVA to compute an erroneous base current of

$$|I_b| = \tfrac{900}{345} = 2.61 \text{ kA}$$

which is off with a factor of $\sqrt{3}$ from the correct value.

The example demonstrates that caution must be exercised in working with pu values in three-phase analyses.

Example 3-4 Work Example 3-3 in per units. Use the following arbitrary base values:

$$\text{MVA-base} \triangleq 300 \text{ MVA, total 3-phase power}$$

$$\text{kV-base} \triangleq 250 \text{ kV, line voltage}$$

SOLUTION As we shall work our problem on a "per-phase" basis we need the following "per-phase" base values:

$$|S_b| = \frac{300}{3} = 100 \text{ MVA/phase}$$

$$|V_b| = \frac{250}{\sqrt{3}} = 144.3 \text{ kV phase-to-neutral}$$

Thus, for current and impedance bases, we get, respectively:

$$|I_b| = \frac{100 \text{ (MVA)}}{144.3 \text{ (kV)}} = 0.693 \text{ kA/phase}$$

$$|Z_b| = \frac{144.3 \text{ (kV)}}{0.693 \text{ (kA)}} = 208.3\ \Omega\text{/phase}$$

In terms of these per-phase base values we have

$$V_{a1} = \frac{220/\sqrt{3}}{144.3} = 0.880 \text{ pu/phase}$$

$$S_1 = \frac{70 + j10}{100} = 0.700 + j0.100 \text{ pu/phase}$$

$$Z_p = \frac{5 + j60}{208.3} = 0.024 + j0.288 \text{ pu/phase}$$

If, as before, V_{a1} is selected as our reference phasor we get for the phase current

$$0.880 I_a^* = 0.700 + j0.100$$
$$\therefore \quad I_a = 0.795 - j0.114 \text{ pu} \tag{3-24}$$

Check: Expressed in kiloamperes per phase we get

$$I_a = 0.693(0.795 - j0.114) = 0.551 - j0.079 \text{ kA}$$

which agrees with the result in Example 3-3.

For the receiving-end voltage we next get:

$$V_{a2} = V_{a1} - I_a Z_p = 0.880 - (0.795 - j0.114)(0.024 + j0.288)$$
$$= 0.828 - j0.226 \text{ pu} \tag{3-25}$$

Check: Expressed in kilovolts per phase

$$V_{a2} = 144.3(0.828 - j0.226) = 119.5 - j32.7 \text{ kV/phase}$$

or in kilovolts rms line

$$|V_{a2}| = 250\sqrt{0.828^2 + 0.226^2} = 214.6 \text{ kV}$$

Both of these values agree with previously computed values.

For the receiving-end power we have

$$S_2 = V_{a2} I_a^* = (0.828 - j0.226)(0.795 + j0.114)$$
$$= 0.684 - j0.086 \text{ pu} \tag{3-26}$$

or in three-phase megavalues

$$S_2 = 300(0.684 - j0.086) = 205.3 - j25.7$$

This is also in agreement with earlier results.

If, in computing the base impedance above, we had made use of formula (2-39) the following numerical rules are of practical significance.

Because the formula can be written

$$|Z_b| = \frac{|V_b|^2}{|S_b|} = \frac{(\sqrt{3}|V_b|)^2}{3|S_b|} = \frac{(1000|V_b|)^2}{1{,}000{,}000|S_b|} \tag{3-27}$$

we realize first that it will give proper value if the *line* voltage and *total three-phase* power were used.

Second, we note that the numerical values come out OK if the voltage and power are inserted with their *kilo* and *mega* values respectively. Using these rules we would obtain in this case

$$|Z_b| = \frac{250^2}{300} = 208.3\ \Omega/\text{phase}$$

as before.

We shall find opportunity to use the per-unit system in many examples in this book. Therefore, the above example will suffice at this time.

3-2 THE UNSYMMETRICAL THREE-PHASE CASE

Phase-symmetry, as shown above, results in relatively simple analysis of three-phase systems. More importantly, symmetrical operation ensures that generators, motors, and transformers operate at their best efficiency, within rated limits, and with nonpulsating power. For these reasons, power systems are normally operated as balanced as practically feasible.

However, fault conditions may create grossly unbalanced conditions often at the highest voltage levels of the power systems. These occurrences are, fortunately, relatively rare but it is important that the phenomena manifesting themselves during these brief periods be well understood so that the faults can be properly and promptly detected and cleared, and the disturbance effects as far as possible localized. In Chap. 11 we shall present analysis methods useful in working with unbalanced (faulted) three-phase systems.

3-2-1 Balancing an Unsymmetrical Resistive Load

Presently we shall demonstrate how it may be possible to "symmetrize" a system which is subject to extremely unbalanced loading. This is not *generally* possible, but can be accomplished if the load is purely resistive. For example, consider the single-phase electric industrial oven represented by the resistance R in Fig. 3-11. Directly energized from, for example, phases a and b of a three-phase system, the

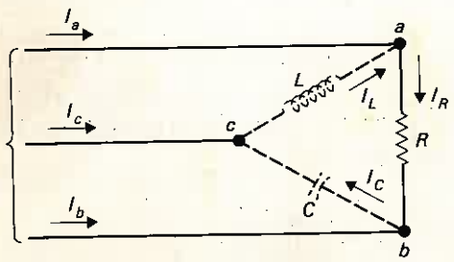

Figure 3-11 Highly unbalanced loading example.

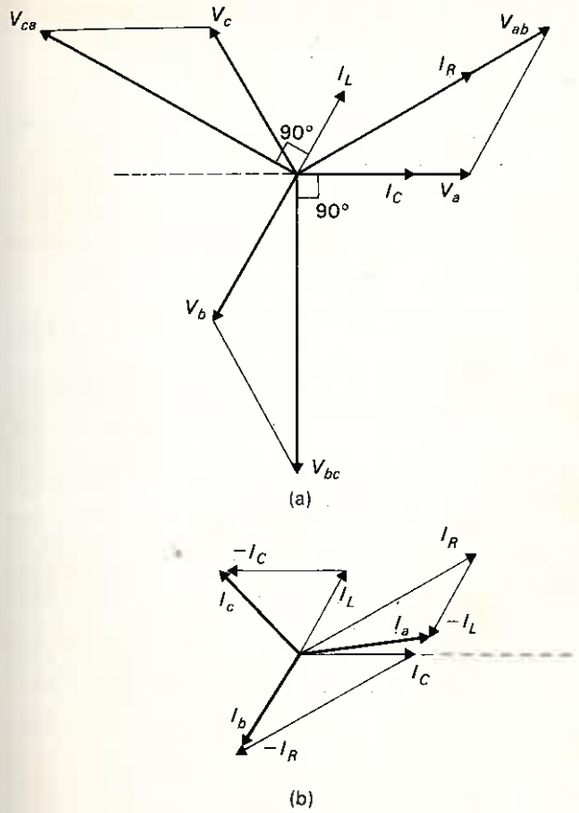

Figure 3-12 Phasor representation of voltages and currents in Fig. 3-11.

oven, the size of which is assumed in the megawatt range, would result in heavy and equal currents in phases a and b, but zero current in phase c. This highly nonsymmetrical loading upon the source would be regarded intolerable (most utility companies would, in fact, not accept it).

We demonstrate now how, by adding the two *reactive* elements L and C to Fig. 3-11 (shown dashed), we can actually make the *total load appear completely three-phase symmetric from the source.* Note that the added reactive elements do not consume megawatts and therefore they do not represent any additional real power drain upon the system.

We could perform the analysis in several ways, but shall choose here, for tutorial purposes, the following graphical method.

The oven current I_R, being purely resistive, must be in phase with the line voltage V_{ab}. The reactor current I_L lags the line voltage V_{ca} by 90°, whereas the capacitor current I_C leads the line voltage V_{bc} by 90°. Accordingly we can construct the phasor diagram in Fig. 3-12*a*.

The source (or phase) currents I_a, I_b, and I_c are related to the above currents through the equations

$$\begin{aligned} I_a &= I_R - I_L \\ I_b &= I_C - I_R \\ I_c &= I_L - I_C \end{aligned} \tag{3-28}$$

These equations are depicted graphically in Fig. 3-12*b* which shows that phase currents now are existing in all three phases *and* that these three currents appear quite symmetric. Actually, as the reader readily verifies, if we make

$$|I_L| = |I_C| = \frac{1}{\sqrt{3}}|I_R| \quad \text{A} \tag{3-29}$$

the phase-current phasors I_a, I_b, and I_c will assume complete three-phase symmetry. In addition, they will line up with the respective phase-voltage phasors V_a, V_b, and V_c respectively.

The conclusion of these findings is *that the three-phase source experiences the three impedances as a symmetrical set of three equal resistors.*

As the power factor of this "symmetrical load" equals unity, the source neither delivers nor receives any reactive power. The explanation is, of course, that with the *LC* tuning expressed by Eq. (3-29), the exact reactive power need by the reactor is delivered by the capacitor.

It should be mentioned that if the phase sequence is reversed or the two reactive elements change place, the above symmetrical features will *not* result. (Compare Prob. 3-7.)

3-3 LOAD CHARACTERISTICS

We have on several occasions referred to "load," "load impedance," etc., without giving much justification for our assumptions. For example, we have assumed symmetry between the phases, which presupposes that whatever the load is, it is equally distributed between the three phases. It is appropriate at this time to present a more detailed discussion of typical load characteristics.

Generally, the term *load* shall refer to a device or a conglomeration of devices that tap energy from the network. In a practical situation the load devices may range from a few-watt night lamp to a multimegawatt induction motor. The power system, if properly designed, shall be capable of supplying energy to all of them. It is possible to divide the various load devices into the following categories:

1. Motor devices (including stationary ones in the industry and portable ones in transportation equipment, i.e., trains, etc.)
2. Heating equipment
3. A diversity of electronic gear
4. Lighting equipment

From an electrical point of view the multitude of devices are characterized by vast differences in regard to:

1. Size
2. Symmetry (single- or three-phase)
3. Load constancy (in respect to time, frequency, and voltage)
4. Use cycle (regular or random use)

For example, industrial loads may have few, if any, resemblances to domestic loads in respect to all the above categories. A certain type of industry load may be made up to 95 percent of large three-phase motors with considerable load constancy and very predictable duty cycle (on at 8 A.M., off at 5 P.M.). A typical domestic load, on the contrary, may consist mostly of single-phase apparatus operated in random manner. How does one logically go about putting any order in such a picture? The fact is that the situation is not as hopeless as it appears at a first glance. *The laws of statistics are on our* (the system engineers') *side.* Whereas the *individual* loads may be entirely random in character, a certain average pattern is recognizable already at the distribution transformers. At the subtransmission level, this averaging effect is still more pronounced. Finally, at the transmission level, we reach an almost predictable situation.

To be fair, we must admit that we help the law of statistics to work their way. For example, on the distribution level we always distribute, by design, the single-phase loads equally between the three phases.

In summary fashion we give the following rules characterizing typical systems loads:

1. Although individually of random type, the *lumped*, or *composite*, loads, as we encounter them at subtransmission or transmission levels, are of highly predictable character.
2. These lumped loads vary in a *predictable* fashion *with time.* Figure 3-13 shows some typical load variations for a small company. In general, there is considerable variation, not only throughout the hours of the day, but also between weekdays and Sundays and holidays and also between different seasons.
3. Although the loads are time-variant, the variations are relatively *slow.* From *minute to minute* we have an almost *constant* load. *A minute is a long time period compared with the electrical time constants of the power system, and this permits us to consider the system operating in steady state—a steady state that slowly "shifts" throughout the hours of the day* ("quasi-static" operation).
4. The typical load always *consumes* reactive power. The reason for this is that motor load is an important (actually *the* most important) ingredient in most cases. Motors are *always* (with the exception of overexcited synchronous machines) *inductive.*
5. The typical load is always *symmetric.* In the case of large motors (greater than

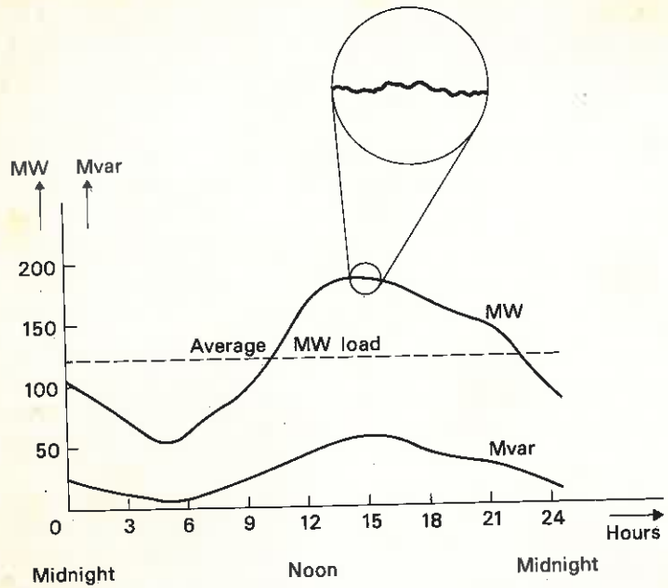

Figure 3-13 Typical daily load fluctuation.

a few horsepowers), this symmetry is automatic, since they are always designed for balanced three-phase operation.

In the case of single-phase devices, the symmetry comes about by statistical effects and intentional distribution between phases.

3-3-1 Voltage and Frequency Load Dependency

An important feature, characterizing all loads, is their dependency on voltage and frequency. During faults and other abnormal situations, the former may vary greatly resulting in major load fluctuations. Even minor changes in voltage and frequency can cause load changes of practical significance. We shall briefly discuss the two important load types, impedance and motor loads.

A. Impedance-type loads Lighting, heaters, ovens, and similar load objects fall in this category. We had summarized this type of load in Table 2-1.

Example 3-5 Consider an inductive load of the type shown in Table 2-1 (item 4). The impedance equals $Z = R + jX$. By how many percent will the real load drop if the voltage is reduced by 1 percent?

SOLUTION From Eq. (2-28) we have

$$P + jQ = |V|^2 Y^* = |V|^2 \frac{1}{R - jX} = |V|^2 \frac{R + jX}{R^2 + X^2} \tag{3-30}$$

$$\therefore \quad P = |V|^2 \frac{R}{R^2 + X^2} \tag{3-31}$$

and

$$Q = |V|^2 \frac{X}{R^2 + X^2}$$

Clearly, the real and reactive loads both are proportional to the square of voltage $|V|$. For a *small* voltage perturbation $\Delta|V|$ we have, for the real power,

$$\frac{\Delta P}{\Delta |V|} \approx \frac{\partial P}{\partial |V|} = 2|V| \frac{R}{R^2 + X^2} = \frac{2}{|V|} P \tag{3-32}$$

The latter expression can be written

$$\frac{\Delta P}{P} \approx 2 \frac{\Delta |V|}{|V|} \tag{3-33}$$

The result tells us that a small relative change in voltage results in twice the relative change in megawatts. Thus, in our case, a 1 percent drop in voltage causes a 2 percent drop in load.

Example 3-6 How would a 1 percent drop in frequency affect the real load in the previous example? The load is assumed to have a power factor of $\cos \phi = 0.8$.

SOLUTION The reactance X depends upon frequency f according to

$$X = 2\pi f L$$

From Eq. (3-31) we thus have

$$\frac{\Delta P}{\Delta f} \approx \frac{\partial P}{\partial f} = -|V|^2 \frac{4RX\pi L}{(R^2 + X^2)^2} = -|V|^2 \frac{2RX^2}{f(R^2 + X^2)^2}$$

$$= -P \frac{2X^2}{f(R^2 + X^2)}$$

$$\therefore \quad \frac{\Delta P}{P} \approx -2 \frac{X^2}{R^2 + X^2} \frac{\Delta f}{f} \tag{3-34}$$

For $\cos \phi = 0.8$ we have

$$\frac{X^2}{R^2 + X^2} = \sin^2 \phi = 0.36$$

$$\therefore \quad \frac{\Delta P}{P} \approx -0.72 \frac{\Delta f}{f}$$

A one percent frequency *drop* thus results in a 0.72 percent load *increase*.

B. Motor load Induction motor load dominates this group. Its dependence upon voltage and frequency is somewhat more complicated to analyze. We exemplify.

Example 3-7 A 480-volt, three-phase induction motor powers a compressor, whose torque is assumed speed-independent. The motor runs at an initial speed corresponding to a per-unit slip of $s = 0.03$. How will the motor load change if the voltage drops by one percent?

SOLUTION It is assumed that the reader has a basic understanding of the induction motor (see Refs. 1 & 2). We will perform the analysis under these simplifying assumptions:

1. The equivalent, per-phase, circuit of the motor is the one shown in Fig. 3-14. We neglect the magnetizing impedance Z_m.
2. The motor torque is of the well-known type shown in Fig. 3-15. We shall assume that we operate, as is typically the case, on the linear portion of the curve.

The motor torque T_m in this linear region equals

$$T_m \approx \frac{90}{\pi n_s}\frac{|V|^2}{R_2}s \qquad \text{N}\cdot\text{m} \tag{3-35}$$

where n_s = synchronous speed in r/min
s = pu slip
V = phase voltage

Initially, the motor operates in point A' (Fig. 3-15) at slip $s' = 0.03$. Following the voltage drop the torque curve changes to the dashed one and the motor will now operate in point A'' at the larger slip s''. From Eq. (3-35) we obtain

$$s'' = s'\frac{|V'|^2}{|V''|^2} = 0.03 \times \left(\frac{1.00}{0.99}\right)^2 = 0.0306 \text{ pu}$$

The real load P drained from the network equals, according to Fig. 3-14,

$$P = \left(R_1 + \frac{R_2}{s}\right)|I|^2 \qquad \text{W/phase} \tag{3-36}$$

where the stator current I is obtained from

$$|I| = \frac{|V|}{\sqrt{(R_1 + R_2/s)^2 + (X_1 + X_2)^2}} \tag{3-37}$$

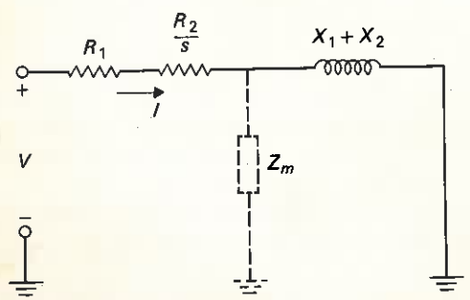

R_1 = stator resistance, 0.290 Ω/phase
X_1 = stator reactance, 0.500 Ω/phase
R_2 = rotor resistance, 0.150 Ω/phase } both referred to
X_2 = rotor reactance, 0.200 Ω/phase } stator side

Figure 3-14 Equivalent circuit of three-phase induction motor. Parameters are given per phase.

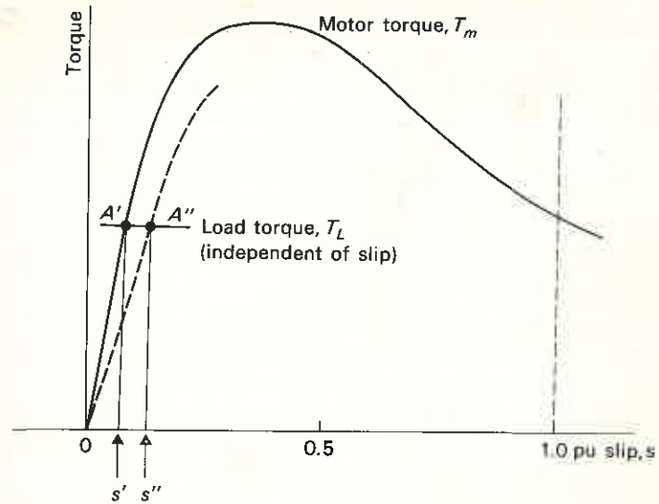

Figure 3-15 Torque versus slip of induction motor in Fig. 3-14.

Using numerical values given in Fig. 3-14 we obtain

$$|I''| = 1.0084|I'|$$

Note that the voltage *drop* causes a 0.8 percent current *rise*, a quite typical situation in the case of induction motor load. (Remember the opposite situation in the case of an impedance load.)

From Eq. (3-36) we finally get

$$\frac{P'}{P''} = \frac{(0.290 + 0.150/0.0300)}{(0.290 + 0.150/0.0306)}\left(\frac{1}{1.0084}\right)^2$$

$$\therefore \quad P'' = 0.998P'$$

Conclusion This motor will reduce its power drain by only 0.2 percent for a voltage drop of 1 percent. (Compare the 2 percent reduction in the case of an impedance load.)

Power companies, in times of generation shortage, will resort to "brownouts" in order to match their load to available generation. They accomplish this by lowering slightly the operating voltage. The above examples should have taught us that impedance loads give a considerably better power reduction than motor loads under such conditions.

3-3-2 Load Management

Historically, power companies considered it their "holy" duty to plan their generating capacity so as to be able to meet every whim of their customers. Over the years this philosophy led to a completely "customer-controlled" load that

took no consideration of the resulting peaks and valleys in the demand curve (Fig. 3-13).

Generator capacity must be available to meet the peak power plus a security margin of the order of 5–15 percent. As the *average load* is considerably less than the peak load it follows that the generators will run at considerably below ratings for most of the time. This is clearly not economically attractive.

As generator capacity has increased in price (to as much as $1000 per kilowatt as of this writing) and as the fuel shortages put an extra squeeze on them, many electric utilities are finding it worthwhile to try to "shave" the load peaks. This is referred as as "load management."

It can be implemented by timer-controlled switching of load objects like hot-water heaters, central radio control of other selected low-priority loads, or by specially designed rate structures that encourage the individual customers to readjust their own electric-use schedules. As this is being written some U.S. power companies are planning the introduction of system-wide load management schemes.

3-4 TRANSMISSION CAPACITY

Quite clearly, in attempting to transmit electric power via a transmission line, one would expect, if for no other reason than purely intuitional, that a limit would be reached beyond which no more power can be "jammed into the line." In this section we shall investigate the limits for power transmission under *static* conditions; i.e., we shall derive the *static transmission capacity* of a transmission line. The assumption we make is that, by *slowly* increasing the load, we force a *slow* increase of the power that is being transmitted via the line under study.

We suggested in Sec. 3-1-8 that a transmission line is characterized by resistance and reactance. In Chap. 6 we shall derive formulas for these parameters. The static transmission capacity depends upon both of these parameters.

3-4-1 Thermal Capacity Limits

The phase resistance R of the line sets a *thermal* transmission limit. As the transmitted power and thus the phase current I_p increase, the ohmic losses grow in proportion to $|I_p|^2$. The conductor temperature rises until the heat dissipation rate is in balance with the conductor heat loss.

Long before the conductor will melt, other permanent damages (for example nonreversible sag) will set in and these then set a *thermal capacity limit* for the line.

The thermal time constant is of the order of several minutes and it therefore takes time to reach the damaging conductor temperatures. For this reason one distinguishes between *short-term* and *long-term* thermal capacity limits, the former exceeding the latter.

3-4-2 Static "Stability" Limits

The thermal capacity limit determines the maximum power transfer on relatively short lines (less than 100–200 miles) and underground cables. The latter are particularly sensitive to thermal overloads because the cable insulation prevents effective cooling of the conductor.

For longer lines the phase impedance sets current and power limits *before* the thermal capacity is reached. When this happens we reach the so-called *static stability limit* of the line. Since the reactance dominates the impedance we shall develop the theory in this section on the assumption that the resistance is zero. This gives limits that are somewhat on the conservative side.

Figure 3-10 gives the relationship between sending-end and receiving-end voltages. If the line resistance is set to zero the voltage phasor diagram is simplified according to Fig. 3-16. We shall find the static stability limit of the line under the following assumptions:

1. The sending-end bus voltage is maintained at *constant* level $|V_1|$ (by controlling the excitation level of the generator at this locality).
2. The real power load P_2 at the receiving end is slowly increased until the power limit is reached.
3. For simplicity the reactive power load Q_2 is zero. (This means that I_p and V_2 are in phase as shown in Fig. 3-16.)

We analyze the following two important cases:

Case I. The voltage level $|V_2|$ uncontrolled For the complex powers in the sending and receiving end we have, respectively

$$S_1 = P_1 + jQ_1 = V_1 I_p^* \tag{3-38}$$

$$S_2 = P_2 + jQ_2 = V_2 I_p^* \tag{3-39}$$

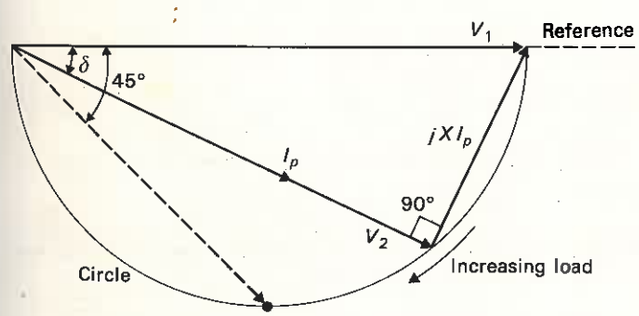

Figure 3-16 Phasor diagram of sending- and receiving-end voltages of transmission line. Resistance neglected. $|V_1|$ = constant.

Because we have neglected the line resistance there are no real line losses and we have

$$P_1 = P_2 = P \tag{3-40}$$

The sending-end voltage equals the sum of the receiving-end voltage and the line drop

$$V_1 = V_2 + jXI_p \tag{3-41}$$

These phasors have been depicted in Fig. 3-16. As V_2 and I_p are of equal phase the voltage drop jXI_p must lead V_2 by 90°. As $|V_1|$ is constant, the tip of the voltage phasor V_2 must thus move along a semicircle of diameter $|V_1|$.

At this juncture we introduce the *power angle*

$$\delta \triangleq \angle V_1 - \angle V_2 \tag{3-42}$$

In terms of δ the current phasor I_p can be written

$$I_p = |I_p| \angle -\delta$$

Upon substitution into (3-38) we obtain

$$P_1 + jQ_1 = |V_1|\,|I_p| e^{j\delta} = |V_1|\,|I_p| \cos\delta + j|V_1|\,|I_p| \sin\delta$$

For the real line power we thus have

$$P_1 = P = |V_1|\,|I_p| \cos\delta \tag{3-43}$$

From Fig. 3-16 we have by inspection

$$|V_2| \sin\delta = X|I_p| \cos\delta \tag{3-44}$$

and also

$$|V_2| = |V_1| \cos\delta \tag{3-45}$$

By combining the last three equations we obtain

$$P = \frac{|V_1|^2}{X} \sin\delta \cos\delta = \frac{|V_1|^2}{2X} \sin 2\delta \tag{3-46}$$

We conclude that the largest real-power flow obtainable in this case is

$$P_{\max} = \frac{|V_1|^2}{2X} \quad \text{MW} \tag{3-47}$$

which will occur for $\delta = 45°$. At this operational point (dashed in Fig. 3-16) the magnitude $|V_2|$ has dropped to 70.7 percent of $|V_1|$.

Example 3-8 A 100-km-long three-phase line has a sending-end voltage of 138 kV and transmits half the maximum real power. Find δ and $|V_2|$.

SOLUTION As $P = \frac{1}{2}P_{\max}$ we obtain

$$\frac{|V_1|^2}{2X} \sin 2\delta = \frac{1}{2}\,\frac{|V_1|^2}{2X}$$

This equation yields

$$\delta = 15°$$

Then, from Eq. (3-45)

$$|V_2| = \frac{138}{\sqrt{3}} \cos 15° = 76.96 \text{ kV/phase}$$

(or 133 kV line-to-line).

Case II. The voltage level $|V_2|$ must remain constant The previous case demonstrated clearly that with no provisions taken the voltage at the receiving-end bus will sag badly for all loadings except very small ones. This is clearly a very unacceptable practical situation. In the real world it is necessary to specify that $|V_2|$ be kept at a *constant* level as the load varies. The tip of the phasor V_2 must thus move along a circle having a radius equal to the specified voltage level (Fig. 3-17).

As the voltage drop phasor jI_pX must lead the current phasor by 90° it becomes immediately clear that no longer can the I_p and V_2 phasors be collinear as in Fig. 3-16. If $|V_2|$ is specified *high* then, as shown in Fig. 3-18*a*, I_p must *lead* V_2. If $|V_2|$ is specified *low*, I_p must *lag* V_2 (Fig. 3-18*b*). *It is obvious that reactive power in a controlled fashion either be injected into or drawn from bus 2 to meet those requirements.*

In analyzing the situation we note first that

$$I_p = \frac{V_1 - V_2}{jX} \tag{3-48}$$

By use of formula (3-39) we get

$$P_2 + jQ_2 = P + jQ_2 = V_2\left(\frac{V_1 - V_2}{jX}\right)^* = \frac{V_2V_1^* - V_2V_2^*}{-jX}$$

$$= \frac{|V_2|e^{j\angle V_2}|V_1|e^{-j\angle V_1} - |V_2|e^{j\angle V_2}|V_2|e^{-j\angle V_2}}{-jX}$$

$$= \frac{j|V_1|\,|V_2|e^{-j\delta} - j|V_2|^2}{X}$$

$$= \frac{|V_1|\,|V_2|}{X} \sin\delta + j\frac{|V_1|\,|V_2| \cos\delta - |V_2|^2}{X}$$

$$\therefore \quad P = \frac{|V_1|\,|V_2|}{X} \sin\delta \quad \text{MW/phase} \tag{3-49}$$

$$Q_2 = \frac{|V_1|\,|V_2| \cos\delta - |V_2|^2}{X} \quad \text{Mvar/phase} \tag{3-50}$$

For completeness we also find Q_1 from Eq. (3-38). The reader may easily confirm the result

$$Q_1 = \frac{|V_1|^2 - |V_1|\,|V_2| \cos\delta}{X} \quad \text{Mvar/phase} \tag{3-51}$$

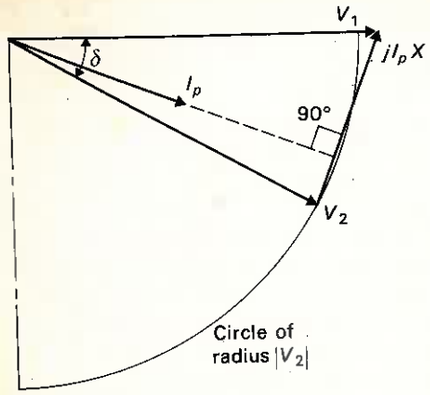

Figure 3-17 Same as in Fig. 3-16 but with *both* $|V_1|$ and $|V_2|$ kept constant.

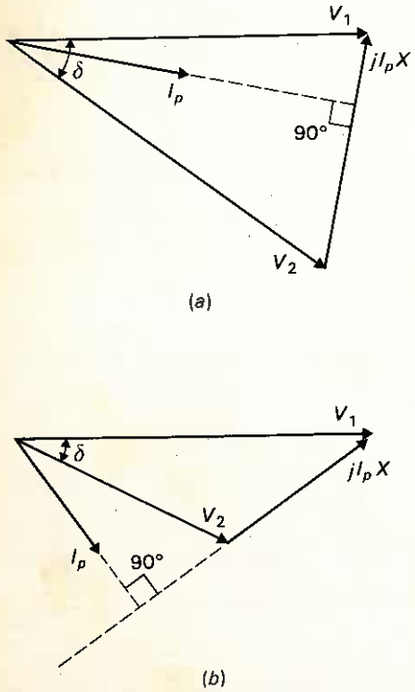

Figure 3-18 Phasor diagram of sending- and receiving-end voltages of transmission line. (*a*) Current leading V_2. (*b*) Current lagging V_2.

The above results are interesting and *very important*. We make the following observations:

The real power P reaches its maximum, the "static transmission capacity"

$$P_{\max} = \frac{|V_1||V_2|}{X} \quad \text{MW/phase} \tag{3.52}$$

for $\delta = 90°$

The transmission capacity increases as the square of the voltage level; one more reason for the need of high transmission voltages.

The *direction* of megawatt flow is determined by sin δ. Positive δ, that is, V_1 leading V_2, results in megawatt flow in direction $1 \to 2$. Negative δ, that is, V_2 leading V_1, means megawatt flow in the opposite direction $2 \to 1$.

Bus voltage magnitudes $|V_1|$ and $|V_2|$ do *not* determine megawatt flow direction. (In an HVDC line they *do*. Compare also Eq. (2-14).)

Although the *real* power is the same in each end, the *reactive* end powers are different. The reactive loss in the line reactance accounts for the difference.

We may define an "average" Q flow thus

$$Q_{\text{ave}} \triangleq \frac{Q_1 + Q_2}{2} = \frac{|V_1|^2 - |V_2|^2}{2X} \tag{3-53}$$

The last step follows directly from Eqs. (3-50) and (3-51). Formula (3-53) indicates that if

$$|V_1| > |V_2|$$

the megavar flow is in direction $1 \to 2$. For $|V_1| < |V_2|$ the megavar flow reverses.† In the case of a "flat" voltage profile, that is, $|V_1| = |V_2|$, formulas (3-50) and (3-51) inform that

$$Q_1 = -Q_2 = \frac{|V_1|^2}{X}(1 - \cos\delta) \tag{3-54}$$

This means that equal amounts of megavars flow *into* the line at both ends.

Example 3-9 The 138-kV line in Example 3-8 is operated with 138 kV in both ends. 100 MW flow in direction $1 \to 2$. Find power angle and reactive flow in line ends. The line reactance equals 80 Ω/phase.

SOLUTION The power angle is solved first:

$$\frac{100}{3} = \frac{(138/\sqrt{3})^2}{80} \sin\delta$$

$$\therefore \quad \delta = 24.84°$$

† Compare with formula (2-14). Note the analogy between the flow of *reactive* power on an *ac* line with the *real* power flow in a *dc* line.

The reactive flow in each end equals

$$Q_1 = -Q_2 = \frac{(138/\sqrt{3})^2}{80}(1 - \cos 24.84°) = 7.34 \text{ Mvar/phase}$$

or 22.02 Mvar total three-phase.

(Note that 44 Mvar are consumed by the line reactance.)

Example 3-10 Let us compute the static stability limit for two different lines, both having an assumed length of 100 miles.

Case A This line is designed for a nominal voltage of 140 kV and consists of one conductor per phase. Line reactance is 0.8 Ω/mi for a total reactance of 80 Ω.

Case B This line is designed for a nominal voltage of 765 kV and consists of four bundled conductors per phase (see Chap. 6). Line reactance is 0.55 Ω/mi for a total reactance of 55 Ω.

SOLUTION From Eq. (3-52), we thus get for case A

$$P_{max} = \frac{(140)^2}{80} = 245 \text{ MW, 3-phase}$$

and for case B

$$P_{max} = \frac{(765)^2}{55} = 10{,}600 \text{ MW, 3-phase}$$

The 765-kV line would thus handle the same power as 43 lines rated at 140 kV.

Example 3-11 A transmission line has a reactance of $X = 0.3$ pu/phase. The load at the receiving-end bus can be represented by a resistor of $R = 1.0$ pu/phase. $|V_1|$ is kept at 1 pu.

Case A Calculate $|V_2|$ if no reactive power is injected at bus 2.

Case B Determine the reactance, X_c, of a capacitor to be placed in parallel with R to make $|V_2|$ equal to $|V_1|$.

SOLUTION **Case A** If the resistor is the only load at bus 2 we have the following ratio between the two bus voltages:

$$\frac{V_2}{V_1} = \frac{R}{R + jX}$$

$$\therefore \quad |V_2| = |V_1| \frac{R}{\sqrt{R^2 + X^2}} = \frac{1.0}{\sqrt{1.0^2 + 0.3^2}} = 0.958 \text{ pu} \tag{3-55}$$

The real load at bus 2 thus equals

$$P_2 = \frac{|V_2|^2}{R} = \frac{0.958^2}{1.0} = 0.917 \text{ pu MW}$$

Case B With $|V_2| = |V_1| = 1$ pu the power consumption in R equals

$$P_2 = \frac{|V_2|^2}{R} = \frac{1^2}{1} = 1 \text{ pu}$$

As $P = P_2$ we can compute the power angle from Eq. (3-49):

$$\frac{1 \times 1}{0.3} \sin \delta = 1$$

$$\therefore \quad \delta = 17.46°$$

Finally, Eq. (3-50) yields

$$Q_2 = \frac{1 \times 1 \times \cos 17.46° - 1^2}{0.3} = -0.1535 \text{ pu Mvar}$$

Conclusion The capacitor must deliver 0.1535 pu Mvar and must thus have a reactance of

$$X_c = \frac{|V_2|^2}{|Q_2|} = \frac{1^2}{0.1535} = 6.51 \text{ pu } \Omega$$

SUMMARY

In this chapter we have familiarized the reader with the important three-phase method of transmitting electric ac power. Its basic advantage is power constancy—which translates into constant torques in electric three-phase motors and generators. The importance of operating three-phase systems symmetrically has been stressed.

Balanced three-phase systems may be analyzed on a "per-phase" basis and many text examples have been worked using this technique. In some important practical situations large single-phase load objects must be supplied from a three-phase system resulting in extreme phase imbalance. It has been demonstrated how added reactive elements can balance such a load.

All electric loads change with voltage level and frequency. We have demonstrated how impedance and motor loads differ in this regard.

Finally, we have given a detailed analysis of the factors that determine the transmission capacity of a three-phase line. The transmission capacity has been proven directly proportional to the square of the voltage level and inversely proportional to the line reactance. We have also found a very useful role for the seemingly "useless" reactive power. By manipulating the generation and flow of megavars on the system we are in fact able to control its voltage profile. More will be said about this in Chap. 7, which deals with power flow analysis.

PROBLEMS

***3-1** Three equal impedances, $Z = 6 + j2$ Ω are connected to form a Y-connected load on a 600-V, three-phase system. Compute the current in each impedance and the total three-phase real, reactive, and apparent powers.

***3-2** Three equal capacitor units are connected Δ at the end of a 600-V, 60-Hz, three-phase line. Determine the capacitance of each unit if the bank is to deliver 900 kvar of reactive power to the system. What will be the current in each unit and in the line?

***3-3** A three-phase transmission line has a phase impedance of $Z_R = 1 + j7$ Ω/phase. It delivers 600 kW at unity power factor and a voltage of 13.2 kV to a symmetric load. What will be the sending-end voltage, kilowatts, kilovars, and kilovoltamperes?

***3-4** Consider the transmission line in Prob. 3-3. The sending-end voltage equals 13.2 kV and it is being loaded at the receiving end by three Y-connected impedances $Z = 10 + j30$ Ω.

A. Compute the receiving-end voltage.

B. As you noted in *A* the load causes a voltage drop. Add three equal capacitors in parallel with the load impedances and select their size so as to boost the receiving-end voltage back to 13.2 kV.

***3-5** Select $|S_b| = 1$ MVA and $|V_b| = 13.2/\sqrt{3}$ kV. Then rework Probs. 3-3 and 3-4 using per-unit analysis. Check your answers with those previously obtained.

3-6 The power equation (3-10) was obtained on the assumption that the three-phase load was *balanced*. Analyze the situation when we have a slight load unbalance as depicted in Fig. 3-19. Show in particular that the total power will now have a small pulsating component, the amplitude of which is approximately proportional to the unbalance ΔR. We make the assumption that the unbalance is relatively small, i.e.,

$$\Delta R \ll R$$

The load voltage is assumed symmetrical.

3-7 The single-phase oven represented by R in Fig. 3-11 is rated 5 MW. The source voltage is 38 kV.

(*a*) Determine the megavar and kilovolt ratings of the reactor and the capacitor required to symmetrize the load.

(*b*) Viewed from the source the actual load can be represented by three identical Y-connected equivalent resistors. Compute the resistance value of these in terms of the oven resistance R.

(*c*) Prove that if the voltage phase sequence is reversed to *acba* . . . the circuit will *not* appear symmetrical from the source.

3-8 Equations (3-32) and (3-34) in the text can be written

$$\Delta P \approx \frac{\partial P}{\partial |V|} \Delta |V|$$

$$\Delta P \approx \frac{\partial P}{\partial f} \Delta f$$

respectively.

If you had a simultaneous change in *both* $|V|$ and f then the *total* change in P would be

$$\Delta P \approx \frac{\partial P}{\partial |V|} \Delta |V| + \frac{\partial P}{\partial f} \Delta f$$

(*a*) Prove this statement.

(*b*) Then compute the total percentage change in real power that will result from a simultaneous one percent drop in voltage *and* frequency in a load consisting of a five-ohm resistor in series with a five-ohm capacitor, all per phase and Y-connected.

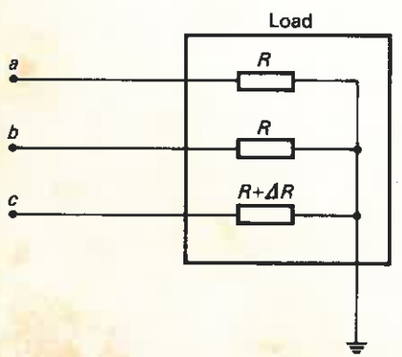

Figure 3-19 Impedance load with slight unbalance.

***3-9** Consider the motor load discussed in Example 3-7. Rework the example but assume now that the compressor torque increases with speed, at the rate of one-half percent torque per one percent speed.

***3-10** Consider the 138-kV transmission line in Example 3-9. The line is operated with 140 kV in the sending end and 130 kV in the receiving end. 120 MW are being transmitted. Compute the reactive flow, magnitude, and direction, in both ends.

***3-11** If the line in Example 3-9 is being operated at its maximum power (that is, $\delta = 90°$) and with 140 kV in both ends what will be (*a*) the reactive flow in each end and (*b*) the voltage midline?

***3-12** Prove that all power formulas derived in Sec. 3-4 are valid if voltages, powers, and reactances are inserted in per unit.

3-13 The line-power formula (3-49) was derived on the assumption of zero real line losses. Add now a resistance R to the line impedance and find a more general P formula. Note that the real powers will now be different in both line ends. Derive the receiving-end power.

Then derive a more general formula for P_{max} and show that maximum power is *not* transmitted when $\delta = 90°$.

Plot P versus δ for the numerical case:

$$|V_1| = |V_2| = 138 \text{ kV (line-to-line)}$$

$$Z_p = 10 + j80 \ \Omega/\text{phase}$$

Plot also Eq. (3-49) for comparison.

3-14 In Example 3-11 it was shown that insertion of a 6.51-pu shunt capacitor boosts the voltage from 0.958 to 1 pu. *

Insert instead a 6.51-pu shunt reactor and show that the result will now be a voltage *drop*.

REFERENCES

1. Van E. Mablekos: *Electric Machine Theory for Power Engineers*, Harper & Row, New York, 1980.
2. Olle I. Elgerd: *Basic Electric Power Engineering*, Addison-Wesley, Boston, 1977.
3. William H. Hayt, Jr. and Jack E. Kemmerly: *Engineering Circuit Analysis*, 2d ed., McGraw-Hill Book Company, New York, 1971.
4. William D. Stevenson, Jr.: *Elements of Power Systems Analysis*, 3d ed., McGraw-Hill Book Company, New York, 1975.
5. M. E. Van Valkenburg: *Network Analysis*, 3d ed., Prentice-Hall, Inc., Englewood Cliffs, N.J., 1974.

CHAPTER

FOUR

THE THREE-PHASE SYNCHRONOUS GENERATOR

4-1 INTRODUCTION

Essentially one hundred percent of the world's bulk electric power is being produced in three-phase synchronous generators, a fact that clearly justifies our designating this device the most important component of an electric power system. As the synchronous machine, or *alternator*, dominates the operating features of a power system and, most importantly, also incorporates the major control functions of the system, it is appropriate that we give it the attention it deserves.

We shall presently develop mathematical models which adequately describe the behavior of the machine under steady-state conditions. The models will be later extended to explain the essential machine behavior under transient or dynamic conditions. We concentrate on those models that possess proven usefulness in system analysis. We shall skip details which, although important to the machine designer, are of only insignificant value to the systems analyst.

A synchronous generator with its many windings, some of which are in motion relative to others, constitutes a rather complex device, the analysis of which may easily become bogged down in a morass of formulas. However, by making ample use of built-in symmetry features and *by limiting the analysis to the all-important fundamental components of flux, mmf, and current* it is possible in the end to arrive at surprisingly simple models. Throughout, we shall try to relate the analytical results to the physical realities of the machine, often by the use of analogs.

14-8-1982 I.I.E.

4-2 BASIC DESIGN FEATURES

Figure 4-1 depicts the basic design of a two-pole synchronous *turbogenerator*. This type of generator, invariably of two- or four-pole design, is used when the *prime mover* is a high-speed steam turbine, a common situation in most industrialized countries. The generator *rotor* and the turbine, which latter typically is divided into several stages, are connected on a single shaft normally mounted in a horizontal arrangement. In order to reduce the magnitudes of centrifugal forces, the cylindrical rotor has a relatively small diameter, but large axial length.

The rotor contains p "belts" of slots ($p = 2$ in Fig. 4-1) in which are placed the *field-winding* conductors. The field winding is energized from a controllable dc *excitation source* (Chap. 9). The rotor-field conductors belonging to the same belt carry dc currents in the same direction, with the current direction alternating in the p belts. The resulting rotor mmf will thus alternate around the periphery, in effect forming p magnetic rotor *poles*. For the two-pole case the resulting magnetic flux paths are shown dashed in Fig. 4-1. The magnetic axis of the rotor-field winding is referred to as the "direct" or "d-axis" and is identified in Fig. 4-1. Perpendicular to the d-axis is found the "quadrature" or "q-axis."

The *stator winding*, or *armature*, is placed in *equidistant* slots which are located around the *total* inner stator surface. (Only the slots belonging to phase a are shown in Fig. 4-1.) The armature is divided into *three identical phase windings* which are placed in $3p$ phase belts, each of which spans $120/p$ degrees of the stator surface. In the two-pole machine shown in Fig. 4-1 there will thus be a total of six belts, each spanning 60°. The three identical phase windings are interconnected to form a "generator neutral" which normally is grounded.

When slower prime movers, e.g., hydroturbines, must be used, and consequently a higher number of poles is required, the rotor is normally designed with *salient poles*. Figure 4-2 shows this type of design for a six-pole machine. The field winding is now placed in coils which are fitted around the rotor poles. Except when extremely large waterheads are utilized, the rotors, or "runners," typically are slow and tend to have very large diameter and relatively small axial length. The turbine-generator shaft assembly is normally vertical, with the turbine placed below the generator.

In addition to the field and armature windings described above, all synchronous machines are provided with rotor *damper* windings (not shown in Figs. 4-1 and 4-2), consisting of short-circuited *cages* quite similar to the "squirrel-cage" induction motor windings. In a salient-pole machine the cage bars are placed in axial slots in the pole faces; in a turbogenerator they are normally situated (usually as conducting wedges) in the same slots as the field winding. The damper windings are idle under normal balanced operation but go automatically into operation during transients (Sec. 4-13).

The magnetic flux in the rotor, under normal conditions, is constant. In the stator, however, it will fluctuate with time. The rotor iron is therefore solid whereas the stator iron is designed laminated in order to reduce iron losses. (The

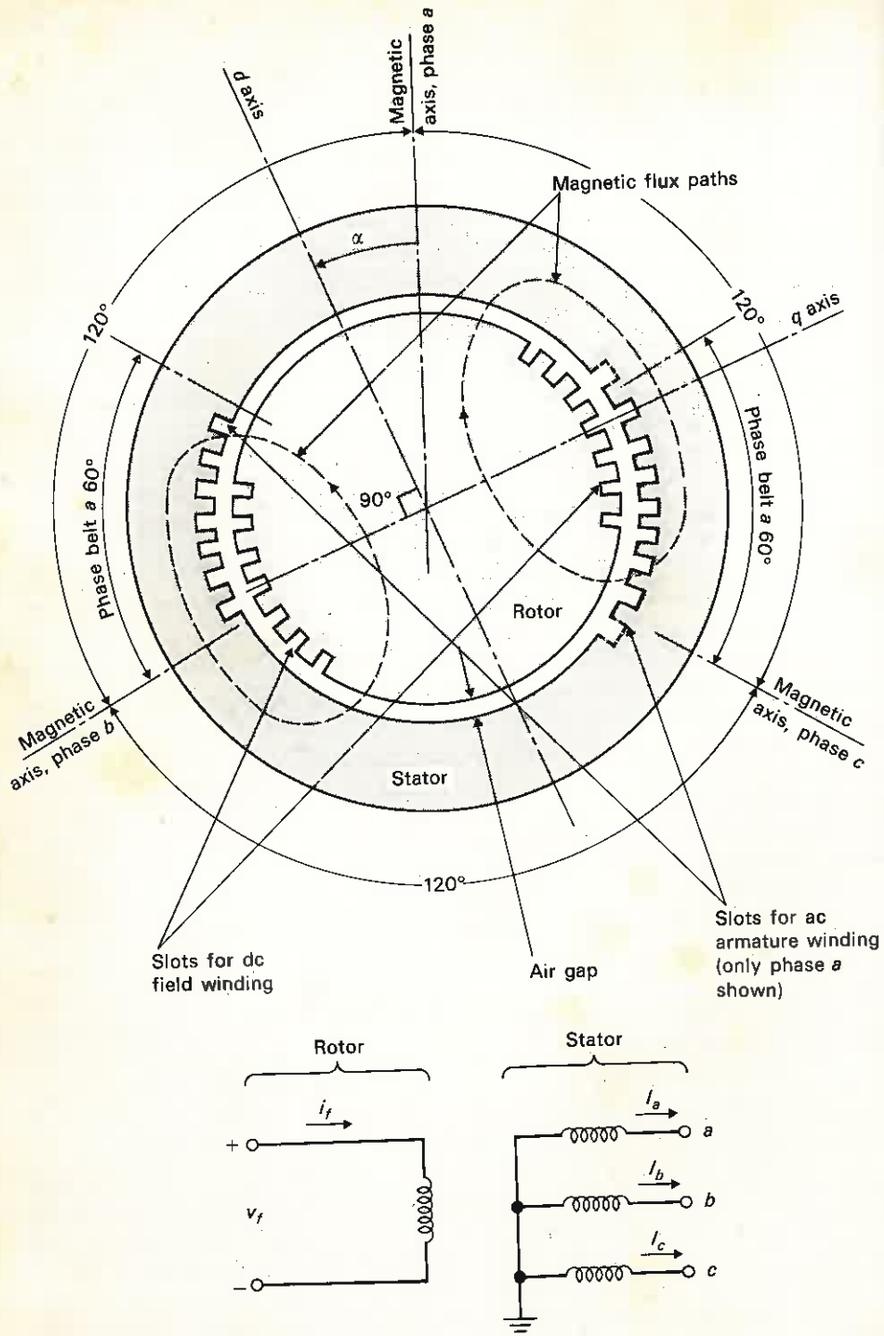

Figure 4-1 Design details of three-phase synchronous turbogenerator.

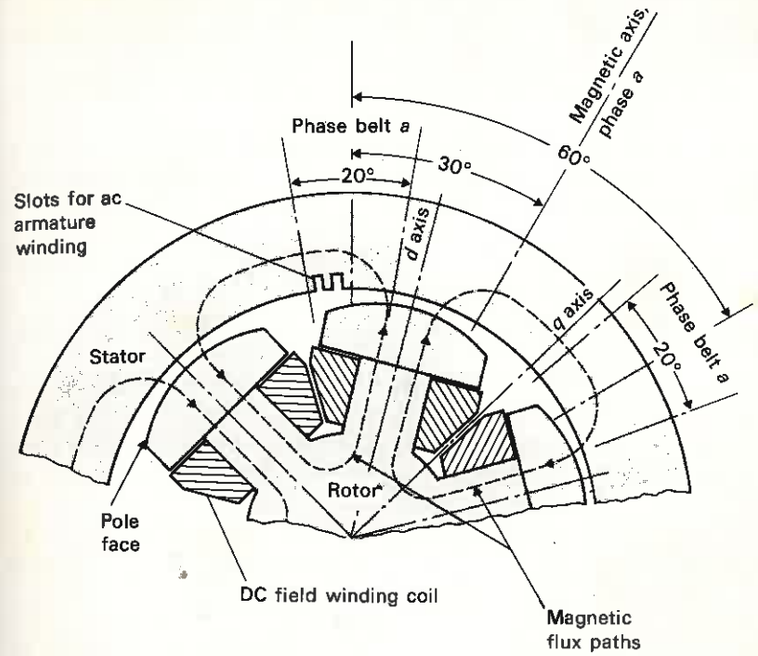

Figure 4-2 Design details of three-phase hydrogenerator.

solid rotor iron provides current paths and does, in reality, act as a separate damper winding during transient conditions.) For more detailed descriptions of the machine, see Refs. 1, 2, or 3.

4-3 INDUCTION OF STATOR EMFs—FLUX AND EMF WAVES

When a dc field current i_f flows in the rotor-field winding, an mmf is set up which causes the formation of a rotor-based *field flux*. In a salient-pole generator (Fig. 4-2) the pole faces are *tapered*, resulting in a maximum flux density along the d axis diminishing to zero in the q direction. By proper tapering one creates, in actuality, a *sinusoidal* flux distribution along the air-gap periphery.

In the case of a turborotor the magnetic flux distribution (Fig. 4-3) has more of a "staircase" look, where each "step" is due to the added mmf contributed by the field current in the discrete rotor slots. However, as seen in Fig. 4-3, the *fundamental* sinusoidal space wave is *dominating* over the harmonics. *Throughout*

this chapter we shall assume the field flux to have a sinusoidal† air-gap distribution in both salient and turbo-type machines.

If the rotor spins at a constant *synchronous* speed, the stator conductors will experience a travelling "flux wave."

When a magnetic flux of density B cuts a perpendicular conductor at a relative speed s, an emf is induced in the conductor, the instantaneous magnitude e of which follows from the formula

$$e = Bs \qquad \text{V/m} \tag{4-1}$$

B is measured in tesla and s in meters per second.

As the flux distribution is assumed sinusoidal so will be the emf distribution. The stator will thus experience an "emf wave" or "E wave" of the same speed as the flux wave. The situation is depicted in Fig. 4-4. (The symbol Φ_{fa} for the flux wave will be explained in the next section.) *Note the polarity of the E wave.*

The two waves consist of $p/2$ full cycles around the full periphery. Thus if the rotor speed is n r/min, each stator conductor will experience an ac emf of frequency

$$f = \frac{p}{2} \times \frac{n}{60} = \frac{pn}{120} \qquad \text{Hz} \tag{4-2}$$

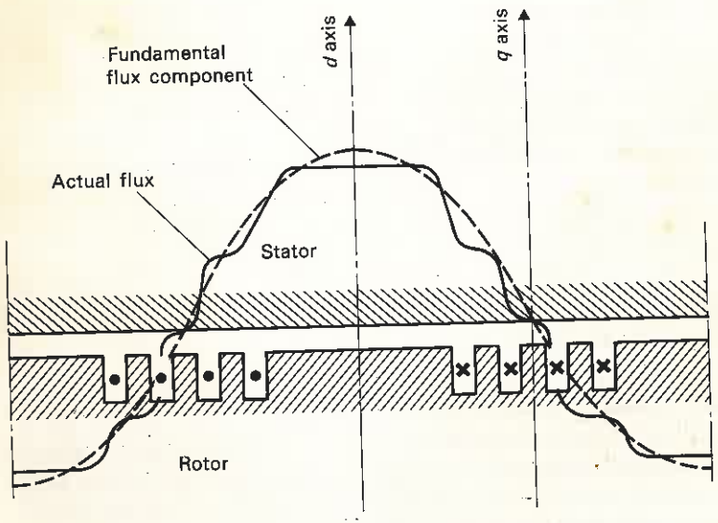

Figure 4-3 Air-gap flux distribution of a turbogenerator.

† The space harmonics induce high-frequency undesired emf components in the armature. However, by various winding designs their effects can be essentially annulled. (Ref. 1, Chap. 4.)

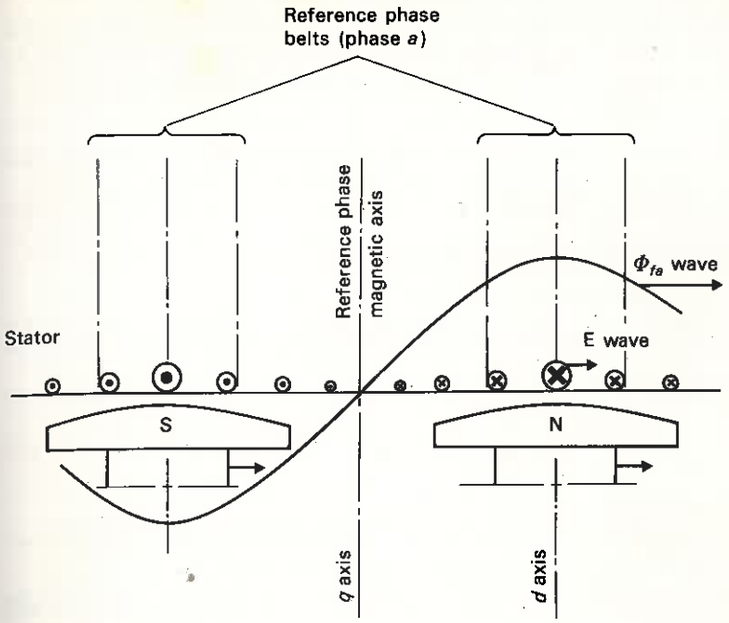

Figure 4-4 The E wave travels synchronously with the rotor poles (and flux).

For example, the 2-pole machine in Fig. 4-1 when rotating at 3600 r/min will generate a 60-Hz emf. It also follows that when the rotor turns one *mechanical* degree, the stator emf completes $p/2$ *electrical* degrees. In a two-pole machine electrical and mechanical degrees are identical.

Due to their winding locations (Fig. 4-1) the emf's induced in phases b and c will lag that in phase a by 120 and 240 electrical degrees respectively. In words: *The generated emf's will constitute a symmetrical three-phase set in accordance with Fig. 3-4.*

4-4 SPEED VOLTAGE

The wave snapshot in Fig. 4-4 is arbitrarily taken at the moment when the emf crests in phase a. Note that this happens when the rotor q axis coincides with the magnetic axis of winding a, i.e., *at the moment when the flux linkage is zero.* We understand this better if we derive the emf from the flux linkage.

In our following analysis we shall be concerned with several flux waves. To properly identify these waves we shall employ a double subscript system. For example, if a flux is created by the rotor *f*ield current (subscript f) but is linked with the stator *a*rmature (subscript a) then the flux is identified by the subscript pair fa.

To a rotor-bound observer the flux wave in Fig. 4-4 will appear as a constant or dc flux (symbol Φ). A stator-bound observer experiences the same wave as an ac flux of frequency f (symbol ϕ). In reference phase a the two fluxes are related by the formula

$$\phi_{fa} = \Phi_{fa} \cos \alpha = \Phi_{fa} \cos \omega t = -\Phi_{fa} \sin (\omega t - \pi/2) \qquad \text{Wb/phase} \quad (4\text{-}3)$$

For the meaning of the angle α see Fig. 4-1. $\alpha = \omega t$ must be measured in *electrical radians.*

Faraday's law yields the emf induced in phase a

$$e = -\frac{d\phi_{fa}}{dt} = \omega \Phi_{fa} \cos (\omega t - \pi/2) \qquad \text{V/phase} \quad (4\text{-}4)$$

The rms value of this emf equals

$$|E| = \frac{\omega \Phi_{fa}}{\sqrt{2}} = \frac{\omega L_{fa} i_f}{\sqrt{2}} \sim n i_f \qquad \text{V/phase, rms} \quad (4\text{-}5)$$

The last step follows from Eq. (4-2).

L_{fa} represents the "mutual inductance coefficient" between rotor field and stator armature as measured *when their magnetic axes coincide.*

Formula (4-4) confirms the earlier finding that the emf lags the linked flux

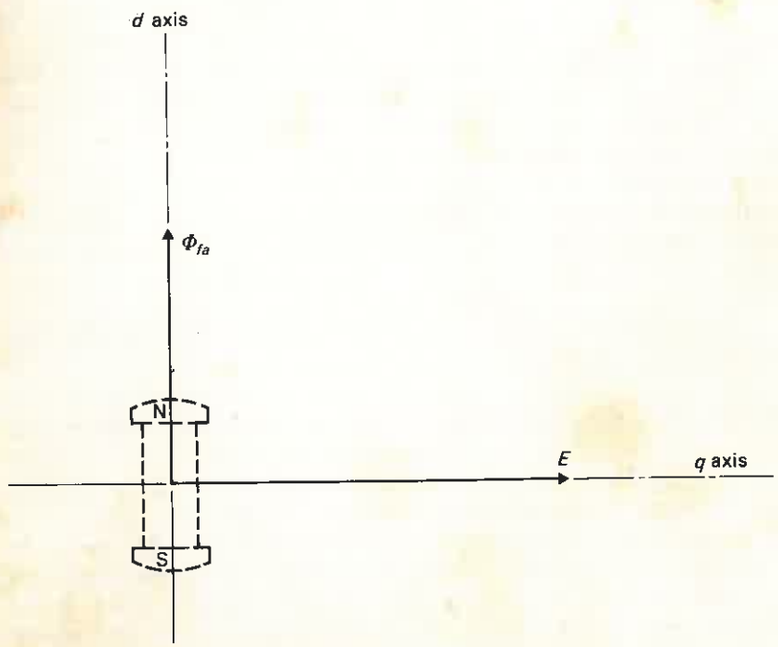

Figure 4-5 Phasor representation of speed emf.

by 90 electrical degrees. Because the rms value of the emf is proportional to rotor speed n it is often referred to as a *speed voltage.*

As both ϕ_{fa} and e are sinusoidal we can express them as *phasors.* Figure 4-5 thus tells in phasor language how the *reference phase* experiences the pole flux. *Note in particular that a d axis flux induces a q axis speed voltage.*

(Why is it that when the flux and emf are expressed as "waves" as in Fig. 4-4 their crests are coinciding but when expressed as phasors as in Fig. 4-5 the one lags the other by 90°?)

4-5 THE CURRENT-LOADED MACHINE—THE "I WAVE"

The synchronous machine can be operated in two distinctly different ways, both of which will be discussed later:

1. Singly, onto a symmetrical load
2. In parallel with other machines as part of a larger system

Both of these modes of operation are identical in one important respect—the phase currents, symbolized by I, will constitute a *symmetrical three-phase set* as described by Eqs. (3-5).

When these three currents pulsate in the three stator phase windings, the total *composite* effect will be what best can be termed a stator "current wave," or "I wave." The proof of this is given in App. B. Here we will only state the following important features of the I wave:

1. In a macro sense it constitutes a surface "sheet current" varying sinusoidally around the periphery with $\rho/2$ full cycles.
2. The wave will travel around the stator periphery at synchronous speed.
3. Its crest will coincide with a phase-belt center at the same instant as the respective phase-current, I, peaks. Its amplitude is proportioned to $|I|$.

The last feature means that if the E phasor leads the I phasor by β degrees then the E wave will lead the I wave by the same angle.

In Fig. 4-6, we have superimposed the I wave upon the wave system earlier shown in Fig. 4-4. (To avoid cluttering we have not shown the E wave. For an explanation of the Φ_{aa} wave see the next section.)

4-6 ARMATURE REACTION

Just as the dc rotor-field current represents a rotating mmf wave that results in the Φ_{fa} wave so does the above stator I wave represent a rotating mmf wave that will, in its turn, create a flux wave named the *armature reaction wave.* As the

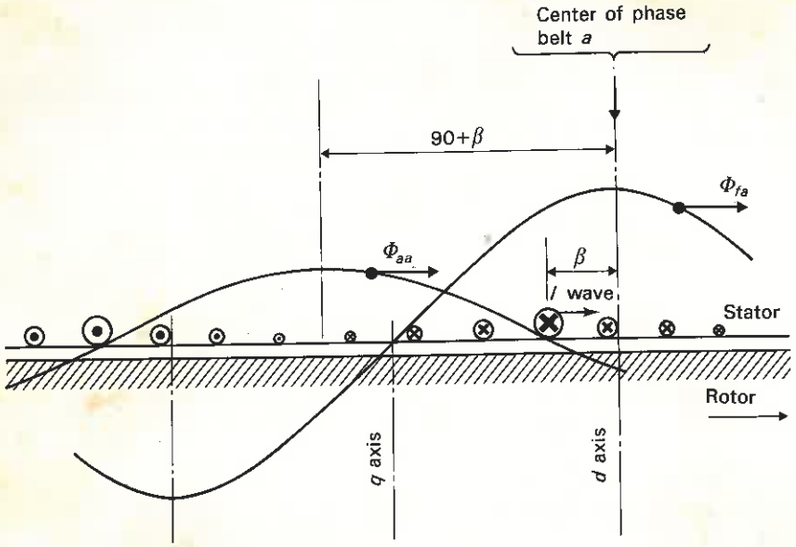

Figure 4-6 *I* wave and armature reaction wave.

latter is caused by the armature current and will induce an emf in the armature it will be symbolized Φ_{aa}. The Φ_{aa} wave, shown in Fig. 4-6, has these features:

1. Its crests are located at the zeros of the I wave. Thus it will lag the Φ_{fa} wave by $(90 + \beta)$ degrees.
2. Its amplitude will be proportional (if magnetic saturation is neglected) to $|I|$.
3. It can be resolved into two wave components, one having its crest along the d axis and the other along the q axis. The components are not shown in Fig. 4-6 but depicted in the phasor diagram in Fig. 4-7.

   For $\beta > 0$ the d axis component will buck, for $\beta < 0$ it will boost Φ_{fa}.

   The stator reference phase a will experience Φ_{aa} as an ac flux ϕ_{aa}.

In similarity with Eq. (4-3) we write for ϕ_{aa}

$$\phi_{aa} = \Phi_{aa} \cos(\omega t - \pi/2 - \beta) \qquad \text{Wb/phase} \tag{4-6}$$

In the stator reference phase the Φ_{aa} wave will induce the speed emf

$$e_I = -\frac{d\phi_{aa}}{dt} = \omega\Phi_{aa} \sin(\omega t - \pi/2 - \beta) \qquad \text{V/phase} \tag{4-7}$$

of rms value

$$|E_I| = \frac{\omega\Phi_{aa}}{\sqrt{2}} = \omega L_{aa}|I| \tag{4-8}$$

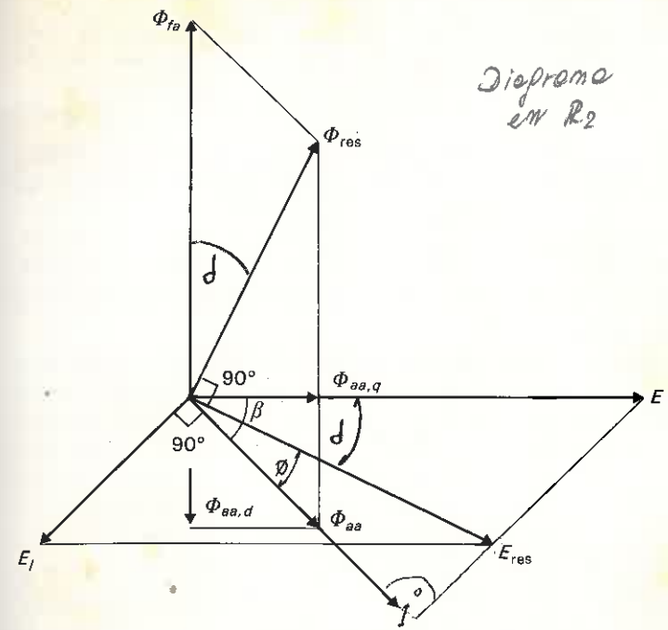

Figure 4-7 Fluxes and speed emf's shown as phasors.

The last step follows as a consequence of the proportionality between the flux Φ_{aa} and its causative current, the proportionality constant being defined as the inductance L_{aa}. Phasor E_I is identified in Fig. 4-7.

4-7 THE TERMINAL VOLTAGE

Physically, the two flux waves Φ_{fa} and Φ_{aa} cannot exist separately. They add up to a resulting flux wave, Φ_{res}. Similarly the two armature emf's E and E_I cannot exist (or be measured) separately but add up, vectorially, to a resulting emf

$$E_{res} = E + E_I \qquad \text{V/phase} \tag{4-9}$$

The situation is shown graphically in the phasor diagram in Fig. 4-7, which is a direct extension of Fig. 4-5. As the wave Φ_{aa} lags the wave Φ_{fa} by $(90 + \beta)$ degrees the Φ_{aa} phasor will obviously coincide with the I phasor. Just as E lags Φ_{fa} by 90° so will E_I lag Φ_{aa} by the same angle. *E_I will thus lag the current I by 90°.*

As E_{res} is the voltage or emf that can actually be measured between terminal a and ground it is referred to as the *terminal voltage, V*, of the generator.

As phasor E_I lags the current phasor I by 90° and as its magnitude $|E_I|$ follows from Eq. (4-8) we can express it as

$$E_I = -j\omega L_{aa} I \triangleq -jX_s I \qquad \text{V/phase} \tag{4-10}$$

The proportional constant $X_s = \omega L_{aa}$ has dimension of reactance, and is named the "synchronous reactance." By substitution of (4-10) into (4-9) we obtain

$$E_{\text{res}} \triangleq V = E - jX_s I \qquad \text{V/phase} \tag{4-11}$$

Equation (4-11) corresponds to the phasor diagram in Fig. 4-8*a* (which is really identical to the one in Fig. 4-7).

The terminal voltage V can hence be considered the result of the field induced "internal emf" E minus the voltage drop across the "internal impedance" jX_s, justifying our representing the machine with the "equivalent

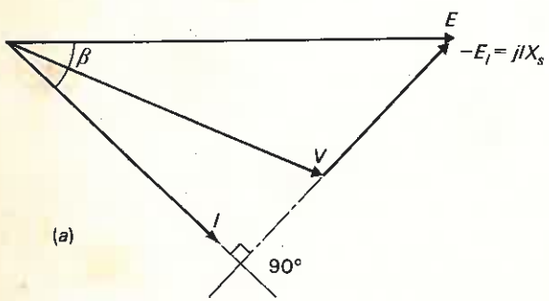

(*a*)

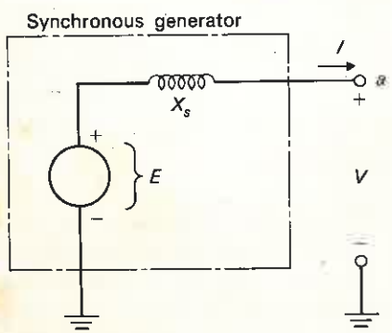

(*b*)

Figure 4-8 Equivalent circuit of synchronous generator.

network" in Fig. 4-8*b*. In reality the internal impedance also has a *resistive* component R_s, representing the phase-winding resistance. However, whereas X_s typically lies in the range 0.60–1.50 pu in terms of machine ratings, R_s is less than 0.01 pu and we may therefore, in most analysis cases, completely neglect it.

The reactance X_s can be readily obtained by the following test. Short circuit the armature and increase the field current until the armature current reaches 1 pu. The short circuit is then removed and the terminal voltage measured *without changing the field current*. The measured value of $|V|$ expressed in per-unit is identical to the per-unit value of X_s. (The reader should draw a phasor diagram and explain the statement.)

4-8 MAGNETIC SALIENCY EFFECTS—TWO-REACTION THEORY

The derivations of the last two sections tacitly neglected "magnetic saliency." Specifically we assumed that the I wave would produce Φ_{aa} and E_I waves, the magnitudes of which would be *independent of the relative phase* β. This assumption is tantamount to saying that the magnetic reluctance is the same along both d or q axes (and all positions in between). This is obviously not true for the salient-pole machine (Fig. 4-2). Even for the "round rotor" turbogenerator the assumption does not hold water. This is explained in Fig. 4-9 that depicts how the slotted segments of the rotor increase the magnetic reluctance in the q direction.

Thus, in all practical generators the position of the I wave relative to the rotor (as measured by the angle β) *will* affect the Φ_{aa} and E_I waves *and thus the value of* X_s. *It now becomes necessary to distinguish between the magnetizing effects in d and q directions.* This is being done by resolving the current I into two components I_d and I_q as depicted in Fig. 4-10. The former component will cause a flux wave $\Phi_{aa,d}$ in the d direction, the latter a flux wave $\Phi_{aa,q}$ in the q direction.

These two flux waves (shown in Fig. 4-7) will cause speed emf's E_{Id} and E_{Iq} respectively which, in analogy with Eq. (4-8), will have magnitudes

$$\begin{aligned} |E_{Id}| &= \frac{\omega\Phi_{aa,d}}{\sqrt{2}} \triangleq \omega L_{aa,d} I_d \triangleq X_d I_d \qquad \text{V/phase} \\ |E_{Iq}| &= \frac{\omega\Phi_{aa,q}}{\sqrt{2}} \triangleq \omega L_{aa,q} I_q \triangleq X_q I_q \qquad \text{V/phase} \end{aligned} \tag{4-12}$$

In analogy with Eq. (4-10) we can express the phasors E_{Id} and E_{Iq} as

$$\begin{aligned} E_{Id} &\triangleq -jX_d I_d \qquad \text{V/phase} \\ E_{Iq} &\triangleq -jX_q I_q \qquad \text{V/phase} \end{aligned} \tag{4-13}$$

where X_d and X_q are the *direct-* and *quadrature-axis synchronous reactances* respectively. Table 4-1 gives typical values of these reactances (in per unit of rated megavoltamperes and kilovolts).

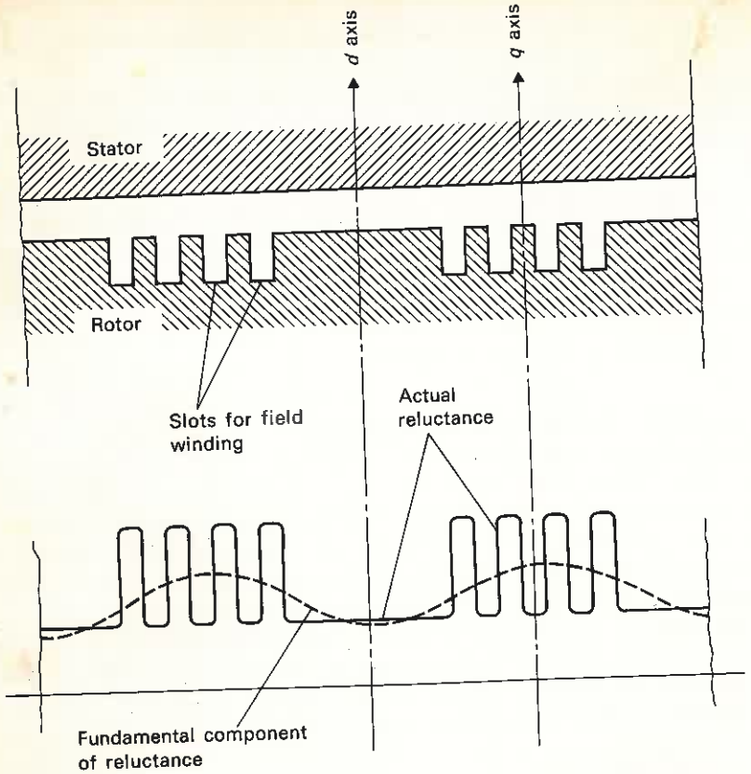

Figure 4-9 Saliency effect in turbo machine.

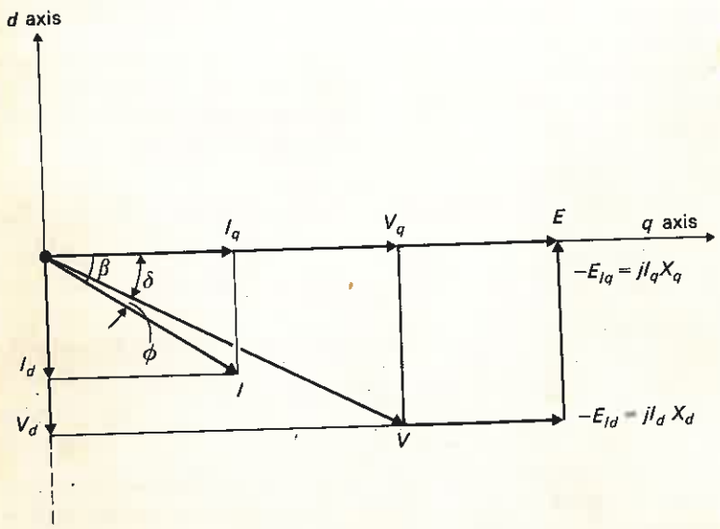

Figure 4-10 Resolution of I into components I_d and I_q.

Table 4-1 Synchronous machine reactances (in per unit of rated MVA)

Reactances	Synchronous motors: High-speed	Synchronous motors: Low-speed	Synchronous capacitors	Hydro-generators	Turbine generators
X_d	0.80	1.10	1.60	1.00	1.15
X_q	0.65	0.80	1.00	0.65	1.00
X'_d	0.30	0.35	0.40	0.30	0.15
X''_d	0.18	0.20	0.25	0.20	0.10
X_-	0.19	0.35	0.25	0.20	0.13
X_0	0.05	0.07	0.08	0.07	0.04

As the resulting stator emf (=terminal voltage) equals the sum of E, E_{Id}, and E_{Iq} we have

$$V = E + E_{Id} + E_{Iq} = E - jX_dI_d - jX_qI_q \qquad \text{V/phase} \tag{4-14}$$

The corresponding phasors are shown in Fig. 4-10.

The phasor diagram that we now have arrived at is very important as it shall serve as the base for many of our continuing discussions. Note that we have identified two new phase angles in our diagram. The angle ϕ is the phase between the terminal phase voltage V and the phase current I. In computing delivered power (megawatts and megavars) it has the same meaning as in formulas (2-21), *defined positive when V leads I*.

The *power angle δ defined positive when E leads V* has in many ways the same meaning as the δ defined by Eq. (3-42).

4-9 POWER AND TORQUE CREATION

The prime job of the generator is to produce megawatts. The electromechanical air-gap torque T_{em} that is developed within the generator constitutes the basic link between the mechanical turbine power P_T and the electrical power P_G delivered from the generator terminals. In this section we study briefly the physical mechanism whereby the air-gap torque is created, and also the qualitative nature of same.

The basic physical law to remember is the force action between a magnetic field B and a perpendicular current i. The force on the current-carrying conductor is shown in Fig. 4-11. If this law is applied to the *rotor-based* Φ_{fa} wave and the *stator-based* I wave (Fig. 4-6) we realize immediately (if $-90° < \beta < 90°$) that the stator is subject to a force (and torque) acting in the direction of rotation.†

† The torque tends to tilt the stator in the direction of rotation and will actually do so if it is not properly bolted down.

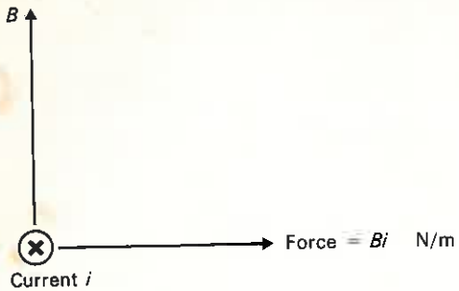

Figure 4-11 Mechanical force on current-carrying conductor placed in magnetic field.

The rotor is subject to an equal and opposite reaction force (and torque). This latter torque clearly tends to decelerate the rotor, but will be prevented from doing so by the accelerating turbine torque, which will always keep exact balance and thus maintain constant rotor speed. How this torque balance is actually achieved will be detailed in Chap. 9.

The I wave has the physical appearance of a "sheet current" flowing in the stator surface. To obtain the total force (or torque) between rotor and stator we must integrate over the total stator surface. Such an integration is not difficult to perform[1] and yields

$$T_{em} = \frac{P_G}{\omega_m} \sim \hat{B}_{fa}\hat{I}\cos\beta \qquad \text{N}\cdot\text{m} \tag{4-15}$$

where $\hat{B}_{fa}$ and $\hat{I}$ are the amplitudes of the Φ_{fa} and I waves respectively. As all the three factors in the above equation are *constants it follows that both the air-gap torque and generator power are constants as well.*

The formula (4-15) is exact only if magnetic nonsaliency can be assumed. As we noted earlier some degree of saliency can always be expected. This fact adds a corrective "saliency term" to our torque and power equations. As we shall see in the next section its effect is small.

4-10 POWER FORMULAS

The power formula (4-15) is very impractical because $\hat{B}_{fa}$, $\hat{I}$, and β are all hard to measure. More practically useful formulas should express the generator power in terms of easily measureable variables. We now set out to find such formulas and start from the well-known formula for complex power

$$S_G = P_G + jQ_G = |V|\,|I|\cos\phi + j|V|\,|I|\sin\phi \tag{4-16}$$

V, I, and ϕ are all defined and appear in Fig. 4-10. Note that because I is defined positive out from the machine, Eq. (4-16) *defines P_G and Q_G positive in a generator sense.* Note also that the equation gives *per-phase* values of power.

From the phasor diagram in Fig. 4-10 we obtain upon projection along and perpendicular to E, respectively:

$$\begin{aligned} |E| - I_d X_d &= |V|\cos\delta \\ I_q X_q &= |V|\sin\delta \end{aligned} \tag{4-17}$$

We also have

$$\begin{aligned} I_q &= |I|\cos\beta \\ I_d &= |I|\sin\beta \end{aligned} \tag{4-18}$$

and for the angles:

$$\phi = \beta - \delta \tag{4-19}$$

From the last equation we derive

$$\begin{aligned} \cos\phi &= \cos(\beta-\delta) = \cos\beta\cos\delta + \sin\beta\sin\delta \\ \sin\phi &= \sin(\beta-\delta) = \sin\beta\cos\delta - \cos\beta\sin\delta \end{aligned} \tag{4-20}$$

Upon multiplying these last equations by $|I|$ and then making use of Eqs. (4-18) we get*

$$\begin{aligned} |I|\cos\phi &= I_q\cos\delta + I_d\sin\delta \\ |I|\sin\phi &= I_d\cos\delta - I_q\sin\delta \end{aligned} \tag{4-21}$$

Finally, upon inserting these last expressions into Eq. (4-16) and at the same time making use of the relations (4-17) we obtain these important formulas for the real and reactive generator powers

$$\boxed{\begin{aligned} P_G &= \frac{|V|\,|E|}{X_d}\sin\delta + \frac{|V|^2}{2}\left(\frac{1}{X_q} - \frac{1}{X_d}\right)\sin 2\delta \\ Q_G &= \frac{|V|\,|E|}{X_d}\cos\delta - |V|^2\left(\frac{\cos^2\delta}{X_d} + \frac{\sin^2\delta}{X_q}\right) \end{aligned}} \quad \begin{aligned} &\text{MW/phase} \\ &\text{Mvar/phase} \end{aligned} \tag{4-22}$$

The first term in the P_G formula dominates. The second term is the "saliency torque" component. If we were to neglect the saliency effect by setting

$$X_d = X_q = X_s \tag{4-23}$$

then the above general power formulas simplify to

$$\boxed{\begin{aligned} P_G &= \frac{|V|\,|E|}{X_s}\sin\delta \\ Q_G &= \frac{|V|\,|E|}{X_s}\cos\delta - \frac{|V|^2}{X_s} \end{aligned}} \quad \begin{aligned} &\text{MW/phase} \\ &\text{Mvar/phase} \end{aligned} \tag{4-24}$$

Formulas (4-22) and (4-24) are particularly useful when the magnitudes of both E and V can be assumed constant, *in which case P_G and Q_G become functions of δ only.*

Note that the above formulas yield *three*-phase *mega*values of power if $|E|$ and $|V|$ are expressed in *kilo*volts *line* voltage.

Often in power-system studies the simpler formulas (4-24) are preferred to the more complex ones (4-22). For the synchronous reactance X_s one would then use the *average* value of X_d and X_q.

Example 4-1 Demonstrate the actual approximations involved by finding exact and approximate P_G expressions for a hydrogenerator having the following ratings:

15 MVA (total 3-phase)
13.6 kV (line), 60 Hz

It is assumed that the generator is operated with $|E| = |V| = 13.6$ kV (line). Define rated megavoltamperes and kilovolts as base values, and express your answers in per unit.

The reactance data are:

$$X_d = 0.80 \text{ pu/phase}$$

$$X_q = 0.65 \text{ pu/phase}$$

$$X_s \cong \frac{0.65 + 0.80}{2} = 0.725 \text{ pu/phase}$$

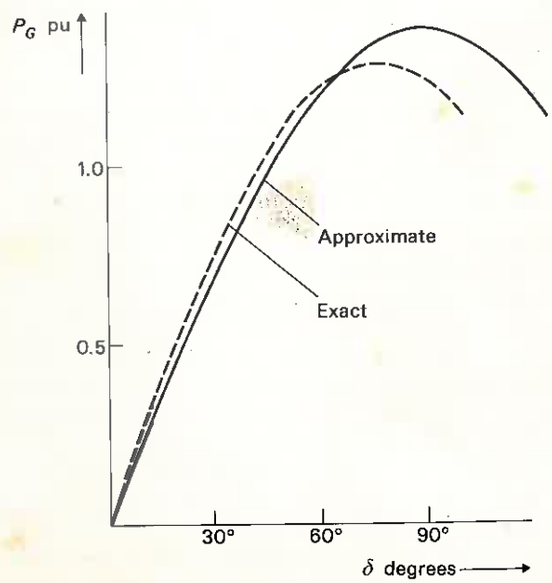

Figure 4-12 A comparison of approximate and exact megawatt formulas.

SOLUTION We first use the exact power formula

$$P_G = \frac{1 \times 1}{0.80} \sin \delta + 0.5\left(\frac{1}{0.65} - \frac{1}{0.80}\right) \sin 2\delta$$

$$= 1.250 \sin \delta + 0.144 \sin 2\delta \quad \text{pu MW} \tag{4-25}$$

The approximate formula reads

$$P_G \approx \frac{1 \times 1}{0.725} \sin \delta = 1.379 \sin \delta \quad \text{pu MW} \tag{4-26}$$

In Fig. 4-12 we have plotted the two P_G-δ graphs for comparison. Note the good agreement obtained in the δ range (0–30°) where the machine normally would be operated.

4-11 CONTROL OF SYNCHRONOUS MACHINES OPERATED SINGLY

As was mentioned in Sec. 4-5, synchronous generators can be operated either onto individual loads or, in parallel with other generators, as part of huge interconnected power grids. In the first mode of operation, the frequency and terminal voltage level must be controlled by means of the prime-mover torque and the field current respectively. The generator power, real and reactive, is essentially determined by the load itself. Although this mode of operation is comparatively uncommon we shall presently study it for the purpose of comparing it with the more common parallel operation.

Consider a synchronous machine initially running at rated speed, zero loading, and with a 100 percent terminal voltage. A load consisting of three Y-connected resistors is connected to its terminals. How will the machine behave? What will be its new frequency, terminal voltage, and power outputs?

As the load is being applied, the resulting stator currents immediately will create a stator I wave and an accompanying air-gap torque. As was explained in Sec. 4-9 the latter will tend to *decelerate* the rotor. *In order to maintain constant speed it is thus necessary to increase the prime-mover torque until torque balance is restored.* The air-gap torque thus constitutes the mechanism whereby mechanical power from the prime mover is transformed into electrical power to the load impedances.

The stator current will also cause a voltage drop across the synchronous reactance. Thus we can expect the terminal voltage to drop below its original 100 percent. *In order to restore constant terminal voltage we must obviously boost the excitation level, thereby increasing the emf magnitude.*

Let us demonstrate with the following example.

Example 4-2 Let the hydrogenerator in Example 4-1 operate at no-load, rated speed and terminal voltage. Three Y-connected resistors of 15 Ω each are connected to its terminals. Find the new terminal voltage and power outputs. Disregard saliency and work with the earlier computed value for X_s (0.725 pu Ω/phase).

SOLUTION If the load resistance is R ohms, we have the relationship

$$I = \frac{V}{R}$$

Upon substitution into Eq. (4-11) we obtain for the terminal voltage

$$V = E\frac{R}{R + jX_s} \tag{4-27}$$

Our numerical values are

$$\text{Reference phasor } E = \frac{13.6}{\sqrt{3}}\underline{/0^\circ} = 7.852\underline{/0^\circ} \quad \text{kV/phase}$$

$$R = 15.0\ \Omega/\text{phase}$$

$$X_s = 0.725\frac{13.6^2}{15} = 8.94\ \Omega/\text{phase}$$

Equation (4-27) yields

$$V = 6.745\underline{/-30.8^\circ} \quad \text{kV/phase}$$

and

$$I = \frac{V}{R} = 0.450\underline{/-30.8^\circ} \quad \text{kA/phase}$$

The terminal voltage obviously experiences a drop from 7.852 to 6.745 kV, that is, 14.1 percent, to the new value of 0.859 pu.

The generator power output is computed from formula (4-16).

As $\phi = 0$ we obtain

$$P_G = 3 \times 0.450 \times 6.745 \times \cos 0^\circ = 9.11 \text{ MW (total 3-phase)}$$

$$Q_G = 0 \text{ Mvar}$$

In order to maintain the speed (and frequency) it is necessary to adjust the steam flow in the turbine so that it outputs 9.11 MW (plus losses).

In order to increase $|V|$ back to 1.00 pu, it is necessary to increase $|E|$ in the ratio $1/0.859 = 1.164$, that is, by 16.4%.

The real power consumed by a resistor is proportional to the square of the voltage and, consequently, the increase in $|V|$ will cause an increase in P_G to the higher value

$$P_G = 1.164^2 \times 9.11 = 12.3 \text{ MW}$$

We need to make a corresponding increase in the prime-mover power to maintain the speed at 100 percent. *Note that the reactive power output of the above generator is zero regardless of what the terminal voltage (or excitation level) is.* (The resistors cannot, of course, accept any reactive power from the generator.)

In summary, when a generator is operating alone onto an individual load the problem of controlling its speed and terminal voltage can become a rather delicate operation. Primarily the real-power output depends upon the load and is controlled by regulating the prime-mover torque so as to achieve torque balance and, as a result, constant speed and frequency. The terminal voltage is controlled by regulating the excitation level. However, there is an *interaction* or "cross-coupling" between these two control channels; an increase in excitation level causes an increase in the real-power output which, in turn, requires a prime-mover adjustment.

Note that formulas (4-22) or (4-24) were of little use in Example 4-2, because of the nonconstancy of $|V|$.

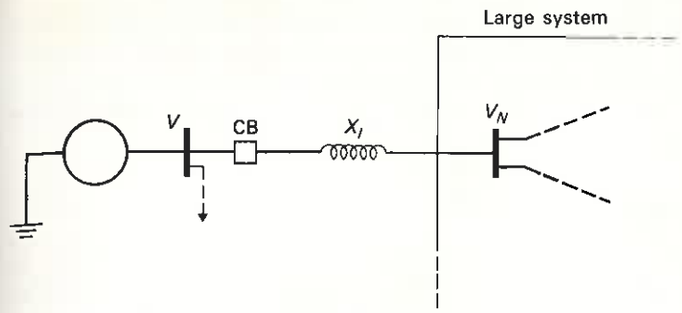

Figure 4-13 Generator operating onto large system via connecting link.

4-12 GENERATOR OPERATED AS PART OF LARGE POWER GRID

This is by far the most important operating case, being the typical way that all large interconnected power systems are operated. In the following analysis we shall assume that our generator unit is connected to the system bus via a connecting link consisting of line and transformers having a total inductive† impedance of jX_l ohms per phase (Fig. 4-13). The voltage of the network bus equals V_N.

Let us first consider one important consequence resulting from the assumption that the external system is "large." For example, were we to operate our 15 MVA example generator onto the U.S. interconnected grid which has a total generating capacity in excess of 500 GVA then we realize immediately that our machine will have no measurable influence on the system speed or frequency.

4-12-1 Synchronization

Before our machine can be operated as part of the grid, it must be *synchronized* onto it, i.e., it must be interconnected with the already operating system. Synchronization can take place if the following conditions are all satisfied:

1. The generator and network frequencies are equal.
2. The phase sequence of the generator matches that of the network.
3. The generator emf E and network voltage V_N are of equal magnitude.
4. E and V_N have equal phase.

If and only if all these conditions are satisfied, the voltages across the three breaker poles of the circuit breaker CB are all zero, and the generator can be smoothly "locked" onto the network by closing the circuit breaker.

† Compare Chaps. 5 and 6.

Once the machine is synchronized onto the network, we can make it either produce or absorb real power. Likewise, we can make it generate or consume reactive power. The magnitude and direction of the megawatt flow is determined by means of the shaft torque. The megavar flow is controlled by the excitation level $|E|$.

4-12-2 Modified Power Formulas

We noted that our generator normally will not affect the system frequency. In most instances its effect on the system bus voltage V_N is likewise quite negligible, as this bus is likely to appear quite "voltage stiff" as viewed from the generator. (In Chap. 10 we shall see that this characteristic of V_N is due to a feature referred to as the "short-circuit capacity" of the bus.)

For our present purpose we will thus assume that $|V_N|$ is essentially a constant.

The earlier phasor diagram in Fig. 4-10 is then modified to incorporate the bus voltage V_N. Note that the difference between V and V_N is due to the voltage drop across the connecting link, i.e.,

$$V_N = V - jX_l I \tag{4-28}$$

Inclusion of V_N changes the diagram in Fig. 4-10 to the one in Fig. 4-14*a* which, if V is deleted, yields the diagram in Fig. 4-14*b* relating the internal emf E

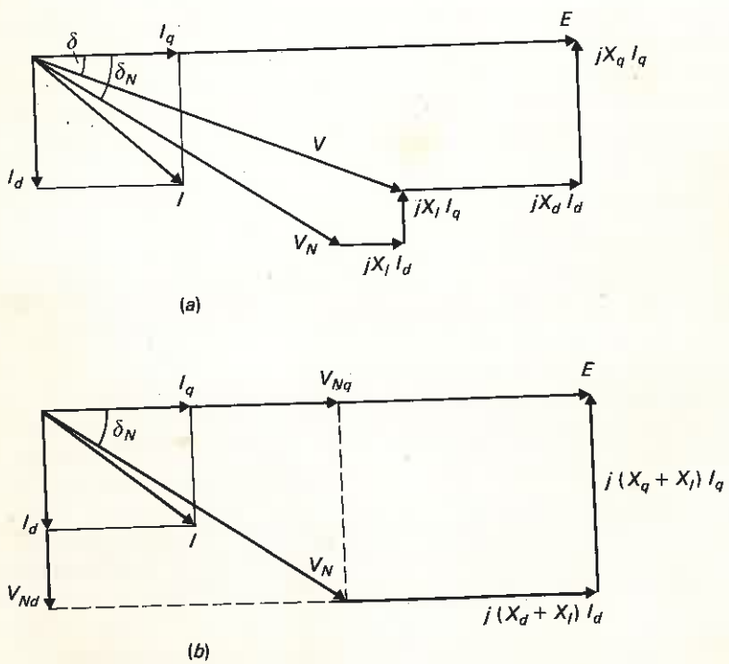

Figure 4-14 Modified phasor diagram.

with the system bus voltage V_N. *The latter phasor diagram is clearly identical to the one in Fig. 4-10 if we make these variable substitutions:*

$$\begin{aligned} V &\to V_N \\ V_d &\to V_{Nd} \\ V_q &\to V_{Nq} \\ \delta &\to \delta_N \\ X_d &\to X_d + X_l \\ X_q &\to X_q + X_l \end{aligned} \tag{4-29}$$

All power formulas that were derived from Fig. 4-10 thus apply if we observe the above parameter and variable changes. Note, however, that P_G and Q_G now must be measured at the system bus.

Example 4-3 Consider the hydrogenerator in Example 4-1. It is connected to a distant bus held at 1 pu voltage. The connecting link has an impedance of $j0.11$ pu based on generator ratings. The generator is excited to $|E| = 1.22$ pu and delivers 10 MW. Find δ, δ_N, I, and V.

SOLUTION From Eq. (4-22) and upon making use of the modifications (4-29) we obtain

$$\begin{aligned} P_G &= \frac{1.00 \times 1.22}{0.80 + 0.11} \sin \delta_N + \frac{1.00^2}{2}\left(\frac{1}{0.65 + 0.11} - \frac{1}{0.80 + 0.11}\right) \sin 2\delta_N \\ &= 1.341 \sin \delta_N + 0.108 \sin 2\delta_N \quad \text{pu MW} \end{aligned} \tag{4-30}$$

Upon setting $P_G = 10/15 = 0.667$ pu this equation yields $\delta_N = 25.7°$.
From Fig. 4-14*b* we have

$$V_{Nd} = |V_N| \sin \delta_N = I_q(X_q + X_l)$$

$$V_{Nq} = E - |V_N| \cos \delta_N = E - I_d(X_d + X_l)$$

For the current components I_q and I_d we thus get

$$I_q = \frac{1.00 \sin 25.7°}{0.65 + 0.11} = 0.571 \text{ pu}$$

$$I_d = \frac{1.22 - 1.00 \cos 25.7°}{0.80 + 0.11} = 0.350 \text{ pu}$$

$$\therefore \quad I = \sqrt{0.571^2 + 0.350^2} \angle -\tan^{-1}\left(\frac{0.350}{0.571}\right) = 0.670 \angle -31.5° \text{ pu}$$

From Eq. (4-28) we obtain the terminal voltage

$$\begin{aligned} V &= V_N + jX_l I = 1.00 \angle -25.7° + j0.11 \times 0.670 \angle -31.5° \\ &= 1.01 \angle -21.5° \text{ pu} \end{aligned}$$

In summary

$$\delta = 21.5°$$

$$\delta_N = 25.7°$$

$$|I| = 0.670 \text{ pu kA}$$

$$|V| = 1.01 \text{ pu kV}$$

4-12-3 Real Power Control

We had assumed $|V_N|$ to be constant. If, in addition, the excitation level is fixed then $|E|$ is also constant. Thus, if nonsaliency is also assumed, the real generator output power equals

$$P_G \approx \frac{|E||V_N|}{X_s + X_l} \sin \delta_N \triangleq P_{\max} \sin \delta_N \tag{4-31}$$

where $P_{\max} \triangleq |E||V_N|/(X_s + X_l)$ is *constant.*

Figure 4-15 depicts how the generator real power P_G varies with the power angle δ_N. A positive δ_N means that E leads V_N and this phase relationship forces P_G to become positive signifying *generator action.* On the other hand, should V_N lead E, then P_G becomes negative, the machine thus taking real power from the network, i.e., *motoring.*

We must remember that the phase of E is tied to the position of the rotor. A positive δ_N thus results when the prime mover *advances* the rotor position by

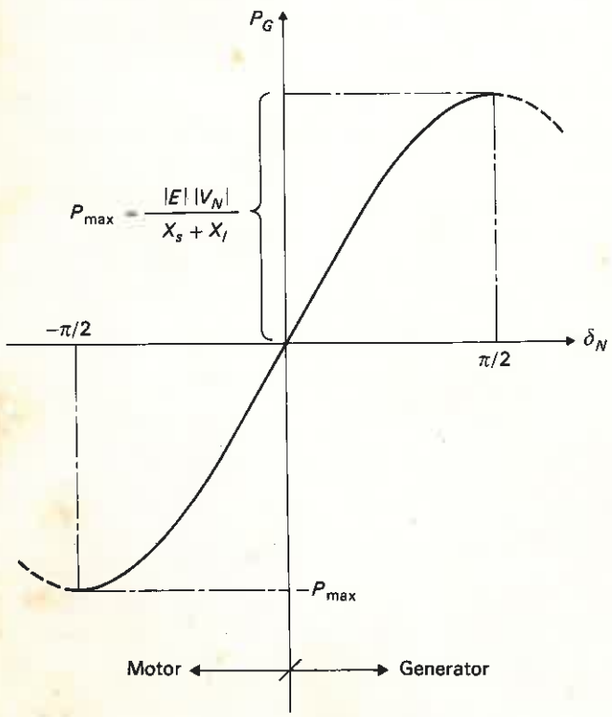

Figure 4-15 P_G versus δ_N of nonsalient machine.

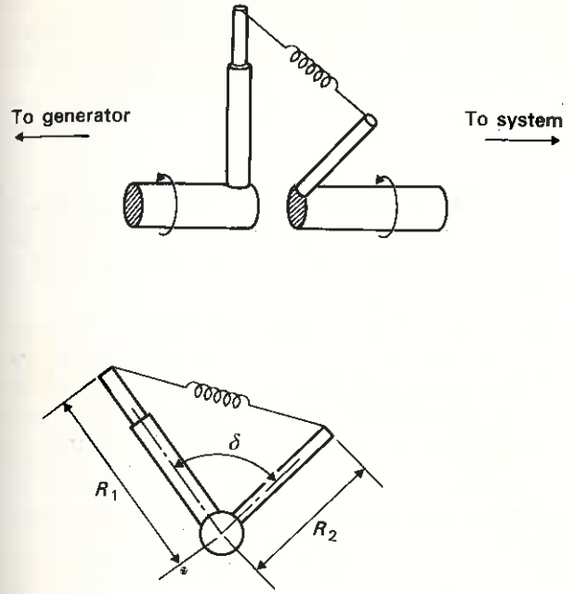

Figure 4-16 A mechanical analog.

delivery of an accelerating torque. A negative δ_N results when the rotor moves into a lagging position due to the decelerating torque emanating from a mechanical shaft load.

4-12-4 A Mechanical Analog

The synchronous generator locked onto a network behaves from a real-power point of view quite similar to the mechanical rod-spring coupling shown in Fig. 4-16. The reader can readily verify that the power (or torque) transmitted via this mechanical system equals

$$T_{\text{mech}} \sim P_{\text{mech}} \sim R_1 R_2 \sin \delta \tag{4-32}$$

The symmetry between formulas (4-31) and (4-32) is obvious.

4-12-5 Electrical Stiffness

The "electrical stiffness" or "synchronizing coefficient" S_y of a synchronous machine is defined as

$$S_y \triangleq \frac{dP_G}{d\delta_N} = \frac{|E||V_N|}{X_s + X_l} \cos \delta_N \qquad \text{MW/rad} \tag{4-33}$$

and indicates the differential power increase obtained per differential power-angle increase. *We can evidently make our machine stiffer by either increasing*

$|E|$ *(that is, using high-magnitude pole flux), by decreasing the synchronous reactance* X_s, *or by operating the machine at a small power angle.* The second method can, of course, be employed only as a *design tool.*†

4-12-6 Pullout Power

As the electrical stiffness decreases with increasing angle δ_N we seldom operate a synchronous machine above $\delta_N = 30°$. Should we operate at power angles close to 90° the machine would lose its stiffness. (Note that the same thing happens in the rod-spring coupling in Fig. 4-16.)

If the shaft torque increases so as to force δ_N to approach 90° the transmission collapses. The real power generated or consumed by a synchronous machine cannot exceed the value P_{max} in Fig. 4-15. This power is referred to as the *pullout power.* Should the turbine power exceed P_{max} the generator will "pull out" of synchronism. (Note that at the point of pullout the stiffness is zero.)

Example 4-4 Consider the generator in Example 4-3. It has been synchronized onto the 13.6 kV network. The prime-mover torque is adjusted until P_G measures 9 MW or 0.60 pu.

(*a*) Find power angle δ_N if $|E|$ is kept at the synchronization value.
(*b*) Compute S_y.
(*c*) Find pullout power.
(*d*) Find current at point of pullout. Is current loading acceptable?

SOLUTION (*a*) With $|E| = |V_N| = 13.6/\sqrt{3} = 1$ pu we get directly from Eq. (4-31)

$$0.6 = \frac{1 \times 1}{0.725 + 0.11} \sin \delta_N$$

This equation yields $\delta_N = 30.1°$

(*b*) From Eq. (4-33) we get

$$S_y = \frac{1 \times 1}{0.835} \cos 30.1° = 1.04 \text{ pu MW/rad} = 0.27 \text{ MW/degree}$$

(*c*)
$$P_{pullout} = P_{max} \approx \frac{1 \times 1}{0.835} = 1.20 \text{ pu} = 18.0 \text{ MW}$$

(*d*) At the point of pullout the relationship between V_N, E, and I is shown in Fig. 4-17. From this diagram we obviously have

$$(X_s + X_l)|I| = \sqrt{|E|^2 + |V_N|^2}$$

$$\therefore \quad |I| = \frac{\sqrt{|E|^2 + |V_N|^2}}{X_s + X_l} = \frac{\sqrt{1.00^2 + 1.00^2}}{0.835} = 1.69 \text{ pu}$$

At point of pullout the generator is 69 percent current-overloaded, but only 20 percent power-overloaded.

† The most effective way of building a machine with low-magnitude X_s is by using relatively large air gaps. We pay a price for this: a very powerful dc excitation source must be used to overcome the air-gap reluctance in order to obtain required flux density.

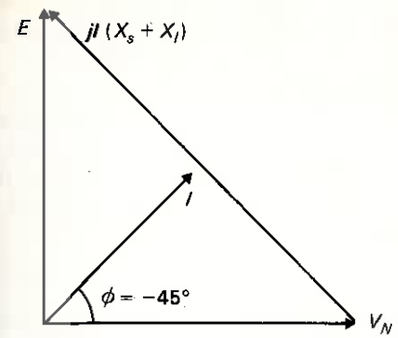

Figure 4-17 Phasor relations at point of pullout.

Example 4-5 Determine power angle, stiffness, and pullout power for the machine in Example 4-4 if we increase its excitation level by 30 percent. It is assumed that the prime-mover setting is unchanged at 9 MW.

SOLUTION The emf now takes on the new rms value $|E| = 1.3$ pu.

The increased flux levels will boost the stiffness of the machine resulting in a smaller power angle.

From Eq. (4-31) we actually obtain

$$0.6 = \frac{1.3 \times 1.0}{0.835} \sin \delta_N$$

which yields $\delta_N = 22.7°$.

Equation (4-33) yields the new stiffness value

$$S_y = \frac{1.3 \times 1.0}{0.835} \cos 22.7° = 1.44 \text{ pu MW/rad}$$

And, finally for the pullout power

$$P_{max} = \frac{1.3 \times 1.0}{0.835} = 1.56 \text{ pu MW} = 23.4 \text{ MW}$$

4-12-7 Control of the Reactive Generator Power

We have so far said nothing about how to control the *reactive power* Q_G delivered by the machine. In the discussion that follows we shall make use of the second of Eqs. (4-24), modified according to Sec. 4-12-2. (Remember that Q_G shall be measured at the system bus.)

The formula tells us that Q_G becomes positive if

$$|E| \cos \delta_N > |V_N| \tag{4-34}$$

This means that the generator *produces* reactive power, i.e., *acts, from the network point of view, as a capacitor.* The inequality (4-34) evidently depends upon δ_N, that is, upon the *real* power P_G.† Generally, however, the inequality is

† However, since $\cos \delta_N$ is an *even* function of δ_N, it does not matter whether we have motor or generator action.

satisfied for high-magnitude $|E|$, that is, for *strong* excitation. We refer to this as *overexcitation.*

We therefore have the following important rule.

An overexcited synchronous machine (operated either as motor or generator) produces reactive power and acts as a shunt capacitor as viewed from the network.

On the contrary an *underexcited* machine *consumes* reactive power from the network and in consequence acts as a shunt coil, if viewed from the network. Underexcitation is defined by the inequality

$$|E| \cos \delta_N < |V_N| \tag{4-35}$$

This feature of an overexcited synchronous machine, of actually generating reactive power, is taken advantage of in a so-called *synchronous capacitor*. In this mode of operation the machine usually carries no real load;† that is, $\delta_N = \delta = 0$. From Eq. (4-24) we then have

$$Q_G = \frac{|V_N|\,|E| - |V_N|^2}{X_s + X_l} \quad \text{Mvar} \tag{4-36}$$

The beauty of this arrangement is that Q_G can be *continuously* and *simply* controlled in both magnitude and direction by changing $|E|$, that is, by varying the dc excitation current.

It is important to realize that a change in excitation level *will not affect the real-power output* P_G of the generator. The excitation change will, however, affect the magnitude of P_{max}, and thus the stiffness of the machine. This means that the power angle δ_N, *but not the power* P_G, will vary. For example, a reduction in the field current will increase the magnitude of δ_N, even possibly to the point of pullout.

A change in the shaft torque, as earlier reasoned, will immediately affect the power P_G. At the same time the power angle δ_N will also change, and since Q_G depends on $\cos \delta_N$, *we therefore also experience a change in* Q_G. We usually work with power angles below 30°. For such small angles, $\cos \delta_N$ is rather insensitive to changes in δ_N and therefore we do not experience too large a fluctuation in Q_G. We say that the cross-coupling is weak.

Example 4-6 Determine the reactive power situation in the two operating conditions discussed in Examples 4-4 and 4-5.

SOLUTION We first study the situation in Example 4-4. As the excitation level satisfies the inequality (4-35) we have here an *underexcited* case. Equation (4-24) yields

$$Q_G = \frac{1.00^2 \cos 30.1° - 1.00^2}{0.835} = -0.161 \text{ pu Mvar}$$

† It may seem strange, at a first glance, that the generator carries armature current but neither receives nor delivers megawatts. Note, however, that if you let δ_N be zero in Fig. 4-14*b*, the current component I_q must also be zero. The current I must therefore have a phase β of $\pm 90°$ the sign depending upon over- or underexcitation. (Compare also Figs. 4-18*e* and *f*.) Cos β is therefore zero and according to formula (4-15) so is the torque.

telling us that the machine (including X_l) *absorbs* 2.42 Mvar.

After boosting $|E|$ by 30 percent the reactive power formula gives

$$Q_G = \frac{1.3 \times 1.0 \times \cos 22.7° - 1.00^2}{0.835} = +0.239 \text{ pu Mvar}$$

The machine is now operating in an *overexcited* mode and *supplies*† 3.59 Mvar to the grid. The reader is encouraged to draw the phasor diagrams for the two cases and confirm how the excitation boost changes the current phasor from a leading to a lagging position.

4-12-8 A Summary of Operating Cases

Based upon magnitude and direction of real and reactive powers one can distinguish between the six important practical operating combinations shown in Fig. 4-18. As a *generator*, driven by a prime mover, the machine can be operated either as a producer or consumer of reactive power (cases *a* and *b*). Two similar cases (*c* and *d*) exist when the machine is being used as a *motor*, delivering torque to a mechanical load.

Often the machine is operated with zero real power. If overexcited it then performs the same job as a set of three shunt capacitors. In this mode of operation (case *e*) it is referred to as a "synchronous capacitor." If underexcited (case *f*) it would consume reactive power. This last mode of operation is used when there is a need in a network to dispose of surplus reactive power, for example during night hours when the real load is light but the high-voltage lines still must be energized and produce large amounts of reactive power (see Chap. 6).

Example 4-7 Consider our 15-MVA example machine. It must be run as a synchronous capacitor producing 7.5 Mvar to the grid. What should be its level of excitation? The system bus voltage equals 1 pu.

SOLUTION Since it must produce 0.5 pu reactive power at 1 pu voltage the current must equal 0.5 pu.

From Fig. 4-18*e* we have

$$|E| - |V_N| = |I|(X_s + X_l) = 0.5(0.725 + 0.11) = 0.418 \text{ pu}$$

$$\therefore \quad |E| = 1.00 + 0.418 = 1.418 \text{ pu}$$

or 19.3 kV, line-to-line.

Example 4-8 In this example we study how the real and reactive power outputs of a generator change when the machine is subject to manipulation of *both* control inputs, the shaft torque and the excitation current.

We shall consider our example hydrogenerator feeding power into the network bus which is held at 1 pu voltage. Our computations are in per unit of rated generator power and voltage.

Let us assume that the generator initially runs overexcited, with $|E| = 1.50$ pu and a real-power output corresponding to $P_G = 0.25$ pu.

† How much reactive power does it generate as measured at its terminals?

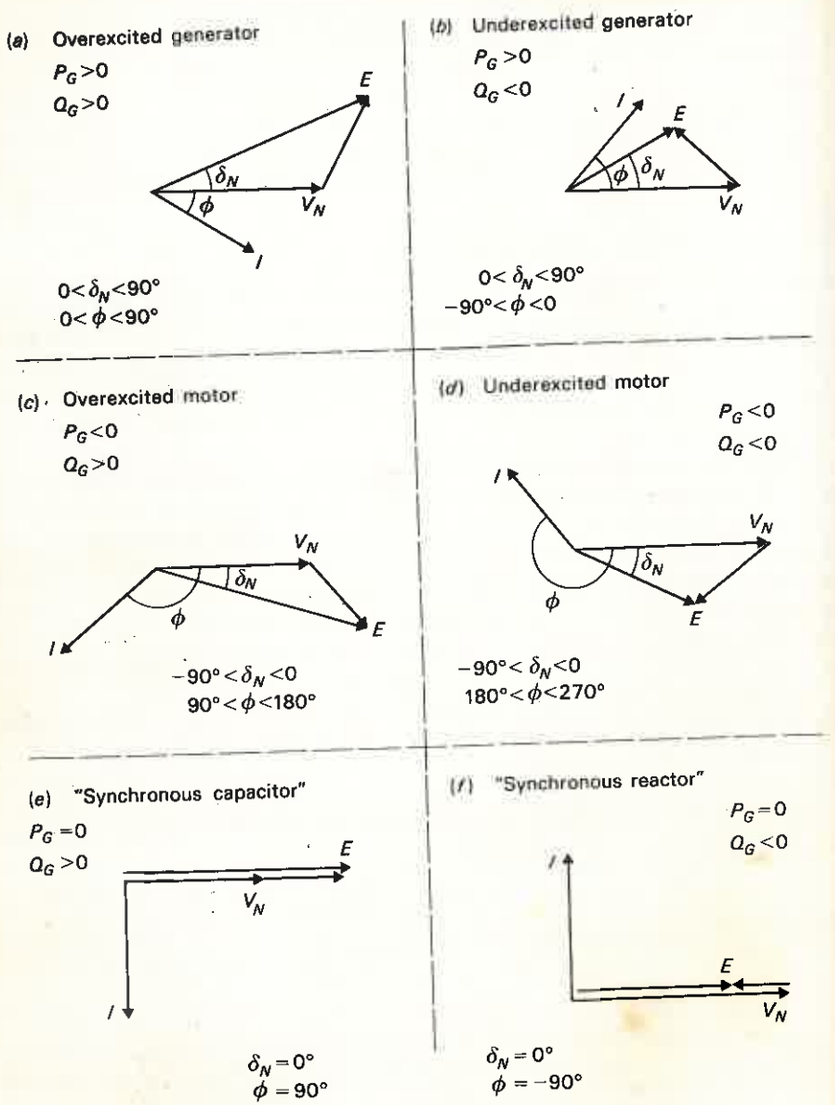

Figure 4-18 The six operating cases of a synchronous machine.

From Eq. (4-31) we can now compute the power angle δ_N

$$0.25 = \frac{1.5 \times 1.0}{0.835} \sin \delta_N$$

which yields

$$\delta_N = 8.00°$$

From the Q_G equation we then compute the reactive power output

$$Q_G = \frac{1.5 \times 1.0 \times \cos 8.00° - 1.0^2}{0.835} = 0.581 \text{ pu Mvar}$$

The megavoltampere output of the generator is thus

$$\sqrt{0.250^2 + 0.581^2} = 0.633 \text{ pu MVA}$$

as measured at the network bus, indicating that the generator is running at slightly above half-current load.

We shall now subject the machine to (*a*) torque control and (*b*) excitation control, and study the output changes in both cases.

Case a. Torque control Let us assume that we open the steam valve corresponding to a 100-percent increase in the turbine torque; i.e., the real-power output will increase to 0.5 pu. The power angle will now increase, and we compute the new value

$$0.5 = \frac{1.5 \times 1.0}{0.835} \sin \delta_N$$

i.e.,

$$\delta_N = 16.16°$$

For this new rotor position the reactive power will ***decrease*** to

$$Q_G = \frac{1.5 \times 1.0 \cos 16.16° - 1.0^2}{0.835} = 0.528 \text{ pu Mvar}$$

measured at network bus. We thus conclude that a 100-percent *increase* in the torque input (and thus the P_G output) results in a 9.2-percent *decrease* in the Q_G output. We have here, obviously, a cross-coupling between the torque input and the Q output, but a weak one.

Case b. Excitation control Let use now assume that we start from the same initial state as before, keeping the steam valve setting unchanged but varying the field current. For example, let us assume a 20-percent increase of field current, which (if we assume no saturation) means that $|E|$ increases to $1.20 \times 1.50 = 1.8$ pu. This increase of the pole flux results in a stiffer machine, and from the P_G equation we compute the new and smaller power angle

$$0.25 = \frac{1.8 \times 1.0}{0.835} \sin \delta_N$$

i.e.,

$$\delta_N = 6.66°$$

There will, of course, be no change in the P_G output. The new Q_G output will be

$$Q_G = \frac{1.8 \times 1.0 \times \cos 6.66° - 1.00^2}{0.835} = 0.944 \text{ pu Mvar}$$

measured at network bus, i.e., a 62-percent increase from the original value of 0.581.

The generator reactive output is thus very sensitive to changes in excitation level.

4-12-9 Machine Operating Limits

The basic job of a synchronous generator is to produce megawatts. However, in addition, depending upon the load and operating situation, the machine may be called upon to either generate or absorb megavars. One may then ask what the generating limits are in a specific case. For example, could a generator with the name-plate capacity of 250 MVA deliver it all in megavars?

The physical limits of a generator are reached when the operating temperature attains a prescribed maximum value. The temperature rise is due to core losses and ohmic losses in the windings.

A generator is always asked to generate the power at an *essentially constant* terminal voltage. A constant terminal voltage requires a constant flux wave B_{res} (Sec. 4-6) and thus essentially constant core losses. *Thus the ohmic winding losses will in reality determine the loading limits.*

Ohmic losses occur in both stator and rotor windings, but the former dominate. According to Eq. (4-16) we have

$$P_G^2 + Q_G^2 = |V|^2 |I|^2 \tag{4-37}$$

As the ohmic-stator losses are proportional to $|I|^2$ and, as we noted above, the terminal voltage $|V|$ is constant we conclude that

$$\text{Armature losses} \sim P_G^2 + Q_G^2 \tag{4-38}$$

In a P_G-Q_G diagram (Fig. 4-19) the equation (4-37) means that loci for constant armature losses are *circles* with centers in origin. *If the armature losses were the only ohmic losses of consequence then the region within the contour abcd would represent permissible P_G-Q_G loading of the machine.* (Note that we have excluded the region for $P_G < 0$ because a typical generator cannot operate as a motor.)

However, there are additional constraints that must be observed in practice:

1. Unless we take a generator unit off-line it is not desirable to reduce the real power output below a certain minimum value $P_{G\,\min}$. (For example, in a fossil plant constant boiler temperature must be maintained to prevent slagging.) This constraint reduces our permissible region to within the new bounds $a'bc'd'$.
2. If the generator is strongly *over*excited and *producing* large quantities of reactive power Q_G, then, according to Fig. 4-18*a*, a large internal emf E is needed. This will require heavy rotor current resulting in extreme ohmic rotor losses. As a result we must cut down on stator losses, which means the imposition of a lower reactive bound $a''e$ in Fig. 4-19.
3. If the generator is strongly *under*excited and *absorbing* large quantities of reactive power Q_G, then, according to Fig. 4-18*b* a very small internal emf is required. But this means a reduction of the electrical stiffness (Eq. 4-33) and a resulting increase in the power angle δ_N, that is, less stability margins. In practice we want to prevent "too soft" a machine by imposing limits to the degree of underexcitation. This results in the additional boundary $c''f$ in Fig. 4-19.

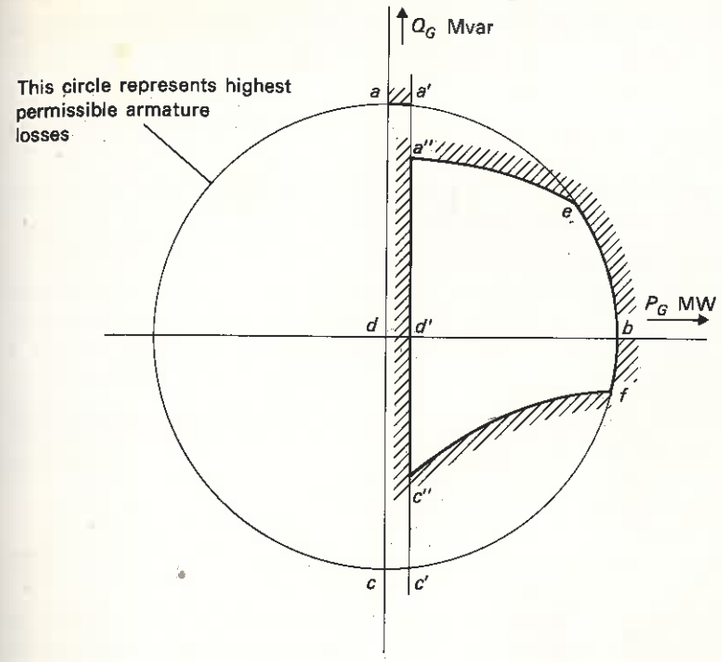

Figure 4-19 Real and reactive power limits of generator.

Upon taking all above constraints into account we have thus, in summary, ended up with the shaded contour $a''ebfc''d'$ in Fig. 4-19 within which our generator can be satisfactorily operated.

4-13 TRANSIENT MACHINE BEHAVIOR

All the previous theory was based upon the assumption that steady-state conditions prevail within the machine. The basic phasor diagram in Fig. 4-10 and the important power formulas (4-22) are valid only if the various flux waves are fully developed and of constant magnitudes. During periods of change the relationships between currents, voltages, and emf's are quite different and new "transient power formulas" apply.

Since the load is slowly drifting over periods of minutes and hours (Fig. 3-13), in a true sense a generator never is in a constant steady state. However, the drift is so slow that the transient effects can be neglected during

normal operation. The "transients" that we are mostly concerned with may be initiated by the following types of disturbances:

1. *Sudden* and *large* network changes or "faults," exemplified by a solid terminal short circuit.
2. *Sudden* but relatively *small* load changes. For example a 100-kW motor may be connected to an already loaded 100-MVA generator.

We present in this section a theory for transient phenomena. It will be based upon the assumptions first that the magnetic circuits are linear, i.e., all saturation effects can be neglected. Second, all disturbances *possess three-phase symmetry*. A general theory of transients in synchronous machines exists ("The Park equations") but is quite unwieldy, certainly on a textbook level. We rather present this material from a physical point of view even if, in the process, it will suffer somewhat in rigor.

4-13-1 Transients in Magnetically Coupled Circuits

To better understand the magnetic coupling phenomena in our machine we study first the transient characteristics of the two magnetically coupled circuits in Fig. 4-20. Coil 1 (the "primary") is connected to a "network" whereas coil 2 (the "secondary") is energized by a constant dc emf, E_2.

The disturbance or "fault" will be due to some sudden change in the network portion. We shall assume the "prefault" variables in both circuits to be *constants* symbolized by $(\ )^0$. The "postfault" variables will be symbolized $(\ )^f$. They will in general be nonconstants which, however, with passing of time will settle down to new postfault constant steady states. The difference between $(\ )^f$ and $(\ )^0$ represent the variable *change* due to the fault. This change will be symbolized by the prefix Δ.

The two coils have resistances R_1 and R_2 and self-inductances L_1 and L_2 respectively. Their mutual inductance is M. If ϕ_1 and ϕ_2 represent the two

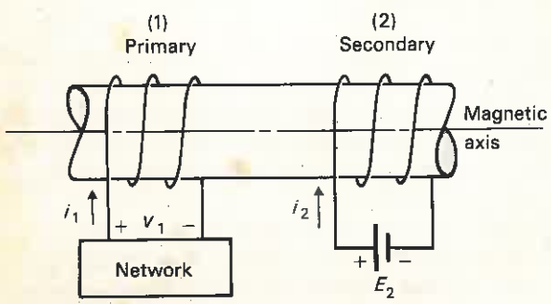

Figure 4-20 Two magnetically coupled coils wound on low-reluctance core.

linked coil fluxes, Kirchhoff's voltage law yields the following general postfault equations:

$$v_1^f = R_1 i_1^f + \frac{d\phi_1^f}{dt} \tag{4-39}$$

$$E_2 = R_2 i_2^f + \frac{d\phi_2^f}{dt} \tag{4-40}$$

The linked fluxes are related to the currents through the two equations

$$\phi_1^f = L_1 i_1^f + M i_2^f \tag{4-41}$$

$$\phi_2^f = L_2 i_2^f + M i_1^f \tag{4-42}$$

4-13-2 Magnetic Inertia

Consider Eq. (4-40). For the linked secondary flux we write

$$\phi_2^f = \phi_2^0 + \Delta\phi_2 \tag{4-43}$$

where ϕ_2^0 is constant.

For the secondary current we similarly write

$$i_2^f = i_2^0 + \Delta i_2 = \frac{E_2}{R_2} + \Delta i_2 \tag{4-44}$$

By substitution of Eqs. (4-43) and (4-44) into (4-40) the latter equation reduces to

$$0 = R_2\, \Delta i_2 + \frac{d}{dt}(\Delta\phi_2) \tag{4-45}$$

The coils in Fig. 4-20 have iron cores resulting in comparatively large flux magnitudes. In addition we shall assume that the secondary coil has a particularly low resistance R_2 in relation to its inductance. In Eq. (4-45) the second term will therefore be dominating and we can set with good accuracy

$$\frac{d}{dt}(\Delta\phi_2) \approx 0 \tag{4-46}$$

This equation integrates into

$$\Delta\phi_2 = \text{constant} = \Delta\phi_2\,(0) = 0 \tag{4-47}$$

In words: *The magnetic flux linked with a low resistance–high inductance coil tends to remain constant throughout a disturbance. The coil is said to be characterized by high "magnetic inertia."*

The sudden disturbance causes a sudden change Δi_1 in the primary current. To preserve secondary flux constancy a corresponding sudden current change

Δi_2 will be induced in the secondary. Equation (4-42) yields the following relationship between $\Delta\phi_2$ and the changes in currents:

$$\Delta\phi_2 = L_2\,\Delta i_2 + M\,\Delta i_1 \tag{4-48}$$

To keep $\Delta\phi_2$ equal to zero the induced secondary current change thus must equal

$$\Delta i_2 = -\frac{M}{L_2}\,\Delta i_1 \tag{4-49}$$

Figure 4-21 gives a graphic display of the unfolding of a typical disturbance. In the prefault state the two coil currents have constant steady-state values i_1^0 and i_2^0 respectively. Due to a sudden change in the "network" a sudden "transient component" Δi_1 is added to the primary current. A *proportional* "transient" Δi_2 is induced in the secondary in *opposite direction.*

If R_2 (and R_1) were *exactly* zero, those initial current changes would retain their magnitudes indefinitely. However, there will always be a nonzero R_2 which

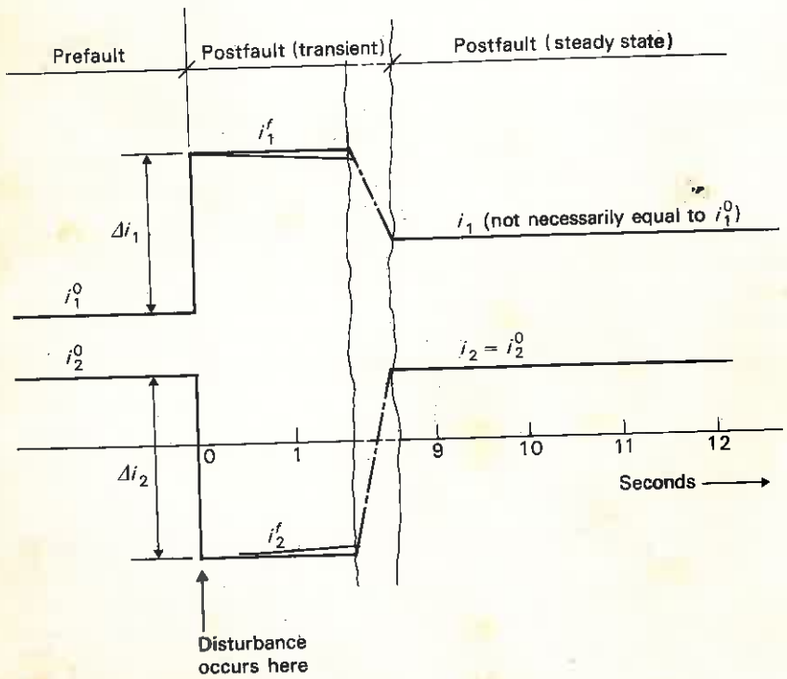

Figure 4-21 "Transients" following a disturbance in the "network" portion of Fig. 4-20.

will cause a decay, albeit a slow one, of Δi_2 to an eventual zero value. Δi_1 will also decay at the same rate but not necessarily to zero.

4-13-3 Transients along *d* Axis

We are now adequately prepared to interpret the transient behavior of the synchronous machine. The magnetic characteristics of the two coupled dc circuits in Fig. 4-20 closely resemble those that exist along the *d* axis of the three-phase synchronous machine. The primary coil corresponds to the stator armature. The ac armature current causes a dc magnetization along the *d* axis measured by the *d*-axis component I_d, which current component thus corresponds to the primary i_1. The secondary coil and its current i_2 correspond to the field winding and its current i_f respectively. The linked field flux ϕ_f is characterized by large magnetic inertia and in analogy with Eq. (4-47) must satisfy the equation

$$\Delta\phi_f \approx 0 \tag{4-50}$$

When sudden disturbances occur in the power network the armature current I undergoes rapid adjustments in both its *d*-axis and *q*-axis components. Figure 4-22 indicates the changes ΔI_d in the former. Proportional and opposite polarity

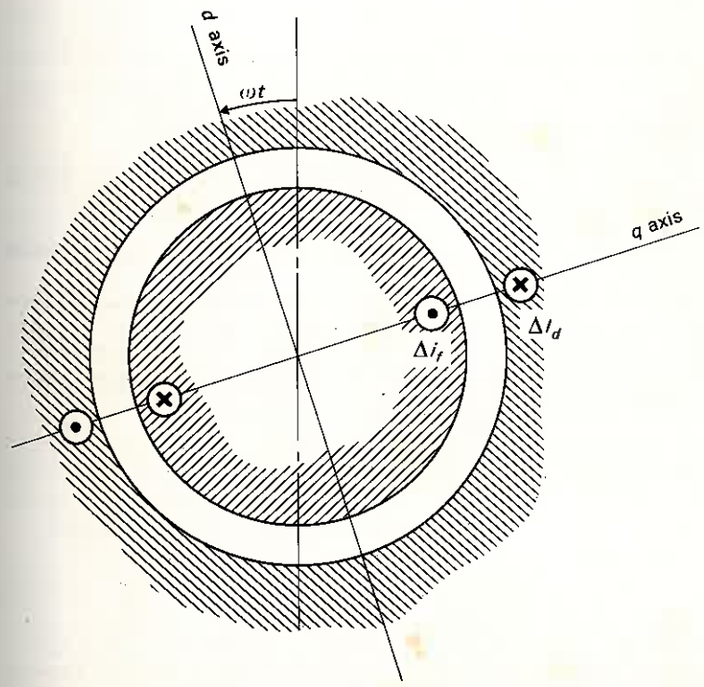

Figure 4-22 The transient components of I_d and i_f are of opposite polarity.

increments Δi_f are instantaneously induced in the field winding. The very high magnetic inertia of this winding will cause these transients to linger for 10 seconds and longer (Fig. 4-21) before a new postfault steady state sets in.

4-13-4 Transients along q Axis

Due to the absence of a q-axis field winding there are not any q-axis phenomena that correspond directly to the d-axis transients discussed in the previous section. In a first approximation we may thus assume that in the postfault state the q axis steady state conditions set in immediately following the disturbance.

Example 4-9 A synchronous generator is operating at 1 pu speed, 1 pu excitation but zero load when a symmetrical short circuit is placed across its stator terminals. Find the postfault currents.

SOLUTION From Fig. 4-10 we first find the postfault *steady-state* current picture. As V is zero both V_d and V_q must also be zero. Thus we obtain

$$E = jI_d X_d \tag{4-51}$$

and

$$V_d = jI_q X_q = 0 \tag{4-52}$$

i.e.,

$$I_q = 0 \tag{4-53}$$

and

$$I_d = \frac{E}{jX_d} = I \tag{4-54}$$

Figure 4-23 depicts the postfault *steady-state* phasor diagram. As the angle β equals 90° the postfault steady-state armature current is *totally demagnetizing* (compare Fig. 4-6).

Figure 4-24 depicts the postfault *transient* current picture. The sudden appearance of the *demagnetizing* I_d component calls for an equally sudden *boost* in the field current. Both these components are then subject to a subsequent slow decay. Note that although I_d has dc characteristics (viewed by a rotor-bound observer) the actual armature current (viewed by stator-bound observer) is of course of ac type.

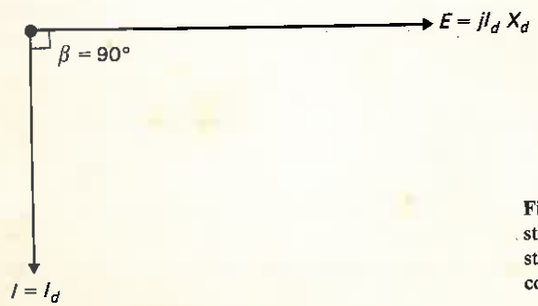

Figure 4-23 The postfault steady-state phasor diagram following stator short circuit. Note that I contains only I_d component.

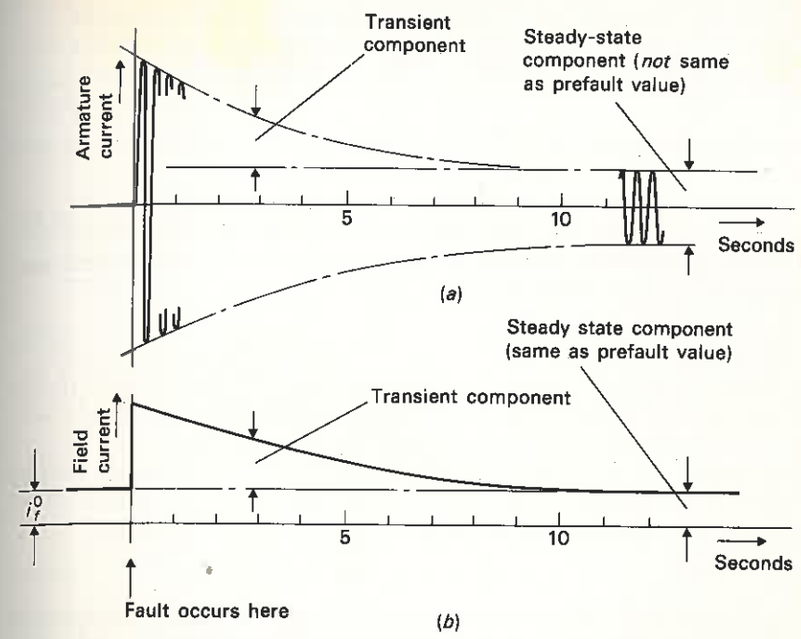

Figure 4-24 The armature and field current transients following a symmetrical terminal short circuit. (Note that the ac cycles in the former are not drawn to proper time scale.)

4-13-5 Transient Reactance X'_d

According to Eq. (4-51) the postfault steady-state armature current has an rms value

$$|I| = |I_d| = \frac{E}{X_d} \tag{4-55}$$

and is identified in Fig. 4-24*a*.

What will the rms value be in the transient period? This is important to know as the transient period covers many seconds and the *transient* current components thus in a decisive way will determine what happens in the system during these critical moments.

Return for a moment to Sec. 4-13-1. From Eq. (4-41) we have

$$\Delta\phi_1 = L_1\,\Delta i_1 + M\,\Delta i_2 \tag{4-56}$$

which, in view of Eq. (4-49), can be written

$$\Delta\phi_1 = L_1\,\Delta i_1 - \frac{M^2}{L_2}\,\Delta i_1 \triangleq \sigma L_1\,\Delta i_1 \tag{4-57}$$

where

$$\sigma \triangleq 1 - \frac{M^2}{L_1 L_2} \tag{4-58}$$

is the *magnetic leakage coefficient* of the coupled circuits. For typical iron core circuits

$$\sigma \ll 1 \tag{4-59}$$

For *slow* "steady-state" changes no secondary currents Δi_2 are induced and ϕ_1 will increase with the amount

$$\Delta\phi_1 = L_1 \, \Delta i_1 \tag{4-60}$$

For *rapid* "transient" changes ϕ_1 will increase with the lesser amount (4-57). *We conclude that the "effective" primary inductance which is measured by the ratio $\Delta\phi_1/\Delta i_1$ has been reduced from L_1 to the quite smaller value σL_1.*

If we translate this observation to the armature of our synchronous machine, we conclude that the stator "steady-state d-axis inductance" $L_{aa,d}$ (Eq. 4-12) for rapid changes will reduce to the much lower value

$$L'_d \triangleq \sigma L_{aa,d} \tag{4-61}$$

The parameter L'_d is referred to as the "d-axis transient inductance". Expressed as *reactance* (compare Eq. 4-12) we talk about a "d-axis transient reactance"

$$X'_d \triangleq \sigma X_d \tag{4-62}$$

Typical values for X'_d are given in Table 4-1.

The low values for X'_d result in the relatively high current values immediately following the fault as demonstrated in fig. 4-24a. As time passes the reactance will increase and the current will decrease at the exponential tempo set by the field circuit. We proceed to investigate these rates.

4-13-6 Transient Decay Rates

The rotor field winding has a self-inductance L_{ff} and resistance R_f, and its *open-circuit d-axis time constant* is defined by

$$T'_{do} = \frac{L_{ff}}{R_f} \quad \text{s} \tag{4-63}$$

"Open-circuit" refers to the armature winding. With the latter winding open no induced currents exist in it, the effective field inductance equals L_{ff} and transients in the rotor field will thus decay at the exponential rate

$$\exp\left(-\frac{t}{T'_{do}}\right)$$

As T'_{do} typically assumes values in the range 5–10 s, "open-circuit" field transients may last for about a minute.

When the armature is shorted (Example 4-9) the "effective" inductance as felt in the field is reduced in the same ratio as that in the stator, i.e., in the ratio σ. The *transient short-circuit d-axis time constant* T'_d will thus be reduced from T'_{do} in the same ratio, i.e.,

$$T'_d \triangleq \sigma T'_{do} = \frac{X'_d}{X_d} T'_{do} \quad \text{s} \tag{4-64}$$

T'_d determines the decay rate in Fig. 4-24.

Example 4-10 The generator in the previous example has $X_d = 0.95$ pu and $X'_d = 0.30$ pu. Describe the transient armature current in Fig. 4-24. $T'_{do} = 7.0$ s.

SOLUTION We have

$$|I^f| = I_d = \frac{1.0}{0.95} = 1.05 \text{ pu in steady state}$$

$$|I^f| = \frac{1.0}{0.30} = 3.33 \text{ pu immediately following the fault}$$

The transient portion of the armature current is thus

$$3.33 - 1.05 = 2.28 \text{ pu}$$

We also have

$$T'_d = \frac{0.30}{0.95} \times 7.0 = 2.21 \text{ s}$$

$$|I^f| = 1.05 + 2.28 \exp\left(-\frac{t}{2.28}\right) \text{ pu} \tag{4-65}$$

4-13-7 Transient Phasor Diagram

The phasor diagram in Fig. 4-10 proved very useful in developing power formulas valid in the steady state. We develop now a similar phasor diagram (Fig. 4-25) depicting the relations between voltage and current phasors during transients. The diagram will serve as a basis (Sec. 4-13-8) for developing power formulas during transient operation.

A. Prefault phasors As the prefault phasors are constants they can be obtained directly from Fig. 4-10. The prefault voltage phasors V^0, V^0_d, V^0_q and E^0 are shown in Fig. 4-25*a*. To avoid cluttering the prefault current phasors I^0, I^0_d and I^0_q are shown separately in Fig. 4-25*b*. The latter two are computed from

$$I^0_d = \frac{E^0 - V^0_q}{X_d} \tag{4-66}$$

$$I^0_q = \frac{V^0_d}{X_q} \tag{4-67}$$

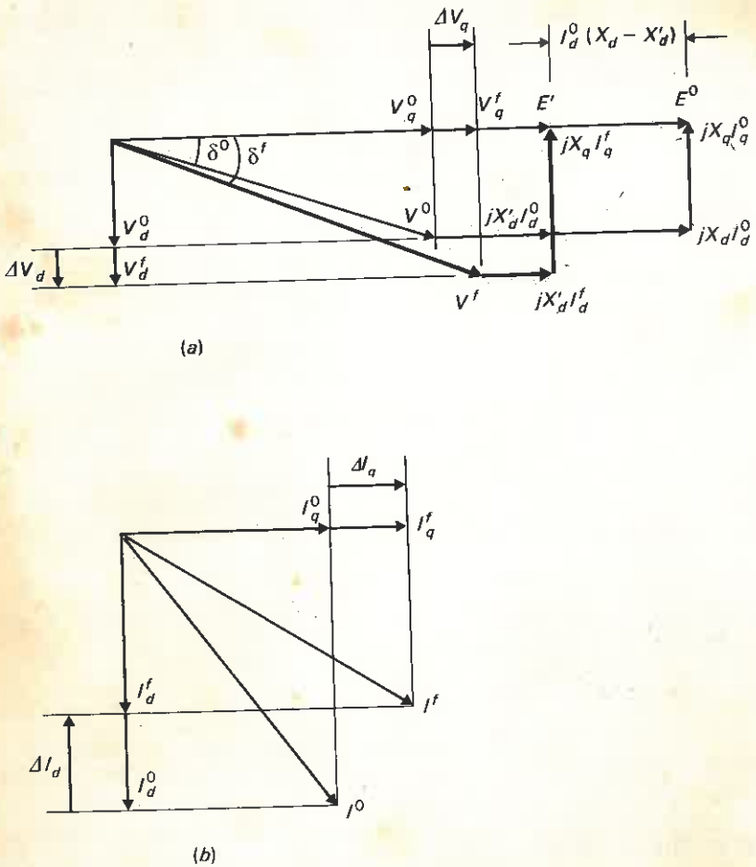

Figure 4-25 Prefault and postfault voltage and current phasors: (*a*) voltages; (*b*) currents.

B. Postfault phasors The fault causes the terminal voltage suddenly to change to the postfault value V^f, thus making the *d*- and *q*-axis voltage components change with the amounts ΔV_d and ΔV_q respectively. According to our earlier reasoning the *d*- and *q*-axis current components *as measured immediately following the fault* will change with the amounts

$$\Delta I_d = -\frac{\Delta V_q}{X'_d} \tag{4-68}$$

$$\Delta I_q = \frac{\Delta V_d}{X_q} \tag{4-69}$$

Note that a positive change ΔV_q causes a reduction in I_d, that is, a negative value ΔI_d.

C. Assembling the transient phasor diagram By definition we have

$$V_d^f = V_d^0 + \Delta V_d \tag{4-70}$$

Substitution of V_d^0 and ΔV_d from Eqs. (4-67) and (4-69), respectively, yields

$$V_d^f = I_q^0 X_q + \Delta I_q X_q = I_q^f X_q \tag{4-71}$$

Also, by definition we have

$$V_q^f = V_q^0 + \Delta V_q \tag{4-72}$$

Substitution of ΔV_q from Eq. (4-68) into Eq. (4-72) yields the voltage relation

$$V_q^f + X'_d I_d^f = V_q^0 + X'_d I_d^0 \triangleq E' \tag{4-73}$$

Equations (4-71) and (4-73) together fully define the sought transient phasor diagram shown boldface in Fig. 4-25*a*. Equation (4-71) tells us that the postfault voltage component V_d^f is related to the current I_q^f in identically the same way as the *steady-state* voltage V_d is related to I_q.

Equation (4-73) similarly informs us that the voltage V_q^f plus the drop $X'_d I_d^f$ add up to emf E' in exactly the same way as the *steady-state* speed voltages V_q^0 and $X_d I_d^0$ add up to the emf E^0.

We thus make this important conclusion: The *transient postfault* voltage phasors V^f, $jX'_d I_d^f$, $jX_q I_q^f$, and E' are related to each other in a similar manner as are the *steady-state prefault* voltage phasors V^0, $jX_d I_d^0$, $jX_q I_q^0$, and E^0. *In fact, the steady-state and transient phasor diagrams become identical if we make the substitutions*

$$\begin{aligned} E^0 &\rightarrow E' \\ X_d &\rightarrow X'_d \end{aligned} \tag{4-74}$$

4-13-8 The EMF Behind the Transient Reactance

Obviously the emf or speed voltage that was defined by Eq. (4-73) and which was designated the symbol E' is of great importance in transient studies. It is referred to as the "emf behind the transient reactance."

The importance of E' is due to its *constancy throughout the fault*, a feature that follows directly from Eq. (4-73). In this regard it has the same character as the field flux ϕ_f.† We find E' as follows.

From Fig. 4-25 we note that

$$E' = E^0 - (X_d - X'_d)I_d^0 \tag{4-75}$$

† In Ref. 3 it is shown how E' is in fact proportional to ϕ_f.

Upon substitution of I_d^0 from Eq. (4-66) we have the alternate formula

$$E' = \frac{X'_d E^0 + (X_d - X'_d)V_q^0}{X_d} \tag{4-76}$$

4-13-9 Transient Power Formulas

The steady-state power formulas (4-22) were obtained from the phasor diagram in Fig. 4-10. By making use of the substitutions (4-74) these formulas thus yield the transient powers as well. We obtain

$$P'_G = \frac{|V^f|\,|E'|}{X'_d}\sin\delta + \frac{|V^f|^2}{2}\left(\frac{1}{X_q} - \frac{1}{X'_d}\right)\sin 2\delta \qquad \text{MW} \tag{4-77}$$

where $\delta \triangleq \underline{/E'} - \underline{/V^f}$

Often we neglect the second term and have then the simpler formula

$$P'_G \approx \frac{|V_f|\,|E'|}{X'_d}\sin\delta \qquad \text{MW} \tag{4-78}$$

We work the following two examples:

Example 4-11 A turbogenerator is characterized by the reactance parameters

$$X_d = X_q = 1.00 \text{ pu}$$

$$X'_d = 0.20 \text{ pu}$$

Its excitation level equals $E^0 = 1.50$ pu. The generator delivers 0.75 pu MW to a strong bus which maintains a constant voltage of 1 pu. Sudden changes in the prime-mover torque or the generator loading are disturbing the torque balance causing changes in the power angle δ. How does the subsequent megawatt output vary with δ?

SOLUTION In prefault steady state the megawatt output follows from Eq. (4-24):

$$P_G = \frac{1.5 \times 1.0}{1.00}\sin\delta = 1.5\sin\delta \text{ pu MW} \tag{4-79}$$

This is curve A in Fig. 4-26. By setting $P_G = P_G^0 = 0.75$ we obtain the steady-state power angle $\delta^0 = 30°$.

The steady-state operating point is identified in Fig. 4-26. From a knowledge of δ^0, we now get

$$V_q^0 = |V^0|\cos\delta^0 = 1.00\cos 30^0 = 0.866 \text{ pu kV}$$

Equation (4-76) then yields

$$E' = \frac{0.20 \times 1.50 + (1.00 - 0.20)0.866}{1.00} = 0.993 \text{ pu kV}$$

From Eq. (4-77) we get directly the transient generator power

$$P'_G = 4.96\sin\delta - 2.00\sin 2\delta \qquad \text{pu MW} \tag{4-80}$$

This power is plotted versus δ in Fig. 4-26 (curve B).

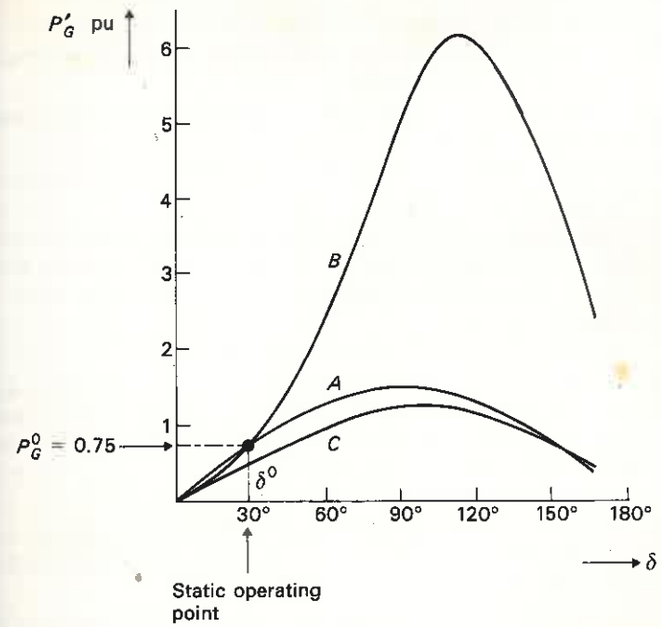

Figure 4-26 Steady-state and transient generator powers. The three cases are described in the text.

This power curve would for example apply if we wish to study the small transient oscillations of the generator rotor that occur following power imbalances due to suddenly applied *small* load objects. See Chap. 9 for details.

Example 4-12 The terminal voltage of the generator in the previous example experiences a sudden 75 percent drop. Find an expression for the subsequent generator power.

SOLUTION We have now $|V^f| = 0.25$ pu. As before $E' = 0.993$ pu. From Eq. (4-77) we thus have

$$P'_G = 1.24\sin\delta - 0.13\sin 2\delta \tag{4-81}$$

This is curve C in Fig. 4-26.

This curve would apply for example when we wish to study the *large* oscillations of the rotor following a fault large enough to cause a 75 percent voltage drop. See Chap. 12 for more details.

We make the following summary observations in regard to the last two examples:

1. For very slow (quasi-static) changes, curve A tells us the relationship between power output and rotor position.
2. For sudden changes in the prime mover torque or generator loading *but constant terminal voltage*, curve B applies.

3. For a sudden 75 percent drop in terminal voltage, curve C applies.
4. The static-torque curve does not have a "saliency" term because we assumed $X_d = X_q$.
5. The transient torque contains a saliency term, the magnitude of which is of second order. It is also *negative*.†
6. *The transient power may attain very large peaks compared with the steady-state power* (due to the high armature currents).
7. As time passes the transient components of i_f and I_d decay, resulting in a gradual change of E'. If the exciter source voltage v_f *is held constant*, E' will eventually approach E^0 and the transient power P'_G will then equal the steady-state power P_G.

Example 4-13 In this final example we return to Example 4-3. We wish to develop a formula for the *transient* power of the 15-MVA generator operated onto the distant bus of constant voltage $|V_N| = 1.0$ pu. The generator is assumed to operate in a prefault steady state identical to the one in Example 4-3. Its transient reactance equals 0.33 pu.

SOLUTION The voltage V^f in power formula (4-76) is the terminal generator voltage. As we now must express the generator power in terms of the *bus* voltage V_N^f we must not only observe the substitutions (4-74) but also the modifications (4-29), to which is added

$$X'_d \to X'_d + X_l \tag{4-82}$$

From Example 4-3 we have

$$|V_N^0| = |V_N^f| = 1.0 \text{ pu}$$

$$\therefore \quad V_{Nq}^f = V_{Nq}^0 = 1.0 \times \cos \delta_N^0 = 1.0 \times \cos 25.7° = 0.901 \text{ pu}$$

From Eq. (4-76) we obtain after modification

$$E' = \frac{(0.33 + 0.11)1.22 + [(0.80 + 0.11) - (0.33 + 0.11)]0.901}{0.80 + 0.11} = 1.055 \text{ pu}$$

Equation (4-77) yields upon modification

$$P'_G = \frac{1 \times 1.055}{0.33 + 0.11} \sin \delta_N + \frac{1^2}{2}\left(\frac{1}{0.65 + 0.11} - \frac{1}{0.33 + 0.11}\right) \sin 2\delta_N$$

$$= 2.398 \sin \delta_N - 0.478 \sin 2\delta_N \text{ pu MW} \tag{4-83}$$

We shall make further use of this formula in Chap. 9.

4-13-10 Additional Transient Phenomena

For simplicity we took a few analytical shortcuts in developing the above theory. Our coarse analysis neglected some transient effects that we now summarize briefly.

† In the *static* power formula the saliency term comes out *positive*. Compare Eq. (4-25).

A. "Subtransients" We noted in Sec. 4-2 the presence of rotor *damper* windings. The real reason for their inclusion is to provide damping of the *mechanical* rotor swings that will occur when a generator suddenly is subject to severe torque imbalances. More will be said about this in Chaps. 9 and 12.

The damper windings will of course also influence transients. Actually, due to their physical location—close† to the armature—their magnetic coupling to the latter is stronger than that between armature and field. Consequently, the leakage coefficient between armature and dampers is *smaller* than that between armature and field.

When the stator disturbance hits, the flux which at that moment is linked with the damper winding will "freeze" just as the flux ϕ_f freezes in the field winding. The freezing is accomplished in the same way as in the field—by the induction of a dc current. Whereas the induced dc current in the field will take seconds to decay, the one in the damper winding will disappear in 50 to 100 milliseconds. But in the few moments it does exist its effect on the armature will manifest itself in the lowering of the effective reactance below X'_d to the so-called *subtransient reactance* X''_d (see Table 4-1). The ac short-circuit current (Fig. 4-24) will have a couple of very high peaks immediately following the onset of the short (not shown in Fig. 4-24).

B. Armature dc components A "flux freezing" will also take place in all the three stator phases at the moment of fault. The resulting dc-current components will be of different magnitudes in each phase (depending upon the rotating flux position at the moment of fault). Like the dc component in the damper winding the three dc components in the armature phases will die out very fast, but while they last they will add to the currents depicted in Fig. 4-24*a* giving all three stator currents an unbalanced offset lasting for a few cycles. Also, these stator dc fluxes will induce in the rotor field winding an ac voltage of frequency f which will cause a rapidly decaying ac current component riding on top of the slowly decaying "transient" component of i_f in Fig. 4-24*b*.

C. Transients in the q axis We had neglected totally any transient effects in q direction thus assuming that the steady state sets in instantaneously. This is not quite correct. The solid rotor iron does in effect offer a path for transiently induced dc components which then give rise to a q-axis transient armature reactance X'_q. This effect will be relatively short lived but must be taken into account in more careful modeling.

D. Saturation effects Particularly in large-scale disturbances the nonlinear magnetic saturation will make its presence known. Most simulation studies of major faults (Chap. 12) will use different modeling techniques to take these effects into account.

† This fact improves their damping efficiency.

SUMMARY

We have presented in this chapter the theory of a symmetrically loaded three-phase synchronous machine. First, we have discussed its basic design features. Then we demonstrated how the operating characteristics of the machine could be explained in terms of synchronously traveling flux, mmf, emf, and current waves.

Real and reactive power formulas were derived and a physical base for the air-gap torque was given. Considerable emphasis has been placed on the control of a synchronous machine which is part of a large interconnected network. We have studied the response of the machine to variations in the two basic control inputs, the prime-mover torque, and the field current. We have concluded that these two inputs are essentially decoupled; i.e., a change in torque affects the real power output whereas a change in the field current controls the reactive output.

All models developed in this chapter were based upon the assumption of sinusoidal traveling waves. Harmonics do exist but their influence is normally minimized by various design tricks.

The models are also based upon the simplifying assumption of linearity. Since all synchronous machines operate in a region of magnetic saturation, the models must of necessity be characterized by some approximation. We do not, in our introductory type of presentation, enter into a detailed discussion of the effect of these nonlinearities. We wish to point out, however, that the linear models presented form the basis for *all* practical system studies. It is often possible to take account of the nonlinear effects by adding first-order corrective terms to our linear parameters. Some comments on these procedures will be given in Chap. 12.

Finally, we have presented a brief theory of transient generator phenomena. We concluded that the high magnetic inertia of the rotor field winding dominatingly controls the transient currents and power.

PROBLEMS

4-1 We found in the text an expression for the pullout torque based on the assumption that $X_d = X_q$. Find, using Eq. (4-22), an expression for the pullout torque for a machine when we do not assume nonsaliency. For what δ-value does pullout occur?

4-2 Show what the phasor diagrams in Figs. 4-8 and 4-10 will look like if the armature resistance R_s is not neglected. Use the new diagrams and correct the power formulas (4-22) and (4-24).

***4-3** A generator having a synchronous reactance of 0.90 pu based on its own rating is connected via a transmission line to a remote bus, the voltage of which we may assume held constant at a value of 100 percent. The line has an impedance of $j0.15$ pu per phase, based upon the machine megavolt-amperes. The internal emf E of the machine is kept at a constant magnitude of 135 percent.

(*a*) Compute the pullout power of the machine.

(*b*) At the moment of pullout, determine magnitude and direction of the reactive power at *both* the generator terminal and the remote bus.

(*c*) At the moment of pullout, what is the terminal voltage of the generator?

(*d*) Is the machine current-overloaded at pullout?

***4-4** A synchronous machine is running overexcited with $|E| = 150$ percent. The synchronous reactance has the value 120 percent, and the machine delivers a real power of 0.4 pu. Terminal voltage is 1 pu, independent of excitation level. If the prime-mover torque is increased by 1 percent, by how many percent will P_G and Q_G change?

4-5 Consider the two-bus system shown in Fig. 4-27. The load S_{D2} drawn from bus 2 is in its entirety supplied by generator $G1$ and transported via the line. The latter, as will be demonstrated in Chap. 6, may be represented by an equivalent π network, the impedances of which, in a chosen base system, are as follows:

$$Z_s = j0.05 \text{ pu}$$

$$Z_p = -j3.00 \text{ pu}$$

The synchronous reactance equals 18 percent in the chosen base system.

The magnitude $|V_2|$ of the voltage of bus 2 must equal 1.00 pu.

(*a*) Determine the voltage level, $|V_1|$, that we must maintain at bus 1 in order to achieve the above objective.

(*b*) Compute the required reactive generation Q_{G1}.

(*c*) Compute the generator emf $|E|$.

***4-6** A synchronous machine has been synchronized onto a large network. All four conditions for a smooth "lock-in" were satisfied. Without changing the field current, we now make the machine generate real power. Will it, at the same time, generate or consume reactive power? Explain.

4-7 Figure 4-28 depicts a simple arrangement for synchronization of a generator to a network. A, B, and C are three light bulbs (or voltmeters). If the generator speed (or frequency) is different from that of the network, the lights of each bulb will pulsate in sequence $ABCA \ldots$ or $ACBA \ldots$.

(*a*) Relate the pulsation sequence with over- or underspeed of the generator.

(*b*) State the conditions that must be satisfied for closing the circuit breaker.

***4-8** A synchronous hydrogenerator is rated at 60 Hz, 21 kV, and 80 MVA. Based upon its own ratings it is characterized by the following reactance values:

$$X_d = 1.00 \text{ pu}$$

$$X_q = 0.65 \text{ pu}$$

It is delivering 60 MW at a 1 pu terminal voltage. It is overexcited with $|E| = 1.45$ pu.

(*a*) Find δ.

(*b*) Find Q_G.

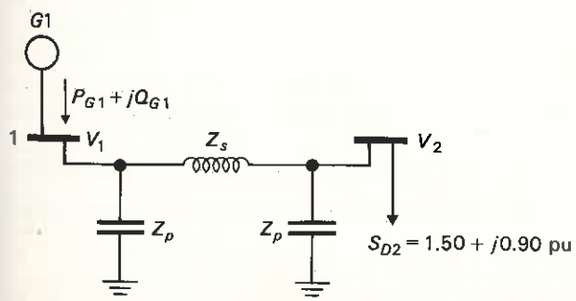

Figure 4-27 A two-bus example system.

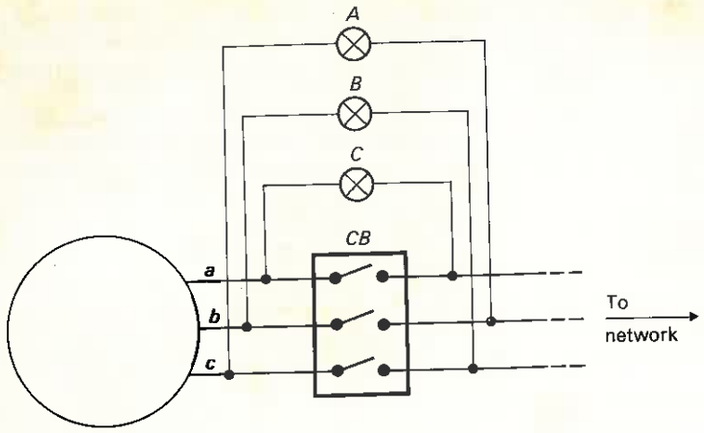

Figure 4-28 Simple synchronizing arrangement.

***4-9** A synchronous *motor* has X_d and X_q reactance values of 1.10 and 0.80 pu respectively. It is being run at a real-power output of 0.61 pu and overexcited so as to deliver 0.36 pu megavars to the network. Terminal voltage = 1 pu.

(*a*) Find δ.

(*b*) Find $|E|$.

(*c*) Show that the motor, as viewed by the network, can be represented by an equivalent circuit of type 7 in Table 2-1. Give the resistance R and reactance $1/\omega C$ expressed per phase and in per unit of machine ratings.

4-10 Consider Example 4-4 and Fig. 4-17.

(*a*) Indicate in this phasor diagram the position of the terminal voltage V.

(*b*) Compute $|V|$ at the moment of pullout.

***4-11** Work Example 4-8 but use the exact power formulas (4-22). Compare the accuracy.

4-12 A generator operates onto a constant bus voltage V^0 at a power angle $\delta°$. Without changing the turbine torque the excitation level is given the small perturbation $\Delta|E|$. Prove that the reactive power increases by the amount

$$\Delta Q_G = \frac{V^0}{X_s \cos \delta°} \Delta|E| \tag{4-84}$$

REFERENCES

1. Olle I. Elgerd: *Basic Electric Power Engineering*, Addison-Wesley Publishing Company, Boston, 1977.
2. Fitzgerald, Kingsley, and Kusko: *Electric Machinery*, 3d ed., McGraw-Hill Book Company, New York, 1971.
3. Edward W. Kimbark: *Power System Stability: Synchronous Machines*, Dover Publishing Inc., New York, 1956.
4. C. C. Concordia: *Synchronous Machines*, J. Wiley & Sons, New York, 1957.
5. V. J. Vickers: "Recent Trends in Turbogenerators," *Proceedings IEE*, vol. 121, November 1974.
6. F. P. de Mello and J. R. Ribeiro: "Derivation of Synchronous Machine Parameters from Tests," *IEEE Transactions*, vol. PAS-96, no. 4, July/August 1977, pp. 1211–1218.

CHAPTER

FIVE

THE POWER TRANSFORMER

5-1 INTRODUCTION

In Chaps. 2 and 3 we noted that the need for high power transmission capacity and effective reduction of transmission losses requires high transmission voltages. It is not practically feasible to generate voltages of magnitudes in the hundreds of kilovolts directly in synchronous generators. The required insulation thickness prohibits generation in excess of about 25 kV. To achieve the transmission capabilities called for in the systems of today and the near future, we must make use of transmission voltages as high as 500 to 1000 kV. The role of the power transformer is therefore an important one.

The transformer, in addition, isolates the expensive generator from the exposed overhead power grid. The transient overvoltages caused by atmospheric disturbances (Chap. 10) will propagate along the lines as waves, having high crests and steep voltage fronts and velocities slightly less than that of light. As these waves are being reflected at the transformer terminals, high-voltage amplitudes will be built up which will stress the insulation of the transformer. It is much easier and cheaper to insulate for these waves in a transformer than in a generator winding.

Power transformers come in sizes ranging from distribution transformers rated at a few kilovoltamperes to huge transmission transformers with three-phase ratings in excess of 1000 MVA. We shall be most concerned with large units which can be divided into the following categories:

1. Generator transformers
2. Transmission transformers
3. Regulating (or control) transformers

The first type, having a typical voltage rating of, say 20/345 kV, serves as a step-up device, transforming the power directly from generator to transmission level. The second type, having a typical voltage rating of, say, 345/500 kV, is used for transformation of power between the different voltage levels in the transmission system. Often this will be a so-called "autoconnected" transformer. The third type of transformer is used as a power flow and voltage control device. From an operating engineer's viewpoint this is a particularly important transformer function that we shall explore in some detail. Unlike generators and most load objects which are unidirectional as far as the power flow is concerned, transformers accept power flows in either direction.

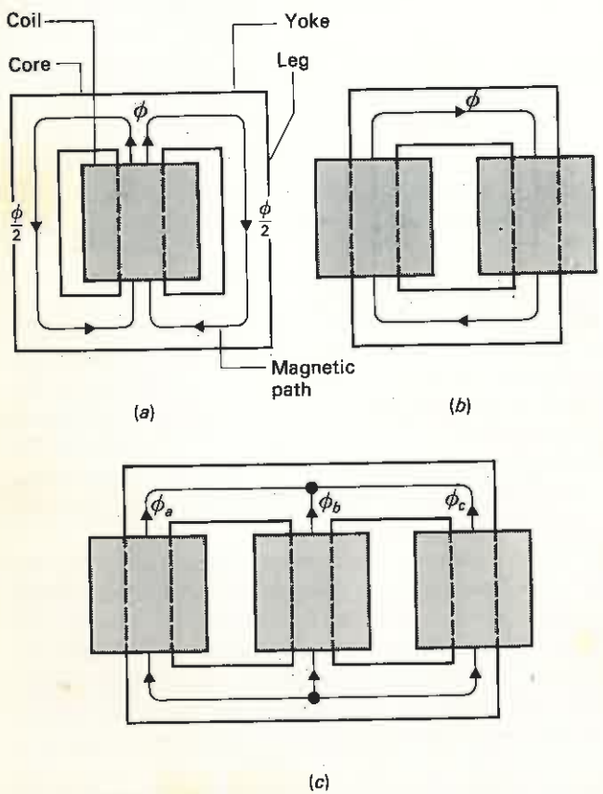

Figure 5-1 Various core and coil arrangements: (*a*) single-phase, split core; (*b*) single-phase, split coil; (*c*) three-phase.

5-2 DESIGN FEATURES

As a *static* device a transformer, compared with a generator, is characterized not only by simpler design but also less complicated behavior and theory. The heart of the transformer is the *magnetic core* which conducts the *ac* flux. To reduce eddy current and hysteresis losses the core is stacked by about 0.3-mm thick laminations of cold-rolled silicon alloyed iron. Typical core geometries are shown in Fig. 5-1, indicating how the magnetic paths are closed via the "leg" and "yoke" portions of the core.

The windings, typically made of insulated copper, are formed into coils which are placed onto the core legs. Figure 5-2 shows a common arrangement where the coils are of concentric cylindrical shape. The low-voltage (LV) coils are placed closest to the iron, with the high-voltage (HV) coils outermost. If intermediate-voltage (IV) windings exist they are placed in between.

Three-phase transformers may consist either of three separate single-phase units of the types shown in Fig. 5-1*a* or *b*, or of one unit of the "three-phase core" type shown in Fig. 5-1*c*.

The core-winding assembly is placed into a steel *tank* filled with *oil* which serves a triple function.

First, it adds to the electrical insulation between the windings. Second, it helps conduct the heat away from core and windings to external heat exchangers. The oil circulation is either natural or forced. Third, the oil helps damp the noise generated by magnetostriction in the core. The electric power is being led into and out of the tank via *bushings*.

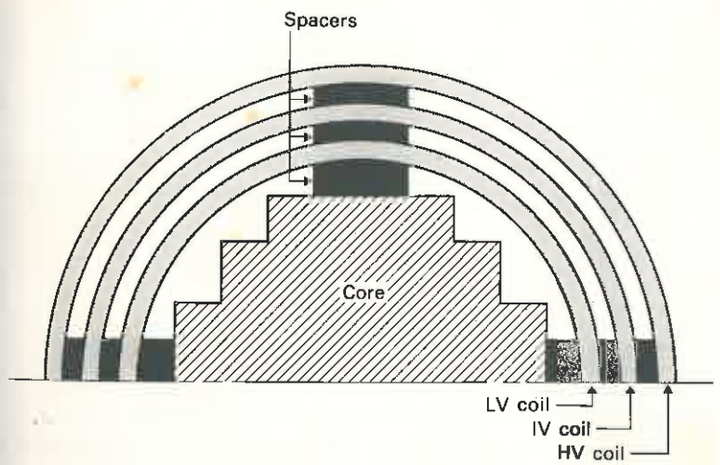

Figure 5-2 Section through core and coils.

5-3 THE n-WINDING "IDEAL TRANSFORMER"

Figure 5-3 depicts schematically an n-winding power transformer. We shall presently develop performance equations for this device assuming it to be an "ideal transformer" (IT) a device characterized by the following features:

1. Zero winding resistances.
2. The transformer flux ϕ is totally confined to the magnetic core, i.e., there are no "leakage" fluxes (Sec. 5-4-2).
3. The core material has zero magnetic reluctance, i.e., it is characterized by a magnetic permeability $\mu = \infty$.
4. Zero hysteresis and eddy current losses in the core.

None of these requirements are totally satisfied in a physical transformer, and an IT thus becomes a mathematical artifice. However, the simple IT model gives a surprisingly accurate picture of the real device and IT models are, therefore, in fact very useful in a number of systems studies.

A note about the definition of current directions in Fig. 5-3. We have arbitrarily designated winding 1 our "primary" winding and have assumed its current to enter at the positive voltage terminal, i.e., electric power is *entering* this

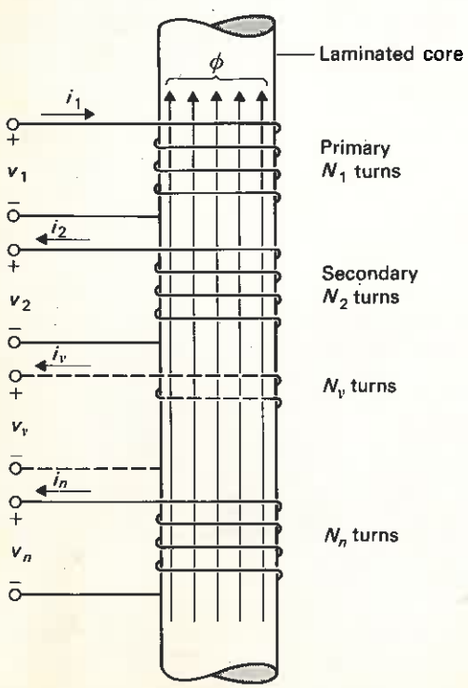

Figure 5-3 n-winding transformer. Note voltage and current polarities.

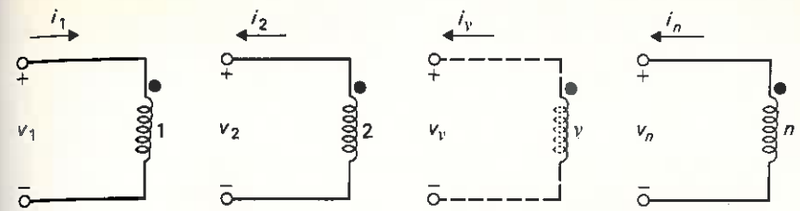

Figure 5-4 Polarity marking by dot symbols.

winding. The current directions at the remaining $n - 1$ windings are defined such that the corresponding powers are *exiting* from the transformer.

Winding polarities are very important in transformers. It is impractical to always indicate winding directions as we have done in Fig. 5-3. A simpler *dot symbol* is used in Fig. 5-4 to indicate polarity. The "dot rule" is very simple: *When currents are entering the "dotted" terminals they will encircle the core flux in the same direction.*

5-3-1 IT Voltage Relations

The following voltage equilibrium equations apply to the IT in Fig. 5-3:

$$\begin{aligned} v_1 &= N_1 \frac{d\phi}{dt} \\ v_2 &= N_2 \frac{d\phi}{dt} \\ &\vdots \\ v_n &= N_n \frac{d\phi}{dt} \end{aligned} \tag{5-1}$$

We shall be primarily interested in operating the transformer with sinusoidally varying voltages. By replacing the time functions v and ϕ by the phasors V and Φ, and the operator d/dt by $j\omega$, equations (5-1) transform to

$$\begin{aligned} V_1 &= j\omega N_1 \Phi \\ V_2 &= j\omega N_2 \Phi \\ &\vdots \\ V_n &= j\omega N_n \Phi \end{aligned} \tag{5-2}$$

Upon dividing the first equation (5-2) by the second, third, etc., we obtain the following $n - 1$ voltage relations:

$$\frac{V_1}{V_i} = \frac{N_1}{N_i} = a_{1i} \qquad \text{for } i = 2, 3, \ldots, n \tag{5-3}$$

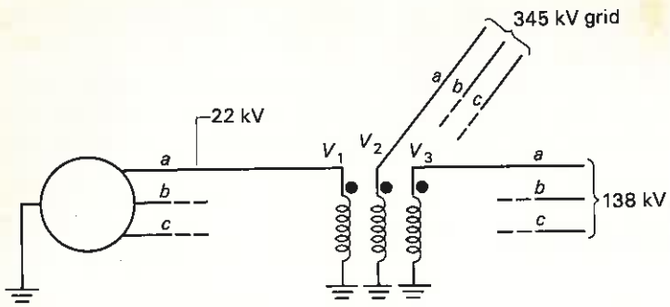

Figure 5-5 A three-winding transformer.

The $n-1$ parameters a_{1i} are known as the "transformation ratios" of the transformer.

One talks about "referring the voltage V_i to the primary" by the voltage transformation

$$V_i' \triangleq a_{1i} V_i \qquad \text{for } i = 2, 3, \ldots, n \tag{5-4}$$

As all transformation ratios are *real* numbers it follows that all n voltage phasors have equal phase.

Example 5-1 A three-winding, three-phase transformer feeds power from a 22-kV three-phase generator to both a 345-kV grid and a local industry served at 138 kV. The three-phase transformer is made up of three identical single-phase transformer units of the type depicted in Fig. 5-1*a*, each unit containing three windings which are connected between the phase terminals and neutral as shown in Fig. 5-5 (only one phase shown). Determine the required transformation ratios a_{12} and a_{13}.

SOLUTION As V_1, V_2, and V_3 now represent the phase voltages we have

$$V_1 = \frac{22}{\sqrt{3}} = 12.70 \text{ kV}$$

$$V_2 = \frac{345}{\sqrt{3}} = 199.2 \text{ kV}$$

$$V_3 = \frac{138}{\sqrt{3}} = 79.67 \text{ kV}$$

$$a_{12} = \frac{12.70}{199.2} = 0.06377$$

$$a_{13} = \frac{12.70}{79.67} = 0.1594$$

5-3-2 Core Flux and "VPT"

In the previous example we could only compute the transformation ratios but *not* the individual numbers of turns. To do so we must know the iron "flux load," or the flux density used. Consider the first of Eqs. (5-2). The rms values of

flux and voltage are related by

$$|V_1| = \omega N_1 |\Phi|$$

The sinusoidal transformer flux lags the voltage by 90° and has a maximum value of

$$\phi_{\max} = \sqrt{2}|\Phi| = \sqrt{2}\,\frac{|V_1|}{\omega N_1} = \sqrt{2}\,\frac{|V_1|}{2\pi f N_1} \qquad \text{Wb} \tag{5-5}$$

If the effective† core area is A m^2 we obtain for the maximum flux *density*

$$B_{\max} = \frac{\phi_{\max}}{A} = \sqrt{2}\,\frac{|V_1|}{2\pi f A N_1} \qquad \text{T} \tag{5-6}$$

tension espira

This formula is often written in terms of "voltage-per-turns" (VPT)

$$\text{VPT} \triangleq \frac{|V_1|}{N_1} = 4.443\, A f B_{\max} \qquad \text{V/t} \tag{5-7}$$

In normal transformers the maximum flux densities lie in the range 1.3–1.7 T.

Example 5-2 The transformer in the previous example has an effective core area of 0.70 m^2. Frequency is 60 Hz. $B_{\max} = 1.5$ T. Find VPT and N_1, N_2, and N_3.

SOLUTION Formula (5-7) gives directly

$$\text{VPT} = 4.443 \times 0.700 \times 60 \times 1.5 = 279.9 \text{ V/t}$$

and

$$N_1 = \frac{|V_1|}{\text{VPT}} = \frac{12{,}700}{279.9} \approx 45 \text{ t}$$

Equations (5-3) finally yield N_2 and N_3:

$$N_2 = \frac{45}{0.06377} \approx 706 \text{ t}$$

$$N_3 = \frac{45}{0.1594} \approx 282 \text{ t}$$

(We have adjusted the N-values to satisfy the requirements that all turns must be integers.)

5-3-3 IT Current and Power Relations

"Ohm's law" for the magnetic core in Fig. 5-3 states

$$\sum mmf = i_1 N_1 - i_2 N_2 - \cdots - i_n N_n = \mathscr{R}\phi \tag{5-8}$$

or

$$i_1 N_1 = i_2 N_2 + \cdots + i_n N_n + \mathscr{R}\phi$$

where $\mathscr{R}$ is the total magnetic path reluctance.

† Some iron area is lost due to the insulation between the laminations.

If the currents and flux are sinusoidal, then the current and flux phasors must satisfy

$$I_1 N_1 = I_2 N_2 + \cdots + I_n N_n + \mathscr{R}\Phi \tag{5-9}$$

In an IT the permeability μ was assumed infinite which means that $\mathscr{R}$ is zero. For an IT we therefore have

$$I_1 N_1 = I_2 N_2 + \cdots + I_n I_n \tag{5-10}$$

This is an important relationship sometimes referred to as the *mmf balance equation.* We shall find it particularly important as we study three-phase transformers in later sections.

From the last equation we also get for the conjugate currents

$$I_1^* N_1 = I_2^* N_2 + \cdots + I_n^* N_n \tag{5-11}$$

If we multiply this equation by V_1/N_1 and at the same time observe the voltage relations (5-3) we obtain:

$$V_1 I_1^* = V_2 I_2^* + \cdots + V_n I_n^* \tag{5-12}$$

or in words: *In an IT the power (real* and *reactive) entering the primary equals the sum of the powers exiting from the other windings.*

Example 5-3 Consider the transformer in Fig. 5-5. 600 MW and 150 Mvar are flowing out on the 345-kV line. The local power demand from the 138-kV bus is 150 MW at cos $\phi = 1$. Find currents and powers in all three windings.

SOLUTION We choose V_1 as the reference phasor. V_1, V_2, and V_3 are all of equal phase and shown (not to scale) in Fig. 5-6. The powers flowing from windings 2 and 3 equal respectively

$$S_2 = V_2 I_2^* = 200 + j50 \text{ MW and Mvar/phase}$$

$$S_3 = V_3 I_3^* = 50 + j0 \text{ MW and Mvar/phase}$$

$$I_2 = \frac{200 - j50}{199.2} = 1.004 - j0.251 = 1.035\angle{-14.0^\circ} \text{ kA/phase}$$

$$I_3 = \frac{50 + j0}{79.67} = 0.628 + j0 = 0.628\angle{0^\circ} \text{ kA/phase}$$

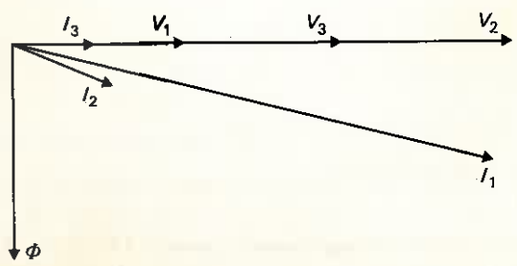

Figure 5-6 Phasor representation of core flux, terminal voltages, and coil currents.

Equation (5-12) gives the generator power

$$S_1 = V_1 I_1^* = S_2 + S_3 = 250 + j50 \text{ MW and Mvar/phase}$$

The generator current is solved from the last equation

$$I_1 = \frac{250 - j50}{12.70} = 19.69 - j3.94 = 20.1\angle{-11.3^\circ} \text{ kA/phase}$$

We have added these current phasors to Fig. 5-6. For completeness we have also shown the flux phasor which, according to Eq. (5-2), will lag the voltage by 90°.

Example 5-4 Figure 5-7 depicts a distribution transformer, the primary (HV) winding of which is connected to the line voltage of a 23-kV, three-phase network. There are two separate but interconnected LV windings each of 120-V rating. The midtap is grounded. With the indicated polarities the two voltages V_2 and V_3 will add to give a total voltage of 240 volts between the outer terminals. The latter voltage serves larger load objects.

A resistor heater is connected across one of the 120-V branches, a small drill motor across the other. A larger pump motor is connected across the 240-V terminals. Using IT models find all primary and secondary currents if the loads are as follows:

Drill:	0.500 kW, pf = 0.81
Pump:	2.53 kW, pf = 0.92
Heater:	1.5 kW, pf = 1.0

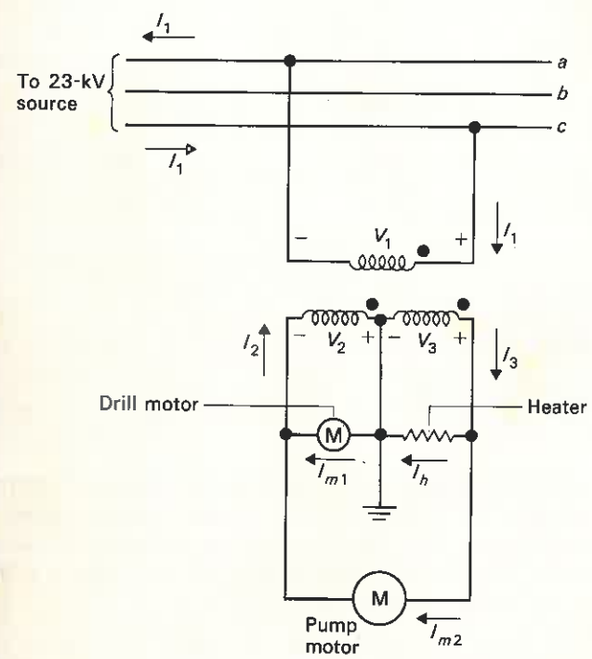

Figure 5-7 Distribution transformer of voltage rating 23,000/240/120 volts.

FAC. DE CIENCIAS EXACTAS Y TECNOLOGIA
BIBLIOTECA

SOLUTION With V_1 as our reference phasor we compute first the currents:

$$I_h = \frac{1500}{120} = 12.5\angle 0^\circ \text{ A}$$

For the motors the real power (P) and power factor ($\cos\phi$) are given. As $Q = P\tan\phi$ we get for the

Drill motor: $Q = 0.362$ kvar
Pump motor: $Q = 1.078$ kvar

$$I_{m1} = \frac{500 - j362}{120} = 4.167 - j3.017 = 5.14\angle -35.9^\circ \text{ A}$$

$$I_{m2} = \frac{2530 - j1078}{240} = 10.54 - j4.492 = 11.46\angle -23.1^\circ \text{ A}$$

From Fig. 5-7 we note that

$$I_2 = I_{m1} + I_{m2} = 14.71 - j7.51 = 16.5\angle -27.1^\circ \text{ A}$$

$$I_3 = I_h + I_{m2} = 23.04 - j4.49 = 23.5\angle -11.0^\circ \text{ A}$$

As we have

$$\frac{N_1}{N_2} = \frac{N_1}{N_3} = \frac{23{,}000}{120} = 191.7$$

we finally obtain the HV current from Eq. (5-10):

$$I_1 = \frac{N_2}{N_1} I_2 + \frac{N_3}{N_1} I_3 = \frac{I_2 + I_3}{191.7} = 0.197 - j0.0626 = 0.207\angle -17.6^\circ \text{ A}$$

Check: The primary power equals

$$S_1 = V_1 I_1^* = 23{,}000 \times 0.207 e^{j17.6^\circ} = 4530 + j1440$$

which equals the sum of the three loads.

5-3-4 Equivalent IT Circuit

The current equation (5-10) can be written

$$I_1 = \frac{I_2}{a_{12}} + \frac{I_3}{a_{13}} + \cdots + \frac{I_n}{a_{1n}} \triangleq I'_2 + I'_3 + \cdots + I'_n \tag{5-13}$$

The currents I'_2, I'_3, etc., are the secondary, tertiary, etc., currents "referred to the primary." The last equation justifies the IT *equivalent diagram* shown in Fig. 5-8. For the practically important case of $n = 2$, the equivalent IT circuit simplifies to the one in Fig. 5-9*a*. Because there is only *one* turn ratio, a_{12}, in a two-winding transformer we set for simplicity

$$a_{12} = \frac{N_1}{N_2} \triangleq a \tag{5-14}$$

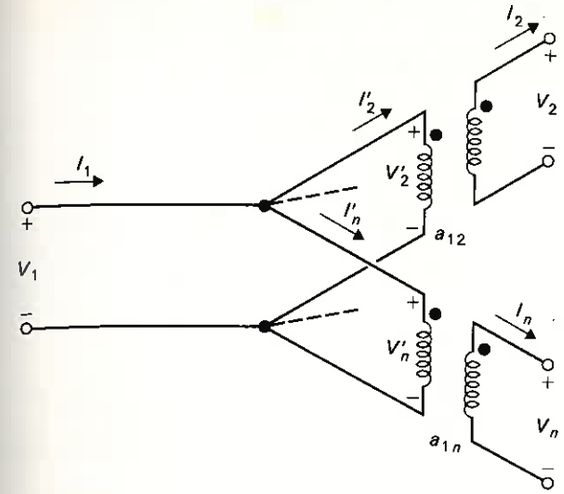

Figure 5-8 Equivalent diagram of n-winding "ideal transformer."

In this case the voltage and current relations read

$$V_1 = \frac{N_1}{N_2} V_2 = aV_2 \triangleq V'_2 \tag{5-15}$$

and

$$I_1 = \frac{N_2}{N_1} I_2 = \frac{I_2}{a} \triangleq I'_2 \tag{5-16}$$

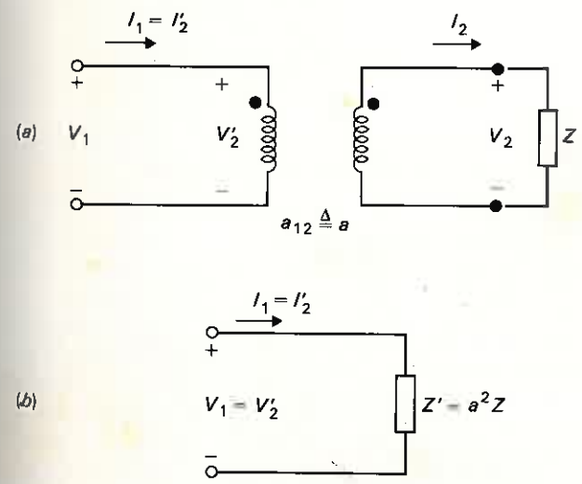

Figure 5-9 Two-winding IT.

5-3-5 Impedance Transformations in IT's

Assume that the secondary in Fig. 5-9*a* is loaded with an impedance Z. We thus have

$$\frac{V_2}{I_2} = Z$$

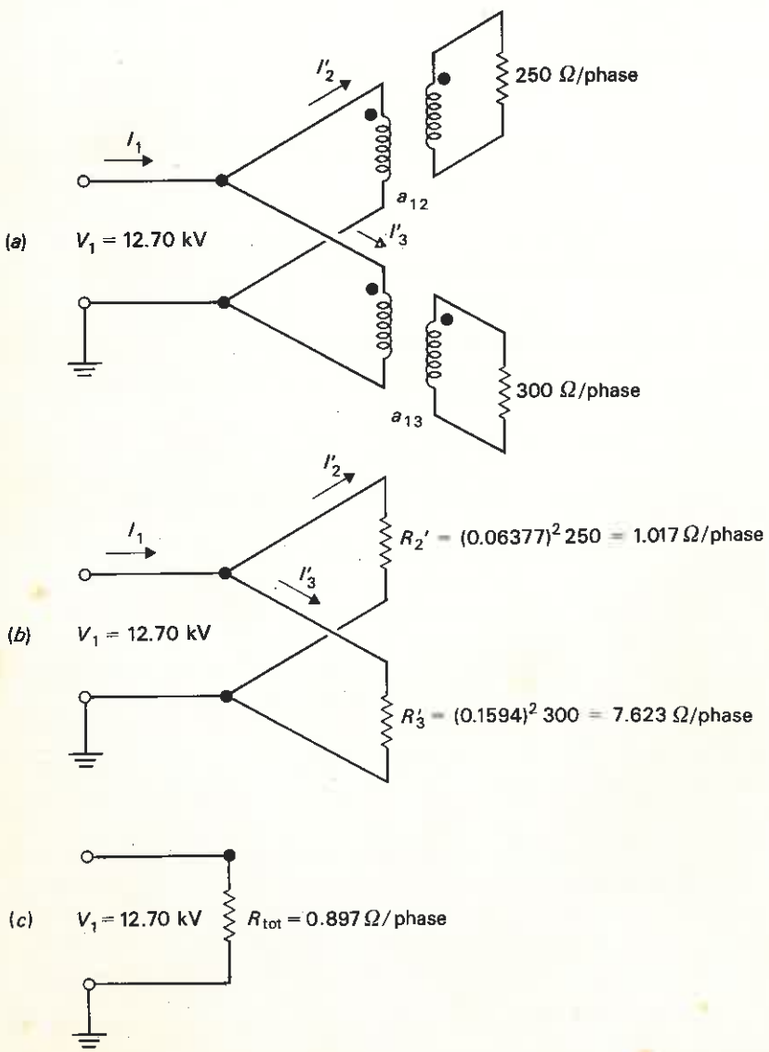

Figure 5-10 Resistive loading of three-winding transformer.

However, in view of Eqs. (5-15) and (5-16) this can alternately be stated

$$\frac{V_2}{I_2} = \frac{V_1/a}{aI_1} = Z \tag{5-17}$$

or

$$\frac{V_1}{I_1} = a^2 Z \triangleq Z' \tag{5-18}$$

The impedance Z' (Fig. 5-9*b*) indicates how Z is "felt" on the primary side and is known as the "secondary impedance Z referred to the primary side." Note that

$$Z' = \frac{V'_2}{I'_2} \tag{5-19}$$

The above "impedance transformation rule" can be readily generalized to an n-winding IT.

Example 5-5 In the three-winding transformer in Fig. 5-5 250-Ω resistors load each phase on the 345-kV secondary, and 300-Ω resistors each phase on the 138-kV tertiary. What will be the load felt by the generator?

SOLUTION On a per-phase basis we have the loading as seen in Fig. 5-10*a*. Using the rule (5-18) we then directly obtain the equivalent loading in Fig. 5-10*b*. The two parallel resistances represent a total load (Fig. 5-10*c*) on the generator of

$$R_{tot} = \frac{1.017 \times 7.623}{1.017 + 7.623} = 0.897\ \Omega/\text{phase}$$

The total generator load is thus

$$P_1 = \frac{12.70^2}{0.897} = 179.8\ \text{MW/phase}$$

or 539 MW total three-phase.

5-4 THE PHYSICAL POWER TRANSFORMER

As demonstrated in several examples the IT models yield important information with simple means. The analysis results obtained from the IT models are often off only a few percentage points from the correct values.

However, because of their simplicity, IT models hide important facts. For example, an IT is lossless and as it consequently cannot be subject to overheating it can accommodate an infinite power transfer whereas, in reality, losses actually set a definite power limit for a physical transformer. Also an IT will not be subject to voltage drops. The terminal voltages (and the flux) will remain constant regardless of the current magnitudes. A physical transformer will be subject to voltage drops which, although relatively small, may in some instances have important operational consequences.

In this section we shall augment the IT model so that it more accurately

represents the physical device. For simplicity we shall limit our discussion to a two-winding transformer. We will justify our model corrections by physical reasoning.

5-4-1 Accounting for Magnetizing Current and Core Losses

The IT formula (5-13) suggests that if windings 2, ..., n are open circuited the primary current I_1 will be zero, i.e., the impedance as viewed from the source would be infinite. This was due to the assumption of zero magnetic reluctance $\mathscr{R}$. In reality, $\mathscr{R}$ is nonzero and as a consequence an open-circuited transformer will draw a nonzero *magnetization current* I_m from the source. This can actually be predicted from formula (5-9) which reads in this case

$$I_1 \triangleq I_m = \frac{\mathscr{R}\Phi}{N_1} \tag{5-20}$$

According to Eq. (5-2) the flux phasor equals

$$\Phi = \frac{V_1}{j\omega N_1}$$

Thus

$$I_1 \triangleq I_m = -j\frac{\mathscr{R}}{\omega N_1^2} V_1 \triangleq Y_m V_1 \tag{5-21}$$

where

$$Y_m = -j\frac{\mathscr{R}}{\omega N_1^2} \tag{5-22}$$

is the *magnetizing admittance* viewed from the primary.

We can obviously account for the magnetizing current by adding the shunt admittance Y_m to the IT circuit in Fig. 5-9, thus obtaining the corrected equivalent circuit in Fig. 5-11*a*.

The above analysis resulted in a magnetizing admittance of the purely reactive form

$$Y_m = -jB_m$$

However, as can be readily confirmed by an *open-circuit test*†, Y_m will in reality be of the form

$$Y_m = G_m - jB_m$$

i.e., the transformer absorbs both *real* and *reactive* magnetizing power. The real power component is due to *hysteresis* and *eddy current* core losses. The former can be thought of as an "internal magnetic friction" that needs to be overcome in reorienting the elementary magnets twice per flux cycle.

The eddy current losses are ohmic in nature due to the induced currents flowing in the iron perpendicular to the flux ϕ. Laminating the iron reduces

† Compare Example 5-6.

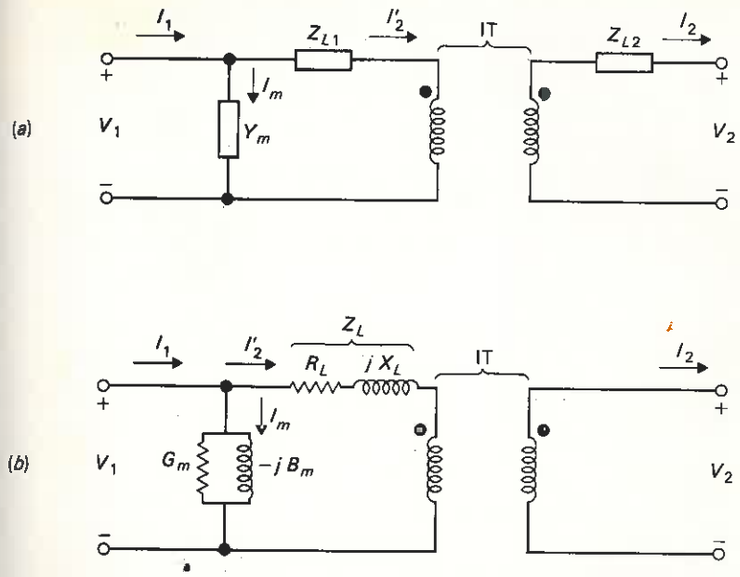

Figure 5-11 Adding leakage and magnetizing impedances to the IT circuit.

these losses to a minimum but not to zero. One may represent those losses with an $n+1$st winding with a *fixed* resistive impedance added to the circuit in Fig. 5-8. This, then, in effect will add a resistive part G_m to the magnetizing admittance as shown in Fig. 5-11*b*.

5-4-2 Accounting for Winding Resistances and Leakage Fluxes

The ohmic losses in the windings are taken into account by means of resistances R_1 and R_2. Both coils are associated with "leakage fluxes," ϕ_{L1} and ϕ_{L2}, as shown in Fig. 5-12. These fluxes result in *leakage reactances* X_1 and X_2. Consequently the two impedances

$$Z_{L1} = R_1 + jX_1$$

and

$$Z_{L2} = R_2 + jX_2$$

are added to the series branches in Fig. 5-11*a* to account for these nonideal features.

As an impedance can be moved across an IT by observing the equation (5-18) it is customary to lump the two series impedances into *one* "leakage impedance"

$$Z_L = Z_{L1} + a^2 Z_{L2}$$

as shown in Fig. 5-11*b*.

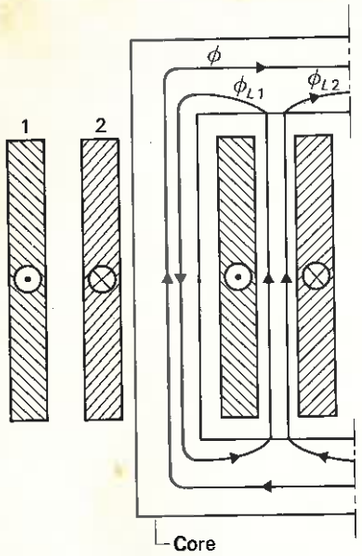

Figure 5-12 Leakage flux paths.

Example 5-6 A 60-Hz, 30-MVA, two-winding transformer has the following voltage and current ratings:

HV side: 66.4 kV, 451.8 A
LV side: 13.2 kV, 2273 A
Transformation ratio, $a = 66.4/13.2 = 5.03$

The transformer is made subject to the following two tests designed to find Y_m and Z_L:

1. Opencircuit (OC) test Full voltage is applied to the HV side with the LV side *open*. One measures:

$$|I_1| = |I_m| = 14.0\ A\ (= 3.1\%\ \text{of rated HV current})$$

$$P_1 = 41.0\ \text{kW}\ (= 0.1367\%\ \text{of rated MVA})$$

2. Shortcircuit (SC) test The LV side is *shorted* and one increases the HV voltage until rated currents flow in both windings. One measures:

$$|V_1| = 7.97\ \text{kV}\ (= 12.0\%\ \text{of rated HV voltage})$$

$$P_1 = 206\ \text{kW}\ (= 0.687\%\ \text{of rated MVA})$$

On the basis of these tests compute Y_m and Z_L.

SOLUTION *OC test* With a current of only 3.1% of rated, the copper losses are negligible, meaning that the measured P_1 consists essentially of core losses only. Thus, by use of formula (2-28) we get

$$G_m \cdot |V_1|^2 = P_1 \tag{5-23}$$

$$\therefore\ G_m = \frac{P_1}{|V_1|^2} = \frac{41{,}000}{(66{,}400)^2} = 9.30\ \mu\mho$$

We also have

$$|I_m| = \sqrt{G_m^2 + B_m^2} \cdot |V_1| \tag{5-24}$$

$$\therefore\ B_m = \sqrt{\frac{|I_m|^2}{|V_1|^2} - G_m^2} = \sqrt{\frac{(14.0)^2}{(66{,}400)^2} - 9.30^2 \times 10^{-12}} = 210.6\ \mu\mho$$

SC test In this test the voltage, *and thus the core flux*, is only 12 percent of rated. We can thus neglect core losses, meaning that the measured P_1 is only winding losses. Thus, from Fig. 5-11:

$$P_1 = R_L\,|I_1|^2 \tag{5-25}$$

$$\therefore\ R_L = \frac{206 \times 10^3}{(451.8)^2} = 1.01\ \Omega$$

and

$$|V_1| = \sqrt{R_L^2 + X_L^2} \cdot |I_1| \tag{5-26}$$

$$\therefore\ X_L = \sqrt{\frac{|V_1|^2}{|I_1|^2} - R_L^2} = \sqrt{\left(\frac{7970}{451.8}\right)^2 - 1.01^2} = 17.6\ \Omega$$

Referred to the HV side the leakage impedance equals

$$Z_L = 1.01 + j17.6 = 17.6\underline{/87^\circ}\ \Omega$$

Having thus developed a corrected transformer model we will use it for a couple of examples where the simple IT model would prove useless.

Example 5-7 Find a formula for the efficiency of the above transformer when operated at 30 percent of rated load and at a power factor of $\cos\phi = 0.8$.

SOLUTION The output megavoltamperes would be $30 \times 0.30 = 9$ MVA and the real power output thus

$$P_2 = 9 \times 0.8 = 7.2\ \text{MW} \tag{5-27}$$

The input power equals output power plus core and copper losses, i.e.,

$$P_1 = P_2 + P_{Fe} + P_{Cu} = 7.2 + 0.041 + 0.206 \times 0.3^2 = 7.2595\ \text{MW} \tag{5-28}$$

(Core losses are independent of loading since the voltage and flux remain essentially constant. Winding losses are proportional to the square of current.)

$$\therefore\ \text{Efficiency}\ \eta = \frac{P_2}{P_1} = \frac{7.2}{7.2595} = 0.992\ \text{pu} \tag{5-29}$$

Power transformers are quite efficient.

Example 5-8 The LV side of the above transformer is loaded with a resistive load corresponding to 6 Ω. Its HV terminals are connected to a 40-km transmission line which in turn is fed from a 66.4-kV network (Fig. 5-13*a*). Use appropriate approximations and find the input and output transformer voltages V_1 and V_2, and also the primary and secondary currents I_1 and I_2. The line impedance is $j50\ \Omega$.

SOLUTION If we express the magnetizing admittance as an impedance it will equal

$$Z_m = \frac{1}{Y_m} = 209 + j4740\ \Omega \tag{5-30}$$

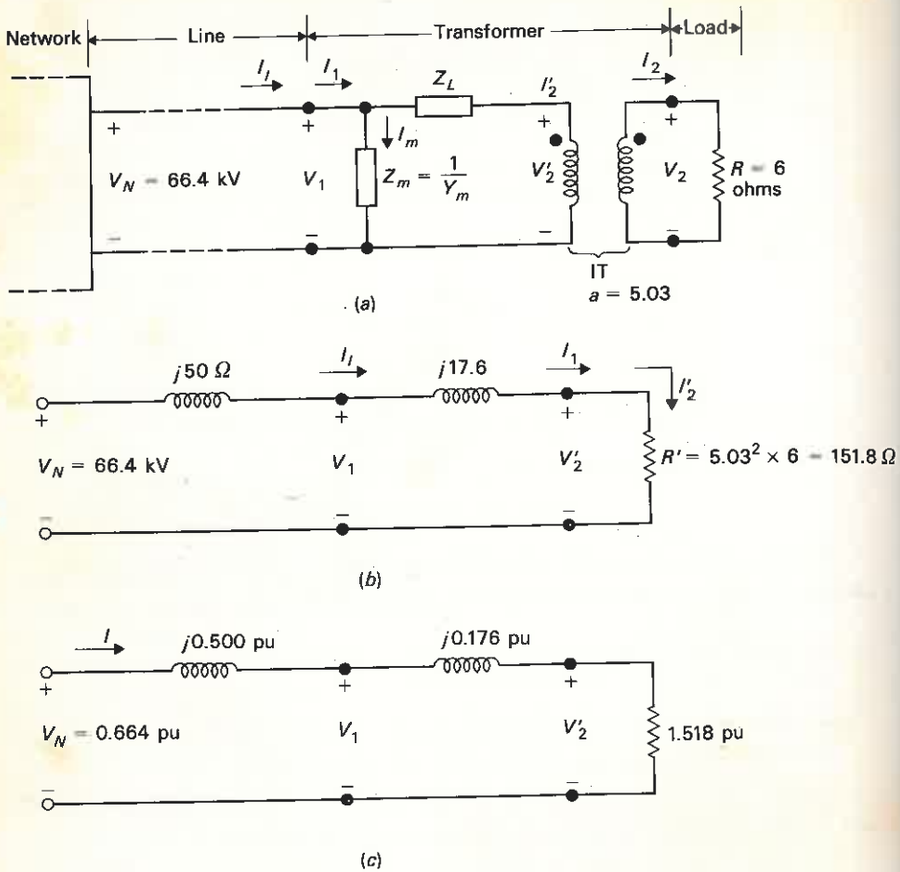

Figure 5-13 Simple transmission system.

This impedance is much larger than R', that is, the load impedance referred to the HV side. I_m will therefore be negligible, compared with the "load component" I'_2 of the transformer current. It is customary in many systems studies to neglect I_m besides I'_2, that is, we set $Z_m = \infty$.

Furthermore, the leakage impedance is mainly inductive (Example 5-6) and we neglect its resistive part. Similarly, we shall find in the next chapter that the line impedance is mainly inductive and we therefore neglect its resistance also. With all these approximations the equivalent circuit of line, transformer, and load takes on the form in Fig. 5-13*b*.

From this circuit we have for currents

$$I_l \approx I_1 \approx I'_2 = \frac{66.4\angle 0^\circ}{151.8 + j67.6} = 0.3996\angle -24.0^\circ \text{ kA}$$

$$I_2 \approx 5.03 \times 0.3996\angle -24.0^\circ = 2.010\angle -24.0^\circ \text{ kA}$$

and for the voltages

$$V'_2 = 151.8 \times 0.3996\angle -24.0^\circ = 60.66\angle -24.0^\circ \text{ kV}$$

$$V_2 = \frac{1}{5.03} \times 60.66\angle -24.0^\circ = 11.45\angle -24.0^\circ \text{ kV}$$

$$V_1 = (151.8 + j17.6) \times 0.3996\angle -24.0^\circ = 61.07\angle -17.4^\circ \text{ kV}$$

At no-load the currents would be zero. With no voltage drops the transformer secondary voltage would thus equal 66.4/5.03 = 13.2 kV. The 6-Ω load thus causes a voltage drop of

$$\frac{13.2 - 11.45}{13.2} \times 100 = 13.3\%$$

5-4-3 Transformer Rating

Clearly, the core losses (P_{Fe}) and winding losses (P_{Cu}) determine the power limit of a physical transformer. When the *sum* of these losses exceeds a certain value, the temperature rise of the device becomes excessive. P_{Fe} depends upon flux density B_{max} which in turn is directly proportional to voltage level. P_{Cu} is determined by the current.

In conclusion, $|V|$ and $|I|$ are thus determining for the temperature level of the transformer. It is customary to let the product $|V| \cdot |I|$ be a measure of the power rating, i.e., a transformer is rated in apparent power, kilovoltamperes or megavoltamperes.

5-5 PER-UNIT ANALYSIS

In Chap. 2 we stated that one of the reasons for the usage of per-unit analysis is the simplification resulting when transformers are involved. We will now clarify this point.

5-5-1 Transformer Variables in Per Unit of Ratings

We have noted that voltage, current, and impedance levels all change between the various windings of a transformer. Only the powers remain invariant. Were we to express voltage, current, and impedance in volts, amperes, and ohms then we would have to contend with the unavoidable need of changing the V, I, and Ω values depending upon what winding they would all be "referred" to. This was exemplified in Example 5-8. When many transformers are involved (and this is generally the case in actual systems studies) this can be a nuisance. Use of the per-unit system simplifies matters considerably.

Consider for a moment our 30-MVA example transformer in Example 5-8. Its primary current was computed to be 399.6 A. In terms of rated primary current (451.8 A) its primary current loading is thus

$$|I_1| = \frac{399.6}{451.8} = 0.884 \text{ pu}$$

Similarly, the secondary current loading in terms of rated secondary current (2273 A) equals

$$|I_2| = \frac{2010}{2273} = 0.884 \text{ pu}$$

In per-unit values the primary and secondary currents have the same numerical values.†

The primary and secondary voltages expressed in terms of their respective rated values are

$$|V_1| = \frac{61.07}{66.4} = 0.920 \text{ pu}$$

$$|V_2| = \frac{11.45}{13.2} = 0.867 \text{ pu}$$

Finally, if we compute the input and output megavoltamperes in terms of rated megavoltamperes we obtain

$$|S_1| = \frac{0.3996 \times 61.07}{30} = 0.813 \text{ pu}$$

$$|S_2| = \frac{2.010 \times 11.45}{30} = 0.767 \text{ pu}$$

Note that we could have obtained the per-unit values of $|S_1|$ and $|S_2|$ directly from the per-unit values of currents and voltages

$$|S_1| = 0.884 \times 0.920 = 0.813 \text{ pu}$$

$$|S_2| = 0.884 \times 0.867 = 0.767 \text{ pu}$$

All of these computed per-unit values are more meaningful than those absolute values computed in Example 5-8 because they relate directly to the rated values of the transformer.

We obtained the per-unit values in two steps:

First we computed the absolute values from the equivalent circuit in Fig. 5-13*b*. Second we recomputed the absolute values into per-unit values in terms of the device rating.

5-5-2 Transformer Impedance in Per Units

It is more practical to perform the *whole* analysis in per units. In order to do this it is necessary to recompute the transformer impedance in per units. Consider again our 30-MVA example transformer.

† This would, of course, not be exactly so if the magnetizing current were included.

Its leakage impedance (resistance neglected) had been computed to

$$Z_L = j17.6\ \Omega \text{ in terms of HV}$$

Were we to choose the rated base value pair

$$|S_b| = 30 \text{ MVA}$$

$$|V_b| = 66.4 \text{ kV (HV)}$$

then, according to formula (2-39) the per-unit leakage impedance would equal

$$Z_L = \frac{j17.6}{(66.4)^2/30} = j0.120 \text{ pu}$$

Assume instead that Z_L had been referred to the LV side of the transformer. Its ohmic value would then be

$$Z_L = \frac{j17.6}{(5.03)^2} = j0.696\ \Omega$$

If we now were to choose the base pair

$$|S_b| = 30 \text{ MVA}$$

$$|V_b| = 13.2 \text{ kV (LV)}$$

the per-unit value of Z_L would equal

$$Z_L = \frac{j0.696}{(13.2)^2/30} = j0.120 \text{ pu}$$

In words: *If the voltage base is changed in the ratio $a = N_1/N_2$ ("floating" voltage base) the numerical value*† *of the transformer per-unit impedance will be the same on primary and secondary sides.*

In our above discussions we chose the *rated* values of the transformer as base values. Clearly, when we have a number of transformers involved we must employ a *common* base system. The above rule still will apply.

Example 5-9 Work Example 5-8 in per units. Use the arbitrarily selected base pair

$$|S_b| = 100 \text{ MVA}$$

$$|V_b| = 100 \text{ kV}$$

SOLUTION From this base value pair we first compute base current and base impedance;

$$|I_b| = \frac{100 \text{ MVA}}{100 \text{ kV}} = 1 \text{ kA}$$

$$|Z_b| = \frac{100 \text{ kV}}{1 \text{ kA}} = 100\ \Omega$$

† Note also that the numerical value (0.120 pu = 12% in this case) also equals the voltage value during the SC test (Example 5-6). Explain this.

We then compute the line, transformer, and load impedances in per unit of the given base system:

Line: The impedance, $j50\ \Omega$, equals

$$Z_l = \frac{j50}{100} = j0.500 \text{ pu}$$

Transformer: Its impedance, $j0.120$ pu, was computed on the base pair 66.4 kV and 30 MVA. On the base pair 100 kV and 100 MVA its new per-unit value equals (see Eq. 2-42)

$$jX_L = j0.12\frac{100}{30}\left(\frac{66.4}{100}\right)^2 = j0.176 \text{ pu}$$

Load: The 6-Ω resistor is felt on the HV side as a resistor of magnitude

$$(5.03)^2 \times 6 = 151.8\ \Omega$$

or in per unit

$$R = \frac{151.8}{100} = 1.518 \text{ pu}$$

We have summarized all these per-unit impedance data in Fig. 5-13*c*. Realizing that the network voltage equals

$$V_N = \frac{66.4\angle 0^\circ}{100} = 0.664\angle 0^\circ \text{ pu}$$

we obtain directly for the current

$$I = \frac{0.664\angle 0^\circ}{1.518 + j(0.500 + 0.176)} = 0.3996\angle -24.0^\circ \text{ pu}$$

As $|I_b| = 1$ kA the computed current corresponds to 399.6 A which agrees with the value computed in Example 5-8. The reader is recommended to complete the example by computing the voltages V_1 and V_2, and to check with earlier results.

5-6 THREE-PHASE TRANSFORMERS

Transformation of three-phase power can be accomplished in several ways by the use of "single-phase" transformers of the type discussed in earlier sections. For example, we learned in Example 5-1 how power can be transformed between the voltage levels 22, 345, and 138 kV by using three 3-winding single-phase units where the individual windings were connected to the phase voltages respectively. Other possibilities exist and we shall presently discuss the more important ones.

5-6-1 Single-Phase versus Three-Phase Cores

Three-phase transformers may consist either of a "bank" of three identical single-phase units of the type shown in Figs. 5-1*a* or *b* or of one unit of the type in Fig. 5-1*c*, a "three-phase core." As the voltages in the three phases possess the

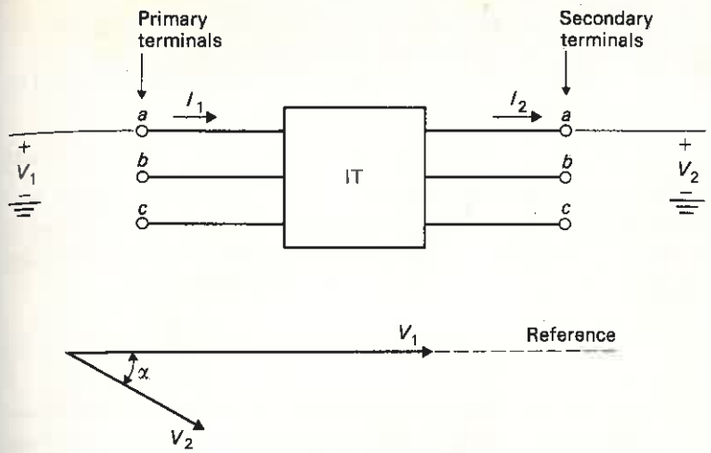

Figure 5-14 Three-phase two-winding transformer.

three-phase symmetry of Fig. 3-5 so will the core fluxes. Consequently, the three fluxes will add up to zero at any moment of time, and this explains the absence of a magnetic return path† in the core depicted in Fig. 5-1*c*.

Clearly, the "three-phase core" contains less iron than three single-phase units and is therefore cheaper. On the other hand, a winding failure would require a replacement need for the total three-phase unit, whereas in the case of the "bank" arrangement only one phase-unit needs replacement. As far as the electrical characteristics go the two types are almost identical.

5-6-2 General Three-Phase Transformer Relationships

Figure 5-14 depicts a two-winding three-phase transformer. We develop presently some general relationship between the primary and secondary currents and voltages of this device. We state first some basic assumptions and make also some agreements about symbols used:

1. The transformer is "ideal."
2. The primary and secondary voltages possess three-phase symmetry.
3. The loading is balanced so that the primary and secondary currents also possess three-phase symmetry.
4. Subscripts 1, 2, 3, ..., will be used to identify "primary," "secondary," "tertiary," etc., variables.
5. Superscripts *a*, *b*, and *c* will be used when there is a need to distinguish

† Compare the normal deletion of a neutral current return path in a balanced three-phase circuit.

between phases. When no such need exists, they will be deleted, and the variables then (as in Fig. 5-14) will always refer to phase a.

6. Line voltages will, when needed, be symbolized by double superscripts. The order of the superscripts defines polarity, for example,

$$V_1^{ab} = V_1^a - V_1^b \tag{5-31}$$

In a single-phase transformer the transformation ratios were *always* real numbers, i.e., the primary and secondary voltage phasors are colinear. This is generally *not* true for a three-phase transformer. As will be demonstrated the "three-phase transformation ratio" may be complex, i.e., of the form

$$\frac{V_1}{V_2} \triangleq a = |a|\underline{/\alpha} \tag{5-32}$$

indicating that primary and secondary phase voltages are of unequal time phase. A positive angle α indicates that V_2 lags V_1, that is, the transformer imparts a voltage *lag*.

Being an IT the transformer in Fig. 5-14 is lossless. This means that

$$V_1 I_1^* = V_2 I_2^* \tag{5-33}$$

For the currents we thus have

$$\frac{I_1}{I_2} = \frac{V_2^*}{V_1^*} = \frac{1}{a^*} = \frac{1}{|a|}\underline{/\alpha^{j\alpha}} \tag{5-34}$$

Comparing Eqs. (5-32) and (5-34) we conclude that

$$\underline{/I_1/I_2} = \underline{/V_1/V_2} = \alpha \tag{5-35}$$

or in words: *A three-phase transformer always imparts the same phase shift upon currents and voltages.*

An important practical consequence of the phase-shift situation is that *parallel operation of three-phase transformers is possible only if both their ratio magnitude and phase shift are identical.*

In view of the above findings we conclude that the earlier derived equivalent circuit (Fig. 5-11) can be made to represent a three-phase transformer if a "phase shifter" is added, which imparts a phase shift of α degrees to *both* current and voltages.

The result is the circuit in Fig. 5-15 which may also be made to incorporate nonideal features by adding leakage and magnetization impedances in the primary branch, as shown dashed in the figure.

5-6-3 Y-Connected Transformers

In Example 5-1 we encountered a situation where electric three-phase power was to be transformed between three 3-phase buses. Three separate single-phase transformers were interconnected to form a "three-phase transformer." The three windings on each separate core were connected to the phase voltages of the three different buses as indicated in Fig. 5-5.

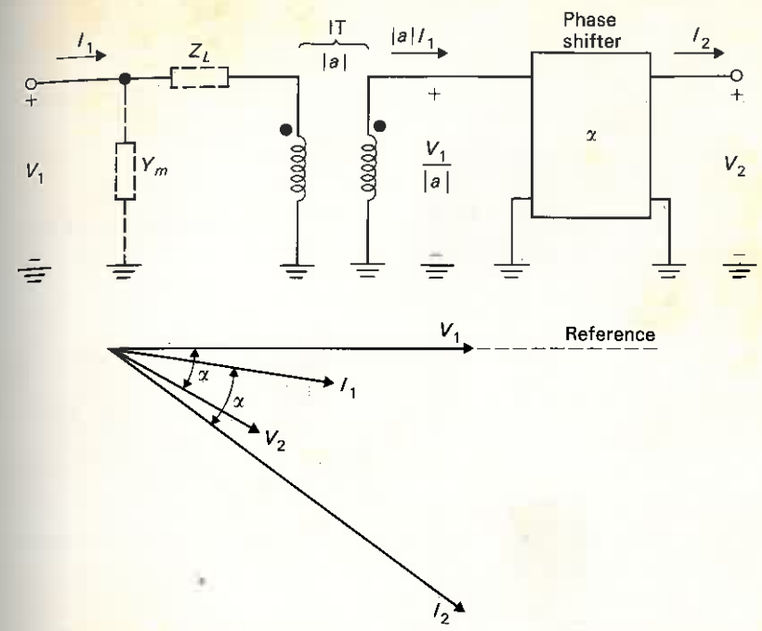

Figure 5-15 Equivalent diagram of three-phase transformer, with losses included.

We now examine closer this type of transformer and limit our attention to a *two*-winding three-phase transformer, intended to transform power between *two* 3-phase buses. It consists of three identical single-phase two-winding units interconnected as shown in Fig. 5-16*a*. The reader should take careful note of the winding polarity. In Fig. 5-16*b* the same transformer is shown in a simpler symbol. Finally, in Fig. 5-16*c* another symbol yet is used. In what follows we shall prefer the use of this latter symbol type which is *characterized by the fact that its windings are given an angular orientation coinciding with that of its voltage phasors.*

For example the two windings marked 1 and 2 are physically located on the "a core." The primary winding, 1, is connected to the voltage $V_1^a = |V_1|\underline{/0°}$. The winding 2 experiences the voltage $V_2^a = |V_2|\underline{/0°}$. The symbolic picture in Fig. 5-16*c* thus by inspection reveals the transformation ratio of the three-phase transformer. Its "three-phase transformation ratio" is obviously

$$a = \frac{V_1^a}{V_2^a} = \frac{|V_1|}{|V_2|}\underline{/0°}$$

$$\therefore \quad |a| = \frac{|V_1|}{|V_2|} = \frac{N_1}{N_2}$$

and

$$\alpha = 0°$$

(N_1 and N_2 are the number of turns of windings 1 and 2.)

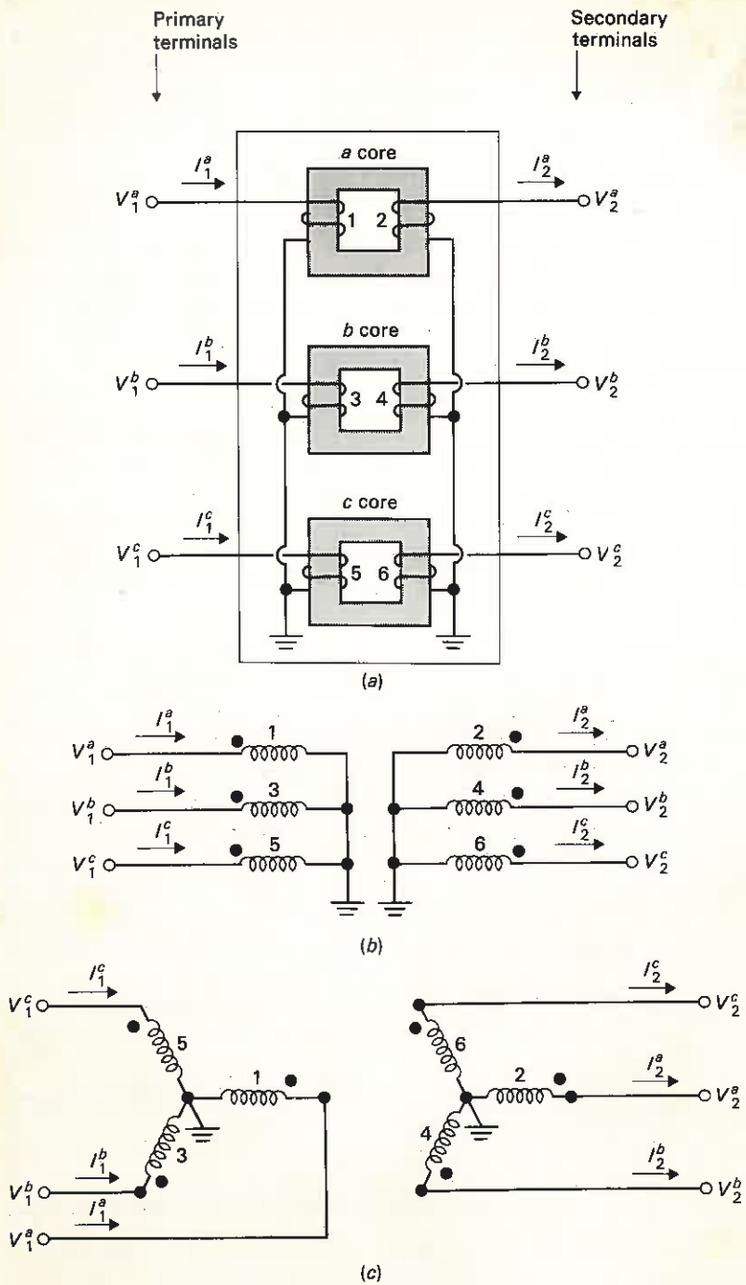

Figure 5-16 Y-Y connected two-winding three-phase transformer: (*a*) core and coil arrangements; (*b*) dot symbol representation; (*c*) symbol representation exposing the voltage phasor relations.

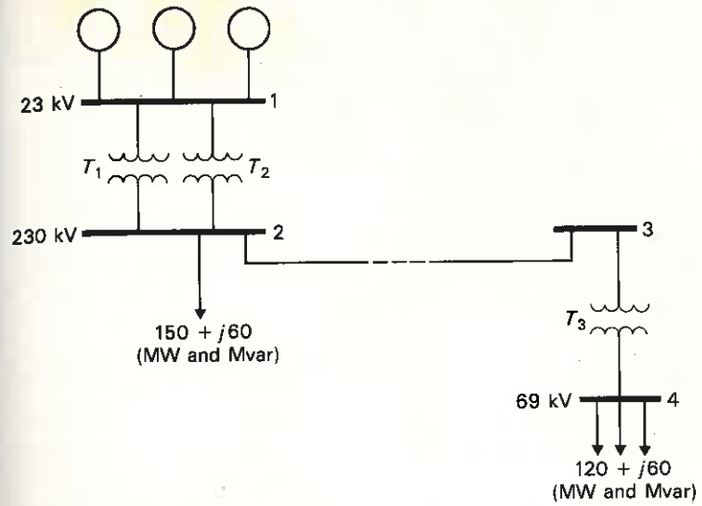

Figure 5-17 A transmission system.

The symbol in Fig. 5-16*c* also explains the designation "Y-Y" for this type of three-phase connection.

When the three-phase transformer in Fig. 5-16 is loaded *symmetrically* on the secondary, all single-phase units will be subject to the same rms currents, voltages, and voltage drops. The only thing that will be different between the three units is the time phase. We can therefore use "per-phase" analysis. Each unit will handle one-third of the total three-phase power. Each winding will be subject to $1/\sqrt{3}$ of the respective line voltages. The "three-phase transformer" is always rated in *total* three-phase power and *line* voltages.

Example 5-10 Consider the three-phase system in Fig. 5-17. From a 23-kV generator bus (1) power is transformed in two identical parallel three-phase transformers *T*1 and *T*2 to a 230-kV bus (2), thereupon transmitted via a 230-kV line to a 50-mile distant bus (3). A third transformer, *T*3, transforms the power to a 69-kV substation bus (4).

It is required to hold the latter bus voltage at exactly 69 kV. What voltage must be maintained at bus 1 if the system loading is as indicated in Fig. 5-17?

System data:

T1 and T2: 150 MVA, 60 Hz, Y-Y, 23/230 kV each.
T3: 150 MVA, 60 Hz, Y-Y, 230/69 kV.

All three transformers have a leakage impedance of *j*0.1 pu based on their respective ratings.† The line has a reactance of 60 ohms per phase. (All resistances and magnetization currents are neglected.)

† This means that each individual single-phase unit has a *j*0.1 pu impedance.

SOLUTION We shall work this problem in per units with $|S_b| = 100$ MVA per phase. The voltage base will be "floating." If we refer to bus 1, $|V_b|$ will equal $23/\sqrt{3}$ kV phase-to-neutral. If we refer to buses 2 and 3 (or the transmission line), then $|V_b|$ will be $230/\sqrt{3}$ kV. Finally, if we refer to bus 4, $|V_b|$ will equal $69/\sqrt{3}$ kV per phase.

Note that the variable voltage base brings with it a variable current base. For example, at the 23-kV level 1 pu current corresponds to

$$\frac{100}{23/\sqrt{3}} = 7.531 \text{ kA/per phase}$$

At the 230- and 69-kV levels 1 pu current means 0.753 and 2.510 kA/phase respectively.

From the transformer and line data we directly obtain the per-phase representation in Fig. 5-18*a*. We make these clarifications:

1. A transformer that has 10 percent reactance on a 50-MVA basis will have a 20 percent reactance on 100-MVA base (compare Eq. 2-42).
2. The base impedance on 230-kV level equals $230^2/300 = 176.3\ \Omega$.
   The line reactance, 60 Ω, thus equals $60/176.3 = 0.340$ pu.

The diagram in Fig. 5-18*a* is readily simplified to the one in Fig. 5-18*b*. From this diagram we now compute V_1 in these steps:

Step 1 Choose $V_4 = 1\angle 0°$ pu (reference phasor)

Step 2 From equation

$$1 \cdot I_4^* = 0.4 + j0.2$$

solve

$$I_4 = 0.4 - j0.2$$

Step 3 $V_2 = V_4 + j0.540 I_4 = 1 + j0.540(0.4 - j0.2) = 1.108 + j0.216$

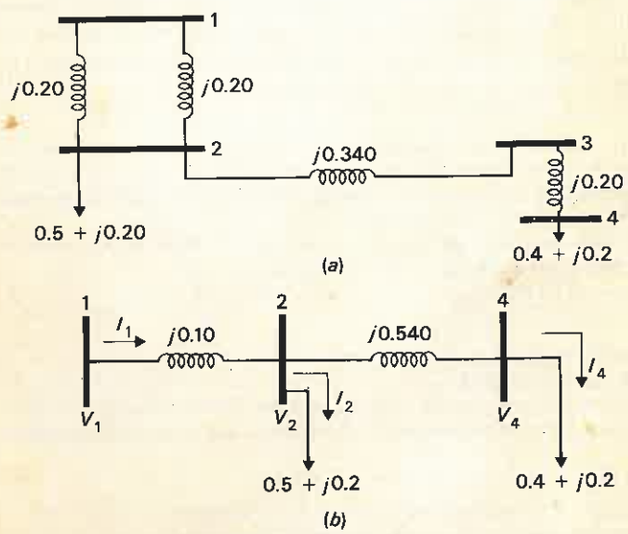

Figure 5-18 Equivalent diagram of system in Fig. 5-17.

Step 4 From equation

$$V_2 I_2^* = 0.5 + j0.2$$

solve

$$I_2 = \frac{0.5 - j0.2}{1.108 - j0.216} = 0.4686 - j0.0891$$

Step 5 $I_1 = I_2 + I_4 = 0.8686 - j0.2891$

Step 6 $V_1 = V_2 + j0.10 I_1 = 1.177\angle 14.9°$

Conclusion: The generator bus must be held at $1.177 \times 23 = 27.07$ kV to maintain a voltage of 69 kV at bus 4.

5-6-4 Δ-Connected Transformers

The Y-connected transformer is very simple but it has some serious practical drawbacks. For example, in Ref. 1 is shown how, due to the nonlinear magnetic

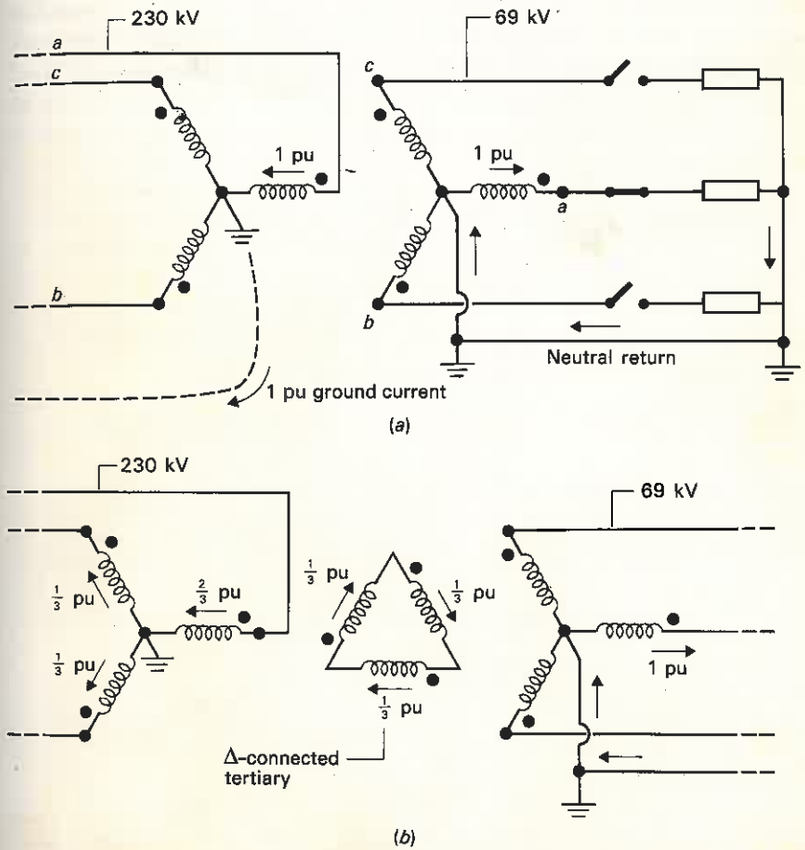

Figure 5-19 Severe transformer unbalancing: (*a*) of Y-Y transformer with solidly grounded neutrals; (*b*) with Δ-connected tertiary added.

characteristics of the core material, this type of transformer will generate harmonics (particularly 180 Hz) that will exit via the neutrals and cause trouble in communication networks.

Y-connected transformers are also very "unforgiving" in cases of even slight unbalancing of load. Consider for example the transformer $T3$ in Fig. 5-17. Assume that it is subject to a load unbalance. Figure 5-19*a* depicts the worst possible case; phase *a* carrying a 1-pu load current with phases *b* and *c* carrying zero. The neutral return of the 69-kV secondary provides the return path for the load current. On the primary side, phase *a* will respond with a 1-pu current. No portion of this current can return via phases *b* and *c* as this would upset the mmf balance in these cores. As a consequence, the full 1-pu primary current will be forced into ground to seek its way back to the 50-mile distant neutrals of $T1$ and $T2$. On the way this "vagabonding" current can play dirty tricks with communication and other networks.

Compare what would happen if we provided $T3$ with a tertiary set of windings connected in *closed* Δ as shown in Fig. 5-19*b*. For the same 1-pu unbalanced secondary load as in the previous case a 0.33-pu tertiary circulating current will now arise which will permit primary currents to flow in all three phases. "*Mmf*"

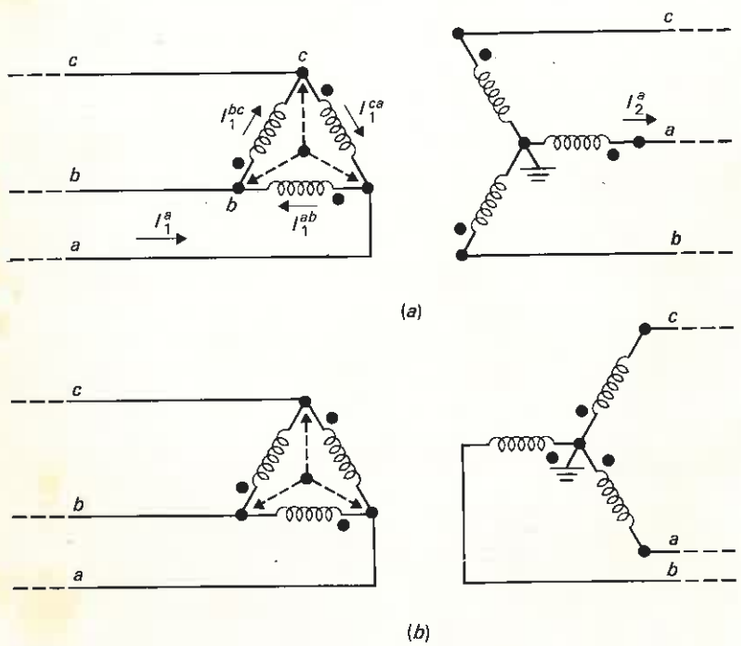

Figure 5-20 Δ-Y connected transformer: (*a*) This connection results in a 30° phase advancement; (*b*) This connection yields a 30° phase lag.

balance is achieved in all three cores and no primary ground current is created.

It is not necessary to provide a special tertiary. One or the other (or both) of the primaries or secondaries may serve as a closed Δ. Figure 5-20 depicts a common arrangement. Note that two possibilities exist depending upon which polarity is chosen for the Y-connected secondary.

The reader is urged to check how a single-phase loading (of the type in Fig. 5-19*a*) results in primary currents in two of the phases. Which two?

5-6-5 Analysis of Δ-Y Transformers under Balanced Loading

We present now a brief analysis of the Δ-Y type transformer. We limit our discussion to the polarity case in Fig. 5-20*a*. We immediately find by inspection that the secondary phase voltage *leads*† the primary by 30°, i.e.,

$$\alpha = \angle\frac{V_1^a}{V_2^a} = -30° \tag{5-37}$$

According to Eq. (5-35) the secondary phase current, I_2^a, will thus also lead the primary, I_1^a, by 30°. As far as the "delta currents," I_1^{ab} and I_1^{ca}, are concerned we note that they are related to the phase current I_1^a by the equation

$$I_1^a = I_1^{ab} - I_1^{ca} \tag{5-38}$$

Due to the assumed existing three-phase symmetry the currents I_1^{ab}, I_1^{bc}, and I_1^{ca} constitute a symmetrical three-phase set, i.e.,

$$I_1^{ca} = I_1^{ab} e^{j120°}$$

In view of this last relation, Eq. (5-38) yields

$$I_1^a = I_1^{ab}(1 - e^{j120}) = \sqrt{3}\, I_1^{ab} e^{-j30°} \tag{5-39}$$

In words: *The magnitude of the phase current is* $\sqrt{3}$ *times the Δ-current.*

Example 5-11 Connect three of the 30-MVA single-phase transformers treated in Example 5-6 into a Δ-Y three-phase bank to be used for transforming power from a 90-MVA, 13.2-kV generator to a 115-kV bus. Find all primary and secondary currents in the fully loaded transformer.

SOLUTION At full load the secondary phase current magnitude equals

$$|I_2| = \frac{30}{115/\sqrt{3}} = 0.452 \text{ kA/phase}$$

The "three-phase transformation ratio" equals

$$|a| = \frac{13.2}{115} = 0.1148$$

† As the reader discovers from Fig. 5-20*b* the second alternative yields $\alpha = +30°$.

Thus, the primary full-load *phase* current equals

$$|I_1| = \frac{0.452}{0.1148} = 3.936 \text{ kA/phase}$$

The "Δ current" has a magnitude of

$$\frac{3.936}{\sqrt{3}} = 2.273 \text{ kA}$$

Note that the two winding current values, 452 and 2273 A, agree with the rated values computed in Example 5-6.

In Chap. 11 we shall study more closely power systems subject to unbalanced loading and fault conditions. We shall then have further opportunity to learn of the importance of Δ-connected three-phase transformers.

5-6-6 Three-phase Multiwinding Transformers

It is quite common that three-phase transformers are of multiwinding type used for transforming power between several voltage levels. The windings may be of mixed type, containing both Y and Δ connections. The following example

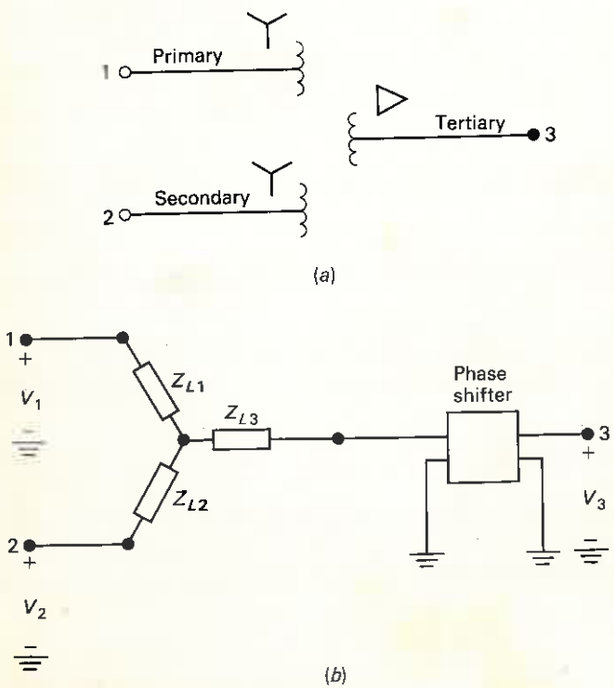

Figure 5-21 A three-winding Y-Y-Δ transformer.

Table 5-1

Winding	Rated voltage, line-to-line, kV	Rated megavoltamperes total three-phase	Impedance based on 15 MVA, 3-ϕ
Primary (1)	13.8	15.0	$Z_{L1} = j6.02\%$
Secondary (2)	69.0	15.0	$Z_{L2} = j0.88\%$
Tertiary (3)	4.80	5.25	$Z_{L3} = j9.97\%$

demonstrates how analysis may proceed when multiwinding transformers are involved.

Example 5-12 A three-winding-three-phase transformer is equipped with Y-connected primaries (1) and secondaries (2) and a Δ-connected tertiary (3). It is schematically depicted in Fig. 5-21*a*. Its equivalent circuit is shown in Fig. 5-21*b*. (As all impedances will be given in per unit the IT has been deleted.) Table 5-1 summarizes the voltage, power, and impedance data for the three windings.

We note that all windings do not necessarily have equal power ratings. The tertiary, in this case, is designed for only about a third of the power that may be routed via the primaries and the secondaries.

(The three impedances can be obtained by three separate short-circuit tests. For example, by keeping the tertiary open and the secondary shorted the sum $Z_{L1} + Z_{L2}$ can be obtained from measurements on the primary (compare Example 5-6).)

The transformer acts as shown in Fig. 5-22*a* as a connecting link between three buses in a substation. Another 30-MVA transformer is also connected between the 69- and 13.8-kV buses. Energy is fed from the 69-kV bus to the two other buses. The 69-kV bus can, for practical purposes, be considered "infinite."† Assume that a symmetric solid three-phase short circuit occurs on the 4.8-kV bus. Find the short-circuit current, I_{sh}, fed to the faulted bus from the tertiary winding. The 30-MVA transformer has an impedance of $j8.00$ percent based on its own rating.

SOLUTION As we are interested only in the rms value of the short-circuit current we can neglect the phase shifter and the two transformers will therefore be represented as shown in Fig. 5-22*b*. Note that the impedance of the 30-MVA transformer has been recomputed to 15-MVA (3-phase).

In two self-explanatory steps the circuit in Fig. 5-22*b* is reduced to the simple one in Fig. 5-22*d*.

† We talk in power lingo of an *infinite bus*. Such a bus will maintain a 100 percent voltage *independently of how much current we drain from it*. In other words, it is assumed to be connected to an impedanceless voltage source. No physical network bus is, of course, that strong. There is a great need to know just how strong a bus really is. This information has important bearing upon the magnitude of fault currents that the system will experience in that particular locality, and thus is determining for the dimension of bus bars, circuit breakers, switches, etc. The so-called *short-circuit capacity* (SCC) is a measure of the strength of a bus. We shall return to this concept later, in Chap. 10, in connection with network fault studies.

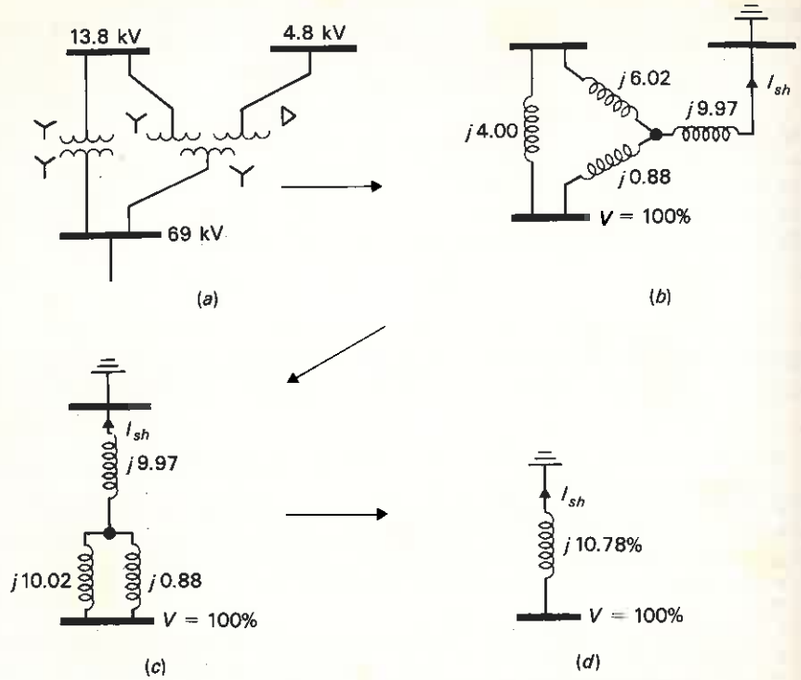

Figure 5-22 Equivalent circuit representation of the transformer in Fig. 5-21.

From this latter circuit we compute the short-circuit current

$$|I_{sh}| = \frac{100}{10.78} = 9.28 \text{ pu} \tag{5-40}$$

This current value is based on 15 MVA. In terms of the *rated* megavoltamperes of the tertiary, the short-circuit current amounts to

$$|I_{sh}| = 9.28 \times \frac{15}{5.25} = 26.5 \text{ pu} \tag{5-41}$$

In other words, the short-circuit current is 26.5 times the rated value. This example demonstrates a conflicting feature of transformer impedances:

From a voltage-drop point of view, we wish the impedances to be small.

From a short-circuit current point of view, we would like them to be large.

5-7 AUTOTRANSFORMERS

Consider the two-winding single-phase transformer depicted in Fig. 5-23*a*. It has a power rating of 100 kVA and a voltage rating of 1000/200 V. The rated currents are thus 100 and 500 A in the high-voltage and low-voltage windings,

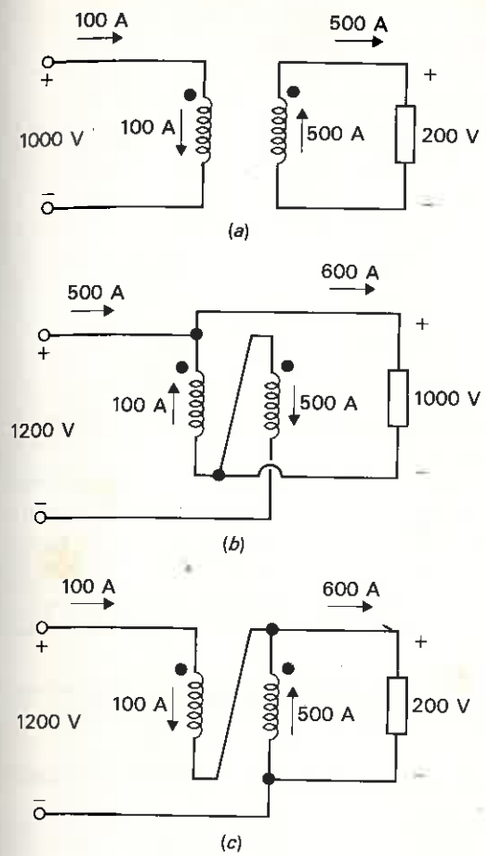

Figure 5-23 Autoconnected transformers.

respectively, as indicated in the figure. Let us now interconnect the windings as shown in Figs. 5-23*b* and *c*. *Without changing the voltage per turn, and thus the core flux*, we obviously have now obtained a 1200-V winding.

We can then designate the former 1000-V terminals as our "secondaries" and thus obtain a 1200/1000-V *autotransformer* (Fig. *b*), or we can use the former 200-V terminals for the same purpose and obtain a 1200/200-V autotransformer (Fig. *c*). In either case we can load these new secondary terminals with maximum 600 A and still limit the coil currents to their rated values, as shown in Fig. 5-23*b* and *c*. *Without increasing the core and copper losses, and thus not overloading the transformer, we have in effect increased its rating to 600 and 120 kVA, respectively, i.e., with 600 and 20 percent, respectively.*

This substantial gain in power rating is bought at a price. To appreciate this let us study the effect that the interconnection of windings has had on the impedance and short-circuit currents in the transformer. Let us assume that the

Table 5-2

Transformer type	MVA rating	Voltage ratio	Impedance in per units of ratings
Two-winding type	$\lvert S_r \rvert$	$a:1$	Z_L
Autotransformer, case I	$(a+1)\lvert S_r \rvert$	$\frac{a+1}{a}:1$	$\frac{1}{1+a}Z_L$
Autotransformer, case II	$\frac{a+1}{a}\lvert S_r \rvert$	$(a+1):1$	$\frac{a}{1+a}Z_L$

original transformer in Fig. 5-23*a* has a typical impedance value of $j0.06$ pu. A short circuit would thus render a short-circuit current of $1/0.06 = 16.7$ pu.

Let us then turn our attention to the case shown in Fig. 5-23*b*. Assume that a short circuit occurs on the 1000-V secondary. This means that the primary voltage, 1200 V, is now applied across the 200-V winding. Since the impedance has not changed, the short-circuit current will now be $1200/200 = 6$ times its previous value, i.e., 100 times rated value. We may express the situation thus:

The per-unit impedance has decreased in the ratio 1:6 to the new value 0.01 pu.

One additional disadvantage of the autotransformer is the metallic† connection between primary and secondary (permitting easy transmission of disturbance overvoltages).

In Table 5-2 we summarize the characteristics of autotransformers in regard to ratings and impedance values.

We note that the greatest increase in megavoltampere rating, and also the greatest increase in short-circuit current, take place when the voltage ratio of the resulting autotransformer is close to unity. Autotransformers are used with advantage in such cases when the voltage ratio is of the order of 2 : 1 or lower.

All the foregoing discussions have referred to single-phase transformers. They can be directly applied to the per-phase situation in three-phase systems. Figure 5-24 shows the winding connections for the most common three-phase arrangement. Usually, a Δ-connected tertiary is added which will be idle under normal balanced operation but gets into operation in unbalanced fault and loading situations.

A typical application of a three-phase autotransformer would be as a tie

† It is this metallic connection that explains the increased power rating of the autotransformer. As the reader probably has already realized, we do not really increase the *power transformation ability* of a transformer by connecting it "auto." For example, when we increased the *rating* from 100 to 600 kVA in the above example, the autotransformer is actually only *transforming* 100 kVA (i.e., the old value). 600 − 100 = 500 kVA is simply passing the transformer untransformed.

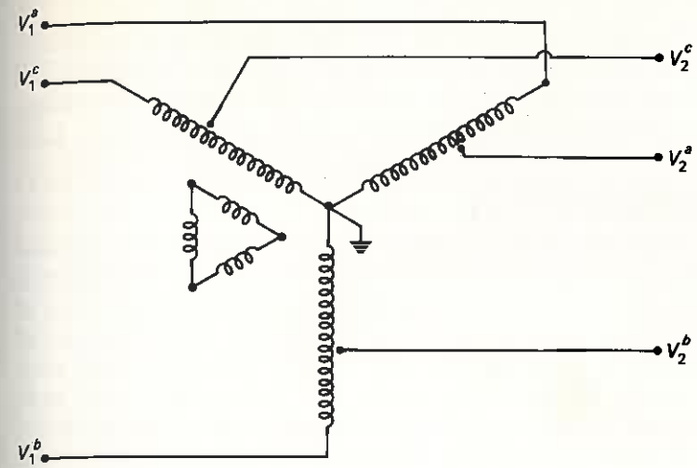

Figure 5-24 Y-Y auto-connected three-phase transformer with Δ-connected tertiary.

between the 500- and 345-kV levels of a transmission system. A 500/345-kV autotransformer with a 1000-MVA rating would be of much smaller size (and cost) than a two-winding transformer of equal ratings.

5-8 THE TRANSFORMER AS A CONTROL DEVICE

5-8-1 TCUL Transformers

Transforming energy between different voltage levels is the primary job of a power transformer. Practically every transformer is provided with taps for ratio control, and is thus equipped to perform a secondary duty, i.e., controlling the secondary voltage level. On most transformers these taps can be changed only in deenergized state. In many instances this ratio control can be performed by *tap changing under load* (TCUL).

We recall from our discussions in Chap. 3 that, due to the changing power flow, the voltage profile of the transmission network tends to vary slowly throughout the day, dropping during peak load hours and rising during night hours. It is theoretically possible, of course, to maintain the level perfectly constant by providing every bus of the transmission system with controllable Q sources. However, this is neither a practical nor an economical approach, and as a result the transmission voltage profile will vary within certain tolerable limits. TCUL transformers make it possible to maintain a constant voltage level on important subtransmission- and distribution-level buses, in spite of fluctuations in the voltage level of the transmission system.

For example, a 5 percent drop of the primary voltage of a TCUL transformer can be completely compensated by a 5 percent decrease of the transforma-

tion ratio. The tap-changing equipment of TCUL transformers is usually motor-operated, and by letting the motors be commanded from voltage sensors, we can provide closed loop control of the secondary voltage level. A less sophisticated arrangement employs manual operation.

5-8-2 Regulating Transformers

Regular ratio control, as discussed, is a feature that can be incorporated into any transformer, including distribution transformers. We now turn our attention to a type of transformer which is almost exclusively used on the transmission levels of our systems, the so-called *regulating*, or *control*, transformer. The primary job of these transformers is not to transform a large amount of energy. Indeed, their megavoltampere ratings are often quite limited. The primary function of these devices is to change, by usually a relatively *small* amount, the voltage in a point of the system, as shown in Fig. 5-25. The voltage change ΔV, introduced by these devices, can in general be changed in both magnitude and phase.

As we shall see, the added voltage ΔV, although of small magnitude, will have a drastic effect on the *power flow* in the link in question. *Regulating transformers are therefore in effect means for controlling the power flow in our system.*

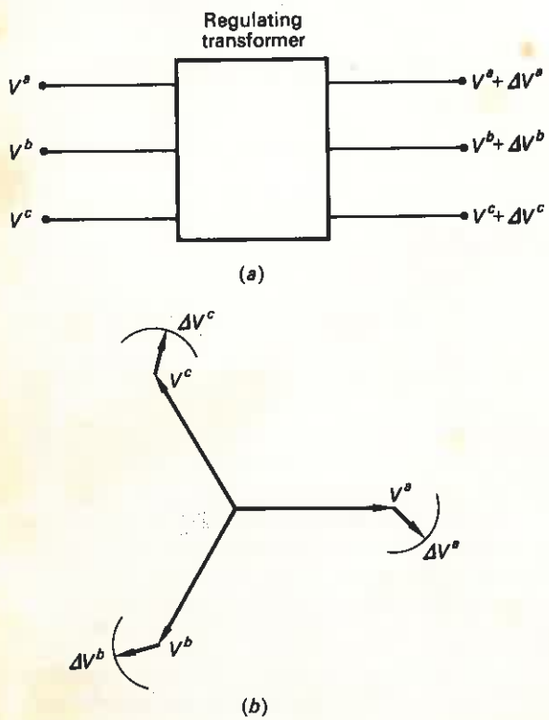

Figure 5-25 A three-phase regulating transformer (RT) adds a voltage increment of variable phase or magnitude or both.

Before we prove this statement, let us present some typical examples on regulating transformers.

5-8-3 Regulating Transformer for Voltage Magnitude Control

There are a number of different schemes by means of which it is possible to obtain *magnitude* control of the added voltage ΔV. Figure 5-26*a* depicts one common arrangement. From a three-phase autotransformer (*exciting transformer*) an adjustable voltage is picked off and used as a primary voltage in a *series transformer* which is placed at the point in our network where we wish to add the voltage ΔV. To comprehend the operation of the device, consider phase *a* of the system. The voltage picked off by means of the tap changer T_a is obviously in phase with V^a. Therefore the series transformer in phase *a* must add a voltage ΔV^a to V^a which is in phase with V^a itself, illustrated by the phasor diagram in Fig. 5-26*b*. The magnitude $|\Delta V|$ is obviously dependent upon the tap changer position.

We shall confirm later that the effect of this type of regulating transformer is to control the flow of *reactive* power in the link in question.

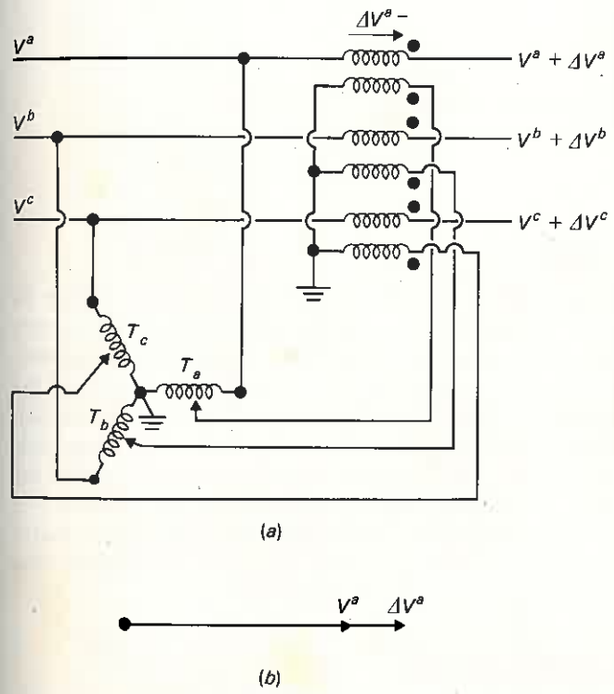

Figure 5-26 Voltage magnitude RT.

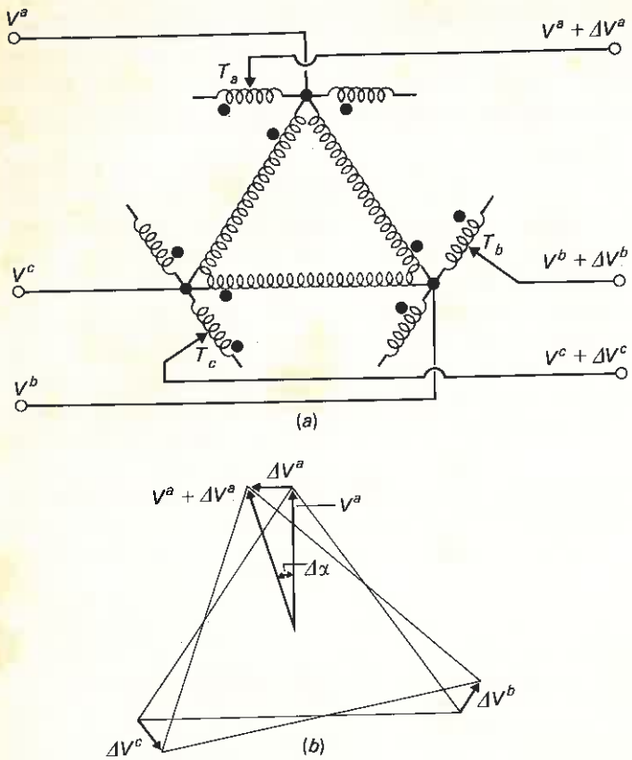

Figure 5-27 Voltage phase RT.

5-8-4 Regulating Transformer for Voltage Phase Angle Control

If the added voltage ΔV has a phase of $\pm 90°$ relative to the system voltage V, then the effect of the added voltage is to change the phase angle of the system voltage, as depicted in the phasor diagram of Fig. 5-27*b*. A possible arrangement to accomplish this type of control is shown in Fig. 5-27*a*. The operation of the device should be self-explanatory. The associated phasor diagram indicates that the phase angle adjustment $\Delta\alpha$ is approximately proportional to the magnitude of the added regulator voltage ΔV. The approximation is better, the smaller the adjustments we work with. It is also easily confirmed from the geometry of the phasor diagram that, for small angular adjustments, the arrangement leaves the voltage magnitude practically unaffected. Later examples will confirm that this type of device will control the *real power* flow in the line.

5-8-5 Examples on Power Flow Control

We shall finish this chapter by working two problems exemplifying the use of transformers for control of power flow.

Example 5-13 Phase Angle Control In our first problem we consider the system in Fig. 5-28*a*. Two parallel 230-kV transmission lines carry 600 MW of power from a generator bus 1 to a distant bus 2 whence it is delivered to a city. The line $L1$ has a reactance of 40 Ω/phase, $L2$ a reactance of 60 Ω. By excitation control of the generators the bus 1 is kept at 230 kV. A variable shunt capacitor at bus 2 delivers reactive power to stabilize $|V_2|$ at 230 kV also.

The lesser line reactance makes $L1$ carry the larger share of the power. By use of formula (3-49) we compute the actual megawatt flows as follows:

$$P_1 = \frac{230^2}{40} \sin \delta$$

$$P_2 = \frac{230^2}{60} \sin \delta \qquad (5\text{-}42)$$

$$P_1 + P_2 = 600$$

where δ is the power angle defined by Eq. (3-42)

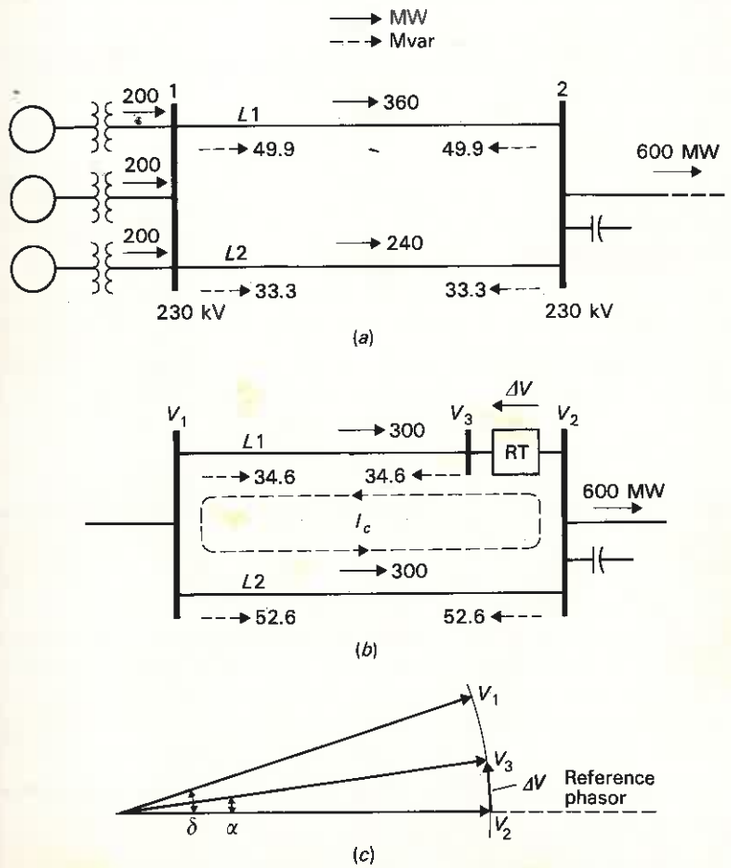

Figure 5-28 Example on use of phase angle RT.

These equations yield

$$\delta = 15.796°$$

$$P_1 = 360 \text{ MW}$$

$$P_2 = 240 \text{ MW}$$

From formulas (3-50) and (3-51) we also compute the reactive line flows

$$Q_1 = -Q_2 = 49.9 \text{ Mvar} \qquad (\text{line } L1)$$

$$Q_1 = -Q_2 = 33.3 \text{ Mvar} \qquad (\text{line } L2)$$

We have summarized these power flows in Fig. 5-28*a*.

By inserting a phase-angle regulating transformer (RT) in line $L1$ at bus 2 we intend to shift real power from $L1$ to $L2$ so that the two lines carry *equal* power amounts. We can obviously accomplish this by making the power angle of $L1$ *less* than the power angle of $L2$. The RT should thus add a voltage component ΔV to V_2 such that V_3, the voltage of the receiving end of $L1$, is *ahead* of V_2 as shown in Fig. 5-28*c*. With this relative phase position of the voltages V_1, V_2, and V_3, it is clear that the power angle of $L2$ will be δ but that of $L1$ only $\delta - \alpha$.

As before, we assume that $|V_1|$ and $|V_2|$ be kept at 230 kV by proper reactive power injection at the two buses. From the above stated megawatt requirements we find the δ- and α-values from these equations:

$$P_1 = 300 = \frac{230^2}{40} \sin(\delta - \alpha)$$

$$P_2 = 300 = \frac{230^2}{60} \sin \delta \tag{5-43}$$

These two equations yield

$$\delta = 19.89°$$

$$\alpha = 6.75° = 0.118 \text{ rad}$$

The power angles for the lines $L1$ and $L2$ are thus 13.14 and 19.89 degrees respectively. Using formulas (3-50) and (3-51) we then recompute the reactive line flows

$$Q_1 = -Q_2 = 34.6 \text{ Mvar} \qquad (\text{line } L1)$$

$$Q_1 = -Q_2 = 52.6 \text{ Mvar} \qquad (\text{line } L2)$$

Figure 5-28*b* summarizes the new power flow picture. The added voltage, ΔV, has a magnitude

$$|\Delta V| \approx |V_2|\alpha = \frac{230}{\sqrt{3}} 0.118 = 15.6 \text{ kV/phase} \tag{5-44}$$

The addition of ΔV has in effect superimposed a circulating current I_c (shown dashed in Fig. 5-28*b*) upon the existing line currents. According to Thevenin's theorem† this current will equal

$$I_c = \frac{\Delta V}{Z_{\text{loop}}} \tag{5-45}$$

where Z_{loop} is the impedance of the loop formed by the two lines. Since ΔV has a phase of

† For a discussion of this theorem see Chap. 10.

approximately 90° we obtain

$$I_c \approx \frac{j15.6}{j100} = 0.156\underline{/0°} \text{ kA/phase}$$

Note that I_c, approximately, is in phase with V_2 and therefore represents a *real power* increment of magnitude

$$\Delta P = |V_2|\,|I_c| = \frac{230}{\sqrt{3}} 0.156 = 20.7 \text{ MW/phase} \tag{5-46}$$

or

$$\approx 60 \text{ MW total 3-phase}$$

We have thus subtracted 60 MW from the original 360 MW in line $L1$ for a new real power of 300 MW.

Similarly, we have added 60 MW to the old 240 in line $L2$ which now will also carry 300 MW.

Example 5-14 Voltage Magnitude Control Consider the network portion depicted in Fig. 5-29*a*. Two transformers, designated $T1$ and $T2$ are operated in parallel and transforming power between an 11-kV generator bus and a 69-kV substation bus, from which a load of $S_L = 80 \text{ MW} + j60 \text{ Mvar}$ must be supplied at 69 kV. The two transformers have identical megavoltampere ratings of 50 MVA each, and their voltage ratings, 11/69 kV, are of course also equal.

The load corresponds to $\sqrt{(80)^2 + (60)^2} = 100$ MVA, and it would therefore seem feasible for the transformers mutually to supply it. However, there is a complication: the two transformers have different impedances, $j6$ and $j8$ percent, respectively, and they will therefore *not* divide their loads in the proper ratio 1 : 1. Transformer $T1$ will, in effect, be overloaded; and $T2$ underloaded. We wish to see to what extent we can improve the load division *by manipulation of the transformer ratios.* Each transformer ratio can be varied from 90 to 110 percent of the nominal ratio $a^0 = 11/69$ in 32 discrete steps of 5/8 percent each. Clearly, this ratio change will

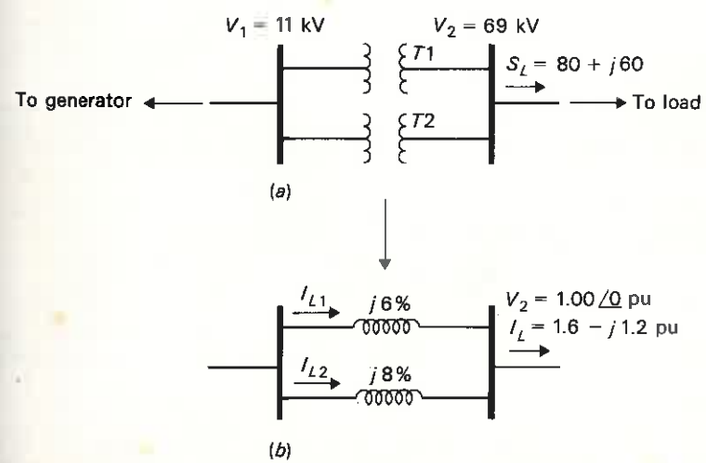

Figure 5-29 Parallel operation of transformers.

provide us with voltage *magnitude* control only, which of course right away puts constraints on us.

We approach this problem in the following manner:

1. We determine first the load division with no corrective action taken.
2. We make then appropriate tap changes, within the limits given, and investigate the effects on the load division.

1. Load division before ratio change For analysis purposes we represent the network portion in Fig. 5-29*a* by the equivalent diagram in Fig. 5-29*b*. We shall work with per-unit values and settle first for the following base values:

Power base = 50/3 MVA per phase
Voltage bases = $11/\sqrt{3}$ and $69/\sqrt{3}$ kV respectively

(The 69-kV bus voltage is also chosen as our reference phasor.)

The actual load is therefore

$$S_L = \tfrac{80}{50} + j\tfrac{60}{50} = 1.6 + j1.2 \text{ pu}$$

and since the 69-kV bus is held at 100 percent voltage, the corresponding load current, I_L, is calculated from

$$1.6 + j1.2 = 1.0 I_L^* \tag{5-47}$$

Hence

$$I_L = 1.6 - j1.2 \text{ pu} \tag{5-48}$$

This load current is divided between the two transformers as follows:

$$I_{L1} = \frac{j8}{j6 + j8} I_L = \tfrac{8}{14}(1.6 - j1.2) = 0.914 - j0.686 \text{ pu}$$

$$I_{L2} = \frac{j6}{j6 + j8} I_L = \tfrac{6}{14}(1.6 - j1.2) = 0.686 - j0.514 \text{ pu} \tag{5-49}$$

The two transformer load currents have, evidently, the rms ratio

$$\frac{|I_{L2}|}{|I_{L1}|} = \tfrac{6}{8} = 0.75 \tag{5-50}$$

instead of the desired ratio 1.00. Actually, since $|I_{L1}| = 1.14$ pu and $|I_{L2}| = 0.86$ pu, we note that transformer $T1$ would be 14 percent current overloaded, and transformer $T2$, 14 percent underloaded. This is an unacceptable situation which we now set out to correct.

2. Effects of ratio change What we will be doing, in effect, is *deliberately* making the ratios of the two transformers different. This results in a *circulating current* I_c in the two transformers, as explained in Fig. 5-30. First, we have the load currents that were computed above, and which would be the *only* transformer currents *if the transformation ratios were equal.* If, however, these ratios are set slightly different and in such manner that the secondary voltage of $T2$ would be somewhat *higher* than that of $T1$ then, upon closing the circuits in Fig. 5-30*a* (i.e., upon paralleling the transformers) circulating currents would flow† in primary and secondary wind-

† In reality a certain portion of this circulating current will also pass through the load. As the load shunt impedance is much greater than the transformer series impedance we neglect this portion. Note that I_c will flow even if the load is disconnected.

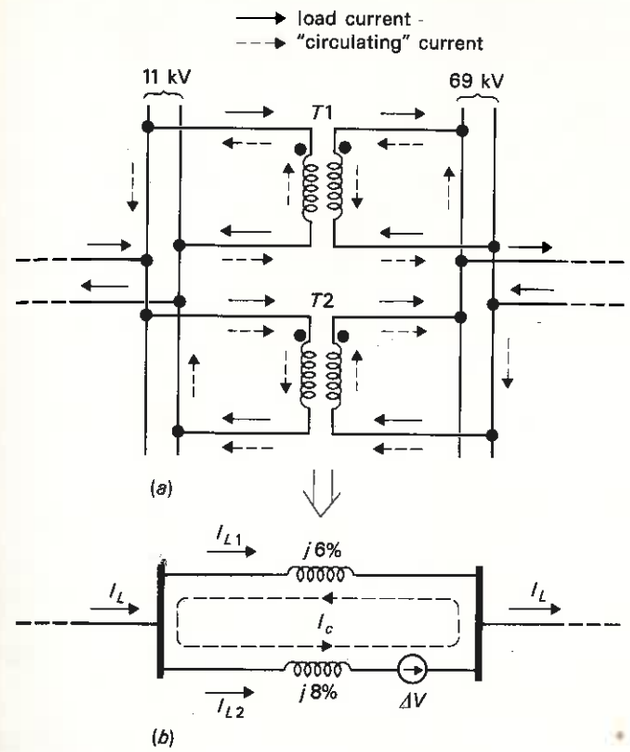

Figure 5-30 Tracing the circulating currents in parallel operated transformers of unequal ratios.

ings as indicated by dashed arrows. *Note that these currents will add to the load currents in T2 but subtract from them in T1.*

Figure 5-30*b* gives a simplified per-unit current picture. According to Thévenin the circulating current will follow from Eq. (5-45). The driving voltage, ΔV, is the difference between the (open-circuit) secondary voltages of $T2$ and $T1$, expressed in *per units.* If $T2$ is set at the nominal transformation ratio $a^0 = 11/69$ and $T1$ at the slightly higher ratio $a^0 + \Delta a$ then ΔV would equal

$$\Delta V = \frac{V_1}{a^0} - \frac{V_1}{a^0 + \Delta a} \approx \frac{V_1\,\Delta a}{(a^0)^2} \quad \text{V} \tag{5-51}$$

or, if expressed in per units,

$$\Delta V \approx \frac{\Delta a}{a^0} \quad \text{pu V} \tag{5-52}$$

From Fig. 5-30*b* we then get

$$I_c = \frac{\Delta V}{j0.14} = \frac{\Delta a/a^0}{j0.14} \quad \text{pu} \tag{5-53}$$

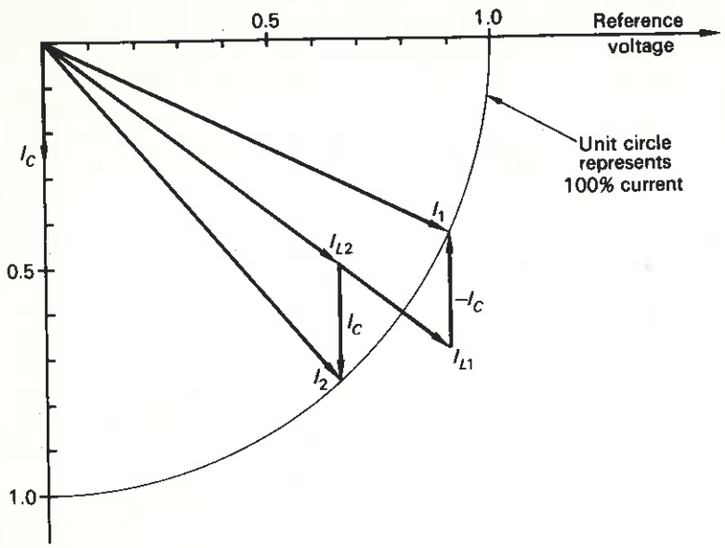

Figure 5-31 Graphical determination of circulating current.

Note that because ΔV is *in phase* with our reference voltage V_2 the current I_c will be lagging it by 90°. Upon using the superposition theorem we have from Fig. 5-30*b*

$$I_1 = I_{L1} - I_c \qquad I_2 = I_{L2} + I_c \tag{5-54}$$

We note that, since we can control I_c within certain limits, we may be able to arrange it so that these new transformer currents result in a better loading of the transformers.

In the current phasor diagram of Fig. 5-31, we have drawn to proper scale the currents I_{L1} and I_{L2} from Eqs. (5-49). The circle represents 1 pu current. A current phasor extending outside of this circle thus represents an *overloaded* transformer. By adding and subtracting the circulating current vector I_c to I_{L2} and from I_{L1}, respectively, in accordance with Eqs. (5-54), we find that the new currents I_1 and I_2 tend toward the circle from the outside and inside, respectively. By trial and error (or more sophisticated analysis if we wish), we find that if $|I_c|$ is chosen approximately equal to 0.25 pu, the currents I_1 and I_2 fall approximately on the circle.

From Eq. (5-53) we therefore get

$$\frac{\Delta a}{a^0} \approx 0.14 \times |I_c| = 0.14 \times 0.25 = 0.035 \text{ pu}$$

As the adjustments can be made only in 5/8 percent steps, the proper thing to do is to *increase* the ratio of transformer $T1$ in six steps for a total ratio increase of 0.0375 perunit. A still better solution would be to increase it only by three steps and *reduce* the ratio of transformer $T2$ by three steps. This would give the same ΔV as before, but also result in a 69-kV bus voltage closer to the required 100 percent. Why?

Having completed our solution, we make this observation: Since the phase angle of the circulating current I_c is either $\pm 90°$ relative to the voltage, we can control only the *reactive component* of the transformer current. This is tantamount to saying that we can control only the *reactive* power flow; the *real* power flow being beyond our control.

5-9 SUMMARY

In this chapter we have exposed the essential features of the power transformer to the extent that this device concerns the systems engineer. We have followed the same philosophy as we applied in our discussion of synchronous machines; relatively unimportant design details have been left out of our story.

The systems engineer is particularly interested in simple models of the transformer, and we have presented those equivalent diagrams that are of particular value in subsequent systems studies. Considerable emphasis has been put on the three-phase transformer and we have noted the pros and cons of Δ and Y connections. The per-unit system of analysis has been employed and it is demonstrated how, by use of a floating voltage base, the per-unit system can considerably simplify the analysis when transformers are involved.

The advantages and disadvantages of autotransformers have been pointed out. Considerable emphasis has been placed on the transformer as a control device. We have noted that phase-angle- and voltage-magnitude-regulating transformers can be used in controlling the routing of real and reactive power within the network. More will be said about this aspect of transformers in Chap. 7.

PROBLEMS

orrollam.

***5-1** A three-winding, 60-Hz, single-phase transformer has the voltage ratings

600/1200/10,000 V

The three windings are rated respectively

400, 100, 400 kVA

The transformer is fed from a 600-V source and loaded with a 15-Ω resistor on the 1200-V side, and a 260-Ω capacitor on the 10-kV side.

Use IT modeling and determine:

(*a*) All three winding currents

(*b*) Kilovoltampere loading in each winding

Is the transformer operated within limits?

***5-2** A single-phase transformer has the ratings

100 kVA, 60 Hz
13,200/200 V

Explain what would happen if, by mistake, the transformer were to be used at rated voltage but at 50 Hz.

***5-3** The transformer in Prob. 5-2 is by test found to have a core loss of 340 W and a leakage impedance of $0.0039 + j0.0612$ pu (based on ratings). If the transformer is loaded by a resistive load at what per-unit loading (compare Example 5-7) will it run at maximum efficiency?

***5-4** One has two identical 100 kVA transformers with data as described in Probs. 5-2 and 5-3. In working them in parallel one can transform 200 kVA of power. If the primary voltage is 13.4 kV and if the secondary load impedance equals $0.585 + j0.380\ \Omega$ determine:

(A) Total secondary load (kilowatts and kilovars)
(B) Total source load
(C) Secondary voltage

***5-5** If, in paralleling the two transformers in Prob. 5-4 one would accidentally use wrong polarity, by how many percent would each of the four windings be overloaded?

5-6 The U.S. Navy possesses a self-cooled transformer type, intended for use in arctic surroundings and having the ratings

500 kVA, 60 Hz
1000/500 V

What will be the new ratings of this transformer if used in tropical climate with the same voltage as before but at 50 Hz? Work with the following assumptions:

1. In the new installation we tolerate only 80 percent of the *total* losses accepted in the arctic installation.
2. In the original installation the total losses amounted to 0.5 percent of rated power and were distributed as follows:
   Copper losses 1.25 kW measured at 100 percent current
   Eddy current losses 0.625 kW } measured at 100 percent voltage
   Hysteresis losses 0.625 kW }
3. The hysteresis and eddy-current losses depend upon frequency f and maximum core flux density B_{max} according to these formulas:

$$P_{hyst} \sim f \cdot B_{max}^{1.6} \tag{5-55}$$

$$P_{ec} \sim f^2 \cdot B_{max}^2 \tag{5-56}$$

***5-7** A 500-kVA single-phase transformer has the voltage ratings 800/200 V. If you reconnect it for 800/1000 V to serve a 1-kV load, how many kilovoltamperes can it deliver?

5-8 Consider the 100-kVA two-winding transformer depicted in Fig. 5-23. We wish to connect it as an autotransformer. The two windings obviously can be connected together in four different ways, *only two of which are correct.*

Assume that we make the *wrong* connection. In the belief that we have a 1200/1000-V autotransformer, we connect our "autotransformer" to a 1200-V source.

(*a*) What voltage will we measure across the "1000-V" terminals?
(*b*) Explain the effect that our mistake will have on the device.

5-9 As power systems grow one sometimes finds a situation when in the same geographical area network branches of different voltage levels are getting close and one would wish to interconnect them to obtain "double feed" possibilities. Figure 5-32*a* shows two buses, *A* and *B*, which we would like to interconnect by a three-phase transformer *T*. The voltage levels of the two buses are 230 and 138 kV respectively, but there exists a 60° phase shift between them; the phase voltage of *A* leading that of *B* by 60°.

A 250-MVA, 230/138-kV Y-Y connected transformer is available (Fig. 5-32*b*). Can you reconnect its windings so that it could be used? Show the interconnection in full detail marking carefully polarities and phases. All six LV ends are accessible and fully insulated to ground.

5-10 Assume that the two 50-MVA transformers in Example 5-14 have different winding connections, one being Y-Y and the other Y-Δ connected. Their voltage ratings are still assumed to be equal (11/69 kV line-to-line). By mistake they are being parallel-connected. Employ Thévenin's theorem to find the magnitude of the currents (in per unit) that would circulate in the transformers.

5-11 A 230-kV three-phase line connects buses 1 and 2. The line has a reactance of 80 Ω per phase. When operated at 230 kV in each end the line, according to formula (3-52), can transmit a maximum of 661 MW between $1 \rightarrow 2$.

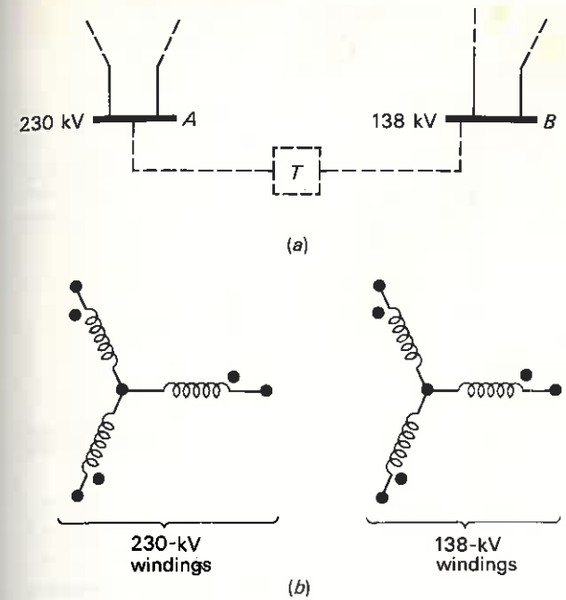

Figure 5-32 A connecting transformer.

A 230/138-kV transformer connects bus 2 with bus 3. If the latter bus is held at 138 kV what maximum power can be transmitted between buses $1 \rightarrow 3$

(*a*) if the transformer is "ideal"
(*b*) if we take the transformer leakage impedance into account, consisting of a reactance of 80 Ω/phase (referred to HV side)

Prove also that if we operate at maximum power in the latter case the voltage of bus 2 drops to 163 kV. Bus 1 is kept at 230 kV in all cases.

5-12 Refer to Example 5-12

(*a*) How much of the computed short-circuit current will flow via the 30-MVA transformer?
(*b*) Will it be current-overloaded?
(*c*) We wish to decrease the short-circuit current in the tertiary winding from the computed value of 9.28 pu to not more than 4.0 pu by placing series reactors between the 69-kV bus and the 69-kV winding of the three-winding transformer. Prove that this is not possible. Explain why.
(*d*) Prove that the objective of part (*c*) can be achieved by adding series reactors to the high-voltage terminals of the 30-MVA transformer *also*.
(*e*) Assume that we insert six identical reactors in accordance with parts (*c*) and (*d*). Compute the minimum reactance, expressed in ohms per reactor, needed to do the job.

***5-13** Two three-phase transformers of identical voltage ratings and winding connections are to be operated in parallel. Their power ratings are $|S_1|$ and $|S_2|$ respectively. Prove that they will share the common load in proper proportions only if their per-unit leakage impedances satisfy the relation

$$|Z_{pu\,1}| = |Z_{pu\,2}| \tag{5-57}$$

The pu impedances are based on $|S_1|$ and $|S_2|$, respectively.

5-14 For metering and relaying purposes one makes use of *current and potential transformers* (CT and PT, respectively) connected to the high-voltage bus to be monitored, as shown in Fig. 5-33. Answer the following questions in regard to these devices:

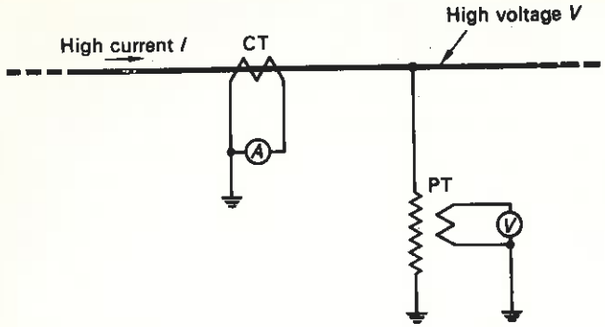

Figure 5-33 Potential and current transformers.

(*a*) If, as usual, we define the transformation ratio in accordance with Eq. (5-14) why is it normally true that

$$a \ll 1 \quad \text{for a CT}$$

$$a \gg 1 \quad \text{for a PT}$$

(*b*) Why should one strive to load a CT with as small, and a PT with as large, an impedance as possible?

(*c*) If a CT secondary is accidentally open circuited, the device will be momentarily destroyed, due to excessive core losses. If a PT secondary is accidentally short circuited, it will be destroyed due to excessive copper losses. Explain.

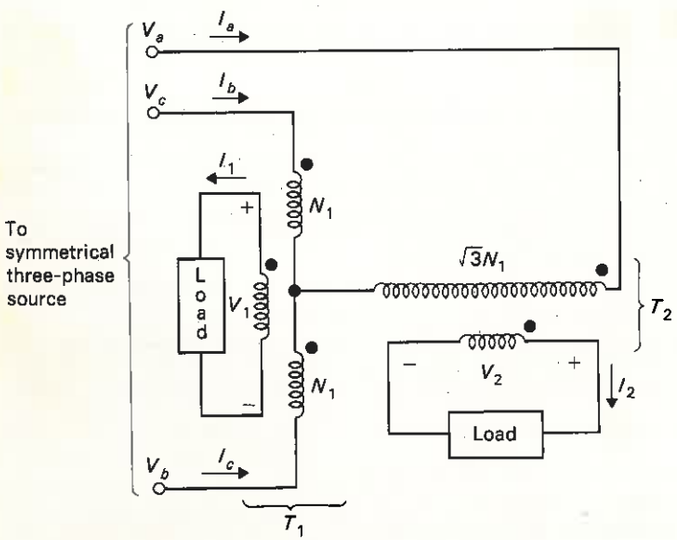

Figure 5-34 Scott-connected transformers.

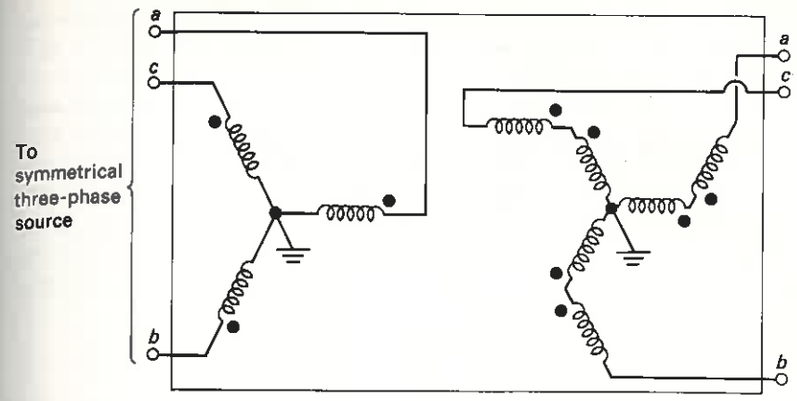

Figure 5-35 Zigzag connected transformer.

5-15 Figure 5-34 depicts two single-phase transformers T_1 and T_2 energized from a symmetrical three-phase source in a so-called "Scott connection." Each secondary has N_1 turns.

1. If the two primaries have $2N_1$ and $\sqrt{3}N_1$ turns respectively prove that both transformers operate with same VPT.
2. Assume that the three-phase source has a 5-kV line voltage. T_1 is unloaded whereas T_2 carries a 100-kW resistive load. Choose V_a as reference phasor and show phasors V_1, V_2, I_a, I_b, and I_c. What are the rms values of these voltages and currents?
3. With T_2 still loaded add a resistive load to T_1. Show that the three phase currents will form a symmetrical three-phase set if the load on T_1 is properly chosen. Find the load that will symmetrize the primary currents.

5-16 The three windings of a three-winding single-phase transformer are rated at 1000, 500, 500 volts respectively. Three such single-phase transformers are connected in "Y-Z" (or "zig-zag") as shown in Fig. 5-35.

1. Find the "three-phase transformation ratio" of this transformer.
2. Apply a load to one phase of the Z side (as was done in Fig. 5-19*a*). Prove that no ground current will flow on the Y side.

5-17 The 15-MVA hydrogenerator in Example 4-1 is connected to a remote 69-kV bus via a step-up transformer *T*1, a 115-kV transmission line, and a step-down transformer *T*2. The line has a reactance of 15 ohms per phase. The transformers *T*1 and *T*2 have the following data:

*T*1: 40 MVA, 13.6/115 kV, 7 percent leakage reactance
*T*2: 20 MVA, 115/69 kV, 8 percent leakage reactance
(The reactances are based upon respective ratings.)

The constant generator excitation level is $E = 1.31$ pu. The remote bus is kept at 69 kV. Find the maximum real power that can be transmitted. Would the generator be overloaded at maximum power transfer? Use generator model in Fig. 4-8.

REFERENCE

1. R. Feinberg: *Modern Power Transformer Practice*, John Wiley & Sons, New York, 1979.

CHAPTER

SIX

THE POWER TRANSMISSION LINE

6-1 INTRODUCTION

The transmission lines constitute the arteries of an electric energy system. The availability of a well-developed, high-capacity system of transmission lines makes it technically and economically feasible to move large blocks of electric energy over large distances. Electric transmission of bulk power can be accomplished either by alternating current or direct current with the line design falling in any one of the following categories:

1. Aerial lines
2. Underground cables
3. Compressed-gas insulated lines

The vast majority of the world's power lines are of three-phase aerial design with bare conductors and with the surrounding air serving as the insulating medium. Because of the dominance of aerial lines they will receive our main attention in this chapter.

The reader will recall the basic reasons for high voltage levels:

1. Reduction of losses—formulas (2-40) and (2-41)
2. Reduction of voltage drops—formula (2-43)
3. Increased power transmittability—formula (3-52)

Insulation requirements and, lately, possible health hazards set practical limits to the voltage level.

An overhead line is characterized by exposed magnetic and electric fields (Fig. 6-13). As the voltage level is increased, concern is being expressed that these fields may have damaging biological effects. In Fig. 6-1 are shown how these fields vary in magnitude at ground level under a 765-kV three-phase transmission line. As of this writing the experimental evidence in regard to the danger of these fields is inconclusive. However, it is probably safe to state that overhead voltage levels do in fact have a very definite practical upper limit.

In densely populated areas when aerial lines cannot be used for safety or other reasons, the power is transmitted in underground cables. Due to the proximity in a cable between the phase conductor and the outer grounded sheath the

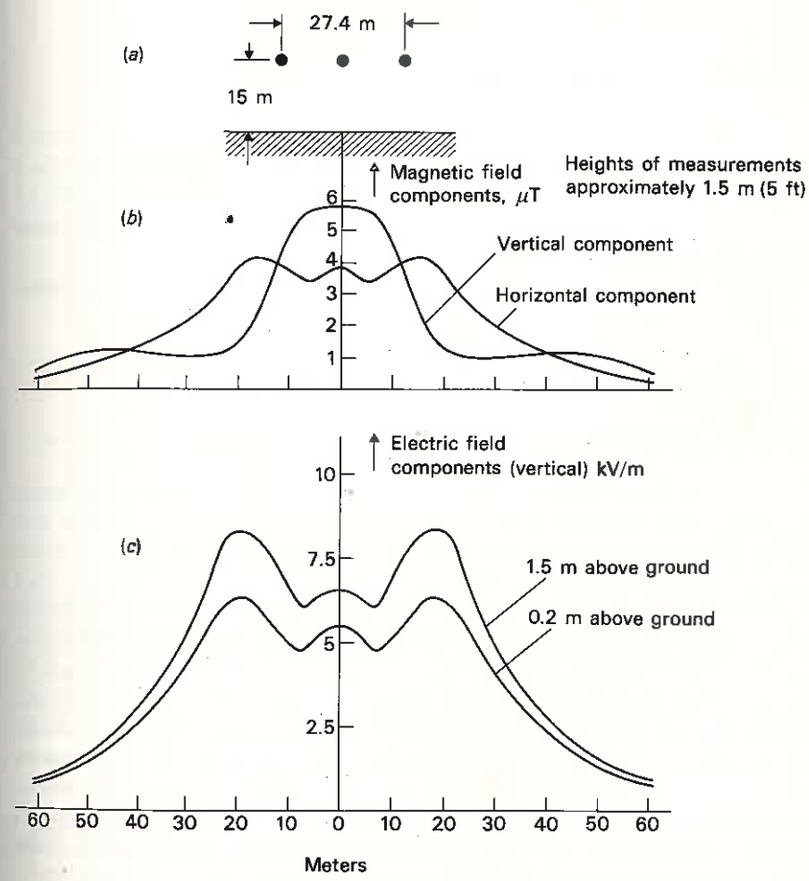

Figure 6-1 Magnetic and electric fields under 765-kV transmission line: (*a*) conductor geometry; (*b*) magnetic field; (*c*) electric field.
(*Source: IEEE Trans., vol. PAS-97, no. 1, 1978, pp. 8–16.*)

shunt capacitance is of very large magnitude giving rise to very excessive capacitive "leakage" currents (Prob. 6-1). Alternating-current cables, therefore, can be used only for relatively short transmission distances, seldom exceeding a few miles.

The capacitive leakage problem does not, of course, exist if high-voltage dc (HVDC) is employed. Underwater HVDC cables of lengths in excess of 100 km have been put in service (between Norway and Denmark). HVDC aerial transmission lines are also used. They are superior to ac lines when electric power must be wheeled over very large distances (> 1000 km).

Transmission lines using compressed gas for insulation find limited use for very short transmission distances mostly in power plants. As of this writing they are in the research and development stage.

6-2 DESIGN CONSIDERATIONS

Although copper has almost twice the conductivity of aluminum, the latter is almost exclusively used for today's conductors. Not only is it characterized by a weight and price advantage, but perhaps more important is the fact that an aluminum conductor has a larger diameter than a copper conductor of equivalent resistance and/or weight.

Figure 6-2 shows the electric field picture around three different conductor types:

(*a*) Single copper conductor
(*b*) Single aluminum conductor
(*c*) "Bundled" aluminum conductor

To make the three cases comparable, we have assumed that all are characterized by the same resistance and voltage (note the equal number of electric flux lines). The closeness of the flux lines at the conductor surface is a measure of the electric field intensity E. Note the decrease of E as we move from $a \rightarrow b \rightarrow c$. This results in less chance for *corona* in the latter cases. This phenomenon is a serious problem in high-voltage technology. It is caused by a breakdown or ionization of the atmosphere when a certain field intensity (≈ 3000 kV/m) is reached. Corona is associated with energy loss, will cause communication interference, and is generally not tolerated. For voltages in excess of about 230 kV it is in fact not possible to use a round single conductor. Instead of going to a hollow conductor, it is more practical to use bundle conductors of two, three, or several conductors per phase spaced about 30–40 cm apart. As we shall see, bundling of conductors also reduces to a considerable extent the line reactance, and therefore gives the added advantage of increased transmission capacity.

For the conductor sizes in use (diameter often exceeding 30 mm) it is not practical to use solid design. Flexible *aluminum-conductor steel-reinforced*

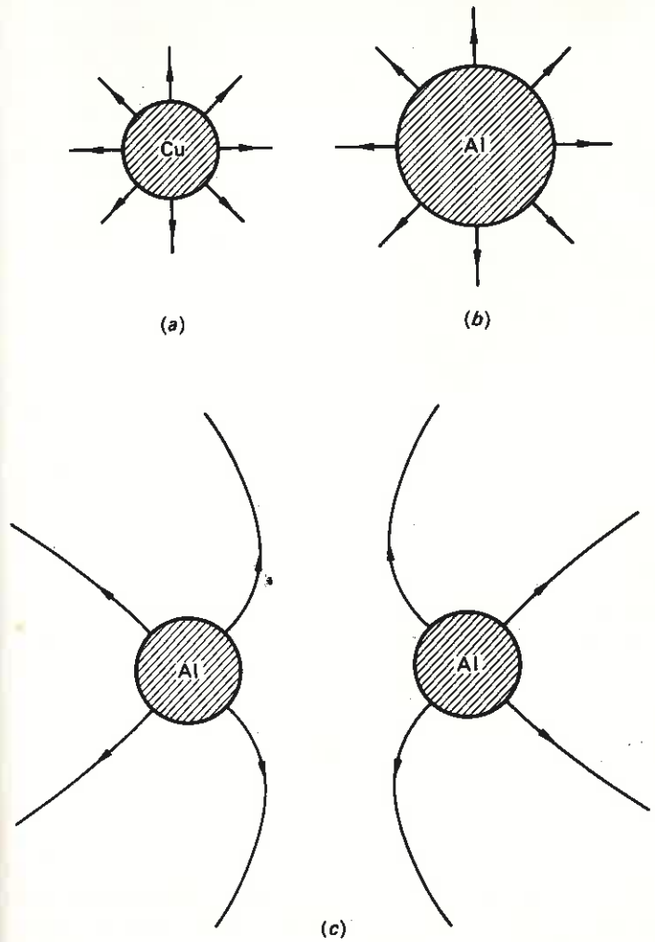

Figure 6-2 Comparison of electric field intensity at conductor surface for (*a*) single Cu conductor; (*b*) single Al conductor; (*c*) bundled Al conductors.

(ACSR) cables, consisting of a central core of *stranded* steel wires for the mechanical strength, surrounded by the current-carrying layers of aluminum strands, are the most common design. The conductors are suspended from the tower crossarms by flexible insulator strings.

Formula (2-40) informs that the cost for lost energy decreases with increased voltage level. However, the fixed costs of towers, insulators, right-of-way, etc., increase with voltage. As shown in Fig. 6-3 the total transmission costs will therefore be minimized at a certain voltage level. This "optimum economic voltage" increases with line length.

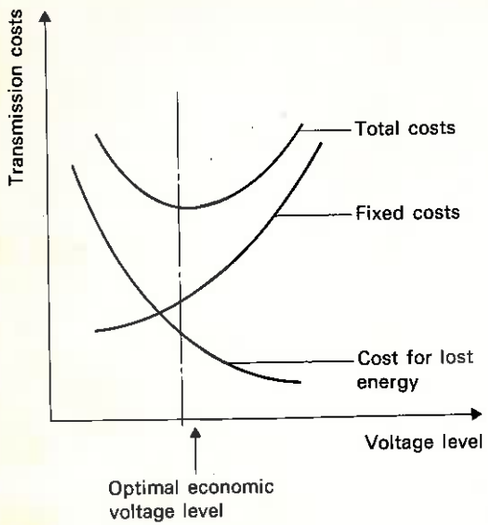

Figure 6-3 Economic choice of voltage level.

A systems engineer is interested primarily in the electric performance characteristics of the transmission line. These can be expressed in terms of the following four line parameters, listed in order of importance:

1. Line inductance
2. Line shunt capacitance
3. Line resistance
4. Line shunt conductance

We shall symbolize these parameters by L, C, R, and G, respectively, and shall in most practical cases express them per unit length (meter) and per phase of the transmission line. If the transmission line is unsymmetrical, it is in general not *theoretically* possible to express some of the parameters on a per-phase basis. However, if we tolerate some slight approximations, it can be done as a *practical* convenience. We shall comment on these matters as we proceed.

6-3 LINE RESISTANCE AND SHUNT CONDUCTANCE

The reason why we classify R and G as "least important" is that they affect the equivalent line impedances, and thus the transmission capacity, to a relatively unimportant degree. They do, of course, *completely* determine the real transmission *losses*, and to the extent that we are interested in the energy losses, we must consider their presence.

The *resistance* is obtained from the formula

$$R = \frac{\rho}{A} \quad \text{ohms per meter and phase} \tag{6-1}$$

where ρ = resistivity of conductor material, $\Omega \cdot$ m,† and A = effective conductor area, m^2. In conductors of ACSR type the most accurate resistance information is obtained from manufacturers' tables.

The resistance losses account for a temperature rise in the conductors that may in fact set a *thermal limit* to the current load (Sec. 3-4-1). High temperatures affect the sag between towers and cause also a loss of conductor tensile strength.

For example, the total electric blackout that hit New York City on July 13, 1977 was the result of several causes. An important contributing factor was the short circuit occurring between one 345-kV line conductor and a tree due to the excessive sag resulting from overheated conductors.

For the *shunt conductance* G there is no reliable formula. The shunt conductance accounts for the resistive leakage current between the phases and ground. This current flowing mainly along the insulator strings varies strongly with the weather, atmospheric humidity, pollution, and salt content. It is customary to neglect its presence under normal operating conditions, partly because it usually is of negligible magnitude, partly because of our ignorance.

6-4 LINE INDUCTANCE

The inductance L of a power line is by far the most important line parameter from a systems engineer's viewpoint. For normal line designs the corresponding reactance, $X = \omega L$, is the dominating impedance element due to its effect upon transmission capacity and voltage drop. It is important, therefore, that we give this parameter proper attention.

The simplest way to determine the inductance of a circuit is to first find its "linked" flux ϕ. The inductance is then computed from the flux linkage per ampere, i.e.,

$$L = \frac{\phi}{i} \quad \text{H} \tag{6-2}$$

In some instances (like inside a conductor) where the linked flux is hard to determine, it becomes easier to find the inductance by first computing the stored magnetic field energy w_{mf}, and then finding the inductance from formula (2-8). The magnetic field energy is stored in a magnetic field B in volume densities

† It should also be added that, because the conductors are of considerable size, the effective ac resistance will be somewhat higher than the dc value, due to "skin effect."

computed from the formula

$$\frac{dw_{mf}}{d\,(\text{volume})} = \frac{1}{2\mu\mu_0} B^2 \qquad \text{J/m}^3 \tag{6-3}$$

where $\mu_0 = 4\pi \times 10^{-7}$ = magnetic permeability of vacuum, and μ = relative magnetic permeability of medium in question.

In developing formulas for the line inductance (and also the capacitance) it is necessary to know accurately the magnetic (and electric) field geometries. Considering that the conductors are made up of mixed strands, that they are often sagging greatly between the towers, and that the line may traverse rough terrain whose electric and magnetic features are not well known, it should be understood from the outset that any models that we choose will be approximate at best. In view of these realities the following assumptions are reasonable, and test results confirm that they render acceptable accuracy:

1. The conductors are assumed straight, parallel, and of infinite length.
2. The conductors are cylindrical and their current densities are uniform.
3. The presence of earth will not affect the *magnetic* field and will therefore not affect inductance formulas.
4. The presence of earth will sometimes measurably affect the *electric* field, requiring that capacitance formulas be modified.

6-4-1 The Single-Phase Line

The single-phase transmission line serves as an appropriate point of departure in our analysis. In order to obtain general results, we assume the two conductors to have different radii, R_1 and R_2 (Fig. 6-4).

In computing the total inductance L per meter line, we shall distinguish between the inductance due to the magnetic field energy *inside* the conductors L_i and *outside* the conductors L_o. We then have

$$L = L_i + L_o \tag{6-4}$$

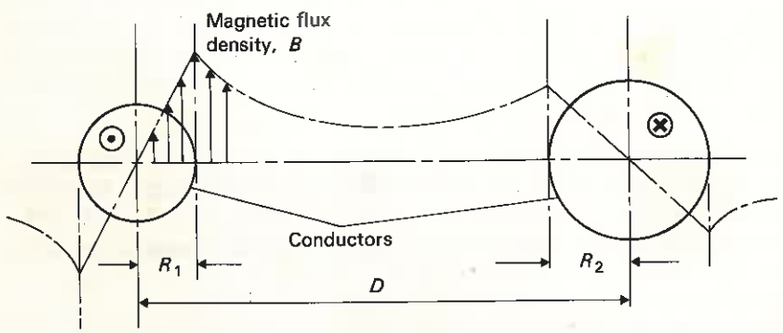

Figure 6-4 Magnetic flux density around conductors forming single-phase line.

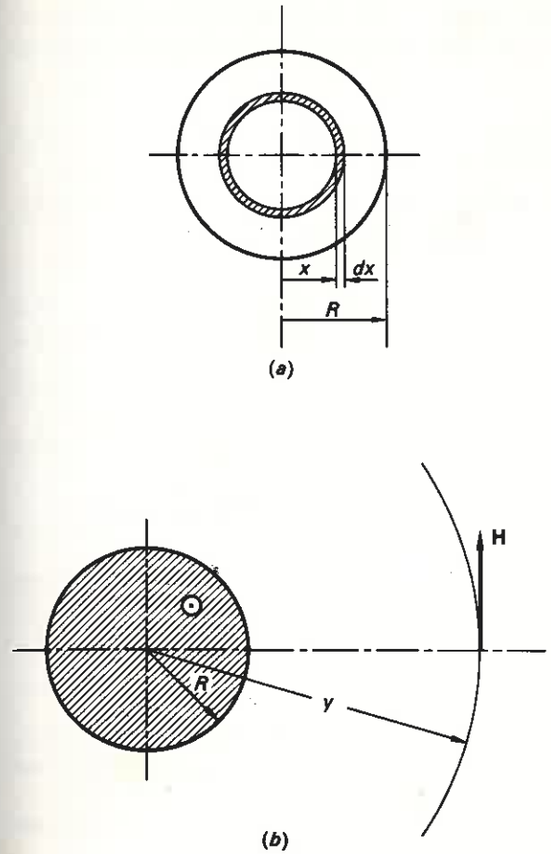

Figure 6-5 Finding the inside and outside magnetic flux densities in a cylindrical conductor.

6-4-2 Inside Inductance L_i

Consider a conductor of radius R (Fig. 6-5). If the total conductor current is i amperes, the current inside radius x, where $x < R$, will equal $(x/R)^2 i$. The magnetic field forms concentric circles and by performing a line integration $\int H\,dl$ around the circle of radius x, we thus obtain

$$H \cdot 2\pi x = \left(\frac{x}{R}\right)^2 i \tag{6-5}$$

Hence

$$B = \mu\mu_0 H = \mu\mu_0 \frac{x}{2\pi R^2} i \qquad \text{T} \tag{6-6}$$

i.e., the magnetic field intensity increases linearly with x, as shown in Fig. 6-4.

The volume element shown shaded in Fig. 6-5*a* has the volume $2\pi x\,dx$ per meter of line, and the total magnetic field energy inside the conductor is thus, in accordance with Eq. (6-3)

$$w_{mf} = \frac{\mu\mu_0}{2}\int_0^R \left(\frac{x}{2\pi R^2}i\right)^2 2\pi x\,dx = \frac{\mu\mu_0}{16\pi}i^2 \qquad \text{J/m} \tag{6-7}$$

Note that the stored energy is *independent of wire size*. For the *two* conductors in Fig. 6-4 the totally stored magnetic energy therefore equals

$$w_{mf} = \frac{\mu\mu_0}{8\pi}i^2 \qquad \text{J/m} \tag{6-8}$$

From Eq. (2-8) we thus have

$$\tfrac{1}{2}L_i i^2 = \frac{\mu\mu_0}{8\pi}i^2 \tag{6-9}$$

Hence, the internal inductance for the double conductor line equals

$$L_i = \frac{\mu\mu_0}{4\pi} \qquad \text{H/m} \tag{6-10}$$

6-4-3 Outside Inductance L_o

We could obtain the outside inductance in the same manner as we computed L_i. As this would lead to unwieldy integrals, it is *considerably* simpler to approach the problem by using formula (6-2).

We compute first the total *outside* magnetic flux ϕ_o inside the loop formed by the two conductors.

The magnetic flux lines due to the current in *one* conductor form concentric circles, as depicted in Fig. 6-5*b*. By performing a line integration around a circle of radius y, where $y > R$, we therefore obtain for the H contribution from the left conductor in Fig. 6-4

$$2\pi y \cdot H = i$$

The flux density due to the left conductor is therefore

$$B = \mu_0 H = \mu_0 \frac{i}{2\pi y} \qquad \text{T} \tag{6-11}$$

The total magnetic flux per meter of line between the two conductors due to the current in the left conductor is thus

$$\int_{R_1}^{D-R_2} \mu_0 \frac{i}{2\pi y}\,dy = \mu_0 \frac{i}{2\pi}\ln\frac{D-R_2}{R_1} \approx \mu_0\frac{i}{2\pi}\ln\frac{D}{R_1} \qquad \text{Wb/m} \tag{6-12}$$

The approximation in the last step is valid, since we usually have $D \gg R_2$. The total flux contributed by *both* conductor currents is finally obtained:

$$\phi_o = \mu_o\frac{i}{2\pi}\ln\frac{D}{R_1} + \mu_o\frac{i}{2\pi}\ln\frac{D}{R_2} = \mu_o\frac{i}{\pi}\ln\frac{D}{\sqrt{R_1R_2}} \qquad \text{Wb/m} \tag{6-13}$$

ϕ_o is the *linked* outside flux and from Eq. (6-2) we then have for the outside inductance

$$L_o = \frac{\mu_o}{\pi}\ln\frac{D}{\sqrt{R_1R_2}} \qquad \text{H/m} \tag{6-14}$$

6-4-4 Total Inductance L

Equation (6-4) finally yields the *total* inductance of the double conductor line

$$L = \frac{\mu_o}{\pi}\left(\frac{\mu}{4} + \ln\frac{D}{\sqrt{R_1R_2}}\right) \qquad \text{H/m} \tag{6-15}$$

Normally, the two conductors have equal radii, that is, $R_1 = R_2 = R$, and formula (6-15) then simplifies to

$$L = \frac{\mu_o}{\pi}\left(\frac{\mu}{4} + \ln\frac{D}{R}\right) \qquad \text{H/m} \tag{6-16}$$

For a nonmagnetic line ($\mu = 1$) we can rewrite the last formula in a simpler form:

$$L = \frac{\mu_0}{\pi}\left(\frac{1}{4} + \ln\frac{D}{R}\right) = \frac{\mu_0}{\pi}\left(\ln e^{1/4} + \ln\frac{D}{R}\right)$$

$$= \frac{\mu_0}{\pi}\ln\frac{D}{R_{eq}} \qquad \text{H/m} \tag{6-17}$$

where $R_{eq} \triangleq e^{-1/4}R = 0.7788\,R$.

Example 6-1 To get a feel for the orders of magnitude involved, let us compute the inductance of a nonmagnetic single-phase transmission line having the following data:

$$R = 0.5 \text{ cm}$$

$$D = 240 \text{ cm}$$

SOLUTION Equation (6-16) yields

$$L = 4\times10^{-7}\left(\frac{1}{4} + \ln\frac{240}{0.5}\right) = 4\times10^{-7}(0.250 + 6.174)$$

$$= 25.7\times10^{-7} \text{ H/m}$$

$$= 25.7\times10^{-4} \text{ H/km}$$

Multiplying by $\omega = 377$, we obtain the 60-Hz reactance

$$X = \omega L = 0.969\ \Omega/\text{km} \qquad (\text{or } 1.56\ \Omega/\text{mile})$$

It is interesting to note that, because of the relative "insensitivity" of the logarithmic function, a change of line dimensions will only slightly change the inductance. For example, a 100 percent increase of the conductor spacing D will result in only an 11 percent increase of the reactance in the case just given. Note also that the inside inductance contributes only about four percent to the total.

6-4-5 Concept of "Apparent" Inductance

As we extend the theory to three-phase lines it becomes analytically advantageous to split up the total or *loop* inductance L into self-inductances of each conductor plus the mutual inductance between them. Consider for a moment the inductive circuit shown in Fig. 6-6*a*, consisting of two magnetically coupled coils. The two coils are characterized by the self-inductances L_1 and L_2 respectively and the mutual inductance M_{12}. The magnetic polarity is indicated by the dot symbols. If we series-connect the coils and inject the current i, their inductive voltage drops Δv_1 and Δv_2 (polarities defined in the figure) will equal, respectively,

$$\Delta v_1 = L_1 \frac{di}{dt} - M_{12} \frac{di}{dt}$$
$$\Delta v_2 = L_2 \frac{di}{dt} - M_{12} \frac{di}{dt} \tag{6-18}$$

The total loop drop thus equals

$$\Delta v_1 + \Delta v_2 = (L_1 + L_2 - 2M_{12}) \frac{di}{dt} \tag{6-19}$$

The expression within parentheses represents the total inductance of the loop formed by the two coils. Had the magnetic polarity been the opposite to that shown in Fig. 6-6*a* then the last term would be positive.

Consider now the single-phase line shown in Fig. 6-6*b*. Its total loop inductance as given by formula (6-15) can be rewritten as follows:

$$L = \frac{\mu_0}{2\pi}\left[\left(\frac{\mu}{4} + \ln\frac{1}{R_1}\right) + \left(\frac{\mu}{4} + \ln\frac{1}{R_2}\right) - 2\ln\frac{1}{D}\right] \quad \text{H/m} \tag{6-20}$$

We define now the *apparent* self- and mutual inductances of the conductors

$$L_1 \triangleq \frac{\mu_0}{2\pi}\left(\frac{\mu}{4} + \ln\frac{1}{R_1}\right)$$
$$L_2 \triangleq \frac{\mu_0}{2\pi}\left(\frac{\mu}{4} + \ln\frac{1}{R_2}\right) \tag{6-21}$$
$$M_{12} \triangleq \frac{\mu_0}{2\pi}\ln\frac{1}{D}$$

In terms of these inductance parameters we can write the loop inductance of the line in the same form as for the two coupled coils, i.e.,

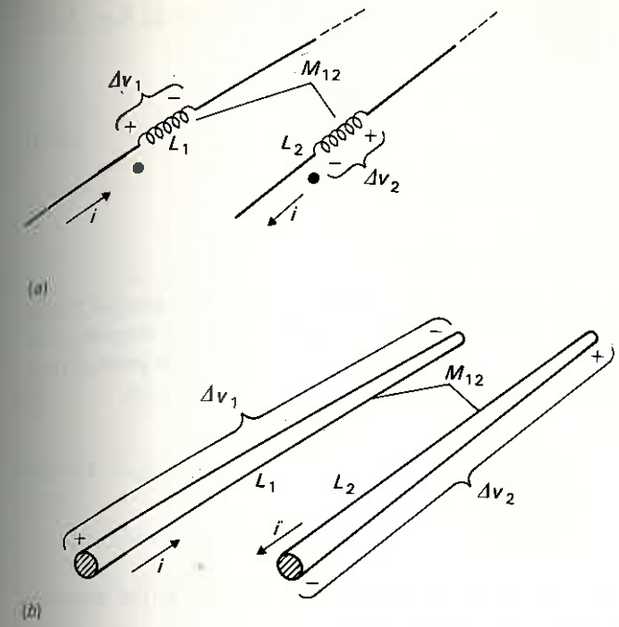

Figure 6-6 The single-phase line viewed as two magnetically coupled coils.

$$L = L_1 + L_2 - 2M_{12} \quad \text{H/m} \tag{6-22}$$

In viewing the line inductance from this point of view, we make the following observations:

1. The apparent inductances contain an "error of dimension," since the logarithmic arguments have the dimension $(\text{length})^{-1}$. They must therefore be considered individually as mathematical artifices that attain physical meaning only when appearing together, in which case the dimensionality error disappears.
2. The last term in Eq. (6-22) has a negative sign because the current directions in the wires are opposite.

The inductive voltage drops Δv_1 and Δv_2 (polarities defined in Fig. 6-6*b*) along one meter of each conductor in analogy with Eq. (6-18) are respectively

$$\Delta v_1 = L_1 \frac{di}{dt} - M_{12}\frac{di}{dt} = \frac{\mu_0}{2\pi}\left(\frac{\mu}{4} + \ln\frac{D}{R_1}\right)\frac{di}{dt} \quad \text{V/m}$$
$$\Delta v_2 = L_2 \frac{di}{dt} - M_{12}\frac{di}{dt} = \frac{\mu_0}{2\pi}\left(\frac{\mu}{4} + \ln\frac{D}{R_2}\right)\frac{di}{dt} \quad \text{V/m} \tag{6-23}$$

In most of the practical applications currents and voltages are sinusoidal. By

replacing v and i by the phasors V and I and d/dt by the operator $j\omega$, Eqs. (6-23) will then take on the form

$$\Delta V_1 = \frac{\mu_0}{2\pi} j\omega\left(\frac{\mu}{4} + \ln\frac{D}{R_1}\right)I$$
$$\Delta V_2 = \frac{\mu_0}{2\pi} j\omega\left(\frac{\mu}{4} + \ln\frac{D}{R_2}\right)I \qquad (6\text{-}24)$$

6-4-6 Extension to the n-Conductor Case

We extend now the concepts of "apparent" self-inductance and mutual inductance to the n-wire transmission line depicted in Fig. 6-7. It should be noted that the single- and three-phase lines are but special cases of this more general case. Taking a cue from Eqs. (6-21) we thus define

$$L_k = \frac{\mu_0}{2\pi}\left(\frac{\mu_k}{4} + \ln\frac{1}{R_k}\right) \quad \text{H/m}$$
$$M_{kl} = \frac{\mu_0}{2\pi}\ln\frac{1}{D_{kl}} \quad \text{H/m} \qquad (6\text{-}25)$$

L_k is the apparent self-inductance of conductor k, and M_{kl} is the apparent mutual inductance between the conductors k and l.

In terms of these "mathematical" inductances we can specify completely the inductive voltage drops in each of the n parallel conductors. Specifically, the inductive voltage drop Δv_k per meter of conductor k can be written, in analogy with Eq. (6-23):

$$\Delta v_k = L_k\frac{di_k}{dt} + \sum_{\substack{\nu=1\\ \nu\neq k}}^{n} M_{k\nu}\frac{di_\nu}{dt} \quad \text{V/m} \qquad (6\text{-}26)$$

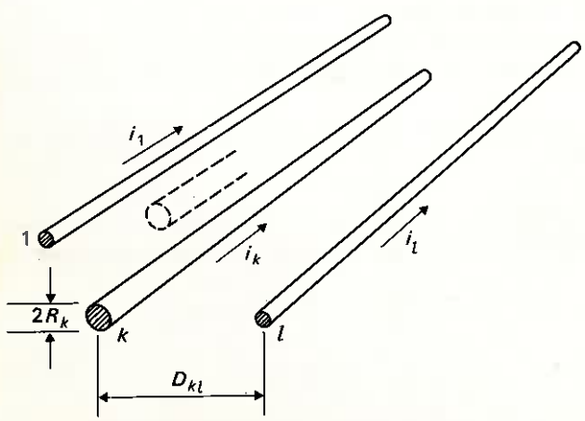

Figure 6-7 Multiconductor line.

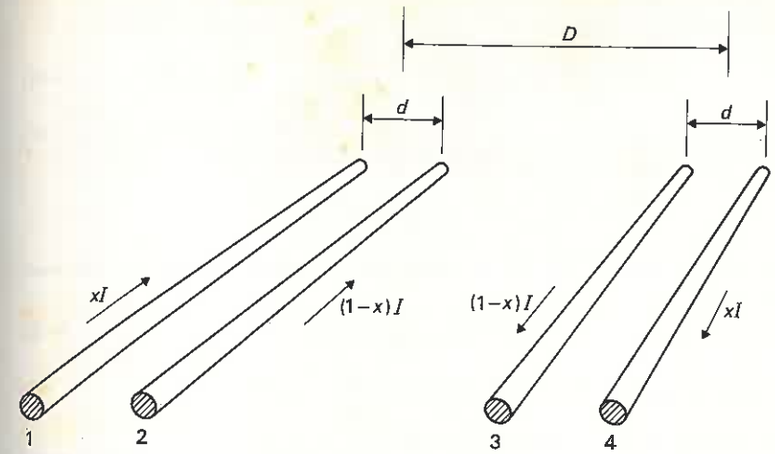

Figure 6-8 Single-phase 4-conductor line.

or, in the case of *sinusoidal* currents,

$$\Delta V_k = L_k\, j\omega I_k + \sum_{\substack{\nu=1\\ \nu\neq k}}^{n} M_{k\nu}\, j\omega I_\nu \quad \text{V/m} \qquad (6\text{-}27)$$

Note that all the mutually coupled voltage terms in these formulas have positive signs because we have assumed all currents positive in the same direction (Fig. 6-7).

Example 6-2 Four identical conductors form a "bundled" single-phase line (Fig. 6-8). The conductor pair of each bundle is held apart by conductive spacers. Find the inductance of the line.

SOLUTION We do not initially know how the total current I divides between the two conductors within each bundle. However, for symmetry reasons conductors 1 and 4 must carry equal current fraction xI. Conductors 2 and 3 carry the remaining fraction $(1-x)I$.

By use of Eq. (6-27) we find the inductive drops ΔV_1 and ΔV_2:

$$\Delta V_1 = j\omega\frac{\mu_0 I}{2\pi}\left[x\left(\frac{1}{4} + \ln\frac{1}{R}\right) + (1-x)\ln\frac{1}{d} - (1-x)\ln\frac{1}{D} - x\ln\frac{1}{D+d}\right]$$
$$= j\omega\frac{\mu_0 I}{2\pi}\left[x\ln\left(\frac{D+d}{R_{eq}}\right) + (1-x)\ln\frac{D}{d}\right] \quad \text{V/m}$$

Similarly

$$\Delta V_2 = j\omega\frac{\mu_0 I}{2\pi}\left[(1-x)\ln\left(\frac{D-d}{R_{eq}}\right) + x\ln\frac{D}{d}\right] \quad \text{V/m}$$

As ΔV_1 must equal† ΔV_2 we obtain

$$x\ln\left(\frac{D+d}{R_{eq}}\right) + (1-x)\ln\frac{D}{d} = (1-x)\ln\left(\frac{D-d}{R_{eq}}\right) + x\ln\frac{D}{d}$$

† We neglect resistance.

We solve this equation for x

$$x = \frac{\ln [d(D-d)/DR_{eq}]}{\ln [d^2(D^2-d^2)/D^2R_{eq}^2]} \tag{6-28}$$

If we can assume that $D \gg d$, Eq. (6-28) yields the simple and obvious result $x \cong 0.5$, informing us that the current divides equally. In this simple case we have

$$\Delta V_1 = \Delta V_2 = j\omega \frac{\mu_0}{2\pi} I \ln \frac{D}{\sqrt{dR_{eq}}}$$

The voltage drop in the return lead doubles the above value. The *total* line inductance will thus equal

$$L_{tot} = \frac{\mu_0}{\pi} \ln \frac{D}{\sqrt{dR_{eq}}} \quad \text{H/m} \tag{6-29}$$

In comparing formulas (6-17) and (6-29) we conclude that

(*a*) The bundling *reduces* the inductance.
(*b*) The bundled line yields the same reactance as a nonbundled line having a conductor radius $\sqrt{dR_{eq}}$.

6-4-7 Inductance Calculations for Three-phase Single-Conductor Lines

We now apply the above theory to some important three-phase line configurations. Presently we consider nonbundled designs.

Example 6-3 Our first case is the *phase-symmetric* case shown in Fig. 3-9a, having the conductors placed in the corners of an equilateral triangle of side D. The conductors all have radius R.

SOLUTION Using formula (6-27) we write first the expression for the inductive voltage drop along phase conductor a

$$\Delta V_a = \frac{\mu_0}{2\pi}\left(\frac{1}{4} + \ln \frac{1}{R}\right) j\omega I_a + \frac{\mu_0}{2\pi} \ln \frac{1}{D} j\omega I_b + \frac{\mu_0}{2\pi} \ln \frac{1}{D} j\omega I_c \tag{6-30}$$

In view of Eq. (3-7) the ΔV_a expression is simplified as follows:

$$\Delta V_a = \frac{\mu_0}{2\pi}\left(\frac{1}{4} + \ln \frac{1}{R}\right) j\omega I_a - \frac{\mu_0}{2\pi} \ln \frac{1}{D} j\omega I_a$$

$$= I_a \cdot j\omega \frac{\mu_0}{2\pi}\left(\frac{1}{4} + \ln \frac{D}{R}\right) \quad \text{V/m} \tag{6-31}$$

Similar expressions can be written for phases b and c. If summarized in vector form the three equations read

$$\begin{bmatrix} \Delta V_a \\ \Delta V_b \\ \Delta V_c \end{bmatrix} = j\omega \frac{\mu_0}{2\pi} \begin{bmatrix} \frac{1}{4} + \ln \frac{D}{R} & 0 & 0 \\ 0 & \frac{1}{4} + \ln \frac{D}{R} & 0 \\ 0 & 0 & \frac{1}{4} + \ln \frac{D}{R} \end{bmatrix} \begin{bmatrix} I_a \\ I_b \\ I_c \end{bmatrix} \tag{6-32}$$

or, in more compact form,

$$\Delta \mathbf{V}_p = j\omega \mathbf{L} \mathbf{I}_p \tag{6-33}$$

where $\mathbf{L}$ is the *inductance matrix* of the three-phase line. *In a phase-symmetric case, the inductance matrix is diagonal with identical diagonal elements.* Thus there exists total decoupling between phases, and in consequence, the line can be analyzed on a "per-phase" basis.

The per-phase inductance equals

$$L = \frac{\mu_0}{2\pi}\left(\frac{1}{4} + \ln \frac{D}{R}\right) \quad \text{H/m and phase} \tag{6-34}$$

which, interestingly, is half the value derived for the two-conductor case (Eq. 6-16).

Numerical case:

$$D = 5 \text{ m}$$

$$R = 1.5 \text{ cm}$$

$$f = 60 \text{ Hz}$$

$$\therefore \quad L = \frac{4\pi \times 10^{-7}}{2\pi}\left(\frac{1}{4} + \ln \frac{500}{1.5}\right) = 12.12 \times 10^{-7} \text{ H/m and phase}$$

The line reactance then follows:

$$X = \omega L = 377 \times 12.12 \times 10^{-7} = 4.569 \times 10^{-4} \ \Omega/\text{m} = 0.457 \ \Omega/\text{km and phase}$$

(or 0.735 Ω/mile).

From tables we find the ac resistance for this conductor to equal $R = 0.074$ Ω/km. The line reactance is therefore six times the resistance, confirming what we said earlier about relative size of R and X.

Example 6-4 In our next example we shall derive the inductance for a three-phase line having the phase conductors placed in a horizontal plane according to Fig. 6-9. In practice this is a fairly common conductor geometry.

SOLUTION For the sake of completeness we shall compare the *untransposed* and *transposed* cases depicted in Figs. 6-9*a* and *b* respectively.

Case A. Untransposed line Using Eq. (6-27) we obtain, for the voltage drop in phase a,

$$\Delta V_a = j\omega I_a \frac{\mu_0}{2\pi}\left(\frac{1}{4} + \ln \frac{1}{R}\right) + j\omega I_b \frac{\mu_0}{2\pi} \ln \frac{1}{D} + j\omega I_c \frac{\mu_0}{2\pi} \ln \frac{1}{2D} \quad \text{V/m} \tag{6-35}$$

By using the current relation (3-7) we can eliminate, for example, I_c from Eq. (6-35):

$$\Delta V_a = I_a j\omega \frac{\mu_0}{2\pi}\left(\frac{1}{4} + \ln \frac{2D}{R}\right) + I_b j\omega \frac{\mu_0}{2\pi} \ln 2 \quad \text{V/m} \tag{6-36}$$

If, in a similar fashion, we compute the voltage drops per meter of phases b and c, we get

$$\Delta V_b = I_b j\omega \frac{\mu_0}{2\pi}\left(\frac{1}{4} + \ln \frac{D}{R}\right) \tag{6-37}$$

$$\Delta V_c = I_c j\omega \frac{\mu_0}{2\pi}\left(\frac{1}{4} + \ln \frac{2D}{R}\right) + I_b j\omega \frac{\mu_0}{2\pi} \ln 2 \tag{6-38}$$

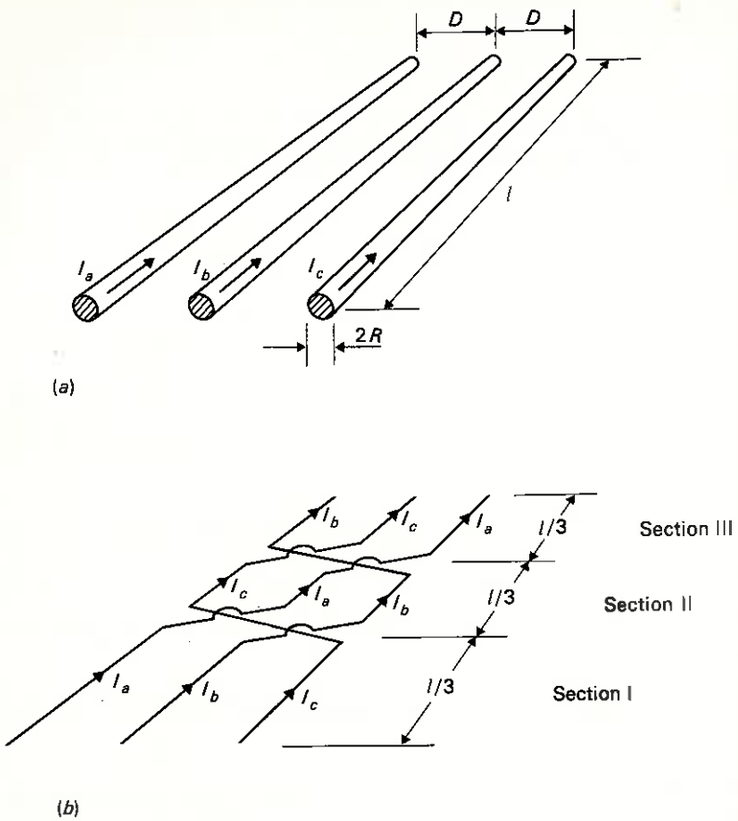

Figure 6-9 Three-phase transmission line with conductors placed in horizontal plane: (*a*) untransposed case; (*b*) transposed case.

We summarize the three last equations in vector form:

$$\begin{bmatrix} \Delta V_a \\ \Delta V_b \\ \Delta V_c \end{bmatrix} = j\omega \frac{\mu_0}{2\pi} \begin{bmatrix} \frac{1}{4} + \ln \frac{2D}{R} & \ln 2 & 0 \\ 0 & \frac{1}{4} + \ln \frac{D}{R} & 0 \\ 0 & \ln 2 & \frac{1}{4} + \ln \frac{2D}{R} \end{bmatrix} \begin{bmatrix} I_a \\ I_b \\ I_c \end{bmatrix} \tag{6-39}$$

Before we comment on this result we treat for comparison

Case B. The transposed (or phase-symmetrical) line We must now consider separately the three different sections of the line in Fig. 6-9*b*.

In section I we obtain the same voltage drops per meter and phase as stated by Eq. (6-39)

For sections II and III we can use the result (6-39) by simply transposing the variable subscripts in accordance with Fig. 6-9*b*, i.e., for Sec. II:

$$\begin{bmatrix} \Delta V_c \\ \Delta V_a \\ \Delta V_b \end{bmatrix} = j\omega \frac{\mu_0}{2\pi} \begin{bmatrix} \text{same as} \\ \text{in Eq. (6-39)} \end{bmatrix} \begin{bmatrix} I_c \\ I_a \\ I_b \end{bmatrix} \tag{6-40}$$

For Sec. III:

$$\begin{bmatrix} \Delta V_b \\ \Delta V_c \\ \Delta V_a \end{bmatrix} = j\omega \frac{\mu_0}{2\pi} \begin{bmatrix} \text{same as} \\ \text{in Eq. (6-39)} \end{bmatrix} \begin{bmatrix} I_b \\ I_c \\ I_a \end{bmatrix} \tag{6-41}$$

For the voltage drop in phase *a* we thus have

$$\begin{aligned} \Delta V_a &= \frac{\Delta V_a^{\mathrm{I}} + \Delta V_a^{\mathrm{II}} + \Delta V_a^{\mathrm{III}}}{3} \\ &= \frac{1}{3} \cdot j\omega \frac{\mu_0}{2\pi} \left\{ \left(\frac{1}{4} + \ln \frac{2D}{R}\right) I_a + \ln 2 I_b + \left(\frac{1}{4} + \ln \frac{D}{R}\right) I_a \right. \\ &\quad \left. + \ln 2 \cdot I_c + \left(\frac{1}{4} + \ln \frac{2D}{R}\right) I_a \right\} \\ &= \frac{1}{3} \cdot j\omega \frac{\mu_0}{2\pi} \left\{ 2\left(\frac{1}{4} + \ln \frac{2D}{R}\right) + \frac{1}{4} + \ln \frac{D}{R} - \ln 2 \right\} I_a \\ &= j\omega \frac{\mu_0}{2\pi} \left\{ \frac{1}{4} + \ln \left(\frac{\sqrt[3]{2}\,D}{R}\right) \right\} I_a \qquad \text{V/m} \end{aligned} \tag{6-42}$$

For ΔV_b and ΔV_c we derive symmetrical expressions

$$\Delta V_b = j\omega \frac{\mu_0}{2\pi} \left\{ \frac{1}{4} + \ln \left(\frac{\sqrt[3]{2}\,D}{R}\right) \right\} I_b \qquad \text{V/m} \tag{6-43}$$

$$\Delta V_c = j\omega \frac{\mu_0}{2\pi} \left\{ \frac{1}{4} + \ln \left(\frac{\sqrt[3]{2}\,D}{R}\right) \right\} I_c \qquad \text{V/m} \tag{6-44}$$

or by summarizing in matrix form

$$\begin{bmatrix} \Delta V_a \\ \Delta V_b \\ \Delta V_c \end{bmatrix} = j\omega \frac{\mu_0}{2\pi} \begin{bmatrix} \frac{1}{4} + \ln \left(\frac{\sqrt[3]{2}\,D}{R}\right) & 0 & 0 \\ 0 & \frac{1}{4} + \ln \left(\frac{\sqrt[3]{2}\,D}{R}\right) & 0 \\ 0 & 0 & \frac{1}{4} + \ln \left(\frac{\sqrt[3]{2}\,D}{R}\right) \end{bmatrix} \begin{bmatrix} I_a \\ I_b \\ I_c \end{bmatrix} \tag{6-45}$$

We pause here to make some observations and comparisons of the transposed and untransposed cases.

1. In the *transposed* line the inductance matrix is diagonal with identical diagonal elements, *thus permitting "per-phase" anaylsis.*
2. In the untransposed line the **L** matrix is *not* diagonal and consequently, in a strict sense, the inductive voltage drops will *not* possess three-phase symmetry even if the currents do.

It is interesting to see what this unsymmetry amounts to for a specific case. Let us, for demonstration purposes, assume

$$R = 1 \text{ cm}$$

$$D = 3 \text{ m}$$

For these specific conductor and spacing dimensions the two 3 × 3 matrices in Eqs. (6-45) and (6-39) take on the numerical values

$$\begin{bmatrix} 6.185 & 0 & 0 \\ 0 & 6.185 & 0 \\ 0 & 0 & 6.185 \end{bmatrix} \quad \text{and} \quad \begin{bmatrix} 6.647 & 0.693 & 0 \\ 0 & 5.954 & 0 \\ 0 & 0.693 & 6.647 \end{bmatrix} \quad \text{respectively}$$

We note that the coupling between the phases, as measured by the elements of value 0.693 in the second matrix, is relatively insignificant as compared with the elements along the main diagonal. Also, we note that these latter elements do not have too wide a spread and have an average value close to that of the transposed line. *For this reason we do not introduce too great an error if, even in the untransposed case, we treat the voltage drop on a per-phase basis.*

The inductance per phase in the transposed case will be

$$L = \frac{\mu_0}{2\pi} \times 6.185 = 12.37 \times 10^{-7} \text{ H/m}$$

and the 60 Hz reactance per phase

$$X = 377 \times 12.37 \times 10^{-4} = 0.466 \ \Omega/\text{km}$$

(or 0.750 Ω/mile).

6-4-8 Inductance Calculations for Bundled Three-Phase Lines

Figure 6-2 informed us that bundling of conductors reduces the risk for corona. As bundling essentially means adding parallel conductors we should also expect a reduction† in line reactance. In our next example we study the situation quantitatively.

Example 6-5 Find the line reactance for the three-phase line shown in Fig. 6-10. The transmission line has the same phase spacing D as the one in Fig. 6-9, but for reasons of reducing corona, we use two conductors per phase, placed the distance d apart. We will assume that the line is transposed.

SOLUTION In finding the inductive voltage drop in, say, phase a we can now consider either one of the two parallel conductors of that phase (we designate them 1 and 2 in Fig. 6-10). The voltage drops along either one will be the same, and we assume that each conductor carries half† the phase current. We choose conductor 1 and obtain the following expression for the voltage drop per meter in section I.

$$\Delta V_1 = \underbrace{j\omega \frac{I_a}{2}\frac{\mu_0}{2\pi}\left(\frac{1}{4} + \ln\frac{1}{R}\right)}_{1} + \underbrace{j\omega \frac{I_a}{2}\frac{\mu_0}{2\pi}\ln\frac{1}{d}}_{2} + \underbrace{j\omega \frac{I_b}{2}\frac{\mu_0}{2\pi}\ln\frac{1}{D}}_{3} + \underbrace{j\omega \frac{I_b}{2}\frac{\mu_0}{2\pi}\ln\frac{1}{D+d}}_{4}$$
$$+ \underbrace{j\omega \frac{I_c}{2}\frac{\mu_0}{2\pi}\ln\frac{1}{2D}}_{5} + \underbrace{j\omega \frac{I_c}{2}\frac{\mu_0}{2\pi}\ln\frac{1}{2D+d}}_{6} \quad \text{V/m} \qquad (6\text{-}46)$$

† Compare Example 6-2.

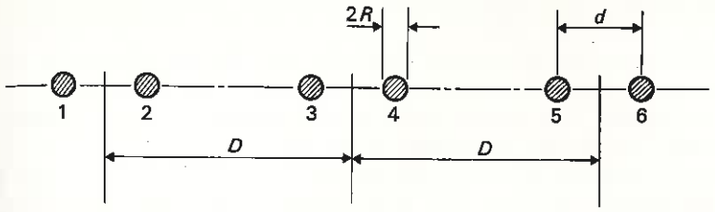

Figure 6-10 Same conductor geometry as in previous figure but with bundled conductor design.

The six terms in this expression represent the contributions to the total drop by the currents in the six conductors 1 to 6, respectively. Since $d \ll D$, we realize that terms 3 and 4 and also 5 and 6 are practically equal, and we can therefore reduce the expression to the following one:

$$\Delta V_1 \cong j\omega \frac{I_a}{2}\frac{\mu_0}{2\pi}\left(\frac{1}{4} + \ln\frac{1}{R} + \ln\frac{1}{d}\right) + j\omega I_b \frac{\mu_0}{2\pi}\ln\frac{1}{D} + j\omega I_c \frac{\mu_0}{2\pi}\ln\frac{1}{2D} \quad \text{V/m} \qquad (6\text{-}47)$$

If we now proceed to find the corresponding voltage drops in sections II and III, for the conductors occupying the positions 3 (or 4) and 5 (or 6), respectively, we get

$$\Delta V_3 \cong j\omega I_a \frac{\mu_0}{2\pi}\left(\frac{1}{8} + \ln\frac{D}{\sqrt{Rd}}\right) \quad \text{V/m} \qquad (6\text{-}48)$$

$$\Delta V_5 \cong j\omega \frac{I_a}{2}\frac{\mu_0}{2\pi}\left(\frac{1}{4} + \ln\frac{1}{R} + \ln\frac{1}{d}\right) + j\omega I_b \frac{\mu_0}{2\pi}\ln\left(\frac{1}{2D}\right) + j\omega I_c \frac{\mu_0}{2\pi}\ln\frac{1}{D} \quad \text{V/m} \qquad (6\text{-}49)$$

By taking the average of ΔV_1, ΔV_3, and ΔV_5, we obtain the total inductive voltage drop per meter in phase a

$$\Delta V_a = \frac{\Delta V_1 + \Delta V_3 + \Delta V_5}{3} = j\omega \frac{\mu_0}{2\pi} I_a \left[\frac{1}{8} + \ln\frac{\sqrt[3]{2}D}{\sqrt{Rd}}\right] \quad \text{V/m} \qquad (6\text{-}50)$$

The reactance per phase is, obviously,

$$X = \omega \frac{\mu_0}{2\pi}\left[\frac{1}{8} + \ln\frac{\sqrt[3]{2}D}{\sqrt{Rd}}\right] \quad \Omega/\text{m} \qquad (6\text{-}51)$$

It is interesting to see how this value compares numerically with the reactance value (0.466 Ω/km and phase) that we obtained for the single-conductor line in Fig. 6-9. We shall use the same phase spacing, $D = 3$ m and, to make the comparison meaningful, we shall assume the same conductor area per phase in both cases, which therefore means that we shall use

$$R = \frac{1}{\sqrt{2}} \times 1 = 0.707 \text{ cm}$$

Finally, let us assume a conductor spacing $d = 35$ cm. From Eq. (6-51) we now get

$$X = 377 \times \frac{4\pi \times 10^{-7}}{2\pi}\left[\frac{1}{8} + \ln\frac{\sqrt[3]{2} \cdot 300}{\sqrt{0.707 \times 35}}\right]$$
$$= 0.336 \ \Omega/\text{km and phase}$$

(or 0.541 Ω/mile and phase)

The bundling has therefore resulted in a 28 percent reduction of the line reactance, a circumstance that we appreciate, in view of the accompanying 39 percent increase in transmission capacity.

6-5 LINE CAPACITANCE

The line resistance and inductance constitute the elements that make up the *series* impedance of the transmission line.

The capacitance that we will now discuss, together with the conductance, forms the *shunt*, or *parallel*, admittance of the line.

The series elements, of which the inductance is the dominating one, set a limit to the current that can flow through the line and therefore physically determine the power transmittability. The parallel elements, of which the capacitance is the dominating one, represent a source for reactive power. The generated megavars are proportional to the square of the line voltage, and the importance of these shunt elements increases, therefore, with the magnitude of the operating voltage. For line voltages of the order 300 to 500 kV and line lengths in excess of 200 km, the impact of these shunt elements becomes of primary concern for the systems engineer. In a high-voltage *cable* the close proximity of the conductors results in a very large shunt capacitance, actually of the order of 20 to 40 times that of an aerial line. The reactive generation can then become a problem for cables only 1 km long.

6-5-1 Capacitance of Single-Phase Line

As in the case of the line inductance we find it convenient to start with a study of the capacitance of the single-phase line. We shall investigate two long parallel conductors (Fig. 6-11), which we initially shall consider very thin; indeed, we shall view them as "mathematical" lines. The conductors are charged with electric charges of opposite signs to the extent of $\pm Q$ C/m of conductor. Since it will serve our purpose, we shall first derive an expression for the electric potential v_P at an arbitrary point P located at a distance of r_1 and r_2 from the two wires, respectively. (Note that P is not necessarily located in the plane containing the two wires.)

Consider two opposite line elements of differential length dz. They may be considered as electric *point charges* containing the charges $\pm Q\,dz$, respectively. An elementary law of electric field theory states that the potential v at the distance r from a point charge q equals†

$$v = \frac{q}{4\pi\varepsilon_0 r} \quad \text{V} \tag{6-52}$$

where $\varepsilon_0 = 8.854 \times 10^{-12}$, dielectric constant for vacuum.

Since the distances from the line elements to the point P equal, respectively, $\sqrt{z^2 + r_1^2}$ and $\sqrt{z^2 + r_2^2}$, we obtain by summation for the potential in point P

$$v_P = \int_{-L}^{+L} \frac{Q\,dz}{4\pi\varepsilon_0\sqrt{z^2 + r_1^2}} + \int_{-L}^{+L} \frac{-Q\,dz}{4\pi\varepsilon_0\sqrt{z^2 + r_2^2}} \quad \text{V} \tag{6-53}$$

† q is in general a function of time. This applies to all variables introduced in this section.

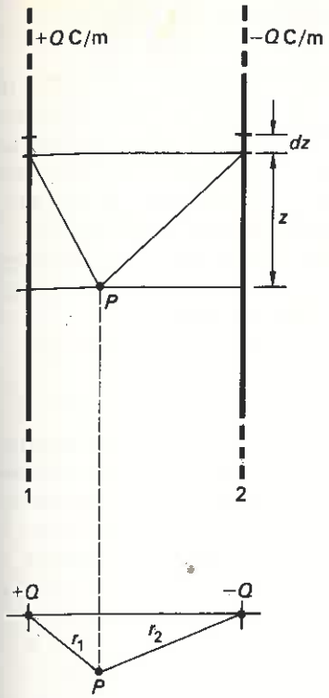

Figure 6-11 Finding the potential in vicinity of single-phase line.

We have integrated over the total line length $2L$. We shall later let L approach ∞. The integrals of Eq. (6-5) are easily evaluated, and upon substitution of the integration limits we get

$$v_P = \frac{Q}{4\pi\varepsilon_0} \ln \left[\frac{(L + \sqrt{L^2 + r_1^2})(-L + \sqrt{L^2 + r_2^2})}{(L + \sqrt{L^2 + r_2^2})(-L + \sqrt{L^2 + r_1^2})}\right] \quad \text{V} \tag{6-54}$$

If $L \to \infty$, the ratio $(L + \sqrt{})/(L + \sqrt{})$ clearly approaches 1, but the second ratio, $(-L + \sqrt{})/(-L + \sqrt{})$, takes on an indeterminate value, and we must therefore study it more carefully. We can write

$$\frac{-L + \sqrt{L^2 + r_2^2}}{-L + \sqrt{L^2 + r_1^2}} = \frac{-1 + [1 + (r_2/L)^2]^{1/2}}{-1 + [1 + (r_1/L)^2]^{1/2}}$$

$$= \frac{-1 + [1 + \frac{1}{2}(r_2/L)^2 + \cdots]}{-1 + [1 + \frac{1}{2}(r_1/L)^2 + \cdots]} = \left(\frac{r_2}{r_1}\right)^2 + \cdots$$

(terms which vanish with increasing L).

For $L \to \infty$, Eq. (6-54) therefore takes on the limit value

$$v_P = \frac{Q}{4\pi\varepsilon_0} \ln \left[1\left(\frac{r_2}{r_1}\right)^2\right] = \frac{Q}{2\pi\varepsilon_0} \ln \frac{r_2}{r_1} \quad \text{V} \tag{6-55}$$

We make several important observations in regard to this result:

1. The potential v_P is constant along contours for which the ratio r_2/r_1 is unchanging. From an important geometrical rule we know that these contours are the so-called *harmonic* circles, a few of which are sketched in Fig. 6-12. The *equipotential surfaces* (i.e., surfaces of same potential) thus are cylinders. (The electric *field* lines are orthogonal to the equipotential surfaces. They are also circles, some of which are shown dashed in Fig. 6-12.)
2. In close proximity to the line charges, the ratio r_2/r_1 is either very large or very small. Consider, for example, the immediate neighborhood of the positive wire. The ratio is now very large, and since we can write

$$\frac{r_2}{r_1} \approx \frac{D}{r_1} \qquad (D = \text{distance between wires})$$

we realize that v_P depends, approximately, only upon r_1, and *the equipotential surfaces adjacent to the conductor therefore form concentric cylinders with centers in the wire.* In Fig. 6-12 we have drawn in boldface one such surface of radius $r_1 = R_1$.

In the immediate neighborhood of the negative line charge we have

$$\frac{r_2}{r_1} \approx \frac{r_2}{D}$$

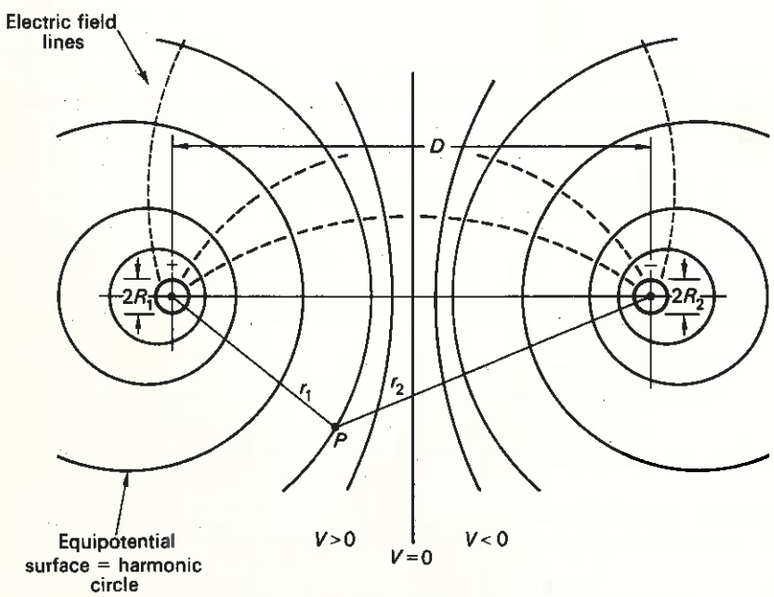

Figure 6-12 Electric field picture and equipotential surfaces around the line in Fig. 6-11.

and we conclude that, even here, the equipotential surfaces have the above-indicated features. In Fig. 6-12 we show one of radius $r_2 = R_2$.

3. The potential v_1 on the cylinder of radius R_1 equals, in accordance with Eq. (6-55)

$$v_1 \approx \frac{Q}{2\pi\varepsilon_0} \ln \frac{D}{R_1} \tag{6-56}$$

Likewise, for the potential v_2 on the cylinder of radius R_2, we have

$$v_2 \approx \frac{Q}{2\pi\varepsilon_0} \ln \frac{R_2}{D} \tag{6-57}$$

The potential *difference* between these two cylindrical surfaces is therefore

$$v_1 - v_2 \approx \frac{Q}{2\pi\varepsilon_0}\left(\ln \frac{D}{R_1} - \ln \frac{R_2}{D}\right) \approx \frac{Q}{\pi\varepsilon_0} \ln \frac{D}{\sqrt{R_1 R_2}} \tag{6-58}$$

4. From this last result we conclude that the voltage between very small cylinders (R_1 and $R_2 \to 0$) is of unlimited magnitude, and this fact, of course, means that line charges in reality are a physical absurdity (but still a mathematical convenience).
5. We can take physical wires of non zero radii R_1 and R_2 and place them so that their outer surfaces coincide with the surfaces shown in Fig. 6-12. If these wires are made of conducting material, we know that their outer surfaces constitute equipotential surfaces, and *the presence of these wires will therefore not change the field picture.*

   We draw from this fact the important conclusion that Eq. (6-58) indeed tells us the voltage between these wires.
6. The charge will in this latter case be found, not in the center of the wire, but rather on its surface. Since the field *outside* the conductor did not change by introducing the conductor, we conclude that the total surface charge of the wires still amounts to $\pm Q$ C/m.
7. Knowing the charge per meter conductor, Q, and the voltage between them, $v_1 - v_2$, we can obviously obtain the capacitance per meter simply from

$$C \triangleq \frac{Q}{v_1 - v_2} = \frac{Q}{(Q/\pi\varepsilon_0) \ln (D/\sqrt{R_1 R_2})} = \frac{\pi\varepsilon_0}{\ln (D/\sqrt{R_1 R_2})} \quad \text{F/m} \tag{6-59}$$

If the conductors have equal radii, $R = R_1 = R_2$, then the formula for the line capacitance will simply be

$$C = \frac{\pi\varepsilon_0}{\ln (D/R)} \tag{6-60}$$

Example 6-6 To get a feel for the magnitudes involved, consider the single-phase transmission line of Example 6-1 characterized by

$$D = 240 \text{ cm}$$

$$R = 0.5 \text{ cm}$$

Its capacitance will be

$$C = \frac{\pi \times 8.854 \times 10^{-12}}{\ln 480} = 4.51 \times 10^{-12} \text{ F/m}$$

Assume that the line is operated at 100 kV and 60 Hz. It will then have a total capacitive shunt *reactance* of

$$X_c = \frac{1}{\omega C} = \frac{1}{377 \times 4.51 \times 10^{-9}} = 5.88 \times 10^5 \ \Omega/\text{km}$$

At the assumed operating voltage the line will take a "charging" current of

$$\frac{100 \times 10^3}{5.88 \times 10^5} = 0.17 \text{ A/km}$$

and it will *generate* reactive power Q in the amount of†

$$Q = \frac{|V|^2}{X_c} = \frac{10^{10}}{5.88 \times 10^5} = 17000 \text{ var} \quad \text{or} \quad 17 \text{ kvar/km}$$

6-5-2 Influence of Earth

The field picture in Fig. 6-12 is valid only if the two wires are far removed from any other conductors, particularly the surface of earth. The presence of earth will change the electric flux lines and equipotential surfaces considerably, which in

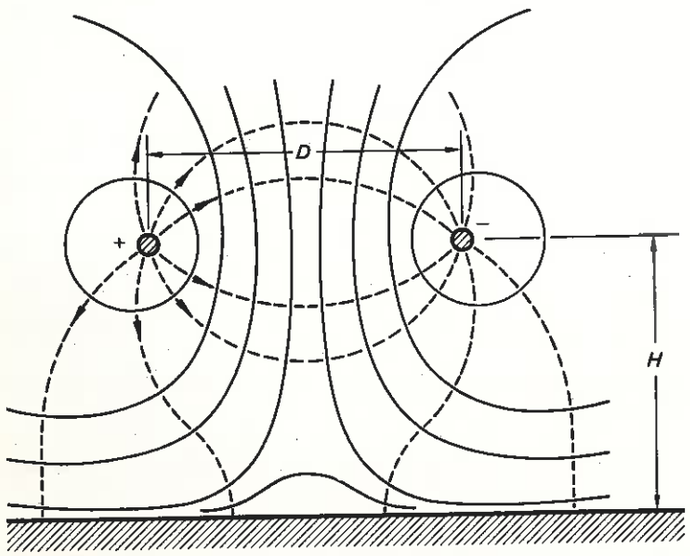

Figure 6-13 Influence of ground on the electric field picture.

† There is an unfortunate "symbol collision" between line charge Q and reactive power Q, which should not be confused.

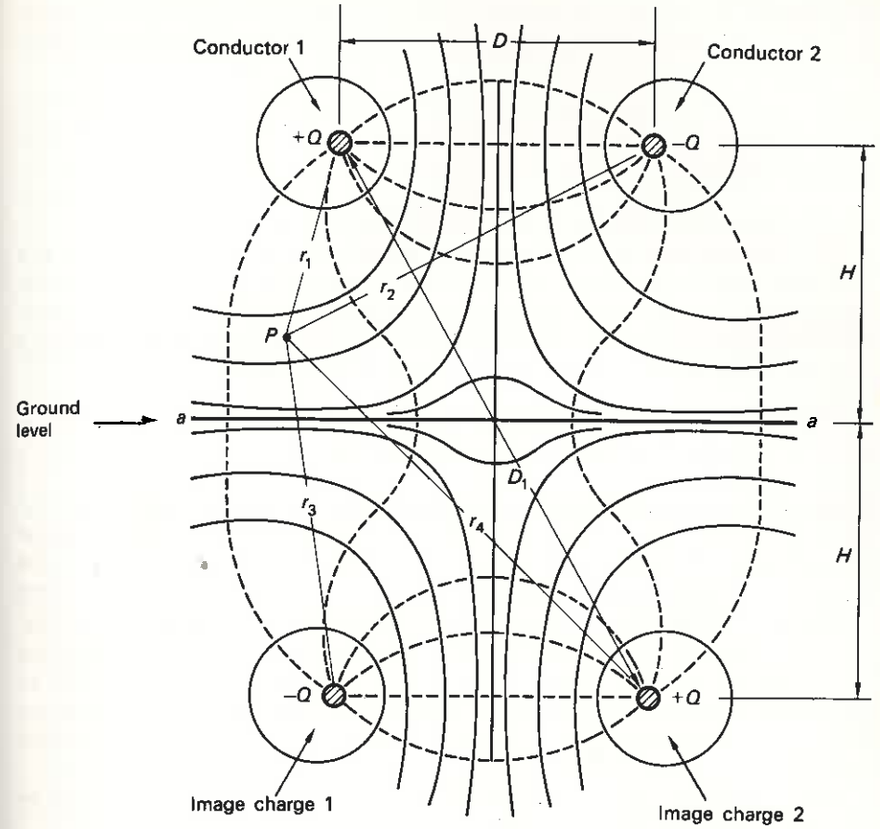

Figure 6-14 Using image charges to find the electric field above ground.

effect will change the effective capacitance between the wires. Since in the case of normal power lines the distances between the phases and between phases and ground are of the same order of magnitude, these effects cannot always be neglected. If the two conductors in Fig. 6-12 are placed over ground, the changes in the electric field picture are as demonstrated in Fig. 6-13. Note that the equipotential surfaces no longer are circular cylinders.

It turns out that the effect of the presence of ground can be accounted for in a very simple way by means of so-called *image charges*. These *imaginary* charges are of the same magnitude as the actual physical charges but of opposite sign, and placed as far underground as the actual charges are placed overhead. The situation is depicted in Fig. 6-14. In making use of this concept the following steps should be followed:

1. Place the image charges in proper location.
2. Remove the ground. Actual and image charges are now surrounded by air.

3. Compute the potential in a general point P by adding the contributions from *both* the actual and image charges. (How this is actually accomplished will be shown in the next section.)
4. The potential as computed in step 3 will, *for any point above the ground level*, be identical with the *actual* potential caused by the two actual charges plus the ground.

The proof of the validity of the above method is very simple:

The ground level is an equipotential surface in Fig. 6-13. In Fig. 6-14 the level *aa* is likewise an equipotential surface, for reasons of *symmetry*. In addition, the conductor configuration above the ground level being identical in both cases, the field configurations *above* this level *must* be the same, since there cannot be two different fields satisfying these same boundary conditions.†

6-5-3 Capacitance of Multiple Conductor Lines

If the effect of ground is taken into account, the two-wire problem evidently grows into a four-wire problem. Computing the capacitance for a three-phase line is clearly a three-wire problem, and if the effect of ground must be taken into account, a six-wire problem (including the three image charges). There is clearly a need here to expand our two-wire theory to include n parallel long conductors.

We remember that the line-inductance derivations valid for a single-phase line could be extended to an n-wire line by introduction of the concepts of "apparent self-inductance and mutual inductance." We can likewise extend our single-phase capacitance derivations to the n-wire case by use of similar concepts.

The potential v_P resulting from the two line charges $+Q$ and $-Q$ can, in accordance with Eq. (6-55), be written

$$v_P = \frac{Q}{2\pi\varepsilon_0} \ln \frac{1}{r_1} + \frac{-Q}{2\pi\varepsilon_0} \ln \frac{1}{r_2} \qquad \text{V} \tag{6-61}$$

The two individual terms in this expression are referred to as *logarithmic potentials*‡ and can be viewed as the individual contributions by each line charge to the total potential in point P.

We now consider a system of n parallel and very long conductors that carry the line charges $Q_1, Q_2, \ldots, Q_n$ C/m, respectively. A point P having the distances

† As is known from the theory of electric fields, the Laplace differential equation

$$\nabla^2 V = 0$$

has *one* solution only for given boundary conditions.

‡ Note that the logarithmic potential thus defined is characterized by the same error of dimension as we found in the case of "apparent inductance." As, in reality, the line charges *always* appear in pairs, this dimensionality error will automatically disappear.

$r_1, r_2, \ldots, r_n$ to the conductors in question has a potential v_P that contains contributions from each line charge, in accordance with the formula

$$v_P = \sum_{\nu=1}^{n} \frac{Q_\nu}{2\pi\varepsilon_0} \ln \frac{1}{r_\nu} \qquad \text{V} \tag{6-62}$$

It is understood that the algebraic sum of all the line charges, including those of the image charges, equals zero; i.e.,

$$\sum_{\nu=1}^{n} Q_\nu = 0 \tag{6-63}$$

If this were not true, we would have (because of the infinite length of the conductors) an infinite surplus of charge, which is physically impossible.

Example 6-7 In our first example on use of logarithmic potentials we shall recompute the capacitance of a single-phase line, taking account of the effect of ground. In the following analysis the symbols refer to those given in Fig. 6-14.

In accordance with Eq. (6-62) and by obeying rules 3 and 4 with respect to using the image charges, we obtain the following expression for the potential in a point P *above* ground level:

$$v_P = \frac{Q}{2\pi\varepsilon_0} \ln \frac{1}{r_1} + \frac{-Q}{2\pi\varepsilon_0} \ln \frac{1}{r_2} + \frac{-Q}{2\pi\varepsilon_0} \ln \frac{1}{r_3} + \frac{Q}{2\pi\varepsilon_0} \ln \frac{1}{r_4} \tag{6-64}$$

If, in particular, the point P is chosen on the surface of conductor 1, the potential v_P will equal v_1, and we get

$$v_1 = \frac{Q}{2\pi\varepsilon_0} \ln \frac{1}{R} - \frac{Q}{2\pi\varepsilon_0} \ln \frac{1}{D} - \frac{Q}{2\pi\varepsilon_0} \ln \frac{1}{2H} + \frac{Q}{2\pi\varepsilon_0} \ln \frac{1}{D_1} \tag{6-65}$$

If P is moved to the surface of conductor 2, we have

$$v_2 = \frac{Q}{2\pi\varepsilon_0} \ln \frac{1}{D} - \frac{Q}{2\pi\varepsilon_0} \ln \frac{1}{R} - \frac{Q}{2\pi\varepsilon_0} \ln \frac{1}{D_1} + \frac{Q}{2\pi\varepsilon_0} \ln \frac{1}{2H} \tag{6-66}$$

We thus get, after some algebra,

$$v_1 - v_2 = \frac{Q}{\pi\varepsilon_0} \ln \left(\frac{D}{R}\frac{2H}{D_1}\right) \tag{6-67}$$

and finally, for the capacitance,

$$C = \frac{Q}{v_1 - v_2} = \frac{\pi\varepsilon_0}{\ln \left(\frac{D}{R}\frac{2H}{D_1}\right)} \qquad \text{F/m} \tag{6-68}$$

The result should be compared with Eq. (6-60). Since $2H < D_1$, it is clear that the proximity to ground has resulted in an *increase* of the line capacitance.† Let us see the numerical effect by considering the line discussed in Example 6-6. We shall assume that the distance above ground, H, equals the spacing between the conductors; i.e., we have

$$H = D$$

† The reader should ask himself why, on physical ground, we get an increase.

and

$$D_1 = \sqrt{D^2 + 4H^2} = \sqrt{5D^2} = \sqrt{5}\,D$$

Since we had, in Example 6-6

$$\frac{D}{R} = 480$$

we now obtain

$$C = \frac{\pi\varepsilon_0}{\ln(480 \times 2/\sqrt{5})} = \frac{\pi 8.854 \times 10^{-12}}{6.062} = 4.59 \times 10^{-12}\ \text{F/m}$$

The presence of ground has thus resulted in two percent increase of the capacitance.

The relatively insignificant effect of the presence of earth demonstrated by this example gives us a good excuse to neglect it on most occasions.

6-5-4 Capacitance of Three-Phase, Single-Conductor Lines

We use now the developed theory to compute the shunt capacitance of a three-phase line. We start with a nonbundled line and for simplicity we ignore the influence of earth.

Example 6-8 Find the capacitance of the *phase-symmetric* three-phase line of Example 6-3.

SOLUTION Using Eq. (6-62) and letting, in turn, the point P coincide with the surface of the phase conductors a, b, and c we obtain

$$\begin{aligned} v_a &= \frac{Q_a}{2\pi\varepsilon_0}\ln\frac{1}{R} + \frac{Q_b}{2\pi\varepsilon_0}\ln\frac{1}{D} + \frac{Q_c}{2\pi\varepsilon_0}\ln\frac{1}{D} \\ v_b &= \frac{Q_a}{2\pi\varepsilon_0}\ln\frac{1}{D} + \frac{Q_b}{2\pi\varepsilon_0}\ln\frac{1}{R} + \frac{Q_c}{2\pi\varepsilon_0}\ln\frac{1}{D} \\ v_c &= \frac{Q_a}{2\pi\varepsilon_0}\ln\frac{1}{D} + \frac{Q_b}{2\pi\varepsilon_0}\ln\frac{1}{D} + \frac{Q_c}{2\pi\varepsilon_0}\ln\frac{1}{R} \end{aligned} \tag{6-69}$$

By making use of Eq. (6-63) the above three equations can be rewritten thusly:

$$\begin{aligned} v_a &= \frac{Q_a}{2\pi\varepsilon_0}\ln\frac{1}{R} - \frac{Q_a}{2\pi\varepsilon_0}\ln\frac{1}{D} = \frac{Q_a}{2\pi\varepsilon_0}\ln\frac{D}{R} \\ v_b &= \frac{Q_b}{2\pi\varepsilon_0}\ln\frac{1}{R} - \frac{Q_b}{2\pi\varepsilon_0}\ln\frac{1}{D} = \frac{Q_b}{2\pi\varepsilon_0}\ln\frac{D}{R} \\ v_c &= \frac{Q_c}{2\pi\varepsilon_0}\ln\frac{1}{R} - \frac{Q_c}{2\pi\varepsilon_0}\ln\frac{1}{D} = \frac{Q_c}{2\pi\varepsilon_0}\ln\frac{D}{R} \end{aligned} \tag{6-70}$$

or, in compact matrix form

$$\begin{bmatrix} v_a \\ v_b \\ v_c \end{bmatrix} = \frac{1}{2\pi\varepsilon_0}\begin{bmatrix} \ln\frac{D}{R} & 0 & 0 \\ 0 & \ln\frac{D}{R} & 0 \\ 0 & 0 & \ln\frac{D}{R} \end{bmatrix}\begin{bmatrix} Q_a \\ Q_b \\ Q_c \end{bmatrix} \tag{6-71}$$

By inversion, the last equations can also be written:

$$\begin{bmatrix} Q_a \\ Q_b \\ Q_c \end{bmatrix} = \frac{2\pi\varepsilon_0}{\ln(D/R)}\begin{bmatrix} 1 & 0 & 0 \\ 0 & 1 & 0 \\ 0 & 0 & 1 \end{bmatrix}\begin{bmatrix} v_a \\ v_b \\ v_c \end{bmatrix} \tag{6-72}$$

We conclude that the phase-symmetric line has complete "decoupling" between phases. Analysis can thus be performed on a "per-phase" basis. If the voltages constitute a symmetrical three-phase set so will the line charges, and also the charging currents.

The capacitance per phase equals

$$C = \frac{Q_a}{v_a} = \frac{Q_b}{v_b} = \frac{Q_c}{v_c} = \frac{2\pi\varepsilon_0}{\ln(D/R)} \quad \text{F/m} \tag{6-73}$$

The "charging current," expressed in amperes per meter line, in phase a is

$$i_a = \frac{dQ_a}{dt} = C\frac{dv_a}{dt} \quad \text{A/m} \tag{6-74}$$

If we assume *sinusoidally* varying voltages the last equation can be written

$$I_a = j\omega C V_a = j\frac{V_a}{1/\omega C} = j\frac{V_a}{X_c} \quad \text{A/m} \tag{6-75}$$

Numerical case Using the same line data as in Example 6-3 we obtain

$$C = \frac{2\pi \times 8.854 \times 10^{-12}}{\ln(500/1.5)} = 9.577 \times 10^{-12} \quad \text{F/m}$$

$$X_c = \frac{1}{\omega C} = \frac{1}{377 \times 9.577 \times 10^{-12}} = 2.770 \times 10^8 \quad \Omega/\text{m}$$

$$= 0.277\ \text{M}\Omega/\text{km}$$

For an assumed line voltage of 230 kV, i.e., a *phase* voltage of 132.8 kV, the charging current will be

$$I_a = \frac{132.8 \times 10^3}{0.277 \times 10^6} = 0.479 \text{ amperes per kilometer and phase}$$

which corresponds to a generated reactive power of $0.479 \times 132.8 = 63.7$ kvar or 191 kvar total three-phase per kilometer.

6-5-5 Capacitance of Bundled Three-Phase Line

We exemplify now the derivation of the shunt capacitance for bundled transmission lines. Again, for simplicity, we ignore influence of earth.

Example 6-9 Consider the 765-kV line having the conductor geometry depicted in Fig. 6-15. The line is designed with four conductors per phase. For the analysis to follow we shall assume that

$$D \gg d \gg R \tag{6-76}$$

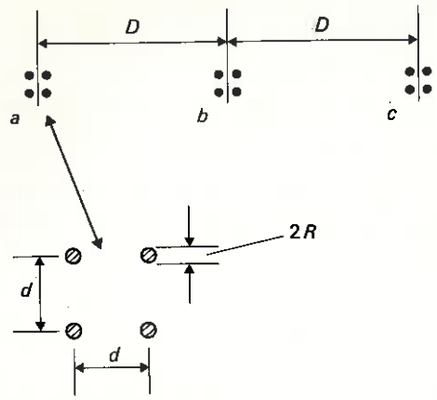

Figure 6-15 A 765-kV line with quadruple bundling of phase conductors.

We shall also assume that the line charge divides equally between the four conductors in each phase. Using Eq. (6-62) and placing the point P on the surface of one of the four conductors of phase a, we obtain:

$$v_a = \frac{Q_a/4}{2\pi\varepsilon_0}\ln\frac{1}{R} + 2\times\frac{Q_a/4}{2\pi\varepsilon_0}\ln\frac{1}{d} + \frac{Q_a/4}{2\pi\varepsilon_0}\ln\frac{1}{\sqrt{2}\,d} + \frac{Q_b}{2\pi\varepsilon_0}\ln\frac{1}{D} + \frac{Q_c}{2\pi\varepsilon_0}\ln\frac{1}{2D} \tag{6-77}$$

Upon making use of Eq. (6-63) we can write the last equation

$$v_a = \frac{1}{2\pi\varepsilon_0}\left[Q_a\ln\left(\frac{2^{7/8}D}{R^{1/4}\cdot d^{3/4}}\right) + Q_b\ln 2\right] \tag{6-78}$$

We similarly obtain for phases b and c

$$v_b = \frac{1}{2\pi\varepsilon_0}Q_b\ln\left(\frac{D}{R^{1/4}d^{3/4}2^{1/8}}\right)$$

$$v_c = \frac{1}{2\pi\varepsilon_0}\left[Q_b\ln 2 + Q_c\ln\left(\frac{2^{7/8}D}{R^{1/4}d^{3/4}}\right)\right] \tag{6-79}$$

It would be somewhat unwieldy to continue the analysis in generalized dimensions. We settle therefore at this stage for the following numerical values:

$$D = 12\text{ m}$$
$$d = 40\text{ cm}$$
$$R = 15\text{ mm}$$

Upon insertion of these numerical data into the last three equations they assume the form

$$\begin{bmatrix} v_a \\ v_b \\ v_c \end{bmatrix} = 10^{10}\begin{bmatrix} 8.680 & 1.246 & 0 \\ 0 & 7.433 & 0 \\ 0 & 1.246 & 8.680 \end{bmatrix}\begin{bmatrix} Q_a \\ Q_b \\ Q_c \end{bmatrix} \tag{6-80}$$

Inversion of the above matrix yields the following set of equations:

$$\begin{bmatrix} Q_a \\ Q_b \\ Q_c \end{bmatrix} = 10^{-11}\begin{bmatrix} 1.152 & -0.193 & 0 \\ 0 & 1.345 & 0 \\ 0 & -0.193 & 1.152 \end{bmatrix}\begin{bmatrix} v_a \\ v_b \\ v_c \end{bmatrix} \tag{6-81}$$

or, in more compact notation,

$$\mathbf{Q} = \mathbf{C}\cdot\mathbf{v} \tag{6-82}$$

We note that the *capacitance matrix* C is not diagonal, thus making "per-phase" analysis slightly approximative.

Just as transposition diagonalized the L matrix (Example 6-4) so it will also make the C matrix diagonal. Let Q^{I}, Q^{II}, and Q^{III} respectively represent the line charges in the three transposed sections shown in Fig. 6-9*b*. In accordance with Eq. (6-81) we can thus write for phase a

$$\begin{aligned} Q_a^{\mathrm{I}} &= 10^{-11}\times(1.152v_a - 0.193v_b) \\ Q_a^{\mathrm{II}} &= 10^{-11}\times 1.345v_a \\ Q_a^{\mathrm{III}} &= 10^{-11}\times(1.152v_a - 0.193v_c) \end{aligned} \tag{6-83}$$

By adding these equations and recalling that $v_a = -(v_b + v_c)$ we obtain

$$Q_a^{\mathrm{ave}} = \frac{Q_a^{\mathrm{I}} + Q_a^{\mathrm{II}} + Q_a^{\mathrm{III}}}{3} = 10^{-11}\times 1.281v_a \tag{6-84}$$

Identical expressions can be derived for phases b and c. In summary, the transposed line can be characterized by the vector equation

$$\begin{bmatrix} Q_a^{\mathrm{ave}} \\ Q_b^{\mathrm{ave}} \\ Q_c^{\mathrm{ave}} \end{bmatrix} = 10^{-11}\begin{bmatrix} 1.281 & 0 & 0 \\ 0 & 1.281 & 0 \\ 0 & 0 & 1.281 \end{bmatrix}\begin{bmatrix} v_a \\ v_b \\ v_c \end{bmatrix} \tag{6-85}$$

The transposed line thus has a capacitance of

$$C = \frac{Q^{\mathrm{ave}}}{v} = 1.281\times 10^{-11}\text{ F per phase and meter}$$

This corresponds to a 60-Hz shunt reactance of magnitude

$$X_c = \frac{1}{\omega C} = \frac{1}{377\times 1.281\times 10^{-11}} = 0.207\times 10^9\ \Omega\text{ per meter and phase}$$

or 0.207 MΩ per kilometer and phase.

If the line is operated at rated voltage of 765 kV the line will generate

$$\frac{765^2}{0.207\times 10^6} = 2.83\text{ Mvar/km (total 3-phase)}$$

6-6 LONG-LINE THEORY

The line parameters presented in preceding sections were derived on a per-phase basis and were obtained per meter of the line. It would seem reasonable, therefore, if we are interested in the performance of a specific line of length l, simply to multiply these parameters by the actual line length in order to obtain the total parameter values for the line. This can indeed be done for short lines. In the case of longer lines, the accuracy of this procedure becomes impaired because of our neglect of the *distributed* effect of the parameters. In this section we shall study this "distribution effect" of the line. We shall develop exact models for lines of arbitrary length, and also approximate models valid under specified conditions.

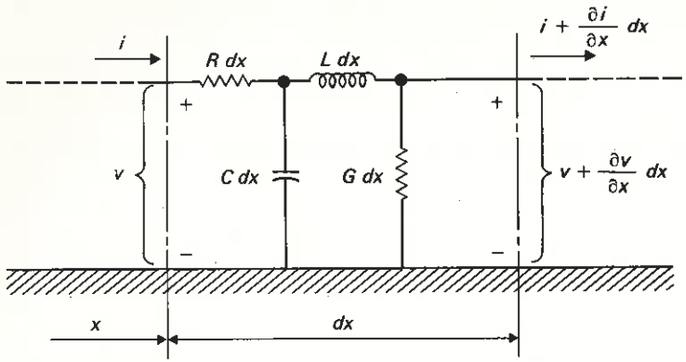

Figure 6-16 Differential section of long continuous-parameter line.

Consider a very long single-conductor line strung above earth. On a per-meter basis the line has the series parameters R and L and the shunt parameters G and C, the latter relative to ground. A differential section of the line may be represented by the four differential circuit elements shown in Fig. 6-16.

The coordinate x defines the position along the line counted from the sending end. The voltage and current along the line are functions of *both* x and time t and should therefore strictly be symbolized $v(x, t)$ and $i(x, t)$ respectively. For brevity we will use the shorter symbols v and i respectively.

In the short distance dx the voltage will change with the amount

$$\frac{\partial v}{\partial x}\,dx \qquad \text{V}$$

This change is due to the resistive and the inductive drops along section dx. We express this mathematically thusly:

$$v - \left(v + \frac{\partial v}{\partial x}\,dx\right) = \left(Ri + L\frac{\partial i}{\partial t}\right)dx$$

Similarly, we can express the change in current resulting from the leakage across the two shunt elements

$$i - \left(i + \frac{\partial i}{\partial x}\,dx\right) = \left(Gv + C\frac{\partial v}{\partial t}\right)dx$$

We can reduce these two equations to the simpler pair

$$\begin{aligned} -\frac{\partial v}{\partial x} &= Ri + L\frac{\partial i}{\partial t} \\ -\frac{\partial i}{\partial x} &= Gv + C\frac{\partial v}{\partial t} \end{aligned} \tag{6-86}$$

6-6-1 Long-line Equations in the Sinusoidal Case

In Chap. 10 the partial differential equation pair (6-86) will guide us to an understanding of the *traveling wave phenomena* on transmission lines during lightning strikes and other abnormal situations. Presently we shall use the equations to study the line performance under steady state when voltage and current both are *sinusoidal* functions of time.

At the same time we shall interpret the model in Fig. 6-16 to represent one phase of a *symmetric* three-phase line. R, L, G, and C thus represent the earlier studied "per-phase" parameters of the line, and v and i represent voltage to ground and phase current respectively. In sinusoidal steady state the latter will be of the form

$$\begin{aligned} v &= V(x)e^{j\omega t} \\ i &= I(x)e^{j\omega t} \end{aligned} \tag{6-87}$$

$V(x)$ and $I(x)$ are phasors which are functions of the space variable x only.

For the partial derivatives we obtain:

$$\begin{aligned} \frac{\partial v}{\partial t} &= j\omega V(x)e^{j\omega t} \\ \frac{\partial i}{\partial t} &= j\omega I(x)e^{j\omega t} \end{aligned} \tag{6-88}$$

and

$$\begin{aligned} \frac{\partial v}{\partial x} &= \frac{dV(x)}{dx}e^{j\omega t} \\ \frac{\partial i}{\partial x} &= \frac{dI(x)}{dx}e^{j\omega t} \end{aligned} \tag{6-89}$$

By substitution of (6-87) and (6-89) into Eqs. (6-86) we obtain

$$\begin{aligned} -\frac{dV(x)}{dx} &= (R + j\omega L)I(x) \\ -\frac{dI(x)}{dx} &= (G + j\omega C)V(x) \end{aligned} \tag{6-90}$$

Note that the *partial* differential equations (6-86) now have turned into *ordinary* differential equations.

By separation of variables we obtain the following "long-line" differential equations for $V(x)$ and $I(x)$:

$$\frac{d^2V(x)}{dx^2} = (R + j\omega L)(G + j\omega C)V(x)$$
$$\frac{d^2I(x)}{dx^2} = (R + j\omega L)(G + j\omega C)I(x) \tag{6-91}$$

We introduce at this juncture the *propagation constant* γ and *wave* (or *surge*) *impedance* Z_w, defined as follows:

$$Z_w \triangleq \sqrt{\frac{R + j\omega L}{G + j\omega C}} \qquad \text{(dimension = ohms)}$$
$$\gamma \triangleq \sqrt{(R + j\omega L)(G + j\omega C)} \qquad \text{(dimension = } m^{-1}\text{)} \tag{6-92}$$

In terms of these parameters we can now write the differential equations (6-91) in shorter form

$$\frac{d^2V}{dx^2} = \gamma^2 V$$
$$\frac{d^2I}{dx^2} = \gamma^2 I \tag{6-93}$$

6-6-2 Solution of Differential Equations

Equations (6-93) are easily integrated. The reader can, by back substitution, confirm that the general solutions are of the form

$$V(x) = C_1 \cosh \gamma x + C_2 \sinh \gamma x$$
$$I(x) = C_3 \cosh \gamma x + C_4 \sinh \gamma x \tag{6-94}$$

Of the four integration constants $C_1 \cdots C_4$ only *two* can be chosen independently, because the *original* equations (6-90) are *two first*-order differential equations. We find it convenient to express $V(x)$ and $I(x)$ in terms of $V(0)$ and $I(0)$, i.e., the voltage and current at the sending end.

By setting $x = 0$ in the above equations we obtain

$$V(0) = C_1 \cdot 1$$
$$I(0) = C_3 \cdot 1$$

Hence

$$C_1 = V(0)$$
$$C_3 = I(0) \tag{6-95}$$

To find C_2 and C_4 we substitute the solutions (6-94) into the original equations (6-90):

$$C_1\gamma \sinh \gamma x + C_2\gamma \cosh \gamma x = -(R + j\omega L)(C_3 \cosh \gamma x + C_4 \sinh \gamma x)$$
$$C_3\gamma \sinh \gamma x + C_4\gamma \cosh \gamma x = -(G + j\omega C)(C_1 \cosh \gamma x + C_2 \sinh \gamma x)$$

By setting $x = 0$ in the last equations we get:

$$C_2\gamma = -(R + j\omega L)C_3$$
$$C_4\gamma = -(G + j\omega C)C_1$$

which yield

$$C_2 = -\frac{R + j\omega L}{\gamma} C_3 = -Z_w I(0)$$
$$C_4 = -\frac{G + j\omega C}{\gamma} C_1 = -\frac{1}{Z_w} V(0) \tag{6-96}$$

In terms of $V(0)$ and $I(0)$ the solutions thus are

$$V(x) = V(0) \cosh \gamma x - Z_w I(0) \sinh \gamma x$$
$$I(x) = I(0) \cosh \gamma x - \frac{V(0)}{Z_w} \sinh \gamma x \tag{6-97}$$

The last equation pair expresses $V(x)$ and $I(x)$ in terms of $V(0)$ and $I(0)$. We can actually write Eqs. (6-97) in the vector form

$$\begin{bmatrix} V(x) \\ I(x) \end{bmatrix} = \begin{bmatrix} \cosh \gamma x & -Z_w \sinh \gamma x \\ -\dfrac{1}{Z_w} \sinh \gamma x & \cosh \gamma x \end{bmatrix} \begin{bmatrix} V(0) \\ I(0) \end{bmatrix} \tag{6-98}$$

By inverting the 2×2 matrix in Eqs. (6-98) we can express $V(0)$ and $I(0)$ in terms of $V(x)$ and $I(x)$. The reader may readily check that this process yields the equation pair

$$\begin{bmatrix} V(0) \\ I(0) \end{bmatrix} = \begin{bmatrix} \cosh \gamma x & Z_w \sinh \gamma x \\ \dfrac{1}{Z_w} \sinh \gamma x & \cosh \gamma x \end{bmatrix} \begin{bmatrix} V(x) \\ I(x) \end{bmatrix} \tag{6-99}$$

The last two equations are often written in the form

$$V(0) = AV(x) + BI(x)$$
$$I(0) = CV(x) + DI(x) \tag{6-100}$$

where

$$A = D = \cosh \gamma x$$
$$B = Z_w \sinh \gamma x \qquad (6\text{-}101)$$
$$C = \frac{1}{Z_w} \sinh \gamma x$$

6-6-3 Equivalent Circuit of Long Line

We show now that by proper choice of the series impedance Z_s and the two shunt admittances Y_{1p} and Y_{2p} the π network in Fig. 6-17 will represent an *equivalent circuit* of the long line. For this to be true the relationships between the "output" variables $V(x)$ and $I(x)$ and the "input" variables $V(0)$ and $I(0)$ in Fig. 6-17 must be identical with those expressed by Eqs. (6-97).

By inspection we write the following equations for voltages and currents in Fig. 6-17:

$$V(x) = V(0) - Z_s[I(0) - Y_{1p}V(0)]$$
$$I(x) = I(0) - Y_{1p}V(0) - Y_{2p}V(x) \qquad (6\text{-}102)$$

These equations are then put in a form that resembles Eqs. (6-97), i.e.,

$$V(x) = V(0)(1 + Z_s Y_{1p}) - Z_s I(0) \qquad (6\text{-}103)$$

and

$$I(x) = I(0) - Y_{1p}V(0) - Y_{2p}\{V(0) - Z_s[I(0) - Y_{1p}V(0)]\}$$
$$= I(0)(1 + Z_s Y_{2p}) - V(0)(Y_{1p} + Y_{2p} + Z_s Y_{1p} Y_{2p}) \qquad (6\text{-}104)$$

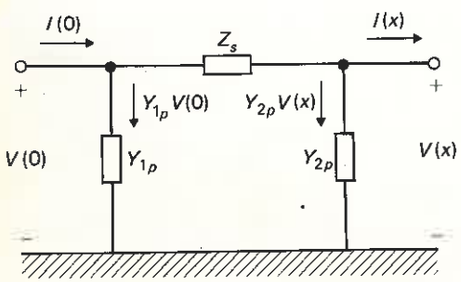

$Z_s = Z_w \sinh \gamma x$

$Y_{1p} = Y_{2p} = \frac{1}{Z_w} \tanh \frac{\gamma x}{2}$

Figure 6-17 Equivalent circuit of "long line."

If we compare this last pair of equations with Eqs. (6-97) we conclude that they can be made identical by setting

$$1 + Z_s Y_{1p} = 1 + Z_s Y_{2p} = \cosh \gamma x$$
$$Z_s = Z_w \sinh \gamma x \qquad (6\text{-}105)$$
$$Y_{1p} + Y_{2p} + Z_s Y_{1p} Y_{2p} = \frac{1}{Z_w} \sinh \gamma x$$

We readily confirm that Eqs. (6-105) will be satisfied by choosing

$$Z_s = Z_w \sinh \gamma x$$
$$Y_{1p} = Y_{2p} = \frac{1}{Z_w} \frac{\cosh \gamma x - 1}{\sinh \gamma x} = \frac{1}{Z_w} \tanh \left(\frac{\gamma x}{2}\right) \qquad (6\text{-}106)$$

which parameter values therefore constitute the branch elements for the equivalent circuit.

6-6-4 Computational Considerations

In using the above equations we must realize that, generally, both γ and Z_w are complex numbers. For computational purposes it is helpful to express Z_w and γ in terms of the *real* line parameters, defined as follows:

$$Z_w \triangleq R_w + jX_w$$
$$\gamma \triangleq \alpha + j\beta \qquad (6\text{-}107)$$

The hyperbolic sines and cosines of the complex argument γx can be separated into real and imaginary parts by use of the formulas

$$\cosh \gamma x = \cosh (\alpha + j\beta)x = \cosh \alpha x \cos \beta x + j \sinh \alpha x \sin \beta x$$
$$\sinh \gamma x = \sinh (\alpha + j\beta)x = \sinh \alpha x \cos \beta x + j \cosh \alpha x \sin \beta x \qquad (6\text{-}108)$$

Example 6-10 A phase-symmetric three-phase line having the data computed in Examples 6-3 and 6-8 has a total length of 500 km. It is being operated at a receiving-end voltage of 220 kV and delivers a three-phase power of $S = 90 + j30$ MW and Mvar. Find sending-end voltage and powers, real transmission losses, and reactive generation of the line. $f = 60$ Hz.

SOLUTION The line parameters for this line had been found to be

$R = 74 \times 10^{-6}$ Ω/m
$L = 1.212 \times 10^{-6}$ H/m
$C = 9.577 \times 10^{-12}$ F/m
G is set equal to zero.

Based on this data we compute γ

$$\gamma = \sqrt{(74 + j377 \times 1.212)j377 \times 9.577 \times 10^{-9}} = (0.1037 + j1.2886) \times 10^{-6}$$

In our case $x = l = 0.5 \times 10^6$ m and we thus have

$$\alpha l = 0.1037 \times 10^{-6} \times 0.5 \times 10^6 = 0.05185$$

$$\beta l = 1.2886 \times 10^{-6} \times 0.5 \times 10^6 = 0.6443$$

Next we find the wave impedance

$$Z_w = \sqrt{\frac{74 + j377 \times 1.212}{j377 \times 9.577}} \times 10^3 = 358.05 \angle -4.5997^\circ$$

$$= 356.90 - j28.71$$

From Eqs. (6-108) we then have

$$\cosh \gamma l = 0.8006 + j0.03116$$

$$\sinh \gamma l = 0.04148 + j0.6015$$

We can now determine the equivalent circuit elements

$$Z_s = (356.90 - j28.71)(0.04148 + j0.6015) = 32.08 + j213.5\ \Omega/\text{phase}$$

$$Y_{1p} = Y_{2p} = \frac{0.8006 + j0.03116 - 1}{32.08 + j213.5} \approx j0.0009349\ \mho/\text{phase}$$

(Had we calculated the equivalent circuit data by simply multiplying the per-meter parameter data by the line length, we would have obtained the following *erroneous* values:

$$Z_s = (74 + j377 \times 1.212)10^{-6} \times 0.5 \times 10^6 = 37.0 + j228.5\ \Omega$$

$$Y_{1p} = Y_{2p} = j377 \times 9.577 \times 10^{-12} \times 0.250 \times 10^6 = j0.000903\ \mho)$$

Having thus obtained the equivalent circuit we are now ready to find the sending-end variables. The analysis proceeds in the following steps:

Step 1 First we compute the receiving-end current. Receiving-end power equals $S(l) = 30 + j10$ megawatts and megavars per phase.

With $V(l)$ chosen as reference phasor we obtain

$$I(l) = \frac{30 - j10}{220/\sqrt{3}} = 0.2362 - j0.0787 \text{ kA/phase}$$

Step 2 The current through the impedance Z_s (Fig. 6-17) equals

$$I(l) + V(l)Y_{2p} = 0.2362 - j0.0787 + \frac{220}{\sqrt{3}} \times j0.0009349 = 0.2362 + j0.0400 \text{ kA/phase}$$

Step 3 The voltage drop in the line is computed next

$$\Delta V = (0.2362 + j0.0400)(32.08 + j213.5) = -0.96 + j51.71 \text{ kV/phase}$$

Step 4 We then find sending-end voltage

$$V(0) = \frac{220}{\sqrt{3}} + \Delta V = 126.06 + j51.71 = 136.25\angle 22.30^\circ \quad \text{kV/phase}$$

Step 5 For the sending-end current we have

$$I(0) = 0.2362 + j0.0400 + Y_{1p}V(0) = 0.1879 + j0.1579 \quad \text{kA/phase}$$

Step 6 And finally, for the sending-end power,

$$S(0) = V(0)I^*(0) = 31.86 - j10.18 \text{ MW and Mvar/phase}$$

In summary: Sending-end voltage: $136.25 \times \sqrt{3} = 236.0$ kV, line-to-line.
Sending-end power: $95.58 - j30.54$, MW and Mvar, total three-phase.
Real losses: $95.58 - 90.00 = 5.58$ MW, total three-phase.
Total line reactive generation: $30.00 + 30.54 = 60.54$ Mvar, total three-phase.
(This is *net* generation, i.e., generation in line capacitance minus losses in line inductance.)

Example 6-11 With the load, $90 + j30$, delivered at the receiving end in the previous example, the line "regulation" equals

$$\frac{|V(0)| - |V(l)|}{|V(0)|} = \frac{236.0 - 220}{236.0} = 0.068 \text{ pu}$$

This is not a bad voltage drop for a 500-km line. Clearly, the shunt capacitance of the line helps keep the voltage level up. But what happens at light load? For example, what would happen to $V(l)$ if the load were suddenly dropped?

SOLUTION With $I(l) = 0$ the "output" voltage in Fig. 6-17 is simply obtained by "voltage division":

$$|V(l)| = \frac{|1/Y_{2p}|}{|Z_s + 1/Y_{2p}|}|V(0)| = \frac{|-j1070|}{|32.08 + j213.5 - j1070|} \times \frac{236.0}{\sqrt{3}}$$

$$\therefore \quad |V(l)| = \frac{1070}{856.5} \times \frac{236.0}{\sqrt{3}} = \frac{294.8}{\sqrt{3}}$$

In words: *The voltage regulation is* minus *25 percent.*

The example demonstrates the tendency of "empty" lines to run at excessively high voltage. Clearly, a 25 percent voltage boost cannot be tolerated. In reality, one would "compensate" the line, by adding shunt reactors, that would consume the megavars produced by the line. (See Sec. 6-6-8.)

6-6-5 Surge Impedance Loading

Surge Impedance Loading (SIL) is said to exist when the line is terminated in a load impedance equalling the surge impedance Z_w. SIL is characterized by very simple voltage and current relations along the line. With the terminating impedance equalling Z_w we clearly have

$$V(l) = I(l)Z_w \tag{6-109}$$

By setting $x = l$ and upon substituting this expression for $V(l)$ into Eqs. (6-99) the latter equations yield the simple voltage and current relationships

$$\begin{aligned} V(0) &= V(l)(\cosh \gamma l + \sinh \gamma l) = V(l)e^{\gamma l} \\ I(0) &= I(l)(\cosh \gamma l + \sinh \gamma l) = I(l)e^{\gamma l} \end{aligned} \tag{6-110}$$

and also

$$\frac{V(0)}{I(0)} = \frac{V(l)}{I(l)} = Z_w \tag{6-111}$$

Equations (6-110) can be written

$$\frac{V(l)}{V(0)} = \frac{I(l)}{I(0)} = e^{-\gamma l} \tag{6-112}$$

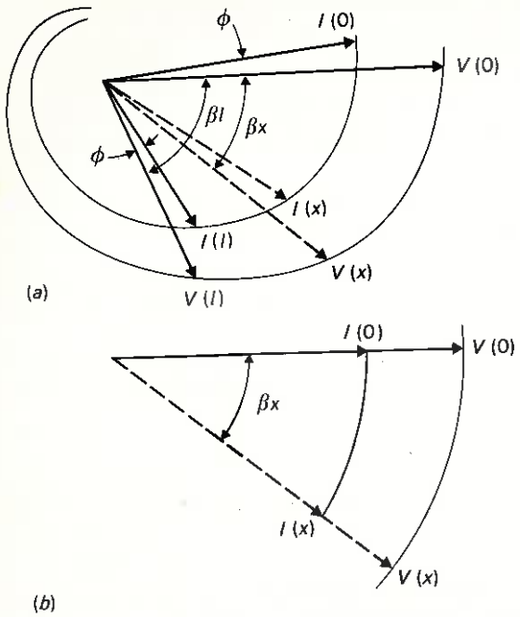

Figure 6-18 Voltage and current phasors along line terminated in its surge impedance: (*a*) lossy line; (*b*) lossless line.

These equations are complex. By separating the real and imaginary parts the following magnitude and phase relations result:

$$\frac{|V(l)|}{|V(0)|} = \frac{|I(l)|}{|I(0)|} = e^{-\alpha l} \tag{6-113}$$

$$\angle V(0) - \angle V(l) = \angle I(0) - \angle I(l) = \beta l \tag{6-114}$$

The physical meaning of these equations is graphically illustrated in Fig. 6-18*a*. Moving down the line in positive x direction the voltage and current phasor tips follow spiraling loci. As was demonstrated in Example 6-10 the surge impedance is typically slightly capacitive, meaning that at any point along the line the current leads the voltage by a small angle ϕ.

Example 6-12 Assume the line in Example 6-10 to be SIL loaded. Find the phase lag βx and attenuation $e^{-\alpha x}$ along the 500-km line. Also study the voltage, current, and power situation if the receiving-end voltage equals 220 kV.

SOLUTION For the phase lag we have

$$\beta l = 0.6443 \text{ rads} = 36.9°$$

The attenuation equals

$$e^{-\alpha l} = e^{-0.05185} = 0.9495$$

At the receiving end we compute (with $V(l)$ as reference phasor)

$$I(l) = \frac{220/\sqrt{3}\angle 0°}{358.05\angle -4.60°} = 0.3547\angle 4.60°$$

$$S(l) = 3 \times \frac{220}{\sqrt{3}} \times 0.3547\angle -4.60° = 134.71 - j10.84 \text{ MW and Mvar, 3-phase}$$

At the sending end we have

$$I(0) = \frac{0.3547}{0.9495}\angle 4.60° + 36.9° = 0.3736\angle 41.5° \text{ kA/phase}$$

$$V(0) = \frac{220/\sqrt{3}}{0.9495}\angle 0° + 36.9° = 133.8\angle 36.9° \text{ kV/phase}$$

$$\therefore \quad S(0) = 3 \times 133.8 \times 0.3736\angle -4.60° = 149.4 - j12.0 \text{ MW and Mvar, 3-phase}$$

6-6-6 Lossless Line; Concept of Wavelength

Examples 6-10 and 6-12 illustrate that the real losses in a typical power line are comparatively insignificant. If we set $R = G = 0$ in our mathematical line models they become particularly simple and we can easily expose some interesting physical features of such a *lossless line.* With losses neglected the surge impedance becomes purely resistive and the propagation constant purely imaginary in accordance with

$$Z_w = R_w = \sqrt{\frac{L}{C}} \qquad \Omega \tag{6-115}$$

and

$$\gamma = j\beta = j\omega\sqrt{LC} \tag{6-116}$$

Equations (6-97) simplify to

$$\begin{aligned} V(x) &= V(0)\cos\beta x - jR_w I(0)\sin\beta x \\ I(x) &= I(0)\cos\beta x - j\frac{V(0)}{R_w}\sin\beta x \end{aligned} \tag{6-117}$$

In the case of SIL loading of a lossless line the voltage and current attenuation become zero. The spiraling loci of Fig. 6-18*a* change into circular ones as shown in Fig. 6-18*b*. This means that the voltages and currents along an SIL loaded line are constant—or of "flat profile."

For a more general loading situation the voltages and currents will not be constant but will, according to Eqs. (6-117) *vary sinusoidally along the line with respect to the space coordinate x.*

A full voltage and current cycle along the line corresponds to a change in the angular argument βx of 2π rad. The length corresponding to one full cycle is

referred to as the *wavelength* λ. The wavelength evidently is obtained from the equality

$$\lambda = \frac{2\pi}{\beta} = \frac{2\pi}{\omega\sqrt{LC}} = \frac{1}{f\sqrt{LC}} \tag{6-118}$$

For example, at 60 Hz the line in Example 6-10 has a wavelength of

$$\lambda = \frac{1}{60\sqrt{1.212 \times 10^{-6} \times 9.577 \times 10^{-12}}} = 4.89 \times 10^6 \text{ m}$$

(or 3000 miles approximately.)

The equivalent circuit representation of a lossless line is obtained from Fig. 6-17 by replacing Z_w and γ by the simplified expressions (6-115) and (6-116). The resulting circuit is depicted in Fig. 6-19. Note that in this diagram the argument βx has been replaced by the expression

$$\beta x = \frac{x}{\lambda} 2\pi \tag{6-119}$$

which is obtained directly from Eq. (6-118).

6-6-7 Electrically "Short" and "Long" Lines

All branch elements in Fig. 6-19 are *purely reactive*. Furthermore, it is seen that Z_s is *inductive* and Y_p *capacitive* if

$$x < \frac{\lambda}{2} \tag{6-120}$$

i.e., for a line length less than a half-wave. Should the line length be in excess of $\lambda/2$ then the series impedance will become capacitive and the shunt admittance inductive.

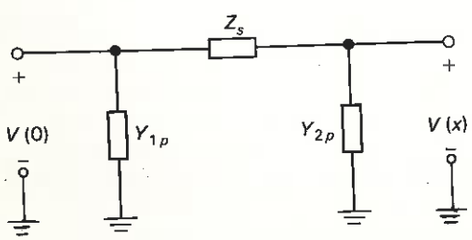

$$Z_s = j\sqrt{\frac{L}{C}} \sin\left(\frac{x}{\lambda} 2\pi\right)$$

$$Y_{1p} = Y_{2p} = j\sqrt{\frac{C}{L}} \tan\left(\frac{x}{\lambda}\pi\right)$$

Figure 6-19 The equivalent circuit of long lossless line.

Of course, in reality, an ac power line never reaches half-wavelengths. In fact, few lines exceed $\lambda/8$ ($\approx$ 600 km at 60 Hz).

If the line is sufficiently short, the magnitude of the factor x/λ is so small that we can set with good accuracy

$$\sin \frac{x}{\lambda} 2\pi \approx \frac{x}{\lambda} 2\pi$$
$$\tan \frac{x}{\lambda} \pi \approx \frac{x}{\lambda} \pi \tag{6-121}$$

The impedance and admittance elements of Fig. 6-19 can then be written

$$Z_s = j\sqrt{\frac{L}{C}} \sin \frac{x}{\lambda} 2\pi \approx j\sqrt{\frac{L}{C}} \frac{x}{\lambda} 2\pi = j\omega L x \tag{6-122}$$

$$Y_{1p} = Y_{2p} = j\sqrt{\frac{C}{L}} \tan \frac{x}{\lambda} \pi \approx j\sqrt{\frac{C}{L}} \frac{x}{\lambda} \pi = j\frac{\omega C x}{2} \tag{6-123}$$

We note that for lines so short that Eqs. (6-121) apply the series impedance is simply obtained by multiplying the reactance per meter by the length of the line. The shunt admittance is obtained in an analogous manner (and divided into two equal parts at each end). We had earlier noted that typical lines have, at 60 Hz, wavelengths of about 3000 miles. For a line length of 100 miles we have $x/\lambda = 1/30$, and the foregoing approximations will be less than one percent. *We conclude therefore, that for line lengths below approximately 100 miles, we can neglect the distribution effect and actually "lump" the line parameters.* We refer to the line in this case as "*electrically short.*"

Figure (6-19) also gives a clue as to when a power line becomes "too long," electrically speaking. It is noted that a "quarter-wave" line which is characterized by $x/\lambda = 0.25$ (which corresponds to about 1200 km at 60 Hz) will have series and shunt reactances of equal magnitude ($=\sqrt{L/C}$). This obviously sets the stage for resonance phenomena that may result in unacceptable voltage profiles.

Example 6-13 Let the three-phase transmission line of Example 6-10 have a length of 1000 km. What sending-end voltage is required to keep the line energized so as to measure 220 kV at the receiving end? Receiving-end power is assumed zero.

SOLUTION We neglect for simplicity the line resistance and work with the equivalent circuit in Fig. 6-19. We had earlier computed

$$\lambda = 4890 \text{ km}$$

The wave impedance equals

$$\sqrt{\frac{L}{C}} = \sqrt{\frac{1.212}{9.577}} \times 10^3 = 356 \ \Omega/\text{phase}$$

As

$$\frac{x}{\lambda} = \frac{1000}{4890} = 0.204$$

the equivalent circuit parameters equal

$$Z_s = j356 \cdot \sin 73.4° = j341\ \Omega/\text{phase}$$

$$Y_{1p} = Y_{2p} = \frac{j1}{356} \tan 36.7° = j0.00209\ \mho/\text{phase}$$

From Fig. 6-19 we obtain (for open line)

$$\frac{V(x)}{V(0)} = \frac{1/Y_{2p}}{Z_s + 1/Y_{2p}} = \frac{-j478}{j341 - j478} = \frac{478}{137} = 3.49 \tag{6-124}$$

$$\therefore \quad |V(0)| = \frac{|V(x)|}{3.49} = \frac{220/\sqrt{3}}{3.49} = \frac{63}{\sqrt{3}}\ \text{kV/phase}$$

$V(0)$ must be held at 63 kV to keep the remote end at 220 kV. This lopsided voltage profile will be improved if the line is loaded but the example clearly demonstrates the difficulties associated with keeping very long lines at an acceptable voltage level.

6-6-8 Line Compensation

We have noted that long lines operated under variable load conditions are subject to greatly varying voltage. Loading at the SIL level results in an ideal line voltage profile which, if losses can be neglected, actually is perfectly flat. Seldom if ever does one have this situation in practice.

Either the load is generally heavy, in which case the voltage drop across the series line reactance may result in a low receiving-end voltage level, or the load is generally light, in which case the shunt capacitive current dominates, causing a negative drop across the series inductance with a resulting high receiving-end voltage. The problem becomes more serious as the line length increases and could, if not counteracted, greatly limit the operating range of the line.

The reactive megavar generation of the lines, which under light load periods cannot be consumed by the loads, presents an additional problem. Where will it go? We remember (Chap. 4) that the system generators have only a limited ability to absorb reactive power.

Series and *shunt compensation* are the normally employed means whereby the above problems can be minimized. The former consists of series capacitors placed, for example, midline during heavy load. Shunt compensation is accomplished by means of reactors, typically placed at the ends of the line during light load, and also when taking a line in service. If the line is very long, compensation may have to be performed at several points along the line to keep the voltages within certain tolerances. Both series capacitors and shunt reactors can be switched in and out as required.

Example 6-14 Consider the 500-km line, the line parameters of which were computed in Example 6-10. Determine the size of two banks of shunt reactors to be placed at each end and having the exact megavar rating to reduce the line reactive generation to zero.

SOLUTION Figure 6-20*a* shows the equivalent, per-phase network as we earlier computed it. We have indicated the *impedance* value, $-j1070\ \Omega$, of the shunt capacitors. Were we to connect shunt reactors at each end, each having the reactance

$$X_L = j1070\ \Omega/\text{phase}$$

then *total* compensation would be achieved, i.e., the reactive line generation would be exactly consumed by the reactors.

The equivalent network of the compensated line would be the one shown in Fig. 6-20*b*. As viewed from either end the line impedance would be infinite. The no-load current would be zero and the no-load voltage in both ends would be equal. *Note, however, that the midpoint voltage would not equal the end voltage.* (Would we also like the midpoint voltage to be equal to the end-point value then we need a midpoint reactor as well. Compare Prob. 6-16.)

For an operating voltage of 240 kV the reactors must have a megavar rating of

$$Q_{\text{react}} = \frac{(240/\sqrt{3})^2}{1070} = 17.94\ \text{Mvar/phase}$$

or 53.83 Mvar total three-phase.

The total installed reactor capacity would equal 108 Mvar for the total line.

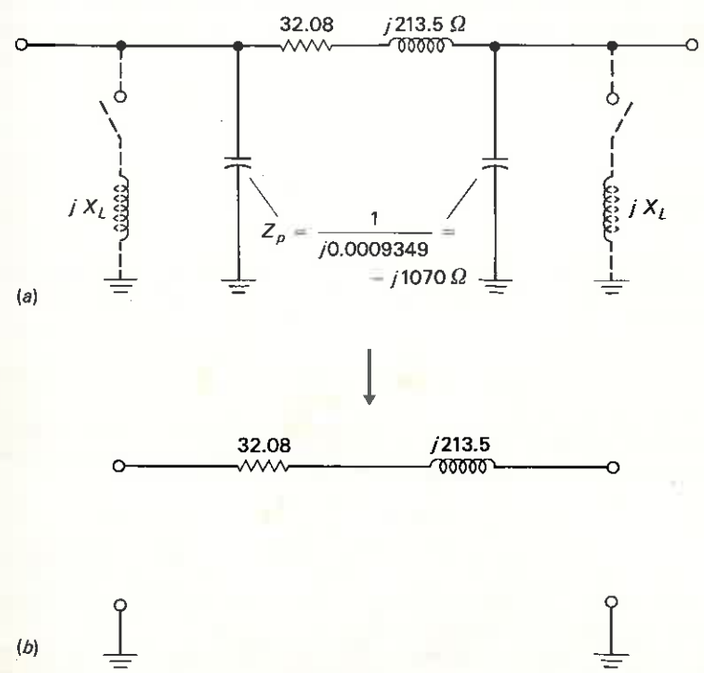

Figure 6-20 Totally reactor-compensated line.

6-7 SUMMARY

The most important design parameters of a transmission line from a systems analysis point of view are the series inductance and the shunt capacitance. Methods for computing these parameters have been developed in this chapter, first for a single-phase line, then for a three-phase line. We have confirmed under balanced operation that it is possible to define per-phase parameters. We earlier concluded that this could be done for generators and transformers, and therefore we know at this stage that per-phase analysis is permissible for the overall system *under balanced load conditions.*

The advantages of bundle conductor design have been pointed out. It may be commented at this time that bundling of conductors is a "cheap" substitute for adding a parallel line to an existing one. One obviously saves the cost of a new right-of-way plus the construction cost of the line itself. However, whereas bundling reduces the reactance by about 30 percent (Example 6-5), and thus increases the power capacity of the line by about 40 percent, the new line would reduce the total reactance by 50 percent and thus double the power capacity.

For lines having a length in excess of about 100 miles, it becomes necessary to take the distribution effect of parameters into account. We have derived the so-called "long-line" equations and presented the corresponding equivalent network. The large series reactance and considerable reactive power generation of long lines cause particular operating problems that may require special compensation techniques.

PROBLEMS

6-1 Figure 6-21 depicts the typical design of a high-voltage cable. The dielectric is characterized by the relative dielectric constant ε. Prove that the capacitance between the cylindrical conductor and the outer shield equals

$$C = \frac{2\pi\varepsilon\varepsilon_0}{\ln (R_2/R_1)} \quad \text{F/m} \tag{6-125}$$

Assume that three of these cables are used for three-phase transmission at 230 kV, 60 Hz. Find the charging current in amperes per kilometer and the reactive generation in kilovars per kilometer. Compare with Example 6-7. Use the numerical data

$$R_1 = 1.5 \text{ cm}$$
$$R_2 = 4 \text{ cm}$$
$$\varepsilon = 3.5$$

***6-2** A single-phase line (Fig. 6-22) consists of five identical conductors, two of which carry current in one direction, the other three in the opposite direction.

(*a*) Make reasonable assumptions for the current division. Find a formula for the line inductance expressed in henrys per meter.

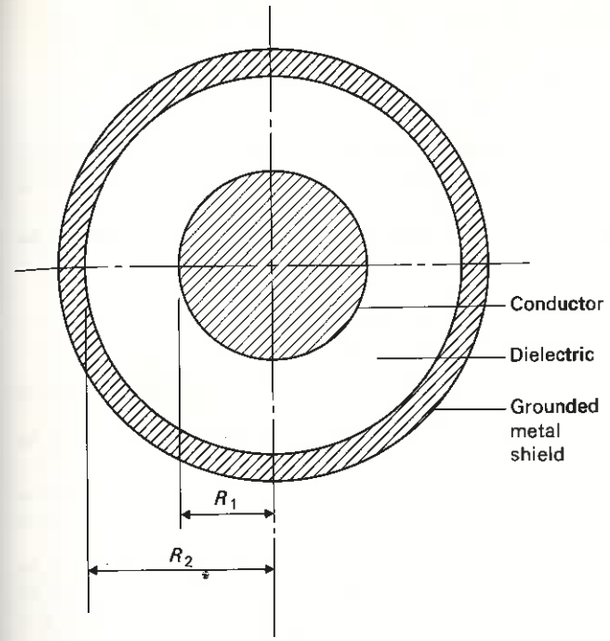

Figure 6-21 Cable conductor.

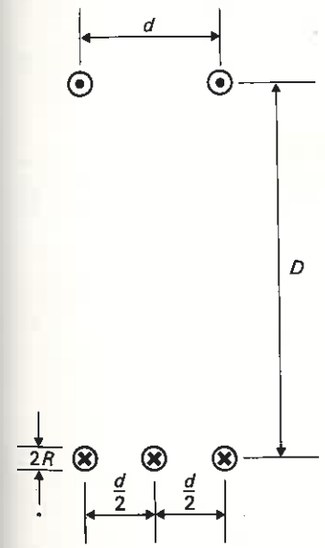

Figure 6-22 Five-conductor single-phase line.

(*b*) Obtain a numerical value using these numerical conductor and line dimensions:

$$D = 1 \text{ m}$$
$$d = 0.1 \text{ m}$$
$$R = 2 \text{ mm}$$

***6-3** Compare your inductance formula in Prob. 6-2 with the two-conductor formula (6-16). In the latter case what would be the equivalent wire radius to render the same inductance as that of the five-wire line. D is assumed the same in both cases.

***6-4** Consider the phase-symmetric 230-kV three-phase line studied in Examples 6-3 and 6-8. We summarize the line parameters:

$$R = 0.074\ \Omega/\text{km}$$
$$L = 12.12 \times 10^{-4}\ \text{H/km}$$
$$C = 9.577 \times 10^{-9}\ \text{F/km}$$

(*a*) The line is 150 km long and can be assumed "electrically short." Find the equivalent circuit elements.

(*b*) The line is open circuited and energized to a voltage level of 230 kV as measured at the sending end. Find the voltage at the open end. $f = 60$ Hz.

6-5 The 150-km open-circuited line in Prob. 6-4 is being energized from a 500-MVA, 20-kV generator via a 500-MVA, 20/230-kV stepup transformer. The generator has a 90 percent synchronous reactance and the transformer a 14 percent leakage reactance, all based upon the device ratings.

It is assumed that the generator excitation is adjusted until the voltage measures 230 kV on the transformer HV side. The line is suddenly deenergized by opening the circuit breakers located on the transformer HV side. Compute the new voltage on the transformer HV side assuming that the generator excitation is unchanged. Neglect all resistances in your analysis, and model the transformer as an IT.

6-6 We assume now that the line in Prob. 6-5 is being energized and that the *sending-end* voltage of the line is kept at 230 kV by automatic voltage regulation (AVR) of the generator (see also Chap. 9). Three 220-Ω Y-connected load resistors are suddenly switched to the receiving end.

(*a*) By how many percent will the voltage $|V(l)|$ drop from its open-circuit value computed in Prob. 6-4*b*?

(*b*) How many megawatts will the resistors consume?

(*c*) Compute the megawatt and megavar flows at the sending end.

6-7 In Probs. 6-4 to 6-6 control of the line voltage can be achieved by excitation control of the generator in the sending end. This limits voltage control to *one* end of the line only. If independent voltage control is desired in *both* ends it is necessary to provide controllable reactive power sources in both line ends.

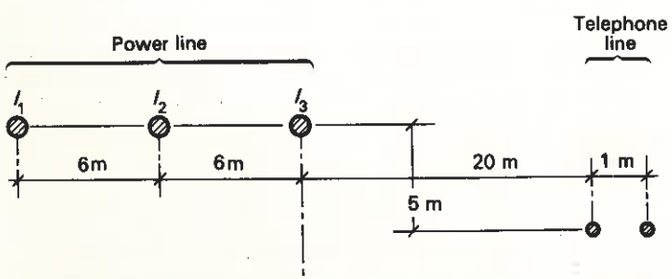

Figure 6-23 Magnetic coupling between power and telephone lines.

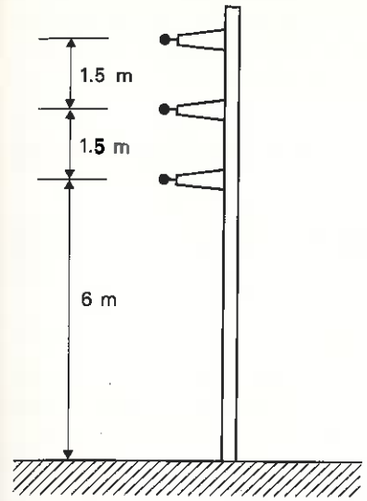

Figure 6-24 Phase conductors placed in vertical plane.

Assume that we specify in Prob. 6-6 that the sending-end voltage must be 230 kV *and the receiving-end voltage 240 kV*. Prove that this voltage profile can be achieved by installing a shunt capacitor bank in parallel with the 220-Ω load resistors. What megavar rating must the bank have?

***6-8** A telephone line runs parallel with an untransposed power line. Figure 6-23 gives the dimensions of the two. The power line carries a balanced three-phase current of 500 A (rms) per phase. Compute the 60-Hz voltage induced in the telephone line per meter.

Hint: Use the apparent mutual inductances and compute the voltage induced in each telephone wire. The difference is your answer. Note that you will have to compute a *small* difference between relatively large terms, so you must be careful to obtain sufficient accuracy.

***6-9** A 132-kV urban line has the conductor geometry shown in Fig. 6-24. Conductor diameter is 10 mm.

(*a*) Find inductance per kilometer and phase, transposed.

(*b*) Find capacitance per kilometer and phase, transposed and no earth.

(*c*) As in (*b*) but add now influence of earth.

6-10 Two identical transmission lines are carried on the same towers. The conductors belonging to each line are contained in the same vertical planes, the distance between which is 4 m. The distance between phase conductors is 2 m with the phase order *a*, *b*, *c* counted from top. Each line is untransposed and carries a balanced set of three-phase currents of 500 A/phase. The lines run parallel for a distance of 30 km. Compute the voltages (magnitude *and* phase) induced in phases *a*, *b*, and *c* in one line by the currents in the other. What would be your answer if transposition existed every 10 km?

6-11 Each phase of a proposed three-phase 1200-kV transmission line consists of a conductor bundle composed of 12 conductors symmetrically spaced around a circle 100 cm in diameter. Each conductor has a diameter of 12 mm. Each phase bundle is placed in a corner of an equilateral triangle of 15 m side. Compute the inductance and capacitance per phase and meter of the line. Also find the megavar generation per kilometer.

***6-12** Connect a load resistor of value $\sqrt{L/C}$ across one end of the line in Fig. 6-19. Prove that the impedance as measured from the other end equals $\sqrt{L/C}$ *independent of the line length x.*

***6-13** Consider the three-phase line in Fig. 6-9*a*. The two outer conductors are interconnected in each end and used as a combined return conductor of a single-phase line. Find the per-meter inductance and capacitance of the line.

*6-14 Find the line inductance per phase of the 765-kV line in Fig. 6-15. Assume line transposed.

6-15 The shunt capacitance of a long transmission line can be of such a magnitude as to make it impossible to energize it. The reactive power produced by the line would flow back into the generator and "overwhelm" it.

Consider the 765-kV line discussed in Example 6-9 and Prob. 6-14. Assume the line to be 650 km long and operated at 60 Hz. One wishes to energize it to a voltage level of 765 kV at the sending end with the receiving end open.

(*a*) How many megavars would the line produce? Neglect resistance in your analysis.

(*b*) We assume that the reactive generation of the line computed in (*a*) would exceed the megavar absorption capacity of available generators. In order to facilitate the energizing process of the line one would connect shunt reactors in each end. What megawar rating must these reactors have if we wish to accomplish a complete compensation of the reactive line generation?

6-16 Consider Example 6-14. The open-line voltage was 240 kV at both ends of the *compensated* line.

(*a*) What is it midline?

(*b*) To make the open-line voltage equal 240 kV in all *three* points we propose to install three banks of reactors instead of two, one in each end plus one midline. Can this be done and, if so, what will be the megavar rating of each bank?

6-17 An electrically "short" transmission line is characterized by a series reactance of 30 Ω/phase. To increase the power transmission capacity, we wish to reduce this impedance by 40 percent per phase by inserting series capacitors in each phase. The largest-magnitude current that is expected to flow in the line is 1 kA per phase. Frequency is 60 Hz.

(*a*) Determine the capacitance per phase that must be installed in order to accomplish the desired compensation.

(*b*) It is assumed that commercially available capacitors have a voltage and current rating of 2 kV and 50 A/unit. How would you combine such units into a bank to achieve the desired compensation? What must be the individual capacitance per unit?

(*c*) How many kilovars would be produced totally in all three phases when maximum current is flowing?

6-18 It was stated in Example 6-14 that "the no-load current would be zero." This refers to the generator current. What will be the *line* current?

REFERENCES

1. EHV Transmission Line Reference Book. Edison Electric Institute, 1968.
2. Hallen, E., "Electromagnetic Theory" (book), John Wiley & Sons Inc., New York, 1962.
3. J. E. Bridges: "Environmental Considerations Concerning the Biological Effects of Electric Fields", *IEEE Trans.*, vol. PAS-97, no. 3, Jan/Feb. 1978.
4. "Transmission Line Reference Book—345 kV and Above", Electric Power Research Institute, 1975, Palo Alto, Calif.

CHAPTER

SEVEN

THE ENERGY SYSTEM IN ITS NORMAL STATE —SYSTEM MODELING AND POWER-FLOW ANALYSIS

In previous chapters we have attempted to clarify some basic concepts of electric power engineering. We also have discussed the theory and operating features of the most important system components. We are now prepared to approach the central topic of our study: the operational features of the overall system.

7-1 OPERATING STATES

As first suggested by Dy Liacco,[9,10] depending on its condition, a power system may be operated in several different *states*. Fink and Carlsen[11] clarified further this concept and proposed the *state transition* diagram shown in Fig. 7-1.

For more than 99 percent of the time, a typical system is found in its *normal state*. In this state the frequency and bus voltages are kept at prescribed values. As we shall see later this frequency and voltage constancy results from a carefully maintained balance between the real and reactive power demanded by the loads and those supplied by the real and reactive power sources.

This match or "equality" between generation and demand is a fundamental prerequisite for system "normalcy" and is indicated by the symbol E in Fig. 7-1. The second symbol, I, indicates that certain "inequalities" must also be observed in the "normal" state. For example, generator and transformer loads must not exceed the rated values and transmission lines must not be loaded above their thermal or static stability limits.

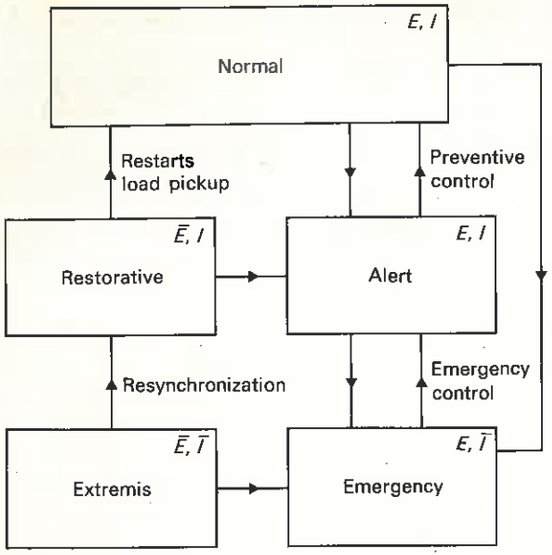

E = Equality constraint
I = Inequality constraint
$^{-}$ = Negation

Figure 7-1 State transition diagram.

The normal state must also be characterized by a certain level of *security* which requires a certain margin of generation in the form of *spinning reserve*.

Should the generating margin fall below some threshold or should a disturbance be deemed imminent then the security level is reduced and the system enters the *alert state*. However, all equalities (E) and inequalities (I) are still observed, and the system still operates fully synchronized and—with luck—could continue to do so for any length of time. However, one would now initiate *preventive control actions* to restore proper generation margin and/or eliminate disturbances so as to return the system to its normal state.

If preventive control fails or if a sufficiently severe disturbance occurs, the system on occasion will enter the *emergency state*. Actually, this state can be reached either directly from the normal state or via the alert state. In the emergency state the generation still tracks the load and the system is still synchronized (symbol E unchanged). But one or several components are now overloaded (note the negation of symbol I) and as these components eventually fail, the system will start to disintegrate. It is most urgent that the system be returned to the normal (or alert) state by means of *emergency control actions*, i.e., disconnection of faulted section, rerouting of power or, if everything else fails, *load shedding*.

If emergency control actions should fail the system will go into the *extremis state*, i.e., disintegrating into sections or *islands*. Some of these islands may

contain sufficient generation to meet the load. Typically, however, the generators will be strained beyond their capacities. Note that both E and I are negated in this state. We *never* tolerate generator overload and in this state we will therefore see considerable generator tripping, maybe to the point of total *blackout*. The chain of events that will transfer the system from "normal" to "extremis" may typically last anywhere from a few seconds to several minutes. To bring it back to normal, i.e., going through the *restorative state*, is a much slower process, lasting hours, sometimes days. A large steam turbine that has been shut down requires many hours for restart. Lost loads can be picked up only gradually and resynchronization of operating islands is likewise a slow undertaking.

In this and the next two chapters we shall address the various problems associated with operation in the normal state. In the last three chapters of the book we will be concerned with the abnormal states and the various control actions available for bringing the system back to normal operation.

One could easily identify a large number of problem areas that have some bearing upon the overall objective of keeping a power system operating in its "normal" state. The textbook space is limited and we therefore limit our coverage to these five topics:

1. Megawatt-frequency interaction
2. Megavar-voltage interaction
3. Power-flow problem
4. Optimum dispatch
5. The control problem

7-2 MEGAWATT-FREQUENCY ($P - f$) INTERACTION

Constant frequency is identified as the primary mark of a normally operating system. There are at least four reasons why the system frequency must not be allowed to deviate from a chosen constant value:

1. Most types of ac motors run at speeds that are directly related to the frequency.
2. The generator turbines, particularly steam-driven ones, are designed to operate at a very precise speed.
3. The overall operation of a power system can be much better controlled if the frequency error is kept within strict limits.
4. A large number of electrically operated clocks are used. They are all driven by *synchronous* motors, and the accuracy of these clocks is a function not only of the frequency error but actually of the *integral* of this error. (Eq. 9-52.)

The first of the above reasons does not put particularly strict bounds on the frequency swings. The vast majority of ac motor-driven loads probably would not be sensitive to frequency fluctuations of the order of 60 ± 2 Hz.

Constant turbine speed is an important requirement. The velocity of the expanding steam is beyond our control and the turbine efficiency requires that we have perfect speed match.

A turborotor with its many huge turbine blades constitutes a mechanical system of many natural frequencies. These frequencies are quite undamped and they are each subject to resonance at various rotor speeds. It is important *under load* that the rotor never drifts into a speed range where dangerous amplitude buildup would result. Hydroturbines are not subject to this danger.

The third reason is equally important. Unusual deviations in frequency indicate that something is basically wrong with a system. By reducing *normal* frequency fluctuations to a faint ripple, we are able to detect the frequency disturbances following a fault at an early stage. In modern energy systems the frequency constancy is normally kept within ± 0.05 Hz.

7-2-1 Load-Frequency Mechanism

Before we attempt to explain the means we have at our disposal to control the system frequency, it is appropriate that we should examine the reasons why it tends to vary in the first place.

The frequency is closely related to the real power balance in the overall network. Under normal operating conditions the system generators run *synchronously* and generate together the power that at each moment is being drawn by all loads *plus* the real transmission losses. The latter, amounting usually to a few percent, consist of ohmic losses in the various transmission components, corona losses on the lines, and core losses in transformers and generators. We must remember that the energy is being transmitted at almost the velocity of light, and since it is not being stored† somewhere in the system in *electric* form we *conclude that the electric energy production rate must equal the consumption rate at each moment of time.*

Should power balance not exist then the difference would enter into or exit from kinetic energy storage. As the kinetic energy depends upon generator speed, a power imbalance will thus translate into a speed (and frequency) deviation. As an analog, consider a freight train consisting of many engines and a string of freight cars. It is desired to keep the velocity of the train controlled at constant speed in spite of the fact that the train will experience fluctuating grades along its course.

The engine power corresponds to the generator power output in the electric system and the freight cars represent the electric loads.

If the total engine power exceeds the total pull exerted by the freight cars the speed will increase as the difference is transformed into kinetic storage. A shortage of engine power results in a slowdown. The rate of the speed change depends upon the magnitude of the power imbalance and train inertia.

† The storage that actually takes place in the reactive elements (coils and capacitors) at the rate of twice per cycle amounts, as we recall, to zero average, and therefore does not enter into our discussion.

In the electric system, should we have a momentary surplus of generator power over load the total speed (frequency) will increase. The rate of the speed (and frequency) increase would depend upon the amount of surplus power and the total moment of inertia of the running equipment. All tens of thousands of motors which during these moments were being supplied by the network would speed up, and they would all meet higher load torques, thus requiring the motors to pull more power from the network. The resulting load increase would soon balance out the load decrease that started the whole chain of events, and the frequency would level off at a new higher value.

Example 7-1 All the generators and motors in a power system represent a total kinetic energy of 1500 MJ (or MWs) as measured at rated frequency, 60 Hz. The system experiences a momentary power surplus at 5 MW. At what rate will the frequency increase?.

SOLUTION A system of inertia I kg/m^2 rotating at the speed ω rad/s possesses a kinetic energy w_{kin} that can be written in any one of the following forms:

$$w_{kin} = \tfrac{1}{2}I\omega^2 = w_{kin}^0\left(\frac{\omega}{\omega^0}\right)^2 = w_{kin}^0\left(\frac{f}{f^0}\right)^2 \quad \text{J (or Ws)} \tag{7-1}$$

where ω^0 = "normal" speed, rad/s
f^0 = "normal" frequency, Hz
w_{kin}^0 = kinetic energy as measured at normal frequency, J (or Ws).

If a *torque* imbalance ΔT, or a corresponding *power* imbalance ΔP, exists then, according to Newton, the system will experience an angular acceleration $d\omega/dt$ that follows from the equation

$$\Delta T = \frac{\Delta P}{\omega} = I\,\frac{d\omega}{dt}$$

In view of Eq. (7-1) the last relation can be put in the form

$$\Delta P = I\omega\,\frac{d\omega}{dt} = \frac{d}{dt}(w_{kin}) = \frac{d}{dt}\left[w_{kin}^0\left(\frac{f}{f^0}\right)^2\right] \quad \text{W} \tag{7-2}$$

In our case we have

$$\Delta P = +5 \text{ MW}$$
$$w_{kin}^0 = 1500 \text{ MJ}$$
$$f^0 = 60 \text{ Hz}$$

From Eq. (7-2) we thus have

$$5 = \frac{d}{dt}\left[1500\left(\frac{f}{60}\right)^2\right] = 2 \times \frac{1500}{3600} \times f\,\frac{df}{dt} = 50\,\frac{df}{dt}$$
$$\therefore\ \frac{df}{dt} = 0.1 \text{ Hz/s}$$

7-2-2 Load-Frequency Control, LFC

As the system load changes it thus becomes necessary to adjust the generation so that the power imbalance is continuously zeroed or at least minimized. Controlling the power generation thus becomes a "load-tracking" problem. The attentive reader probably has already reached the important conclusion that *inasmuch as the frequency constitutes a sensitive indicator of the energy balance in the system, it should indeed be used as the sensor portion of the control system, the job of which is to provide such a balance automatically.*

Load-frequency control (LFC) is in fact a basic control function in a power system. It is invariably performed automatically and because of its great importance we shall devote more detailed discussion to it in Chap. 9.

7-3 MEGAVAR-VOLTAGE ($Q - |V|$) INTERACTION

Practically all equipment used in or operating off a power system is designed for a certain voltage level, the *rated*, or *nameplate*, voltage. If the system voltage should deviate from that value, the performance of the device suffers, and its life expectancy drops. For example, the torque of an induction motor is proportional to the square of the terminal voltage (Eq. 3-35), the light flux from a lamp varies strongly with the voltage, etc.

The motivations for controlling the voltage level on a power system are thus strong. However, there is no need to regulate it to within the same narrow margins as was the case with system frequency. Industry-wide standards exist, specifying tolerable voltage variations on a network.

There is an additional important reason for voltage control. We have learned (Eq. 2-40) that the real line losses depend as much upon the *reactive* as upon the *real* line power flow. It is possible to minimize these losses by selecting an optimum power flow, in terms of real *and* reactive powers. Formula (3-53) informs us that the reactive line flow depends greatly upon line-end voltages, which thus become a means of controlling the real losses.

Normally one designates certain key buses throughout the system the voltage levels of which one then tries to maintain at specified values. These specified values will change as the load shifts. In summarizing our earlier findings these are our means for voltage control:

1. Excitation control of generators. This is the foremost means of control and it focuses on maintaining good voltage control at the generator buses. (More details will be given in Chap. 9.)
2. Switched shunt capacitors and/or reactors. These provide the capability of controlled reactive power injection into, or drain from, a bus.
   (The most modern version consists of thyristor controlled switching which permits continuous rather than step control.)

3. Synchronous capacitors which permit both continuous and sign-sensitive control of reactive power.
4. Tap-changing of transformers.

The common feature of all these control actions relates to the fact that the voltage level of a bus is strongly related to the reactive power injection at the bus. Added reactive power translates into a rise in voltage. This $Q - |V|$ mechanism was explained in Sec. 3-4-2, expressed quantitatively in formulas (3-50), (3-51), and (3-53), and depicted graphically in Fig. 3-18.

7-3-1 Cross-Coupling Between $P - f$ and $Q - |V|$ Control Channels

A surplus of megawatts tends to increase the frequency of a system. The frequency is a system-wide variable so the change will therefore be felt *uniformly throughout the system.*

A surplus of megavars tends to increase the voltage level of a system. The changes are not uniform but will be greatest at the buses where the Q surplus is the greatest. This is one distinct difference between $P - f$ and $Q - |V|$ control.

Another important difference relates to the "cross-coupling" between the two control channels. As we change the megawatt output of one or several generator units in order to maintain frequency constancy no resulting measurable changes occur in voltage levels.† On the contrary, as we change the Q input at a certain bus thereby affecting its voltage level $|V|$ *we do immediately also change the real load of the bus in question* (compare Sec. 3-3-1). This megawatt change will, of course, have an immediate effect on the LFC.

We conclude that whereas there is no discernible coupling from the $P - f$ channel to the $Q - |V|$ channel there is considerable coupling in the opposite direction. This coupling can, as will be demonstrated in Chap. 9, cause instabilities in the smooth megawatt flow on a grid.

7-4 THE POWER-FLOW PROBLEM

An interconnected power system represents an electric network with a multitude of branches and nodes, where the transmission lines typically constitute the branches. In power lingo the nodes are referred to as "buses." Even a medium-sized power company serving a mixed urban and rural population of 2 to 3 million people operates a network that may contain typically hundreds of buses and thousands of branches, not even counting the distribution network.

At some of the buses power is being injected into the network, whereas at

† A megawatt increase will result in a frequency increase which, according to formula (4-5), should increase $|E|$ and thus the terminal voltage $|V|$. However, the automatic voltage regulator, AVR (Chap. 9), has a much faster response. By reducing the field current it cancels the effect of the speed increase resulting in constant $|V|$.

FAC. DE CIENCIAS EXACTAS Y TECNOLOGIA
BIBLIOTECA

most other buses it is being tapped by the system loads. In between, the power will flow in the network meshes. *A given set of loads can be served from a given set of generators in an infinite number of "power-flow" or "load-flow" configurations.* Power-flow analysis concerns itself not only with the actual physical mechanism which controls the power flow in the network meshes but also how to select a "best" or "optimum" flow configuration from among the myriad of possibilities.

We summarize here the more important aspects of power-flow analysis:

1. The total amount of real power in the network emanates from the generator stations, the location and size of which are fixed. The generation must equal the demand at each moment, and since this power must be divided between the generators in a *unique* ratio (Chap. 8) in order to achieve optimum economic operation, we conclude that the individual generator outputs must be closely maintained at predetermined set points. It is important to remember that the demand undergoes *slow but wide changes* throughout the 24 h of the day. We must therefore slowly, either continuously or in discrete steps, change these set points as the hours wear on. This means that a load-flow configuration that fits the demand of a certain hour of the day may look quite different the next hour.
2. Transmission links can carry only certain amounts of power and we must make sure that we do not operate these links too close to their stability or thermal limits.
3. It is necessary to keep the voltage levels of certain buses within close tolerances. This can be achieved by proper scheduling of reactive powers.
4. If the power system is part of a larger pool, it must fulfill certain contractual power-scheduling commitments via its "tie-lines" to neighboring systems.
5. The disturbances following a massive network fault can cause system outages, the effects of which can be minimized by proper prefault power-flow strategies.
6. Power-flow analyses are very important in the planning stages of new networks or additions to existing ones.

The overall power-flow problem can be divided into the following subproblems, each of which we shall discuss separately:

1. Formulation of a suitable mathematical network model. The model must describe adequately the relationships between voltages and powers in the interconnected system.
2. Specification of the power and voltage constraints that must apply to the various buses of the network.
3. Numerical computation of the power-flow equations subject to the above constraints. These computations give us, with sufficient accuracy, the values of all bus voltages.
4. When all bus voltages have thus been determined, we must, finally, compute the actual power flows in all transmission lines.

7-5 A TWO-BUS DEMONSTRATION EXAMPLE

We can best demonstrate the key features of power-flow analysis by discussing the simple two-bus system shown in Fig. 7-2*a*. A real power system never is this simple; nevertheless, it will serve the demonstration purpose well.

Each bus is being fed from generator units which inject the powers S_{G1} and S_{G2}, respectively, into the buses. For simplicity we measure these generator powers on the HV sides of the step-up transformers. Demanded loads are tapped from each bus in the amounts S_{D1} and S_{D2}. The two buses are interconnected via a transmission line that is characterized (Fig. 7-2*b*) by a π network consisting of a series admittance Y_s and two parallel admittances Y_p. The two bus voltages are symbolized V_1 and V_2, respectively.

In the following analysis (and we shall retain this praxis throughout the book), it is convenient to lump the generator power and the load power of a particular bus into a *net* power, referred to as the *bus power* for the bus in question. For bus i we give this bus power the symbol S_i and define it as the

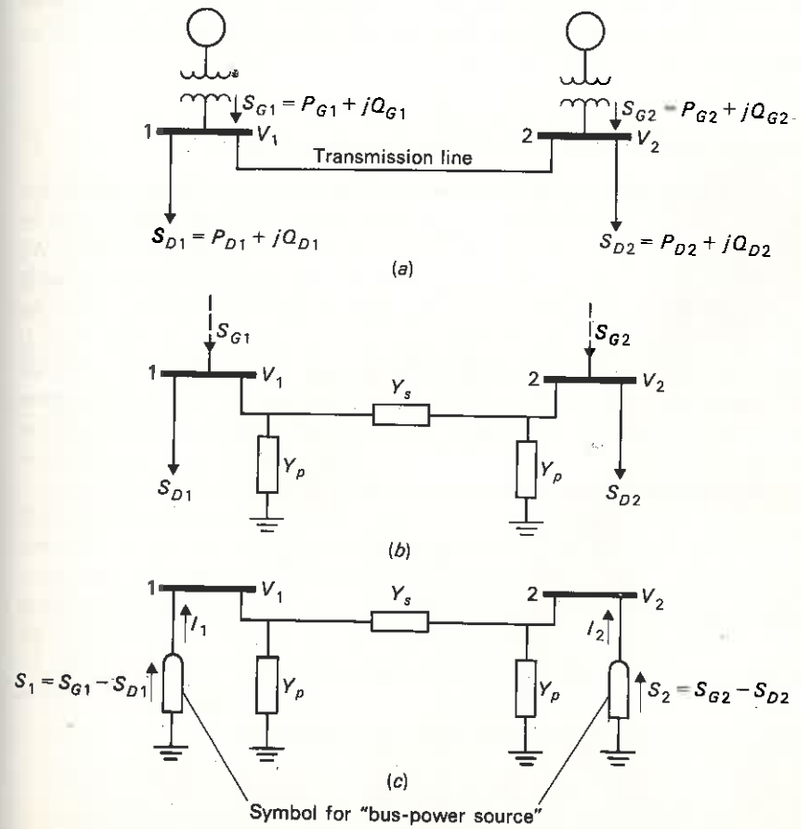

Figure 7-2 A two-bus example system.

difference between the generator and load powers. For our two-bus system we thus have the two bus powers

$$S_1 = P_1 + jQ_1 \triangleq P_{G1} - P_{D1} + j(Q_{G1} - Q_{D1})$$
$$S_2 = P_2 + jQ_2 \triangleq P_{G2} - P_{D2} + j(Q_{G2} - Q_{D2}) \tag{7-3}$$

The bus power can be considered as injected into the bus by a "bus power source," the symbol of which we have introduced in Fig. 7-2*c*.

The given system would be operated in the following manner:

By automatic manipulation of the prime mover torques, we would keep an exact balance between the total generated *real* power and the total demanded *real* power plus *real* losses. *A constant frequency is the criterion that such a balance is being kept.*

By manipulation of the field current in each rotor, and thus the stator emf, we keep each bus voltage at a predetermined level, independent of the variations in loads.

The function of the transmission line is to provide a route for the surplus power on one bus to the surplus load on the other, and/or to serve as an emergency link.

7-5-1 System Model—The Power-Flow Equations (PFE)

Basic to an understanding of the power-flow mechanism on a power grid is the establishment of the mathematical model from which the flow picture can be predicted. We shall refer to this model as the "power-flow equations," PFE. We presently develop this model for the demonstration example by using well-known network theory. The bus power S_1 injected into bus 1 follows from the equation $S_1 = V_1 I_1^*$ where I_1 is the *net* or *bus current* entering bus 1. This current must equal the current entering the line. The latter current consists of two components,† one component $V_1 Y_p$ flowing into the shunt admittance, and one component $(V_1 - V_2)Y_s$ flowing into the series admittance of the equivalent line network.

Thus, for current balance at bus 1, we have

$$I_1 = \frac{S_1^*}{V_1^*} = V_1 Y_p + (V_1 - V_2)Y_s$$

and similarly, for bus 2, (7-4)

$$I_2 = \frac{S_2^*}{V_2^*} = V_2 Y_p + (V_2 - V_1)Y_s$$

Both equations are, of course, on a per-phase basis.

† Neither of which can be individually measured. Why?

We can write the last two equations more simply:

$$I_1 = \frac{S_1^*}{V_1^*} = y_{11} V_1 + y_{12} V_2$$
$$I_2 = \frac{S_2^*}{V_2^*} = y_{21} V_1 + y_{22} V_2 \tag{7-5}$$

where, for brevity, we have introduced the *bus admittance elements*

$$y_{11} \triangleq Y_p + Y_s$$
$$y_{12} \triangleq y_{21} = -Y_s \tag{7-6}$$
$$y_{22} \triangleq Y_p + Y_s$$

We introduce at this stage the following vectors and matrix

$$\mathbf{I}_{\text{bus}} \triangleq \begin{bmatrix} I_1 \\ I_2 \end{bmatrix} \quad \textit{bus current vector} \tag{7-7}$$

$$\mathbf{V}_{\text{bus}} \triangleq \begin{bmatrix} V_1 \\ V_2 \end{bmatrix} \quad \textit{bus voltage vector} \tag{7-8}$$

$$\mathbf{Y}_{\text{bus}} \triangleq \begin{bmatrix} y_{11} & y_{12} \\ y_{21} & y_{22} \end{bmatrix} \quad \textit{bus admittance matrix} \tag{7-9}$$

Equations (7-5) can then be written in the more compact form:

$$\mathbf{I}_{\text{bus}} = \mathbf{Y}_{\text{bus}} \mathbf{V}_{\text{bus}} \tag{7-10}$$

which, if inverted, yields the alternative form

$$\mathbf{V}_{\text{bus}} = \mathbf{Z}_{\text{bus}} \mathbf{I}_{\text{bus}} \tag{7-11}$$

where

$$\mathbf{Z}_{\text{bus}} = \mathbf{Y}_{\text{bus}}^{-1} = \begin{bmatrix} z_{11} & z_{12} \\ z_{21} & z_{22} \end{bmatrix} \tag{7-12}$$

is the *bus impedance matrix.*

Equations (7-10) and (7-11) represent a *complex, linear, simultaneous equation set.* The linearity feature assures an easy solution of the unknowns. For example, if the bus voltages are assumed known the unknown bus currents are computed by direct substitution into (7-10). Vice versa, if currents are the knowns then the unknown voltages are computed from (7-11). We need to invert the matrix $\mathbf{Y}_{\text{bus}}$, of course, but this is routine on a digital computer.

However, in reality *powers*, not currents, are known and this changes the form of Eqs. (7-5) to

$$S_1^* = P_1 - jQ_1 = y_{11} V_1 V_1^* + y_{12} V_2 V_1^*$$
$$S_2^* = P_2 - jQ_2 = y_{21} V_1 V_2^* + y_{22} V_2 V_2^* \tag{7-13}$$

These are our sought PFE's.

Their solution is considerably more difficult than that of the linear sets (7-10) and (7-11) because the equations (7-13) are *nonlinear*.

Example 7-2 The transmission line in Fig. 7-2 is a 230-kV, 200-km line of the phase symmetric type analyzed in Examples 6-3 and 6-8. Find the $\mathbf{Y}_{bus}$ matrix for the two-bus system if we assume the line to be "electrically short." Also express all admittances in per unit referred to the base values:

$$|S_b| = \frac{300}{3} = 100 \text{ MVA/phase}$$

$$|V_b| = \frac{230}{\sqrt{3}} = 132.79 \text{ kV/phase}$$

We shall use this two-bus system to test the iterative computation methods to be presented later in the chapter. For this reason all computations shall be carried out to six significant figures.

SOLUTION We summarize the line parameters from Chap. 6:

$$R = 0.074 \ \Omega/\text{km}$$

$$\omega L = 0.457 \ \Omega/\text{km}$$

$$\frac{1}{\omega C} = 0.277 \ \text{M}\Omega/\text{km}$$

From the given base values we first compute the base admittance

$$|Y_b| = \frac{300}{230^2} = 0.00567108 \ \mho/\text{phase}$$

We then compute

$$Y_s = \frac{1}{Z_s} = \frac{1}{200(0.074 + j0.457)}$$

$$= 0.00172635 - j0.0106614 \ \mho/\text{phase}$$

$$= 0.304413 - j1.879956 \text{ pu } \mho/\text{phase}$$

$$Y_p = \frac{1}{-j2770} = j0.000361011 \ \mho/\text{phase}$$

$$= j0.0636582 \text{ pu } \mho/\text{phase}$$

$$\therefore \quad y_{11} = y_{22} = 0.304413 - j1.879956 + j0.0636583$$

$$= 0.304413 - j1.816298 = 1.841631\angle{-80.485610^\circ}$$

$$y_{12} = y_{21} = -0.304413 + j1.879956 = 1.904443\angle{99.197819^\circ}$$

The $\mathbf{Y}_{bus}$ matrix thus equals

$$\mathbf{Y}_{bus} = \begin{bmatrix} 1.841631\angle{-80.485610^\circ} & 1.904443\angle{99.197819^\circ} \\ 1.904443\angle{99.197819^\circ} & 1.841631\angle{-80.485610^\circ} \end{bmatrix} \text{ pu} \tag{7-14}$$

7-5-2 Writing the PFE's in Real Form

We can write Eqs. (7-13) as follows:

$$P_1 - jQ_1 = V_1^* \sum_{k=1}^{2} y_{1k} V_k \tag{7-15}$$

$$P_2 - jQ_2 = V_2^* \sum_{k=1}^{2} y_{2k} V_k \tag{7-16}$$

or, more compactly,

$$P_i - jQ_i = V_i^* \sum_{k=1}^{2} y_{ik} V_k \qquad \text{for } i = 1, 2 \tag{7-17}$$

Each bus voltage V_i has a magnitude $|V_i|$ and a phase angle δ_i relative to some as of yet nondefined *reference phasor*. The bus admittance element is in general complex (compare Eq. (7-14)) and can be written

$$y_{ij} = |y_{ij}|\angle{\gamma_{ij}} \tag{7-18}$$

We thus can write the PFE's (7-17) in the form

$$P_i - jQ_i = \sum_{k=1}^{2} |y_{ik}|\,|V_i|\,|V_k| e^{j(\delta_k - \delta_i + \gamma_{ik})} \qquad \text{for } i = 1, 2 \tag{7-19}$$

From this last form we can readily separate the real and imaginary parts:

$$P_i = \sum_{k=1}^{2} |y_{ik}|\,|V_i|\,|V_k| \cos(\delta_k - \delta_i + \gamma_{ik}) \triangleq f_{ip} \qquad \text{for } i = 1, 2 \tag{7-20}$$

$$Q_i = -\sum_{k=1}^{2} |y_{ik}|\,|V_i|\,|V_k| \sin(\delta_k - \delta_i + \gamma_{ik}) \triangleq f_{iq} \qquad \text{for } i = 1, 2 \tag{7-21}$$

It is instructive to write out these equations in detail for our two-bus example system. There will be a total of four and they read:

$$\begin{aligned}
P_1 &= P_{G1} - P_{D1} \\
&= |y_{11}|\,|V_1|^2 \cos\gamma_{11} + |y_{12}|\,|V_1|\,|V_2| \cos(\delta_2 - \delta_1 + \gamma_{12}) \triangleq f_{1p} \\
P_2 &= P_{G2} - P_{D2} \\
&= |y_{21}|\,|V_2|\,|V_1| \cos(\delta_1 - \delta_2 + \gamma_{21}) + |y_{22}|\,|V_2|^2 \cos\gamma_{22} \triangleq f_{2p} \\
Q_1 &= Q_{G1} - Q_{D1} \\
&= -|y_{11}|\,|V_1|^2 \sin\gamma_{11} - |y_{12}|\,|V_1|\,|V_2| \sin(\delta_2 - \delta_1 + \gamma_{12}) \triangleq f_{1q} \\
Q_2 &= Q_{G2} - Q_{D2} \\
&= -|y_{21}|\,|V_2|\,|V_1| \sin(\delta_1 - \delta_2 + \gamma_{21}) - |y_{22}|\,|V_2|^2 \sin\gamma_{22} \triangleq f_{2q}
\end{aligned} \tag{7-22}$$

The reader should verify these equations.

7-5-3 Important Characteristics of PFE

We make the following observations relating to Eqs. (7-22):

1. The equations are *algebraic* because they represent a model of a *static* system, or a system operating in steady state.
2. The equations are *nonlinear*, which circumstance will generally make it impossible to obtain *analytical* solutions. However, we shall be content to obtain *numerical* solutions and shall have no difficulty doing so by digital computer.
3. The "real-power balance" can be demonstrated by adding the first two of Eqs. (7-22), i.e.,

$$P_{G1} + P_{G2} = P_{D1} + P_{D2} + f_{1p} + f_{2p} = P_{D1} + P_{D2} + P_L \qquad (7\text{-}23)$$

   This equation states that the sum of the real generation equals the sum of the real demand plus the real losses P_L, the latter equalling the sum of f_{1p} and f_{2p}.
4. The "reactive-power balance" can be similarly demonstrated by adding the last two of Eqs. (7-22):

$$Q_{G1} + Q_{G2} = Q_{D1} + Q_{D2} + f_{1q} + f_{2q} = Q_{D1} + Q_{D2} + Q_L \qquad (7\text{-}24)$$

   The "loss" Q_L in the latter equation equals the actual reactive power loss in the line series inductance *minus* the reactive power generated in the line shunt capacitance.
5. Since the four functions $f_{1p}, \ldots, f_{2q}$ defined in Eq. (7-22) are functions of the voltage variables *only* the same will apply to the losses which thus can be written

$$\begin{aligned} P_L &= P_L(|V_1|, |V_2|, \delta_1, \delta_2) \\ Q_L &= Q_L(|V_1|, |V_2|, \delta_1, \delta_2) \end{aligned} \qquad (7\text{-}25)$$

6. Note that in all four of Eqs. (7-22) the phase angles δ_1 and δ_2 appear in *difference form*, $\delta_1 - \delta_2$.
7. In addition to the fixed network parameters, Eqs. (7-22) contain 12 variables. Consequently, it is not possible to obtain a solution for any of the variables unless we reduce the number of "unknowns" by fixing the values for some of the variables. *We must, in fact, reduce the number of "unknowns" from twelve to four to match the number of equations.* Thus we must a priori specify eight of the variables. The remaining four can then, at least in principle, be solved† from Eqs. (7-22).

† Even in this case we have, of course, no guarantee that we obtain a *unique* solution, since it is possible that a nonlinear set of equations of this type has *several* solutions. (Recall, for example, that the nonlinear equation

$$\sin x = 0$$

has an infinite number of solutions.)

As a rule, however, there is only *one* solution that is of stable practical significance.

7-5-4 Classification of System Variables

The last observation brings into focus one of the most important features of the problems to be discussed in this chapter. Since we wish to obtain a feel for the cause-effect relationship of the system, it is imperative that we bring some measure of order into the abundance of variables. For this purpose we divide them into the following natural groups.

Uncontrollable or disturbance variables Of the 12 variables we agree that the demand variables P_{D1}, P_{D2}, Q_{D1}, and Q_{D2} are completely *beyond our control since they are determined by the power user.* We shall find it convenient to symbolize, for distinguishing purposes, these *uncontrollable*, or *disturbance*, variables by the symbols $p_1, \ldots, p_4$. The latter name refers to the fact that the unpredictable changes in these variables cause the system to deviate from its nominal state.

The disturbance variables thus defined constitute the components of a four-dimensional *disturbance vector* **p**, defined as follows:

$$\mathbf{p} = \begin{bmatrix} p_1 \\ p_2 \\ p_3 \\ p_4 \end{bmatrix} \triangleq \begin{bmatrix} P_{D1} \\ P_{D2} \\ Q_{D1} \\ Q_{D2} \end{bmatrix} \qquad (7\text{-}26)$$

State and control variables The eight variables that are left, $|V_1|$, $|V_2|$, δ_1, δ_2, P_{G1}, P_{G2}, Q_{G1}, and Q_{G2}, can easily be grouped into two categories, "independent" and "dependent" variables, which in control theory are given the names *control* and *state variables*, respectively. In the former category we include those variables that, physically, are used to manipulate, or "control," the latter. Clearly, then, the generator outputs P_{G1}, P_{G2}, Q_{G1}, and Q_{G2} are our control variables.

As we have noted earlier by manipulation of Q_{G1} and Q_{G2} we strongly affect the voltage magnitudes $|V_1|$ and $|V_2|$. P_{G1} and P_{G2} similarly affect δ_1 and δ_2.

To summarize, we define the variables $|V_1|$, $|V_2|$, δ_1, and δ_2 as state variables. To conform with accepted symbol practice, they will be represented by the symbols $x_1 \ldots, x_4$. The variables P_{G1}, P_{G2}, Q_{G1}, and Q_{G2} are our control variables, for which we shall prefer to adopt the usual symbols $u_1, \ldots, u_4$.

We introduce, therefore, the *state vector* **x** and the *control vector* **u**, defined as follows:

$$\mathbf{x} = \begin{bmatrix} x_1 \\ x_2 \\ x_3 \\ x_4 \end{bmatrix} \triangleq \begin{bmatrix} \delta_1 \\ \delta_2 \\ |V_1| \\ |V_2| \end{bmatrix} \qquad \mathbf{u} = \begin{bmatrix} u_1 \\ u_2 \\ u_3 \\ u_4 \end{bmatrix} \triangleq \begin{bmatrix} P_{G1} \\ P_{G2} \\ Q_{G1} \\ Q_{G2} \end{bmatrix} \qquad (7\text{-}27)$$

7-5-5 Solution of PFE—A Basic Dilemma

Having thus classified the 12 variables in Eqs. (7-22) the solution of these equations could seemingly proceed in the following steps:

Step 1 From an assumed knowledge of the customer demand, we possess an a priori knowledge of the four p parameters.

Step 2 We make an a priori assumption about the four control variables, i.e., we specify the bus generations.

Step 3 The remaining four state variables constitute, then, our "unknowns." With exactly four equations, we should in principle be able to solve for these unknowns.

At a closer examination we find, however, that there are two basic roadblocks that prevent us from proceeding along the outlined steps:

1. *The PFE will never permit us to solve for the individual phase angles δ_1 and δ_2, but only their difference, $\delta_1 - \delta_2$.* The truth of this statement becomes immediately obvious if it is realized that *any arbitrary* value added to both δ_1 and δ_2 in Eq. (7-22) will not affect the equations.
2. *We cannot,* a priori, *specify all the four generation variables because the losses P_L and Q_L are not known.* The latter, as shown by Eqs. (7-25), are functions of the *state* variables, which as yet are unknown. Consequently, we do not a priori know the *total* real and reactive generations $P_{G1} + P_{G2}$ and $Q_{G1} + Q_{G2}$, respectively. We can, of course, specify two of the individual generations, for example, P_{G2} and Q_{G2}, which would then leave P_{G1} and Q_{G1} as unknowns.

7-5-6 Modified Specifications—Solution of Our Dilemma

We can bypass the above two problems in the following way. Since we realize that $\delta_1 - \delta_2$, rather than δ_1 and δ_2, must be treated as an unknown, we choose to fix either δ_1 or δ_2 at some arbitrary value.

In this book we shall always choose $\delta_1 = 0$, thereby in effect designating the voltage of bus 1 as our reference phasor. We thus have reduced the number of *unknown* state variables from four to three ($|V_1|$, $|V_2|$, and δ_2).

Included with the two unknown control variables we thus have now a total of *five* unknowns:

$$|V_1|,\ P_{G1},\ Q_{G1},\ |V_2|, \text{ and } \delta_2$$

One of these must clearly be specified before we can attempt a solution of the remaining four. Which one? *Mathematically any one* would do. *Physically,* however, we are quite limited. The choice will actually be between $|V_1|$ and Q_{G1}. We know that these two are strongly coupled. Increase Q_{G1} and $|V_1|$ will rise. As none of the bus voltages are specified so far we take now the opportunity to do so. We therefore specify $|V_1|$ and are consequently left with these four unknowns:

$$P_{G1},\ Q_{G1},\ |V_2|,\ \delta_2$$

We could in addition have specified $|V_2|$. In such a case we must, however, drop Q_{G2} from the list of a priori "knowns" and add it to our list of "unknowns." In either case, the number of unknowns will match the number of equations and solution of the PFE can proceed. Two examples will demonstrate the difference.

Example 7-3 The transmission line in Fig. 7-2 is assumed *lossless* having a series impedance

$$Z_s = j0.1 \text{ pu}$$

In addition, we neglect the line capacitance, i.e., we set

$$Y_p = 0$$

In this case we thus have

$$y_{11} = y_{22} = -y_{12} = -y_{21} = -j10 \text{ pu}$$

Voltage and power specifications are chosen as follows:

$$|V_1| = 1 \text{ pu}$$
$$P_{G2} = Q_{G2} = 0$$
$$P_{D1} = Q_{D1} = 0$$

Write the PFE and solve them.

SOLUTION The four equations (7-22) reduce to

$$\begin{aligned} P_{G1} &= -10|V_2| \sin \delta_2 \\ Q_{G1} &= 10 - 10|V_2| \cos \delta_2 \\ -P_{D2} &= 10|V_2| \sin \delta_2 \\ -Q_{D2} &= -10|V_2| \cos \delta_2 + 10|V_2|^2 \end{aligned} \tag{7-28}$$

Equations (7-22) do not generally possess analytical solutions. However, in this simple case they actually do. To find the solutions we first eliminate δ_2 between the third and fourth of the equations and, after some algebra, obtain

$$|V_2| = \sqrt{\frac{\sqrt{25 - P_{D2}^2 - 10Q_{D2}^2} - (Q_{D2} - 5)}{10}} \tag{7-29}$$

Then we can obtain δ_2 from the third equation

$$\delta_2 = -\sin^{-1}\left(\frac{P_{D2}}{10|V_2|}\right) \tag{7-30}$$

Finally, P_{G1} and Q_{G1} are obtained directly from the first and second equations (7-28).†

† Actually, by adding the first and third equation we have $P_{G1} = P_{D2}$. This means that Eqs. (7-28) represent *three* not *four* equations, the reason being that the system is *lossless.*

Numerical example Assume the load equals $P_{D2} = Q_{D2} = 1$ pu. We then obtain

$$|V_2| = 0.8799 \text{ pu kV}$$
$$\delta_2 = -6.5260°$$
$$Q_{G1} = 1.2580 \text{ pu Mvar}$$
$$P_{G1} = 1.0 \text{ pu MW}$$

In other words, to accommodate a load demand of $1 + j1$ at bus 2, the power angle of the line will be 6.5° and the bus voltage $|V_2|$ drops to 0.88 pu. Should the load demand grow to $1.5 + j1.5$ pu $|V_2|$ would drop to 0.63 pu and the power angle increase to 13.7°. Were we to increase the load demand to $2 + j2$ then Eq. (7-29) would not yield a real value for $|V_2|$ *telling us, in fact, that such a load cannot be transmitted.*

The reader may find it interesting to find the actual power limits for this line under the assumed specifications. *Explain what happens physically.*

In reviewing the results in Example 7-3 we may conclude that we cannot tolerate the severe drop in $|V_2|$ as evidently will occur. We might, therefore, specify even $|V_2|$.

Example 7-4 Consider the same system as in Example 7-3 but change now the specs as follows:

$$|V_1| = |V_2| = 1 \text{ pu}$$
$$P_{G2} = P_{D1} = Q_{D1} = 0$$

The PFE's now take on the form:

$$\begin{aligned} P_{G1} &= -10 \sin \delta_2 \\ Q_{G1} &= 10 - 10 \cos \delta_2 \\ -P_{D2} &= 10 \sin \delta_2 \\ Q_{G2} &= 10 - 10 \cos \delta_2 + Q_{D2} \end{aligned} \tag{7-31}$$

Solution of this set is quite simple. From the third equation we get

$$\delta_2 = -\sin^{-1}\left(\frac{P_{D2}}{10}\right) \tag{7-32}$$

From a knowledge of δ_2 the three other unknowns Q_{G1}, Q_{G2}, P_{G1} are then immediately computed.

Numerical example Let $P_{D2} = Q_{D2} = 2$ pu. (Recall that this load could *not* be transmitted in Example 7-3. Why can it be handled now?)

Results:

$$\delta_2 = -\sin^{-1}\left(\frac{2}{10}\right) = -11.54°$$
$$Q_{G1} = 10 - 10 \cos \delta_2 = 0.202 \text{ pu Mvar}$$
$$Q_{G2} = 2.202 \text{ pu Mvar}$$
$$P_{G1} = 2 \text{ pu MW}$$

Table 7-1

Bus type	A priori known variables						Unknowns obtained from PFE			
	P_D	Q_D	P_G	Q_G	$\lvert V\rvert$	δ	P_G	Q_G	$\lvert V\rvert$	δ
Reference bus	•	•			•	•	•	•		
Load bus	•	•	•	•					•	•
Voltage control bus	•	•	•		•			•		•

7-5-7 Bus Classification on the Basis of Specification

The above examples demonstrate that we can classify buses into at least three types depending upon the variable specifications used:

1. "Reference" ("swing," "slack") bus
2. "Load" bus
3. "Voltage control" bus

We have summarized in Table 7-1 what variables are "knowns" and "unknowns" for the three bus types.

In a typical system the load buses dominate. Normally 80 to 90 percent of all buses fall in this category. The rest are voltage control buses plus one reference bus.

7-6 GENERALIZATION TO n-BUS SYSTEM

In terms of the three vectors **x**, **u**, and **p**, we can evidently write the four equations (7-22) in the form

$$f_i(\mathbf{x}, \mathbf{u}, \mathbf{p}) = 0 \qquad \text{for } i = 1, 2, 3, 4 \tag{7-33}$$

Upon introducing the function vector

$$\mathbf{f} \triangleq \begin{bmatrix} f_1 \\ f_2 \\ f_3 \\ f_4 \end{bmatrix} \tag{7-34}$$

we can write Eq. (7-33) in the very compact form

$$\mathbf{f}(\mathbf{x}, \mathbf{u}, \mathbf{p}) = \mathbf{0} \tag{7-35}$$

referred to as *the vector form of the PFE.*

In our two-bus sample system the vector equation is four-dimensional, but realistic-size power systems may contain hundreds of buses and generators and

thousands of lines. We wish now to extend the foregoing discussions valid for a two-bus system to the general case of an n-bus system. For such a system we have the following $6n$ variables:

n bus voltage magnitudes $|V_i|$
n bus voltage phase angles δ_i
n real power generations P_{Gi}
n reactive power generations Q_{Gi}
n real power demands P_{Di}
n reactive power demands Q_{Di}

Since we can write one complex current equation of the type of Eqs. (7-5) for each bus, we will in effect have a total of $2n$ real equations of the type of Eqs. (7-22), i.e., our vector form of PFE will be $2n$-dimensional.

7-6-1 General Form of the PFE

To determine the PFE's in the general case consider the general bus i depicted in Fig. 7-3. Its generation and load are assumed to equal S_{Gi} and S_{Di}, respectively. The bus power S_i thus equals

$$S_i = S_{Gi} - S_{Di} = P_{Gi} - P_{Di} + j(Q_{Gi} - Q_{Di}) \tag{7-36}$$

Transmission lines connect bus i with other buses, k, in the system. At most there can be $n-1$ such outgoing lines, each of which can be represented by a π-equivalent, having the series and parallel admittances Y_{sik} and Y_{pik} respectively. If a line is nonexistent, its admittances simply are set at zero. In analogy with Eq. (7-4) we have the current balance equation.

$$I_i = \frac{S_i^*}{V_i^*} = V_i \sum_{\substack{k=1\\k\neq i}}^{n} Y_{pik} + \sum_{\substack{k=1\\k\neq i}}^{n} Y_{sik}(V_i - V_k)$$

$$= V_i \sum_{\substack{k=1\\k\neq i}}^{n} (Y_{pik} + Y_{sik}) + \sum_{\substack{k=1\\k\neq i}}^{n} (-Y_{sik})V_k \qquad \text{for } i = 1, 2, \ldots, n \tag{7-37}$$

We can obviously write these equations in the form

$$I_i = \frac{S_i^*}{V_i^*} = y_{i1}V_1 + y_{i2}V_2 + \cdots + y_{ii}V_i + \cdots + y_{in}V_n \qquad \text{for } i = 1, 2, \ldots, n \tag{7-38}$$

where

$$y_{ii} \triangleq \sum_{\substack{k=1\\k\neq i}}^{n} (Y_{pik} + Y_{sik}) \tag{7-39}$$

and

$$y_{ik} = y_{ki} \triangleq -Y_{sik} \tag{7-40}$$

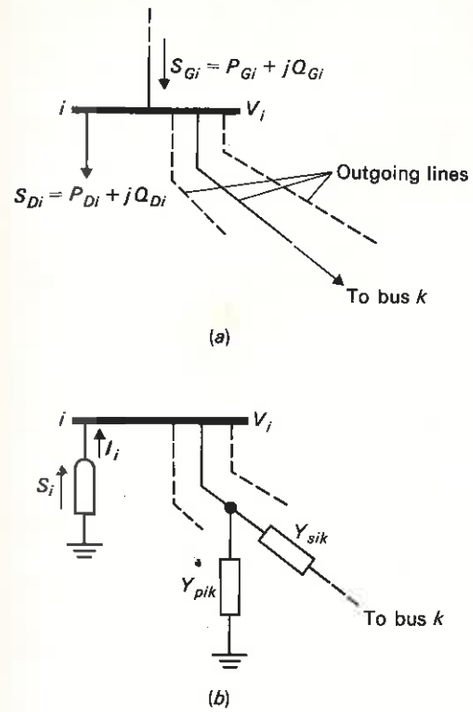

Figure 7-3 General bus with generation, load, and outgoing lines.

We introduce now the n-dimensional *bus current* and *bus voltage* vectors:

$$\mathbf{I}_{\text{bus}} = \begin{bmatrix} I_1 \\ \vdots \\ I_n \end{bmatrix} \qquad \mathbf{V}_{\text{bus}} = \begin{bmatrix} V_1 \\ \vdots \\ V_n \end{bmatrix} \tag{7-41}$$

and the $n \times n$ dimensional *bus admittance* and *bus impedance* matrices

$$\mathbf{Y}_{\text{bus}} = \begin{bmatrix} y_{11} & \cdots & y_{1n} \\ \cdots & \cdots & \cdots \\ y_{n1} & \cdots & y_{nn} \end{bmatrix} \qquad \mathbf{Z}_{\text{bus}} = \mathbf{Y}_{\text{bus}}^{-1} = \begin{bmatrix} z_{11} & \cdots & z_{1n} \\ \cdots & \cdots & \cdots \\ z_{n1} & \cdots & z_{nn} \end{bmatrix} \tag{7-42}$$

The matrix $\mathbf{Y}_{\text{bus}}$ represents the model of the passive portions of the n-bus network, *in systematic form*. From Eqs. (7-39) and (7-40) we conclude the following simple rules for finding the elements of the $\mathbf{Y}_{\text{bus}}$ matrix:

The diagonal element y_{ii} is obtained as the algebraic sum of all admittances incident to node i.

The off-diagonal elements $y_{ik} = y_{ki}$ are obtained as the negative of the admittance connecting nodes i and k.

In terms of these vectors and matrices we can obviously write the general equations (7-38) in the compact linear forms (7-10) and (7-11). If, however, as is usually the case *powers* rather than *currents* are known then the equations take on the nonlinear form

$$S_i^* = P_i - jQ_i = V_i^* \sum_{k=1}^{n} y_{ik} V_k \qquad \text{for } i = 1, 2, \ldots, n. \tag{7-43}$$

This is the general form of the PFE.

It should be noted that the n power-flow equations (7-43) are *complex*. These n equations therefore represent $2n$ *real* equations.

In analogy with Eqs. (7-20) and (7-21) we immediately write down these $2n$ real PFE's:

$$P_i = \sum_{k=1}^{n} |y_{ik}|\,|V_i|\,|V_k| \cos(\delta_k - \delta_i + \gamma_{ik}) \triangleq f_{ip} \tag{7-44}$$

$$Q_i = -\sum_{k=1}^{n} |y_{ik}|\,|V_i|\,|V_k| \sin(\delta_k - \delta_i + \gamma_{ik}) \triangleq f_{iq} \qquad \text{for } i = 1, 2, \ldots, n \tag{7-45}$$

Equations (7-44) and (7-45) express balance of real and reactive powers respectively at bus i.

Example 7-5 Consider the three-bus system depicted in Fig. 7-4. You can assume all three lines L_1, L_2, and L_3 as "electrically short." Find the $\mathbf{Y}_{bus}$ matrix for this system.

All lines are assumed to have these parameter data:

$$R = 0.075\ \Omega/\text{km and phase}$$

$$\omega L = 0.511\ \Omega/\text{km and phase}$$

$$\frac{1}{\omega C} = 0.311\ \text{M}\Omega/\text{km and phase}$$

SOLUTION We first compute the line impedances and admittances. Note that in computing Z_s we use the *full* line length, but for Z_p only *half*-length. The computed data is given in Table 7-2.

Table 7-2

Line	Length, km	$Z_s\ \Omega$	$Y_s \times 10^3$ ℧	$Z_p\ \Omega$	$Y_p \times 10^3$ ℧
1	190	$14.25 + j97.09$	$1.48 - j10.08$	$-j3274$	$j0.3054$
2	95	$7.125 + j48.55$	$2.96 - j20.16$	$-j6547$	$j0.1527$
3	125	$9.375 + j63.88$	$2.25 - j15.32$	$-j4976$	$j0.2010$

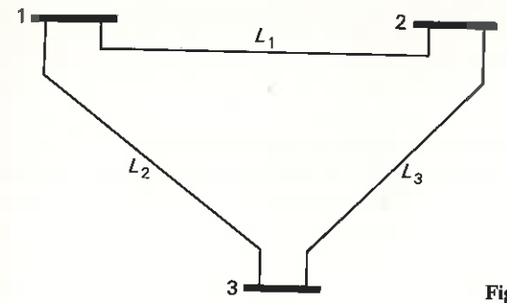

Figure 7-4 A three-bus example system.

In finding the bus admittance elements y_{ik} we use the rules given above. The computational details for one diagonal and one off-diagonal element follow:

$$y_{11} = [j0.3054 + j0.1527 + (1.48 - j10.08) + (2.96 - j20.16)] \times 10^{-3}$$
$$= (4.44 - j29.8) \times 10^{-3}\ \text{℧/phase}$$

$$y_{12} = y_{21} = -(1.48 - j10.08) \times 10^{-3} = (-1.48 + j10.1)10^{-3}\ \text{℧/phase}$$

The bus admittance matrix equals

$$\mathbf{Y}_{bus} = 10^{-3} \begin{bmatrix} 4.44 - j29.8 & -1.48 + j10.1 & -2.96 + j20.2 \\ -1.48 + j10.1 & 3.73 - j24.9 & -2.25 + j15.3 \\ -2.96 + j20.2 & -2.25 + j15.3 & 5.21 - j35.1 \end{bmatrix} \tag{7-46}$$

7-7 COMPUTATIONAL ASPECTS OF THE POWER-FLOW PROBLEM

Taking stock of our progress, we conclude that we have so far covered ground as follows:

1. We have developed systematic methods of assembling the network models and obtaining the PFE for general-size networks.
2. We have discussed the general characteristics of the PFE and, in particular, performed a logic classification of the large number of system variables.
3. We have discussed the important matter of a priori specification of control and state variables and have identified three types of buses based on variable specification.

We have not, however, tried to *solve* the power-flow equations except in a couple of unrealistically simple cases where, in addition, we neglected the line losses. Actually we did arrive at an *analytical* solution for the two-bus system in Example 7-3 and would, in fact, have been able to do so even if we had not neglected losses. Had we attempted a solution of the PFE for the three-bus system in Example 7-5 we would *not* be able to arrive at an analytical solution. Since looking for *analytical* solutions is clearly a hopeless task, we will instead

take the more practical approach of finding *numerical* solutions. Let us enumerate the necessary requirements that must be met by any computational technique that we propose:

1. It must be able to handle nonlinear algebraic equations.
2. It must be able to handle systems having hundreds of buses and thousands of lines.
3. It should not be limited to loss-free systems.
4. It must have sufficient accuracy.
5. It should not be too time-consuming since we may wish, in a practical situation, to perform many series of computations for various combinations of bus power and voltage specifications in order to obtain the best possible flow picture.
6. The n power flow equations (7-43) are complex equations. Our computer programs must take this fact into account if possible.

Historically, the power-flow problem was solved on special analog computers, referred to as "network analyzers." These were miniature replicas of the system to be studied, some of them operated on direct, some on alternating current. The vast majority of today's network computations are performed with digital computers.

We will devote our efforts exclusively toward digital methods.

7-7-1 Iterative Computation of the PFE

When we are faced with the problem of obtaining numerical solutions for a system of simultaneous nonlinear algebraic equations, the method of "systematic guessing" becomes a practical necessity. A great many methods have been proposed in the vast literature on numerical techniques; we shall look closer at two specific methods that have proved very useful in power-flow studies. Each method approaches the problem of solution in the following manner:

1. An initial solution, $V_i^{(0)}$, is guessed.
2. This solution is used in conjunction with the original equations (7-43) to compute a new *and better* first solution, $V_i^{(1)}$.
3. The first solution is used for finding a second one, etc.

This repetitive process of converging on the solution is referred to as an *iterative method*. The different methods utilize somewhat different schemes in computing the new estimates. By the term *algorithm* we mean a list of computer instructions specifying the sequence of operations used. Clearly, the quality of the algorithm must be judged by the *speed of convergence*. The two methods to be presented here differ considerably in this respect. *Generally, we obtain an increase in speed of convergence by paying a price in terms of algorithm complexity.*

In all iterative processes it is necessary to instruct the computer to stop grinding out better and better values *when the accuracy of all computed variables is deemed sufficient.* Typically in a power-flow computation one would stop the computations when *all* bus voltages in the $(\nu + 1)$st iteration would not be different from those in the νth iteration by more than a specified *convergence index* ε, typically of magnitude 10^{-4} pu. The voltages are *phasors* so we must therefore instruct the computer to stop when the difference phasor magnitudes are less than ε, i.e.,

$$|V_i^{(\nu+1)} - V_i^{(\nu)}| < \varepsilon \qquad \text{for } i = 2, \ldots, n \tag{7-47}$$

(For example, the criterion

$$|V_i^{(\nu+1)}| - |V_i^{(\nu)}| < \varepsilon$$

would assure us that the voltage *magnitudes* are within specified accuracy limits but the voltage *angles* might be way off.)

7-7-2 Computational Procedure Depends upon Bus Type

We outline now the computational sequencing. The computations to be performed at a certain bus, i, will depend upon bus type. A priori we know $V_1 = |V_1| \angle 0°$ for the reference bus plus the specified magnitudes $|V_i|$ for all voltage control buses. In our 0th iteration ($\nu = 0$) we designate (by intelligent guess) *all* the *missing* information about *all* n bus voltages. In other words, before any computations begin, numerical values $V_i^{(0)} = |V_i^{(0)}| \angle \delta_i^{(0)}$ must be assigned to *all* n bus voltages.

In the next iteration ($\nu = 1$) we perform computations to obtain new updated values $V_i^{(1)} = |V_i^{(1)}| \angle \delta_i^{(1)}$. We do this by letting the computer scan the PFE's (7-43) in order, performing those computations the chosen algorithm calls for. The nature of the computations depends upon bus type. Let us see how the three bus types differ in this regard.

1. Reference bus For this bus we know *both* $|V_1|$ and δ_1. Therefore *no* computations are needed here, i.e., we can skip bus 1 at every bus scan.

2. Load bus At this type of bus *both* $|V_i|$ and δ_i are unknown. Thus computations must be performed that yield upgraded values for *both* voltage *magnitude* and *phase*.

3. Voltage control bus Here we know the magnitude $|V_i|$ but must compute upgraded value for δ_i. Also, as Q_{Gi} is an unknown for this type of bus, we compute Q_{Gi} in each iteration cycle in order to check that it lies within the capability range of the reactive generation source at the bus in question. Should it fall *outside* the range then, from that iteration on, we let Q_{Gi} assume the limit value. *With Q_i thus fixed the bus in effect becomes a load bus.*

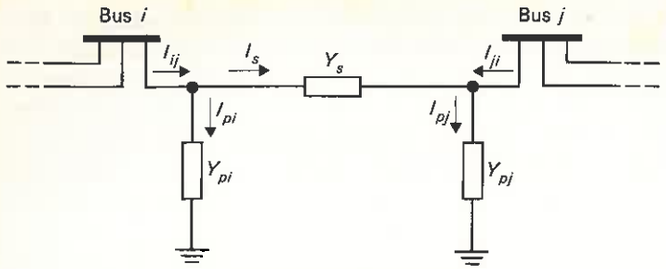

Figure 7-5. Model for finding line power in line connecting buses i and j.

The formula for computing Q_{Gi} is obtained from Eq. (7-45):

$$Q_{Gi} = Q_{Di} + Q_i = Q_{Di} - \sum_{k=1}^{n} |y_{ik}|\,|V_i|\,|V_k| \sin\,(\delta_k - \delta_i + \gamma_{ik}) \tag{7-48}$$

In Summary: When we have scanned all the buses *except 1* a certain number of times the convergence criterion (7-47) eventually is satisfied.† At this point *all bus voltages are known to within acceptable ε limits.* Also, at the voltage control buses, the required reactive generations are likewise known.

Two items remain before our computations are complete:

Item 1. Computation of slack bus powers. The first of Eqs. (7-43) reads

$$P_1 - jQ_1 = V_1^* \sum_{k=1}^{n} y_{1k} V_k \tag{7-49}$$

Since all the voltages are known we can compute P_1 and Q_1, and thus P_{G1} and Q_{G1}, which are our unknowns at this bus.

Item 2. Computation of line flows. With full knowledge of *all* bus voltages the final step in the power-flow analysis is the computation of the power flows on the various transmission lines of the network. Consider the line connecting the two buses i and j in Fig. 7-5. The line (plus reactors if any) can be represented by the series admittance Y_s and the two shunt admittances Y_{pi} and Y_{pj}.

The line current I_{ij}, measured at bus i and defined positive in the direction $i \to j$, equals

$$I_{ij} = I_s + I_{pi} = (V_i - V_j)Y_s + V_i Y_{pi} \tag{7-50}$$

(For definition of I_s and I_{pi} see Fig. 7-5). The line powers S_{ij} and S_{ji} measured at buses i and j respectively and both defined positive *into* the line are now

† Assuming, of course, that our chosen algorithm is any good.

obtained:

$$\begin{aligned} S_{ij} &= P_{ij} + jQ_{ij} = V_i I_{ij}^* = V_i(V_i^* - V_j^*)Y_s^* + |V_i|^2 Y_{pi}^* \\ S_{ji} &= P_{ji} + jQ_{ji} = V_j I_{ji}^* = V_j(V_j^* - V_i^*)Y_s^* + |V_j|^2 Y_{pj}^* \end{aligned} \tag{7-51}$$

This completes our power-flow study. Now let us turn our attention to the choice of algorithms.

7-8 GAUSS-SEIDEL (G-S) ITERATIVE TECHNIQUE

This is one of the simplest iterative methods known. It was also one of the most popular methods used in the early days of digital power-flow analysis. The more powerful Newton-Raphson (N-R) method is today dominating the field. We do, however, include the G-S method here for these reasons:

1. Because of its simplicity it has a definite tutorial value.
2. It is still used for small power systems where program simplicity is more important than computing costs.
3. It is used in many cases for large-scale systems to obtain a first approximate solution which is then used as the "initial solution" for the N-R program.

7-8-1 The G-S Algorithm

Although we shall be primarily interested in solving an n-dimensional equation of type

$$\mathbf{f}(\mathbf{x}) = \mathbf{0} \tag{7-52}$$

we introduce this method by first solving iteratively the scalar equation

$$f(x) = 0 \tag{7-53}$$

Preparatory to finding the G-S algorithm we always need to reshape the given function $f(x)$ into the alternative form

$$x = F(x) \tag{7-54}$$

For a given function f it is always possible to find a function F.

Example 7-6 Consider the second-order equation

$$f(x) = x^2 - 5x + 4 = 0$$

The function $f(x)$ represents the parabola in Fig. 7-6. We can obviously write $f(x)$ as

$$x = \underbrace{\tfrac{1}{5}x^2 + \tfrac{4}{5}}_{F(x)}$$

which is of the form (7-54).

The function $F(x)$ is plotted in Fig. 7-6.

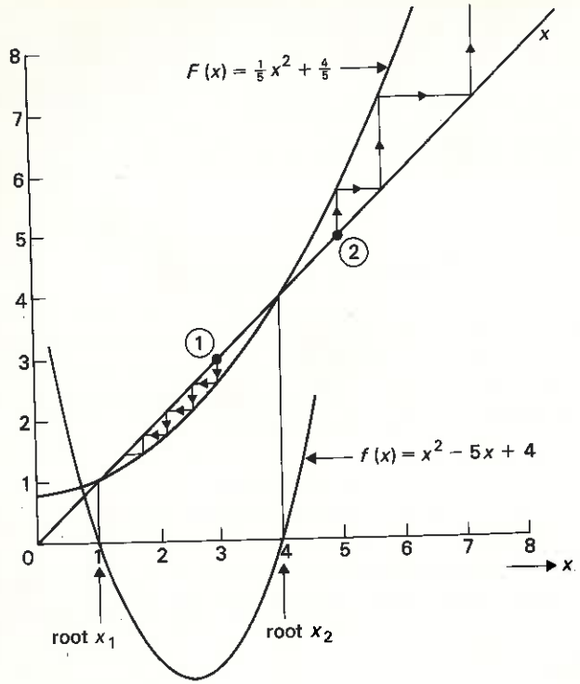

Figure 7-6 Graphical demonstration of the Gauss-Seidel algorithm.

Note that $F(x)$ is not unique. In the present example we could also have written

$$x = \underbrace{\frac{5x - 4}{x}}_{F(x)}$$

How would this function $F(x)$ plot in Fig. 7-6?

The sought algorithm is now obtained by the following empiric reasoning.

The equations $x - F(x) = 0$ and $f(x) = 0$ must have identical roots. The function $x - F(x)$ represents a "boxed in" region between the sloping line x and the function $F(x)$. As this region "thins out" to zero close to a root we can reach that root by a zigzag search process indicated in Fig. 7-6. Starting in the point $x^{(0)}$ marked ① we obtain in order the upgraded values $x^{(1)}$, $x^{(2)}, \ldots, x^{(\nu)}$ which values obviously are computed from the formula

$$x^{(\nu+1)} = F(x^{(\nu)}) \tag{7-55}$$

which thus becomes our algorithm.

We demonstrate the procedure by presenting the first few steps of the process as applied to our above example function.

Iteration 0 Make the arbitrary initial guess $x^{(0)} = 3$

Iteration 1 From the iteration equation (7-55) compute

$$x^{(1)} = F(3) = \tfrac{1}{5} \times 3^2 + \tfrac{4}{5} = 2.600$$

Iteration 2

$$x^{(2)} = F(2.600) = \tfrac{1}{5} \times 2.600^2 + \tfrac{4}{5} = 2.152$$

etc.

The iterative process is ended when the improvements between two consecutive iterations is less than a certain tolerance ε, that is, when

$$|x^{(\nu+1)}| - |x^{(\nu)}| < \varepsilon$$

We note from Fig. 7-6 that we probably will need quite a few iterations to reach sufficiently close to the root. *The slow convergence is one disadvantage of this method.*

Another disadvantage is that the process may not converge at all. This is demonstrated in Fig. 7-6 in an attempt to find the second root, $x_2 = 4$. Starting from $x^{(0)} = 5$, in the point marked ② we actually diverge.

The above method can readily be extended to the n-dimensional equation (7-52). We write the equation first in the form

$$\mathbf{x} = \mathbf{F}(\mathbf{x}) \tag{7-56}$$

and select, then, in analogy with Eq. (7-55), the iteration formula

$$\mathbf{x}^{(\nu+1)} = \mathbf{F}(\mathbf{x}^{(\nu)}) \tag{7-57}$$

7-8-2 The G-S Method Applied to the PFE's

We choose the *complex* form (Eq. 7-43) of the power-flow equations as our point of departure. We rewrite the equation in two steps:

Step 1

$$P_i - jQ_i = V_i^* y_{ii} V_i + V_i^* \sum_{\substack{k=1 \\ k \neq i}}^{n} y_{ik} V_k \qquad \text{for } i = 2, \ldots, n$$

Step 2

$$V_i = \frac{1}{y_{ii}} \left[\frac{P_i - jQ_i}{V_i^*} - \sum_{\substack{k=1 \\ k \neq i}}^{n} y_{ik} V_k \right] \qquad \text{for } i = 2, \ldots, n$$

As the last equation obviously is of the form (7-56) we then have one† possible G-S algorithm

$$V_i^{(\nu+1)} = \frac{1}{y_{ii}} \left[\frac{P_i - jQ_i}{(V_i^{(\nu)})^*} - \sum_{\substack{k=1 \\ k \neq i}}^{n} y_{ik} V_k^{(\nu)} \right] \qquad \text{for } i = 2, \ldots, n \tag{7-58}$$

Note that as V_1 is known a priori, computations need only be performed for buses $2, \ldots, n$.

Before we try out this method on the PFE's let us first decide on a suitable test system.

† Others can be found. This one is chosen for the very simple reason that experience confirms that it yields an algorithm that converges in most cases.

7-8-3 A Two-Bus Test System

As we compare the G-S and N-R computational methods in this chapter we shall test their effectiveness on the simple two-bus system depicted in Fig. 7-7.

This system has the advantage of simplicity. As we demonstrate the computations in detail they will not become unwieldy—as they would even for a three-bus system. It is obviously not possible to exemplify *simultaneously* all three bus types on a two-bus test system. This slight problem can be circumvented by the switched *controllable* capacitor at bus 2. When the capacitor is not energized, the bus 2 becomes a "load" bus. When energized its controllable reactive generation will make bus 2 a "voltage control" bus.

The 230-kV line is assumed to have the $\mathbf{Y}_{\text{bus}}$ data in Eq. (7-14). Figure 7-7 also depicts the specified loads at each bus and the voltage specification at bus 1.

7-8-4 The G-S Method Applied to "Load" Buses

As we apply the G-S iterative technique to our two-bus test system we shall exemplify the two cases when bus 2 is either a "load" bus or a "voltage control" bus. We start with the former.

Example 7-7 In this case the switched capacitor at bus 2 is out. From the bus loads specified in Fig. 7-7 we find the bus powers

$$S_1 = P_{G1} - 1.15 + j(Q_{G1} - 0.31) \text{ pu}$$

$$S_2 = -0.45 - j0.20 \text{ pu}$$

Our problem here is to find $V_2 = |V_2| \underline{/\delta_2}$.

SOLUTION In this case $n = 2$ and Eqs. (7-58) reduce to *one* complex equation

$$V_2^{(\nu+1)} = \frac{1}{y_{22}}\left[\frac{P_2 - jQ_2}{(V_2^{(\nu)})^*} - y_{21}V_1\right] \tag{7-59}$$

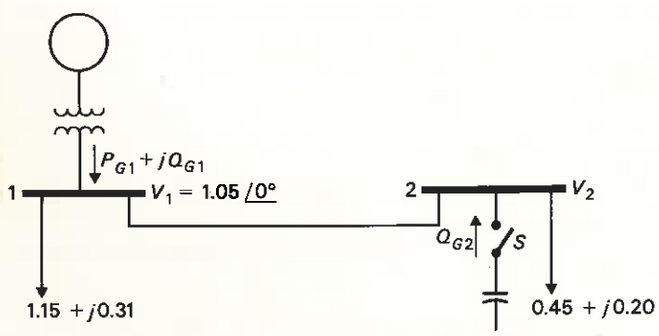

Figure 7-7 Power-flow computations performed on this two-bus example system. All voltage and load data in per units.

Note that $V_1 = 1.05$ pu. Note also that because the equation is *complex* it actually consists of *two real* equations. The G-S algorithm will read (with numerical values substituted)

$$V_2^{(\nu+1)} = (0.542997\underline{/80.485610°})\left[\frac{0.492443\underline{/156.037511°}}{(V_2^{(\nu)})^*} - 1.999665\underline{/99.197819°}\right]$$

Before we can start the iterations we must estimate† an initial value $V_2^{(0)}$. We guess that $|V_2|$ will drop about 10 percent below $|V_1|$ as a result of the specified load, i.e., we set

$$|V_2^{(0)}| = 0.95 \text{ pu kV}$$

As 0.45 pu MW (= 135 MW) shall be transmitted via the 91 Ω series reactance we use formula (3-49) to find the power angle:

$$135 = \frac{241 \times 219}{91} \sin \delta$$

$$\therefore \quad \delta = 13.5°$$

Thus a reasonable starting value would be

$$V_2^{(0)} \doteq 0.95 \underline{/-13.5°} \text{ pu kV}$$

and our algorithm yields

$$V_2^{(1)} = (0.542997\underline{/80.485610°})\left[\frac{0.492443\underline{/156.037511°}}{0.95\underline{/13.5°}} - 1.999665\underline{/99.197819°}\right]$$

$$= 0.902029\underline{/-12.682785°} \text{ pu kV}$$

One additional iteration yields

$$V_2^{(2)} = (0.542997\underline{/80.485610°})\left[\frac{0.492443\underline{/156.037511°}}{0.902029\underline{/12.682785°}} - 1.999665\underline{/99.197819°}\right]$$

$$= 0.897226\underline{/-13.623066°} \text{ pu kV}$$

The above computations were made on a hand calculator. If actually programmed on a digital computer voltage convergence to within $\varepsilon = 10^{-4}$ pu will require seven iterations. The final solution will be

$$V_2 = 0.89103\underline{/-13.6448°} \text{ pu kV}$$

With full knowledge of the two bus voltages we can now compute the line flows and the slack-bus powers.

Equation (7-51) yields

$$S_{12} = 0.47377 + j0.22607 \text{ pu}$$

$$S_{21} = -0.45000 - j0.20000 \text{ pu}$$

Equation (7-49) gives

$$P_1 - jQ_1 = 0.47377 - j0.22607 \text{ pu}$$

Thus

$$P_{G1} = P_1 + P_{D1} = 0.47377 + 1.15 = 1.62377 \text{ pu MW}$$

$$Q_{G1} = Q_1 + Q_{D1} = 0.22607 + 0.31 = 0.53607 \text{ pu Mvar}$$

Figure 7-8 depicts in summary fashion the total load-flow picture.

† Often one would simply start the computations by setting all voltages equal to the reference bus voltage, a so-called "flat voltage start."

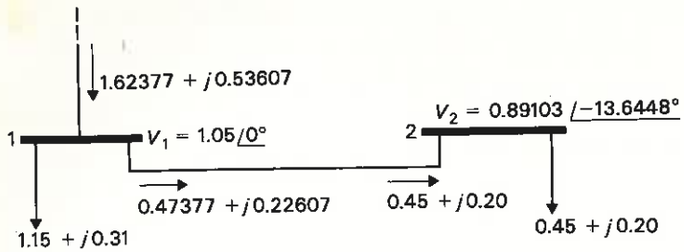

Figure 7-8 Power-flow picture for load configuration in Fig. 7-7. Bus 2 is a load bus.

7-8-5 The G-S Method Applied to "Voltage Control" Buses

Example 7-8 In this case we energize the capacitor at bus 2. With the *same* bus loads and reference bus voltage as in Example 7-7 we now, in addition, specify the bus voltage magnitude $|V_2|$ to equal

$$|V_2| = 1.00 \text{ pu kV}$$

Find δ_2, Q_{G2}, slack-bus powers and total power flow picture.

SOLUTION We again make use of the algorithm (7-59) but it must be corrected in two ways:

1. The bus power Q_2 now equals $Q_2 = Q_{G2} - 0.20$ and is computed from Eq. (7-48).
2. Whenever V_2^* is substituted its magnitude must be adjusted to the specified value $|V_2| = 1.00$ pu.

Our algorithm thus reads

$$V_2^{(\nu+1)} = (0.542997\underline{/80.485610°})\left[\frac{-0.45 - jQ_2^{(\nu)}}{1.00\underline{/-\delta_2^{(\nu)}}} - 1.999665\underline{/99.197819°}\right] \tag{7-60}$$

For $Q_2^{(\nu)}$ we have

$$Q_2^{(\nu)} = -\sum_{k=1}^{2} |y_{2k}|\,|V_2^{(\nu)}|\,|V_k| \sin(\delta_k - \delta_2^{(\nu)} + \gamma_{2k})$$

$$= 1.816298 - 1.999665 \sin(99.197819° - \delta_2^{(\nu)}) \tag{7-61}$$

We start with the guess

$$V_2^{(0)} = 1.00\underline{/-10°} \text{ pu kV}$$

From Eq. (7-61) we compute

$$Q_2^{(0)} = -1.999665 \sin(99.197819° + 10°) + 1.816298$$

$$= -0.072163 \text{ pu Mvar}$$

Upon substitution into (7-60) we obtain

$$V_2^{(1)} = (0.542997\underline{/80.485610°})\left[\frac{-0.45 + j0.072163}{1.00\underline{/10°}} - 1.999665\underline{/99.197819°}\right]$$

$$= 0.992663\underline{/-12.995362°} \text{ pu kV}$$

and then from Eq. (7-61)

$$Q_2^{(1)} = 1.816298 - 1.999665 \sin(99.197819° + 12.995362)$$

$$= -0.035223 \text{ pu Mvar}$$

Two additional iterations yield the value pairs:

$$V_2^{(2)} = 1.000083\underline{/-12.967073°} \text{ pu kV}$$

$$Q_2^{(2)} = -0.035596 \text{ pu Mvar}$$

and

$$V_2^{(3)} = 1.000001\underline{/-12.966859°} \text{ pu kV}$$

$$Q_2^{(3)} = -0.035598 \text{ pu Mvar}$$

To check if convergence is acheived we compute the magnitude of the difference phasor:

$$|V_2^{(3)} - V_2^{(2)}| = 0.000082 \text{ pu kV}$$

Thus we satisfy the specified $\varepsilon = 0.0001$, and will accept the last computed V_2 value.† In summary, our bus voltages are

$$V_1 = 1.05000\underline{/0°} \text{ pu kV}$$

$$V_2 = 1.00000\underline{/-12.9669°} \text{ pu kV}$$

With both bus voltages known to desired accuracy we complete our power-flow study by also computing:

1. Reactive bus power Q_2 from Eq. (7-61)

$$Q_2 = -0.03560 \text{ pu Mvar}$$

2. Reactive generation Q_{G2}

$$Q_{G2} = Q_2 + Q_{D2} = -0.03560 + 0.20 = 0.16440 \text{ pu Mvar}$$

3. Slack-bus powers, from Eq. (7-49),

$$P_{G1} = 1.61706 \text{ pu MW}$$

$$Q_{G1} = 0.31713 \text{ pu Mvar}$$

4. Line-power flows, from Eq. (7-51),

$$S_{12} = P_{12} + jQ_{12} = 0.46706 + j0.00713 \text{ pu}$$

$$S_{21} = P_{21} + jQ_{21} = -0.45000 - j0.03560 \text{ pu}$$

5. Total real losses

$$P_{12} + P_{21} = 0.01706 \text{ pu MW}$$

We have summarized the power-flow picture in Fig. 7-9.

† It is really unusual that convergence is achieved with the G-S algorithm in only three iterations. For multibus systems (and poorer initial voltage guess) 50–100 iterations often are required.

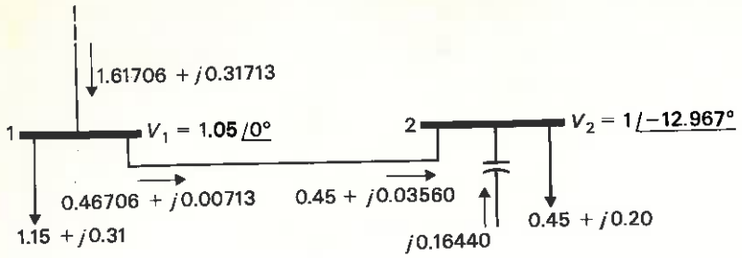

Figure 7-9 Power-flow pictures for load configuration in Fig. 7-7. Bus 2 is voltage controlled.

7-8-6 Convergence Improvements of the G-S Algorithm

The relatively slow convergence of the G-S method can be improved upon by a couple of simple means.

Assume for example that the G-S method is employed for finding the solution to the PFE's for the three-bus system in Example 7-5. According to Eq. (7-58) the algorithms for finding the bus voltages V_2 and V_3 would read

$$\begin{aligned} V_2^{(\nu+1)} &= F_2(V_2^{(\nu)}, V_3^{(\nu)}) \\ V_3^{(\nu+1)} &= F_3(V_2^{(\nu)}, V_3^{(\nu)}) \end{aligned} \tag{7-62}$$

As $V_2^{(\nu+1)}$ and $V_3^{(\nu+1)}$ are computed *sequentially* and because $V_2^{(\nu+1)}$ is more accurate than $V_2^{(\nu)}$ a better algorithm would be as follows†

$$\begin{aligned} V_2^{(\nu+1)} &= F_2(V_2^{(\nu)}, V_3^{(\nu)}) \\ V_3^{(\nu+1)} &= F_3(V_2^{(\nu+1)}, V_3^{(\nu)}) \end{aligned} \tag{7-63}$$

Experience shows that the latter algorithm converges faster than the former.

Another method for speeding up the convergence process consists of using an *acceleration factor* the effect of which on the iterative process is analogous to that of the loop gain in a servo mechanism. Those readers familiar with the characteristics of closed-loop control systems know that by increasing the loop gain, we generally increase the speed of response of the servo, *but if we increase it too much, the servo may go unstable.*

Consider the example in Fig. 7-6. We introduce the difference variable

$$\Delta x = x^{(\nu+1)} - x^{(\nu)} \tag{7-64}$$

Δx is the variable change between the νth and the $(\nu + 1)$st iteration. Let us now multiply this difference by a factor α, *which is larger than unity*, and let us then

† Equation (7-62) is actually *Gauss* algorithm, whereas the improvement (7-63) is due to *Seidel*.

compute the new *accelerated* iterates on the basis of these magnified difference variables in accordance with the algorithm

$$x_{\text{acc}}^{(\nu+1)} = x_{\text{acc}}^{(\nu)} + \alpha\,\Delta x \tag{7-65}$$

The actual effect of the acceleration factor is shown graphically in Fig. 7-10*a* showing how the process in Fig. 7-6 is speeded up. But the graph in Fig. 7-10*b* also shows how too large an α value actually will cause "overshoot." Experience shows that an α value in the range 1.5–1.7 gives the best results in work with power-flow equations.

7-8-7 Computational Flow Chart

The above Examples 7-7 and 7-8 demonstrated the use of the G-S algorithm when, in addition to the reference bus, the system contains either load or voltage control buses. In a more general case we have all three types of buses represented. In Fig. 7-11 we give a flow chart showing the sequencing of the required

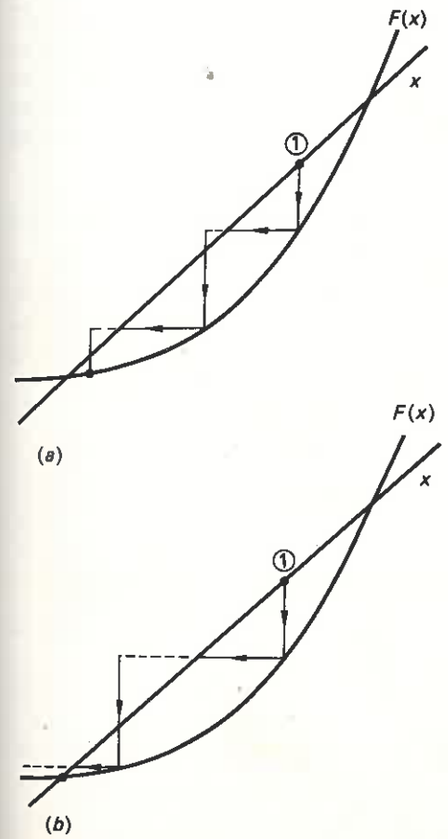

Figure 7-10 Gauss-Seidel algorithm using convergence factors.

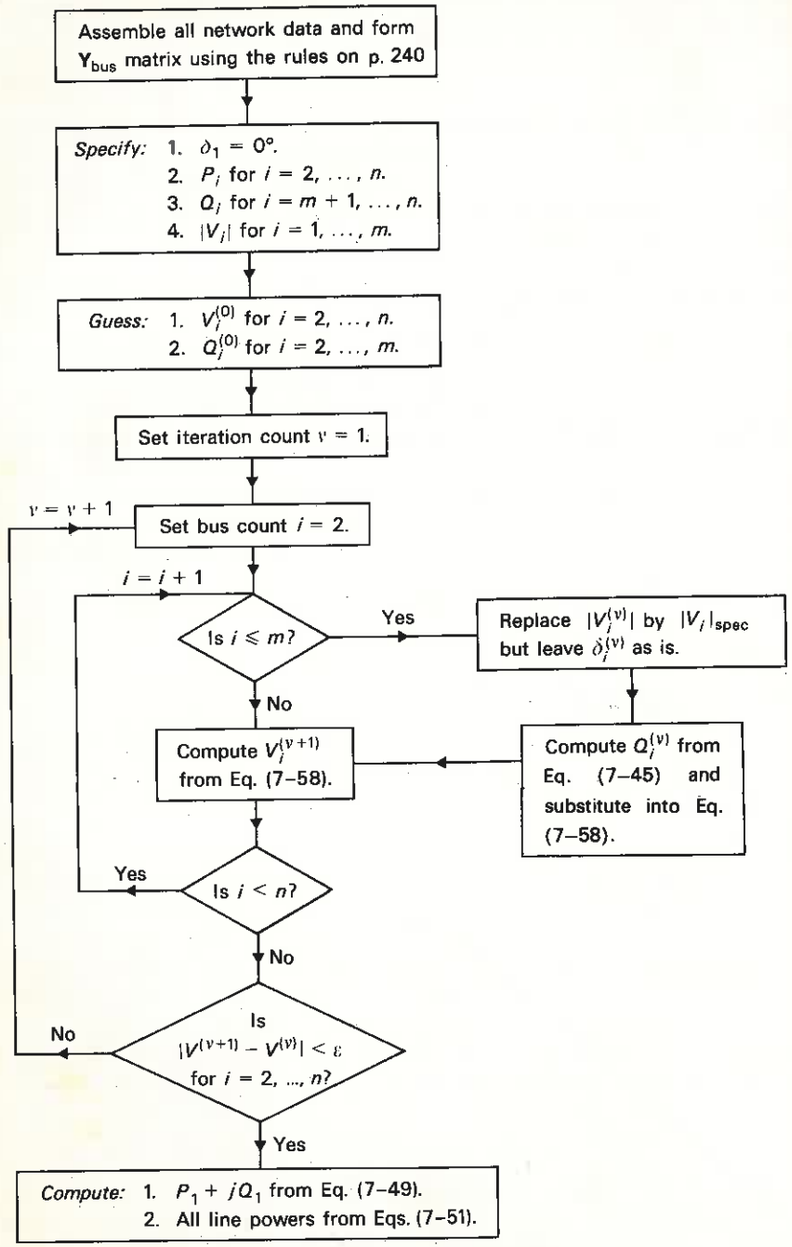

Figure 7-11 Flow chart for power-flow computations using the Gauss-Seidel algorithm.

computations in this general case. The diagram is based on the following coding of buses:

$i = 1$:	reference bus
$i = 2, \ldots, m$:	voltage control buses
$i = m + 1, \ldots, n$:	load buses

Note that the iterations must continue until the ε criterion is satisfied at *all* buses.

For sake of simplicity we have not included in the chart the additional blocks required if, during the iteration process, the reactive source limits should be reached. The reader is encouraged to amend the chart for this possibility.

7-9 THE NEWTON-RAPHSON (N-R) METHOD

The G-S algorithm is very simple but the convergence becomes increasingly slow as the system size grows. The Newton-Raphson technique, now to be discussed, converges equally fast (as measured in number of iterations) for large as well as small systems, usually in less than 4 to 5 iterations. It therefore has become very popular for large system studies.

7-9-1 The N-R Algorithm in Scalar Case

As in Sec. 7-8 we introduce this method by starting with the *scalar* equation (7-53). Assume that we have guessed a solution $x^{(0)}$. We pose now the question how much of an error $\Delta x^{(0)}$ is associated with our guess? As $x^0 + \Delta x^{(0)}$ by definition is the correct root then we must require that

$$f(x^{(0)}) + \Delta x^{(0)} = 0 \tag{7-66}$$

If we expand $f(\ )$ in a Taylor series around the guessed value we obtain

$$f(x^{(0)}) + \Delta x^{(0)}\left(\frac{df}{dx}\right)^{(0)} + \tfrac{1}{2}(\Delta x^{(0)})^2\left(\frac{d^2f}{dx^2}\right)^{(0)} + \cdots = 0 \tag{7-67}$$

All derivatives are computed for $x = x^{(0)}$.

Assuming that the error is relatively small then the higher-order terms can be neglected and we have

$$f(x^{(0)}) + \Delta x^{(0)}\left(\frac{df}{dx}\right)^{(0)} \approx 0 \tag{7-68}$$

from which we then compute an *approximate* value for the error

$$\Delta x^{(0)} = -\frac{f(x^{(0)})}{(df/dx)^{(0)}} \tag{7-69}$$

We add this error to the original guess and should thus obtain an improved value $x^{(1)}$ for the root, i.e.,

$$x^{(1)} = x^{(0)} + \Delta x^{(0)} = x^{(0)} - \frac{f(x^{(0)})}{(df/dx)^{(0)}}$$

Repeated use of this procedure thus yields the N-R algorithm:

$$x^{(\nu+1)} = x^{(\nu)} - \frac{f(x^{(\nu)})}{(df/dx)^{(\nu)}} \tag{7-70}$$

Example 7-9 Find the larger root of the quadratic equation in Example 7-6. Use the initial guess $x^{(0)} = 6$.

SOLUTION We have

$$f(x) = x^2 - 5x + 4$$

$$\frac{df}{dx} = 2x - 5$$

The computations proceed in the following steps:

1. $f(x^{(0)}) = f(6) = 6^2 - 5 \times 6 + 4 = 10$
2. $(df/dx)^{(0)} = 2 \times 6 - 5 = 7$
3. $\Delta x^{(0)} = -10/7 = -1.429$
4. $x^{(1)} = 6 - 1.429 = 4.571$

Two more iterations yield

$$x^{(2)} = 4.079$$

$$x^{(3)} = 4.002$$

The exact value is 4 and we have thus arrived within 0.05 percent in only three iterations. In Fig. 7-12 is shown graphically how the algorithm works. As in the case with the G-S algorithm one does not have a full convergence guarantee. For example if one starts at the value B the algorithm will, as shown, converge on the lower root.

7-9-2 The N-R Algorithm in n-Dimensional Case

Consider now the solution of the n-dimensional equation (7-52). By expanding each equation in a Taylor series around the initial guess

$$\mathbf{x}^{(0)} = \begin{bmatrix} x_1^{(0)} \\ \vdots \\ x_n^{(0)} \end{bmatrix} \tag{7-71}$$

and upon retaining only the first derivative terms we have

$$\begin{aligned} f_1(\mathbf{x}^{(0)}) + \left(\frac{\partial f_1}{\partial x_1}\right)^{(0)} \Delta x_1 + \cdots + \left(\frac{\partial f_1}{\partial x_n}\right)^{(0)} \Delta x_n &\approx 0 \\ \vdots \qquad\qquad\qquad\qquad\qquad\qquad\qquad\qquad &\quad \vdots \\ f_n(\mathbf{x}^{(0)}) + \left(\frac{\partial f_n}{\partial x_1}\right)^{(0)} \Delta x_1 + \cdots + \left(\frac{\partial f_n}{\partial x_n}\right)^{(0)} \Delta x_n &\approx 0 \end{aligned} \tag{7-72}$$

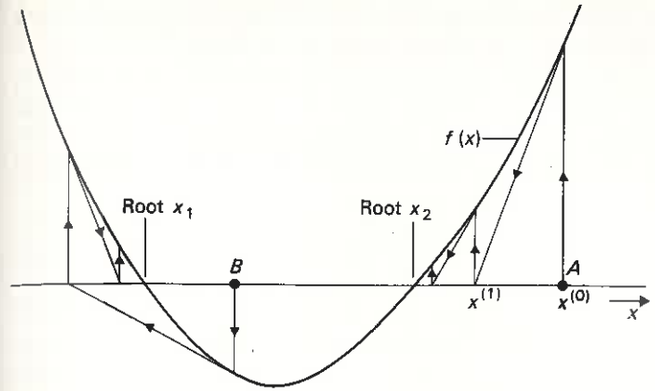

Figure 7-12 Graphical demonstration of N–R algorithm.

We can write this system of n linear equations as follows:

$$\begin{bmatrix} f_1(\mathbf{x}^{(0)}) \\ \vdots \\ f_n(\mathbf{x}^{(0)}) \end{bmatrix} + \begin{bmatrix} \left(\frac{\partial f_1}{\partial x_1}\right)^{(0)} & \cdots & \left(\frac{\partial f_1}{\partial x_n}\right)^{(0)} \\ \vdots & & \vdots \\ \left(\frac{\partial f_n}{\partial x_1}\right)^{(0)} & \cdots & \left(\frac{\partial f_n}{\partial x_n}\right)^{(0)} \end{bmatrix} \begin{bmatrix} \Delta x_1 \\ \vdots \\ \Delta x_n \end{bmatrix} \approx \begin{bmatrix} 0 \\ \vdots \\ 0 \end{bmatrix}$$

Or, in compact matrix-vector notation,

$$\mathbf{f}(\mathbf{x}^{(0)}) + \mathbf{J}^{(0)}\, \Delta\mathbf{x}^{(0)} \approx \mathbf{0} \tag{7-73}$$

From this last equation we then solve for the error vector

$$\Delta\mathbf{x}^{(0)} \approx -[\mathbf{J}^{(0)}]^{-1}\mathbf{f}(\mathbf{x}^{(0)}) \tag{7-74}$$

Upon adding this vector to the original guess and at the same time indicating a repetitive process we obtain the N-R algorithm

$$\mathbf{x}^{(\nu+1)} = \mathbf{x}^{(\nu)} - [\mathbf{J}^{(\nu)}]^{-1}\mathbf{f}(\mathbf{x}^{(\nu)}) \tag{7-75}$$

The $n \times n$ matrix $\mathbf{J}$, having as its elements the partial derivatives $\partial f_i/\partial x_j$, is referred to as a *jacobian*. Use of this algorithm obviously necessitates the need of *inverting* an $n \times n$ matrix in each iteration.

7-9-3 The N-R Algorithm Applied to the PFE

Whereas the G-S algorithm could be applied to the complex form (7-43) of the PFE's, this is not possible in the present case. Some of the required partial derivatives of complex variables do not exist. We must therefore make use of the

real versions [(7-44) and (7-45)] of the PFE. At this time we also make the temporary assumption that all buses, except bus 1, are of "load" type.

Our unknowns thus consist of the $n-1$ voltage phasors $V_2 \cdots V_n$ which in terms of *real* variables means $n-1$ voltage *angles* $\delta_2, \ldots, \delta_n$ and $n-1$ voltage magnitudes $|V_2|, \ldots, |V_n|$.

Our initial guess thus can be assembled in the $(2n-2)$-dimensional *state* vector (compare Eq. 7-27):

$$\mathbf{x}^{(0)} = \begin{bmatrix} \delta_2^{(0)} \\ \delta_3^{(0)} \\ \vdots \\ |V_{n-1}^{(0)}| \\ |V_n^{(0)}| \end{bmatrix} \tag{7-76}$$

By expanding f_{ip} and f_{iq} in Taylor series around the initial guess we obtain from Eqs. (7-44) and (7-45)

$$\begin{aligned} P_i &\approx f_{ip}^{(0)} + \left(\frac{\partial f_{ip}}{\partial \delta_2}\right)^{(0)} \cdot \Delta\delta_2^{(0)} + \cdots + \left(\frac{\partial f_{ip}}{\partial |V_n|}\right)^{(0)} \cdot \Delta|V_n^{(0)}| \\ Q_i &\approx f_{iq}^{(0)} + \left(\frac{\partial f_{iq}}{\partial \delta_2}\right)^{(0)} \cdot \Delta\delta_2^{(0)} + \cdots + \left(\frac{\partial f_{iq}}{\partial |V_n|}\right)^{(0)} \cdot \Delta|V_n^{(0)}| \end{aligned} \quad \text{for } i = 2, \ldots, n \tag{7-77}$$

$f_{ip}^{(0)}$ and $f_{iq}^{(0)}$ represent the real and reactive powers leaving bus i if the bus voltages are set at guessed values. The difference powers

$$\begin{aligned} \Delta P_i^{(0)} &\triangleq P_i - f_{ip}^{(0)} \\ \Delta Q_i^{(0)} &\triangleq Q_i - f_{iq}^{(0)} \end{aligned} \tag{7-78}$$

thus represent the real and reactive bus-power "mismatches" at bus i.

We can write Eqs. (7-77) as follows

$$\begin{bmatrix} \Delta P_2^{(0)} \\ \vdots \\ \Delta Q_n^{(0)} \end{bmatrix} \approx \begin{bmatrix} \left(\frac{\partial f_{2p}}{\partial \delta_2}\right)^{(0)} & \cdots & \left(\frac{\partial f_{2p}}{\partial |V_n|}\right)^{(0)} \\ \vdots & & \vdots \\ \left(\frac{\partial f_{nq}}{\partial \delta_2}\right)^{(0)} & \cdots & \left(\frac{\partial f_{nq}}{\partial |V_n|}\right)^{(0)} \end{bmatrix} \begin{bmatrix} \Delta\delta_2^{(0)} \\ \vdots \\ \Delta|V_n|^{(0)} \end{bmatrix} \tag{7-79}$$

If the $(2n-2)$-dimensional vector of power mismatches is symbolized $\Delta\mathbf{u}^{(0)}$ we can write Eqs. (7-79) in the more compact form

$$\Delta\mathbf{u}^{(0)} \approx \mathbf{J}^{(0)} \cdot \Delta\mathbf{x}^{(0)} \tag{7-80}$$

The computation of the bus voltages would now proceed as follows:

Step 1 Guess at an initial voltage state vector $\mathbf{x}^{(0)}$.
Step 2 Compute the bus power mismatches $\Delta\mathbf{u}^{(0)}$ using Eqs. (7-44) and (7-45).

Step 3 Compute and assemble the jacobian matrix $\mathbf{J}^{(0)}$.
Step 4 Solve the voltage error vector by inverting Eq. (7-80), i.e.,

$$\Delta\mathbf{x}^{(0)} \approx (\mathbf{J}^{(0)})^{-1} \cdot \Delta\mathbf{u}^{(0)} \tag{7-81}$$

Step 5. Add the voltage errors to the initial guess to obtain an upgraded state vector

$$\mathbf{x}^{(1)} = \mathbf{x}^{(0)} + \Delta\mathbf{x}^{(0)} \tag{7-82}$$

Step 6 Repeat the above steps, etc.

When using the G-S algorithm we found it natural to use the voltage error as a convergence measure. Now the power mismatches, real and reactive, will better serve this purpose.

Example 7-10 Use the N-R algorithm to compute the PFE's in Example 7-7. We recall that bus 2 is a "load bus" with the specified bus powers

$$P_2 = -0.45 \text{ pu MW}$$
$$Q_2 = -0.20 \text{ pu Mvar}$$

The reference bus has the specified voltage $|V_1| = 1.05$ pu.

SOLUTION We must now solve simultaneously the second and fourth of Eqs. (7-22) for the two unknowns $|V_2|$ and δ_2. The jacobian matrix is of dimension 2×2 and contains the four partial derivatives

$$\mathbf{J} = \begin{bmatrix} \frac{\partial f_{2p}}{\partial \delta_2} & \frac{\partial f_{2p}}{\partial |V_2|} \\ \frac{\partial f_{2q}}{\partial \delta_2} & \frac{\partial f_{2q}}{\partial |V_2|} \end{bmatrix} \tag{7-83}$$

These derivatives are:

$$\begin{aligned} \frac{\partial f_{2p}}{\partial \delta_2} &= -|y_{21}||V_1||V_2| \sin(\delta_2 - \gamma_{21}) \\ \frac{\partial f_{2p}}{\partial |V_2|} &= |y_{21}||V_1| \cos(\delta_2 - \gamma_{21}) + 2|y_{22}||V_2| \cos \gamma_{22} \\ \frac{\partial f_{2q}}{\partial \delta_2} &= |y_{21}||V_1||V_2| \cos(\delta_2 - \gamma_{21}) \\ \frac{\partial f_{2q}}{\partial |V_2|} &= |y_{21}||V_1| \sin(\delta_2 - \gamma_{21}) - 2|y_{22}||V_2| \sin \gamma_{22} \end{aligned} \tag{7-84}$$

Here follow the computational steps:

Step 1 Select the same initial guess as in Example 7-7, that is, $V_2^{(0)} = 0.95 \underline{/-13.5°}$

$$\therefore \quad \mathbf{x}^{(0)} = \begin{bmatrix} -0.235619 \\ 0.950000 \end{bmatrix} \begin{matrix} \text{rad} \\ \text{pu kV} \end{matrix}$$

Step 2 Find the bus power mismatch

$$\Delta\mathbf{u}^{(0)} = \begin{bmatrix} -0.45 + 0.458299 \\ -0.20 + 0.113348 \end{bmatrix} = \begin{bmatrix} 0.008299 \\ -0.086652 \end{bmatrix} \begin{matrix} \text{pu MW} \\ \text{pu Mvar} \end{matrix}$$

Step 3 Compute the jacobian

$$\mathbf{J}^{(0)} = \begin{bmatrix} 1.752557 & -0.193228 \\ -0.733032 & 1.606169 \end{bmatrix}$$

and its inverse (see App. A)

$$(\mathbf{J}^{(0)})^{-1} = \begin{bmatrix} 0.600828 & 0.072282 \\ 0.274209 & 0.655588 \end{bmatrix}$$

Step 4 Find $\Delta\mathbf{x}^{(0)}$ using Eq. (7-81)

$$\Delta\mathbf{x}^{(0)} = \begin{bmatrix} 0.600828 & 0.072282 \\ 0.274209 & 0.655588 \end{bmatrix} \begin{bmatrix} 0.008299 \\ -0.086652 \end{bmatrix} = \begin{bmatrix} -0.001277 \\ -0.054532 \end{bmatrix}$$

Step 5 Find updated state vector

$$\mathbf{x}^{(1)} = \begin{bmatrix} -0.235619 \\ 0.950000 \end{bmatrix} + \begin{bmatrix} -0.001277 \\ -0.054532 \end{bmatrix} = \begin{bmatrix} -0.236896 \\ 0.895468 \end{bmatrix} \begin{matrix} \text{rad} \\ \text{pu kV} \end{matrix}$$

The corresponding power mismatch vector equals

$$\Delta\mathbf{u}^{(1)} = \begin{bmatrix} -0.001034 \\ -0.005349 \end{bmatrix} \begin{matrix} \text{pu MW} \\ \text{pu Mvar} \end{matrix}$$

Repeated computations yield the state vectors

$$\mathbf{x}^{(2)} = \begin{bmatrix} -0.238133 \\ 0.891064 \end{bmatrix} \qquad \mathbf{x}^{(3)} = \begin{bmatrix} -0.238146 \\ 0.891030 \end{bmatrix}$$

and the power mismatches

$$\Delta\mathbf{u}^{(2)} = \begin{bmatrix} -0.000016 \\ -0.000033 \end{bmatrix} \qquad \Delta\mathbf{u}^{(3)} = \begin{bmatrix} 0.000000 \\ 0.000000 \end{bmatrix}$$

In summary, in three iterations we have converged upon the solution

$$V_2 = 0.89103 \underline{/-13.6448^\circ} \text{ pu kV}$$

which is in agreement with Example 7-7.

7-9-4 Accounting for Voltage Controlled Buses

For every bus where the voltage magnitude is a priori specified, the voltage error $\Delta|V_i|$ is zero and the corresponding row in Eq. (7-79) can be eliminated. *Each voltage control bus thus reduces the dimension of the jacobian by one unit.* As the reactive generation is unknown at all such buses, it must be computed from Eq. (7-48).

Example 7-11 Rework Example 7-8 by use of the N-R algorithm. We recall that the specified bus voltages are

$$|V_1| = 1.05 \text{ pu kV}$$
$$|V_2| = 1.00 \text{ pu kV}$$

The load demand at bus 2 equals

$$P_{D2} = 0.45 \text{ pu MW}$$
$$Q_{D2} = 0.20 \text{ pu Mvar}$$

SOLUTION The dimensionality of the jacobian will be $4 - 2 - 1 = 1$, i.e., it is a *scalar*

$$\mathbf{J} = J = \frac{\partial f_{2p}}{\partial \delta_2} = -|y_{21}||V_1||V_2| \sin(\delta_2 - \gamma_{21}) \tag{7-85}$$

We demonstrate the computational steps starting with the same initial guess as in Example 7-8, that is, $V_2^{(0)} = 1.0 \underline{/-10^\circ}$ pu.

Step 1 $\delta_2^{(0)} = -10^\circ = -0.174533$ rad
Step 2 Compute $Q_{G2}^{(0)}$ from Eq. (7-48)

$$Q_{G2}^{(0)} = 0.20 - 1.904443 \times 1.05 \times 1.00 \sin(109.197819^\circ)$$
$$- 1.841631 \times (1.00)^2 \times \sin(-80.485610^\circ) = 0.127836 \text{ pu Mvar}$$

Step 3 Find power mismatch ΔP_2

$$f_{2p}^{(0)} = 1.904443 \times 1.05 \times 1.00 \cos(109.197819^\circ)$$
$$+ 1.841631 \times (1.00)^2 \times \cos(-80.485610^\circ) = -0.353138 \text{ pu MW}$$
$$\therefore \Delta P_2^{(0)} = -0.45 + 0.353138 = -0.096862 \text{ pu MW}$$

Step 4 Compute jacobian

$$J^{(0)} = -1.904443 \times 1.05 \times 1.00 \times \sin(-109.197819^\circ) = 1.888462$$

and its inverse.

$$(J^{(0)})^{-1} = 0.529532$$

Step 5 Find

$$\Delta x^{(0)} = \Delta\delta_2^{(0)} = 0.529532 \times (-0.096862) = -0.051291 \text{ rad}$$

Step 6 Find undated state

$$x^{(1)} = \delta_2^{(1)} = -0.174533 - 0.051291 = -0.225824 \text{ rad}$$

Two mote iterations yield

$$\delta_2^{(3)} = -0.226314 \text{ rad}$$
$$Q_{G2}^{(3)} = 0.164401 \text{ pu Mvar}$$

This is the same result we obtained in Example 7-8. The corresponding power-flow picture was shown in Fig. 7-9.

Note the need for computing the reactive generation in each iteration. Should the computations reveal that the reactive-power need exceeds the source capacity then, from that iteration on, Q_{G2} must be fixed at the limit value. The bus now becomes a load bus, with both $\Delta\delta_2$ and $\Delta|V_2|$ unknowns. The computations then would be performed as in Example 7-10.

7-10 COMPUTATIONAL ASPECTS OF LARGE-SCALE SYSTEMS

The two- and three-bus systems used above as example systems are not truly representative of real-life systems in several important regards. For one thing, all the elements of the $\mathbf{Y}_{\text{bus}}$ matrices (7-14) and (7-46) are nonzero. This follows as a consequence of the fact that transmission lines exist between *all* buses. A matrix containing no zero elements is termed *full.*

Consider in comparison the six-bus system in Fig. 7-13. Using the rules on p. 240 for the formation of $\mathbf{Y}_{\text{bus}}$ we conclude that its bus admittance matrix equals

$$\mathbf{Y}_{\text{bus}} = j\begin{bmatrix} 15 & -10 & -5 & 0 & 0 & 0 \\ -10 & 10 & 0 & 0 & 0 & 0 \\ -5 & 0 & 25 & -12 & -8 & 0 \\ 0 & 0 & -12 & 12 & 0 & 0 \\ 0 & 0 & -8 & 0 & 23 & -15 \\ 0 & 0 & 0 & 0 & -15 & 15 \end{bmatrix} \tag{7-86}$$

Of the 36 matrix elements 20 are zeros. We say that the matrix *sparsity S* equals

$$\mathbf{S} = \frac{Z}{n^2} = \frac{20}{36} = 0.556 \text{ pu} \qquad (\text{or } 55.6\%) \tag{7-87}$$

A more realistic-size system may have in excess of 100 buses. In such a system, on the average, each bus may be connected with only two or three of the remaining buses. This means that, on the average, only three or four of the elements in each row or column will be nonzero. (Note that *all* diagonal elements will be nonzero.) *The vast majority of the elements of a real world* $\mathbf{Y}_{\text{bus}}$ *matrix will thus be zero.* We often find sparsities as high as 97 percent. Note, however, that whereas $\mathbf{Y}_{\text{bus}}$ is a highly sparse matrix its inverse, $\mathbf{Z}_{\text{bus}}$, is always full.

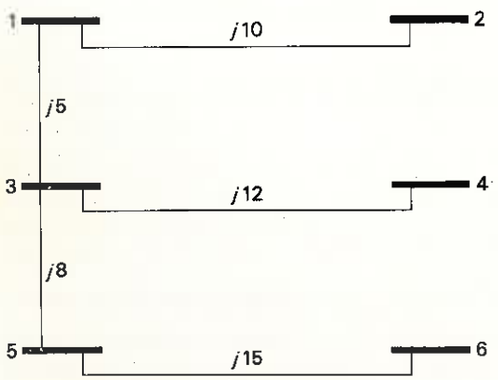

Line admittances in per unit

Figure 7-13 A six-bus example system.

The normally very large order of real-life systems ($n > 100$) combined with the sparsity feature of their admittance matrix will affect the computational methods.

7-10-1 Effects of System Size upon Convergence Characteristics

In our two-bus example system, we found that the G-S algorithm converged faster in the case of a voltage control bus than for a load bus. Also the N-R and G-S methods appeared to converge in about equal number of iterations. Experience confirms that the former feature also applies to large-scale systems.

However, the convergence speed starts to tilt in favor of the N-R method already for $n = 3$. Stagg and El-Abiad[1] have made an extensive comparison of the two methods. They conclude that whereas the required number of iterations are independent of system size for the N-R method they grow in proportion to the number of buses for the G-S method.

The N-R method has another important advantage. We recall that the power "mismatch" expressed by the values $f_{ip}^{(\nu)}$ and $f_{iq}^{(\nu)}$ tells how far off we are in our iteration process. Thus the analyst, by monitoring these values, has a real physical feel for how the iterations progress.

7-10-2 Sparsity of Jacobian Matrix

The sparsity feature of the $\mathbf{Y}_{\text{bus}}$ matrix extends to the jacobian matrix as well. We see this immediately from the expressions for the partial derivatives that constitute the elements of the latter matrix.

Each additional voltage control bus (i) that we need to include in our iteration process involves the additional four partial derivatives

$$\frac{\partial f_{ip}}{\partial \delta_i}, \frac{\partial f_{ip}}{\partial \delta_j}, \frac{\partial f_{iq}}{\partial \delta_i}, \frac{\partial f_{iq}}{\partial \delta_j}$$

where $j \neq i$.

Should the added bus be a load bus, four additional partials of the type $\partial(\ )/\partial|V|$ are added for a total of eight per bus. The expressions for these partials can be readily obtained from Eqs. (7-44) and (7-45). The reader is urged to do so and confirm that all partials except $\partial f_{ip}/\partial\delta_i$ and $\partial f_{iq}/\partial|V_i|$ consist of sums of terms each of which contain as factors the *off-diagonal* elements $|y_{ij}|$ of the $\mathbf{Y}_{\text{bus}}$ matrix. This means, in effect, that the jacobian tends to be almost as sparse as $\mathbf{Y}_{\text{bus}}$.

7-10-3 Sparsity-oriented Computer Programming

It is obvious that the extreme degree of sparsity as exhibited in typical power-system matrices should be taken advantage of in the computational process. Early work by Carpentier, Edelman, Sato, and Tinney[2,3,4] has been followed by

many later contributions. "Sparsity-oriented" programming is today a standard feature in most production-type industry programs. We indicate here briefly the main features of such programs.

7-10-4 Reducing Storage Requirements

If we were to store directly the $\mathbf{Y}_{\text{bus}}$ matrix in Eq. (7-76) 20 of the 36 entries would be zeros. In a very large matrix maybe in excess of 95 percent of the entries would be zeros, obviously a very inefficient use of computer memory. We need to employ some method of "compacting" the matrix so that

1. No zero element is included.
2. Full position identification can take place.

Consider the sparse matrix in Eq. (7-86). Let us define two vectors:

$$ZDIAG = [15, 10, 25, 12, 23, 15]$$

$$ZOFFD = [-10, -5, -10, -5, -12, -8, -12, -8, -15, -15]$$

The first vector contains the ordered diagonal elements, the second the off-diagonal ones, with all zeros excluded. To position the elements in the latter vector in their proper place in $\mathbf{Z}_{\text{bus}}$ we need two more vectors

$$IROW = [1, 3, 4, 7, 8, 10]$$

$$ICOL = [2, 3, 1, 1, 4, 5, 3, 3, 6, 5]$$

The vector $IROW$ identifies where each *row* starts in the vector ZOFFD. For example, row 3 starts with the off-diagonal element -5, which is the *fourth* element in ZOFFD.

The vector $ICOL$ identifies the *column* position of each element in ZOFFD. For example, the above fourth element, -5, is positioned in row 1.

What memory savings do we achieve with this method? The vectors ZDIAG and $IROW$ contain n elements each, and the vectors ZOFFD and $ICOL$, $n^2 - n - Z$ elements each for a total number of elements

$$E_{\text{tot}} = 2n + 2(n^2 - n - Z) = 2(n^2 - Z) \tag{7-88}$$

In view of Eq. (7-87), we thus have

$$E_{\text{tot}} = 2n^2(1 - S) \qquad \text{elements} \tag{7-89}$$

The memory saving is not very impressive for small matrices. In the above example $E_{\text{tot}} = 32$. However, for a matrix of order $n = 300$ and a sparsity of 96 percent, E_{tot} will equal 7200. This figure should be compared with $n(n+1)/2 = 45{,}150$, the required memory size without packing.

7-10-5 Gaussian Elimination and Optimal Ordering

In our two-bus example system, we inverted the jacobian by first computing the *adjoint* and *determinant* of **J** using methods outlined in App. A. For a sparse matrix of large dimensionality this is a very computer-inefficient approach.

Considerable savings can be achieved by performing the necessary inversion by using the so-called gaussian-elimination (G-E) method on an "optimally ordered" jacobian. As the G-E method is basic for all schemes that have been suggested, we present it here in reference to Example 7-10.

We recall that the crucial step in the N-R algorithm is the solution of Eq. (7-79). In Example 7-10 this equation reads (in the first iteration)

$$\begin{bmatrix} 1.752557 & -0.193228 \\ -0.733032 & 1.606169 \end{bmatrix} \begin{bmatrix} \Delta\delta_2^{(0)} \\ \Delta|V_2^{(0)}| \end{bmatrix} = \begin{bmatrix} 0.008299 \\ -0.086652 \end{bmatrix} \tag{7-90}$$

The objective of the G-E solution technique is to "triangularize" the 2×2 matrix in the above equation. We do this in the following three steps:

Step 1 Divide the first equation by 1.752557, thus making the 11-element unity

$$\begin{bmatrix} 1 & -0.110255 \\ -0.733032 & 1.606169 \end{bmatrix} \begin{bmatrix} \Delta\delta_2^{(0)} \\ \Delta|V_2^{(0)}| \end{bmatrix} = \begin{bmatrix} 0.004735 \\ -0.086652 \end{bmatrix}$$

Step 2 Divide the second equation by 0.733032 and add it to the first equation thus creating a zero of the 21-element

$$\begin{bmatrix} 1 & -0.110255 \\ 0 & 2.080875 \end{bmatrix} \begin{bmatrix} \Delta\delta_2^{(0)} \\ \Delta|V_2^{(0)}| \end{bmatrix} = \begin{bmatrix} 0.004735 \\ -0.113475 \end{bmatrix}$$

Step 3 Divide the last equation by 2.080875 thus making the 22-element unity

$$\begin{bmatrix} 1 & -0.110255 \\ 0 & 1 \end{bmatrix} \begin{bmatrix} \Delta\delta_2^{(0)} \\ \Delta|V_2^{(0)}| \end{bmatrix} = \begin{bmatrix} 0.004735 \\ -0.054532 \end{bmatrix}$$

From the last equation we have directly

$$\Delta|V_2^{(0)}| = -0.054532$$

Upon "back-substitution" of this value into the first equation, we obtain

$$\Delta\delta_2^{(0)} = 0.004735 + 0.110255 \times (-0.054532) = -0.001277$$

We note that we have arrived at the same solutions for $\Delta\delta_2^{(0)}$ and $\Delta|V_2^{(0)}|$ as we obtained by matrix inversion in Example 7-10.

The G-E method can readily be extended to an n-dimensional case. Using

essentially the same approach as in the above two-dimensional case we transform the initial n-dimensional jacobian into an "upper triangular" matrix of the form

$$\begin{bmatrix} 1 & a_{12} & \cdots & \cdots & \cdots & a_{1n} \\ 0 & 1 & a_{23} & \cdots & \cdots & a_{2n} \\ 0 & 0 & 1 & \cdots & \cdots & \cdots \\ \cdots & \cdots & \cdots & \cdots & \cdots & \cdots \\ 0 & 0 & \cdots & 0 & 0 & 1 \end{bmatrix} \tag{7-91}$$

The unknown Δ-variables can then be solved in inverse sequence by back-substitution. If the original $\mathbf{J}$ matrix were full [as was the case in Eq. (7-90)] the G-E method would not offer any great computational advantages over the direct inversion approach. The advantages become apparent when the G-E method is combined with "optimal ordering" of a sparse matrix.

Consider the 8×8 jacobian shown in Fig. 7-14*a*. Each dot indicates a nonzero element. The matrix has a 73 percent sparsity. In Fig. 7-14*b* we show the same matrix but with half of the rows reordered. The reordering process is quite simple in that we arrange that as many as possible of the nonzero elements will be located to the right of the main diagonal. Clearly, the reordered matrix can be triangularized in fewer operations than the original one. No transformations need be performed on the first six rows which already appear in the desired form.

7-10-6 "Decoupled" Power-Flow Algorithms

The system operator is often faced with the need for performing "contingency calculations." For example, it would be useful to know what changes would occur in the power-flow picture if a certain transmission line were lost. Answers to this and similar questions are needed in "real time" in order to make it possible to anticipate the consequences of sudden structural changes and to be able to foresee the best operating strategies.

What is needed in such a situation is obviously a "fast" power-flow algorithm that can yield answers in seconds. Many such methods have been proposed[11] of which so-called "decoupled" power-flow algorithms seem to be

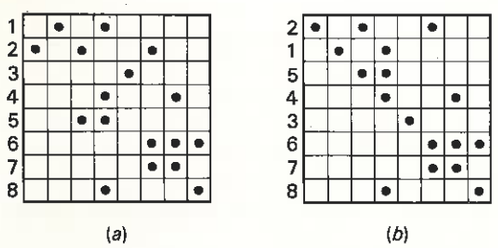

Figure 7-14 $\mathbf{Y}_{\text{bus}}$ matrix for eight-bus system demonstrating the sparsity feature.

the most useful variety. All fast power-flow methods trade off accuracy for speed. Obviously it is preferable to have an answer in five seconds even at the price of 5 percent error rather than waiting one minute for an accurate solution that arrives too late to be useful.

Most fast computational schemes focus on the jacobian, the inversion of which at each iterative step represents the major numerical load. Let us see how "decoupled" algorithms accomplish a reduction of this load.

Consider the relationships between bus-power mismatches and voltage errors as expressed by Eq. (7-79). By *partitioning* we can write this equation in the form

$$\begin{bmatrix} \Delta P_2^{(0)} \\ \vdots \\ \Delta P_n^{(0)} \\ \hline \Delta Q_2^{(0)} \\ \vdots \\ \Delta Q_n^{(0)} \end{bmatrix} \approx \left[\begin{array}{c|c} A & B \\ \hline C & D \end{array}\right] \begin{bmatrix} \Delta\delta_2^{(0)} \\ \vdots \\ \Delta\delta_n^{(0)} \\ \hline \Delta|V_2^{(0)}| \\ \vdots \\ \Delta|V_n^{(0)}| \end{bmatrix} \tag{7-92}$$

We have obviously divided the unknowns $\Delta\delta_i$ and $\Delta|V_i|$ into two separate state vectors $\boldsymbol{\Delta\delta}$ and $\Delta|\mathbf{V}|$. Likewise the bus-power mismatches are divided into their real and reactive components which we can arrange in the vectors $\boldsymbol{\Delta}\mathbf{P}$ and $\boldsymbol{\Delta}\mathbf{Q}$ respectively. In more compact notation Eqs. (7-92) can then be written

$$\begin{bmatrix} \boldsymbol{\Delta}\mathbf{P} \\ \boldsymbol{\Delta}\mathbf{Q} \end{bmatrix} = \begin{bmatrix} \mathbf{A} & \mathbf{B} \\ \mathbf{C} & \mathbf{D} \end{bmatrix} \begin{bmatrix} \boldsymbol{\Delta\delta} \\ \Delta|\mathbf{V}| \end{bmatrix} \tag{7-93}$$

or in component form

$$\begin{aligned} \boldsymbol{\Delta}\mathbf{P} &= \mathbf{A}\,\boldsymbol{\Delta\delta} + \mathbf{B}\Delta|\mathbf{V}| \\ \boldsymbol{\Delta}\mathbf{Q} &= \mathbf{C}\,\boldsymbol{\Delta\delta} + \mathbf{D}\Delta|\mathbf{V}| \end{aligned} \tag{7-94}$$

The matrices $\mathbf{A} \cdots \mathbf{D}$ are submatrices of the jacobian.

At this point we make use of a network property that we have learned about and taken advantage of in earlier chapters (compare Example 4-8). As we change the flows of real and reactive powers we have noted the strong "coupling" between the *real*-power components and the bus-power *phase angles*. A similar link exists between the *reactive* powers and the bus voltage *magnitudes*. This decoupling feature which is of great importance in control and operation of power systems (we shall make further use of it in Chap. 9) can now be given a very obvious numerical interpretation:

The submatrices **B** *and* **C** *are numerically less important than* **A** *and* **D** *meaning that the Eqs. (7-94) can be approximately stated*

$$\begin{aligned} \boldsymbol{\Delta}\mathbf{P} &\approx \mathbf{A}\,\boldsymbol{\Delta\delta} \\ \boldsymbol{\Delta}\mathbf{Q} &\approx \mathbf{D}\Delta|\mathbf{V}| \end{aligned} \tag{7-95}$$

(The reader may confirm this in Example 7-10 where all four submatrices are scalars.)

Considerable reduction in computer time is achieved by basing our algorithm on an alternating iteration of the two equations (7-95) rather than the original equation (7-92).

But this is not all that can be achieved. As exemplified by Eqs. (7-84) the individual elements of the jacobian contain as factors the admittances y_{ij} and sine and cosine of the angles $(\delta_i - \gamma_{ij})$. In typical systems the resistive portions are small relative to the reactive portions and can be neglected. Also most cosines can be set equal to unity.

Combined with the earlier described sparsity feature all of these simplifications can yield an approximate solution technique that finds considerable use in "on-line" control.

7-10-7 Variants of the N-R Method

With a total of m specified bus voltage magnitudes and with δ_1 set equal to zero we are left with the $2n - m - 1$ voltage unknowns $\delta_2, \ldots, \delta_n$ and $|V_{m+1}|, \ldots, |V_n|$. The jacobian thus will be of dimension $(2n - m - 1) \times (2n - m - 1)$. Were we to add the two slack-bus powers P_1 and Q_1 and the $m - 1$ reactive bus powers $Q_2, \ldots, Q_m$ to our vector of unknowns, then the jacobian would have dimension $2n \times 2n$. In this problem formulation we are left with a larger matrix but are spared the need for a separate computation of the slack-bus powers and the reactive bus powers at the voltage controlled buses.

7-11 CONTROL OF THE POWER FLOW

Seldom is one content with simply being able to *compute* the power flow in a system. Typically, we wish to *control* it. These are the means at our disposal:

1. Torque and excitation control of the generators
2. Switching in and out of series and shunt capacitors and reactors
3. Regulating transformers including tap changing of regular transformers

7-11-1 Power-Flow Control by Source Adjustment

Generators typically are available only at a relatively few number of buses. As we learned in Chap. 4 the megawatt output of a generator is essentially proportional to the turbine torque, the latter thus becoming our basic means of real-power-flow control. The generator emf $|E|$ is likewise essentially proportional to the rotor field current which thus becomes our basic means for voltage control and, indirectly, also megavar generation control.

A certain system load can be shared by the generators in an infinite number of ways, each generation configuration corresponding to a certain power-flow picture. In the next chapter we shall discuss means of selecting the *best* or *optimal* configuration.

Capacitors and reactors represent an important secondary means of controlling the system megavar flow and thus the voltage profile.

In determining the effect that changes in the above real and reactive generation sources will have on the overall power flow the simplest approach is by "trial and error." Based upon best engineering judgment, the various generators are maintained at megawatt and kilovolt levels that would match desired load and voltage profile. A power-flow analysis is made and the corresponding flow picture is examined. If line, cable, and transformer loadings are not within desired limits, adjustments are made in the set points and a new flow analysis is made. One would thus converge upon a suitable power-flow picture in an iterative fashion.

7-11-2 Power-Flow Control by Transformer Regulation

In using the third means of power-flow control—transformer ratio or angle setting—one would proceed essentially as above. Based again upon engineering judgment one would choose ratio and angular settings that would seem to meet best the specified requirements. As one then would proceed to analyze the resulting flow picture one finds a basic difference between this type of control and the above-described source control. Whereas changes in generation settings will not effect the $\mathbf{Y}_{\text{bus}}$ matrix, the adjustment of transformer settings will do so. We show this by working a last example.

Example 7-12 Consider the two-bus system in Fig. 7-2. We place a regulating transformer RT at bus 2 as shown† in Fig. 7-15*a*. The RT has a complex transformation ratio

$$a = |a| \underline{/\alpha} \tag{7-96}$$

Model the RT as an ideal transformer and find its effect upon the $\mathbf{Y}_{\text{bus}}$ matrix.

SOLUTION By making use of formulas (5-32) and (5-34) we conclude (see Fig. 7-15*b*) that the voltage and current on the primary side of RT equal aV_2 and I_2/a^* respectively, V_2 and I_2 being the secondary variables.

Current balance at the two buses demands that

$$I_1 = \frac{S_1^*}{V_1^*} = V_1 Y_p + (V_1 - aV_2)Y_s$$

and

$$\frac{I_2}{a^*} = \frac{S_2^*}{(aV_2)^*} = aV_2 Y_p + (aV_2 - V_1)Y_s \tag{7-97}$$

We rewrite the last equation and obtain the pair

$$\begin{aligned} I_1 &= (Y_p + Y_s)V_1 + (-aY_s)V_2 \\ I_2 &= (-a^*Y_s)V_1 + aa^*(Y_p + Y_s)V_2 \end{aligned} \tag{7-98}$$

† In practice, one would hardly bother with a regulating transformer in such a simple system.

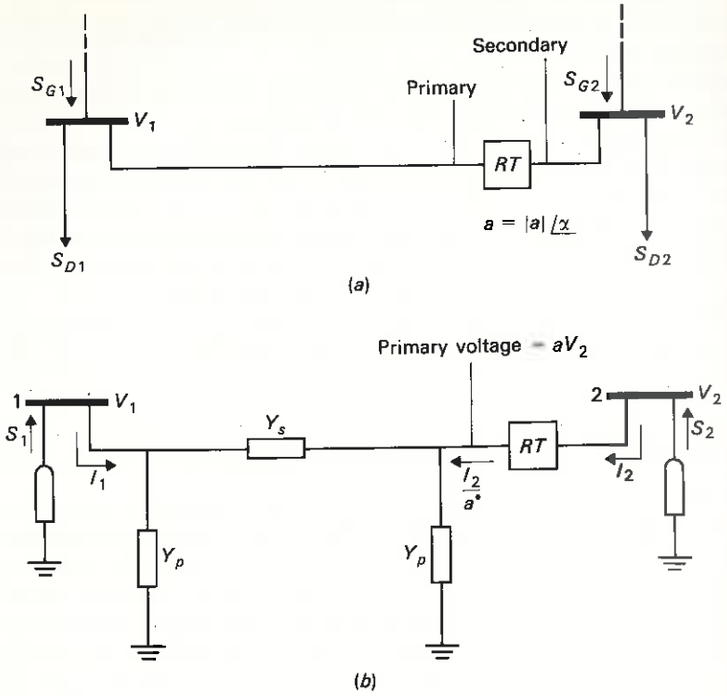

Figure 7-15 Two-bus example system demonstrating the use of regulating transformer.

Clearly, the addition of RT has changed the $\mathbf{Y}_{\text{bus}}$ as given by Eq. (7-6) to the new value

$$\mathbf{Y}_{\text{bus}} = \begin{bmatrix} Y_p + Y_s & -aY_s \\ -a^*Y_s & aa^*(Y_p + Y_s) \end{bmatrix} \tag{7-99}$$

The addition of the RT has added the two additional variables $|a|$ and α to the previous ones and the linearized power balance equations (7-72) will contain the added difference variables $\Delta|a|$ and $\Delta\alpha$. The jacobian matrix will grow correspondingly larger.

In a practical situation (compare Sec. 5-8) the RT is designed for either voltage *magnitude* or *phase* control. In the former case $\alpha = 0$ and $|a|$ can be changed in discrete steps $\Delta|a|$. In the latter case $|a|$ is constant and α can be changed in steps $\Delta\alpha$.

SUMMARY

After a brief discussion of load-frequency and megavar-voltage control this entire chapter has been devoted to the important topic of power-flow analysis.

A power system is in static flow equilibrium when real and reactive power balance exists at all buses. The power-flow equations (PFE's) were derived and found to consist of a coupled set of complex nonlinear algebraic equations. A

total of six voltage and power variables per bus are involved in the power balance mechanism and a basic problem is to group these variables into "knowns" and "unknowns."

Two different iterative computation schemes have been discussed by means of which the PFE's can be numerically solved. Our example systems have been by necessity low-order, but we have discussed the extension to large-scale systems.

Finally, the various means available for control of the power flow have been summarized.

PROBLEMS

***7-1** In Example 7-1 the kinetic energy w_{kin} of a system was expressed in megajoules or megawatt-seconds. It is more common to express the kinetic energy in terms of a *per unit inertia constant H* defined as

$$H \triangleq \frac{w_{\text{kin}}^0}{P_r} \tag{7-100}$$

where P_r is the total megawatt rating of all running generators. H has the physical unit megawatt-second per megawatt, i.e., seconds.

Typical H values line in a fairly narrow range of two to eight seconds.

A power system, having an H value of four seconds, suddenly loses a generator unit that represents eight percent of the total installed capacity. At what rate, in hertz per second, will the system lose frequency?

***7-2** Find the $\mathbf{Y}_{\text{bus}}$ matrix of the two-bus system in Example 7-2 if you *don't* assume the line to be "electrically short."

7-3 The $\mathbf{Y}_{\text{bus}}$ matrix, Eq. (7-14), was derived on the assumption that buses 1 and 2 were the HV buses (230 kV) at each line end. Assume instead that we let 1 and 2 represent the LV buses. The transformers at each end of the line are rated 300 MW each. They have an impedance of $0.60 + j13.1$ percent based on rating. Find the $\mathbf{Y}_{\text{bus}}$ for the two-bus system, assuming the line "electrically short."

***7-4** Consider Example 7-3.

(*a*) How many megawatts can be transmitted if the voltage $|V_2|$ cannot drop below 0.9 pu and the load power factor is unity?

(*b*) Same question as in part *a* but now the load power factor is 0.8 lagging. $|V_1| = 1$ pu in both cases.

7-5 Assume that in Prob. 7-4*b* we had specified pf = 0.8 *leading*. Prove (by phasor diagram or otherwise) that as the load is being increased the voltage magnitude $|V_2|$ will first *increase*, then reach a *maximum*, and finally decrease.

(*a*) Find the maximum value of $|V_2|$.

(*b*) At what megawatt load will $|V_2|$ have dropped to 0.9 pu?

***7-6** Consider the three-bus system in Fig. 7-4. All lines are identical and can each be represented by a series impedance of $j0.1$ pu per phase. Find $\mathbf{Y}_{\text{bus}}$.

***7-7** A load of $1 + j0$ pu per phase is drawn from each of buses 2 and 3 in the three-bus system in Prob. 7-6. Bus 1 is a generator bus. We specify a flat voltage profile $|V_1| = |V_2| = |V_3| = 1$ pu.

(*a*) Write the PFE's for the three buses. Which are your five unknowns? Why don't we have six unknowns?

(*b*) Explore the possibility of solving the PFE's *analytically* and *exactly*. If you think it is possible find the solution of the five unknowns.

(*c*) If you cannot find an exact analytical solution try an *approximate* one by using the relations:

$$\sin x \approx x$$

$$\cos x \approx 1 - x^2/2$$

7-8 Having tried your analytical abilities in Prob. 7-7 delegate now the job to a digital computer. Specifically, write a program using the G-S algorithm that will yield voltage solutions within an accuracy limit of $\varepsilon = 10^{-5}$ pu.

When the iterations have converged compare your solutions with those you derived in Prob. 7-7.

7-9 Consider the four-bus system in Fig. 7-16. All three lines are identical, and each can be represented by a series impedance of $7 + j35$ ohms per phase. Bus 1 is kept at 230 kV. 100 MW of pf = 0.8 lagging is drawn from each of the other three load buses.

There may be a possibility that the voltages V_2, V_3, and V_4 drop so low that the specified loads cannot be delivered. Check this possibility by writing a computer program (G-S algorithm) that will yield a solution. If a solution exists find it and make a plot of all line flows and voltages.

7-10 We add a Q source to bus 4 in Fig. 7-16. We then specify $|V_4| = |V_1| = 230$ kV. The loading is the same as in Prob. 7-9. Write a program using the N-R algorithm for solution of the PFE. "Invert" the jacobian by the Gauss elimination method and attempt to take advantage of the matrix sparsity.

7-11 In Example 7-10 we computed the voltage at load bus 2 and concluded that it had dropped to a value of 0.891 pu. By adding an RT at bus 2 we wish to increase the voltage to 1.0 pu. The RT is of voltage magnitude type where the ratio $|a|$ can be varied in steps of $\Delta|a| = 0.01$ pu around the nominal setting $|a^0| = 1.00$.

Develop a computer program by means of which you can compute proper ratio setting. $|V_1| = 1.05$ pu and the loading is assumed the same as in Example 7-10.

7-12 Write a computer program that will give the total bus voltage and power-flow picture for the three-bus system in Fig. 7-4. Use the G-S method.

1. Use the bus power and bus voltage specifications given in Table 7-3.
2. Use the $\mathbf{Y}_{\text{bus}}$ data in Eq. (7-46)
3. Utilize the convergence improvement techniques presented in Sec. 7-8-6. Write the program so that you can experiment with different values for the acceleration factor α.
4. Use a convergence index of $\varepsilon = 10^{-5}$ for *both* V_2 and V_3. How many iterations are required for $\alpha = 1, 1.2, 1.4, 1.6, 1.8, 2.0$?
5. Start computations with $V_2^{(0)} = V_3^{(0)} = 240/\sqrt{3}\underline{/0^\circ}$

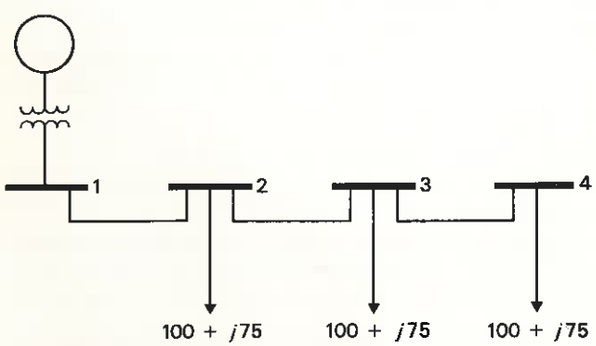

Figure 7-16 Four-bus example system.

Table 7-3

Bus	Bus type	Bus power, total 3-phase		Bus voltage, kV line-to-line
		MW	Mvar	
1	Reference	$P_{G1} - 120$	$Q_{G1} - 60$	240
2	Load	-350	-100	
3	Voltage control	-400	$Q_{G3} - 130$	240

6. What are the total real line losses expressed in three-phase megawatts?
7. Indicate the computed line flows (total three-phase) and bus voltages (line-to-line) in a one-line diagram.
8. Work the problem in per units using the base values

$$|S_b| = 100 \text{ MVA/phase}$$
$$|V_b| = \frac{230}{\sqrt{3}} \text{ kV/phase}$$

REFERENCES

1. G. W. Stagg and A. H. El-Abiad: *Computer Methods in Power Systems Analysis*, McGraw-Hill Book Company, New York, 1968.
2. J. Carpentier, "Application of Newton's Method to the Load Flow Problem," *Proc. Power Syst. Computations Conf.*, Queen Mary College, September, 1963.
3. N. Sato and W. F. Tinney: "Techniques for Exploiting the Sparsity of the Network Admittance Matrix," *IEEE Trans.*, vol. 82, pt. III, December, 1963, pp. 944-949.
4. H. Edelmann: "Ordered Triangular Factorization of Matrices: A Multipurpose Approach for Treating Problems in Large Electric Networks," *Proc. Power Syst. Computation Conf.*, rept. 4.12, Stockholm, 1966.
5. W. F. Tinney and J. W. Walker: "Direct Solutions of Sparse Network Equations by Optimally Ordered Triangular Factorizations," *Proc. IEEE*, November 1967, vol. 55, pp. 1801-1809.
6. C. A. Gross: *Power System Analysis*, John Wiley & Sons, New York, 1979.
7. R. L. Sullivan: *Power System Planning*, McGraw-Hill Book Co., New York, 1977.
8. H. E. Brown: *Solution of Large Networks by Matrix Methods*, John Wiley & Sons, New York, 1975.
9. T. E. Dy Liacco: "The Adaptive Reliability Control System," *IEEE Trans.*, vol. PAS-86, no. 3, May 1967, pp. 517–531.
10. ———: "Control of Power Systems Via the Multi-Level Concept," SRC-68-19, Systems Research Center, Case Western Reserve University, 1968.
11. L. Fink and K. Carlsen: "Operating Under Stress and Strain," *IEEE Spectrum*, March 1978, pp. 48–50.

CHAPTER

EIGHT

OPTIMUM OPERATING STRATEGIES

In the preceding chapter, we learned that a certain system load may be supplied in an infinite number of operating configurations. Determining what generating units to commit and what their individual megawatt and megavar settings should be falls under the general topic of "optimum dispatch." In this chapter we shall explore some of the analytical methods available for calculating optimal operating strategies.

8-1 GENERATION MIX

Figure 8-1 illustrates how a typical utility may meet its daily load demand. The *base load* is carried by generators that run at 100 percent of capacity on a 24-hour basis. *Intermediate*, or "controllable" generators run most of the time but not necessarily fully loaded. *Peaking* units are kept on line only for a few hours every day. *Reserve* capacity is needed to meet unforeseen emergencies.

Base-load units. Nuclear units typically fall in this category. Due to the need for keeping the nuclear reactor and steam system in thermal balance, it is desirable to maintain the megawatt output of such units at as constant a level as possible. Huge fossil-fired units should likewise be run at constant megawatt setting.

Intermediate units. When the megawatt output must be regulated, hydropowered units are the most convenient choice. The power output of a hydrogenerator

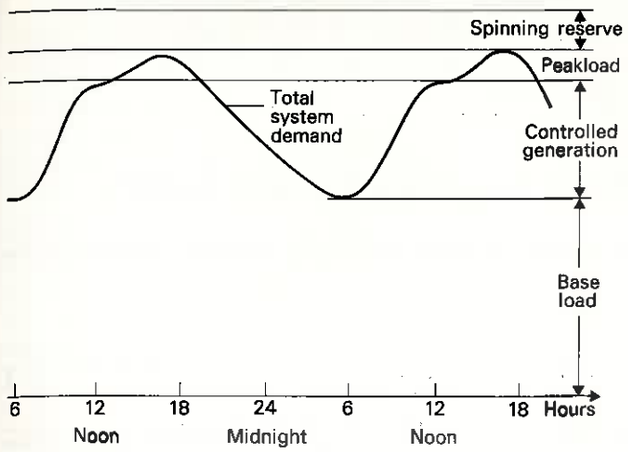

Figure 8-1 Generation strategy for typical power company.

is controlled simply by changing the water flow through the turbine. Not all electric utilities have hydropower available and must then use controllable thermal units. Due to the thermal time constants of the steam system, it is always necessary to regulate such units within their *rate* limits, i.e., the highest rate expressed in megawatts per minute at which the power level can be changed.

Peaking units. Gas-turbine-driven generators can pick up load very fast and are therefore often used for peaking purposes. Hydropowered generators are also an excellent choice when available. Pumped hydro storage and compressed gas are special types of peaking equipment.

Reserve units. The required generator margin can consist of generators maintained at partial output ("spinning reserve") or generators standing by at various levels of readiness.

The energy cost, expressed in dollars per megawatthour, will vary greatly between the above types of units. Peaking units are the most expensive because, on the average, they are greatly underused. If a utility can shave its peak demand by load management, it may be possible to postpone for years the need for acquisition of such units.

Maintaining a proper *generation mix* is a most important requirement for a power company of any size. The problem is not only due to the hourly shifting power demand as indicated in Fig. 8-1. All generating units must be regularly maintained and, in case of nuclear units, also refueled. The operating success of a utility company depends to a great extent upon the ability optimally to match the generation to the load not only over the 24-hour daily time span but over seasons and years.

Pool operation can benefit the individual members in terms of reduced

margin need, peaking capacity, and better use of load and generation diversity. But in the final analysis each individual company will be judged by its own economic and security performance.

8-2 OPTIMUM DISPATCH—PROBLEM FORMULATION

One may formulate an optimum dispatch problem in a number of ways. Let us exemplify.

Example 8-1 A power system has most of its generating capacity in the form of hydro units strung along a major river. The reservoirs can be partly controlled, the overflow water being released over the spillways. Also, water may have to be wasted through bypass tunnels when a station must decrease its megawatt output during periods of light load.

Optimum dispatch is achieved when, over a yearly water cycle, a minimum amount of water is wasted. Differently stated, optimum dispatch permits us to squeeze a maximum amount of megawatthours out of the available seasonal water.

Example 8-2 A power system generates most of its energy in coal-fired units. Atmospheric conditions are favorable for pollution buildup. How should the generations be optimally divided between the different stations to reduce to a minimum the concentration of pollutants in certain critical areas?

Example 8-3 Of the two generators in the two-bus system in Fig. 7-2 one is oil- the other coal-fired. The total system load is 600 MW. In what optimal ratio should the two generators share this load to minimize overall generation cost? How do the real line losses and choice of voltage profile affect the operating strategy?

If we were to specify in all of the above three cases the added requirement that "optimal" must also take into account a measure of security (for example in terms of probability of generator outage) then we obviously have a new dimension of optimum dispatch.

Were we to put the above problems in mathematical clothing so as to make analysis possible it is obvious that each case would look quite different. Example 8-1 would necessitate constructing a hydraulic flow model of the river in question—a not too difficult job. Example 8-2 requires the assembly of a regional atmospheric dispersal model and the choice of a quantitive measure of "pollution," both very difficult and hard-to-define tasks.

Measuring "security" and constructing a mathematical model from which it can be predicted is extremely hard. Work in this field is, at the time of writing, at the research stage.

The simplest type of optimum dispatch is the purely economical variety exemplified in Example 8-3. It has been practiced for some time, is well studied and is, of course, in times of energy shortages and inflation a practically very important case. Also, in the United States the great majority of electric power is produced from fossil fuel. We shall devote the rest of the chapter to *economic optimum dispatch.*

8-3 OPTIMUM ECONOMIC DISPATCH—THE LOSSLESS CASE

We consider presently a power system containing N controllable generators. We assume the system to be geographically compact with relatively short transmission lines (urban system) and negligible real-power losses.

We choose as our dispatch criterion the dollar cost of operation, measured systemwide. We do not concern ourselves with those cost components that are *fixed,* like salaries, plant installation costs, and generating costs in base-loaded units. We consider only those costs that, by proper strategy, we can *control,* i.e., the fuel costs in the controllable generator units.

8-3-1 Cost Function

Let c_i mean the cost, expressed for example in dollars per hour, of producing energy in the generator unit i. The total controllable system production cost therefore will be

$$C = \sum_{i=1}^{N} c_i \qquad \$/\text{h} \tag{8-1}$$

The generated real power P_{Gi} accounts for the major influence on c_i. The individual real generations are raised by increasing the prime mover torques, and this requires an increased expenditure of fuel. The reactive generations Q_{Gi} do not have any measurable influence on c_i because they are controlled by varying the field current.

The individual production cost c_i of generator unit i is therefore for all practical purposes a function only of P_{Gi}, and for the overall controllable production cost, we thus have

$$C = \sum_{i=1}^{N} c_i(P_{Gi}) = c_1(P_{G1}) + \cdots + c_N(P_{GN}) \qquad \$/\text{h} \tag{8-2}$$

When the cost function C can be written as a sum of terms where each term depends only upon one independent variable, we say that C is *separable.*

The cost functions c_i are always determined *empirically.* The fuel costs, of course, constitute the major portions, but operation and maintenance, etc., also enter in. Figure 8-2 depicts a typical cost-versus-megawatt plot. The general nature of the cost functions (but of course not the magnitudes) are the same for coal, oil, or gas-fired stations. Nuclear stations are typically base-loaded and do not enter the analysis. Hydro units, as exemplified in Example 8-1, are optimized on other bases.

8-3-2 Constraint Relations

A set of real generation variables P_{Gi} must now be selected that will minimize the cost function (8-2). The selection cannot be arbitrary *as it is necessary to observe simultaneously certain equality and inequality constraints.*

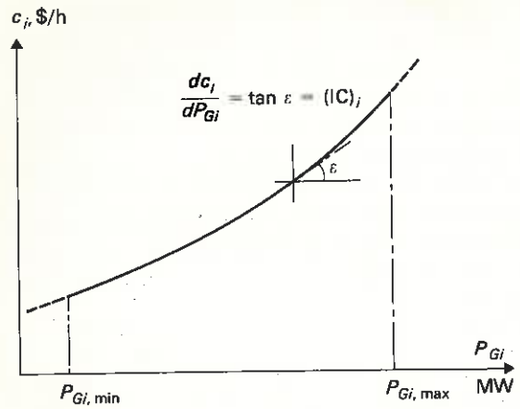

Figure 8-2 Typical production cost-versus-megawatt chart for fossil-fueled generator unit.

A. Equality constraints As the choice of the P_{Gi}'s must be consistent with the static power balance of the system *it is clear that the static power-flow equations must be observed.*

Searching for an optimum set of P_{Gi}'s and simultaneously making sure that the $2n$ PFE's are satisfied is a rather formidable mathematical task. We can achieve considerable simplification by making use of our earlier observation that the reactive powers do not affect C. By thus freeing ourselves from the need for monitoring the *reactive-power balance* and associated voltage profile, we turn our full attention to the *real-power balance* in the system.

Assume that $P_{D,\,\mathrm{tot}}$ represents the total system megawatt demand. Assume further that $P_{G,\,\mathrm{base}}$ represents the total *constant* base generation. The difference

$$P_D \triangleq P_{D,\,\mathrm{tot}} - P_{G,\,\mathrm{base}} \tag{8-3}$$

thus represents the real power that must be supplied from the generator units *under control.* Power balance requires that the controlled generation variables P_{Gi} obey the *constraint equation*

$$\sum_{i=1}^{N} P_{Gi} = P_D \tag{8-4}$$

Due to the relatively slow change in demand (Fig. 8-1) we may consider P_D a *constant* for periods of maybe 2 to 3 minutes. For our later analysis purposes we prefer to put Eq. (8-4) in the form

$$\sum_{i=1}^{N} P_{Gi} - P_D \triangleq f(P_{G1}, P_{G2}, \ldots, P_{GN}) = 0 \tag{8-5}$$

B. Inequality constraints Since each generator must not be operated above its rating or below some minimum value (compare Fig. 4-19) we must observe these inequalities

$$P_{Gi,\,\min} < P_{Gi} < P_{Gi,\,\max} \qquad \text{for } i = 1, \ldots, N \tag{8-6}$$

There are, of course, additional inequalities that must be observed in the optimization process. For example, the real generation must not be set so as to cause overloads on certain lines.

8-3-3 Incremental Generation Costs

In summary, the optimization problem can now be stated thusly.

Select the N generator settings $P_{G1}, \ldots, P_{GN}$, so that the overall cost function C defined by Eq. (8-2) is minimized. Simultaneously observe the equality constraint (8-5) and the inequalities (8-6) plus any additional inequality constraint that may apply.

As we can write Eq. (8-2) in the form

$$C = C(P_{G1}, P_{G2}, \ldots P_{GN}) \tag{8-7}$$

we may initially conclude that we are faced with the problem of optimizing a scalar function of N independent variables. However, due to the constraint equation (8-5) we note that when $N-1$ of the generation variables P_{Gi} have been selected the remaining one (usually the slack-bus power) becomes fixed. *Of the N controllable generation variables thus only $N-1$ can be selected independently.*

The mathematical procedure for finding a *constrained optimum* of this type has been summarized in App. C, to which the reader is referred for details. The solution procedure is as follows:

First, form the *augmented* cost function

$$C^* \triangleq C - \lambda \cdot f \tag{8-8}$$

where f is the equality constraint equation (8-5) and λ the *Lagrange multiplier.*

Second, solve the N equations

$$\frac{\partial C^*}{\partial P_{Gi}} = \frac{\partial C}{\partial P_{Gi}} - \lambda \frac{\partial f}{\partial P_{Gi}} = 0 \qquad i = 1, \ldots, N \tag{8-9}$$

By making use of the relations (8-2) and (8-5) the partial derivatives are computed in our case:

$$\frac{\partial C}{\partial P_{Gi}} = \frac{dc_i}{dP_{Gi}} \triangleq (\mathrm{IC})_i \qquad \text{for } i = 1, \ldots, N \tag{8-10}$$

$$\frac{\partial f}{\partial P_{Gi}} = 1 \qquad \text{for } i = 1, \ldots, N \tag{8-11}$$

The derivatives dc_i/dP_{Gi} are referred to as *incremental costs* (IC) of generation. They represent the slope of the cost curve, as shown in Fig. 8-2. As the unit for c_i is dollars per hour, the IC unit must be dollars per hour per kilowatt, or dollars per kilowatthour. For typical generator sizes, a better unit is dollars per megawatthour.

We mentioned earlier that the cost curves c_i typically are determined *empirically*. To make them better suited for computer work, one must put them into analytical form by some "curve-fitting" method. A common method is to express the cost curves as polynomials of the form

$$c_i = \alpha_i + \beta_i P_{Gi} + \gamma_i P_{Gi}^2 + \cdots \tag{8-12}$$

where the parameters α, β, γ, ... are adjusted to give best possible curve fit.

Example 8-4 Find the incremental cost $(\mathrm{IC})_i$ in the case when c_i is "curve-fitted" with a second-order polynomial, a so-called "quadratic" cost curve.

SOLUTION If only three terms are included in Eq. (8-12) we have

$$c_i = \alpha_i + \beta_i P_{Gi} + \gamma_i P_{Gi}^2 \qquad \$/\mathrm{h} \tag{8-13}$$

and

$$(\mathrm{IC})_i = \frac{dc_i}{dP_{Gi}} = \beta_i + 2\gamma_i P_{Gi} \qquad \$/\mathrm{MWh} \tag{8-14}$$

A *quadratic* cost curve thus corresponds to a *linear* IC-graph (compare Fig. 8-5).

8-3-4 Optimum Dispatch Equations

With all the partial derivatives in Eqs. (8-9) known we can now readily solve the latter equations. Upon substitution of the derivatives given be Eqs. (8-10) and (8-11) we obtain our *optimum dispatch equations* (ODE)

$$\lambda = (\mathrm{IC})_1 = (\mathrm{IC})_2 = \cdots = (\mathrm{IC})_N \tag{8-15}$$

or stated in words: *For optimum dispatch we must make sure that all the individual controllable generators operate at equal incremental production costs. In addition they must individually add up to the demand power P_D.*

Example 8-5 Consider the two-bus system in Fig. 8-3. There are no base-loaded units with $G1$ and $G2$ both being under control. The units are assumed to have quadratic cost functions of the type (8-12). How should the two units share the total load P_D?

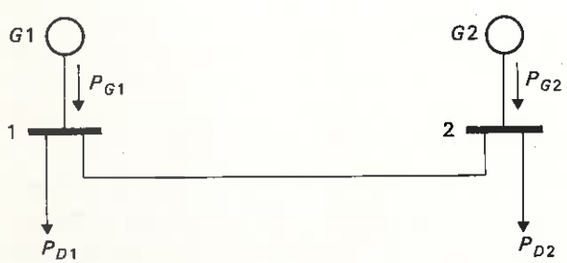

Figure 8-3 A two-generator example system.

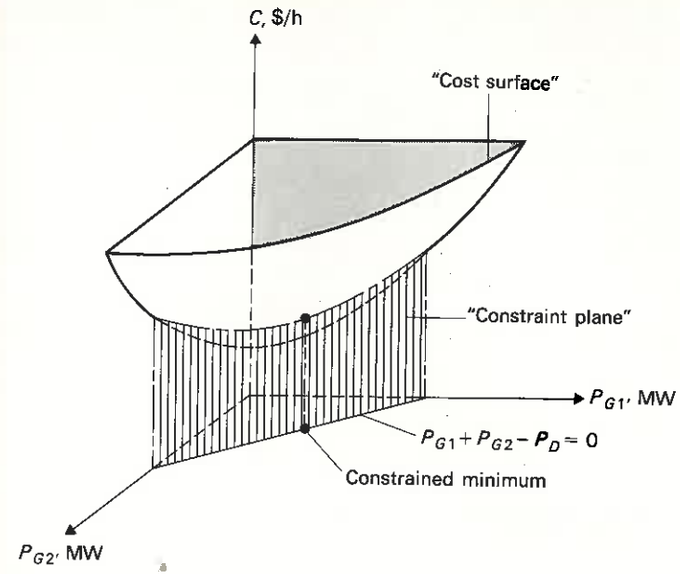

Figure 8-4 Three-dimensional cost surface.

SOLUTION In this case the cost functions and the constraint equations read

$$C = C(P_{G1}, P_{G2}) \qquad \$/\mathrm{h} \tag{8-16}$$

$$P_{G1} + P_{G2} = P_{D1} + P_{D2} = P_D \tag{8-17}$$

As we have only two generation variables we can represent C as a "cost-surface" in three-dimensional space as shown in Fig. 8-4. Note that we have shown the surface for only positive P_{G1} and P_{G2}. The surface resembles a parabolic mirror facing upward.

We can now give the ODE's a simple geometrical interpretation.

If we had *no* imposed constraints we would be operating optimally if we were at the lowest point of the cost surface. This would take us to the bottom, corresponding to the trivial case $P_{G1} = P_{G2} = 0$. The constraint equation (8-17) represents the vertical "constraint plane" identified in Fig. 8-4. *The lowest point on the intersection between this plane and the cost surface represents our sought optimum solution.*

By substitution of the IC expression (8-14) into Eq. (8-15) we obtain

$$\lambda = \beta_1 + 2\gamma_i P_{G1} = \beta_2 + 2\gamma_2 P_{G2} \tag{8-18}$$

Combined with Eq. (8-17) the latter equations yield the optimum solutions

$$\begin{aligned} P_{G1,\,\mathrm{opt}} &= \frac{2\gamma_2 P_D + \beta_2 - \beta_1}{2(\gamma_1 + \gamma_2)} \qquad \mathrm{MW} \\ P_{G2,\,\mathrm{opt}} &= \frac{2\gamma_1 P_D + \beta_1 - \beta_2}{2(\gamma_1 + \gamma_2)} \qquad \mathrm{MW} \end{aligned} \tag{8-19}$$

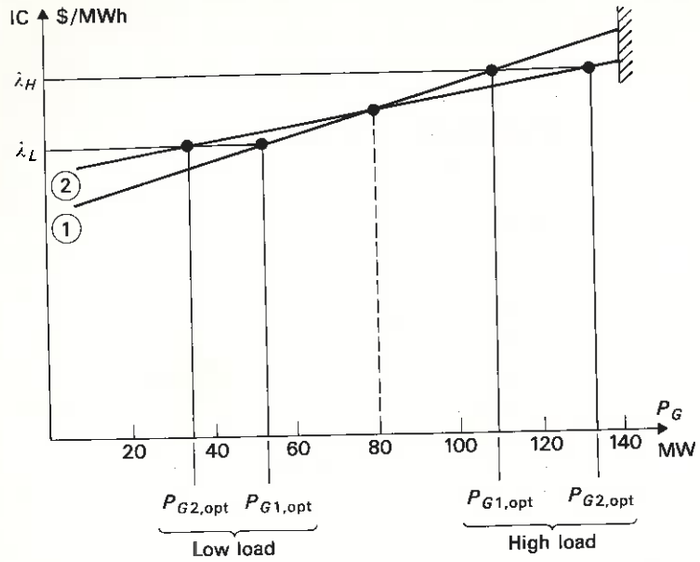

Figure 8-5 Linear incremental cost curves.

At the optimal generator settings the incremental costs are

$$\lambda = (\mathrm{IC})_1 = (\mathrm{IC})_2 = \frac{2\gamma_1\gamma_2 P_D + \beta_1\gamma_2 + \beta_2\gamma_1}{\gamma_1 + \gamma_2} \quad \text{\$/MWh} \tag{8-20}$$

If the two units are identical in costs, i.e., if $\beta_1 = \beta_2$ and $\gamma_1 = \gamma_2$, then the optimal solutions (8-19) simplify to

$$P_{G1,\,\mathrm{opt}} = P_{G2,\,\mathrm{opt}} = \frac{P_D}{2} \tag{8-21}$$

i.e., the generators should share the common load equally.

The incremental costs are in this case

$$\lambda = (\mathrm{IC})_1 = (\mathrm{IC})_2 = \beta + \gamma P_D \tag{8-22}$$

Example 8-6 The two generator units in the previous example are rated at 140 MW each. They burn different fuels and a cost analysis reveals that the two units have the linear IC data shown graphically in Fig. 8-5.

At a loading of about 80 MW both units have the same incremental costs. At lower loadings, unit 1 has a cost advantage over unit 2. At higher loadings the opposite is true.

Determine graphically how the two units should share

(*a*) a heavy load of 240 MW

(*b*) a light load of 90 MW

SOLUTION At optimum dispatch the two generators must have equal IC. We adjust the horizontal "equal IC" line until the sum of P_{G1} and P_{G2} equal the specified loads. The final results are read from the graphs:

(*a*) $P_{G1,\,\mathrm{opt}} = 108$ MW, $P_{G2,\,\mathrm{opt}} = 132$ MW

(*b*) $P_{G1,\,\mathrm{opt}} = 55$ MW, $P_{G2,\,\mathrm{opt}} = 35$ MW

8-3-5 Optimum Dispatch Formula—Inequality Constraints Considered

In deriving the optimum dispatch equations, we tacitly assumed that each generator output remained within permissible limits; i.e., all inequalities (8-6) were observed. As the total load demand increases and, as shown in Fig. 8-6, we move upward on the IC graph, we reach the rated power limit on one of the N generators. For example, in Example 8-6 we find that, as the load increases, generator 2 reaches this limit first.

When one or several generators thus reach their limit values, the question is: How should we operate the remaining units? (In Example 8-6 this, of course, poses no problem, since there is only one unit left and it *must* generate the difference $P_D - P_{G2,\,\max}$. We conclude, therefore, that in the two-generator case, the inequality constraint is of trivial consequence.)

Without proof we give the following operating strategy which seems heuristically plausible:

*If one or several generators reach their limit values, the optimum strategy calls for the remaining ones to operate so as to satisfy the equal-*IC*-rule.*

8-3-6 Computational Considerations

In a practical situation the IC curves are obtained empirically. Not only are they always nonlinear, but they may also show discontinuities. A simple analytical procedure for finding the optimum strategy is not possible in such a case.

Before we suggest a numerical computer approach, let us, with reference to Fig. 8-6, see how we may obtain a solution *graphically*. Since we know that the

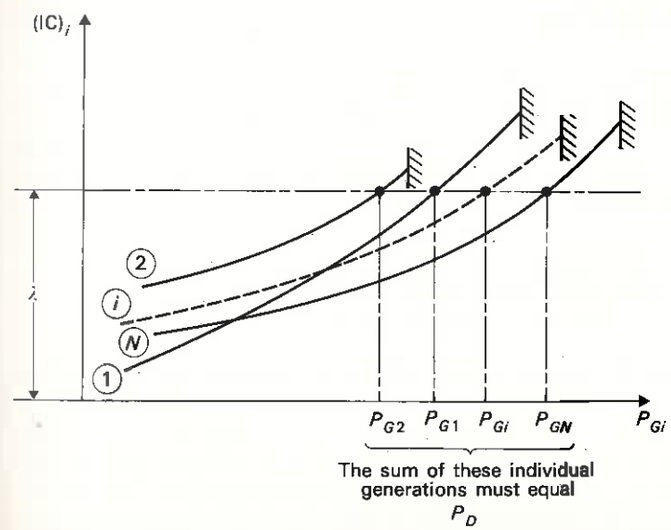

Figure 8-6 Graphical depiction of Eq. (8-15).

optimum strategy calls for equal IC values at all controlled generators, the individual generator settings must be found on the horizontal line shown in the figure. We can, therefore, in trial fashion guess a reasonable λ value and read off the corresponding values for P_{Gi}. They must together add up to the total demand P_D. If they do not, we must make a second better guess for λ, and again check whether the power balance constraint is satisfied. We converge thus on the optimum value in an iterative fashion.

Such a "λ iteration" could be performed in the following steps:

Step 1 Make an initial guess $\lambda^{(0)}$ for the Lagrange multiplier.

Step 2 Compute the individual generations $P_{G1}^{(0)}, P_{G2}^{(0)}, \ldots, P_{GN}^{(0)}$, corresponding to $(\mathrm{IC})^{(0)} = \lambda^{(0)}$. It is assumed that the IC curves are stored in the computer in the polynomial form†:

$$P_{Gi} = \alpha_i + \beta_i(\mathrm{IC})_i + \gamma_i(\mathrm{IC})_i^2 + \cdots \qquad i = 1, 2, \ldots, N \tag{8-23}$$

Step 3 Check if the relationship (8-4) is satisfied.

Step 4 If not, make a second guess, $\lambda^{(1)}$, and repeat the above steps. This guess must, of course, be guided by the results in step 3. For example, if we find that the total generation exceeds P_D, then we know that $\lambda_{\text{correct}} < \lambda^{(0)}$.

In concluding this section we make the following observations:

1. The power demand P_D has been tacitly assumed constant in our analysis. In reality, it will slowly change as the hours wear on. It is therefore necessary to reset the generator outputs at regular intervals, normally every few (2–5) minutes.
2. The Lagrange multiplier λ in this case simply equals the IC. It is usually possible, in constrained optimization problems of this type, to attach physical significance to λ.
3. In a simple "textbook" problem we have shown how, in a two-generator system and with *linear* IC curves, it is possible to obtain by *analytical* means the optimum generator settings. Clearly, in a general N-generator system with nonlinear IC curves (and they usually are), we must resort to iterative computational techniques.

8-4 OPTIMUM GENERATOR ALLOCATION—TRANSMISSION LOSSES CONSIDERED

When it is necessary to transmit energy over large distances, or when a vast area of relatively low load density is served, the transmission losses may in extreme cases amount to 15 to 20 percent of the total load. It then becomes

† *Caution:* The α, β, and γ parameters in Eq. (8-23) do *not* have the same meaning as in Eq. (8-12).

necessary to take them into account when developing an optimal dispatch strategy.

It is obvious that the presence of losses means that we no longer can make use of the simple "equal-incremental-cost" formula. For example, consider, for simplicity, the two-bus system in Fig. 8-3 where the generators at both buses are identical (including identical IC curves). Consider a loading configuration such that the lossy line carries power in direction $1 \to 2$. The "equal-IC" equation (8-2) tells us that we should let each generator carry half of the total load. However, common sense tells us that it must be more economical to let generator 2 supply more than half, thus reducing the transmission losses. In this section we investigate how the best load division is found in a case like the one just mentioned.

Before we develop general analysis methods we find it useful to study in more detail the two-bus system in Fig. 8-3.

8-4-1 Analysis of Two-Bus System

We shall assume that the two generators are identical and have identical IC curves of the earlier discussed linear form (8-14).

We neglect the shunt capacitance of the line, the latter thus being represented by only the series impedance

$$Z_s = R + jX$$

The bus admittance matrix for the two-bus system equals in this case

$$\mathbf{Y}_{\text{bus}} = \frac{1}{R + jX}\begin{bmatrix} 1 & -1 \\ -1 & 1 \end{bmatrix} \tag{8-24}$$

From the first two of Eqs. (7-22) we obtain, after some simple trigonometry,

$$P_{G1} = P_{D1} + \frac{1}{R^2 + X^2}[R|V_1|^2 + |V_1||V_2|(X \sin\delta - R\cos\delta)] \tag{8-25}$$

$$P_{G2} = P_{D2} + \frac{1}{R^2 + X^2}[R|V_2|^2 - |V_1||V_2|(R\cos\delta + X\sin\delta)] \tag{8-26}$$

where $\delta = \delta_1 - \delta_2$ is the power angle of the line.

By adding the above equations we obtain an expression for the line losses:

$$\begin{aligned} P_L &= P_{G1} + P_{G2} - P_{D1} - P_{D2} \\ &= \frac{R}{R^2 + X^2}[|V_1|^2 + |V_2|^2 - 2|V_1||V_2|\cos\delta] \end{aligned} \tag{8-27}$$

Case A. Optimization with Voltages Fixed *We note from the formulas derived that P_L, P_{G1} and P_{G2} depend upon the three variables δ, $|V_1|$ and $|V_2|$. Were we to fix the voltages the three real powers would depend only upon δ.* To treat this

simplest case first, let us presently fix $|V_1|$ and $|V_2|$. To make the above equations less unwieldy, let us also at this time assign the following numerical values:

$$R = 0.02 \text{ pu}$$
$$X = 0.10 \text{ pu}$$
$$|V_1| = |V_2| = |V| = 1.00 \text{ pu}$$
$$\beta = 2.00 \text{ kilodollars/h and pu MW}$$
$$2\gamma = 1.00 \text{ kilodollars/h and (pu MW)}^2$$
$$P_{D1} = 1.00 \text{ pu MW}$$
$$P_{D2} = 3.00 \text{ pu MW}$$

Substitution of these values into the above equations yields

$$\begin{aligned}(\text{IC})_1 &= 2 + P_{G1}\\ (\text{IC})_2 &= 2 + P_{G2}\end{aligned} \tag{8-28}$$

$$\begin{aligned}P_{G1} &= 1.0 + 1.9231(1 - \cos\delta) + 9.6154 \sin\delta\\ P_{G2} &= 3.0 + 1.9231(1 - \cos\delta) - 9.6154 \sin\delta\end{aligned} \tag{8-29}$$

$$P_L = 3.8462(1 - \cos\delta) \tag{8-30}$$

We proceed now to minimize the total generation cost. From Eq. (8-3) we have

$$C = c_1(P_{G1}) + c_2(P_{G2}) \tag{8-31}$$

As P_{G1} and P_{G2} depend only upon the *one* variable δ we write

$$\frac{dC}{d\delta} = \frac{dc_1}{d\delta} + \frac{dc_2}{d\delta} = \frac{dc_1}{dP_{G1}} \cdot \frac{dP_{G1}}{d\delta} + \frac{dc_2}{dP_{G2}} \cdot \frac{dP_{G2}}{d\delta}$$

For minimum we thus require

$$\frac{dC}{d\delta} = (\text{IC})_1 \frac{dP_{G1}}{d\delta} + (\text{IC})_2 \frac{dP_{G2}}{d\delta} = 0 \tag{8-32}$$

Upon derivation of $dP_{G1}/d\delta$ and $dP_{G2}/d\delta$ from (8-29) and substitution of the IC's, Eq. (8-32) takes on the form

$$\sin\delta - 0.8441 \cos\delta + 3.8961 \sin 2\delta = 0 \tag{8-33}$$

We readily solve this equation by trial and error and obtain the numerical solution $\delta = 5.507°$ which, upon substitution into Eq. (8-29), finally yields the optimal generator settings

$$P_{G1,\,\text{opt}} = 1.9316 \text{ pu MW}$$
$$P_{G2,\,\text{opt}} = 2.0861 \text{ pu MW}$$

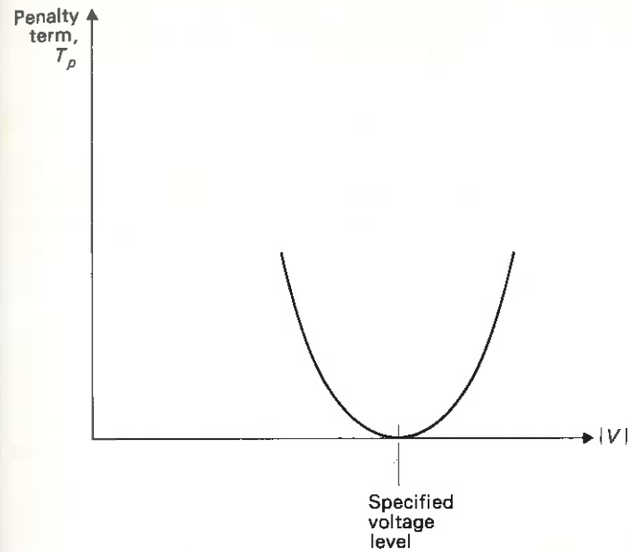

Figure 8-7 Voltage penalty function.

The losses amount to

$$P_L = 1.9316 + 2.0861 - 4.0000 = 0.0177 \text{ pu MW}$$

For comparison, had we neglected losses the optimal generator settings would be 2 pu MW at each machine.

Case B. Optimization with Voltages Considered Variable We recall that P_{G1}, P_{G2}, and P_L depended not only upon δ but also upon $|V_1|$ and $|V_2|$. We may thus conceivably attempt to further reduce the generation costs by manipulating not only the *real* generations but also the *reactive* generations of the two machines. Physically, this should clearly be possible as increasing the voltages definitely will reduce† the losses.

However, as we vary the voltages we are clearly violating the conflicting requirement that their levels stay constant.

Additional constraints are thus entering the scene. In reality, keeping a voltage at a specified level $|V_i|_{\text{spec}}$ is not a "hard" constraint. For example, if we specify in the above two-bus example that $|V_1|$ and $|V_2|$ be held at 1 pu we would not worry too much if they would change to 1.02 or even 1.05 pu. Objections are raised in increasing degree as they would deviate by 5 to 10 percent and up. The voltage constraints are thus "soft" and we can put them into quantitative form by means of a penalty term T_p of the type shown in Fig. 8-7.

† The loss formula (8-27) seems at first glance to tell us that increasing $|V_1|$ and $|V_2|$ results in an *increase* in losses. What is the fallacy in this conclusion?

If, for example, we would consider a voltage deviation of six percent to be four times as objectionable as a deviation of three percent then the penalty term would be of quadratic form

$$T_p \sim (|V| - |V|_{\text{spec}})^2 \tag{8-34}$$

We can now restate the optimization problem by forming a hybrid cost function consisting both of dollar cost of generation as before *plus* a "voltage deviation cost" proportional to the above penalty term.

For example, assume that the voltages $|V_1|$ and $|V_2|$ are specified at the levels 1.00 and 1.05 pu respectively in our two-bus example. The hybrid cost function would then read:

$$C = c_1(P_{G1}) + c_2(P_{G2}) + a_1(|V_1| - 1.0)^2 + a_2(|V_2| - 1.05)^2 \tag{8-35}$$

The positive weight factors a_1 and a_2 put the voltage deviation cost in relation to the dollar cost of generation. The optimization can now proceed along the lines in case A above. As we now have three independent variables δ, $|V_1|$, and $|V_2|$ we do *not* recommend an *analytical* solution method as in case A. Rather this type of problem is quite suitable for the *iterative gradient search* method discussed in App. C.

8-4-2 Analysis of the N-Generator Case

We shall presently develop a method that will permit us to determine optimum dispatch strategies of large-scale systems with losses taken into account. The assumptions are as follows.

The system contains n buses. Controllable generators exist at N of these buses, and by proper indexing we let these buses correspond to $i = 1, \ldots, N$. We seek that particular set of megawatt settings that will minimize the total generation cost. *All bus voltage magnitudes are assumed fixed.*

8-4-3 Incremental Transmission Loss, ITL

The problem is to minimize the cost function (8-7) by simultaneously observing the real power balance, which in the presence of losses P_L reads

$$\sum_{i=1}^{n} P_{Gi} - \sum_{i=1}^{n} P_{Di} - P_L = 0 \tag{8-36}$$

Note that the summations must extend over all n buses.

Our constrained optimum problem can now be formulated in terms of the Lagrange cost function

$$C^* \triangleq \sum_{i=1}^{N} c_i(P_{Gi}) - \lambda\left[\sum_{i=1}^{n} P_{Gi} - \sum_{i=1}^{n} P_{Di} - P_L\right] \tag{8-37}$$

By partial differentiation of the latter equation we obtain the following equations that must be satisfied for optimum real-power dispatch:

$$\frac{\partial C^*}{\partial P_{Gi}} = \frac{\partial c_i}{\partial P_{Gi}} - \lambda + \lambda\frac{\partial P_L}{\partial P_{Gi}} = 0 \qquad \text{for } i = 1, \ldots, N \tag{8-38}$$

The N optimum dispatch equations (8-38) together with the power balance equation (8-36), suffice for finding the $N + 1$ unknowns $P_{G1}, \ldots, P_{GN}$ plus plus λ. The partial derivative $\partial P_L/\partial P_{Gi}$ is referred to as the "incremental transmission loss $(\text{ITL})_i$, associated with generating unit i."

In terms of the ITL's and the earlier defined IC's the optimum dispatch equations then follow directly from Eqs. (8-38)

$$\lambda = \frac{(\text{IC})_1}{1 - (\text{ITL})_1} = \frac{(\text{IC})_2}{1 - (\text{ITL})_2} = \cdots = \frac{(\text{IC})_N}{1 - (\text{ITL})_N} \tag{8-39}$$

If the losses are zero the ITL's will also be zero and Eqs. (8-39) simplify to our earlier "equal IC" equations (8-15).

8-4-4 Finding the ITL's in the Two-Bus Case

Before deriving general formulas for ITL we return for a moment to the now familiar two-bus example system. With $|V_1|$ and $|V_2|$ fixed Eqs. (8-25) to (8-27) inform us that P_L, P_{G1}, and P_{G2} are all explicit functions of *one* variable, the power angle δ.

This means that we may consider P_L to be a function of *either* P_{G1} *or* P_{G2} *but not both.* We choose† to write $P_L = P_L(P_{G2})$. For the incremental transmission losses we thus obtain

$$(\text{ITL})_1 = \frac{\partial P_L}{\partial P_{G1}} = 0 \tag{8-40}$$

$$(\text{ITL})_2 = \frac{\partial P_L}{\partial P_{G2}} = \frac{dP_L}{dP_{G2}} = \frac{dP_L}{d\delta} \cdot \frac{d\delta}{dP_{G2}} \tag{8-41}$$

The first derivative is obtained from Eq. (8-27)

$$\frac{dP_L}{d\delta} = \frac{2R|V_1||V_2|}{R^2 + X^2}\sin\delta \tag{8-42}$$

† The reason being that bus 1 is the reference or "slack" bus and P_{G1} thus takes on the role of slack power.

and the second derivative from Eq. (8-26)

$$\frac{d\delta}{dP_{G2}} = \frac{(R^2 + X^2)/|V_1||V_2|}{R \sin \delta - X \cos \delta} \tag{8-43}$$

Upon substitution of these two derivatives into Eq. (8-41) we obtain

$$(\mathrm{ITL})_2 = 2R \frac{\sin \delta}{R \sin \delta - X \cos \delta} \tag{8-44}$$

The ODE's will thus read

$$\lambda = \frac{(\mathrm{IC})_1}{1 - 0} = \frac{(\mathrm{IC})_2}{1 - 2R \sin \delta/(R \sin \delta - X \cos \delta)} \tag{8-45}$$

The reader can easily verify that this equation is identical with our earlier optimum equation (8-33) derived without the use of ITL's.

8-4-5 Finding the ITL's in General Case

With the knowledge derived from the two-bus case we proceed now to the general n-bus case. First we observe that the total real loss power P_L equals the *total* generation minus the *total* load, i.e., the sum of the bus powers:

$$P_L = \sum_{i=1}^{n} (P_{Gi} - P_{Di}) = \sum_{i=1}^{n} P_i \tag{8-46}$$

Second, we note from Eq. (7-44) that the individual bus power P_i is a function of the $n - 1$ bus voltage phase angles $\delta_2 \cdots \delta_n$. If we introduce the $(n - 1)$-dimensional vector

$$\boldsymbol{\delta} \triangleq \begin{bmatrix} \delta_2 \\ \vdots \\ \delta_n \end{bmatrix} \tag{8-47}$$

we can thus write

$$P_i = P_i(\boldsymbol{\delta}) \qquad \text{for } i = 1, \ldots, n \tag{8-48}$$

and similarly for the loss power

$$P_L = P_L(\boldsymbol{\delta}) \tag{8-49}$$

(Compare Eq. (8-27) in the two-bus case.)
From Eq. (8-46) we obtain by differentiation

$$dP_L = \sum_{i=1}^{n} dP_i = dP_1 + \sum_{i=2}^{n} dP_i \tag{8-50}$$

The total derivatives dP_i are obtained from Eq. (7-44) and are given by

$$\begin{aligned} dP_1 &= \frac{\partial P_1}{\partial \delta_2} d\delta_2 + \cdots + \frac{\partial P_1}{\partial \delta_n} d\delta_n \\ dP_2 &= \frac{\partial P_2}{\partial \delta_2} d\delta_2 + \cdots + \frac{\partial P_2}{\partial \delta_n} d\delta_n \\ &\vdots \\ dP_n &= \frac{\partial P_n}{\partial \delta_2} d\delta_2 + \cdots + \frac{\partial P_n}{\partial \delta_n} d\delta_n \end{aligned} \tag{8-51}$$

At this stage we introduce the following three vectors, all of dimension $(n - 1)$:

$$d\mathbf{P} \triangleq \begin{bmatrix} dP_2 \\ \vdots \\ dP_n \end{bmatrix} \tag{8-52}$$

$$\frac{\partial P_1}{\partial \boldsymbol{\delta}} \triangleq \begin{bmatrix} \dfrac{\partial P_1}{\partial \delta_2} \\ \vdots \\ \dfrac{\partial P_1}{\partial \delta_n} \end{bmatrix} \tag{8-53}$$

$$d\boldsymbol{\delta} \triangleq \begin{bmatrix} d\delta_2 \\ \vdots \\ d\delta_n \end{bmatrix} \tag{8-54}$$

We also define the $(n - 1) \times (n - 1)$ jacobian matrix

$$\frac{\partial \mathbf{P}}{\partial \boldsymbol{\delta}} \triangleq \begin{bmatrix} \dfrac{\partial P_2}{\partial \delta_2} & \cdots & \dfrac{\partial P_2}{\partial \delta_n} \\ \vdots & & \vdots \\ \dfrac{\partial P_n}{\partial \delta_2} & \cdots & \dfrac{\partial P_n}{\partial \delta_n} \end{bmatrix} \tag{8-55}$$

In terms of these defined vectors and matrix, equations (8-51) can then be written in compact form

$$\begin{aligned} dP_1 &= \left(\frac{\partial P_1}{\partial \boldsymbol{\delta}}\right)^T d\boldsymbol{\delta} \\ d\mathbf{P} &= \frac{\partial \mathbf{P}}{\partial \boldsymbol{\delta}} \cdot d\boldsymbol{\delta} \end{aligned} \tag{8-56}$$

The last equation is first inverted

$$d\boldsymbol{\delta} = \left(\frac{\partial \mathbf{P}}{\partial \boldsymbol{\delta}}\right)^{-1} d\mathbf{P}$$

If $d\boldsymbol{\delta}$ is substituted into the first of Eqs. (8-56) we obtain

$$dP_1 = \left(\frac{\partial P_1}{\partial \boldsymbol{\delta}}\right)^T \left(\frac{\partial \mathbf{P}}{\partial \boldsymbol{\delta}}\right)^{-1} d\mathbf{P} \triangleq \boldsymbol{\alpha} \cdot d\mathbf{P} \tag{8-57}$$

The product matrix

$$\boldsymbol{\alpha} \triangleq \left(\frac{\partial P_1}{\partial \boldsymbol{\delta}}\right)^T \left(\frac{\partial \mathbf{P}}{\partial \boldsymbol{\delta}}\right)^{-1} \tag{8-58}$$

is a *row* matrix of dimension $(n-1)$ that can be written in the form

$$\boldsymbol{\alpha} = [\alpha_2, \alpha_3, \ldots, \alpha_n] \tag{8-59}$$

If Eq. (8-57) is substituted into Eq. (8-50) we obtain

$$dP_L = \boldsymbol{\alpha} \cdot d\mathbf{P} + \sum_{i=2}^{n} dP_i \tag{8-60}$$

or

$$dP_L = (1+\alpha_2)\, dP_2 + (1+\alpha_3)\, dP_3 + \cdots + (1+\alpha_n)\, dP_n \tag{8-61}$$

The latter equation is important as it gives the incremental changes in the total loss power P_L resulting from arbitrary incremental changes in the bus powers P_i or† generation P_{Gi}.

Specifically, if all the generator powers except P_{Gi} are kept constant, Eq. (8-61) yields the *partial* derivative

$$\frac{dP_L}{dP_{Gi}} \triangleq \frac{\partial P_L}{\partial P_{Gi}} \triangleq (\mathrm{ITL})_i = 1 + \alpha_i \qquad \text{for } i = 2, \ldots, N \tag{8-62}$$

(Note that we need to include only the N buses containing *controllable* generators.)

Also, as dP_L is independent of dP_{G1} we have

$$(\mathrm{ITL})_1 = 0 \tag{8-63}$$

8-4-6 Computational Procedure

We discuss briefly the computational details. First we recall that the entire theory was based upon the assumption that the load is *constant*. For a time period of a few minutes this may be a good approximation. However, as shown

† This follows since $P_i = P_{Gi} - P_{Di}$ and thus $dP_i = dP_{Gi}$.

in Fig. 8-1 the load will drift *and the solution to the optimum dispatch equations must therefore be updated at regular intervals*, for example every three minutes.

The computational sequencing for one complete solution of the ODE's could proceed as shown in the flow chart in Fig. 8-8. We clarify presently the purpose of some of the blocks in this chart:

Blocks 2 and 4. Upon specification of bus voltages and powers at the various load and voltage control buses we are in a position to obtain a power-flow solution (see Chap. 7). *Note that the specs must include a first guess of the generator power settings $P_{G2}^{(0)} \cdots P_{GN}^{(0)}$.* Superscript (μ) refers to the "power-flow iteration count."

As we exit from block 4 we possess knowledge of *all* bus powers and voltages required to perform the calculations in blocks 5 to 8.

Blocks 9, 10, 11, 12. These blocks make up the inner "λ loop," the purpose of which is to choose generator settings P_{Gi}^{μ} that will satisfy the power-balance equation (8-36). This is accomplished by an iterative search of a λ value in the following manner: Following an initial λ guess we are able to compute the incremental generation costs IC_i in block 10. We then compute the corresponding generation in block 11 using formula (8-23). In block 12 we check that the power balance equation (8-36) is satisfied. If not, we go back to block 9 and pick a better λ value, etc.

Block 13. As we exit from block 12 the new generator settings $P_{Gi}^{(\mu)}$ are closer to the sought optimal values. The μ-iterations are deemed completed when the improvements from previous iteration are less than the tolerance ε.

The above computational loop may be repeated until no further improvements are detected in block 13 in the generator settings. As one complete power flow must be run in each iteration cycle it is obvious that all efforts should be made to reduce the computational needs in every regard. The "fast-power-flow" schemes discussed in Chap. 7 can be useful.

SUMMARY

A power system containing more than one generator unit can provide a specified load demand in an infinite number of generation combinations. Normally, one specific set of generator megawatt settings is "better" in some chosen sense than all the others. If the generators are adjusted to share the common load accordingly the system is said to operate on "optimum dispatch."

Minimum economic generation cost is a relevant criterion and today's power systems are typically operated so as to achieve minimum overall cost. In this chapter we have developed analysis tools by means of which conditions for

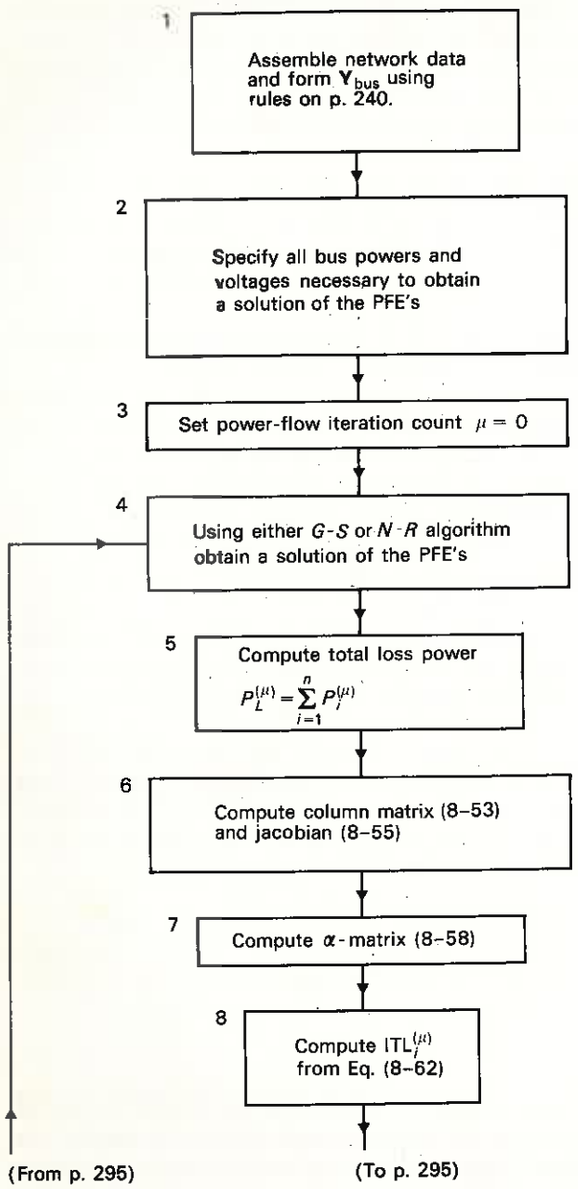

Figure 8-8 Computational flow chart for solving the optimal dispatch equations with losses considered.

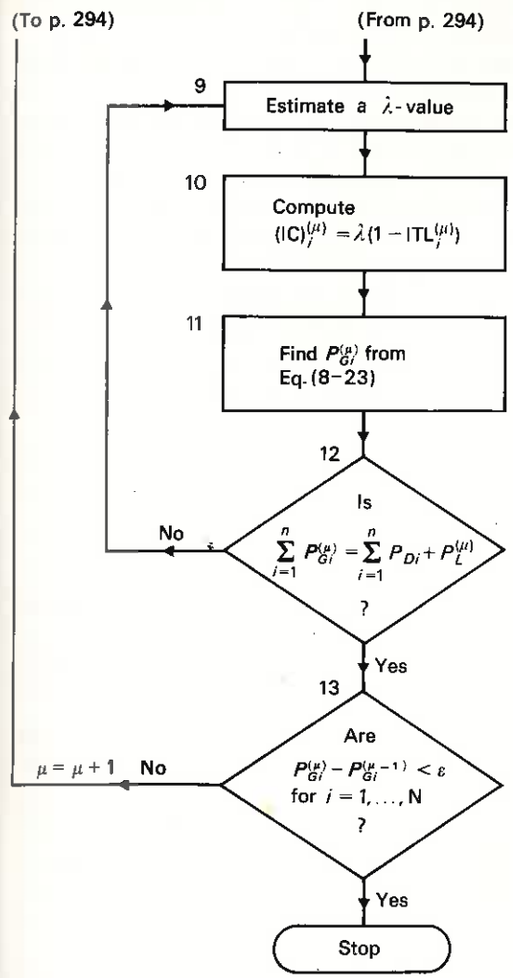

optimum economic dispatch can be determined. Optimum dispatch equations (ODE's) have been derived for both the loss-free and lossy cases.

As the real system losses depend upon real and reactive line flows, it follows that some optimal combination of the reactive line flows may further reduce the losses. The reactive line flows can be varied only by changing the bus voltage magnitudes and since the latter normally should be kept constant this therefore would not seem to be a viable option. However, the voltage constraints are of the "soft" type permitting reactive power adjustment within certain limits. Optimal voltage settings can be obtained with the use of "penalty terms" added to the regular cost function.

Being able to compute the optimum generator megawatt settings is only half the problem; the other half consists of implementing it in "real time." This aspect of optimum control naturally belongs to the general topic of automatic generation control that shall be addressed in the next chapter.

PROBLEMS

***8-1** Consider a situation where the cost functions c_i are *linear* functions of P_{Gi}, that is, of the form

$$c_i = \alpha_i + \beta_i P_{Gi} \qquad \$/\text{h} \tag{8-64}$$

Show that the formulas (8-15) are of little help in trying to find the optimum generator settings in this case.

How does the cost surface look in the two-generator case. Give a graphical explanation why the ODE's don't work in this case. How would you find the optimal generator settings in this case? Assume zero losses.

***8-2** Consider the two-bus system in Example 8-5. Find a formula for the minimum operating losses expressed in dollars per hour.

***8-3** Consider the three-bus system in Fig. 7-4. Each bus is fed from generators, all of which are under control. The IC–P_G curve of each machine has been curve-fitted with polynomials in accordance with

$$\begin{aligned}(\text{IC})_1 &= 9.3 + 0.041P_{G1} + 0.00012P_{G1}^2\\ (\text{IC})_2 &= 7.6 + 0.031P_{G2} + 0.00008P_{G2}^2\\ (\text{IC})_3 &= 8.1 + 0.029P_{G3} + 0.00011P_{G3}^2\end{aligned} \tag{8-65}$$

If P_{Gi} is inserted in MW the formulas yield dollars per MWh. (The formulas are valid only for positive P_{Gi}'s.

The total load demand at a certain hour of the day equals 360 MW. Neglect real losses and develop a computer program that will render a solution for the optimum generator settings within an accuracy of ± 0.1 MW.

8-4 Work Prob. 8-3 without neglecting losses. All three lines are identical; each being represented by a series impedance of $10 + j50\ \Omega$/phase. The 360-MW unity power factor load is divided equally between buses 2 and 3. All three buses are kept at 138 kV.

Develop a computer program that will yield the optimal generator settings.

Show the power flow in all three lines and compute also the total losses.

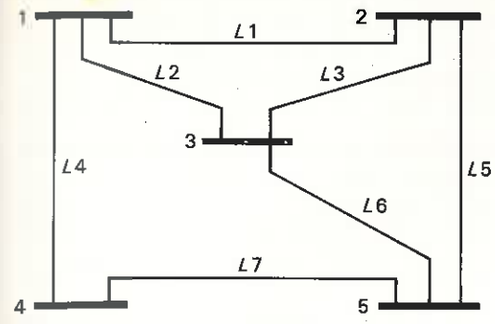

Figure 8-9 A five-bus example system.

8-5 Consider the five-bus system in Fig. 8-9. All seven lines are characterized by a series impedance of $0.211 + j0.851\ \Omega$/mi; and a shunt admittance of $5.21\ \mu\mho$/mi.

The lines are rated at 138 kV and have the following lengths:

$L1$:	70.4 miles
$L2$:	53.1 miles
$L3$:	40.8 miles
$L4$:	71.9 miles
$L5$:	62.8 miles
$L6$:	30.6 miles
$L7$:	98.4 miles

You can consider them all as "electrically short."

Generators are installed at buses 1, 3, and 5. We assume for simplicity that all three generator stations are characterized by equal cost curves

$$(\text{IC})_i = 6.00 + 0.021P_{Gi} \text{ dollars per MWh } (P_{Gi} \text{ to be inserted in MW}).$$

Base values are

100 MVA (total three-phase)
230 kV (line-to-line)

Specified voltages and loads are given in Table 8-1.

Assume all three generators to be under optimal control. Develop a computer program that will yield optimal megawatt settings.

Table 8-1

Bus	Load demand, pu P_{Di}	Load demand, pu Q_{Di}	Bus voltage magnitude, pu	Generation
1	2.31	0.86	1.05	Yes
2	2.01	1.28	Unspecified	No
3	1.61	0.42	1.02	Yes
4	1.71	1.28	Unspecified	No
5	2.11	0.76	1.02	Yes

REFERENCES

1. G. R. Davidson: "Dividing Load between Units," *Electrical World*, Dec. 23, 1922.
2. E. E. George: "Intrasystem Transmission Losses," *AIEE Trans.*, vol. 62, March 1943, pp. 153–158.
3. L. K. Kirchmayer and G. W. Stagg: "Analysis of Total and Incremental Losses in Transmission Systems," *AIEE Trans.*, vol. 70, pt. II, 1951, pp. 1197–1205.
4. L. K. Kirchmayer: *Economic Operation of Power Systems*, John Wiley & Sons, New York, 1958.
5. H. W. Dommel and W. F. Tinney: "Optimal Power Flow Solutions," *IEEE Trans.*, vol. PAS-87, no. 10, October 1968, pp. 1866–1876.
6. J. Peschon et al: "Optimum Control of Reactive Power Flow," *IEEE Trans.*, vol. PAS-87, no. 1, January 1968, pp. 40–48.
7. A. M. Sasson and H. M. Merrill: "Some Applications of Optimization Techniques to Power System Problems," *Proc. IEEE*, vol. 62, July 1974, pp. 959–972.
8. H. H. Happ: "Optimal Power Dispatch—a Comprehensive Survey," *IEEE Trans. Power Apparatus and Systems*, vol. PAS-96, May/June 1977, pp. 841–854.
9. F. Wu et al., "A Two-Stage Approach to Solving Optimal Power Flows," *Proc. 1979 PICA Conf.*, pp. 126–136.
10. B. Stott and O. Alsac: "Fast Decoupled Load Flow," *IEEE Trans.*, Pas vol. 93, May/June 1974, pp. 859–869.

CHAPTER

NINE

THE ENERGY SYSTEM IN STEADY STATE—THE CONTROL PROBLEM

The two preceding chapters were devoted to the problems associated with the selection of a normal operating state for a power system. In this chapter we concern ourselves with the problem of *keeping* the system in this state by means of *continuous automatic closed-loop control.*

As the demand deviates from its normal value with an unpredictable small amount the state of the system will change. The automatic control system must detect these changes, and initiate in "real time" a set of countercontrol actions which will eliminate as quickly and effectively as possible the state deviations.

9-1 BASIC GENERATOR CONTROL LOOPS

Figure 9-1 depicts the two major control loops with which most large generators are equipped. The *automatic voltage regulator* (AVR) loop controls the magnitude of the terminal voltage V. The latter voltage is continuously sensed, rectified, and smoothed. This dc signal, being proportional to $|V|$, is compared with a dc reference $|V|_{\text{ref}}$. The resulting "error voltage," after amplification and signal shaping, serves as the input to the *exciter* which finally delivers the voltage v_f to the generator field winding.

The *automatic load-frequency control* (ALFC) loop regulates the megawatt output and frequency (speed) of the generator. The loop is not a single one as in the case of the AVR. A relatively fast *primary loop* responds to a frequency signal which, as we have noted, is an indirect measure of megawatt balance. Via the *speed governor* and the control valves the steam (or hydro) flow is regulated with

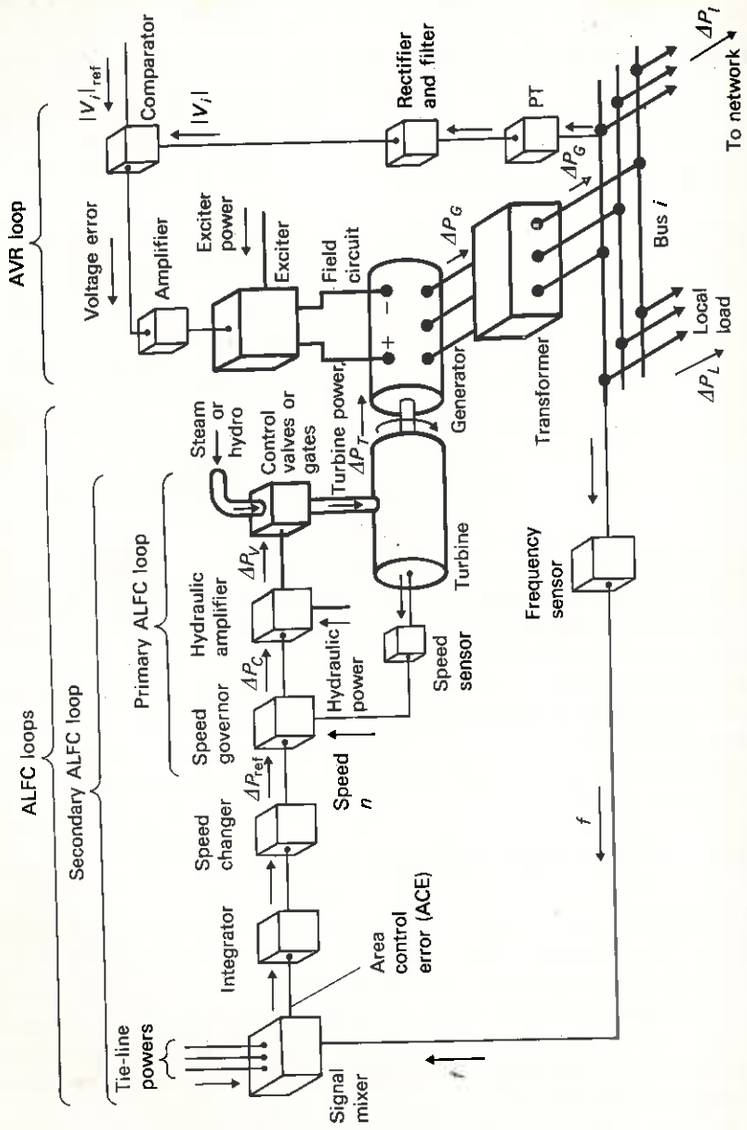

Figure 9-1 The automatic load-frequency and voltage regulator control loops of a synchronous generator.

the intent of matching the megawatt output to relatively fast load fluctuations. By "fast" we mean changes that take place in one to several seconds. By thus tending to maintain a megawatt balance, this primary loop performs indirectly a coarse speed or frequency control.

A slower *secondary* loop maintains the fine adjustment of the frequency, and also by "reset" action maintains proper megawatt interchange with other pool members. This loop is insensitive to rapid load and frequency changes but focuses instead on driftlike changes which take place over periods of minutes.

9-1-1 Cross-Coupling Between Control Loops

The AVR and ALFC loops are not in the truest sense noninteracting; cross-coupling does exist and can sometimes be troublesome. There is little if any coupling from the ALFC loop to the AVR loop, but interaction exists in the opposite direction. We understand this readily by realizing that control actions in the AVR loop affect the magnitude of the generator emf E. As the internal emf determines the magnitude of the real power (Eq. 4-22) it is clear that changes in the AVR loop must be felt in the ALFC loop.

However, the AVR loop is much faster than the ALFC loop and there is therefore a tendency for the AVR dynamics to settle down before they can make themselves felt in the slower load-frequency control channel. In the discussions to follow we shall first study the two loops independently starting with the AVR loop. Later we shall discuss the effects of cross-coupling.

9-1-2 Small-Signal Analysis

In analysis of power system dynamics one distinguishes between *large-signal* and *small-signal* analysis. The former type of analysis is encountered (Chap. 12) when effects of major disturbances are being studied. In such situations generator voltages and powers may undergo sudden changes of magnitudes that may approach 100 percent of normal operating values. Usually this type of analysis leads to differential equations of nonlinear type.

Small-signal analysis is used when variable excursions are relatively small, typically at most a few percent of normal operating values. Differential equations are now mostly linear and the powerful Laplace transform analysis methods can be employed.

We distinguish between the two analysis types by means of variable symbol designations. In large-scale analysis symbols like f, δ, and $|V|$ represent *actual* frequency, power angle, and voltage magnitude respectively. (Compare power-flow analysis in Chap. 7). In small-scale analysis we use the symbols Δf, $\Delta\delta$, and $\Delta|V|$ to mean the *deviations* of frequency, angle, and voltage magnitude from normal operating values. *All analysis in this chapter falls in this latter category.*

9-2 THE AUTOMATIC VOLTAGE REGULATOR (AVR)

The *exciter* is the main component in the AVR loop. It delivers the dc power to the generator field. It must have adequate power capacity (in the low megawatt range for large generators) and sufficient speed of response (rise times less than 0.1 seconds). The basic role of the AVR is to provide constancy of the generator terminal voltage during normal small and slow changes in the load. However, it is common practice to design the exciter with enough margin to give powerful boosts in the excitation level also during emergency situations.

9-2-1 Exciter Types

There exists a variety of exciter types in use, the more important ones described in Refs. 1 and 2.

In older power plants, the exciter consisted of a dc generator driven by the main generator shaft. This arrangement required the transfer of the dc power to the generator field via slip rings and brushes.

Modern exciters tend to be of either *brushless* or *static* design. A typical brushless AVR loop is shown in Fig. 9-2, where the exciter consists of an "inverted" three-phase synchronous generator. The latter has its three-phase armature on the rotor and its field on the stator. Its ac armature voltage is rectified in diodes mounted on the rotating shaft, and then fed directly into the main generator field. This design obviously eliminates the need for slip rings and brushes.

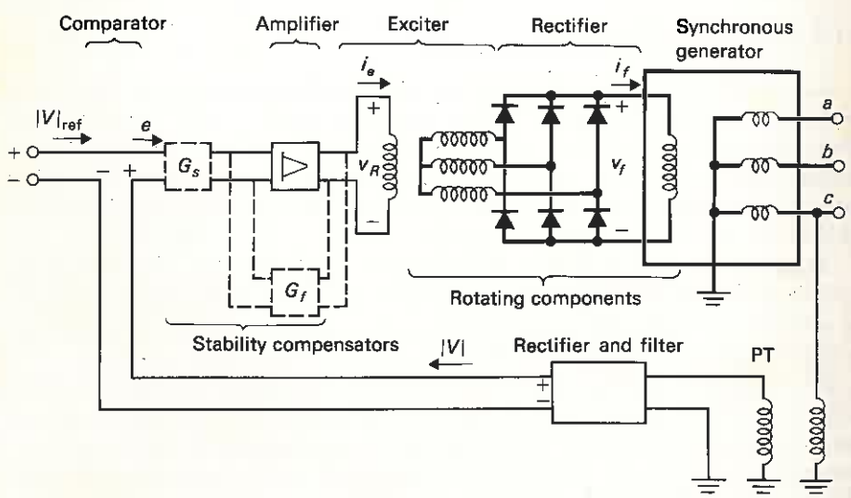

Figure 9-2 Brushless AVR loop.

In a static AVR-loop the excitation power is obtained directly from the generator terminals or from the station service bus. The ac power is rectified in thyristor bridges and fed into the main generator field via slip rings. Static exciters are very fast and contribute to improved "transient stability" (Chap. 12).

9-2-2 Exciter Modeling

Here follows first a brief description of the AVR loop depicted in Fig. 9-2. (The role of the "stability compensators" will be discussed later.)

Assume that for some reason the terminal voltage $|V|$ would decrease. This immediately results in an increased "error voltage" e which, in turn, causes increased values of v_R, i_e, v_f,† and i_f. The d axis generator flux increases as a result of the boost in i_f, thus raising the magnitude of the internal generator emf E and terminal voltage V.

Mathematical modeling of the exciter and its controls follows. If for the moment we disregard the stability compensator (shown dashed in the figure) we have for the comparator and amplifier respectively

$$\Delta|V|_{\text{ref}} - \Delta|V| = \Delta e \tag{9-1}$$

and

$$\Delta v_R = K_A \Delta e$$

where K_A is the amplifier gain.

Laplace transformation of these two equations yields

$$\Delta|V|_{\text{ref}}(s) - \Delta|V|(s) = \Delta e(s)$$

and

$$G_A \triangleq \frac{\Delta v_R(s)}{\Delta e(s)} = K_A \tag{9-2}$$

where G_A is the amplifier transfer function.

The last equation implies *instantaneous* amplifier response. In reality the amplifier will have a delay that can be represented by a time constant T_A, and its transfer function will then be of the form

$$G_A = \frac{\Delta v_R(s)}{\Delta e(s)} = \frac{K_A}{1 + sT_A} \tag{9-3}$$

If R_e and L_e represent respectively the resistance and inductance of the exciter field we have for voltage equilibrium in the latter

$$\Delta v_R = R_e \Delta i_e + L_e \frac{d}{dt}(\Delta i_e) \tag{9-4}$$

† IEEE (see Ref. 1) uses the symbol E_{fd} for the field voltage. We depart from this praxis for two reasons:

(*a*) Capital letter symbols are reserved for phasors;

(*b*) Symbol "e" is reserved for emf and/or "error voltage".

Measured across the main field the exciter produces K_1 armature volts per ampere of field current i_e, that is, we have the proportionality

$$\Delta v_f = K_1 \, \Delta i_e \tag{9-5}$$

Upon Laplace transformation of the last two equations and elimination of Δi_e we obtain the transfer function of the exciter

$$G_e \triangleq \frac{\Delta v_f(s)}{\Delta v_R(s)} = \frac{K_e}{1 + sT_e} \tag{9-6}$$

where

$$K_e \triangleq \frac{K_1}{R_e}$$

$$T_e \triangleq \frac{L_e}{R_e}$$

From these equations and using accepted block symbols we assemble directly the transfer function model shown in Fig. 9-3. The time constants T_A and T_e have values in the ranges 0.02–0.10 and 0.5–1.0 seconds respectively.

(*Note:* Sometimes the exciter block representation is given as

$$\frac{V_F}{V_R} = \frac{1}{K_E + sT_E}$$

We have chosen the form shown in Fig. 9-3 as it conforms with the general control system definitions for "gain" and "time constant.")

9-2-3 Generator Modeling

We need to "close the loop" in Fig. 9-3 by establishing the "missing dynamic link" between the field voltage v_f and the generator terminal voltage $|V|$. As the terminal voltage equals the internal emf minus the voltage drop across the

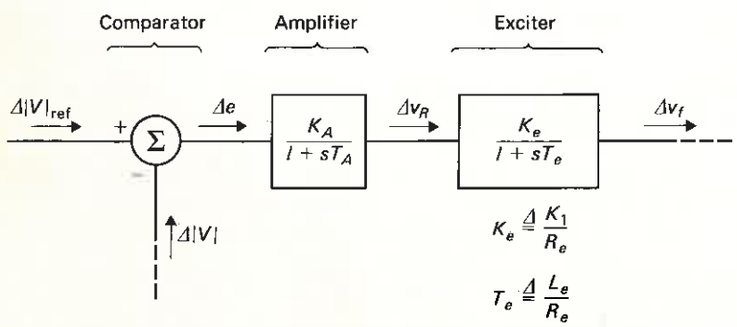

Figure 9-3 Linear model of the comparator-amplifier-exciter portion of the AVR loop in Fig. 9-2.

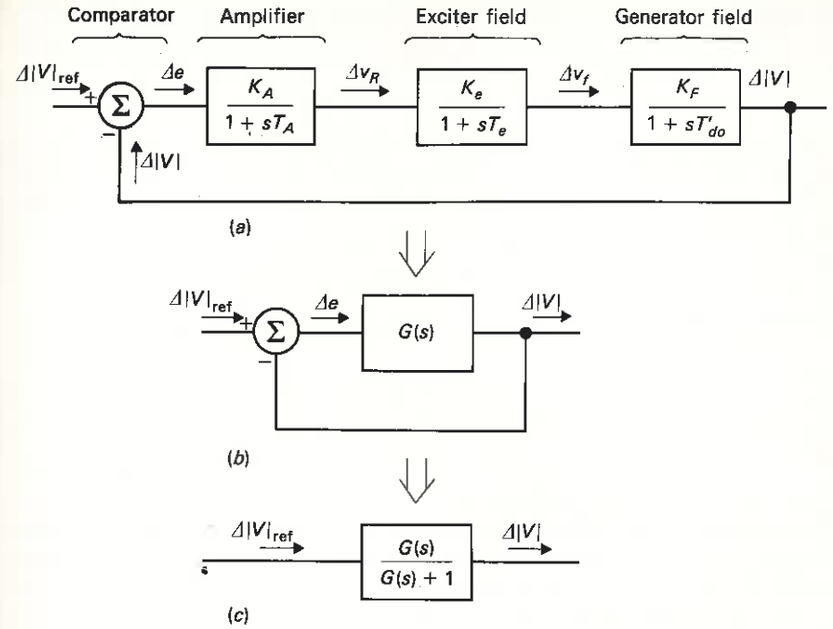

Figure 9-4 Closing the AVR loop; (*a*) individual block representation; (*b*) condensed model; (*c*) closed loop model.

internal impedance it is clear that the relationship between v_f and $|V|$ depends on the generator loading. The simplest possible relationship exists at low or zero loading in which case V equals approximately the internal emf E. Kirchhoff's voltage law applied to the field winding yields in this case:

$$\Delta v_f = R_f \, \Delta i_f + L_{ff} \frac{d}{dt}(\Delta i_f) = \frac{\sqrt{2}}{\omega L_{fa}} \left[R_f \, \Delta E + L_{ff} \frac{d}{dt}(\Delta E) \right] \tag{9-7}$$

The last step follows from Eq. (4-5).

After Laplace transformation the last equation yields the field transfer ratio

$$\frac{\Delta E(s)}{\Delta v_f(s)} \cong \frac{\Delta |V|(s)}{\Delta v_f(s)} = \frac{K_F}{1 + sT'_{do}} \tag{9-8}$$

where

$$K_F \triangleq \frac{\omega L_{fa}}{\sqrt{2} R_f}$$

and T'_{do} was defined by Eq. (4-63).

We can now complete the AVR loop as shown in Fig. 9-4*a*. In two easy-to-follow steps we condense the diagram down to the final form shown in Fig. 9-4*c*.

The *open-loop transfer function* $G(s)$ equals

$$G(s) = \frac{K}{(1 + sT_A)(1 + sT_e)(1 + sT'_{do})} \tag{9-9}$$

where the *open-loop gain* K is defined by

$$K \triangleq K_A K_e K_F \tag{9-10}$$

9-2-4 Static Performance of the AVR Loop

The AVR loop must

1. regulate the terminal voltage $|V|$ to within required static accuracy limit
2. have sufficient speed of response
3. be stable

The static accuracy requirement can be stated thusly:

For a *constant* (subscript 0) reference input the likewise constant error Δe_0 must be less than some specified percentage p of the reference. We thus can write the static accuracy specification as follows:

$$\Delta e_0 = \Delta|V|_{\text{ref, 0}} - \Delta|V|_0 < \frac{p}{100} \cdot \Delta|V|_{\text{ref, 0}} \tag{9-11}$$

For a constant input the transfer function is obtained by setting $s = 0$. From Fig. 9-4*c* we thus obtain

$$\Delta e_0 = \Delta|V|_{\text{ref, 0}} - \Delta|V|_0 = \Delta|V|_{ref,\,0} - \frac{G(0)}{1 + G(0)}\,\Delta|V|_{\text{ref, 0}}$$

$$= \frac{1}{1 + G(0)}\Delta|V|_{\text{ref, 0}} = \frac{1}{1 + K}\,\Delta|V|_{\text{ref, 0}} \tag{9-12}$$

Clearly, the static error decreases with increased loop gain. Substitution of (9-12) into (9-11) yields the minimum gain needed to obtain a specified accuracy:

$$K > \frac{100}{p} - 1 \tag{9-13}$$

For example, if we specify that the static error should be less than one percent the open-loop gain must exceed 99.

9-2-5 Dynamic Response of the AVR Loop

From the theory of linear control systems[12] it is known that the time response $\Delta|V|(t)$ of the loop in Fig. 9-4 equals

$$\Delta|V|(t) = \mathscr{L}^{-1}\left\{\Delta V_{\text{ref}}(s)\frac{G(s)}{G(s) + 1}\right\} \tag{9-14}$$

Mathematically, the response depends upon the *eigenvalues* or *closed-loop poles*, which are obtained from the *characteristic equation*

$$G(s) + 1 = 0 \tag{9-15}$$

In the AVR loop (Fig. 9-4) the open-loop transfer function $G(s)$ is of third order and we thus obtain three eigenvalues, s_1, s_2, and s_3. If these are distinct and real the transient response components are of the form

$$A_1 e^{s_1 t},\ A_2 e^{s_2 t},\ A_3 e^{s_3 t} \tag{9-16}$$

If two of the eigenvalues, for example s_2 and s_3, are conjugate complex, $\sigma \pm j\omega$, then the transient component will contain an oscillatory term of the form

$$A_1 e^{\sigma t} \sin(\omega t + \beta) \tag{9-17}$$

For the AVR loop to be *stable* the transient components must vanish with time. We thus must require that all three eigenvalues be located in the left-hand s plane. For the loop to possess good *tracking ability* the transients must not only vanish but they must do so speedily. As the real parts of the eigenvalues determine the rapidity of the exponential decay, a high-speed loop must possess eigenvalues located well to the left in the s plane.

The amplitude factors A_1, A_2, and A_3 in formulas (9-16) and (9-17) express the relative size of the transient terms. If one or several of the terms are relatively large then the corresponding eigenvalues are said to be *dominant*. Generally the closer the eigenvalue is located to the $j\omega$ axis the more dominant it becomes.

9-2-6 AVR Root Loci

The location in the s plane of the eigenvalues depends upon the open-loop gain K and the three time constants T_A, T_e, and T'_{do}. Of these parameters only the loop gain can be considered adjustable. It is interesting to study how the magnitude of this gain affects the s-plane locations of the three eigenvalues—and thus the transient response.

A *root locus plot* yields valuable information in this regard. Figure 9-5 depicts the root-locus picture for the AVR loop. There are three loci, each starting from an open-loop pole (marked ×). The latter are located at $s = -1/T_A$, $-1/T_e$ and $-1/T'_{do}$ respectively. For low values of the loop gain the eigenvalues (marked □) are located close to the open-loop poles, their positions marked *a*. Because T'_{do} is comparatively large the pole $-1/T'_{do}$ is very close to origin. The dominating eigenvalues s_2 is thus small, resulting in a very slowly decaying exponential term, giving the loop an unacceptably sluggish response. The gain K would not satisfy the inequality (9-13) thus rendering an inaccurate static response as well.

By increasing the loop gain the eigenvalue s_2 travels to the left and the loop response quickens. At a certain gain setting the eigenvalues s_3 and s_2 "collide." Further increase in the loop gain results in s_3 and s_2 becoming conjugate

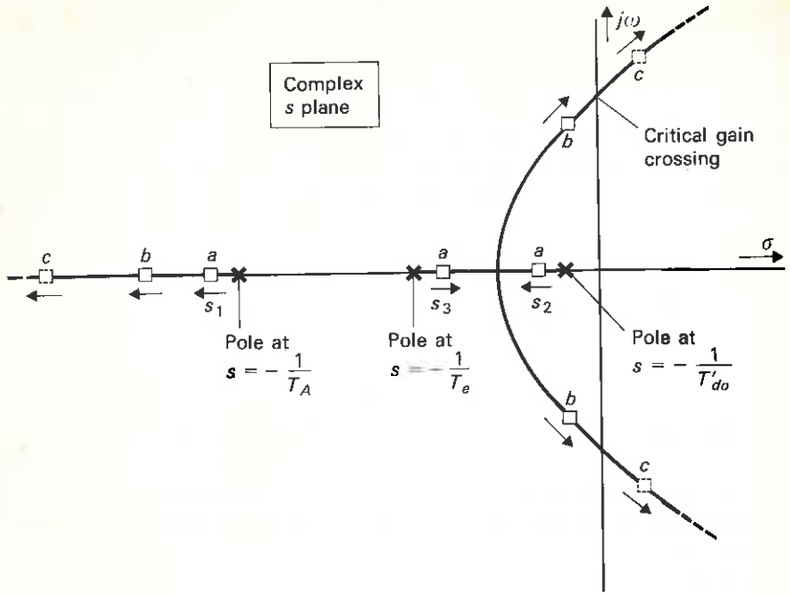

Figure 9-5 Closed-loop root loci for AVR control loop in Fig. 9-4.

complex. This dominant eigenvalue pair (*b*) makes the loop oscillatory, with poor damping. If the gain is increased further the eigenvalues wander into the right-hand *s* plane (*c*). The loop now becomes unstable.

9-2-7 Stability Compensation

High loop gain is needed for static accuracy but this causes undesirable dynamic response, possibly instability. By adding *series* and/or *feedback stability compensation* (Fig. 9-2) to the AVR loop, this conflicting situation can be resolved.

As the stability problems emanate from the three cascaded time constants the compensation networks typically will contain some form of phase advancement. Consider for example the addition of a series *phase* lead compensator, having the transfer function

$$G_s = 1 + sT_c$$

The open-loop transfer function will now contain a zero

$$G(s) = \frac{K(1 + sT_c)}{(1 + sT_A)(1 + sT_e)(1 + sT'_{do})} \tag{9-18}$$

The added network will not affect the static loop gain K, and thus the static accuracy. The dynamic response characteristics will change to the better. Consider for example the case when we would tune the compensator time constant

T_c to equal the exciter time constant T_e. The open-loop transfer function would then equal

$$G(s) = \frac{K}{(1 + sT_A)(1 + sT'_{do})} \tag{9-19}$$

The root loci (there are only two) of the compensated system are depicted in Fig. 9-6. Low loop gain (*a*) still results in negative real eigenvalues, the dominant one of which, s_2, yields a sluggish response term. Increasing loop gain (*b*) results in oscillatory response. The damping of the oscillatory term will, however, not decrease with increasing gain as was the case in the uncompensated system.

In reality a combination of series and feedback compensation is employed. (Compare Prob. 9-5.)

9-2-8 Effects of Generator Loading

The above analysis of the AVR loop was based upon the assumption (Eq. 9-8) that $E \approx |V|$ which holds true only for a lightly loaded generator. How does increased loading affect the above analysis? It should be noted that the ability of the AVR loop to maintain a well regulated terminal voltage under widely shifting load conditions ("robustness") is an absolute prerequisite.

Added load does not change the basic features of the AVR loop as depicted in Fig. 9-4. It will, however, affect the values of both the gain factor K_F and the field time constant. High loading will make the generator work at higher magnetic saturation levels. This means smaller changes in $|E|$ for incremental increases in i_f, translating into a reduction of K_F. The field time constant will likewise decrease as generator loading means closing the armature current paths.

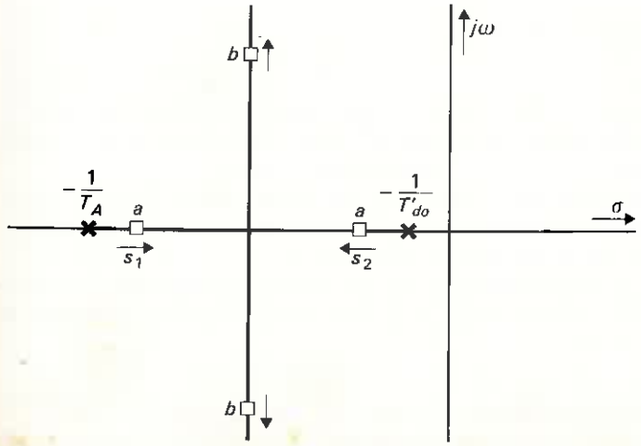

Figure 9-6 Root loci for zero-compensated loop.

This circumstance permits the formation of "transient" stator currents, the existence of which yields a lower "effective" field inductance. The rotor-field time constant, *under load* can be shown to equal

$$T_{d,\,\text{load}} = \frac{X'_d + X_{\text{ext}}}{X_d + X_{\text{ext}}} \cdot T'_{do} \qquad \text{s} \tag{9-20}$$

where X_{ext} is the exterior reactance viewed from generator terminals. Compare also Eq. (4-64).

9-3 AUTOMATIC LOAD-FREQUENCY CONTROL OF SINGLE-AREA SYSTEMS

The basic role of ALFC† is to maintain desired megawatt output of a generator unit and assist in controlling the frequency of the larger interconnection. The ALFC also helps to keep the net interchange of power between pool members at predetermined values. Control should be applied in such a fashion that highly differing response characteristics of units of various types (hydro, nuclear, fossil, etc.) are recognized. Also, unnecessary power output changes should be kept to a minimum in order to reduce wear of control valves.

The ALFC loop will maintain control only during normal (small and slow) changes in load and frequency. It is typically unable to provide adequate control during emergency situations, when large megawatt imbalances occur. Then more drastic "emergency controls" must be applied (Chap. 12).

In the present section we shall first study ALFC as it applies to a single generator supplying power to a local service area. We shall later extend the study to embrace several generators all part of a single "control area."

9-3-1 Speed-Governing System

The real power in a power system is being controlled by controlling the driving torques of the individual turbines of the system. Figure 9-7 shows in a highly schematical fashion the operating features of such a *speed-governing system.*‡ This system constitutes the "primary" control loop in Fig. 9-1.

By controlling the position, measured by the coordinate x_E, of the *control valve* (or *gate*, in the case of a hydroturbine), we can exert control over the flow of high-pressure steam (or water) through the turbine.

A downward small movement of the linkage point E increases the steam (or water) flow by a small amount which, *if measured in valve power*, represents a

† The term "Automatic Generation Control" (AGC) is also commonly used.

‡ The terminology used agrees with the standard accepted by the industry. All systems are, of course, not identical. We chose a representative example for demonstration.

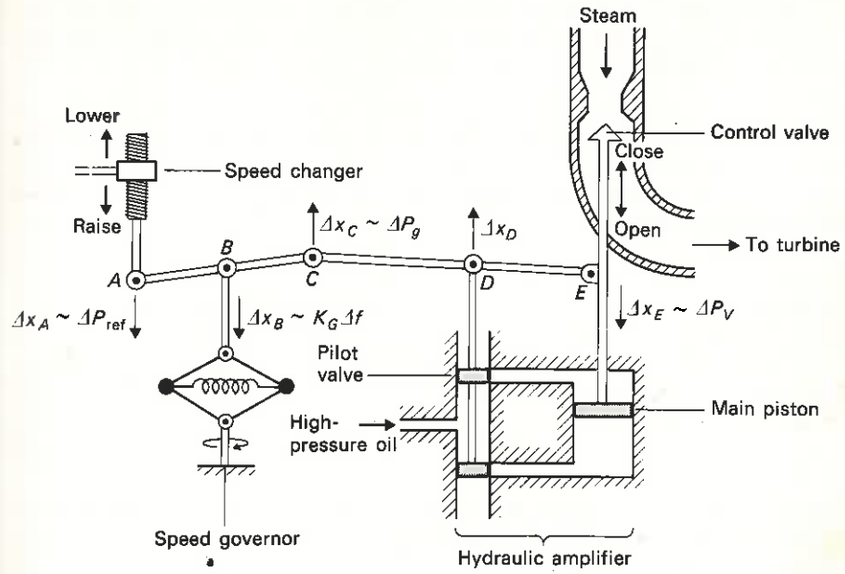

Figure 9-7 Simplified functional diagram of the primary ALFC loop.

megawatt increment ΔP_V. This flow increase translates into a turbine power increment ΔP_T in the turbine (not shown in the figure).

Very large mechanical forces are needed to position the main valve (or gate) against the high steam (or water) pressure, and these forces are obtained via several stages of hydraulic amplifiers. In our simplified version we show only one stage. The input to this amplifier is the position x_D of the *pilot valve*. The output is the position x_E of the *main piston*. Because the high-pressure hydraulic fluid exerts only a slight differential force on the pilot valve, the force amplification is very great.

The position of the pilot valve can be affected via the linkage system in three ways:

1. *Directly*, by the *speed changer*. A small downward movement of the linkage point A corresponds to an increase ΔP_{ref} in the reference power setting.
2. *Indirectly*, via feedback, due to position changes of the main piston.
3. *Indirectly*, via feedback, due to position changes of linkage point B resulting from speed changes.

It should prove a useful exercise for the reader to find, *qualitatively*, the workings of the mechanism. For example, give a "raise" command to the speed changer and prove that this indeed results in an increase in turbine output. Prove also that a speed drop will give the same effect.

Presently we shall give a *quantitative* description of the mechanism.

In the analysis to follow, incremental movements of the five linkage points $A \cdots E$ in Fig. 9-7 are of particular interest. In reality these movements are measured in millimeters but in our analysis we shall rather express them as *power increments* expressed in megawatts or per-unit megawatts as the case may be. The movements are assumed positive in the directions of the arrows. The governor *output command* ΔP_g is measured by the position change Δx_C. The governor has two inputs:

1. Changes ΔP_{ref} in the reference power setting
2. Changes Δf in the speed of frequency of the generator, as measured by Δx_B

An *increase* in ΔP_g results from an *increase* in ΔP_{ref} *and* a *decrease* in Δf. We thus can write for *small* increments

$$\Delta P_g = \Delta P_{ref} - \frac{1}{R}\Delta f \qquad \text{MW} \tag{9-21}$$

The constant R has dimension hertz per megawatt, and is referred to as *regulation* or *droop*. (For numerical values see Example 9-2 below.) Laplace transformation of Eq. (9-21) yields

$$\Delta P_g(s) = \Delta P_{ref}(s) - \frac{1}{R}\Delta f(s) \tag{9-22}$$

Using well-known block diagram symbols we have represented the governor as shown in Fig. 9-8.

9-3-2 Hydraulic Valve Actuator

The input position Δx_D of the valve actuator increases as a result of an increased command ΔP_g but decreases due to increased valve output, ΔP_V. Equal increases in both ΔP_g and ΔP_V should result in $\Delta x_D = 0$. We can thus write

$$\Delta x_D = \Delta P_g - \Delta P_V \qquad \text{MW} \tag{9-23}$$

For small changes Δx_D the oil flow into the hydraulic motor is proportional to position Δx_D of the pilot valve. Thus we obtain the following relationship for the position of the main piston:

$$\Delta P_V = k_H \int \Delta x_D \, dt \tag{9-24}$$

The positive constant k_H depends upon orifice and cylinder geometries and fluid pressure.

Upon Laplace transformation of the last two equations and upon elimination of Δx_D we obtain the actuator transfer function

$$G_H(s) = \frac{\Delta P_V}{\Delta P_g} = \frac{1}{1 + sT_H} \tag{9-25}$$

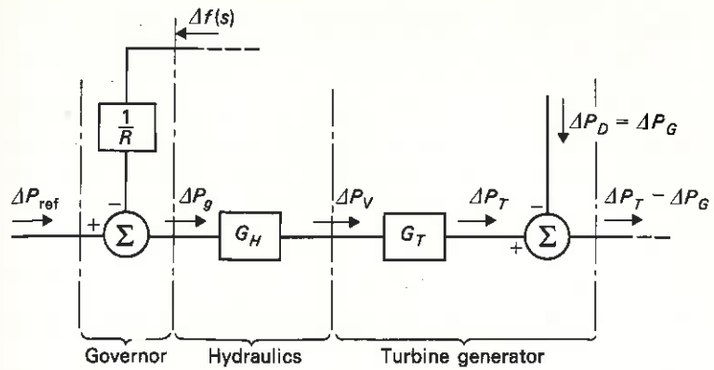

Figure 9-8 Linear model of the primary ALFC loop (minus the power system response).

where the *hydraulic time constant*

$$T_H = \frac{1}{k_H}$$

typically assumes values around 0.1 s.

The hydraulic valve actuator has been represented by the transfer function $G_H(s)$ in Fig. 9-8.

9-3-3 Turbine-Generator Response

In normal steady state and via the mechanism described in Sec. 4-9 the turbine power P_T keeps balance with the electromechanical air-gap power P_G resulting in zero acceleration and a constant speed or frequency. Perturbations ΔP_T and ΔP_G in these powers will upset the above balance. If the difference power, $\Delta P_T - \Delta P_G$, is positive the turbine generator unit will accelerate; if negative it will decelerate.

The turbine power increment ΔP_T depends entirely upon the valve power increment ΔP_V and the response characteristics of the turbine. Different turbine types vary widely in this regard. It is possible to express the turbine dynamics in terms of a turbine transfer function

$$G_T = \frac{\Delta P_T}{\Delta P_V} \tag{9-26}$$

In App. D we have derived G_T for the most common turbine types. A so-called *nonreheat steam turbine* has the simplest transfer function, consisting of a single time constant, i.e.,

$$G_T = \frac{1}{1 + sT_T} \tag{9-27}$$

Other turbine types have more complex transfer functions. In general it can be said *that the turbine response is slow* with response times measured in several seconds.

The generator power increment ΔP_G depends *entirely* upon the changes ΔP_D in the load P_D being fed from the generator. Via the transient mechanism discussed in Sec. 4-13 the generator always adjusts its output so as to meet the demand changes ΔP_D. These adjustments are essentially "instantaneous," certainly in comparison with the slow changes in P_T, and we can therefore set

$$\Delta P_G = \Delta P_D \tag{9-28}$$

In view of Eqs. (9-26) and (9-28) we can thus symbolize the turbine-generator dynamic response as shown in Fig. 9-8.

9-3-4 Static Performance of Speed Governor

At this stage in our analysis the control loop in Fig. 9-8 is "open." We can nevertheless obtain some interesting information about the *static* performance of the speed governor. The relationship between static signals (subscript "0") is obtained by letting $s \to 0$. As $G_H(0) = G_T(0) = 1$ we obtain directly from Fig. 9-8

$$\Delta P_{T,0} = \Delta P_{\text{ref},0} - \frac{1}{R}\Delta f_0 \tag{9-29}$$

We consider three cases.

Case A The generator is synchronized to a network of very large size, so large in fact, that its frequency will be essentially independent of any changes in the power output of this individual generator ("infinite" network).

Since we thus have

$$\Delta f = 0$$

we obtain from Eq. (9-29)

$$\Delta P_{T,0} = \Delta P_{\text{ref},0} \tag{9-30}$$

For a generator operated at a (forced) constant speed, we thus have a direct proportionality between the turbine power and reference power setting.

Example 9-1 A 100-MW generator is operated onto an "infinite" network. How would you make this generator increase its turbine power by 5 MW?

SOLUTION Simply by giving a "raise" signal of 5 MW to the speed-changer motor.

Case B Now we consider the network "finite," i.e., its frequency is variable. We do, however, keep the speed-changer setting constant, that is, $\Delta P_{\text{ref}} = 0$.

From Eq. (9-29) we obtain

$$\Delta P_{T,0} = -\frac{1}{R}\Delta f_0 \tag{9-31}$$

For a constant setting of the speed changer the static increase in turbine power output is directly proportional to the static frequency drop.

This result points out the physical significance of the feedback parameter R. We remember that the physical unit for R is hertz per megawatt. In practice, the power is measured in per units, and in this case the unit for R will be hertz per unit megawatt. If the frequency drop is likewise measured in per units of normal frequency (= 60 Hz), and if the power is measured in per-unit megawatts, then the unit for R will be in per units also.

Example 9-2 Consider the 100-MW generator in the previous example. It has a regulation parameter R of four percent (or 0.04 pu). By how much will the turbine power increase if the frequency drops by 0.1 Hz with the reference unchanged?

SOLUTION A 0.04-pu regulation parameter means that the turbine power will increase 1 pu, or 100 MW for a 0.04-pu, or 2.4-Hz drop in frequency. Thus we have

$$R = \frac{2.4}{100} = 0.024 \text{ Hz/MW}$$

According to Eq. (9-31) for a frequency change of $\Delta f = -0.1$ Hz the turbine power will thus experience a static change of

$$\Delta P_{T,0} = -\frac{1}{0.024} \times (-0.1) = 4.17 \text{ MW}$$

Case C In the general case, changes may occur in both reference setting and frequency in which case the more general relationship (9-29) applies.

In a frequency-generation graph Eq. (9-29) represents a family of sloping lines as depicted in Fig. 9-9, each line corresponding to a specific reference power setting.

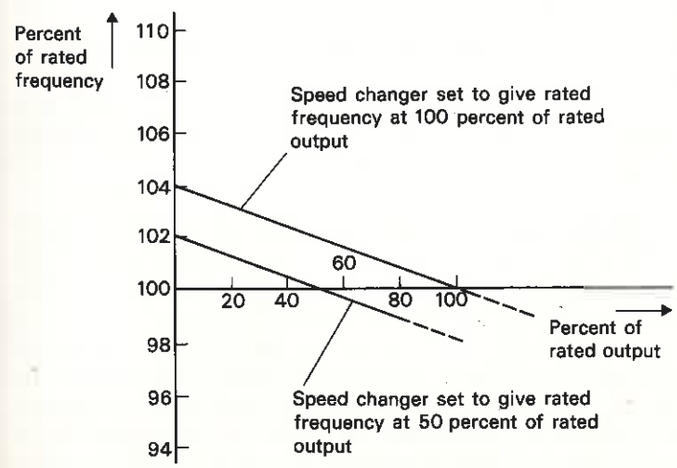

Figure 9-9 Static speed-power response of speed governor (Graphs correspond to $R = 0.04$ pu.)

Example 9-3 Consider again the 100-MW generator in the previous example. If the frequency drops by 0.1 Hz but the turbine power must remain unchanged, by how much should the reference setting be changed?

SOLUTION As $\Delta P_{T,0}$ must be zero we obtain from Eq. (9-29)

$$\Delta P_{\text{ref},0} = \frac{1}{R}\,\Delta f_0 = \frac{1}{0.024} \times (-0.1) = -4.17 \text{ MW}$$

Result: We must command the speed changer to "lower" by 4.17 MW.

Example 9-4 Two generators are supplying power to a system. Their ratings are 50 and 500 MW respectively. The frequency is 60 Hz and each generator is half-loaded. The system load increases by 110 MW and as a result the frequency drops to 59.5 Hz. What must the individual regulations be if the two generators should increase their turbine powers in proportion to their ratings?

SOLUTION The two generators should pick up 10 and 100 MW respectively. From formula (9-31) we thus compute their R values:

$$R = -\frac{-0.5}{10} = 0.05 \text{ Hz/MW} \qquad \text{(smaller unit)}$$

$$R = -\frac{-0.5}{100} = 0.005 \text{ Hz/MW} \qquad \text{(larger unit)}$$

If we express the regulation in per-unit hertz per per-unit megawatt, the R figure will be 0.0417 pu (or 4.17 percent) for *both* units.

This result thus teaches us that generators working in parallel on the same network ought to have the same regulation (expressed in per unit of their own rating) in order to share load changes in proportion to size.

9-3-5 Closing the ALFC Loop

We observed earlier that the loop in Fig. 9-8 is "open." We proceed now to "close" it, i.e., we seek to obtain a mathematical link between ΔP_T and Δf. As our generator is supplying power to a conglomeration of loads in its service area, it is necessary in our following analysis to make reasonable assumptions about the "lumped" area behavior. We make these assumptions:

1. The system is originally running in its normal state with complete power balance, that is, $P_G^0 = P_D^0 +$ losses. The frequency is at normal value f^0. All rotating equipment represents a total kinetic energy of $W_{\text{kin}} = W_{\text{kin}}^0$ megawatt-seconds.
2. By connecting additional load objects to the system the load demand increases by ΔP_D which we shall refer to as "new" load. (If load objects are disconnected then $\Delta P_D < 0$, that is, the "new" load is negative.) The generator immediately increases its output ΔP_G to match the new load, that is, $\Delta P_G = \Delta P_D$.

3. There will now be a power imbalance in the area that equals $\Delta P_T - \Delta P_D$ megawatts. As a result the speed or frequency will change. *This change will be assumed uniform throughout the area.* As the kinetic energy is proportional to the square of the speed we can thus write for the area kinetic energy

$$W_{\text{kin}} = W_{\text{kin}}^0 \left(\frac{f}{f^0}\right)^2 \qquad \text{MWs} \tag{9-32}$$

4. The "old" area load has a frequency dependency $\partial P_D/\partial f$ (compare Example 3-6) that we can lump into one area parameter

$$D \triangleq \frac{\partial P_D}{\partial f} \qquad \text{MW/Hz} \tag{9-33}$$

Area power balance requires that the increase in turbine power equals the sum of "old" and "new" load changes plus the rate of change of kinetic energy. We can thus express this area power balance as follows:

$$\Delta P_T = \Delta P_D + \frac{d}{dt}(W_{\text{kin}}) + D\,\Delta f \qquad \text{MW} \tag{9-34}$$

As

$$f = f^0 + \Delta f$$

and as Δf is small relative to f^0 we can write Eq. (9-32)

$$W_{\text{kin}} = W_{\text{kin}}^0 \left(\frac{f^0 + \Delta f}{f^0}\right)^2 = W_{\text{kin}}^0 \left[1 + \frac{2\,\Delta f}{f^0} + \left(\frac{\Delta f}{f^0}\right)^2\right] \approx W_{\text{kin}}^0 \left(1 + 2\,\frac{\Delta f}{f^0}\right) \tag{9-35}$$

By substitution of Eq. (9-35) into Eq. (9-34) the power-balance equation takes on the form

$$\Delta P_T - \Delta P_D = \frac{2W_{\text{kin}}^0}{f^0}\,\frac{d}{dt}(\Delta f) + D\,\Delta f \qquad \text{MW} \tag{9-36}$$

By dividing this equation by the generator rating P_r and by introducing the *per-unit inertia constant*

$$H \triangleq \frac{W_{\text{kin}}^0}{P_r} \qquad \text{MWs/MW (or s)} \tag{9-37}$$

it takes on the form

$$\Delta P_T - \Delta P_D = \frac{2H}{f^0}\,\frac{d}{dt}(\Delta f) + D\,\Delta f \qquad \text{pu MW} \tag{9-38}$$

The ΔP's are now measured in per unit (on base P_r) and D in per-unit megawatt per hertz.

The H parameter has the advantage over W_{kin}^0 that it is essentially independent of system size. Typical H values lie in the range 2–8 seconds.

[We can rewrite Eq. (9-38) once more

$$\Delta P_T - \Delta P_D = 2H \frac{d}{dt}\left(\frac{\Delta f}{f^0}\right) + Df^0\left(\frac{\Delta f}{f^0}\right) \qquad \text{pu MW} \tag{9-39}$$

The equation is now written in terms of $\Delta f / f^0$, that is, *the per-unit frequency.* Many analysts prefer this.]

Laplace transformation of Eq. (9-38) yields

$$\Delta P_T(s) - \Delta P_D(s) = \frac{2H}{f^0} s\ \Delta f(s) + D\ \Delta f(s) \tag{9-40}$$

which equation can be written in the form

$$\Delta f(s) = G_p(s)[\Delta P_T(s) - \Delta P_D(s)] \tag{9-41}$$

where, for brevity, the following new parameters have been introduced:

$$G_p(s) \triangleq \frac{K_p}{1 + sT_p} \tag{9-42}$$

$$T_p \triangleq \frac{2H}{f^0 D} \qquad \text{s} \tag{9-43}$$

$$K_p \triangleq \frac{1}{D} \qquad \text{Hz/pu MW} \tag{9-44}$$

Equation (9-41) represents the "missing link" in the control loop of Fig. 9-8. By adding a summing junction and a transfer block we close the loop as depicted in Fig. 9-10. (Disregard at this time the dashed portion of the diagram marked "secondary loop.")

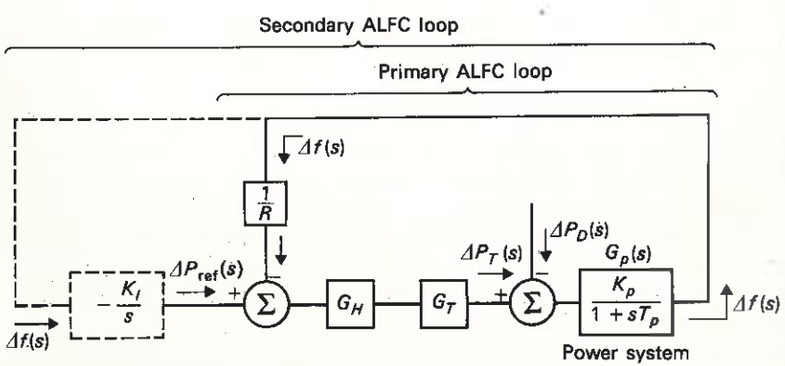

Figure 9-10 Closing the ALFC loop.

9-3-6 Concept of "Control Area"

Our above theory was based upon the assumption of a single generator feeding power to a local service area—a rare situation. In the strictest sense the theory does not apply to the more common case of many parallel-working generators serving a larger area. However, most power systems normally control their generators in *unison.* For reasons mentioned earlier the individual control loops have the same regulation parameters. If also—and this is quite important—the individual generator turbines tend to have the same response characteristics then it is possible to let the control loop in Fig. 9-10 represent the whole system which then would be referred to as a *control area.*

Example 9-5 Determine the primary ALFC loop parameters for a control area having the following data:

Total rated area capacity P_r	= 2000 MW
Normal operating load P_D^0	= 1000 MW
Inertia constant H	= 5.0 s
Regulation R	= 2.40 Hz/pu MW (all area generators)

We shall assume that the load-frequency dependency is *linear,* meaning that the "old" load would increase one percent for one percent frequency increase.

SOLUTION The latter load assumption yields D:

$$D = \frac{\partial P_D^0}{\partial f} = \frac{10}{0.60} = 16.67 \text{ MW/Hz}$$

or in per units of area capacity

$$D = \frac{16.67}{2000} = 8.33 \times 10^{-3} \text{ pu MW/Hz}$$

We then get from Eqs. (9-43) and (9-44)

$$T_p = \frac{2 \times 5.0}{60 \times 8.33 \times 10^{-3}} = 20 \text{ s}$$

$$K_p = \frac{1}{D} = 120 \text{ Hz/pu MW}$$

9-3-7 Static Response of Primary ALFC Loop

Having closed the primary ALFC loop we wish now to study both its static and dynamic features. In this section we shall limit attention to the static characteristics. One of the basic objectives of the loop is to maintain constant frequency in spite of changing loads. How accurately does the loop maintain the frequency?

The primary ALFC loop in Fig. 9-10 has one output Δf and two inputs ΔP_{ref} and ΔP_D. From the block diagram we obtain by inspection

$$\left\{\left[\Delta P_{\text{ref}} - \frac{1}{R}\Delta f\right] G_H G_T - \Delta P_D\right\} G_p = \Delta f \tag{9-45}$$

For a *constant* reference input ($\Delta P_{ref} = 0$) we thus have

$$\Delta f(s) = -\frac{G_p}{1 + (1/R)G_p G_H G_T}\,\Delta P_D(s) \tag{9-46}$$

For a step load change of constant magnitude $\Delta P_D = M$ we have

$$\Delta P_D(s) = \frac{M}{s}$$

Using the final-value theorem, we readily obtain from Eq. (9-46) the static frequency drop

$$\Delta f_0 = \lim_{s\to 0}[s\,\Delta f(s)] = -\frac{K_p}{1 + K_p/R}M = -\frac{M}{D + 1/R} \quad \text{Hz} \tag{9-47}$$

We introduce here the so-called *area frequency response charactertistic* (AFRC) β, defined as

$$\beta \triangleq D + \frac{1}{R} \quad \text{pu MW/Hz} \tag{9-48}$$

and obtain, then,

$$\Delta f_0 = -\frac{M}{\beta} \quad \text{Hz} \tag{9-49}$$

Example 9-6 Find the static frequency drop for the 2-GW system in previous example following a one percent load increase, that is, $\Delta P_D = M = 20$ MW $= 0.01$ pu MW.

SOLUTION For the above numerical data we get

$$\beta = 8.33 \times 10^{-3} + \frac{1}{2.40} = 0.425 \text{ pu MW/Hz}$$

$$\therefore \quad \Delta f_0 = -\frac{0.01}{0.425} = -0.0235 \text{ Hz}$$

or 0.04 percent of normal frequency.

Example 9-7 What would the frequency drop in the previous example have been if the speed-governor loop were nonexistent or open?

SOLUTION Opening the loop is tantamount to setting $R = \infty$. We now would have

$$\beta = D = 8.33 \times 10^{-3}$$

and

$$\Delta f_0 = -\frac{0.01}{0.00833} = -1.20 \text{ Hz}$$

or two percent of normal value.

The reader should contemplate the results of the two last examples.

9-3-8 Dynamic Response of ALFC Loop

The static response of the ALFC loop yielded important information about frequency *accuracy*. The *dynamic* response of the loop will inform about "tracking" ability and stability of the loop.

Finding the dynamic response (for a step load) is quite straightforward. Equation (9-46) upon inverse Laplace transformation yields an expression for $\Delta f(t)$. However, as G_H, G_T, and G_p contain at least one time constant each, the denominator will be of third order, resulting in unwieldy algebra.

We can simplify the analysis considerably by making the reasonable assumption that the action of the speed governor plus the turbine generator is "instantaneous" compared with the rest of the power system. The latter, as demonstrated in Example 9-5 has a time constant of 20 s, and since the other two time constants are of the order of 1 s, we will perform an approximate analysis by setting $T_H = T_T = 0$.

From Eq. (9-46) we then get

$$\Delta f(s) \approx -\frac{\dfrac{K_p}{1 + sT_p}}{1 + \dfrac{1}{R}\dfrac{K_p}{1 + sT_p}}\,\frac{M}{s}$$

$$= -M\frac{RK_p}{R + K_p}\left(\frac{1}{s} - \frac{1}{s + \dfrac{R + K_p}{RT_p}}\right) \tag{9-50}$$

If we make use of the previous numerical values, we obtain

$$\Delta f(s) \approx -0.0235\left(\frac{1}{s} - \frac{1}{s + 2.55}\right)$$

The approximate time response is therefore purely exponential.

$$\Delta f(t) \approx -0.0235(1 - e^{-2.55t}) \quad \text{Hz} \tag{9-51}$$

Figure 9-11 shows an analog computer recording of this response. For comparison, we also simulated the loop response with the inclusion of the time constants T_H and T_T. We make the following observations in regard to our results:

1. The overall *closed-loop* system time constant equals only $1/2.55 = 0.393$ s, which is a considerable reduction from the value $T_p = 20$ s, characterizing the "plant" itself. This speedup is a result of the feedback arrangement of the speed governor. Note that the system can be made still faster by reducing R, that is, by increasing the static loop gain.
2. Reduction of R also reduces the static frequency error.
3. If we performed the above analysis by *not* disregarding the turbine response, then the response would not be purely exponential as above. In Fig. 9-11 we

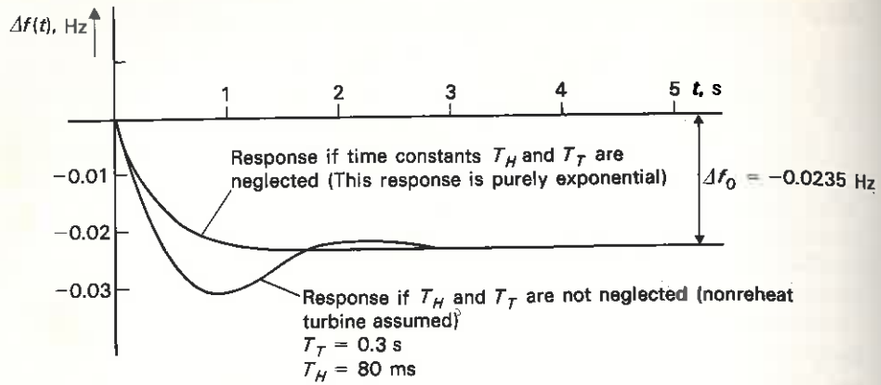

Figure 9-11 Dynamic response of the primary ALFC loop to a step-load increase.

show the difference. Note that the added delays cause a larger transient frequency dip. Why?

4. The speed governor gives a reasonable performance with a static frequency drop of only 2.4 Hz between zero and full load and settling time of the order of 3 s (as depicted in Fig. 9-11). However, with the extremely severe restrictions we in reality impose on frequency constancy (see Sec. 9-3-10), the results are, in fact, entirely unacceptable. We must do much better.
5. The foregoing analysis may not have given the reader a full *physical* understanding of the load frequency mechanism of the single-area system. Since such an understanding is invaluable to appreciate fully so-called bias control in multiarea systems (see Sec. 9-3-10), we shall attempt now to shed some light on the physical mechanism.

9-3-9 Physical Interpretation of Results

When the load suddenly increased by 1 percent (= 20 MW), where did this power come from? Certainly, it must have come from somewhere, as can be certified by the customer who threw the switch and expected *and got instantaneously* the demanded 20 MW.

In the milliseconds following the closure of the switch, the frequency has not changed a measurable amount, and therefore no power increase has had time to develop in the turbine (where the steam valve has not yet moved).

In those first instants the total additional load demand 20 MW is obtained from the stored kinetic energy, which therefore will decrease at an initial rate of 20 MW. The kinetic energy is released by speed reduction. Since the speed is dropping (and from Eq. (9-51) we note that the *initial* deceleration is $0.0235 \times 2.55 = 0.06$ Hz/s), the steam valve is opened up, due to the mechanism described earlier, and this means increased generator output. Also, *and this is important to realize,*

since the speed is now dropping, the "old" load (1000 MW in this case) decreases at the rate of $D = 1000/60 = 16.67$ MW/Hz.

Since the appearance on the scene of this "released" power means that less power needs to be generated, we can in effect consider it to be a direct contribution to the new load demand.

In conclusion, as the speed is dropping, the demand increase of 20 MW is thus made up of three components:

1. "Borrowed" kinetic energy from the rotating system machines
2. Increased generation
3. "Released" old customer load

Initially, the last two components are zero, but as the speed is dropping, they will account for an increased contribution. Consequently, the kinetic energy will be consumed at a decreased rate, and this is confirmed in Fig. 9-11, which shows that the deceleration decreases as time goes on.

Eventually (theoretically, after infinite time), the speed will level off at a new constant lower value. At this time the kinetic energy is constant (at a lower value), and the 20-MW load increase is therefore made up of the last two components only. It is interesting to see in what ratio the last two components contribute.

The static speed drop being 0.0235 Hz, we can compute these contributions as follows:

1. The generator regulation is 4.00 percent, or 2.40 Hz/pu MW, and the increase in generation after the new steady state is reached will be

$$\frac{0.0235}{2.40} = 0.0098 \text{ pu MW}$$

$$= 0.0098 \times 2000 = 19.6 \text{ MW}$$

2. Since the "old" load decreases at the rate of 16.67 MW/Hz, the speed drop of 0.0235 Hz will "release"

$$0.0235 \times 16.67 = 0.4 \text{ MW}$$

These two components evidently add up to 20 MW. Note that the largest contribution, by far, is from new generation.

9-3-10 The Secondary ("Reset") ALFC Loop

It is necessary to achieve much better frequency constancy than is obtained by the speed-governor system itself, as demonstrated above. To accomplish this we must manipulate the speed changer in accordance with some suitable *control strategy*. Before we do so, it is necessary to settle for a set of *control specifications*

the stringency of which will in the end determine the sophistication of the proposed control method.

A. Suggested control system specifications We are presently discussing a single-area system, and the control specifications for such a system are considerably simpler than those imposed upon a multiple-area system (*power pool*).

Here follow some realistic specifications:

1. The control loop must be characterized by a sufficient degree of stability.
2. Following a step load change, the frequency error should return to *zero*. This is referred to as *isochronous control*. The magnitude of the transient frequency deviation should be minimized. (This magnitude depends, of course, upon the magnitude of the load change.)
3. The *integral* of the frequency error should be minimized.
4. The individual generators of the control area should divide the total load for optimum economy (Chap. 8).

Let us comment on each of these requirements:

1. Stability is *always* a problem in closed-loop control. The tighter the error specifications, the greater the risk that the proposed loop will turn unstable.
2. The need for frequency constancy was discussed in Chap. 7. Isochronous (*iso* = equal, *chronos* = time) control gives assurance that the synchronous clocks run on time, *but not without error* (see point 3).
3. Isochronous control guarantees that the *static* frequency error following a *step* load change will vanish. No control system can, however, eliminate the *transient* frequency error (see Fig. 9-12 for a demonstration of this point.) The time error of synchronous clocks is proportional to the *integral of the frequency error*. This integral has the dimension of "cycles." If we divide the integral by f^0 we obtain an expression for time error Δt expressed in seconds, i.e.,

$$\Delta t = \frac{1}{f^0}\int_0^t \Delta f\, dt \qquad \text{s} \tag{9-52}$$

The particular control strategy we shall propose below does not have the ability to reduce the error integral automatically to arbitrarily small values. During the periods of heavy load, the system frequency will have a tendency to be below 60.00 Hz, during periods of the light load above.

For example, assume that the frequency averages 59.99 Hz during a prolonged heavy-load period. In one hour we would now accumulate a time error of

$$\Delta t = \frac{1}{60}\int_0^{3600} (-0.01)\, dt = -\frac{36}{60} = -0.60 \text{ s/h}$$

The customary way to handle such a slowly accumulating time error (in the United States) is as follows.

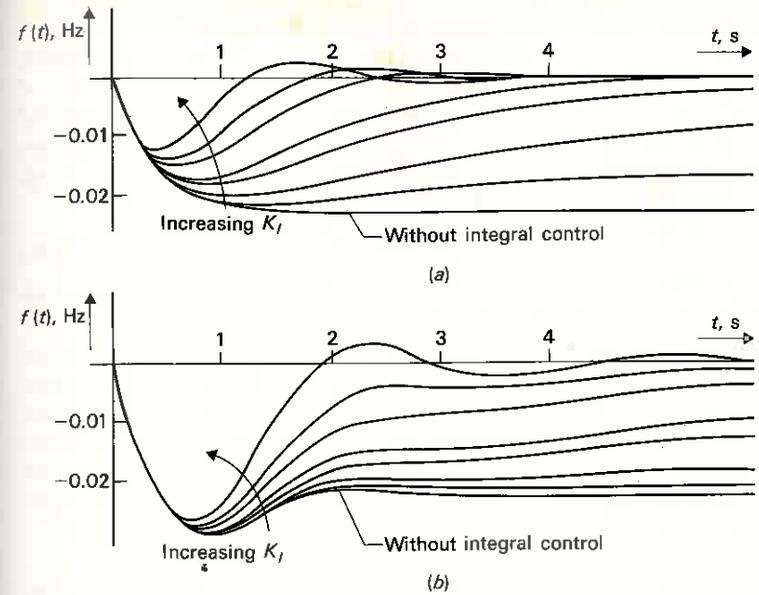

Figure 9-12 Dynamic response of the ALFC loop including the reset action of the secondary loop.

The error is measured by comparing the "system time" with that of the National Bureau of Standards. When an error of ± 3 s has accumulated (and, as exemplified, this may normally take many hours), the speed changer is offset intentionally an amount of, say, 0.02 Hz for a sufficiently long time for the time error to reduce to zero.

In the case of a power pool, one usually designates a pool member to keep track of the time error and inform the other pool members regularly of the need to reduce the error by a *unison* effort.

4. The first three specifications are taken care of by a control system (see below) with a response time of the order of a few seconds or half a minute. When these three control requirements are met, one attends to the fourth economic requirement. This is usually being done by a slower economic dispatch control scheme, having response times of the order of a minute or longer. (Sec. 9-3-11.)

B. Integral control By using the control strategy shown dashed in Fig. 9-10, we obtain an overall system that will meet performance specifications 1 to 2 above. We have added to the primary ALFC loop in Fig. 9-10 so-called *integral control*: i.e., we let the speed changer be commanded by a signal obtained by first amplifying and then integrating the frequency error, i.e.,

$$\Delta P_{\text{ref}} \triangleq -K_I \int \Delta f\, dt \tag{9-53}$$

FAC. DE CIENCIAS EXACTAS Y TECNOLOGIA
BIBLIOTECA

The unit for K_I is "per-unit megawatt per hertz and second."

For example, if the frequency drops by 1 Hz ($\Delta f = -1$) then the integrator calls for an increase in power, with the "call" increasing at the initial rate of K_I pu MW/s. Note the negative polarity of the integral controller. This polarity must be chosen so as to cause a positive frequency error to give rise to a negative, or "decrease," command. The signal fed into the integrator is referred to as *area control error* (ACE), i.e.,

$$\text{ACE} \triangleq \Delta f \tag{9-54}$$

Integral control will give rise to zero static frequency error following a *step* load change, for the following physical reason.

As long as an error remains, the integrator output will increase, causing the speed changer to move. *The integrator output, and thus the speed-changer position, attains a constant value only when the frequency error has been reduced to zero.*

The gain constant K_I controls the rate of integration, and thus the speed of response of the loop. The integration is mostly performed in electronic integrators of the same type as found in analog computers.

C. Analysis of Loop Response Here follows an analysis of the proposed system, subject to a step load change. To avoid cumbersome numerical analysis, we shall as before neglect the turbine dynamics. In addition, we also make the assumption that the speed-changer action is instantaneous. This is not perfectly correct, since the device is electromechanical and will therefore have a nonzero response time. These approximations will make possible relatively simple analysis without distorting the essential features of the response. It is also worth mentioning that the errors we thus introduce into our analysis affect only the transient, *not the static*, response. (This was already demonstrated in Fig. 9-11.)

From Eq. (9-53) we get, upon Laplace transformation,

$$\Delta P_{\text{ref}}(s) = -\frac{K_I}{s}\,\Delta f(s) \tag{9-55}$$

After making use of the block diagram in Fig. 9-10 and Eq. (9-55) we get, after some algebra,

$$\Delta f(s) = -\frac{K_p}{T_p}\,\frac{M}{s^2 + s[(1 + K_p/R)T_p] + K_I K_p/T_p} \tag{9-56}$$

We obtain the time response $\Delta f(t)$ upon inverse transformation of this expression. Since the response depends upon the poles of Eq. (9-56) we must first turn our attention to the second-order-denominator polynomial, which can be written

$$s^2 + s\,\frac{1 + K_p/R}{T_p} + \frac{K_I K_p}{T_p} = \left(s + \frac{1 + K_p/R}{2T_p}\right)^2 + \frac{K_I K_p}{T_p} - \left(\frac{1 + K_p/R}{2T_p}\right)^2 \tag{9-57}$$

Clearly, the nature of the poles depends upon the magnitude of the integral gain K_I. If

$$\frac{K_I K_p}{T_p} > \left(\frac{1 + K_p/R}{2T_p}\right)^2$$

i.e., if

$$K_I > \frac{1}{4T_p K_p}\left(1 + \frac{K_p}{R}\right)^2 \triangleq K_{I,\,\text{crit}} \tag{9-58}$$

then we can write the denominator polynomial in the form

$$(s + \alpha)^2 + \omega^2$$

where α and ω^2 are both positive and real. The expression of $\Delta f(s)$ now has a conjugate-complex pole pair in the stable s plane, and the time response $\Delta f(t)$ therefore contains damped *oscillatory* terms of the types

$$e^{-\alpha t}\sin \omega t \qquad \text{and} \qquad e^{-\alpha t}\cos \omega t$$

If, on the contrary,

$$K_I < K_{I,\,\text{crit}} \qquad (\text{"subcritical" gain setting}) \tag{9-59}$$

then we can write the polynomial in the form

$$(s + \beta_1)(s + \beta_2)$$

where β_1 and β_2 are both positive and real.

Equation (9-56) now has a real pole pair in the stable s plane, and the corresponding *nonoscillatory* time response $\Delta f(t)$ contains terms of the types

$$e^{-\beta_1 t} \qquad \text{and} \qquad e^{-\beta_2 t}$$

In either of the above two cases, $\Delta f(t)$ will thus approach zero, proving that we indeed have both *stable* and *isochronous* frequency control. Our first and second system requirements are thus met. In Fig. 9-12 we depict the actual simulated time responses for different values of the gain setting K_I. The family of curves in Fig. 9-12*a* neglect turbine dynamics, i.e., the case we just analyzed. Figure 9-12*b* includes the effect of turbine and hydraulic motors.

We make the following general comments about integral type control:

1. If we use subcritical gain settings we obtain sluggish nonoscillatory response of the control loop. This means that the integral of $\Delta f(t)$, and thus the time error, will be relatively large. In a practical situation this setting is most often used. The advantage is that the generator now will not unnecessarily "chase" rapid load fluctuations, causing equipment wear.
2. A careful study of the response graphs in Fig. 9-12 reveals the following features:

   As the sudden load increase sets in, the frequency starts falling off *at the same exponential rate as for the system* of Fig. 9-11. During these first instants

the integral controller has not yet had time to go into action, and the system response is determined by the primary ALFC loop which we discussed previously in great detail. After a certain time (the shorter the time, the higher integral gain K_I), the integral controller comes into action and eventually lifts the frequency back to its original value.

3. The reader must realize that in order to keep the analysis of the integral controller simple, we have made several simplifying assumptions. We shall summarize these:
   a. The hydraulic and turbine dynamics were neglected (but they were included in the simulated graphs in Fig. 9-12*b*).
   b. The speed-changer response was assumed instantaneous.
   c. All nonlinearities in the equipment, such as dead zone, etc., have been neglected.
   d. It has been tacitly assumed that the turbine can change its torque as fast as it is commanded by the speed changer to do so. In reality, there is a practical limit to the *rate*, expressed in megawatts per second, at which a steam generator can pick up load. We have neglected this rate limitation during the few seconds we are considering.
   e. We have assumed that the ACE is available as a *continuous* signal. In reality, the measurement of the frequency deviation Δf takes place discontinuously in *sampled-data* fashion. If the sampling rate is relatively high (compared with the fastest changes in the response of Fig. 9-12), then the above analysis gives good results.

9-3-11 Economic Dispatch Control

The integral controller just described results in a system that meets the first three of the specified control requirements. The fourth requirement, i.e., that pertaining to economic dispatch, can be met only by application of the optimal dispatch equations, ODE's (Eq. 8-15).

The *primary* ALFC loop makes the initial coarse readjustment of frequency. By its actions the various generators in the control area track the shifting load and share it in proportion to their size. The speed of response is limited only by the natural time lags of the turbine and the system itself. Depending upon turbine type the primary loop responds in 2 to 20 seconds, typically.

The *secondary* ALFC loop takes over the fine adjustment of the frequency by resetting, through integral action, the frequency error to zero. This loop is considerably slower and goes into action only when the primary loop has done its job. Response time may be of the order of one minute.

Both of the above loops base their simple control decisions upon the frequency error that can be measured locally at the power stations. They can thus be implemented locally in the plants.

Economic dispatch control can be viewed as an additional *tertiary* control loop. As the control decisions in this loop are based upon the solutions of the ODE's it is necessary to incorporate a digital computer as part of this control loop. Typically this computer is located in an "energy control center" which is linked to the various power plants via communication channels (microwave, telephone, etc). Periodically, e.g., every five minutes, the computer is provided with the megawatt settings in the power plants. These settings are compared with the optimal settings derived from a run of the type of "optimal dispatch program" discussed in Chap. 8. If the actual settings are off from the optimal values the computer sends back instructions to the plants to readjust the megawatt outputs accordingly. This readjustment takes place, of course, via the speed changer.

9-4 ALFC OF MULTI-CONTROL-AREA SYSTEMS (POOL OPERATION)

From a practical point of view, the problems of frequency control of interconnected areas, or *power pools*, are more important than those of isolated areas. Practically, all power systems today are tied together with neighboring areas, and the problem of load-frequency control becomes a joint undertaking. Closely associated is the problem of controlling the power flows on the interties.

Many advantages can be derived from pool operation, and they can all be summarized in two words, *mutual assistance*. We should at the outset state the following operating principles, which are basic:

1. Under normal operating conditions each pool member or control area should strive to carry its own load, except such scheduled portions of the other members' loads as have been mutually agreed upon.
2. Each control area must agree upon adopting regulating and control strategies and equipment that are mutually beneficial under both normal and abnormal situations. The advantages of belonging to a pool are particularly evident under emergency conditions.

Let us consider some of the advantages referred to in point 2.

First, consider the effect of *size*. We have seen in the preceding examples in this chapter how the frequency, following a sudden load change, will sag as a result of the fact that, during the first moments following the load increase, the needed energy is being "borrowed" from the kinetic energy of the system. Clearly, the larger the system, the more kinetic energy it possesses, and therefore the more energy can be temporarily borrowed for a given speed drop. For example, the large interconnected group that covers the central and eastern parts of the United States and some Canadian provinces can absorb a sudden load change of about 3000 MW and experience a frequency deviation of less than 0.1 Hz.

A small system of, say, 1000-MW capacity, if it suddenly loses 300-MW capacity (which represents 30 percent), *and if operating alone*, may be in dire trouble. Its frequency will undergo an extensive drop, and chances are that the transient power angle swings that would ensue (Chap. 12) would tear the whole system apart, resulting in a complete blackout.

If the same system were part of a pool of, say, 100,000 MW capacity, the same 300-MW generation failure would represent only a 0.3 percent loss. The frequency would be "saved," and support power to the extent of 300 MW would instantaneously flow into the crippled area via the tie-lines to carry its load until normal generation is restored.

System size also reduces the need for reserve power among the pool members. A system that operates alone as a "single area" must provide power to handle not only the anticipated peaks, but also the sudden requirements due to equipment failures. The reserves are classified on the basis of their readiness. "Spinning" reserves can be called upon for *instantaneous* (at least as fast as the controllers can react) assistance. They are made up of fully operating but only partially loaded units. Hydroelectric-, diesel-, and gas-turbine-operated units can be called upon at a few minutes' notice. Steam reserves range all the way from "low bank" (i.e., idling at pressure and heat levels below that required for service) to "cold reserves" (operative, but not in operation).

Since peak demands occur at various hours of the day in various areas, the ratio between peak and average load for a large pool is smaller than that of the individual systems. It is obvious, therefore, that all pool members can benefit from a reduced need of reserve capacity by a scheduled arrangement of energy interchange.

9-4-1 The Two-Area System

It was possible in Chap. 7 to introduce the reader to the fundamental problems associated with the *static* operation of an n-bus system by discussing, first, the simplest of all multibus systems, the two-bus system. We shall find it equally instructive to introduce the reader to the load frequency dynamics of the n-area system by studying first the dynamics of the two-area system.

Let us therefore turn our attention to a system consisting of two control areas of the type modelled in Fig. 9-10 interconnected via a relatively weak tie-line. The areas are generally of different size and characteristics.

We had earlier made the assumption that a control area is characterized by the same frequency throughout. This is tantamount to saying that the area network is "rigid" or "strong." In the single-area case we could thus represent the frequency deviations by the *single* variable Δf. In the present case we assume each area individually "strong." Having interconnected them with a "weak" tie-line therefore leads us to the assumption that the frequency deviations in the two areas can be represented by *two* variables Δf_1 and Δf_2 respectively.

9-4-2 Modeling the Tie-Line

In normal operation the power on the tie-line follows from equation (3-49), i.e.,

$$P_{12}^0 = \frac{|V_1^0|\,|V_2^0|}{X} \sin(\delta_1^0 - \delta_2^0) \tag{9-60}$$

where δ_1^0 and δ_2^0 are the angles of end voltages V_1 and V_2 respectively. The order of the subscripts indicates that the tie-line power is defined positive in direction $1 \to 2$.

For small deviations in the angles δ_1 and δ_2 the tie-line power changes with the amount

$$\Delta P_{12} \approx \frac{|V_1^0|\,|V_2^0|}{X} \cos(\delta_1^0 - \delta_2^0)(\Delta\delta_1 - \Delta\delta_2) \qquad \text{MW} \tag{9-61}$$

Analogous to the concept of "electric stiffness" of synchronous machines (compare Eq. (4-33)) we now define the "synchronizing coefficient" of a line

$$T^0 \triangleq \frac{|V_1^0|\,|V_2^0|}{X} \cos(\delta_1^0 - \delta_2^0) \qquad \text{MW/rad} \tag{9-62}$$

The tie-line power deviation then takes on the form

$$\Delta P_{12} = T^0(\Delta\delta_1 - \Delta\delta_2) \qquad \text{MW} \tag{9-63}$$

The frequency deviation Δf is related to the reference angle $\Delta\delta$ by the formula

$$\Delta f = \frac{1}{2\pi}\frac{d}{dt}(\delta^0 + \Delta\delta) = \frac{1}{2\pi}\frac{d}{dt}(\Delta\delta) \qquad \text{Hz} \tag{9-64}$$

or inversely

$$\Delta\delta = 2\pi \int^t \Delta f\, dt \qquad \text{rad} \tag{9-65}$$

By expressing tie-line power deviations in terms of Δf rather than $\Delta\delta$ we thus get

$$\Delta P_{12} = 2\pi T^0\left(\int^t \Delta f_1\, dt - \int^t \Delta f_2\, dt\right) \qquad \text{MW} \tag{9-66}$$

Laplace transformation of the last formula yields

$$\Delta P_{12}(s) = \frac{2\pi T^0}{s}(\Delta f_1(s) - \Delta f_2(s)) \tag{9-67}$$

Representing this equation in terms of block diagram symbols yields the diagram in Fig. 9-13.

9-4-3 Block Diagram Representation of Two-Area System

How does the tie-line power enter our area models? Clearly we must go back to our early power-balance equation (9-40). In writing such an equation for area 1 we must clearly *add* ΔP_{12} to the right-hand side. Similarly, for area 2, we must either *subtract* ΔP_{12} or *add* ΔP_{21}, where P_{21} represents the tie-line power in direction $2 \to 1$. We have, if losses are neglected,

$$\Delta P_{21} = -\Delta P_{12} \qquad \text{MW} \tag{9-68}$$

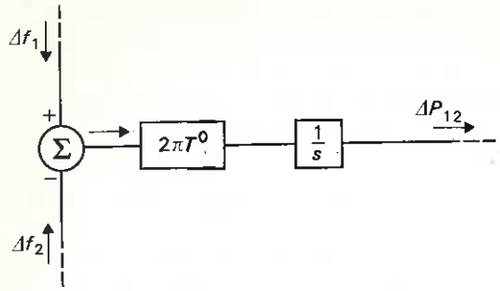

Figure 9-13 Linear representation of tie-line.

We shall find it convenient when we work with multiarea systems *always* to consider the tie-line power positive in the direction *out* from the area in question. We remember that the sum of the right-hand power terms in Eq. (9-40) is represented by the right summing junction of Fig. 9-10. If we thus observe the above tie-line sign rule we can interconnect two single-area diagrams by means of the tie-line symbol in Fig. 9-13. The end result is the block diagram depicted in Fig. 9-14. In reading this diagram the following clarifying points are in order:

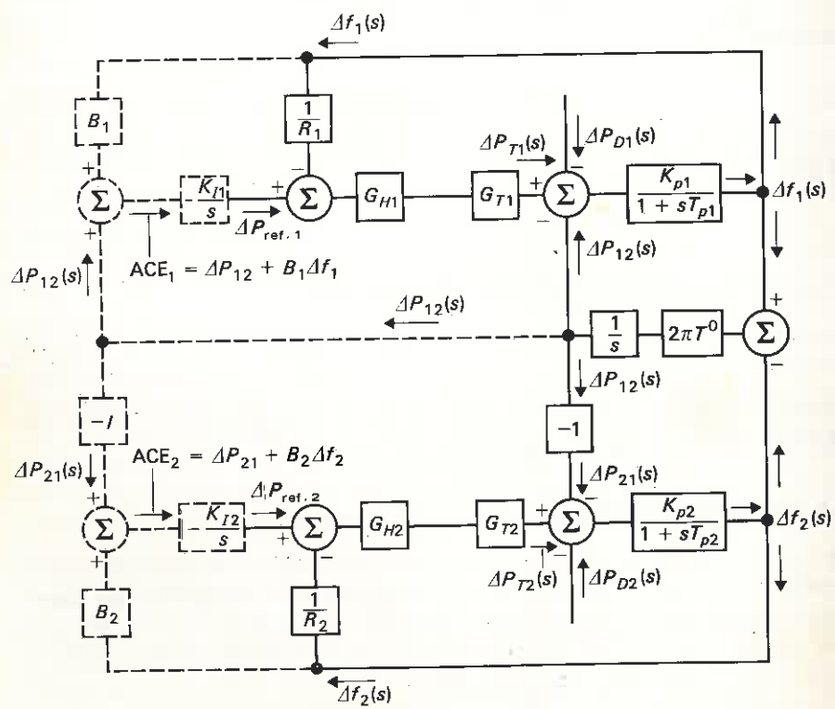

Figure 9-14 Linear model of two-area system.

1. The dashed portions should be disregarded for the time being. (See Sec. 9-4-7.)
2. We remember that the powers in the single-area diagram (Fig. 9-10) were expressed in per unit of area rating. The parameters R, D, and H, likewise were based on the same base power. When two or several areas, generally of different ratings, are involved, we must refer all powers and parameters to the *one* chosen base power.
3. The added blocks of transfer function -1 follow from Eq. (9-68).

9-4-4 Mechanical Analog of Two-Area System

Before we proceed with an analysis of the two-area system, we shall present, without proof, a mechanical system that is a perfect analog of our electrical two-area system. Consider the train in Fig. 9-15. If this train is traveling at a constant speed v^0 and suddenly is subject to incremental load changes, the velocity will change. The two car-assemblies will experience the velocity perturbations Δv_1 and Δv_2, respectively, and the tie-spring power will change with the amount ΔP_{tie}. By writing the incremental dynamic equations for this system, one can readily confirm that they are of the identical form as our electrical system equations. This means that the systems are analogs of each other. The following variables correspond to each other:

$$\Delta v_1 \leftrightarrow \Delta f_1$$

$$\Delta v_2 \leftrightarrow \Delta f_2$$

$$\text{Tie-spring power} \leftrightarrow \text{tie-line power}$$

The train analog can thus be used as an aid in achieving a better feel for the behavior of the electric system.

9-4-5 Static Response of Two-Area System

We shall first investigate the response of the two-area system with fixed speed changer positions; i.e.,

$$\Delta P_{\text{ref},1} = \Delta P_{\text{ref},2} = 0$$

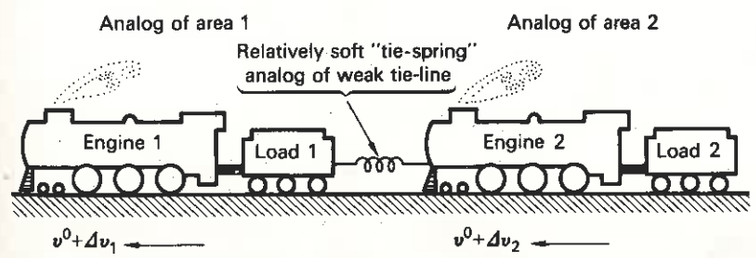

Figure 9-15 A mechanical analog of two-area system.

We assume that the loads in each area are suddenly increased by the constant incremental *steps* $\Delta P_{D1} = M_1$ and $\Delta P_{D2} = M_2$. We shall presently limit our analysis to finding the *static* changes that result in frequency and tie-line power. Let us call those changes† Δf_0 and $\Delta P_{12,0}$ respectively.

Since the incremental increase in turbine dynamics in this static case is determined by the static loop gains‡ we obtain from Fig. 9-14

$$\Delta P_{T1,0} = -\frac{1}{R_1}\Delta f_0$$
$$\Delta P_{T2,0} = -\frac{1}{R_2}\Delta f_0 \tag{9-69}$$

By adding the powers at the summing junctions we obtain

$$-\frac{1}{R_1}\Delta f_0 - M_1 = D_1\,\Delta f_0 + \Delta P_{12,0}$$
$$-\frac{1}{R_2}\Delta f_0 - M_2 = D_2\,\Delta f_0 - \Delta P_{12,0} \tag{9-70}$$

We solve for Δf_0 and $\Delta P_{12,0}$ and obtain

$$\Delta f_0 = -\frac{M_1 + M_2}{\beta_1 + \beta_2} \quad \text{Hz}$$
$$\Delta P_{12,0} = -\Delta P_{21,0} = \frac{\beta_1 M_2 - \beta_2 M_1}{\beta_1 + \beta_2} \quad \text{pu MW} \tag{9-71}$$

where, in analogy with Eq. (9-48), we have defined the AFRC's of each area:

$$\beta_1 \triangleq D_1 + \frac{1}{R_1}$$
$$\beta_2 \triangleq D_2 + \frac{1}{R_2} \tag{9-72}$$

Equations (9-71) become particularly simple if we assume *identical* area parameters; i.e.,

$$D_1 = D_2 = D$$
$$R_1 = R_2 = R$$
$$\beta_1 = \beta_2 = \beta$$

† In steady state the frequency drops in the two areas will be equal (compare graphs in Fig. 9-16).
‡ Obtained by letting $s \to 0$.

We then get

$$\Delta f_0 = -\frac{M_1 + M_2}{2\beta} \quad \text{Hz}$$
$$\Delta P_{12,0} = -\Delta P_{21,0} = \frac{M_2 - M_1}{2} \quad \text{pu MW} \tag{9-73}$$

For example, if a step load change occurs only in area 2, we get

$$\Delta f_0 = -\frac{M_2}{2\beta} \quad \text{Hz}$$
$$\Delta P_{12,0} = \frac{M_2}{2} \quad \text{pu MW} \tag{9-74}$$

These two last equations tell us, in a nutshell, the advantages of pool operation:

1. Fifty percent of the added load in area 2 will be supplied by area 1 via the tie-line.
2. The frequency drop will be only half that which would be experienced if the areas were operating alone (compare Eq. (9-49)).

Example 9-8 A 2-GW control area (1) is interconnected with a 10-GW area (2). The 2-GW area has the system parameters given in Example 9-5, i.e.,

$$R = 2.40 \text{ Hz/pu MW}$$
$$D = 8.33 \times 10^{-3} \text{ pu MW/Hz}$$

Area 2 has the same parameters, *but in terms of the 10-GW base.*

A 20-MW load increase takes place in area 1. Find static frequency drop and tie-line power change.

SOLUTION We will choose the generator capacity of area 1, 2000 MW, as our power base. In Example 9-6 we had already computed $\beta_1 = 0.425$ Hz/pu MW in terms of this base. β_2 has the same numerical value based on 10-GW. Based on 2-GW it must be five times larger numerically, i.e.

$$\beta_2 = 5\beta_1 = 2.125 \text{ Hz/pu MW}$$

Also

$$M_1 = \frac{20}{2000} = 0.01 \text{ pu MW}$$

Equations (9-71) yield the static deviations

$$\Delta f_0 = -\frac{0.01}{0.425 + 2.125} = 0.00392 \text{ Hz}$$

$$\Delta P_{12,0} = \frac{-2.125 \times 0.01}{0.425 + 2.125} = -0.00833 \text{ pu MW} \qquad (\text{or } -16.7 \text{ MW})$$

Note that the frequency drop is now only one sixth of that experienced by area 1 running alone (compare Example 9-6). Note also that this "frequency support" is accomplished by an *added* delivery of 16.7 MW from the larger area.

9-4-6 Dynamic Response of Two-Area System

Even with the very simple turbine model that we have used, the two-area system in Fig. 9-14 is of seventh order. It would therefore be meaningless, in our text, to attempt a direct analytic approach for finding the dynamic response of the system. We perform instead an approximate analysis based upon the following assumptions:

1. Consider the case of two *equal* areas.
2. Consider the turbine controller *fast* relative to the inertia part of the systems, i.e., we set $G_H = G_T = 1$.
3. Neglect the system damping. This means that we assume the load not to vary with frequency; i.e., we set $D_1 = D_2 = 0$. This means, in accordance with Eqs. (9-42) to (9-44), that $G_{p1}(s) = G_{p2}(s) \to f^0/s2H$.

Under these highly simplifying assumptions we can readily derive the following expression for the tie-line power from Fig. 9-14

$$\Delta P_{12}(s) = \frac{\pi f^0 T^0}{H} \frac{\Delta P_{D2}(s) - \Delta P_{D1}(s)}{s^2 + (f^0/2RH)s + 2\pi f^0 T^0/H} \tag{9-75}$$

This expression tells us several important facts:

1. The denominator being of the form
$$s^2 + 2\alpha s + \omega^2 = (s + \alpha)^2 + \omega^2 - \alpha^2$$
where α and ω^2 are both positive, we know that the system is *stable* and *damped*.
2. Following a disturbance, the system will oscillate at the damped angular frequency
$$\omega_0 = \sqrt{\omega^2 - \alpha^2} = \sqrt{\frac{2\pi f^0 T^0}{H} - \left(\frac{f^0}{4RH}\right)^2} \tag{9-76}$$
3. The system damping is strongly dependent upon the α parameter. Since f^0 and H are essentially constants, *the damping will be a function of the R parameters.* Low R values will give strong damping; high R values, weak damping. The system will perform *undamped* oscillations of frequency $\omega_0 = \omega$ if $R = \infty$, that is, if the speed governor is nonexistent.
4. The fact that the system is *inherently* oscillatory could have been immediately predicted from the mechanical analogy in Fig. 9-15.

Example 9-9 Consider two equal areas, each having the parameters

$$R = 3.0 \text{ Hz/pu MW}$$
$$H = 5 \text{ s}$$
$$f^0 = 60 \text{ Hz}$$

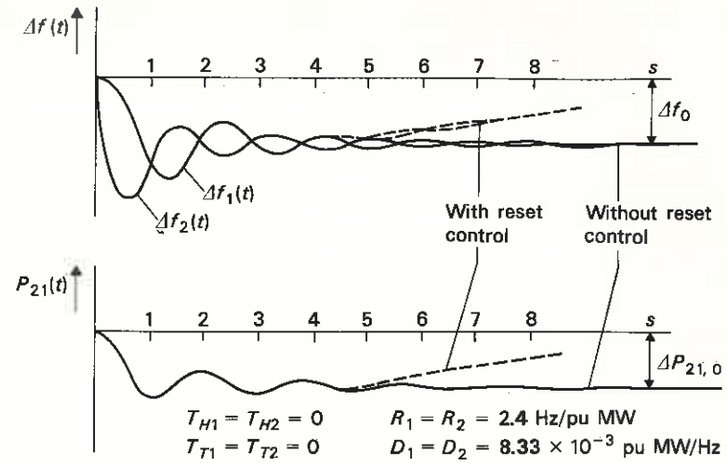

Figure 9-16 Dynamic response of two-area system subject to a step-load increase in area 2.

From Eq. (9-76) we thus get

$$\omega_0 = \sqrt{75.3T^0 - 1.0} \quad \text{r/s}$$

Assume the tie-line has a capacity of 0.1 pu (10 percent of area capacity) and is operating at a power angle of 45°. From Eq. (9-62) we thus have

$$T^0 = 0.1 \cos 45° = 0.0707$$

The oscillating frequency is thus

$$\omega_0 = \sqrt{75.3 \times 0.0707 - 1.0} = 2.1 \text{ r/s} \qquad \text{(or 0.33 Hz approx.)}$$

The graphs in Fig. 9-16 depict the tie-line power and frequency oscillations (in both areas) for a step load increase in area 2. (The dashed portions of the graphs are explained in Sec. 9-4-8.)

9-4-7 Tie-Line Bias Control

The response curves in Fig. 9-16 indicate clearly that some form of reset integral control must be added to the two-area system. The persistent static frequency error is intolerable for the same reason as was the case in the single-area case. Also, a persistent static error in tie-line power flow—so-called "inadvertent exchange"—would mean that one area would have to support the other on a steady-state basis. *A basic guiding principle in pool operation must be that each area, in normal steady state, absorbs its own load* (see p. 329).

Various methods of reset integral control have over the years been tried out—and abandoned—for multiarea systems. For example, in our two-area system we could conceive of the arrangement that area 1 be responsible for

frequency reset and area 2 take care of the tie-line power. We would thus arrange for the following area control errors:

$$\begin{aligned} \mathrm{ACE}_1 &\triangleq \Delta f_1 \\ \mathrm{ACE}_2 &\triangleq \Delta P_{21} \end{aligned} \tag{9-77}$$

These ACE's would be fed via slow integrators on to the respective speed changers. This arrangement would work—but not too good. Actually in the early days of pool operation one area was designated to reset the system frequency and the others would be responsible for zeroing their own "net interchanges" (see also Sec. 9-4-9). The problem with this arrangement proved to be that the central frequency controlling station tended to regulate for everybody trying to absorb everybody else's errors and offsets. As a result it would swing wildly between its generating limits.

As a result of the original work by Cohn[4] a control standard has developed that has been adopted by most operating systems. The control strategy is termed "tie-line bias control" and is based upon the principle that *all operating pool members must contribute their share to frequency control in addition to taking care of their own net interchange.*

9-4-8 Tie-Line Bias Control of Two-Area System

In applying this reset control method to our two-area system we would add the dashed loops shown in Fig. 9-14. The control error for each area consists of a linear combination of frequency and tie-line error:

$$\begin{aligned} \mathrm{ACE}_1 &\triangleq \Delta P_{12} + B_1 \Delta f_1 \\ \mathrm{ACE}_2 &\triangleq \Delta P_{21} + B_2 \Delta f_2 \end{aligned} \tag{9-78}$$

The speed-changer commands will thus be of the form

$$\begin{aligned} \Delta P_{\mathrm{ref},1} &= -K_{I1} \int (\Delta P_{12} + B_1 \Delta f_1)\, dt \\ \Delta P_{\mathrm{ref},2} &= -K_{I2} \int (\Delta P_{21} + B_2 \Delta f_2)\, dt \end{aligned} \tag{9-79}$$

The constants K_{I1} and K_{I2} are integrator gains, and the constants B_1 and B_2 are the *frequency bias* parameters. The minus signs must be included since each area should *increase* its generation if *either* its frequency error *or* its tie-line power increment is negative.

9-4-9 Static System Response

The chosen strategy will eliminate the steady-state frequency *and* tie-line deviations for the following reasons.

Following a step load change in either area, a new static equilibrium, *if such an equilibrium exists*, can be achieved only after the speed-changer commands have reached *constant values*. But this evidently requires that both integrands in Eq. (9-79) be zero; i.e.,

$$\begin{aligned} \Delta P_{12,0} + B_1 \Delta f_0 &= 0 \\ \Delta P_{21,0} + B_2 \Delta f_0 &= 0 \end{aligned} \tag{9-80}$$

In view of Eq. (9-68), these conditions can be met *only* if

$$\Delta f_0 = \Delta P_{12,0} = \Delta P_{21,0} = 0 \tag{9-81}$$

Note that this result is independent of the B_1 and B_2 values. In fact, one of the bias parameters (but not both) can be zero, and we still have a guarantee that Eq. (9-81) is satisfied.

The question what "best" value to choose for the B parameters has been hotly debated. Cohn has shown that choosing $B = \beta$ (i.e., the AFRC) produces satisfactory over-all performance of the interconnected system. The integrator gain constants K_{I1} and K_{I2} are not critical—but they must be chosen small enough not to stimulate the area generators to "chase" load offsets of short duration.

The actual effect on the frequency and tie-line power graphs of the added tie-line bias control is shown in Fig. 9-16 (dashed parts of graphs). Following the immediate excursions which are entirely determined by the primary speed-governor loops of each area, the secondary integrator loops of each area go into action and reset both the frequency and tie-line power back to original values.

9-4-10 Tie-Line Bias Control of Multiarea Systems

In reality a control area is interconnected not with one tie-line to one neighboring area but with several tie-lines to neighboring control areas, all part of the overall power pool. Consider the ith control area. Its *net interchange* equals the sum of the megawatts on all m outgoing tie-lines. As the area control error ACE_i ought to be reflective of the *total* exchange of power it should thus be chosen of the form

$$\mathrm{ACE}_i = \sum_{j=1}^{m} \Delta P_{ij} + B_i \Delta f_i \tag{9-82}$$

Typically, the reset control is implemented by *sampled-data* techniques. At sampling intervals of, say, one second, all tie-line power data are fed into the central energy control center where they are added and compared with predetermined contracted interchange megawatts. In this way is obtained the sum-error of Eq. (9-82). This error is added to the biased frequency error and the ACE results. The ACE is communicated with all area generators that are participating in the secondary ALFC. If optimum dispatch is employed, a tertiary slower "OD loop" is added of the type discussed in Sec. 9-3-11.

9-5 "STEADY-STATE" INSTABILITIES

The control methods outlined above—or variants thereof—are incorporated as standard in most of the interconnected power systems around the world. The operating experience has been good—exceptionally good in view of the vast geographical spread and different generator mix characterizing many of the systems.

However, on occasion, a power system may experience stability problems usually in the form of self-excited low-frequency oscillations. Power engineers are referring to these as "steady-state" instabilities as they occur, mostly unexpected, as the system is running in what appears as a smooth steady state. Figure 9-17 depicts a graph of the frequency of the peninsular Florida grid. It is operating normally at 60 Hz with a slight unavoidable "noise" (which is always characteristic of the ALFC loop action) when, gradually, an oscillation starts to build of frequency typically less than 1 Hz. The oscillation is detected not only in the system frequency but also in the tie-line which will experience power "sloshings" of increasing magnitude. This type of instability is actually caused by cross-coupling between the AVR and ALFC loops. The phenomenon has been detected in many parts of the world. It is directly associated with the so-called *natural oscillatory modes* of the network and it is therefore fitting that we start this section with a discussion of the latter.

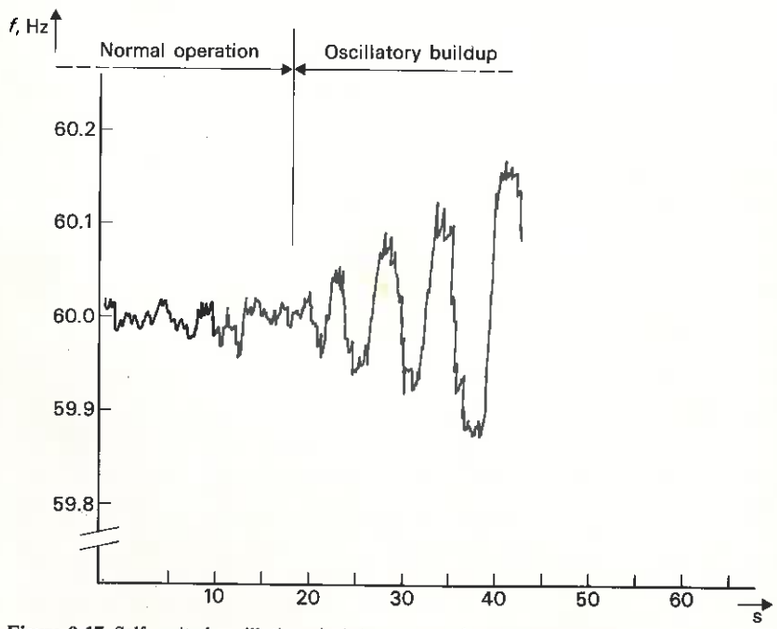

Figure 9-17 Self-excited oscillations in interconnected power system.

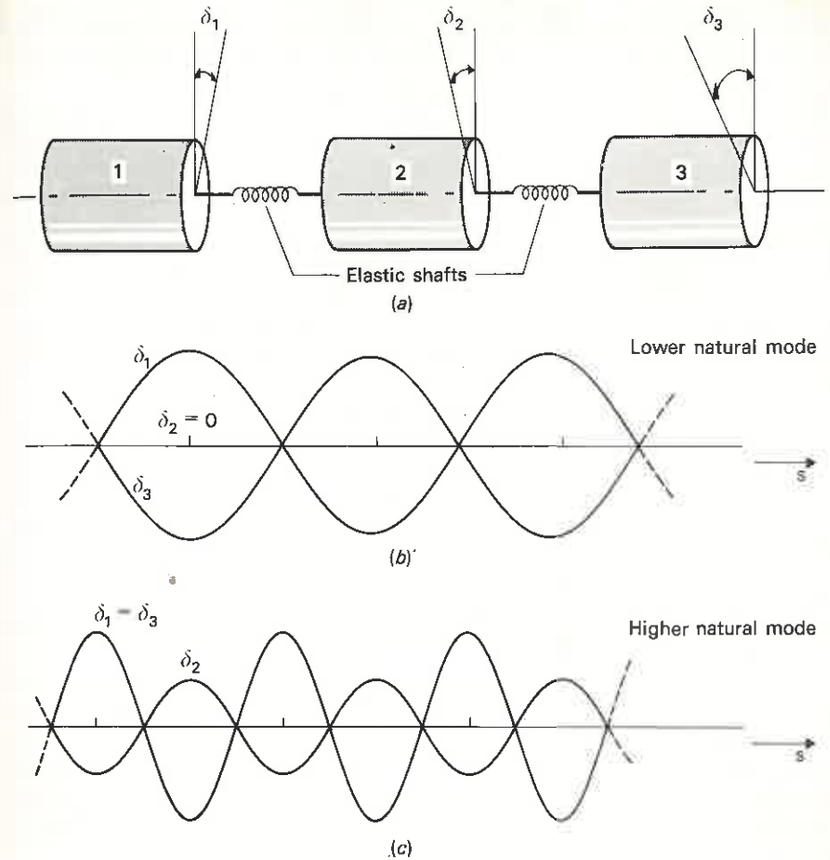

Figure 9-18 Torsional oscillatory system: (*a*) identical masses and shaft elasticities; (*b*) lower natural mode; (*c*) higher natural mode.

9-5-1 Natural Torsional Oscillatory Modes in a Power System

In Fig. 9-18*a* are shown three rotational masses interconnected with elastic shafts. The masses can perform torsional dynamics, describable in terms of the three angular coordinates δ_1, δ_2, and δ_3.

The *three* masses possess *two* torsional *natural modes*, each characterized by the *natural* (or *eigen*) *frequencies* f_1 and f_2 respectively.

If we assume the masses to have equal inertia and the shafts equal elasticity coefficients the natural modes become particularly simple. In the "lower mode" (Fig. 9-18*b*) masses 1 and 3 swing against each other with mass 2 nonparticipating. In the "higher mode" masses 1 and 3 swing against mass 2 (Fig. 9-18*c*).

The natural modes can be excited in one of three ways:

1. By proper choice of initial position settings. For example, if initially the system is held so that $\delta_1^0 = -\delta_3^0$ and $\delta_2^0 = 0$, it will oscillate in the lower mode upon release.
2. By some oscillatory source that is "pumping" the system. Natural oscillations will arise if the source frequency coincides with one of the natural frequencies.
3. Sudden major fault-induced torque imbalances.

The natural oscillations can take place around a fixed reference, as in Fig. 9-18, or around a reference system rotating at a *constant* speed. The latter case is analogous to what happens in a power system. The individual masses are here the generator rotors (including the fixed turbine rotors). The elastic "shafts" are the transmission lines of the grid. The position coordinates are the power angles δ (compare Example 9-9).

If the system contains N generators then there exists, in the strictest sense, $N-1$ natural modes. However, many subgroups of generators, particularly those belonging to the same power stations, are swinging as *coherent groups* rather than individually. Their close proximity makes their connecting "electric shafts" very stiff. These natural frequencies typically lie in the range 0.1–5 Hz. When one of them is being excited the power system is said to perform *intermachine oscillations*. Every individual generator rotor including its directly coupled turbine rotors (and excitor rotor, if present) participate in the oscillations as one unit. The oscillations shown in Fig. 9-17 are of this type.

For a turbogenerator unit of very large rating the shaft is very long and generator rotor, exciter rotor, and the often three to four different turbine rotors† constitute a rotational system which by itself possesses maybe half a dozen natural modes. The eigenfrequencies of these modes typically lie in the frequency range 20–50 Hz. One of these modes can on occasion also be excited, particularly when the electric network contains very long lines with series capacitors. Such an instability is referred to as *subharmonic resonance*.

It is important to realize that both the low-frequency "intermachine" and the high-frequency "subharmonic" oscillations are *poorly* damped. This means that a relatively weak "pumping" source can excite oscillations which may grow to amplitudes of destructive magnitudes causing the "elastic shafts" to break.

In the "subharmonic" phenomenon the elastic shaft consists of the generator shaft itself. In a classic accident this shaft broke causing 100-million-dollar damage.

In the "intermachine" phenomenon the "elastic shafts" are the transmission lines of the grid. They "break" when the tie-line power swings become so large that the power angle δ goes beyond 90 electrical degrees causing loss of synchronism and "island" formation.‡

† High, low, and intermediate pressure sections.

‡ When peninsular Florida experiences the swings depicted in Fig. 9-17, and if the oscillation buildup cannot be stopped, the end result usually is a breakup of the tie-lines to Georgia. The whole peninsular grid will thereupon run isolated. One talks in such cases about "interarea" oscillations.

9-5-2 Natural Mode of a Single Generator Operating onto Infinite Bus

It is instructive to study the factors that determine the natural modes in a power system. Because the intermachine oscillation is the most common one we shall select it for our study. As our "textbook case" we shall choose the simplest of all generator configurations—a single machine operating onto an "infinite" bus. This is analogous to the case of two rotational masses (Fig. 9-18) one of which being of infinite size. With $N = 2$ the system possesses only *one* natural mode, the characteristics of which we now explore.

The single-generator case was extensively studied in Sec. 4-12 where we derived *static* characteristics. In Sec. 4-13 we derived formulas for the *transient* generator power which will now prove useful.

In the study of "area" frequency dynamics in Sec. 9-3-5 we derived the pertinent differential equation (Eq. 9-38) from a "power-balance" expression (Eq. 9-34). We use the same approach now but need to slightly modify it in the following regard:

1. We study the power balance of one rotating unit—not an entire "lumped" area.
2. As we shall later use our derived equations for *large-scale* dynamics (Chap. 12) we do not limit our derivations to incremental excursions.

As the differences between the turbine power P_T and the generator bus power P_G is used for increasing the kinetic energy of the unit we obtain the power balance equation

$$P_T - P_G = \frac{d}{dt}(W_{\text{kin}}) \qquad \text{MW} \tag{9-83}$$

Note that the last term in Eq. (9-34) is nonexistent here, as we assume that no local load is served from the generator.†

Following the same steps as in Sec. 9-3-5 we transform Eq. (9-83) to

$$P_T - P_G = \frac{2H}{f^0}\frac{df}{dt} \qquad \text{pu MW} \tag{9-84}$$

We shall find it more useful to let power angle, δ, rather than frequency, f, be our independent variable. In view of Eq. (9-65) we thus get

$$\boxed{P_T - P_G = \frac{H}{\pi f^0}\frac{d^2\delta}{dt^2}} \qquad \text{pu MW} \tag{9-85}$$

† Later we shall add a term corresponding to the (relatively small) power loss in the generator damper winding (Sec. 9-5-3).

This is the famous *generator swing equation* (GSE) that plays an extremely important role in all types of studies of power-system dynamic phenomena. If we want to use the GSE to study *incremental* dynamics around an operating point (P_T^0, P_G^0, δ^0) then we readily prove it to be of the form

$$\Delta P_T - \Delta P_G = \frac{H}{\pi f^0} \frac{d^2}{dt^2} (\Delta\delta) \tag{9-86}$$

This is the form we find useful in the present case.

Example 9-10 Write the GSE in form (9-86) for study of incremental dynamics of the 15-MVA generator being operated as specified in Example 4-3. The generator has $H = 5$ s, $f^0 = 60$ Hz. Find natural frequency.

SOLUTION We approach the problem in the following steps:

Step 1 Find the steady-state operating point. This was done in Example 4-3 for the power level $P_T^0 = P_G^0 = 0.667$ pu, an excitation level $E^0 = 1.22$ pu and with the network voltage held at $|V_N| = 1.0$ pu. It was found that the steady-state power angle equals

$$\delta_N^0 = 25.7° \text{ electrical degrees}$$

Step 2 Find the transient generator power valid for transient deviations around the above operating point.

This was done in Example 4-13. The *transient* generator power was found to be of the form (4-83).

Step 3 Find ΔP_G.

For small angular deviations around $\delta_N = \delta_N^0$ we can write

$$P_G = P_G^0 + \Delta P_G \approx P_G^0 + \left(\frac{dP_G}{d\delta_N}\right)^0 \Delta\delta_N \tag{9-87}$$

$$\therefore \quad \Delta P_G \approx \left(\frac{dP_G}{d\delta_N}\right)^0 \Delta\delta_N \qquad \text{pu MW} \tag{9-88}$$

or

$$\Delta P_G = S' \, \Delta\delta_N \qquad \text{pu MW} \tag{9-89}$$

where S' is the "transient stiffness" of the generator. Compare also Eq. (4-33). The power component (Eq. 9-89) is referred to as *synchronizing power*.

From Eq. (4-83) we obtain

$$S' = \left(\frac{dP_G}{d\delta_N}\right)^0 = 2.398 \cos \delta_N^0 - 2 \times 0.478 \cos 2\delta_N^0$$

$$= 2.161 - 0.596 = 1.565 \text{ pu MW/electric rad} \tag{9-90}$$

Step 4 Write the incremental GSE. We set for simplicity $\Delta P_T = 0$. Substitution of (9-89) into (9-86) yields

$$\frac{d^2}{dt^2}(\Delta\delta_N) + \frac{\pi f^0 S'}{H} \Delta\delta_N = 0 \tag{9-91}$$

or shorter

$$\frac{d^2}{dt^2}(\Delta\delta_N) + \omega_1^2 \, \Delta\delta_N = 0 \tag{9-92}$$

where

$$\omega_1^2 \triangleq \frac{\pi f^0 S'}{H} \tag{9-93}$$

Step 5 Solve the GSE.

The solution of the second-order *linear, constant-parameter* differential equation (9-92) is of the form

$$\Delta\delta_N = A \sin (\omega_1 t + \psi) \tag{9-94}$$

The integration constants A and ψ depend upon the initial conditions, i.e., upon how the oscillations are started.

In our numerical case

$$\omega_1 = \sqrt{\frac{\pi \times 60 \times 1.565}{5}} = 7.68 \text{ rad/s}$$

corresponding to a "natural" frequency of 1.22 Hz.

It is interesring to note that increased inertia lowers the natural frequency. Increased stiffness (caused by lower generator and line reactances) will increase the synchronizing power and thus the frequency.

9-5-3 Effect of Damper Winding

Equation (9-94) implies that the inertial oscillations are *undamped*. In actuality, the oscillations in all probability would be *damped* and would actually vanish after some time. The system evidently possesses *positive damping*. This damping originates mainly in the rotor "damper" winding (Sec. 4-1).

As the rotor performs incremental dynamics relative to the synchronously running "infinite" system its damper windings will no longer be stationary relative to the armature reaction flux wave. The relative motion will, in fact, induce currents in the damper bars and according to Lenz' law these currents will have a direction *such as to try to stop the relative motion.*

The damper winding will in fact dissipate power and the dissipation rate is almost proportional to the relative velocity, $d(\Delta\delta)/dt$. The presence of the damper winding thus adds a *positive* term on the right-hand side of the power balance equation (9-85). The incremental form of the GSE will change from (9-92) to

$$\frac{d^2}{dt^2}(\Delta\delta_N) + 2b \frac{d}{dt}(\Delta\delta_N) + \omega_1^2 \, \Delta\delta_N = 0 \tag{9-95}$$

The general solution of this equation is

$$\Delta\delta_N = Ae^{-bt} \sin (\omega_1' t + \psi) \tag{9-96}$$

where

$$\omega_1' = \sqrt{\omega_1^2 - b^2} \tag{9-97}$$

Typically, $\omega_1 \gg b$, and therefore

$$\omega_1' \approx \omega_1$$

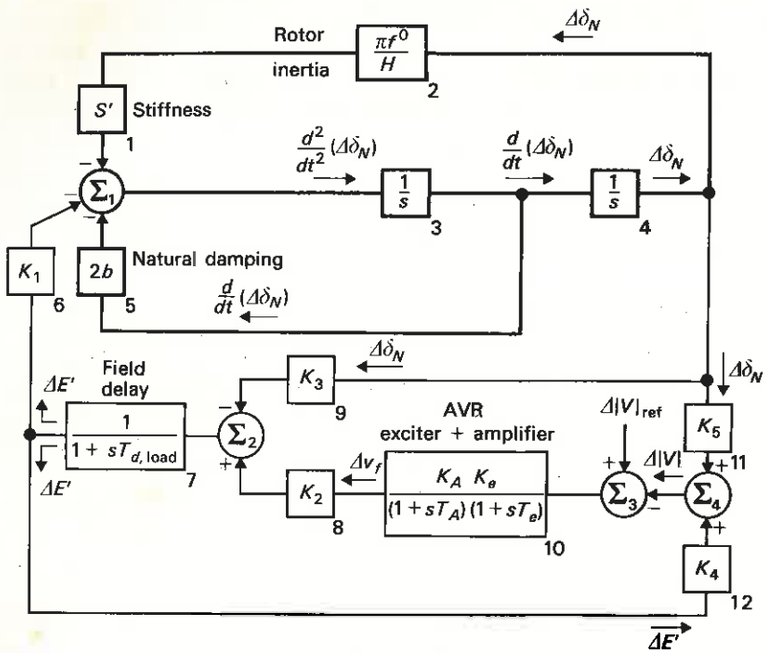

Figure 9-19 A linearized dynamic model of the single generator–infinite bus system including the AVR coupling effects.

In conclusion: *Under the influence of the damper winding, the generator is "oscillatorily stable," meaning that if subject to any small disturbance it will return to its steady-state equilibrium by a damped oscillation.*

This "natural" damping of the system is further enhanced by the resistances of the network, which we have neglected in our analysis.

It is instructive to visualize the rotor dynamics by means of the boldface portion† of the block diagram in Fig. 9-19. The blocks 1 through 4, plus the summing junction $\sum_1$, model the basic undamped "inertia" dynamics of Eq. (9-92). The damper loop (block 5) takes into effect the natural damping of the system, as expressed by Eq. (9-95).

9-5-4 Extension to Large-Scale System

It is possible to extend the above theory to the N-generator case. An "inertial" angular reference is chosen (Chap. 12) relative to which all N machine rotors are measured. A swing equation is then written for every generator. These GSE's will be mathematically coupled via the line powers.

† The remaining part of the diagram will be commented on in Sec. 9-5-5.

In performing a study of the incremental dynamics around some operating point one can conclude that:

1. The response consists not of *one* radian natural frequency ω_1, as in the above case, but $N-1$ natural frequencies $\omega_1, \ldots, \omega_{N-1}$.
2. Under the influence of damper windings and line resistances all $N-1$ natural modes are positively damped.
3. The system would thus be "oscillatorily stable."

9-5-5 Negative Damping

If the "natural" tendency for the interconnected machines is to be "oscillatorily stable" how then can phenomena of the type depicted in Fig. 9-17 be explained? Clearly, our above analysis must have neglected some important system mechanism that will be present in real life. To understand this let us return for a minute to Eq. (9-95). Assume that somehow the damping coefficient b becomes negative. In that case the factor e^{-bt} will *grow* with time rather than *decay*, and the inertial oscillations will be of the type in Fig. 9-17. Furthermore, the system will *self-excite*, i.e., the oscillations will be initiated by any infinitesimal disturbance that is always present.

The damper winding and line resistances will, of course, never yield a negative b. *It is entirely possible, however, that signals emanating from other sources will enter the loop at the summing junction $\sum_1$ in Fig. 9-19.* These signals may, like the damper signal, be proportional to $d(\Delta\delta)/dt$. If they, like the latter, are positive they will further help damp the inertial oscillations. *If, on the contrary, they are negative they will reduce the natural damping, possibly to the point of eliminating it altogether.*

It is instructive to show how such signals may be generated and how they enter into the dynamic picture. For this reason we will in the next few sections give a qualitative, step-by-step presentation of these added effects.

9-5-6 Effect of Changing E'

In deriving the formula (9-89) for ΔP_G we made use of a transient power expression that was derived from Eq. (4-77). *It is important to realize that we tacitly assumed $|V^f|$ and $|E'|$ to be constant thus making P_G a function of the power angle δ_N only,* i.e.,

$$P_G = P_G(\delta_N) \tag{9-98}$$

This yielded the expression (9-89).

In reality the emf E' *will* change and this means that Eq. (9-98) changes to

$$P_G = P_G(\delta_N, E') \tag{9-99}$$

Thus we have for the incremental transient power output

$$\Delta P_G = \left(\frac{\partial P_G}{\partial \delta_N}\right)^0 \Delta\delta_N + \left(\frac{\partial P_G}{\partial E'}\right)^0 \Delta E' \tag{9-100}$$

or shorter

$$\Delta P_G = S' \, \Delta\delta_N + K_1 \, \Delta E' \tag{9-101}$$

where K_1 has the unit "per-unit megawatt per per-unit kilovolt."

The added term will clearly be represented in our block diagram in Fig. 9-19 as the new input via block 6.

9-5-7 Factors Causing Changes in E'

Why will E' change? There are two reasons:

1. Manipulation (via AVR) of the field voltage v_f
2. Changes in relative rotor position δ_N.

An *increase* in v_f will clearly tend to *increase* E'. Not so clearly, an increase in rotor angle tends to *decrease* E'. The latter statement is, however, easily confirmed from Fig. 4-25. As δ increases, the voltage $X'_d I_d$ and thus I_d will increase. But since I_d is *demagnetizing* (Fig. 4-25*b*) the end result is a *decrease* in the emf.

The relationship between increments of $\Delta\delta_N$, Δv_f, and $\Delta E'$ will thus read

$$\Delta E' = K_2 \Delta v_f - K_3 \Delta\delta_N \tag{9-102}$$

The transfer blocks 8 and 9 plus the summing juncton $\sum_2$ account for the effects stated in Eq. (9-102). Equation (9-102) expresses the *steady-state* changes in E' resulting from the changes in Δv_f and $\Delta\delta_N$.

Dynamically, the change in E' can take place *only after* Δv_f and $\Delta\delta_N$ have overcome the field winding time constant, the value of which (under load) was given by formula (9-20). The added delay transfer block 7 takes this field delay into consideration.

9-5-8 Inclusion of the AVR Loop

At this stage the increment Δv_f in Eq. (9-102) must be accounted for. Returning to the AVR block diagram in Fig. 9-4 we obtain Δv_f directly as the output from the exciter. This results in the addition of block 10 plus the third summing junction $\sum_3$ to the growing diagram of Fig. 9-19.

We finally are left with only $\Delta|V|$, the incremental change in the generator terminal voltage. $\Delta|V|$ consists (see Fig. 4-25) of the two components ΔV_q and ΔV_d. The former increases as E' increases, the latter as δ increases. Thus we have the incremental relationship:

$$\Delta|V| = K_4 \, \Delta E' + K_5 \, \Delta\delta_N \tag{9-103}$$

In Fig. 9-19, we symbolize this equation with the summing junction $\sum_4$ and the transfer blocks 11 and 12. The block diagram is now complete with all signal branches, except $\Delta|V|_{\text{ref}}$, fully accounted for.

9-5-9 Discussion of Results

The boldface portion of the diagram in Fig. 9-19 is readily understood. Under the influence of the synchronizing power the generator rotor when disturbed tends to perform undamped natural oscillations much like the spring-mass system of an auto when hitting a bump. The damping power emanating from the damper winding serves as the system "shock absorber." Note that the synchronizing power is in negative phase with the swing amplitude $\Delta\delta_N$, whereas the damping power is 90° out of phase.

What can we make out of the lower portion of the diagram in Fig. 9-19?

Without getting involved in analytical details we summarize these observations:

1. The swing amplitude $\Delta\delta_N$ is fed back via a dual-path system, i.e., directly via blocks 6, 7, and 9 and indirectly via the AVR. This feedback can result in "parasitic" power components in phase with either the synchronizing power or the damping power. The actual phase is determined by the frequency-dependent blocks 7 and 10.
2. DeMello and Concordia analyzed the actual nature of these parasitic power components in a classic paper[5] and contributed quantitative data. Andersson and Fouad[6] applied Routh's stability criterion to find conditions for stability. The resulting formulas are too complex to be included here.
3. The parameters S', K_1, ..., K_5 are partial-derivative expressions (compare Eq. (9-100)) and *are therefore depending upon the loading*. DeMello and Concordia made the following comment: "It is important to recognize that . . . the parameters change with loading. Since they change in rather complex manner, it is difficult to reach general conclusions based on parameter values for one operating point only."
4. In some systems the combination of long lines, fast AVR's, and heavy loading can result in a situation where the parasitic feedback power annuls the natural damping thus making the system "oscillatorily unstable" as demonstrated in Fig. 9-17.
5. It should be realized that Fig. 9-19 in its complexity models only a single generator operating onto an infinite network. The results obtained from this diagram either by analysis or simulation are useful but may not be directly applicable to the conditions existing in an interconnected network.

   A recent EPRI sponsored project[7] has resulted in a computer program for simulation of intermachine oscillations in large systems.
6. When a system experiences self-excited oscillations addition of so-called

"power system stabilizers" (PSS) will quench the oscillations.[8,9] A PSS injects stabilizing "supplementary" signals to the summing junction $\sum_3$ in Fig. 9-19. These signals typically are derived from the generator shaft speed and shaped in special networks.[10] See also Prob. 9-14.

9-6 AGC DESIGN USING KALMAN METHODS

The reader must realize by now that design of generator controllers as we know them today has followed "classical" lines. Root-locus methods, block-diagram representation, intuition, trial and error, empiricism are but a few of the "classical" design tools. The high degree of reliability and general excellent functioning of today's power systems is proof of the soundness of design. In view of this fact is there really any room for improvements?

The phenomenon of intermachine oscillations discussed in the previous section demonstrates that our present power systems are not immune to instabilities. It also accentuates an inherent weakness of classical design—its inability fully to anticipate and adequately to cope with all dynamic features in systems of high dimensionality.

A modern gigawatt generator with its multistage reheat turbine, including its ALFC and AVR controllers, is characterized by an impressive complexity. When all its nonnegligible dynamics are taken into account, including cross-coupling between control channels, the overall dynamic model may be of 20th order.

This "dimensionality barrier" can be nicely overcome by means of computer-aided *optimal control* design methods originated by Kalman.[11,12] Yu, Fosha, and Elgerd[13,14] made early attempts to apply these methods to power systems. A recent survey[15] classifies the many contributions that have later followed. "Optimal control" covers today a widening spectrum of computer-oriented techniques of which the so-called *optimum linear regulator* (OLR) design has proven particularly useful.

Compactly stated, the OLR design results in a controller that *minimizes both transient variable excursions and control efforts.* In practical power systems terms this means optimally damped oscillations with minimum wear and tear of control valves. OLR design proceeds as follows:

Step 1 Casting the system dynamic model in *state variable form* and introduction of appropriate *control forces*

Step 2 Choosing an *integral-squared-error control index*, the minimization of which is the control goal

Step 3 Finding the structure of the *optimal controller* that will minimize the chosen control index

We demonstrate briefly the use of OLR design by applying it to the single-area ALFC system depicted in Fig. 9-10. We propose to find a control force u

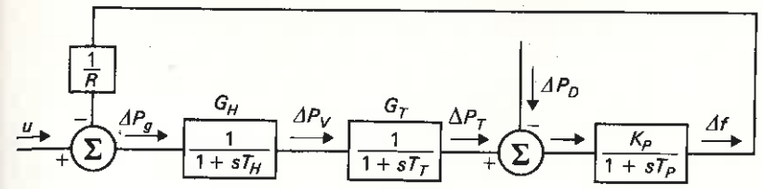

Figure 9-20 OLR control of primary ALFC loop.

(depicted in Fig. 9-20) which in an "optimal" manner steers or controls the system. We define "optimal" later; presently we develop an appropriate model for the system.

9-6-1 Putting the Dynamic Model in State Variable Form

OLR design is based entirely upon the availability of a dynamic system model in so-called *state-variable form.* We demonstrate how this form can be obtained from the block diagram model in Fig. 9-20.

For this system we have the transform equations:

$$\Delta P_V(s) = \frac{1}{1+sT_H}\left(u(s) - \frac{1}{R}\Delta f(s)\right)$$

$$\Delta P_T(s) = \frac{1}{1+sT_T}\Delta P_V(s) \tag{9-104}$$

$$\Delta f(s) = \frac{K_p}{1+sT_p}(\Delta P_T(s) - \Delta P_D(s))$$

Or, if expressed in the time domain,

$$\Delta P_V + T_H \frac{d}{dt}(\Delta P_V) = u - \frac{1}{R}\Delta f$$

$$\Delta P_T + T_T \frac{d}{dt}(\Delta P_T) = \Delta P_V \tag{9-105}$$

$$\Delta f + T_p \frac{d}{dt}(\Delta f) = K_p\,\Delta P_T - K_p\,\Delta P_D$$

At this juncture we introduce the three *state variables* x_1, x_2, and x_3 forming the *state vector*

$$\mathbf{x} = \begin{bmatrix} x_1 \\ x_2 \\ x_3 \end{bmatrix} \triangleq \begin{bmatrix} \Delta P_V \\ \Delta P_T \\ \Delta f \end{bmatrix} \tag{9-106}$$

We also define the *disturbance force*:

$$p \triangleq \Delta P_D \tag{9-107}$$

Equations (9-105) can, upon rearrangement, be put in the form

$$\begin{bmatrix} \dot{x}_1 \\ \dot{x}_2 \\ \dot{x}_3 \end{bmatrix} = \begin{bmatrix} -\dfrac{1}{T_H} & 0 & -\dfrac{1}{RT_H} \\ \dfrac{1}{T_T} & -\dfrac{1}{T_T} & 0 \\ 0 & \dfrac{K_p}{T_p} & -\dfrac{1}{T_p} \end{bmatrix} \begin{bmatrix} x_1 \\ x_2 \\ x_3 \end{bmatrix} + \begin{bmatrix} \dfrac{1}{T_H} \\ 0 \\ 0 \end{bmatrix} u + \begin{bmatrix} 0 \\ 0 \\ -\dfrac{K_p}{T_p} \end{bmatrix} p \tag{9-108}$$

This is the sought "state-variable form." Using matrix and vector symbols it can be put in more compact form:

$$\dot{\mathbf{x}} = \mathbf{A}\mathbf{x} + \mathbf{B}u + \mathbf{\Gamma}p \tag{9-109}$$

The single-area system had only one control force and also one disturbance force. The two-area system in Fig. 9-14 has two control and disturbance forces. Were we to write its state model we would have to define control force and disturbance force *vectors*

$$\mathbf{u} = \begin{bmatrix} u_1 \\ u_2 \end{bmatrix} \qquad \mathbf{p} = \begin{bmatrix} p_1 \\ p_2 \end{bmatrix} \triangleq \begin{bmatrix} \Delta P_{D1} \\ \Delta P_{D2} \end{bmatrix} \tag{9-110}$$

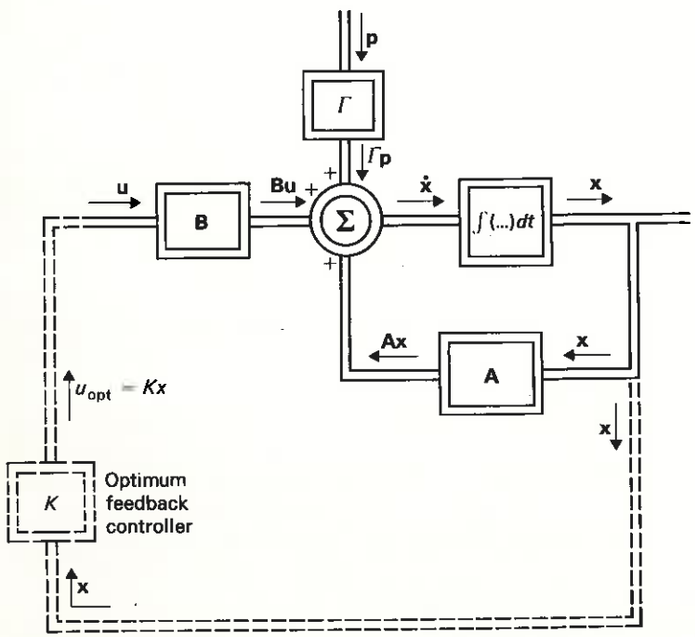

Figure 9-21 Block diagram of linear state model. Dashed feedback portion represents the "optimum" controller.

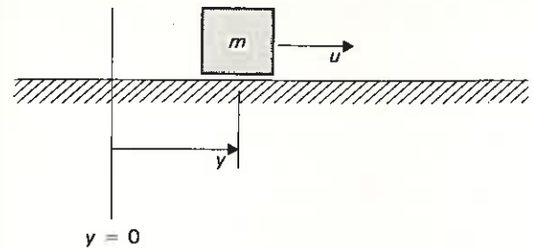

Figure 9-22 Simple controlled system.

The state equations then would be written in the more general form:

$$\dot{\mathbf{x}} = \mathbf{A}\mathbf{x} + \mathbf{B}\mathbf{u} + \mathbf{\Gamma}\mathbf{p} \tag{9-111}$$

In the general case we shall assume $\mathbf{x}$ to be n-dimensional and $\mathbf{u}$ of dimension m.

Figure 9-21† depicts a block symbolic representation of Eq. (9-111).

Example 9-11 A mass of $m = 1$ kg lies on a frictionless table (Fig. 9-22). It is acted upon by the force u. Its position coordinate is y. Write the state equations for this system.

SOLUTION Newton's equation reads

$$1\,\ddot{y} = u \tag{9-112}$$

Define now

$$\mathbf{x} = \begin{bmatrix} x_1 \\ x_2 \end{bmatrix} \triangleq \begin{bmatrix} y \\ \dot{y} \end{bmatrix} = \begin{bmatrix} \text{position} \\ \text{velocity} \end{bmatrix} \tag{9-113}$$

Substitution into (9-112) yields

$$\begin{aligned} \dot{x}_1 &= x_2 \\ \dot{x}_2 &= u \end{aligned} \tag{9-114}$$

or in state-variable form:

$$\begin{bmatrix} \dot{x}_1 \\ \dot{x}_2 \end{bmatrix} = \begin{bmatrix} 0 & 1 \\ 0 & 0 \end{bmatrix} \begin{bmatrix} x_1 \\ x_2 \end{bmatrix} + \begin{bmatrix} 0 \\ 1 \end{bmatrix} u \tag{9-115}$$

In this case we have

$$\mathbf{A} = \begin{bmatrix} 0 & 1 \\ 0 & 0 \end{bmatrix} \quad \mathbf{B} = \begin{bmatrix} 0 \\ 1 \end{bmatrix} \quad \text{and} \quad \mathbf{\Gamma} = \mathbf{0}$$

9-6-2 Optimum Control Index I

Our next concern is to select an *optimum control index*. OLR design is based upon an *integral-squared-error* index of the form

$$I = \int_0^\infty (q_1 x_1^2 + \cdots + q_n x_n^2 + r_1 u_1^2 + \cdots + r_m u_m^2)\, dt \tag{9-116}$$

where the q's and r's are positive *penalty factors*.

† Disregard for the present the dashed part of the figure.

For example, in our single-area example system the I index would read

$$I = \int_0^\infty [q_1(\Delta P_V)^2 + q_2(\Delta P_T)^2 + q_3(\Delta f)^2 + ru^2]\, dt \tag{9-117}$$

As we shall find in the next section, the whole idea of "optimum" control is to *minimize* the I index. Consider for example the term $q_3\ (\Delta f)^2$. Due to the squaring a frequency error will contribute to I independent of its sign. Furthermore if Δf is doubled its contribution to I will quadruple. The integral causes Δf to add to I during its entire duration. The *penalty factors* q_i distribute the penalty weight among the state-variable errors. Should the error in a certain state variable be of little practical signifiance then we simply set its penalty factor equal to zero.

What has been said about state errors applies equally to control-force increments. The penalty factors r_i distribute the penalties among the m control forces. *It is important that none of the r's be set equal to zero.* Should this be the case the corresponding control force could assume infinite magnitude without affecting I. An infinite control force could do its correcting job in zero time. This would obviously be a very unrealistic regulator.

If all the q's and r's constitute the diagonal elements of the two *penalty matrices*

$$\mathbf{Q} \triangleq \begin{bmatrix} q_1 & & 0 \\ & q_2 & \\ & & \ddots \\ 0 & & q_n \end{bmatrix} \quad \text{and} \quad \mathbf{R} \triangleq \begin{bmatrix} r_1 & & 0 \\ & r_2 & \\ & & \ddots \\ 0 & & r_m \end{bmatrix} \tag{9-118}$$

then the I index in Eq. (9-116) can be written (compare App. A) in the compact form

$$I = \int_0^\infty (\mathbf{x}^T\mathbf{Q}\mathbf{x} + \mathbf{u}^T\mathbf{R}\mathbf{u})\, dt \tag{9-119}$$

9-6-3 State Space and State Trajectories

By the term *state space* we mean the n-dimensional coordinate space in which $\mathbf{x}$ ranges. For example, the two-dimensional system in Example 9-11 has a two-dimensional state space often referred to as a *state plane*† as shown in Fig. 9-23. As this system, under the influence of the control force u, is being controlled from the initial state $\mathbf{x}_1 = (1, 1)$ to the end state $\mathbf{x}_2 = (2, 2)$, the *state transfer* can be visualized by a controlled *state trajectory*. In Fig. 9-23 two such trajectories, T_1 and T_2, are shown each corresponding to two different control strategies, u_1 and u_2.

† The term *space plane* is also used.

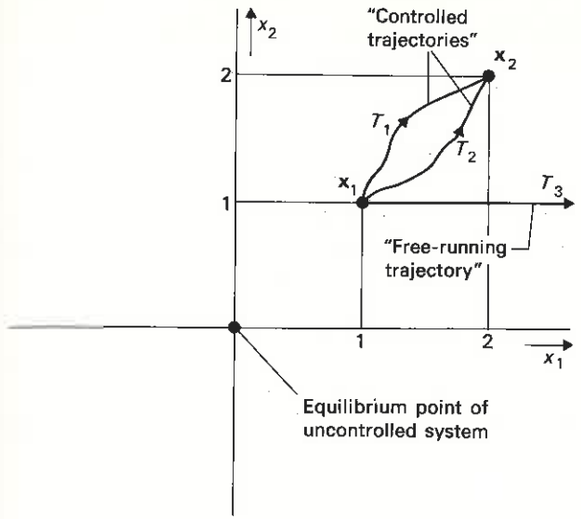

Figure 9-23 Control trajectories.

Origin of the state space is of particular importance, as we realize by setting both $\mathbf{u}$ and $\mathbf{p}$ equal to zero in Eq. (9-111). The state model now reduces to

$$\dot{\mathbf{x}} = \mathbf{A}\mathbf{x} \tag{9-120}$$

which is the model of a *linear, uncontrolled,* or *free-running* system. If we set $\mathbf{x} = \mathbf{0}$, i.e., placing the system in origin, then Eq. (9-120) yields

$$\dot{\mathbf{x}} = \mathbf{0} \tag{9-121}$$

In words: In origin all state variables of a free-running system have zero time rates. *If the state variables and their time rates both are zero, origin must be an equilibrium point.*

For example, if the mass in Fig. 9-22 is given zero position and zero velocity it will remain in this state indefinitely (if $u = 0$). Likewise, if all the three state variables of the above single-area power system are set equal to zero, then the system (if $u = p = 0$) will remain in this state—the *normal state* of the power system—indefinitely.

In contrast, if the free-running system is put in a nonzero initial state it will not remain there. For example if the system in Example 9-11 is put in the state $\mathbf{x}_1 = (1, 1)$ it will move from there on a *free-running trajectory* T_3. In this case the free-running trajectory ends in infinity indicating that the uncontrolled system is *unstable*. If the uncontrolled system were *stable* its free-running trajectory would lead it back to origin.

9-6-4 Optimally Controlled Trajectories

We are now in a position to define what is meant by an "optimum" linear regulator. Consider the three-dimensional single-area power system that we earlier modeled. Consider it initially in its *normal* operating state. As all three "errors" (Eq. 9-106) are thus zero we find the system in equilibrium in state-space origin.

Some disturbance moves the system suddenly away from origin and we begin our study of the system at time $t = 0$ when we thus find it in the *nonzero* state $\mathbf{x}(0)$. If the system were uncontrolled it would continue from $\mathbf{x}(0)$ on a free-running trajectory. *But our system is controlled and if properly designed the control force, u, ought to take it back to origin.*

This state transfer back to origin can take place along an infinite variety of state trajectories. *If our system is designed in such a unique way that the I index (9-117) is minimized along the state trajectory then our control system constitutes an OLR.*

The state trajectory in question is unique and is termed "optimal," $\mathbf{x}(t) = \mathbf{x}_{\text{opt}}(t)$. It would correspond to an "optimal" control force, $u(t) = u_{\text{opt}}(t)$.

9-6-5 OLR Structure—The Riccati Equation

How do we find the optimal trajectory? What will be the structure of the optimal regulator? Kalman's work provided the answers to these important questions. His results can be summarized in the following two-item list:

1. The linear regulator is optimal if the m control forces are linearly dependent upon the n state variables, i.e.,

$$\begin{aligned} u_1 &= k_{11}x_1 + \cdots + k_{1n}x_n \\ &\vdots \\ u_m &= k_{m1}x_1 + \cdots + k_{mn}x_n \end{aligned} \tag{9-122}$$

   or in compact vector-matrix notation

$$\mathbf{u}_{\text{opt}} = \mathbf{K}\mathbf{x}_{\text{opt}} \tag{9-123}$$

   where the gain matrix $\mathbf{K}$ is of order $m \times n$. Equation (9-123) settles immediately the question of structure. The system in Fig. 9-21 is obviously turned into an OLR by "closing the loop" via $\mathbf{K}$ as shown dashed in the figure.

2. The elements of the gain matrix $\mathbf{K}$ are computed by first solving the *matrix Riccati equation*

$$\mathbf{PA} + \mathbf{A}^T\mathbf{P} - \mathbf{PBR}^{-1}\mathbf{B}^T\mathbf{P} + \mathbf{Q} = \mathbf{0} \tag{9-124}$$

   for the unknown $n \times n$ matrix $\mathbf{P}$. With $\mathbf{P}$ known the $\mathbf{K}$ matrix is then obtained from the matrix product

$$\mathbf{K} = -\mathbf{R}^{-1}\mathbf{B}^T\mathbf{P} \tag{9-125}$$

Note that all matrices $\mathbf{A}$, $\mathbf{B}$, $\mathbf{Q}$, and $\mathbf{R}$ that appear in Eqs. (9-124) and (9-125) have been earlier defined. Superscript $(\ )^T$ means transposition.

Example 9-12 Find the gain matrix $\mathbf{K}$ that will make the system in Example 9-11 an OLR. Also find the optimum trajectory $\mathbf{x}_{\text{opt}}$ if the initial system state is $\mathbf{x}(0) = \begin{bmatrix} 1 \\ 1 \end{bmatrix}$.

SOLUTION We had found in Example 9-11

$$\mathbf{A} = \begin{bmatrix} 0 & 1 \\ 0 & 0 \end{bmatrix} \quad \text{and} \quad \mathbf{B} = \begin{bmatrix} 0 \\ 1 \end{bmatrix}$$

$$\therefore \quad \mathbf{A}^T = \begin{bmatrix} 0 & 0 \\ 1 & 0 \end{bmatrix} \quad \text{and} \quad \mathbf{B}^T = [0 \quad 1]$$

Before we can solve the problem we must settle for suitable penalty factors. We choose for simplicity equal penalty weight on x_1, x_2, and u, and thus obtain

$$\mathbf{Q} = \begin{bmatrix} 1 & 0 \\ 0 & 1 \end{bmatrix} \qquad \mathbf{R} = r = 1$$

$$\therefore \quad \mathbf{R}^{-1} = r^{-1} = 1$$

(Note that $\mathbf{R}$ and $\mathbf{R}^{-1}$ are scalars in this case.)

The triple product $\mathbf{BR}^{-1}\mathbf{B}^T$ appearing in the third term of the Ricatti equation equals

$$\begin{bmatrix} 0 \\ 1 \end{bmatrix} \times 1 \times [0 \quad 1] = \begin{bmatrix} 0 & 0 \\ 0 & 1 \end{bmatrix}$$

The Riccati equation thus takes on the form.

$$\begin{bmatrix} p_{11} & p_{12} \\ p_{21} & p_{22} \end{bmatrix}\begin{bmatrix} 0 & 1 \\ 0 & 0 \end{bmatrix} + \begin{bmatrix} 0 & 0 \\ 1 & 0 \end{bmatrix}\begin{bmatrix} p_{11} & p_{12} \\ p_{21} & p_{22} \end{bmatrix} - \begin{bmatrix} p_{11} & p_{12} \\ p_{21} & p_{22} \end{bmatrix}\begin{bmatrix} 0 & 0 \\ 0 & 1 \end{bmatrix}\begin{bmatrix} p_{11} & p_{12} \\ p_{21} & p_{22} \end{bmatrix} + \begin{bmatrix} 1 & 0 \\ 0 & 1 \end{bmatrix} = \begin{bmatrix} 0 & 0 \\ 0 & 0 \end{bmatrix} \tag{9-126}$$

After performing the multiplications called for this 2×2 matrix equation reduces to a set of the four scalar equations:

$$\begin{aligned} -p_{12}p_{21} + 1 &= 0 \\ p_{11} - p_{12}p_{22} &= 0 \\ p_{11} - p_{21}p_{22} &= 0 \\ p_{21} + p_{12} - p_{22}^2 + 1 &= 0 \end{aligned} \tag{9-127}$$

Their solution is simple and yields matrix

$$\mathbf{P} = \begin{bmatrix} \sqrt{3} & 1 \\ 1 & \sqrt{3} \end{bmatrix}$$

We can now compute the $\mathbf{K}$ matrix:

$$\mathbf{K} = -1 \times [0 \quad 1]\begin{bmatrix} \sqrt{3} & 1 \\ 1 & \sqrt{3} \end{bmatrix} = -[1 \quad \sqrt{3}] \tag{9-128}$$

The optimal feedback controller thus is characterized by the control strategy

$$u = u_{\text{opt}} = -[1 \quad \sqrt{3}]\begin{bmatrix} x_1 \\ x_2 \end{bmatrix} = -x_1 - \sqrt{3}\,x_2 \tag{9-129}$$

It is left as an exercise for the reader to determine and then plot the optimal trajectory that will transfer the system from $\begin{bmatrix} 1 \\ 1 \end{bmatrix}$ to $\begin{bmatrix} 0 \\ 0 \end{bmatrix}$. How would the response look in the time domain?

9-6-6 Concluding Comments

In the above simple text example the Riccati equation could be solved *analytically*. In practice, of course, we can only expect to obtain *numerical* solutions. Effective computer programs exist that can solve for the **P** matrix of any reasonable dimensionality.

The optimum solution and gain matrix **K** will depend, of course, upon the choice of penalty matrices **Q** and **R**. Such a choice will always be a subjective one. Here the skill and good system knowledge of the designer becomes invaluable. Typically, at the initial stage of the design process the designer is quite ignorant about the magnitude ranges for the **x** and **u** vectors. Consequently it is difficult to properly balance penalty between the **x** and **u** variables.

A first "guess" is made of the **Q** and **R** matrices, based upon which a first optimal controller is computed. If its response does not square well with the practical hardware constraints a second choice of **Q** and **R** is made. The design thus becomes an iterative process that will converge on an "optimal" OLR.

SUMMARY

In this chapter we have tried to give a balanced presentation of automatic generation control. Generator controls are naturally divided into ALFC's and AVR's each of which is designed under the assumption that little if any channel interaction exists.

Under normal operation the controllers keep the generator operating around a preselected "normal" state with minimal excursions. The dynamic models of all controllers that have been discussed have therefore been linear.

On occasion many of today's power systems experience instabilities of the oscillatory type. We have explored the reasons behind such instabilities and found that cross-coupling between AVR and ALFC channels are to be blamed.

Finally, we have briefly described the more modern computer-aided "optimal" design techniques due to Kalman. The true advantage of such designs is a full guarantee that the system will be stable, assuming of course that the design is based upon a correct dynamic model of the system.

PROBLEMS

***9-1** According to Fig. 1-1 the total installed U.S. generating capacity in 1982 amounts to about 600 GW. Assume that on a particular occasion generators of a total capacity of 550 GW are actually running. To get a feel for the total kinetic energy that these machines collectively represent find the dimensions of a flywheel storing the same amount of kinetic energy. Make these assumptions:

1. The average inertia of all U.S. generators corresponds to a per-unit inertia constant of 5 seconds.
2. The flywheel runs at 1800 r/min.
3. It is made of solid steel.
4. Its shape is cylindrical with the diameter equaling its length.

***9-2** Consider the AVR loop discussed in the text having the block representation shown in Fig. 9-4. The time constants have the following numerical values:

$$T_A = 0.050 \text{ s}$$

$$T_e = 0.50 \text{ s}$$

$$T'_{d0} = 3.0 \text{ s}$$

Assume the loop uncompensated. We would like the static "error" not to exceed one percent which means, according to Eq. (9-13), that the open-loop gain K must exceed 99.

(*a*) Construct a carefully drawn root-locus plot (Fig. 9-5) and prove that the static accuracy requirement conflicts with the requirement for stability.

(*b*) Specifically, compute the closed-loop poles (eigenvalues) if K is set at 99.

(*c*) Reduce K by 50 percent and repeat part *b*.

9-3 In working the previous problem you have now determined that the time response will contain a dominant response term of the oscillatory type

$$e^{\sigma t} \sin(\omega t + \alpha)$$

For stability we not only want σ to be negative but also *sufficiently* negative to make the response term decay fast. Specifically, we require that

$$\sigma < -0.6$$

From the root-locus plot in Prob. 9-2 determine the constraints that this will put on the open-loop gain K.

9-4 It is most desirable that a control loop be "robust," meaning that the loop should retain its stability even if its parameters will undergo wide ranging changes. Consider the above AVR loop with the gain set at the value computed in Prob. 9-3. We assume now that the generator load increases resulting in a decrease in the effective field inductance according to Eq. (9-20). Specifically, let us assume that the field time constant decreases from 3 to 1 s. All other loop parameters (including K) remain unchanged.

Adjust your root-locus plot and determine whether the AVR loop remains stable.

9-5 The previous problems have demonstrated the need for loop stabilization. Figure 9-24 depicts a circuit often used for this purpose. It consists of a *stabilizing* or *damper* transformer, the primary of which is connected to the regulator voltage v_R or (as shown dashed) to the field voltage v_f. (The latter voltage is obviously not easily accessible in a brushless exciter.) Compare Fig. 9-2.

The transformer has the primary parameters R and L and a mutual inductance M. If it feeds into an amplifier with high input impedance its secondary current is zero and we can model its response with the following two equations:

$$v_R = Ri + L\frac{di}{dt} \tag{9-130}$$

$$v_0 = M\frac{di}{dt} \tag{9-131}$$

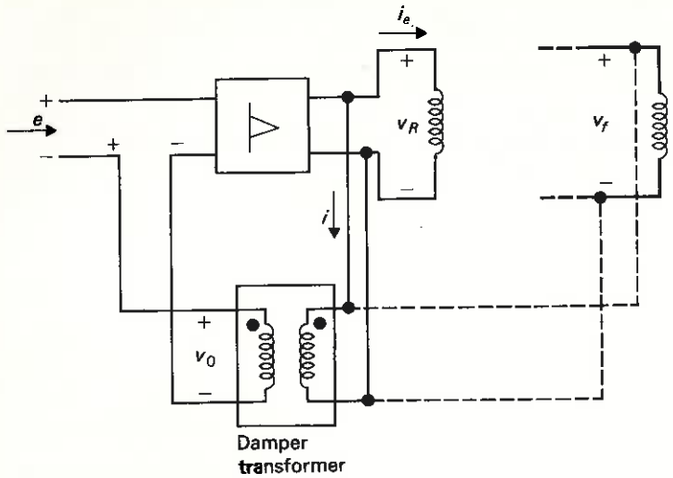

Figure 9-24 Damper transformer.

These equations yield the feed-back stabilizing transfer function

$$G_f = \frac{V_0(s)}{V_R(s)} = \frac{sM}{R + sL} \tag{9-132}$$

If the resistance is dominating we have

$$G_f \approx \frac{M}{R} s \triangleq K_f s \tag{9-133}$$

which then exposes the *derivative feed-back* character of the device.

(*a*) In view of Eq. (9-133) give a *physical* reasoning why this transformer would introduce damping.

(*b*) Use the transfer function (9-133) and study how the device changes the character of the root loci in Fig. 9-5.

(*c*) Same as in (*b*) but change now the input to the field voltage.

***9-6** Three generators rated 100, 200, and 300 MW respectively are operating in parallel feeding energy into a large network. The generators have 3, 4, and 5 percent regulation parameters respectively, expressed in terms of their respective ratings. If the frequency drops by 0.5 percent determine the load increase in each unit *expressed in megawatts.*

***9-7** Consider the primary ALFC loop the parameters of which were given in Example 9-5. By assuming $T_H = T_T = 0$ we found (Eq. (9-51)) the loop to be stable.

By letting T_H and T_T be *nonzero* we obviously have a loop with three cascaded time constants. As we learned in Prob. 9-2 above such a loop can easily be made unstable.

Assume

$$T_H = T_T = 0.5 \text{ s}$$

(*a*) Carefully draw a root-locus plot of the ALFC loop.

(*b*) With the parameters as given in Example 9-5 will the loop be stable? Show in particular the location of the three eigenvalues.

9-8 In the previous problem we had assumed the turbine to be of nonreheat type. Let us now assume the turbine to be of hydrotype with the transfer function given by Eq. (D-5). Let us assume $T_w = 2$ s. We still assume $T_H = 0.5$ s and all other loop parameters the same as in the previous problem.

Make a root-locus plot and determine if the loop would be stable. In your analysis note that

$$\frac{1 - 2sT_w}{1 + sT_w} = -2\frac{s - 1/2T_w}{s + 1/T_w} \tag{9-134}$$

9-9 Same as in Prob. 9-8 but the turbine is now assumed to be of the reheat type with response given by Eq. (D-4). Set

$$T_{CH} = 0.5 \text{ s}$$

$$T_{RH} = 4 \text{ s}$$

$$\alpha = 0.5$$

(*a*) Make root-locus plot and discuss stability.

(*b*) For a step load of 0.01 pu compute $\Delta f(t)$.

9-10 Consider the hypothetical case that the fulcrum B in Fig. 9-7 would get "stuck," meaning that a frequency change would result in zero Δx_B. This is tantamount to saying that R in Fig. 9-10 would be ∞ (or the primary ALFC loop be open).

The "secondary" ALFC loop would now be solely responsible for the frequency control. Would it work? Would the loop be stable? Check the situation in the reheat and nonreheat cases studied in Probs. 9-7 and 9-9.

9-11 A generator has a primary ALFC loop characterized by $R = 5\%$. The secondary loop is open. It is feeding a load consisting of three equal resistors R, connected Y. The frequency equals 60 Hz. The resistances are decreased until the frequency drops to 59 Hz. By how many percent did you have to change R? The AVR loop keeps the voltage constant.

9-12 Replace the three resistors in Prob. 9-11 by three impedances $X = R + j\omega L$. Initially $R = \omega L$ and the frequency equals 60 Hz. By how many percent must you decrease R for the frequency to drop to 59 Hz?

Hint: Find the D parameter.

9-13 Each of the three forsional masses in Fig. 9-18 has an inertia constant of 100 kgm^2. Each of the two elastic shafts has a restoring torque of 200 newtonmeters per radian of twist angle. Find the two natural frequencies expressed in Hz.

9-14 Assume that E' is *not* constant in Example 4-13 on p. 112. Since

$$\left(\frac{\partial P_G}{\partial E'}\right)^0 = \frac{1 \times \sin \delta_N^0}{0.44} = 0.986$$

Eq. (9-101) would yield

$$\Delta P_G = 1.565\ \Delta\delta_N + 0.986\ \Delta E' \tag{9-135}$$

By using the last equation the swing equation (9-92) would read

$$\frac{d^2}{dt^2}(\Delta\delta_N) + 59.0\ \Delta\delta_N + 37.2\ \Delta E' = 0 \tag{9-136}$$

(*a*) Prove that by arranging so that $\Delta E' \sim d/dt\,(\Delta\delta_N)$ we introduce positive damping into the system.

(*b*) Suggest at least two ways by means of which this can be practically implemented.

REFERENCES

1. "Computer Representation of Excitation Systems," IEEE Committee Report, *IEEE Trans.*, vol. PAS-87, no. 6, June, 1968, pp. 1460–1464.
2. T. L. Dillman *et al.*: "A High Initial Response Brushless Excitation System," *IEEE Trans.*, vol. PAS, Sept/Oct., 1971.
3. IEEE Committee Report, "Dynamic Models for Steam and Hydro Turbines in Power System Studies," *IEEE Trans. Power Appar. Syst.*, vol. PAS-92, no. 6, November/December 1973, pp. 1904–1915.
4. N. Cohn: *Control of Generation and Power Flow on Interconnected Systems*, John Wiley & Sons, New York, 1971.
5. F. P. DeMello and C. Concordia: "Concepts of Synchronous Machine Stability as Affected by Excitation Control," *Stability of Large Power Systems*, IEEE Press, New York.
6. P. M. Andersson and A. A. Fouad: *Power System Control and Stability*, The Iowa University Press, Ames, Iowa, 1977.
7. R. T. Byerly, D. E. Sherman, and R. J. Bennon: "Frequency Domain Analysis of Low-Frequency Oscillations in Large Electric Power Systems, Part 1—Basic Concepts, Mathematical Models, and Computing Methods," EPRI EL-727, Project 744-1, Final Report, April 1979.
8. F. R. Schleif, H. D. Huskins, G. E. Martin, and E. E. Hattan: "Excitation Control to Improve Power Line Stability," *IEEE Trans.* (Power Apparatus and Systems), vol. 87, 1968, pp. 1426–1434.
9. F. W. Keay: "Design of a PSS Sensing Frequency Deviation," *IEEE Trans.*, vol. PAS, March/April 1971.
10. P. L. Dandeno, A. N. Karas, K. R. McClymont, and W. Watson: "Effect of High Speed Rectifier Excitation Systems on Generator Stability Limits," *IEEE Trans. Power Appar. Syst.*, vol. PAS 87, January 1968, pp. 190–196.
11. R. E. Kalman: "The Theory of Optimal Control and the Calculus of Variations," *Mathematical Optimization Techniques*, R. Bellman (ed.), University of California Press, Berkeley, California, 1963.
12. Andrew P. Sage: *Optimum Systems Control*, Prentice-Hall, Inc., Englewood Cliffs, N.J., 1968.
13. Y. Yu and H. A. M. Moussa: "Optimal Stabilization of Multimachine Systems," *IEEE Trans. Power Appar. Syst.*, vol. PAS-91, no. 3, May/June 1972, pp. 1174–1182.
14. O. I. Elgerd and C. E. Fosha, "Optimum Megawatt-Frequency Control of Multiarea Electric Energy Systems," and "The Megawatt-Frequency Control Problem: A New Approach Via Optimal Control Theory," *IEEE Trans. Power Appar. Syst.*, vol. PAS-89, no. 4, April 1970, pp. 556–576.
15. T. W. Reddoch: "Load-Frequency Control Performance Criteria with Reference to the Use of Advanced Control Theory," *Systems Engineering For Power: Status and Prospects*, Henniker, New Hampshire, Aug. 17–22, 1975.

CHAPTER

TEN

ENERGY SYSTEM TRANSIENTS—SURGE PHENOMENA AND SYMMETRICAL FAULT ANALYSIS

The material contained in the last three chapters may, for purposes of classification, be grouped in the following two categories:

1. The theory of the energy system operated in *static* equilibrium. The system models turned out to be *nonlinear algebraic* equations.
2. The theory of *small-scale dynamic* perturbations around the static equilibrium point. The system models in this case were found to be *linear differential* equations with constant parameters.

In this and the following two chapters we shall discuss the energy system subject to major faults or disturbances resulting in dynamic state fluctuations which must be classified as *large scale*. System dynamics in this category will collectively be referred to as *transients*.

10-1 CLASSIFICATION OF SYSTEM TRANSIENTS

Depending upon the *speed* of these transients, we can group them in the following three classifications.

10-1-1 Class A. Ultrafast Transients—Surge Phenomena

This type of transient is caused by atmospheric discharges on the exposed transmission lines and by the abrupt but normal network changes resulting from regular switching operations. These transients are entirely electric in nature and involve, essentially, only the transmission lines themselves. Physically, a disturbance of this type causes an electromagnetic wave that travels with almost the speed of light along the lines, giving rise to reflected waves at the line terminations.

In the case of a 90-mile line, a disturbance wave traveling at 180,000 mils will complete a round trip in 1 ms. *The phenomena associated with these waves take place, therefore, during the first few milliseconds after their initiation.* Due to the always present line losses, the waves attenuate fast and die out after a few reflections.

The high inductances of the transformers in most instances effectively "fence out" these disturbances from the generator windings, but in the reflection process high surge voltages will be built up that can destroy the insulation of the high-voltage equipment. The traveling charges can be discharged to ground via *lightning arresters* that serve as fast-acting "safety valves." However, should the insulation be destroyed at some point, either in a transformer or between the phases of the lines, then this type of transient can lead to a *short circuit*, which is an abrupt and abnormal structural change of the network which will give rise to a new, slower type of transient that belongs to our next classification.

Our major reason for studying class A transients is to provide a basis for selection of the insulation level of the line equipment.

10-1-2 Class B. Medium-Fast Transients—Short-Circuit Phenomena

Under this classification we list those system transients that are caused by abrupt abnormal structural changes—short circuits—in the system.

The vast majority of the short circuits occur on the exposed transmission lines due to insulation breakdowns following surge voltages described above, salt sprays on insulators, birds, and other mechanical causes. In order of severity, the short circuits can be divided into the following types:

1. *Solid, symmetric* short circuit of all three phases. A "symmetric" short circuit is caused by the application of three equal *fault impedances* Z^f between each phase and ground. The short circuit is said to be "solid" if $Z^f = 0$.
2. Short circuit of two phases, with the third phase remaining healthy. The shorted phases may or may not be simultaneously grounded.
3. Short circuit between one phase and ground, with the two remaining phases healthy.

The power transmission capacity of a line subjected to the first type of short circuit will be instantaneously reduced to zero; short circuits of types 2 and 3 will partially cripple the line. As in the case of class A transients, the class B transients are also entirely *electric* in nature, and are determined by the magnetic interplay between the generator windings. The time constants of these windings range from a few cycles of the 60-Hz wave for the "damper" windings to, perhaps, 5 s for the field winding. These transients therefore will be considerably slower than the class A variety. *Since, usually, the first 10 cycles of the short-circuit currents are of greatest practical importance, we will be studying a time range of from 10 to 100 ms following the fault.*

In addition to destroying or reducing the energy-transmitting ability of parts of the system, the short-circuit currents may reach magnitudes far beyond the rated values for generators and transformers. Such high currents, if permitted to persist, may cause *thermal damage* to the equipment. In some instances the resulting high dynamic forces can damage windings or buses. It is important, therefore, to *isolate* a faulty section as soon as possible. Usually, we should not disconnect a larger portion of the system than necessary, and we should not keep it disconnected for longer periods than needed. A large percentage of short circuits are "self-healing"; i.e., upon extinguishing the fault current, the short-circuit path will be deionized, and the insulation is restored. In practice, therefore, one utilizes *reclosure breakers* that automatically close once, twice, or several times, to test whether the line has recovered. Only if the fault persists does the breaker open permanently. Such a closing-opening-closing cycle may take of the order of 1 s or longer.

There are several reasons why we wish to have as accurate data as possible about short-circuit currents and voltages in a system:

1. The interrupting capacity of each circuit breaker in every switching locality must be based upon the most severe short-circuit case.
2. The protective relaying system which is intended to sense the fault and initiate selective switching bases its operation upon the magnitude and directions of fault currents.
3. The magnitude of bus voltages during short circuits determines the transient generator power outputs and thus the "transient stability" of the system.

10-1-3 Class C. Slow Transients—"Transient Stability"

A short circuit is always accompanied by an instantaneous collapse, total or partial, of the bus voltages throughout the system. With the generator voltages thus suddenly dropping, we find an equally sudden reduction of the generator power output. Since the power *input* to the generator stays constant during those first instants before the mechanical turbine controllers come into play, each generator will be subject to a surplus accelerating torque, which, if sustained, can develop into the most dangerous type of transient situation to which a power system can be subjected—mechanical oscillations of the synchronous machine rotors. These *electromechanical* transients may, under unfortunate circumstances, pull some or all of the machines out of synchronism. Such an occurrence constitutes a partial or complete breakdown of the energy system. The system is said

to have reached its *transient-stability limit*. It may take hours to resynchronize a fully "blacked-out" system, and a systems engineer will go to almost any length to avoid such a nightmare. It is therefore extremely important that we be able to simulate such occurrences on computers and learn how to develop switching and load-shedding strategies that will minimize the effects of faults.

These rotor swings, being mechanical in nature, are relatively slow. The actual speed depends upon the *mode* of oscillations. For example, if one machine swings against another in the same power station, the rotors may complete three to four swing cycles per second. If all the machines in the Eastern United States swing as a coherent *block* against the western block, we may measure only three to four swing cycles per minute. A transient-stability study thus may concern itself with time periods that last for a fraction of a second to one minute or longer. In the latter case the thermal processes in the nuclear core or the boiler will change, and it now becomes necessary to take even these portions of the system into account in the simulation.

In this chapter we shall discuss class A transients, and also those class B transients which result from *symmetrical three-phase* short circuits.

In Chap. 11 we shall discuss class B transients following *unbalanced* faults. Finally, in Chap. 12, we shall discuss the transient-stability problems belonging to our class C category.

10-2 TRANSMISSION LINE TRANSIENTS

Overvoltages caused by atmospheric discharges and switching operations are of primary importance as a basis for selection of insulation level and surge protection. A systems engineer also needs to estimate their effect on the protective relaying.

We give a *brief* exposé of these phenomena, with the objective of conveying a general understanding of their nature. Our mathematical models are based on the following simplifying assumptions:

1. Line resistance and shunt conductance are neglected. Omission of these parameters results in equations that have analytical solutions. In addition, the numerical answers typically lie on the "safe side."
2. A three-phase line contains three phase conductors plus one or two protective overhead ground wires, all of which may be involved in a lightning discharge. The magnetic and capacitive coupling between the conductors results in a very complex transient picture. We simplify the analysis by using a "per-phase" model. This assumption leads, under certain conditions, to rather large errors, but on the whole is quite reliable in systems that have solidly grounded neutral. Certainly, in view of our limited objective and the considerable model simplification that it will entail, this is a logical assumption to make in an introductory text.

10-2-1 The Wave Equation and Its Solution

We use Eqs. (6-86) as our point of departure. Upon first setting $R = G = 0$ and then differentiating the first equation with respect to x and the second with respect to t and finally adding the two, we get

$$\frac{\partial^2 v(x, t)}{\partial x^2} = \frac{1}{\kappa^2}\frac{\partial^2 v(x, t)}{\partial t^2} \tag{10-1}$$

For brevity we have introduced

$$\kappa \triangleq \frac{1}{\sqrt{LC}} \tag{10-2}$$

Note that this new parameter has the physical dimension of meters per second, i.e., velocity.

Equation (10-1) is the famous *wave equation*. It has the general solution

$$v(x, t) = v_1(x - \kappa t) + v_2(x + \kappa t) \tag{10-3}$$

where $v_1(\ldots)$ and $v_2(\ldots)$ are *arbitrary* functions of the arguments $x - \kappa t$ and $x + \kappa t$, respectively. The actual shape of these functions is determined by the *initial voltage and current distributions* along the line (compare Example 10-1).

PROOF From the solution equation (10-3) we obtain

$$\frac{\partial^2 v}{\partial x^2} = v_1'' + v_2'' \tag{10-4}$$

$$\frac{\partial^2 v}{\partial t^2} = \kappa^2 v_1'' + \kappa^2 v_2'' \tag{10-5}$$

where the symbols v_1'' and v_2'' mean $d^2 v_1(\ldots)/d(x - \kappa t)^2$ and $d^2 v_2(\ldots)/d(x + \kappa t)^2$ respectively.

Substitution of (10-4) and (10-5) into (10-1) yields an identity. QED.

Equation (10-3) represents the *voltage* solution. The *current* solution is obtained in the following manner.

From our voltage solution we first compute the partial derivative

$$\frac{\partial v}{\partial x} = v_1' + v_2'$$

We thereupon substitute this derivative into the first of Eqs. (6-86)

$$v_1' + v_2' = -L\frac{\partial i}{\partial t} \tag{10-6}$$

Integration with respect to t gives

$$\int^t v_1'\, dt + \int^t v_2'\, dt = -Li(x, t) \tag{10-7}$$

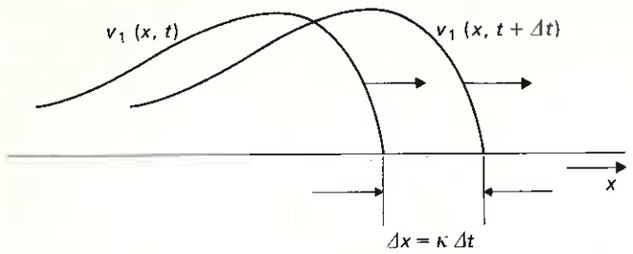

Figure 10-1 Traveling voltage wave.

Evaluation of the integrals gives the result

$$-\frac{1}{\kappa} v_1(x - \kappa t) + \frac{1}{\kappa} v_2(x + \kappa t) = -Li(x, t)$$

Since $L\kappa = \sqrt{L/C} = R_w$ (the *wave impedance* defined by Eq. (6-115)) we finally have the current solution

$$i(x, t) = \frac{1}{R_w} v_1(x - \kappa t) - \frac{1}{R_w} v_2(x + \kappa t) \tag{10-8}$$

10-2-2 Physical Interpretation of Results

Consider the first component v_1 of the voltage solution (10-3). Since the argument $x - \kappa t$ will not change if we increase t and x by the amounts Δt and $\kappa\, \Delta t$, respectively, it is clear that the function $v_1(x - \kappa t)$ represents a wave traveling in positive x direction with the velocity

$$\frac{\Delta x}{\Delta t} = \kappa \qquad \text{m/s} \tag{10-9}$$

We have demonstrated the situation in Fig. 10-1. The component v_2 similarly can be shown to represent a wave traveling in the negative x direction with the same velocity.

Example 10-1 Take, for example, the transmission line in Examples 6-3 and 6-8. It was characterized by the parameters

$$L = 1.21 \times 10^{-6} \text{ H/m and phase}$$

$$C = 9.58 \times 10^{-12} \text{ F/m and phase}$$

The wave velocity is thus

$$\kappa = \frac{1}{\sqrt{LC}} = 2.94 \times 10^8 \text{ m/s (or 180,000 mi/s, approx)}$$

The wave impedance is

$$R_w = \sqrt{\frac{L}{C}} = 356\ \Omega$$

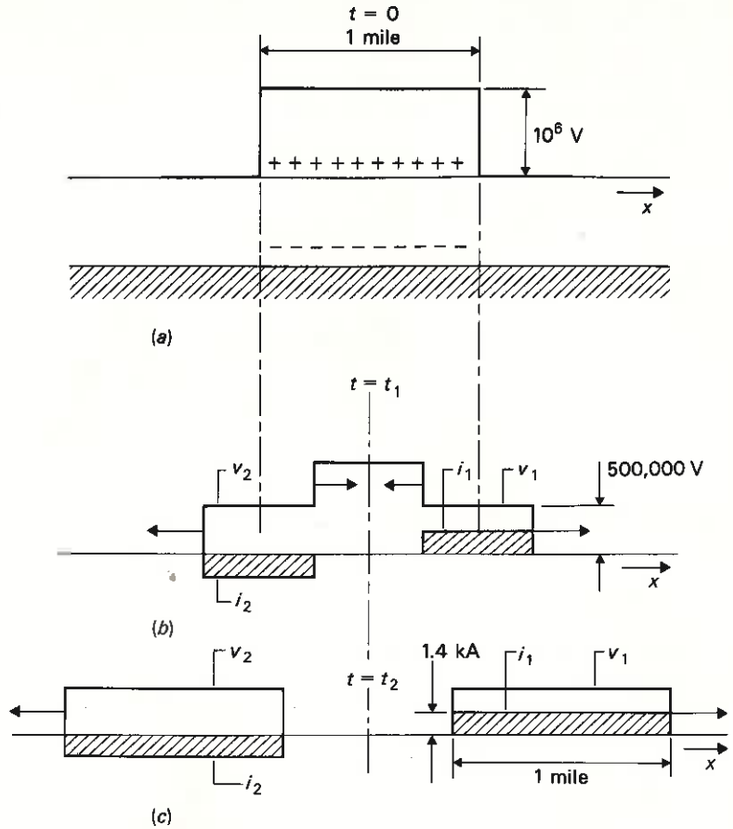

Figure 10-2 Origin of two oppositely traveling voltage-current waves.

Assume that a lightning bolt discharges a uniform positive charge along a one-mile stretch of the line, as shown in Fig. 10-2*a*. Initially, at $t = 0$, we thus find a constant voltage along the one-mile stretch. Let us assume that its magnitude is 1 MV.

The wave equation tells us that the charge just cannot "sit there"; it must travel at the speed κ. For symmetry reasons, half the charge travels to the left and half to the right, and at two different moments later, the voltage picture will be as shown in Fig. 10-2*b* and *c*.

Each voltage wave is accompanied by a current wave of magnitude 500,000/356 = 1.4 kA. Note that the i_1 wave is positive, corresponding to a positive charge traveling in the assumed positive current direction. A positive charge traveling in the negative x direction represents a negative current.

10-2-3 Wave Reflections

When a wave system, here called the *incoming wave*, consisting of a voltage v_i and associated current i_i hits a discontinuity it will result in a *reflected* wave pair v_r and i_r and a *continuing* (or refracted) pair v_c and i_c (Fig. 10-3). The discontinu-

ity may consist of a joint of two lines of different wave impedances R_{w1} and R_{w2}, a junction, or simply a line termination.

We must require that the currents and voltages as measured at the point of discontinuity are the same on each side. The three wave pairs must thus satisfy the equations

$$i_i + i_r = i_c \tag{10-10}$$

$$v_i + v_r = v_c \tag{10-11}$$

But according to Eq. (10-8) we also have

$$\frac{v_i}{i_i} = -\frac{v_r}{i_r} = R_{w1} \tag{10-12}$$

and

$$\frac{v_c}{i_c} = R_{w2} \tag{10-13}$$

By combining the two last equations with Eqs. (10-10) and (10-11) we obtain the reflected and refracted waves in terms of the incoming wave

$$v_r = \alpha v_i \tag{10-14}$$

$$v_c = \beta v_i \tag{10-15}$$

where for brevity we have defined respectively the *reflection* and *refraction coefficients* α and β:

$$\alpha \triangleq \frac{R_{w2} - R_{w1}}{R_{w2} + R_{w1}} \tag{10-16}$$

$$\beta \triangleq \frac{2R_{w2}}{R_{w2} + R_{w1}} \tag{10-17}$$

Example 10-2 Consider the 500 kV/1.4 kA wave pair in Fig. 10-2 that travels in *positive x*-direction. It is hitting the *open-circuited* end of the line. Study the reflection process.

SOLUTION As no line exists beyond the termination point the wavepair v_c/i_c does not exist and we limit our attention to the reflected pair v_r/i_r. The reflection coefficient is obtained by setting $R_{w2} = \infty$ and we get $\alpha = 1$, that is, the reflected and incoming waves have equal voltage magnitudes. Their current magnitudes are thus also equal but of opposite signs.

Figure 10-4 shows how the reflection process unfolds in five easy-to-follow steps. Note the doubling of the voltage for a few dangerous moments.

Due to the ever-present resistance the waves will attenuate as they travel. Their profile will also change.

Note that we have not shown in Figs. 10-2 to 10-4 the regular 60-Hz voltage and currents upon which the waves are superimposed. Due to the extreme speed of the wave phenomena (as we said earlier, they will complete five round trips in 5 ms on a 90-mile line and will then, for all practical purposes, be dissipated), the regular 60 Hz *is essentially constant.*

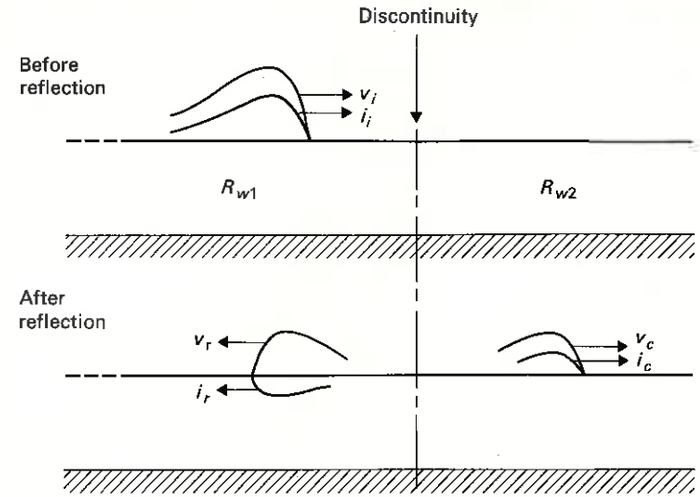

Figure 10-3 Voltage-current wave encountering line discontinuity. Before-and-after wave pictures.

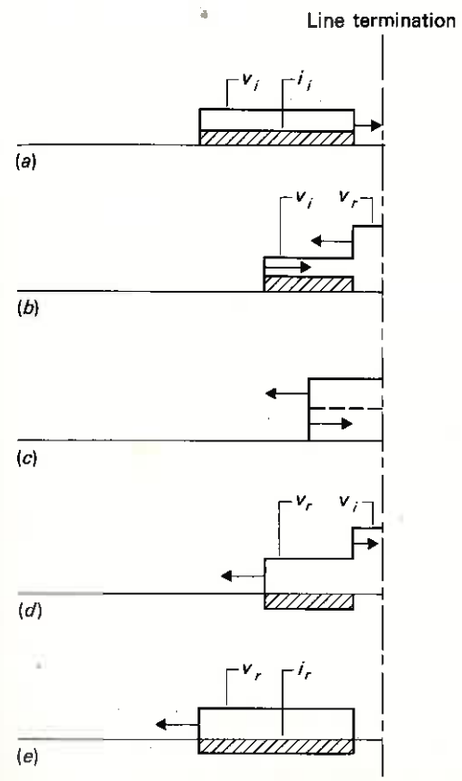

Figure 10-4 Voltage-current wave reflected at open-circuited line end. Reflection process unfolded in step-by-step fashion.

10-2-4 Parameter Lumping

The wave-carrying ability of the transmission line is a consequence of its *continuous-parameter* character. Other physical *continua* (air, water, etc.) also have this capacity.

When simulating line transients on an analog computer, or when performing digital solution of the wave equation, "lumping" of the line parameters becomes a necessity. In Fig. 10-5 we indicate how such a lumping is performed in decreasing degree of coarseness. The LC representation of the line certainly emphasizes its oscillatory character.

Example 10-3 Consider a 90-mile stretch of the line discussed in Example 10-1. If we represent it in the coarsest possible fashion, as shown in Fig. 10-5*b* we get:

$$L_1 = 90 \times 1609 \times 1.21 \times 10^{-6} = 1.75 \times 10^{-1}\ \text{H}$$

$$C_1 = \tfrac{1}{2} \times 90 \times 1609 \times 9.58 \times 10^{-12} = 6.94 \times 10^{-7}\ \text{F}$$

The resonant frequency of the corresponding LC circuit would be $f = 646$ Hz. The "actual" frequency would be $f = 1000$ Hz (since it takes 1 ms for a wave to complete one round trip).

(Compare also Prob. 10-9.)

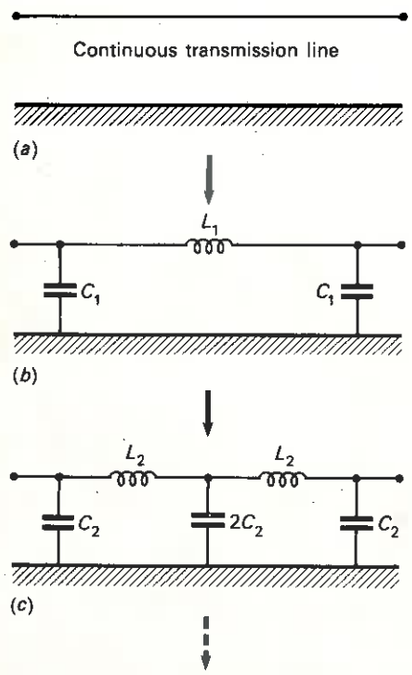

Figure 10-5 Lumped representation of continuous-parameter line.

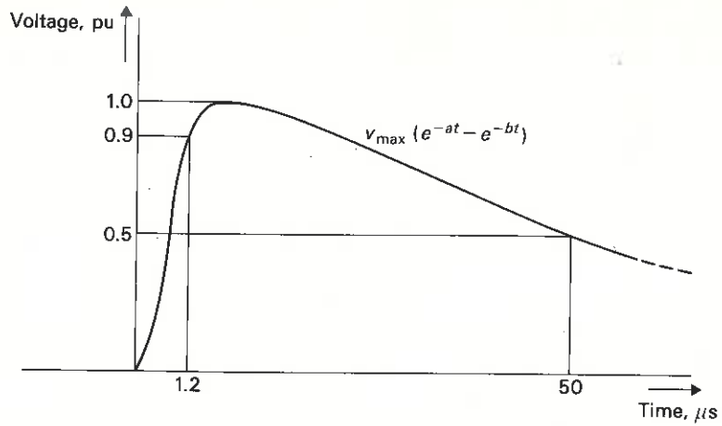

Figure 10-6 Standard test wave.

10-2-5 Overvoltages and Insulation Levels

A three-phase transmission line rated at 345-kV *line* voltage is characterized by an *rms* phase-to-neutral voltage of $345/\sqrt{3} = 199$ kV and a *peak* phase-to-neutral voltage of $199 \times \sqrt{2} = 282$ kV. These are *normally* expected voltage values. Atmospheric disturbances and/or switching transients may subject the apparatus to much higher voltages of impulse type.

All power equipment is normally tested for both the normal ac frequency *and* impulse strength. A typical impulse test wave is the "1.2×50-μs wave" shown in Fig. 10-6. This wave reaches 90 percent of its peak value in 1.2 μs and falls off to 50 percent of peak in 50 μs. Mathematically, this wave consists of two decaying exponentials.

Basic insulation level (BIL) measures the ability to withstand test voltages without disruptive discharge. For example, a transformer intended for use in the above 345-kV system and which has been successfully tested at 800-kV peak, is said to have a BIL of $800/282 = 2.84$ pu.

10-2-6 Circuit Interrupt Devices

As was indicated already in Fig. 1-3, power-switching devices are liberally distributed throughout a power system and constitute in fact one of the most important means of system control. The reader is no doubt familiar with the ease with which low-power circuits can be switched on and off. Interruption of currents in the kiloamp range at voltage levels in the hundreds of kilovolts is a much more difficult problem requiring devices of complicated design and often high cost. We do not intend to discuss here the vast spectrum of *fuses, switches,* and *load-* and *circuit breakers,* etc. that are represented in a modern power system. For our purposes we shall distinguish between *disconnect switches* and

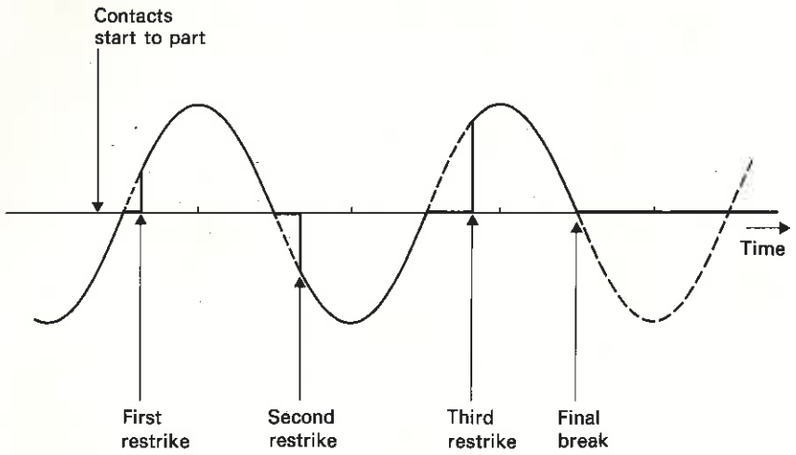

Figure 10-7 Interruption process of alternating current.

circuit breakers. The former device is not designed to interrupt current (except possibly very low loads) but is intended to isolate apparatus that have been disconnected from service.

Circuit interruption under load or fault conditions is accomplished by *circuit breakers,* which are designed to interrupt the largest currents that can conceivably flow in a circuit. CB's can be operated either manually or by automatic command. The current interruption is achieved by movable contacts, which when rapidly parting draw an arc which by various means is forcibly extinguished. The arc extinction can be achieved by an intense stream of air in *air-blast breakers* or by flow of oil in *oil-circuit breakers,* OCB's. Other means like interruption in SF_6 or vacuum or by "magnetic blowout" are also used.

Interruption of an ac current is a "gradual" process as demonstrated in Fig. 10-7 which depicts the deenergizing of a *resistive* load. Following the trip command the movable contacts begin to move apart, and the current is interrupted at the next zero passage. However, enough *dielectric strength* has not developed between the moving contacts and when the voltage across the CB increases to some critical value a first *restrike* occurs. Before final current break is accomplished several similar restrikes will typically take place.

Interrupting time of a CB is measured in cycles and indicates the time interval between energizing the trip coil and final current clearing. Modern air-blast breakers can clear in one cycle whereas old OCB's may require ten or more cycles for total fault clearing.

A faulted synchronous generator supplies the largest currents immediately following the fault, when the stator dc transient adds to the ac "subtransient" component to form one or two extreme current peaks (Sec. 4-13-10). A CB must withstand the destructive effects of these peaks. The actual interruption process

takes place when these two fast decaying components are either partly or completely gone and the slower-decaying "transient" component remains.

The *interrupt capacity* of a CB is expressed either in kiloamps *rms* or in corresponding megavoltamperes. The reason for the latter rating practice is understood when we realize that the total breaker job consists of *first* interrupting the current and, *second,* building up full insulation against the system voltage. For example, consider a CB designed to interrupt 5 kA, rms, in a 66-kV network. Its rated interrupt megavoltampere capacity would equal

$$5 \times \frac{66}{\sqrt{3}} = 191 \text{ MVA/phase} \tag{10-18}$$

or 573 MVA total three-phase.

10-2-7 Switching Transients

Rapidly appearing and fast disappearing waves, caused by atmospheric disturbances like those discussed above, represent one type of transmission line transients. Another type of fast transients of considerable practical significance is generated during normal switching operations. Collectively, we refer to these as *switching transients.* The simplest type of switching transient is generated by CB *closing* operations, when a transmission line is being energized. This situation is depicted in Fig. 10-8. As the circuit breaker is closed, a wave is initiated that will travel down the line in the manner described above. The amplitude of the wavefront depends upon at what instant of the 60-Hz cycle the breaker is closing. The worst case occurs if it closes at the maximum point. If the 60-Hz voltage has an rms value $|V|$, the wave amplitude will then be $\sqrt{2}|V|$. Upon reflection, this wave evidently can cause a voltage of magnitude $2\sqrt{2}|V|$.

Switching transients occurring during CB *opening* maneuvers can also give rise to dangerous overvoltages. For purposes of illustration, consider the case shown in Fig. 10-9*a*. A shunt capacitor C is connected to the end of a transmission line which we have lumped into a single π link. Let us consider the following switching situation.

The capacitor is to be disconnected from the network, and for that purpose we send a trip command to the CB the contacts of which start to move apart. At the moment t_1, when the current wave is going through a zero, the arc is deionized and the current ceases. At this moment, however, the capacitor is

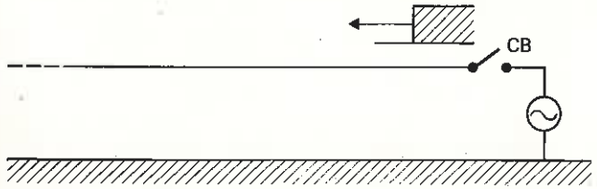

Figure 10-8 Initiation of switching transient.

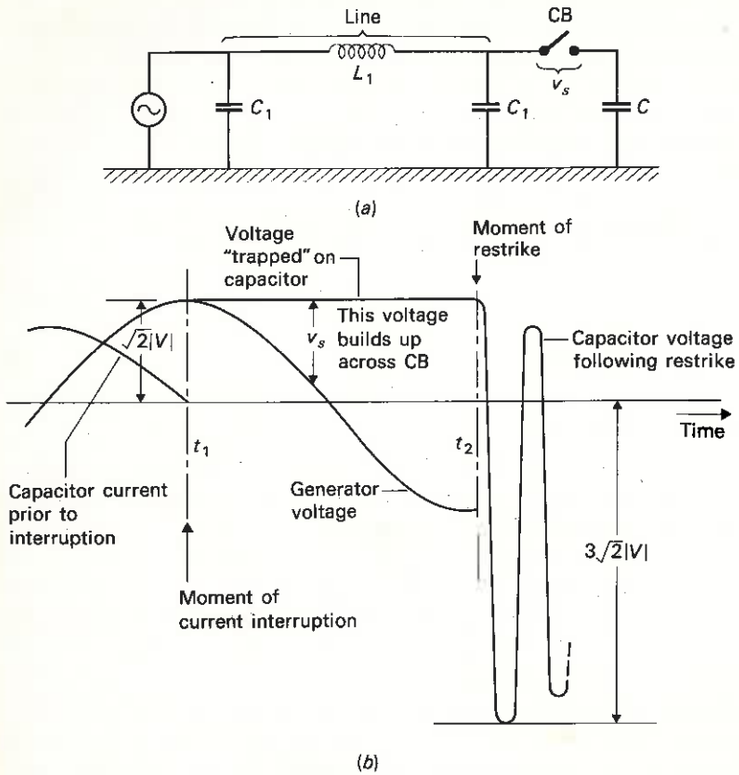

Figure 10-9 Voltage "multiplication" following restrike of switched capacitor.

charged to full peak voltage $\sqrt{2}|V|$. As the network voltage reverses, we therefore build up a voltage v_s across the CB contacts. If the circuit breaker can build up its recovery strength faster than the oncoming voltage v_s, the switching operation will be successful. If not, we will obtain a restrike.

In Fig. 10-9*b* we assume that such a restrike occurs at the most dangerous moment t_2, when the voltage v_s is at its maximum value. The restrike causes a fast oscillatory voltage in the *LC* circuit. The frequency of this transient will, typically, be ten to twenty times the system frequency (compare Example 10-3).

As we show in Fig. 10-9*b*, the voltage overshoot will amount to $3\sqrt{2}|V|$ volts.

10-3 SYMMETRICAL SHORT CIRCUITS

In the remaining sections of this chapter we shall concern ourselves with the study of *symmetrical short circuits* as defined in Sec. 10-1-2. When in addition the symmetric fault is *solid* it constitutes the most severe fault to which a system can

be subject. Although this type of short is much less common than, say, a single-line-to-ground fault, its severity justifies our paying it special attention.

Consider for example a symmetric fault occurring on line L5 in the system depicted in Fig. 1-4. The generators at buses 1 and 2 plus those of the neighboring system, would immediately start feeding current into the fault. The currents would be particularly heavy at each end of the faulted line and the voltages of buses 3 and 5 would be severely depressed. The currents would be heavy throughout the system and all the bus voltages would be sagging, but the severity of these effects would diminish with the distance to the fault.

10-3-1 Thévenin's Theorem

A short circuit represents a *structural network change* equivalent with that caused by the addition of an impedance (or, in the case of a symmetric short, three equal impedances) at the place of fault. The *changes* in voltages and currents that will result from this structural change can be conveniently analyzed by means of *Thévenin's theorem* which states:

The changes that take place in the network voltages and currents due to the addition of an impedance between two network nodes are identical with those voltages and currents that would be caused by an emf placed in series with the impedance and having a magnitude and polarity equal to the prefault voltage that existed between the nodes in question and all other active sources being zeroed.

To obtain the postfault currents and voltages in the network, we must superimpose these changes on the prefault currents and voltages.

We shall find the theorem extremely useful in this chapter and the next in determining the system-wide effects of short circuits.

Example 10-4 Use Thévenin's theorem to find the short-circuit current that will flow through the switch *S* in Fig. 10-10*a* upon closing.

SOLUTION We first seek the "prefault" voltage across *S*. As both prefault currents i_1 and i_2 equal 5 A the voltages of nodes *A* and *B* equal

$$V_A = +5 \cdot 5 = +25 \text{ V}$$

$$V_B = +5 \cdot 15 = +75 \text{ V}$$

respectively.

The prefault voltage across *S* thus equals 50 V with *B* positive relative to *A*. Thus the "fault" current will flow in the direction indicated by the arrow in Fig. 10-10*a*. The impedance as measured between A-B *with E zeroed* equals 7.5 Ω and is found in three easy-to-follow steps in Fig. 10-10*b*. Thus the current through the switch equals

$$i^f = \frac{50}{7.5} = 6.67 \text{ A}$$

The postfault current through the battery equals the sum of the prefault current (10 A) *plus* that portion of i^f (3.33 A) that will flow through the battery. The postfault battery current will thus equal 10 + 3.33 = 13.33 A.

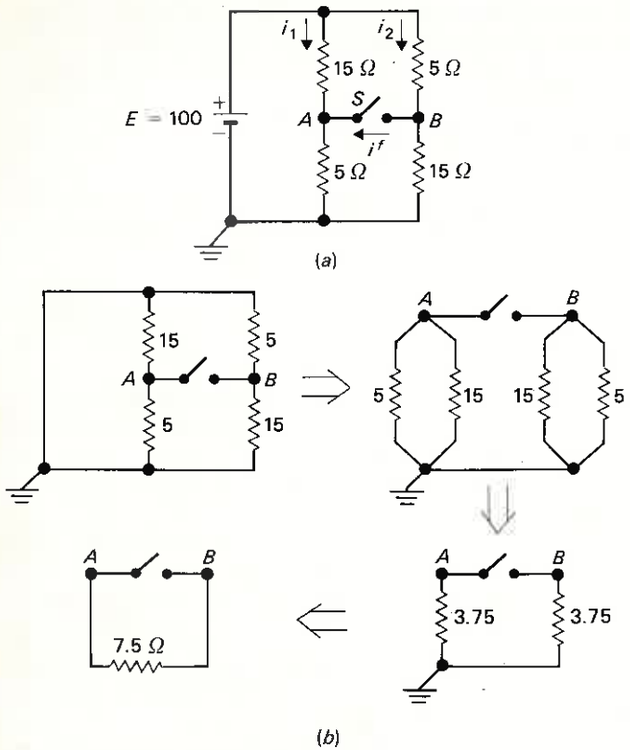

Figure 10-10 Finding the fault current in dc circuit by means of Thévenin's theorem.

10-3-2 SC Analysis of the Two-Bus System

To demonstrate the basic steps in short-circuit analysis we make use of our old friend, the two-bus system. The "prefault" system is depicted in Fig. 10-11. It is assumed that a symmetric short occurs on bus 1 which is structurally equivalent with closing the "fault breaker" CB in our one-line diagram. Z^f is the fault impedance, assumed equal in all three phases.

A. System data and operating specifications The two generators and transformers are assumed of equal rating—300 MVA—which is chosen as our three-phase base power in the following analysis. The line is represented by a series reactance of 0.20 pu Ω/phase.

In the prefault state the loads at buses 1 and 2 have unity power factors and are represented by two shunt resistors of 2 and 0.8 pu Ω respectively. The prefault bus voltages are both kept at $|V_1| = |V_2| = 1$ pu. The generators are sharing the total megawatt load equally.

B. Prefault current and voltage picture From the above data we compute

$$P_{D1} = \frac{1^2}{2} = 0.5 \text{ pu MW}$$

$$P_{D2} = \frac{1^2}{0.8} = 1.25 \text{ pu MW}$$

$$Q_{D1} = Q_{D2} = 0$$

$$P_{G1} = P_{G2} = \frac{1.75}{2} = 0.875 \text{ pu MW}$$

The line will therefore carry $1.25 - 0.875 = 0.375$ pu MW in the direction $1 \to 2$.

Equation (3-49) yields the power angle

$$0.375 = \frac{1 \times 1}{0.2} \sin \delta$$

$$\therefore \quad \delta = 4.30°$$

Equations (3-50) and (3-51) give the reactive flows in each line end

$$Q_1 = -Q_2 = \frac{1 - 1 \cos 4.30°}{0.2} = 0.014 \text{ pu Mvar}$$

Based upon these power data and by using the formula (2-28) we compute the *prefault currents* which have been identified by arrows in Fig. 10-11. *Note that we have defined the prefault bus voltage V_1^0 as reference phasor.*

C. Thévenin's network equivalent In applying Thévenin's theorem we first construct the so-called "Thévenin's network equivalent." The prefault voltage V_1^0 at

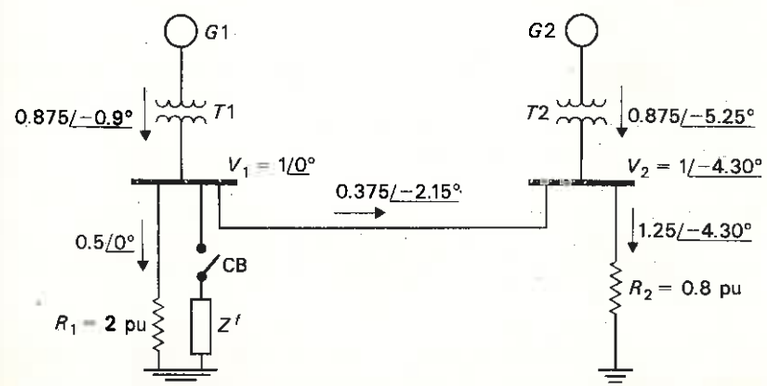

Figure 10-11 Two-bus example system used for symmetrical fault current calculation.

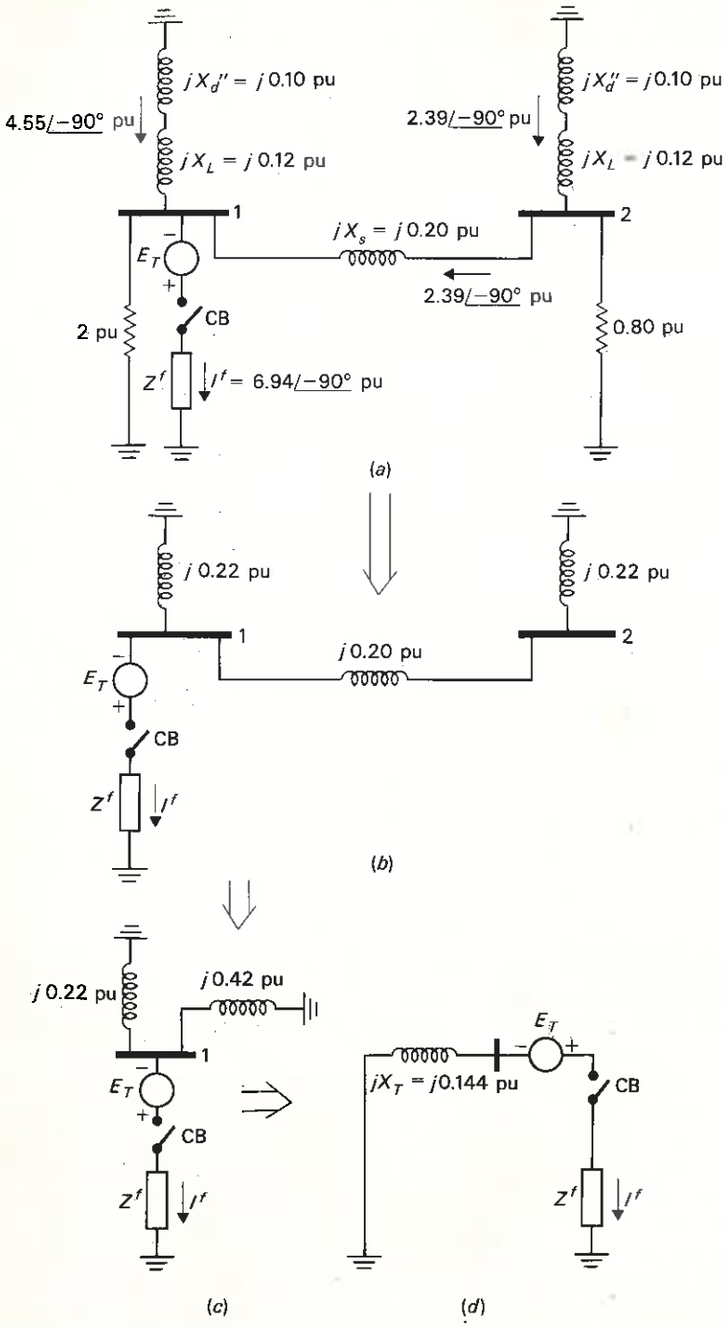

Figure 10-12 Step-by-step development of the "Thévenin's equivalent" for a short at bus 1.

bus 1 equals 1 pu. The theorem says that we must place an emf, the "Thévenin's emf" $E_T = V_1^0$, in series with the short-circuit branch. This we have done in Fig. 10-12*a*. All the other network components are represented with their equivalent impedances. We comment briefly on the network in Fig. 10-12*a*:

1. The load resistances remain the same as in Fig. 10-11.
2. The line resistance and capacitance are omitted and only the series reactance has been included.
3. The transformer leakage impedances are assumed purely reactive, $j0.12$ pu.
4. For the generators we have "zeroed" the emf's and retained only their internal impedances. Assuming that we are interested in the ac component of the current *immediately following the fault* then we should, according to our discussion in Sec. 4-13-10, choose the *subtransient* reactance 0.1 pu Ω (see also Table 4-1).

D. Current changes brought about by E_T Thévenin's theorem states that the actual *changes* in currents resulting from closing of CB in Fig. 10-11 equal those caused by the insertion of the emf E_T in Fig. 10-12. These latter currents are sometimes referred to as "Thévenin's currents." We now proceed to compute these currents.

For this purpose we simplify the equivalent network in Fig. 10-12*a* in three self-explanatory steps. Note that in the first step we omit, for sake of simplicity, the shunt load resistances. For example, at bus 2 we have replaced the parallel combination of 0.80 and $j0.22$ (which in actuality equals $0.056 + j0.205$) by $j0.22$. This seems like a reasonable approximation.

From the final network in Fig. 10-12*d* we obtain for the current through the "fault breaker":

$$I^f = \frac{1}{j0.144} = 6.94\angle{-90°} \text{ pu kA} \tag{10-19}$$

(We have set $Z^f = 0$, corresponding to a *solid* fault.)

This current obviously is the total fault-current from both generators. We find the contribution from each by noting that the total current divides in inverse impedance ratio. For example, the generator $G1$ will contribute

$$\frac{0.42}{0.22 + 0.42} \times (6.94\angle{-90°}) = 4.55\angle{-90°} \text{ pu kA} \tag{10-20}$$

E. Postfault current and voltage picture By superimposing the current and voltage changes caused by E_T upon those existing in the prefault state we obtain the total postfault current and voltage picture. For example, the postfault current supplied by generator $G1$ equals $0.875\angle{-0.9°} + 4.55\angle{-90°} = 4.64\angle{-79°}$ pu. Similarly we compute the remaining postfault currents of interest. We have summarized the postfault currents in the diagram of Fig. 10-13. Note that we have omitted the load resistances, which we earlier concluded influence the situation insignificantly.

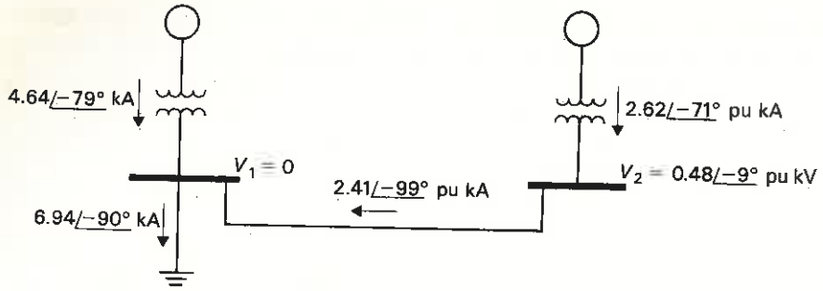

Figure 10-13 Distribution of short-circuit currents for the fault in Fig. 10-11.

In Fig. 10-13 we have also indicated the postfault bus voltages. The bus voltage V_1^f will of course be zero. The bus voltage V_2^f will equal V_2^0 plus the change due to E_T, that is,

$$V_2^f = 1\underline{/-4.30°} - (2.39\underline{/-90°})(j0.22) = 0.48\underline{/-9°} \text{ pu kV} \qquad (10\text{-}21)$$

10-3-3 Discussion of Results

Several important observations can be made from the simple example just treated:

1. The normal prefault "load" current phasors (Fig. 10-10) are predominantly *in phase with the voltage.*
2. The short-circuit gives rise to current *changes* ("Thévenin's currents") having their predominant components *lagging the* voltage by 90°.
3. The magnitudes of the Thévenin currents exceed those of the "load" currents by a significant factor (compare Figs. 10-11 and 10-12).
4. As a result of the above magnitude and phase differences the actual fault currents approximately equal the Thévenin currents (compare Figs. 10-12 and 10-13). *Due to this fact one often completely disregards the prefault load currents in computing the fault currents.*
5. The choice of generator impedance† must be a judicious one. In the above example we chose the *subtransient* reactance. Had we instead been interested in the fault current as measured two to three cycles following the fault then we should have chosen the *transient* reactance X_d'.
6. Although we have claimed that the simultaneous short circuit of all three phases is "symmetric" this is not quite so. The short-lived transient dc components which are generated in a faulted generator (Sec. 4-13-9) and which

† The concept of impedance makes strict mathematical sense only when the network is in sinusoidal steady state. Since the 60-Hz component decays relatively slowly, this approximation is a very good one.

are of different magnitudes in each phase give initially a nonsymmetric short-circuit current set. The effect of this dc component is added in some empiric fashion. For example, in determining the current interrupting capacity of a breaker, we use the computed ac (subtransient) component multiplied by a factor that depends upon the speed of the breaker. The following recommendations are common:

Two-cycle breaker:	1.4
Three-cycle breaker:	1.2
Eight-cycle breaker (or slower):	1.0

10-3-4 Short-Circuit Capacity, SCC

In reducing the network in Fig. 10-12 we obtained in the end the Thévenin's equivalent in Fig. 10-12*d*, consisting of the "Thévenin emf" E_T in series with the "Thévenin reactance" X_T. Ours was a simple system requiring a simple network reduction process. *However, we can obtain the same simple "Thévenin's equivalent" for a general n-bus system* (compare Eq. (10-36)).

For a solid fault ($Z^f = 0$) the fault current magnitude will equal

$$|I^f| = \frac{|E_T|}{X_T} \qquad (10\text{-}22)$$

The product of the *prefault* bus voltage and the *postfault* current is referred to as *short-circuit capacity* (SCC) or *fault level* of the bus in question. By definition it has the value

$$|\text{SCC}| \triangleq |E_T|\,|I^f| = \frac{|E_T|^2}{X_T} \quad \text{MVA} \qquad (10\text{-}23)$$

If $|E_T|$ is measured in kilovolt *phase* voltage the SCC comes out in megavoltamperes per phase. With $|E_T|$ inserted in kilovolt *line* voltage SCC will be expressed in megavoltamperes three-phase. With $|E_T|$ in per unit $|\text{SCC}|$ will also be in per-unit megavoltamperes.

As E_T equals the prefault voltage of the shorted bus and as this voltage normally has a magnitude of approximately 1 pu, Eq. (10-23) yields

$$|\text{SCC}| \approx \frac{1}{X_T} \quad \text{pu MVA} \qquad (10\text{-}24)$$

For example, in the above two-bus example we had found $X_T = 0.144$ pu Ω. Thus the SCC of bus 1 equals 1/0.144 = 6.94 pu MVA. As the base power was 300 MVA this corresponds to 2090 MVA total three-phase. Because of the symmetry bus 2 will have an equal fault level.

The SCC has a direct bearing upon choice of circuit breakers, which obviously must have an interrupt megavoltampere capacity equaling at least the fault level value for the bus in question.

There is a direct relationship between the SCC and the "voltage stiffness" of a system.

The diagram of Fig. 10-12*d* informs us that when a load Z^f is connected to the bus the voltage drop of that bus will be directly proportional to X_T. A perfectly "voltage stiff" (or "infinite") bus requires that $X_T = 0$. However, according to Eq. (10-24) such a bus has an infinite fault level.

Clearly, these are conflicting requirements. The fault levels increase with system voltage. At 230 kV fault levels can reach 15,000 MVA. The strongest networks in the United States have fault levels approaching 100 GVA. The SCC's have a tendency to grow as new generators are added and additional lines are built. Sometimes one must install artificial series reactors to reduce the fault levels.

Example 10-5 In Example 5-12 the short-circuit current at the 4.8 kV tertiary of a three-winding transformer had been computed to equal 9.28 pu on a 15-MVA base. This corresponds to a fault level of 9.28 × 15 = 139 MVA. One wishes to reduce this value to 70 MVA by adding equal series reactor units in each phase of the 69-kV feeder line (see Fig. 5-22). Find the reactance of each unit.

SOLUTION Reduction of the |SCC| from 139 to 70 MVA means a reduction of the short-circuit current from 9.28 to 4.67 pu. The reactance value, 0.1078 pu, in Fig. 5-22*d* must therefore be increased to 1/4.67 = 0.2141 pu, i.e., we must add an extra reactance of 0.2141 − 0.1078 = 0.1063 pu per phase.

At a voltage level of 69 kV and a base power of 15 MVA 1 pu impedance equals $69^2/15 = 317\ \Omega$. Thus we need to install three equal reactors each having a reactance of

$$0.1063 \times 317 = 33.7\ \Omega$$

10-4 SYSTEMATIC SHORT-CIRCUIT COMPUTATIONS

To involve the digital computer in short-circuit computations it is necessary to develop *systematic, general* computational procedures. The network reduction technique used in the preceding example can be used only in "textbook" examples of low dimensionality. We shall presently develop a technique that possesses full generality, i.e., it is directly applicable to an n-bus system.

10-4-1 Network Model

Consider the part of the n-bus system depicted in Fig. 10-14. It contains bus q at which we shall apply the symmetrical three-phase short circuit. The prefault bus voltages constitute an n vector

$$\mathbf{V}^0_{\text{bus}} = \begin{bmatrix} V^0_1 \\ \vdots \\ V^0_q \\ \vdots \\ V^0_n \end{bmatrix} \tag{10-25}$$

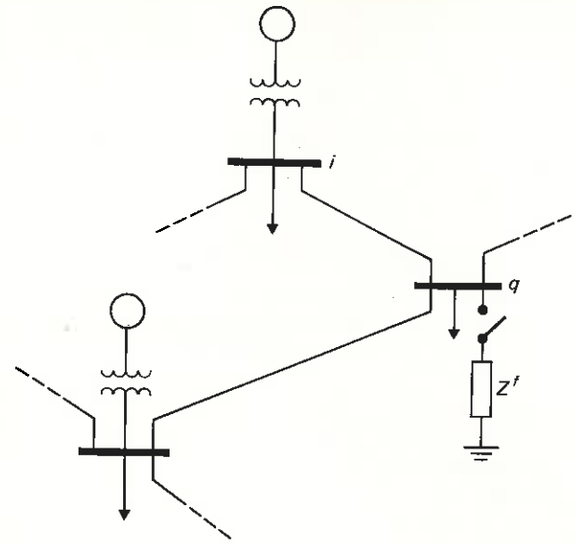

Figure 10-14 Section of general n-bus system.

These prefault voltages can be obtained from a standard power-flow analysis of the type described in Chap. 7.

Upon zeroing all active sources and after representing the generators, transformers, lines, and loads by their appropriate impedances we arrive at the "Thévenin's network" in Fig. 10-15. The effect of the fault is, as usual, represented by the "Thévenin emf" $E_T = V^0_q$.

In this network the bus voltages represent the *changes* caused by the fault. We name these changes† $\Delta V_1, \ldots, \Delta V_n$ and summarize them in the n-dimensional *Thévenin voltage vector*

$$\mathbf{V}_T \triangleq \begin{bmatrix} \Delta V_1 \\ \vdots \\ \Delta V_q \\ \vdots \\ \Delta V_n \end{bmatrix} \tag{10-26}$$

Thévenin's theorem now states that the postfault bus voltages which constitute the components of the n vector $\mathbf{V}^f_{\text{bus}}$ are obtained by superposition, i.e.,

$$\mathbf{V}^f_{\text{bus}} = \mathbf{V}^0_{\text{bus}} + \mathbf{V}_T \tag{10-27}$$

† These changes are not necessarily small (as was the case in Chap. 9).

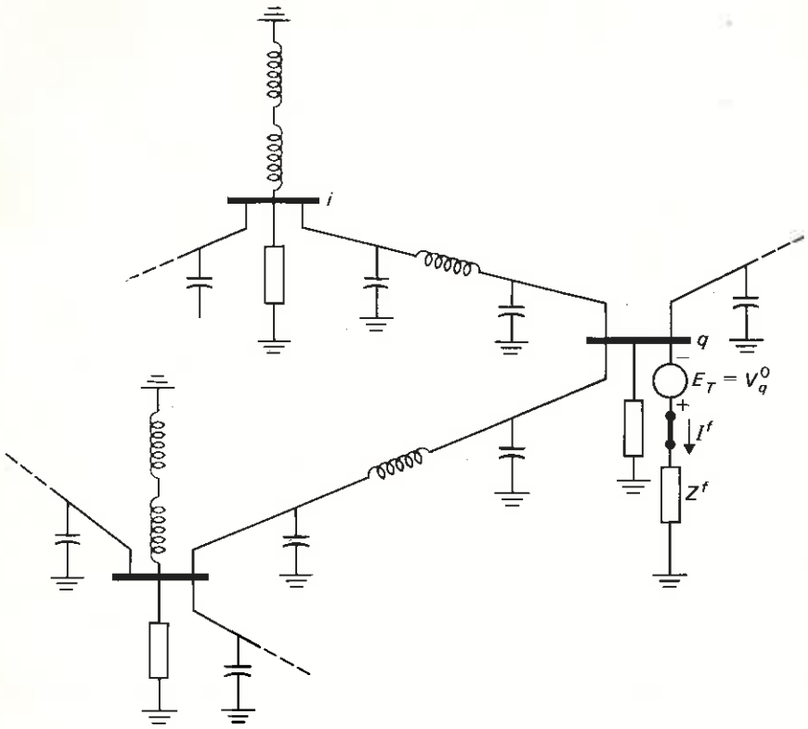

Figure 10-15 "Thévenin equivalent" of the network in Fig. 10-14.

10-4-2 Z_{bus} Network Representation

The n-bus system in Fig. 10-15 can be represented by an $n \times n$ $\mathbf{Z}_{bus}$ matrix.† In terms of this matrix the relationship between bus voltages and injected bus currents are given by Eq. (7-11), i.e.,

$$\mathbf{V}_{bus} = \mathbf{Z}_{bus}\mathbf{I}_{bus} \tag{10-28}$$

In the network of Fig. 10-15 bus currents are injected at *one bus only*, i.e., at bus q in the amount $-I^f$. The bus current vector thus equals the "fault current vector"

$$\mathbf{I}_{bus} \triangleq \mathbf{I}^f = \begin{bmatrix} 0 \\ \vdots \\ -I^f \\ \vdots \\ 0 \end{bmatrix} \leftarrow q\text{th component} \tag{10-29}$$

† It should be noted that it is *not* the same $\mathbf{Z}_{bus}$ matrix as we introduced in Chap. 7. In the present case we have represented the generators and loads with their impedances. In Chap. 7 they were *not* included as part of the network.

We have already observed that the bus voltages equal $\mathbf{V}_T$. From Eq. (10-28) we thus have

$$\mathbf{V}_T = \mathbf{Z}_{bus}\mathbf{I}^f \tag{10-30}$$

Upon substitution into Eq. (10-27) we finally have

$$\mathbf{V}_{bus}^f = \mathbf{V}_{bus}^0 + \mathbf{Z}_{bus}\mathbf{I}^f \tag{10-31}$$

10-4-3 Solution of Vector Equation

The vector equation (10-31) contains $n + 1$ unknowns: the n postfault bus voltages V_i^f plus the fault current I^f. We need therefore one more equation and find it by realizing that the postfault bus voltage V_q^f is related to the fault current I^f through

$$V_q^f = Z^f I^f \tag{10-32}$$

As we proceed with our analysis we shall write the vector equation (10-31) in component form

$$\begin{aligned} V_1^f &= V_1^0 - z_{1q}I^f \\ &\cdots\cdots\cdots \\ V_q^f &= V_q^0 - z_{qq}I^f \\ &\cdots\cdots\cdots \\ V_n^f &= V_n^0 - z_{nq}I^f \end{aligned} \tag{10-33}$$

If Eq. (10-32) is substituted into the qth equation (10-33), we obtain directly the following simple expression for the fault current:

$$I^f = \frac{V_q^0}{Z^f + z_{qq}} \tag{10-34}$$

Since V_q^0 is assumed known, so is the fault current. We therefore substitute I^f into Eq. (10-33) and obtain the following final formulas for the postfault bus voltages:

$$\begin{aligned} V_i^f &= V_i^0 - \frac{z_{iq}}{Z^f + z_{qq}} V_q^0 \qquad i \neq q \\ V_q^f &= \frac{Z^f}{Z^f + z_{qq}} V_q^0 \end{aligned} \tag{10-35}$$

If the short circuit is *solid* (that is, $Z^f = 0$), these formulas simplify to

$$\begin{aligned} I^f &= \frac{V_q^0}{z_{qq}} \\ V_q^f &= 0 \\ V_i^f &= V_i^0 - \frac{z_{iq}}{z_{qq}} V_q^0 \qquad i \neq q \end{aligned} \tag{10-36}$$

(Note that z_{qq} represents the Thévenin reactance X_T in Eq. (10-22).)

Our analysis has rendered the values for the fault current I^f and the n postfault bus voltages V_i^f. We need also to know the postfault currents in all branches of the network. These can be obtained from the same formulas (7-50) as we used in our earlier power-flow studies.

Example 10-6 We shall exemplify the above general analysis method on the three-bus system shown in Fig. 7-4. 100- and 200-MVA generators are feeding, via step-up transformers, power into buses 1 and 2 respectively. The three transmission lines are assumed of equal impedance, $j0.20$ pu on 100 MVA base. Find the SCC at all three buses. Find all short-circuit currents and bus voltages following a solid symmetrical short of bus 3. All three prefault bus voltages are assumed to have 1 pu magnitude. Generator plus transformer reactances equal 0.30 pu based upon respective ratings.

SOLUTION Upon representing the generators, transformers, and lines with their internal reactances the network equivalent in Fig. 10-16 results. All impedances are expressed on a three-phase base power of 50 MVA. Note that we have omitted load impedances and shunt capacitances of the lines. (In a real-life study there is no need to make these simplifications as inclusion of these components represents only a slightly added data increase.)

The network in Fig. 10-16 is actually so simple that we could easily use "longhand" reduction methods of the type we employed for the two-bus system. The reader is encouraged to do so and check the SC data we are about to compute.

We first form the bus admittance matrix for the network in Fig. 10-16. Using Eqs. (7-39) and (7-40) we obtain

$$y_{11} = \frac{1}{j0.15} + \frac{1}{j0.1} + \frac{1}{j0.1} = -j26.67$$

$$y_{22} = \frac{1}{j0.075} + \frac{1}{j0.1} + \frac{1}{j0.1} = -j33.33$$

$$y_{33} = \frac{1}{j0.1} + \frac{1}{j0.1} = -j20.0$$

$$y_{12} = y_{21} = -\frac{1}{j0.1} = j10$$

$$y_{13} = y_{31} = -\frac{1}{j0.1} = j10$$

$$y_{23} = y_{32} = -\frac{1}{j0.1} = j10$$

We can now assemble the bus admittance matrix

$$\mathbf{Y}_{\text{bus}} = \begin{bmatrix} -j26.67 & j10 & j10 \\ j10 & -j33.33 & j10 \\ j10 & j10 & -j20 \end{bmatrix} \tag{10-37}$$

By inversion of $\mathbf{Y}_{\text{bus}}$ we get

$$\mathbf{Z}_{\text{bus}} = \begin{bmatrix} j0.073 & j0.0386 & j0.0558 \\ j0.0386 & j0.0558 & j0.0472 \\ j0.0558 & j0.0472 & j0.1014 \end{bmatrix} \tag{10-38}$$

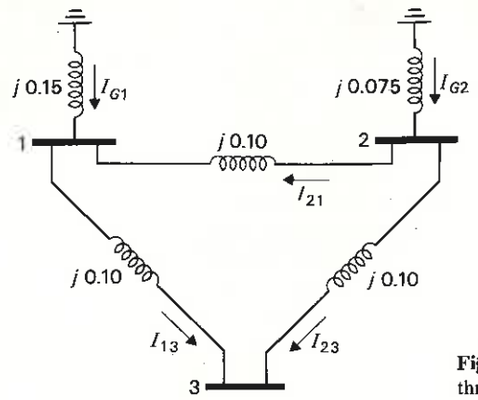

Figure 10-16 "Thévenin equivalent" of three-bus example.

Using the first of formulas (10-36) we compute the magnitude of the short-circuit current in the fault. We obtain, for a short at bus 1

$$|I^f| = \frac{1}{0.073} = 13.7 \text{ pu}$$

for a short at bus 2

$$|I^f| = \frac{1}{0.0558} = 17.9 \text{ pu}$$

for a short at bus 3

$$|I^f| = \frac{1}{0.1014} = 9.86 \text{ pu}$$

Remembering that the base power was 50 MVA, the fault levels of the three buses are 685, 895, and 493 MVA respectively. (Why is a fault on bus 2 most severe?)

For a solid short at bus 3 the last two of Eqs. (10-36) reveal that the bus voltages will drop to the following values:

$$V_1^f = 1.00 - \frac{j0.0558}{j0.1014} \times 1.00 = 0.450 \text{ pu}$$

$$V_2^f = 1.00 - \frac{j0.0472}{j0.1014} \times 1.00 = 0.535 \text{ pu}$$

$$V_3^f = 0$$

The short-circuit currents on the three lines are, respectively,

$$|I_{12}| = \frac{|0.450 - 0.535|}{0.1} = 0.850 \text{ pu}$$

$$|I_{23}| = \frac{|0.535 - 0|}{0.1} = 5.35 \text{ pu}$$

$$|I_{31}| = \frac{|0 - 0.450|}{0.1} = 4.50 \text{ pu}$$

10-5 $\mathbf{Z}_{bus}$ BUILDING ALGORITHMS

The above three-bus example demonstrates the ease with which the short-circuit computations proceed *once the* $\mathbf{Z}_{bus}$ *matrix is known.* We found $\mathbf{Z}_{bus}$ by first assembling the $\mathbf{Y}_{bus}$ matrix and then inverting the latter. $\mathbf{Y}_{bus}$ assembly is quite simple utilizing the formulas we derived in Chap. 7.

For large systems this approach becomes unwieldy because of the need of inverting a very large matrix. It then becomes much more computer efficient to use *direct* assembly methods for $\mathbf{Z}_{bus}$. With such methods one builds the $\mathbf{Z}_{bus}$ matrix "from scratch," adding one network branch at a time until the total network is assembled. We shall introduce the reader to this technique by using again the three-bus system as an example.

10-5-1 Interpretation of the $\mathbf{Z}_{bus}$ Matrix

We have redrawn the Thévenin network in Fig. 10-16 as a "three-port" network shown in Fig. 10-17. For this network the $\mathbf{Z}_{bus}$ formulation reads in detailed form

$$\begin{aligned} V_1 &= z_{11}I_1 + z_{12}I_2 + z_{13}I_3 \\ V_2 &= z_{21}I_1 + z_{22}I_2 + z_{23}I_3 \\ V_3 &= z_{31}I_1 + z_{32}I_2 + z_{33}I_3 \end{aligned} \tag{10-39}$$

The V_i's are the voltages between the ports and the ground reference. The I_i's are the injected port currents.

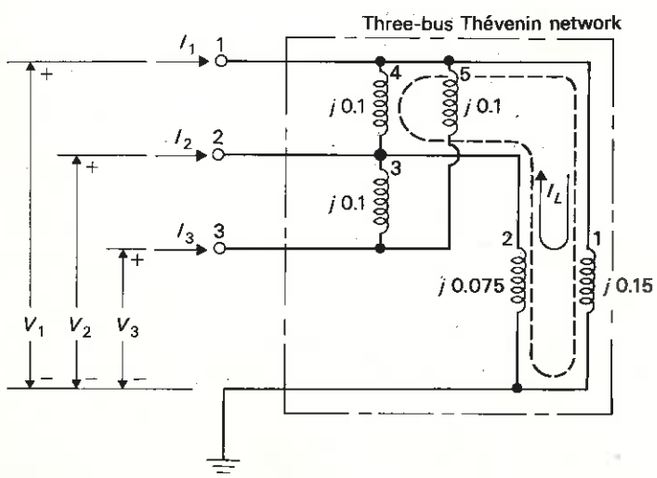

Figure 10-17 Three-bus system in Fig. 10-16 depicted as an "n-port network."

From Fig. 10-17 we now easily interpret the meaning of the nine elements of the $\mathbf{Z}_{bus}$ matrix. For example, if we inject 1 A into port 1 but leave ports 2 and 3 open, Eq. (10-39) simplifies to

$$\begin{aligned} V_1 &= z_{11} \\ V_2 &= z_{21} \\ V_3 &= z_{31} \end{aligned} \tag{10-40}$$

Thus, by computing (or measuring) the three terminal voltages we obtain the first column in the $\mathbf{Z}_{bus}$ matrix. For example, the voltage between port 1 and ground (with ports 2 and 3 open) equals

$$V_1 = j1 \times \frac{(0.06667 + 0.075) \times 0.15}{0.06667 + 0.075 + 0.15} = j0.073 \text{ pu}$$

which checks with element z_{11} in the matrix (10-38).

10-5-2 Step-by-Step $\mathbf{Z}_{bus}$ Assembly

Our example system consists of five branch elements numbered 1 to 5 in Fig. 10-17. We now proceed to assemble the 3×3 $\mathbf{Z}_{bus}$ matrix by adding these elements one by one. As we go from step to step we are particularly interested to find the algorithm which takes us from the "old" bus impedance matrix $\mathbf{Z}_{bus}^{old}$ to the "new" one $\mathbf{Z}_{bus}^{new}$. The impedance of each "new" branch that we add is symbolized z_b in each step.

In the original state ("step 0") we obviously have no network and thus no impedance matrix.

Step 1. Introduce branch 1. Clearly this branch results in a system that obeys the equation

$$V_1 = z_b I_1 = j0.15 I_1 \tag{10-41}$$

The bus impedance matrix is of order 1×1, that is, a scalar. This first step has thus left us with

$$\mathbf{Z}_{bus}^{new} = z_b = j0.15 \tag{10-42}$$

Step 2. Add branch 2. This branch introduces a new bus and the equation (10-41) is now expanded to

$$\begin{aligned} V_1 &= j0.15 I_1 + 0 I_2 \\ V_2 &= 0 I_1 + z_b I_2 \end{aligned} \tag{10-43}$$

The "new" $\mathbf{Z}_{bus}$ matrix is of order 2×2 and is obtained from the "old" one by the extension

$$\mathbf{Z}_{bus}^{new} = \begin{bmatrix} \mathbf{Z}_{bus}^{old} & 0 \\ 0 & z_b \end{bmatrix} = j\begin{bmatrix} 0.15 & 0 \\ 0 & 0.075 \end{bmatrix} \tag{10-44}$$

The first two steps were simple as they both involved addition of branches between "new" buses and the reference ground. No coupling with the "old" buses takes place which explains the zeros in Eq. (10-44). If the "old" $\mathbf{Z}_{\text{bus}}$ is of order $k \times k$ the "new" $\mathbf{Z}_{\text{bus}}$ will be of order $(k+1) \times (k+1)$. The "building algorithm" reads in the general case

$$\mathbf{Z}_{\text{bus}}^{\text{new}} = \left[\begin{array}{c|c} \mathbf{Z}_{\text{bus}}^{\text{old}} & \begin{matrix} 0 \\ \vdots \\ 0 \end{matrix} \\ \hline 0 \cdots 0 & z_b \end{array}\right] \tag{10-45}$$

Step 3. Add branch 3. This branch introduces the third bus to our system. It is different from the branches in the previous two steps inasmuch as it is connected between bus 3 and an "old" bus (2). With the added branch the "old" I_2 changes to $I_2 + I_3$ and we thus write

$$\begin{bmatrix} V_1 \\ V_2 \end{bmatrix} = \mathbf{Z}_{\text{bus}}^{\text{old}} \begin{bmatrix} I_1 \\ I_2 + I_3 \end{bmatrix} \tag{10-46}$$

In addition we have the relation

$$V_3 = V_2 + I_3 z_b \tag{10-47}$$

We rewrite the equations (10-46) and (10-47) as follows:

$$\begin{bmatrix} V_1 \\ V_2 \\ \hline V_3 \end{bmatrix} = \left[\begin{array}{c|c} \mathbf{Z}_{\text{bus}}^{\text{old}} & \begin{matrix} z_{12} \\ z_{22} \end{matrix} \\ \hline z_{21} z_{22} & z_b + z_{22} \end{array}\right] \begin{bmatrix} I_1 \\ I_2 \\ \hline I_3 \end{bmatrix} \tag{10-48}$$

In this case $z_b = j0.10$ pu Ω.

Thus, with the inclusion of branch 3 the bus admittance matrix will change to

$$\mathbf{Z}_{\text{bus}}^{\text{new}} = j \begin{bmatrix} 0.15 & 0 & 0 \\ 0 & 0.075 & 0.075 \\ 0 & 0.075 & 0.175 \end{bmatrix} \tag{10-49}$$

Assume the "old" $\mathbf{Z}_{\text{bus}}$ to be of dimension $k \times k$ and the new branch to be connected between buses $k+1$ and j. The general algorithm will read:

$$\mathbf{Z}_{\text{bus}}^{\text{new}} = \left[\begin{array}{c|c} \mathbf{Z}_{\text{bus}}^{\text{old}} & \begin{matrix} z_{1j} \\ \vdots \\ z_{kj} \end{matrix} \\ \hline z_{j1} \cdots z_{jk} & z_{jj} + z_b \end{array}\right] \tag{10-50}$$

Step 4. Add branch 4. This branch is different from the two types we encountered in the earlier steps. The branch does not create any new bus but adds a new connection between two "old" buses, 1 and 2 in this case. It also creates a loop (shown dashed in Fig. 10-17) in which will circulate a loop current I_L.

As we analyze the effect of this added branch we seek a *general* algorithm. We thus assume that the branch impedance z_b is connected between the general buses i and j in the "old" k-port network. As the "old" current I_i will increase to $I_i + I_L$ and the "old" current I_j will decrease to $I_j - I_L$ we can write

$$\begin{bmatrix} V_1 \\ \vdots \\ V_i \\ V_j \\ \vdots \\ V_k \end{bmatrix} = \begin{bmatrix} & & \\ & \mathbf{Z}_{\text{bus}}^{\text{old}} & \\ & & \end{bmatrix} \begin{bmatrix} I_1 \\ \vdots \\ I_i + I_L \\ I_j - I_L \\ \vdots \\ I_k \end{bmatrix} \tag{10-51}$$

This vector equation can be written

$$\begin{bmatrix} V_1 \\ \vdots \\ V_k \end{bmatrix} = \begin{bmatrix} & & \\ & \mathbf{Z}_{\text{bus}}^{\text{old}} & \\ & & \end{bmatrix} \begin{bmatrix} I_1 \\ \vdots \\ I_k \end{bmatrix} + \underbrace{\begin{bmatrix} z_{1i} - z_{1j} \\ \vdots \\ z_{ki} - z_{kj} \end{bmatrix}}_{\mathbf{a}} I_L \tag{10-52}$$

or in compact notation:

$$\mathbf{V}_{\text{bus}} = \mathbf{Z}_{\text{bus}}^{\text{old}} \mathbf{I}_{\text{bus}} + \mathbf{a} I_L \tag{10-53}$$

where the k-dimensional column matrix $\mathbf{a}$ is defined in Eq. (10-52).

The voltage drop across the branch z_b can be expressed as follows:

$$V_i - V_j + z_b I_L = 0 \tag{10-54}$$

V_i and V_j constitute the ith and jth rows of Eq. (10-52) and can be written

$$\begin{aligned} V_i &= [z_{i1}, \ldots, z_{ik}]\mathbf{I}_{\text{bus}} + (z_{ii} - z_{ij}) I_L \\ V_j &= [z_{j1}, \ldots, z_{jk}]\mathbf{I}_{\text{bus}} + (z_{ji} - z_{jj}) I_L \end{aligned} \tag{10-55}$$

Thus, by substitution into Eq. (10-54), we get

$$\overbrace{[z_{j1} - z_{i1}, \ldots, z_{jk} - z_{ik}]}^{\mathbf{b}}\mathbf{I}_{\text{bus}} + (2z_{ij} - z_{ii} - z_{jj} - z_b) I_L = 0 \tag{10-56}$$

or in compact notation:

$$0 = \mathbf{b}\mathbf{I}_{\text{bus}} + (2z_{ij} - z_{ii} - z_{jj} - z_b) I_L \tag{10-57}$$

where the k-dimensional row matrix $\mathbf{b}$ is defined in Eq. (10-56).

The loop current I_L is solved from this last equation and substituted into Eq. (10-53). The result is

$$\mathbf{V}_{\text{bus}} = \mathbf{Z}_{\text{bus}}^{\text{old}} \mathbf{I}_{\text{bus}} + \frac{1}{z_b + z_{ii} + z_{jj} - 2z_{ij}} \mathbf{a}\mathbf{b}\mathbf{I}_{\text{bus}}$$

which can be written

$$\mathbf{V}_{\text{bus}} = \left\{\mathbf{Z}_{\text{bus}}^{\text{old}} + \frac{\mathbf{ab}}{z_b + z_{ii} + z_{jj} - 2z_{ij}}\right\}\mathbf{I}_{\text{bus}} = \mathbf{Z}_{\text{bus}}^{\text{new}}\mathbf{I}_{\text{bus}} \tag{10-58}$$

The sought algorithm ("Kron's reduction formula") thus reads

$$\mathbf{Z}_{\text{bus}}^{\text{new}} = \mathbf{Z}_{\text{bus}}^{\text{old}} + \frac{\mathbf{ab}}{z_b + z_{ii} + z_{jj} - 2z_{ij}} \tag{10-59}$$

After this brief detour into the mysteries of matrix algebra, we are prepared to finish step 4. The branch impedance is placed between buses $i = 1$ and $j = 2$ and its impedance equals $z_b = j0.10$.

From Eq. (10-49) we have

$$z_{ii} = z_{11} = j0.15$$
$$z_{jj} = z_{22} = j0.075$$
$$2z_{ij} = 2z_{12} = 0$$
$$\therefore \quad z_b + z_{ii} + z_{jj} - 2z_{ij} = j0.3250$$

From Eq. (10-49) we obtain the **a**-matrix

$$\mathbf{a} = j\begin{bmatrix} 0.15 - 0 \\ 0 - 0.075 \\ 0 - 0.075 \end{bmatrix} = j\begin{bmatrix} 0.15 \\ -0.075 \\ -0.075 \end{bmatrix}$$

and the **b**-matrix

$$\mathbf{b} = j[0 - 0.15,\ 0.075 - 0,\ 0.075 - 0] = j[-0.15,\ 0.075,\ 0.075]$$

The second matrix term in Eq. (10-59) thus will assume the value

$$\frac{j}{0.3250}\begin{bmatrix} 0.15 \\ -0.075 \\ -0.075 \end{bmatrix}[-0.15 \quad 0.075 \quad 0.075]$$

$$= j\begin{bmatrix} -0.0692 & 0.0346 & 0.0346 \\ 0.0346 & -0.0173 & -0.0173 \\ 0.0346 & -0.0173 & -0.0173 \end{bmatrix} \tag{10-60}$$

By addition of this matrix to the "old" $\mathbf{Z}_{\text{bus}}$ matrix we obtain

$$\mathbf{Z}_{\text{bus}}^{\text{new}} = j\begin{bmatrix} 0.0808 & 0.0346 & 0.0346 \\ 0.0346 & 0.0577 & 0.0577 \\ 0.0346 & 0.0577 & 0.1577 \end{bmatrix} \tag{10-61}$$

Step 5. Add branch 5. This branch connects buses $i = 1$ and $j = 3$ and is of the same type as the one we just discussed in step 4. We can therefore use the algorithm (10-59) again.

We have now

$$z_b = j0.1$$
$$z_{ii} = z_{11} = j0.0808$$
$$z_{jj} = z_{33} = j0.1577$$
$$2z_{ij} = 2z_{13} = j0.0692$$
$$\therefore \quad z_b + z_{ii} + z_{jj} - 2z_{ij} = j0.2693$$

The column matrix **a**

$$\mathbf{a} = j\begin{bmatrix} 0.0808 - 0.0346 \\ 0.0346 - 0.0577 \\ 0.0346 - 0.1577 \end{bmatrix} = j\begin{bmatrix} 0.0462 \\ -0.0231 \\ -0.1231 \end{bmatrix}$$

The row matrix **b**

$$\mathbf{b} = j[0.0346 - 0.0808,\ 0.0577 - 0.0346,\ 0.1577 - 0.0346]$$
$$= j[-0.0462,\ 0.0231,\ 0.1231]$$

The bus impedance increment matrix thus equals:

$$\frac{j}{0.2693}\begin{bmatrix} 0.0462 \\ -0.0231 \\ -0.1231 \end{bmatrix}[-0.0462, \quad 0.0231, \quad 0.1231]$$

$$= j\begin{bmatrix} -0.0079 & 0.0040 & 0.0211 \\ 0.0040 & -0.0020 & -0.0106 \\ 0.0211 & -0.0106 & -0.0563 \end{bmatrix} \tag{10-62}$$

We add this matrix to the "old" one and obtain our *final* bus impedance matrix

$$\mathbf{Z}_{\text{bus}} = j\begin{bmatrix} 0.0729 & 0.0386 & 0.0557 \\ 0.0386 & 0.0557 & 0.0471 \\ 0.0557 & 0.0471 & 0.1014 \end{bmatrix} \tag{10-63}$$

10-5-3 Comments on Results

We make these brief observations:

1. Our computed value for $\mathbf{Z}_{\text{bus}}$ agrees with the one we earlier obtained by inversion of $\mathbf{Y}_{\text{bus}}$ (Eq. 10-38).
2. The step-by-step method that we have presented in this section seems like a very tedious and roundabout method to obtain a bus impedance matrix that we computed so "conveniently" in Sec. 10-4.
3. The previous observation is certainly pertinent for a three-bus system. However, as the dimensionality increases, the "$\mathbf{Z}_{\text{bus}}$-building method" very soon demonstrates its advantage over the "inversion method."

4. We encountered three different branch types each requiring a special algorithm. In an example more general than our five-branch network we would encounter a fourth type. This happens when a "new" branch is added between an "old" bus and reference ground. The reader is invited to find an algorithm for this situation in Prob. 10-12.
5. When obtaining the $\mathbf{Z}_{bus}$ matrix by inversion, any small change in the network would necessitate a *complete* new inversion of the $\mathbf{Y}_{bus}$ matrix. This is *not* necessary when we use the $\mathbf{Z}_{bus}$ building algorithm. This method is therefore particularly convenient when we want to study the effects of changes in the network.

10-6 SUMMARY

After classification of system transients into the categories "ultrafast," "medium fast," and "slow," we have taken a closer look at the two first classes. The ultrafast transients, usually caused by atmospheric disturbances and switching operations, give rise to overvoltages, which usually disappear within milliseconds but may cause insulation breakdown. We studied methods of estimating the overvoltage magnitudes.

It should be understood that because atmospheric disturbances are difficult to measure, and even estimate, it does not make much sense to employ too sophisticated mathematical techniques in the solution of the wave equation. We made several simplifying assumptions which permitted us to obtain solutions relatively simply.

Of the "medium-fast" transients or "short-circuit" phenomena, we have considered in this chapter only the *balanced* case, i.e., when the short circuit involves *symmetrically* all three phases. Of all the short circuits that may occur, this is by far the rarest occurrence—but the most dangerous one. For this reason the balanced short-circuit computations are the most important.

Systematic, computerized methods for solving this type of short circuit on a general n-bus system have been presented. Reasonable model simplifications have been utilized, of which the most useful one is to represent the generator with an emf behind either the transient or the subtransient reactance.

PROBLEMS

***10-1** In Example 10-6 we concluded that a solid symmetrical short circuit on bus 2 results in a current of 17.9 pu, or differently stated, bus 2 has an SCC of $17.9 \times 50 = 895$ MVA. To reduce the stresses on the circuit breaker, we wish to reduce the SCC to 500 MVA by adding reactors in series with $G2 + T2$. How much reactance per phase must be added? Express your answer (1) in per units, (2) in ohms, assuming the reactors are placed on the low-voltage side of $T2$, and (3) in ohms, assuming the reactors are placed on the high-voltage side of $T2$. (Where would *you* place them?)

The step-up transformer has a nominal voltage rating of 20/115 kV.

***10-2** Use the value of $\mathbf{Z}_{bus}$ computed in Example 10-6 and find in the simplest manner possible the postfault voltages on buses 1 and 3 if the *solid* short circuit occurs on bus 2.

***10-3** Consider the reflected wave in Example 10-2. As it travels to the left it will eventually hit the other end of the line. Assume that end also to be open circuited. What does the wave look like (voltage *and* current) following the *second* reflection?

***10-4** Consider the 500 kV/1.4 kA wave pair in Fig. 10-2 which travels in positive x direction. Assuming that it hits a shorted line end what will the reflected wave pair look like?

***10-5** A 90-mile line is open at both ends. It is characterized by

$$\kappa = 180{,}000 \text{ mi/s}$$

$$R_w = 400\ \Omega$$

A dc battery of 20 kV emf is connected to the sending end at $t = 0$. Plot versus time the voltage and current as measured midline. Your plot should cover at least 3 μs.

***10-6** A line having a wave impedance of R_w ohms forks into two lines of same wave impedance R_W. If a wave pair v_i/i_i hits the fork, describe the waves that continue down the two lines and also the reflected wave pair.

***10-7** Consider the test impulse depicted in Fig. 10-6. If the peak value is 250 kV determine the three parameters v_{max}, a, and b. Time t is measured in seconds.

10-8 Following the restrike in Fig. 10-9 the capacitor voltage swings down to a value which, if damping is neglected, measures $3\sqrt{2}\,|V|$. At the moment the voltage reaches this peak the capacitor current passes through zero. (Why?) Assume that the CB interrupts the current at this moment. The capacitor voltage thus is "trapped" again. As the generator voltage turns around the voltage across the CB will increase and reach a new maximum.

(*a*) What will this maximum voltage be?

(*b*) Assume that a *second restrike* would occur at the moment when this maximum voltage is reached. To what value would the capacitor voltage then swing?

(*c*) Assume a third restrike, etc. To what voltage could the capacitor theoretically swing?

10-9 (This problem requires an analog computer.) In Prob. 10-5 you plotted (hopefully correctly) the *exact* midline voltage versus time on a 90-mile transmission line.

Now divide the line into 10 nine-mile long sections each of which you "lump" into a π link consisting of one series reactor and two shunt capacitors. Write the coupled set of ordinary differential equations that dynamically describe this lumped line. Then simulate it on an analog computer and verify the plot you found in Prob. 10-5.

Note: The physical system is very fast and you need to time scale it at least by a factor of 10^6 before you put it on the computer (1 second on the computer will correspond to 1 microsecond on the line).

***10-10** Consider the four-bus power system depicted in Fig. 7-16. The line data were given in Prob. 7-9. The generator is rated at 500 MVA and has a transient reactance of 0.25 pu based on its own rating. The transformer has equal megavoltampere rating. Its reactance is 12 percent.

Find the SCC of each bus assuming all prefault voltages to be 1 pu.

10-11 A four-bus system has a total of six lines which provide interconnections between each bus and all the other three buses. All lines have the same impedance, $j0.10$ pu.

There are equal generators and step-up transformers at each bus. The combined impedance (transient reactance plus leakage reactance) of each generator/transformer is $j0.17$ pu.

Find the SCC of each bus. All prefault voltages are 1 pu.

10-12 Find the $\mathbf{Z}_{bus}$ "building algorithm" in the case when a "new" branch is added between an "old" bus and the reference ground.

***10-13** In the text we presented two different methods for finding the SCC data in the three-bus example of Fig. 10-16. Both methods used the bus impedance matrix.

Take a simpler approach (like the one we used for the two-bus system) to find the short-circuit current in a solid fault on bus 3.

Hint: Use the "star-mesh" transformation to make a Y out of the Δ in Fig. 10-16.

REFERENCES

1. Homer E. Brown: *Solution of Large Networks by Matrix Methods*, John Wiley & Sons, New York, 1975.
2. John R. Neuenswander: *Modern Power Systems*, International Textbook Company, 1971.
3. G. W. Stagg, and A. H. El-Abiad: *Computer Methods in Power Systems Analysis*, McGraw-Hill Book Company, New York, 1968.
4. Charles A. Gross: *Power System Analysis*, John Wiley & Sons, New York, 1979.
5. P. M. Anderson: *Analysis of Faulted Power Systems*, Iowa State Press, Ames, Iowa, 1973.

CHAPTER

ELEVEN

UNBALANCED SYSTEM ANALYSIS

In all previous work we have based our analysis on the assumption that complete phase symmetry exists. Thus the load (or fault) impedances are the same in all three phases, and the voltages, emf's, and currents are characterized by complete three-phase symmetry. On this assumption we have then studied the system on a per-phase basis, i.e., we have focused attention on one of the phases. Knowledge of the current or the voltage in this *reference phase* implies knowledge of the corresponding variables in the other two phases. The total power, real or reactive, is obtained by multiplying the phase power by three.

As the algebraic sum of the balanced phase currents is zero at all times no current will flow between generator or transformer neutrals and ground. Zero currents produce zero voltage drops and therefore all neutrals in a balanced system are at ground potential (which we arbitrarily define as zero).

11-1 NEUTRAL CURRENTS AND VOLTAGES

In an unsymmetrically faulted or loaded system, neither the phase currents nor the phase voltages possess three-phase symmetry. Per-phase analysis is therefore out of the question. As the algebraic sum of the phase currents no longer may be zero there will be a *neutral current* I_n flowing in the system. This current may flow in specially provided neutral conductors, in overhead ground wires, or in the ground itself.

Often the neutrals are connected to ground via *grounding impedances* (reactors and resistors), the main purpose of which is to limit the magnitudes of the fault current. Consider for example the *single-line-to-ground fault* in Fig. 11-1 resulting in the fault current I^f in phase a. This fault will yield a neutral current of magnitude

$$I_n = I_a + I_b + I_c = I^f \tag{11-1}$$

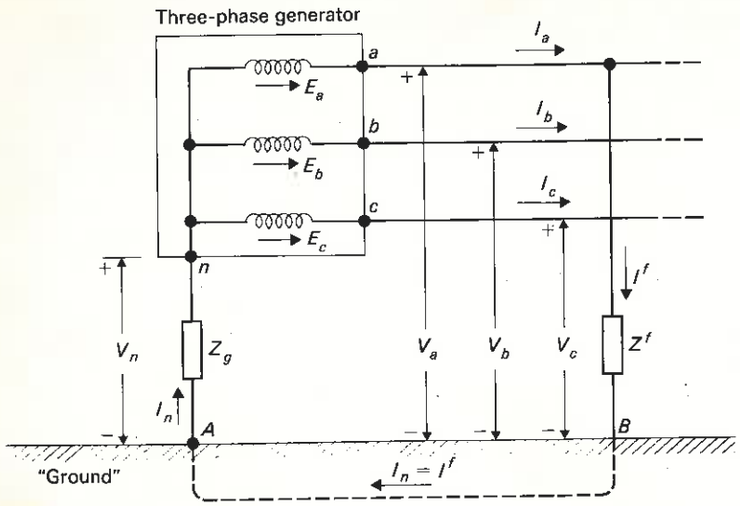

Figure 11-1 Unbalanced generator current loading results in neutral return current I_n.

The potential of the generator neutral V_n will equal the ground potential minus the drop over Z_g, that is

$$V_n = 0 - I_n Z_g = -I_n Z_g = -I^f Z_g \tag{11-2}$$

When we talk about "phase" or "phase-to-ground" or "phase-to-neutral" voltages in a *balanced* system no ambiguity exists because they are all the same. In an unbalanced system we must obviously exercise caution. Unless otherwise stated "phase" voltages in this chapter are symbolized V_a, V_b, and V_c and are defined as the voltages that are measured between machine terminals (see Fig. 11-1) and ground.

The "phase-to-neutral" voltages equal the phase voltages minus the neutral voltage. For example, for phase a

$$V_{an} = V_a - V_n = V_a + I_n Z_g \tag{11-3}$$

11-2 SYMMETRICAL COMPONENTS

11-2-1 Definitions

Consider an arbitrarily unbalanced three-phase set of phasors, exemplified by the currents I_a, I_b, and I_c shown boldface in Fig. 11-2*a*. Fortesque[1] demonstrated how it is possible to resolve this set into three so-called *symmetrical component sets*, namely:

1. The *positive sequence* set consisting of three components of equal magnitude, displaced by 120 and 240° respectively, and having the phase sequence *abca* ... (Fig. 11-2*b*).
2. The *negative sequence* set consisting of three components of equal magnitude, displaced by 240 and 120° respectively, having the phase sequence *acba* ... (Fig. 11-2*c*).
3. The *zero-sequence* set the components of which being of equal both magnitude and phase (Fig. 11-2*d*).

The three components systems are symbolized† by subscripts +, −, and 0 respectively.

† In the literature subscripts 1, 2, and 0 are often used. We avoid this usage as it collides with "primary" and "secondary" transformer variables. Also, we prefer the sequence order (+, −, 0) to the often used (0, +, −), as, unquestionably, the positive sequence is the most common and important of the three.

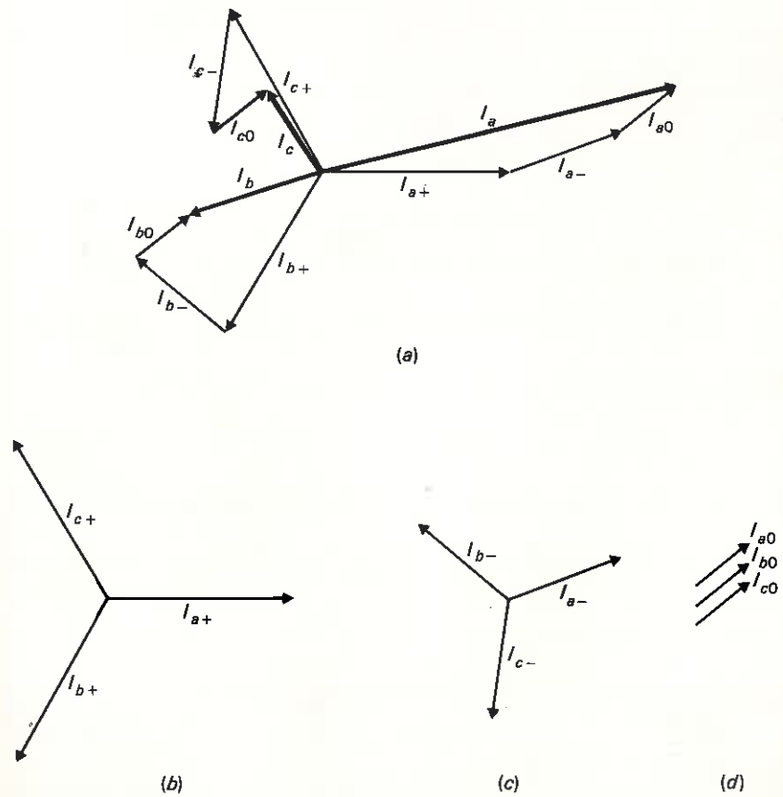

Figure 11-2 Unbalanced set of three-phase currents decomposed into symmetrical components.

11-2-2 The Symmetrical Component Transformation (SCT)

The situation graphically displayed in Fig. 11-2 can mathematically be expressed as follows:

$$\begin{aligned} I_a &= I_{a+} + I_{a-} + I_{a0} \\ I_b &= I_{b+} + I_{b-} + I_{b0} \\ I_c &= I_{c+} + I_{c-} + I_{c0} \end{aligned} \tag{11-4}$$

The three positive sequence components are individually related as follows:

$$\begin{aligned} I_{b+} &= I_{a+}\, e^{-j120^\circ} \\ I_{c+} &= I_{a+}\, e^{j120^\circ} \end{aligned} \tag{11-5}$$

For the negative and zero sequence components we have, respectively

$$\begin{aligned} I_{b-} &= I_{a-}\, e^{-j120^\circ} \\ I_{c-} &= I_{a-}\, e^{-j120^\circ} \end{aligned} \tag{11-6}$$

and

$$I_{a0} = I_{b0} = I_{c0} \tag{11-7}$$

Substitution of relations (11-5) to (11-7) into Eq. (11-4) yields

$$\begin{aligned} I_a &= I_{a+} + I_{a-} + I_{a0} \\ I_b &= \alpha^2 I_{\alpha+} + \alpha I_{a-} + I_{a0} \\ I_c &= \alpha I_{a+} + \alpha^2 I_{a-} + I_{a0} \end{aligned} \tag{11-8}$$

For shorter notation we have here introduced the brevity symbol†

$$\alpha \triangleq e^{j120^\circ} = \cos 120^\circ + j \sin 120^\circ = -\frac{1}{2} + j\frac{\sqrt{3}}{2} \tag{11-9}$$

We easily confirm that the following identities apply for α:

$$\begin{aligned} \alpha^2 &= e^{j240^\circ} = e^{-j120^\circ} = -\frac{1}{2} - j\frac{\sqrt{3}}{2} \\ \alpha^3 &= 1 \\ 1 + \alpha + \alpha^2 &= 0 \\ \alpha^* &= \alpha^2 \\ (\alpha^2)^* &= \alpha \end{aligned} \tag{11-10}$$

Equations (11-8) can be written in compact matrix form

$$\mathbf{I}_p = \mathbf{T}\mathbf{I}_s \tag{11-11}$$

† The symbol a is often used. We have already "reserved" it for transformer ratio.

where the matrix

$$\mathbf{T} \triangleq \begin{bmatrix} 1 & 1 & 1 \\ \alpha^2 & \alpha & 1 \\ \alpha & \alpha^2 & 1 \end{bmatrix} \tag{11-12}$$

is referred to as the *symmetrical component transformation matrix.*

The current vectors

$$\mathbf{I}_p \triangleq \begin{bmatrix} I_a \\ I_b \\ I_c \end{bmatrix} \tag{11-13}$$

and

$$\mathbf{I}_s \triangleq \begin{bmatrix} I_{a+} \\ I_{a-} \\ I_{a0} \end{bmatrix} \quad \text{or shorter} \quad \mathbf{I}_s = \begin{bmatrix} I_+ \\ I_- \\ I_0 \end{bmatrix} \tag{11-14}$$

represent the actual phase currents and the symmetrical current components, respectively.

From Eq. (11-11) we obtain upon inversion

$$\mathbf{I}_s = \mathbf{T}^{-1}\mathbf{I}_p \tag{11-15}$$

where

$$\mathbf{T}^{-1} = \frac{1}{3}\begin{bmatrix} 1 & \alpha & \alpha^2 \\ 1 & \alpha^2 & \alpha \\ 1 & 1 & 1 \end{bmatrix} \tag{11-16}$$

(See Sec. A-2-4.)

Equation (11-15) is so important that we write it out in component form

$$\begin{aligned} I_{a+} &= \tfrac{1}{3}(I_a + \alpha I_b + \alpha^2 I_c) \\ I_{a-} &= \tfrac{1}{3}(I_a + \alpha^2 I_b + \alpha I_c) \\ I_{a0} &= \tfrac{1}{3}(I_a + I_b + I_c) \end{aligned} \tag{11-17}$$

Equations (11-15) and (11-11) define, respectively, the *direct* and *indirect SC transforms.*

We may, of course, apply the SCT to voltage phasors as well. If the vectors

$$\mathbf{V}_p \triangleq \begin{bmatrix} V_a \\ V_b \\ V_c \end{bmatrix} \quad \text{and} \quad \mathbf{V}_s \triangleq \begin{bmatrix} V_{a+} \\ V_{a-} \\ V_{a0} \end{bmatrix} \quad \text{or shorter} \quad \mathbf{V}_s = \begin{bmatrix} V_+ \\ V_- \\ V_0 \end{bmatrix} \tag{11-18}$$

represent the actual voltages and the symmetrical voltage components, respectively, we have the SC transform pair for voltages

$$\mathbf{V}_p = \mathbf{T}\mathbf{V}_s \tag{11-19}$$

$$\mathbf{V}_s = \mathbf{T}^{-1}\mathbf{V}_p \tag{11-20}$$

Example 11-1 In a *single-line-to-ground* fault (Fig. 11-1) current will flow only in phase a. Find the SC's for this current set.

SOLUTION With $I_a = I^f$ and $I_b = I_c = 0$ Eqs. (11-17) yield directly

$$I_{a+} = I_{a-} = I_{a0} = \tfrac{1}{3}I^f \tag{11-21}$$

RESULT A single-line-to-ground fault (or load) produces positive, negative, and zero sequence currents of *equal* magnitudes.

Example 11-2 In a *line-to-line* fault between phases b and c (Fig. 11-3a) the current set is characterized by

$$\begin{aligned} I_a &= 0 \\ I_b &= I^f \\ I_c &= -I^f \end{aligned} \tag{11-22}$$

Find the SC's.

SOLUTION Substitution into Eq. (11-17) yields

$$\begin{aligned} I_{a+} &= \frac{1}{3}(\alpha I^f - \alpha^2 I^f) = \frac{j}{\sqrt{3}} I^f \\ I_{a-} &= \frac{1}{3}(\alpha^2 I^f - \alpha I^f) = -\frac{j}{\sqrt{3}} I^f \\ I_{a0} &= \frac{1}{3}(I^f - I^f) = 0 \end{aligned} \tag{11-23}$$

The SC's are shown in Fig. 11-3b

RESULT A line-to-line fault (or load) produces positive and negative sequence currents of *equal* magnitude. No zero sequence currents exist.

Example 11-3 We may, of course, find the SC's for *any* set of three phasors. Prove that the three *line* voltage phasors V_{ab}, V_{bc}, and V_{ca} *never* can contain a zero sequence component.

PROOF. The three line voltages are defined as follows (compare Eqs. 3-3):

$$\begin{aligned} V_{ab} &= V_a - V_b \\ V_{bc} &= V_b - V_c \\ V_{ca} &= V_c - V_a \end{aligned} \tag{11-24}$$

According to the last of Eqs. (11-20) the zero sequence component of the *line* voltages will equal one-third of the sum $V_{ab} + V_{bc} + V_{ca}$. By adding Eqs. (11-24) we note that this sum *always* is zero, and this means then that this phasor set never will contain a zero sequence component.

Example 11-4 Prove that "neutral" current can flow only if zero sequence currents exist.

PROOF. The phasor sums $I_{a+} + I_{b+} + I_{c+}$ and $I_{a-} + I_{b-} + I_{c-}$ are both zero. *Thus, neither the positive nor the negative sequence currents will contribute any neutral current.* However, from Eq. (11-1) and the last of Eqs. (11-17) we observe that

$$I_n = I_a + I_b + I_c = 3I_{a0} = I_{a0} + I_{b0} + I_{c0} \tag{11-25}$$

informing us that the neutral current is obtained as the sum of the zero sequence currents in each phase. As a corollary we obtain from Eq. (11-2)

$$V_n = -3I_{a0}Z_g \tag{11-26}$$

i.e., *only zero sequence current contributes to the neutral voltage.*

11-2-3 Decoupling Property Between Sequence Currents

We have so far given no motivations for having introduced the symmetrical components. At a first glance it would seem that the involvement of three new current and voltage variables would actually represent a complication of matters. However, the SCT is characterized by a property which renders it a most useful tool in studies of unbalanced systems.

In Chaps. 3, 4, and 5 we learned that systems that possess phase symmetry and are subject to balanced loading can be greatly simplified by use of "per-phase" analysis. This became possible as the result of *zero coupling between phase currents.*

Such a decoupling between phase currents is *not* present if the phase symmetric systems are subject to *unbalanced* loading (or fault). However, as we shall confirm in the next sections, phase-symmetric systems are always characterized by *zero coupling between the sequence currents.* This means that generators,

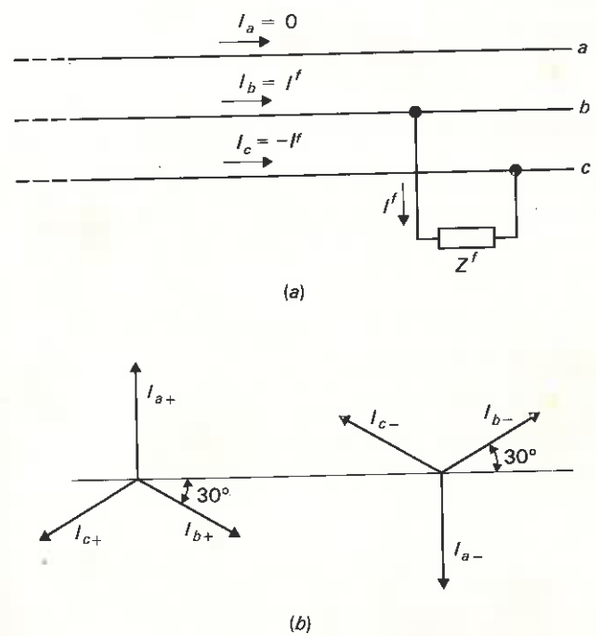

Figure 11-3 Line-to-line fault produces positive and negative current components of equal magnitude.

transformers, and (transposed) lines can be analyzed on a "per-sequence-component" basis.

This "decoupling feature" between sequence currents is reflected in the power formulas as well. In terms of the actual phase voltages and currents, the total power flow equals

$$S = P + jQ = V_a I_a^* + V_b I_b^* + V_c I_c^* = [V_a, V_b, V_c]\begin{bmatrix} I_a^* \\ I_b^* \\ I_c^* \end{bmatrix} = \mathbf{V}_p^T \cdot \mathbf{I}_p^* \tag{11-27}$$

(Compare Eq. A-5.)

By substitution of Eqs. (11-11) and (11-19) into Eq. (11-27), we get

$$S = P + jQ = (\mathbf{TV}_s)^T(\mathbf{TI}_s)^* = \mathbf{V}_s^T\mathbf{T}^T\mathbf{T}^*\mathbf{I}_s^* \tag{11-28}$$

The last step follows from Eq. (A-30). The matrix product $\mathbf{T}^T\mathbf{T}^*$ is then evaluated

$$\mathbf{T}^T\mathbf{T}^* = \begin{bmatrix} 1 & \alpha^2 & \alpha \\ 1 & \alpha & \alpha^2 \\ 1 & 1 & 1 \end{bmatrix}\begin{bmatrix} 1 & 1 & 1 \\ \alpha & \alpha^2 & 1 \\ \alpha^2 & \alpha & 1 \end{bmatrix} = 3\begin{bmatrix} 1 & 0 & 0 \\ 0 & 1 & 0 \\ 0 & 0 & 1 \end{bmatrix} = 3\mathbf{U} \tag{11-29}$$

In view of this result we may write the power formula (11-28) as follows:

$$S = P + jQ = 3\mathbf{V}_s^T\mathbf{I}_s^* = 3V_+ I_+^* + 3V_- I_-^* + 3V_0 I_0^* \tag{11-30}$$

In words: *The total power in the unbalanced system can be computed as the sum of the symmetrical component powers.* It is important to realize that no *cross-terms* (like $V_+ I_-^*$) appear in Eq. (11-30).

11-3 SCT OF THE GENERATOR PERFORMANCE EQUATIONS

Return for a moment to the *symmetrically* operated synchronous machine. If rotor saliency was neglected the *per-phase* relationship between stator emf (E), stator current (I) and terminal voltage (V) was expressed by Eq. (4-11). By writing this equation for all three phases we obtain

$$\begin{aligned} V_a &= E_a - Z_s I_a \\ V_b &= E_b - Z_s I_b \\ V_c &= E_c - Z_s I_c \end{aligned} \tag{11-31}$$

where Z_s is the "synchronous impedance." *By design*† the phase emf's constitute a *symmetrical three-phase set of positive sequence*, i.e., we can write

$$\mathbf{E}_p \triangleq \begin{bmatrix} E_a \\ E_b \\ E_c \end{bmatrix} = \begin{bmatrix} E_a \\ \alpha^2 E_a \\ \alpha E_a \end{bmatrix} \tag{11-32}$$

† Sec. 4-2.

Equation (11-31) can be written in the compact form

$$\mathbf{V}_p = \mathbf{E}_p - \mathbf{Z}_p \mathbf{I}_p \tag{11-33}$$

where the generator *impedance matrix* $\mathbf{Z}_p$ is of the *diagonal* form

$$\mathbf{Z}_p = \begin{bmatrix} Z_s & 0 & 0 \\ 0 & Z_s & 0 \\ 0 & 0 & Z_s \end{bmatrix} \tag{11-34}$$

The zero off-diagonal elements assure zero coupling between phases. The equal diagonal elements make it sufficient to analyze one phase only ("per-phase" analysis).

11-3-1 Performance Equations for Unsymmetrically Loaded Machine

Let us then assume *nonsymmetrical* loading of the generator. An accurate analysis of this mode of operation reveals quite a complex picture. Both the rotor and stator currents will contain harmonics. However, if we limit attention to the currents and voltages† of *fundamental* frequency we find the performance equation (11-33) unchanged *in form*. However, the impedance matrix no longer will be diagonal as all of its nine elements will be nonzero. It will, however, possess *cyclic symmetry*,‡ i.e., it will be of the form

$$\mathbf{Z}_p = \begin{bmatrix} z_1 & z_2 & z_3 \\ z_3 & z_1 & z_2 \\ z_2 & z_3 & z_1 \end{bmatrix} \tag{11-35}$$

With the off-diagonal elements all being nonzero *we have evidently lost the decoupling between phases that characterized the symmetrically loaded machine.*

Here is where the SCT changes the picture to the better. To verify this we first substitute $\mathbf{V}_s$ and $\mathbf{I}_s$ for $\mathbf{V}_p$ and $\mathbf{I}_p$ into Eq. (11-33)

$$\mathbf{TV}_s = \mathbf{E}_p - \mathbf{Z}_p\mathbf{TI}_s \tag{11-36}$$

Then we premultiply by $\mathbf{T}^{-1}$

$$\mathbf{V}_s = \mathbf{T}^{-1}\mathbf{E}_p - \mathbf{T}^{-1}\mathbf{Z}_p\mathbf{TI}_s \tag{11-37}$$

By introducing the "SC transformed" emf vector

$$\mathbf{E}_s \triangleq \mathbf{T}^{-1}\mathbf{E}_p \tag{11-38}$$

† Measured relative to the generator neutral.

‡ This means that phase a is magnetically coupled with phases b and c in the identical way as phase b is coupled with phases c and a, and phase c with phases a and b. This is appreciated if we remember (Fig. 4-1) that the rotor sweeps by the stator phases in order *abca* ... and that the three stator phases are identical.

and the "SC transformed" generator impedance

$$\mathbf{Z}_s \triangleq \mathbf{T}^{-1}\mathbf{Z}_p\mathbf{T} \tag{11-39}$$

we can write Eq. (11-37) in the *same form* as the nontransformed equation (11-33), i.e.,

$$\mathbf{V}_s = \mathbf{E}_s - \mathbf{Z}_s\mathbf{I}_s \tag{11-40}$$

11-3-2 Sequence Network Representation of Generators

What has been gained by the above transformation? To find out we first perform the multiplications called for

$$\mathbf{E}_s = \mathbf{T}^{-1}\mathbf{E}_p = \frac{1}{3}\begin{bmatrix} 1 & \alpha & \alpha^2 \\ 1 & \alpha^2 & \alpha \\ 1 & 1 & 1 \end{bmatrix}\begin{bmatrix} E_a \\ \alpha^2 E_a \\ \alpha E_a \end{bmatrix} = \frac{1}{3}\begin{bmatrix} E_a(1+\alpha^3+\alpha^3) \\ E_a(1+\alpha^4+\alpha^2) \\ E_a(1+\alpha^2+\alpha) \end{bmatrix} = \begin{bmatrix} E_a \\ 0 \\ 0 \end{bmatrix} \tag{11-41}$$

and

$$\mathbf{Z}_s = \mathbf{T}^{-1}\begin{bmatrix} z_1 & z_2 & z_3 \\ z_3 & z_1 & z_2 \\ z_2 & z_3 & z_1 \end{bmatrix}\mathbf{T}$$

$$= \begin{bmatrix} z_1 + \alpha^2 z_2 + \alpha z_3 & 0 & 0 \\ 0 & z_1 + \alpha z_2 + \alpha^2 z_3 & 0 \\ 0 & 0 & z_1 + z_2 + z_3 \end{bmatrix} \tag{11-42}$$

At this point we introduce the generator *sequence impedances*

$$\begin{aligned} z_+ &\triangleq z_1 + \alpha^2 z_2 + \alpha z_3 && \textit{positive-sequence impedance} \\ z_- &\triangleq z_1 + \alpha z_2 + \alpha^2 z_3 && \textit{negative-sequence impedance} \\ z_0 &\triangleq z_1 + z_2 + z_3 && \textit{zero-sequence impedance} \end{aligned} \tag{11-43}$$

and can then, in view of the results (11-41) and (11-42), write Eq. (11-40) in the simple component form

$$\begin{aligned} V_{a+} &= E_a - z_+ I_{a+} \\ V_{a-} &= 0 - z_- I_{a-} \\ V_{a0} &= 0 - z_0 I_{a0} \end{aligned} \tag{11-44}$$

We make these important observations:

1. As the $\mathbf{Z}_s$ matrix turned out to be diagonal there exists zero coupling between the three sequence component systems.
2. Only the positive sequence system has an induced emf. (This, of course, is not surprising as the generators are designed that way.)
3. The sequence impedances are all different. (For more details see Sec. 11-3-3.)

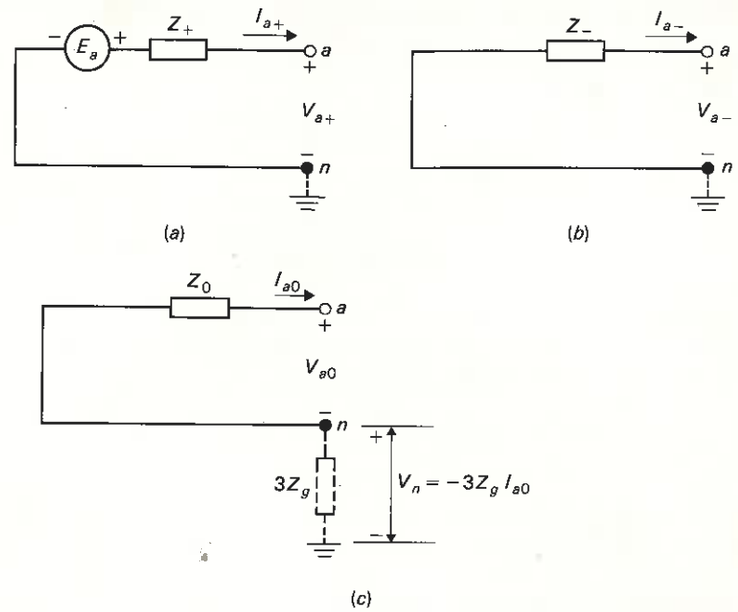

Figure 11-4 Generator sequence networks.

The three equations (11-44) can be represented by the three equivalent "generator sequence networks" shown in Fig. 11-4. Note that the sequence voltages V_{a+}, V_{a-}, and V_{a0} are measured between the terminal a and the generator *neutral* n.

It is more practical in system studies to measure phase voltages relative to *ground* as indicated in Fig. 11-1. Neither positive nor negative sequence currents contribute any neutral current and thus any voltage drop across the grounding impedance Z_g. Thus, for these two sequence systems the neutral point n and ground are equivalent, from a voltage point of view. We have so indicated in Figs. 11-4*a* and *b*.

Should zero sequence current flow, the potential of the neutral n will be lower than that of ground by the amount $3Z_g I_{a0}$ (compare Eqs. 11-26). This explains the addition of the impedance $3Z_g$ between n and ground in Fig. 11-4*c*.

Thus, whenever grounding impedance is used the generator zero sequence impedances z_0 must be changed according to the rule

$$z_0 \to z_0 + 3Z_g \tag{11-45}$$

Example 11-5 Assume that the single-line-to-ground short in Fig. 11-1 is *solid*, i.e., the fault impedance Z^f is zero. Find formulas for the fault current I^f and the voltages V_b and V_c of the two healthy phases.

SOLUTION We borrow the results from Example 11-1 expressed by the formula (11-21).

Equal sequence currents are assured by connecting all three sequence networks in series as shown in Fig. 11-5. From this diagram we obtain directly for the fault current

$$\frac{I^f}{3} = \frac{E_a}{z_+ + z_- + z_0 + 3Z_g}$$

$$\therefore \quad I^f = \frac{3E_a}{z_+ + z_- + z_0 + 3Z_g} \tag{11-46}$$

The voltages V_b and V_c are also readily obtained. From Eq. (11-19) we obtain for V_b

$$V_b = \alpha^2 V_{a+} + \alpha V_{a-} + V_{a0} \tag{11-47}$$

We substitute V_{a+}, V_{a-}, and V_{a0} from Eq. (11-44). As we are now measuring V_{a0} to ground we must add $3Z_g$ to the generator impedance z_0. We thus obtain

$$V_b = \alpha^2\left(E_a - z_+ \frac{I^f}{3}\right) - \alpha z_- \frac{I^f}{3} - (z_0 + 3Z_g)\frac{I^f}{3} \tag{11-48}$$

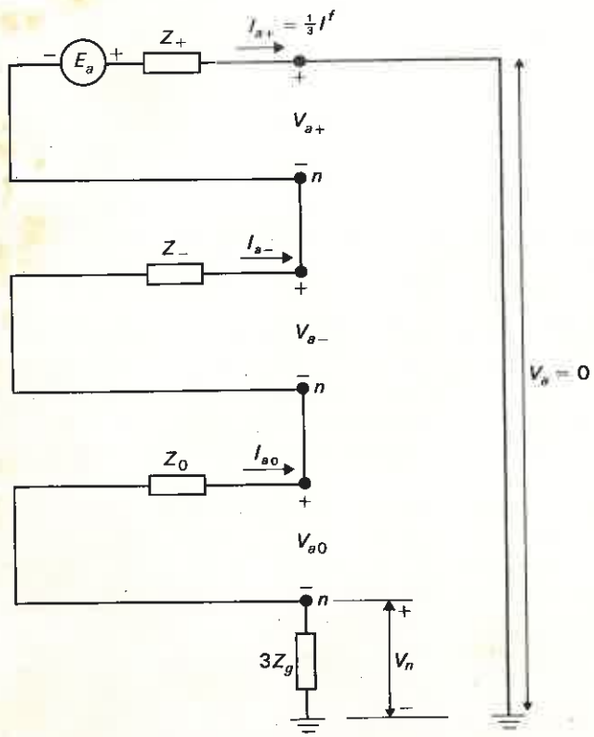

Figure 11-5 Interconnection of sequence networks to simulate single-line-to-ground fault.

By substitution of the value for I^f from Eq. (11-46) we obtain finally

$$V_b = E_a \frac{z_-(\alpha^2 - \alpha) + (z_0 + 3Z_g)(\alpha^2 - 1)}{z_+ + z_- + z_0 + 3Z_g} \tag{11-49}$$

A similar formula can be obtained for V_c.

SPECIAL CASE By setting $Z_g = \infty$ we have a *floating neutral*. According to Eq. (11-46) this reduces the fault current to *zero*. But what happens to the voltages V_b and V_c? According to Eq. (11-49) V_b assumes the value

$$V_b = (\alpha^2 - 1)E_a \tag{11-50}$$

with the magnitude

$$|V_b| = \sqrt{3}\,|E_a| \tag{11-51}$$

Similarly for $|V_c|$. Obviously, *both* healthy phases assume full *line* voltage to ground.

11-3-3 Determination of Generator Sequence Impedances

We comment briefly on how to determine the generator sequence impedances. For both generators, lines, and transformers all sequence impedances are essentially purely reactive. The words "impedance" and "reactance" will thus be used interchangeably. In practice, the impedance data are furnished by the manufacturer.

The procedure for finding these impedances will be the same in all cases. Whether we wish to determine them by test or by analytical means, we must subject the component to a set of currents and voltages satisfying the description for the respective sequence system in question. With the machine operating under those conditions, we then either measure or compute the sought impedances, depending upon whether we seek the parameters by test or analysis.

A. Positive-sequence impedance This is the simplest parameter to determine. A system component operating under balanced conditions of voltages and currents (of phase sequence *abca*...) is in effect in a "positive-sequence mode." In Chap. 4 we have penetratingly discussed the impedance situation for a synchronous machine under balanced load and fault conditions. We summarize our earlier findings:

For *steady state*, use

$$z_+ = jX_d \tag{11-52}$$

For *fault*, if the one-cycle transient is of interest, use

$$z_+ = jX_d'' \tag{11-53}$$

If the three- to four-cycle transient is of interest, use

$$z_+ = jX_d' \tag{11-54}$$

If we wish to obtain z_+ by test, the simplest procedure will be to short-circuit the machine from no load, having excited the machine to a 100 percent emf (compare Fig. 4-24). If from an oscillogram† we measure the per-unit rms values of the 60-Hz current component at $|I''|$, $|I'|$, and $|I_{ss}|$ at one cycle, three to four cycles, and in steady state, respectively, then we obtain the reactances

$$X''_d = \frac{1}{|I''|} \quad \text{pu}$$

$$X'_d = \frac{1}{|I'|} \quad \text{pu} \tag{11-55}$$

$$X_d = \frac{1}{|I_{ss}|} \quad \text{pu}$$

Typical numerical values for these reactances are found in Table 4-1.

B. Negative-sequence impedance Figure 11-6 suggests how we can find z_- from *test*. The test machine should be running at full speed and zero emf. The latter condition is achieved by *shorting*‡ the rotor field. A negative-sequence set of currents is fed into the machine from a generator running at full speed in opposite direction. The negative-sequence impedance is obtained as

$$z_- = \frac{V_a}{I_a} \tag{11-56}$$

† One should take the average in the three phases. By measuring peak to peak, the influence of the dc component is annulled.

‡ *Not* by *opening* it. Both z_- and z_0 (like X'_d and X''_d) are a result of induced *rotor* currents. We must perform the test so as to let these currents freely flow.

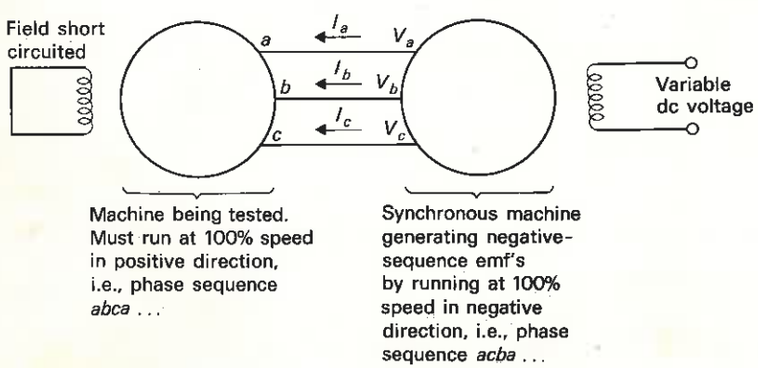

Figure 11-6 Finding generator negative sequence impedance by test.

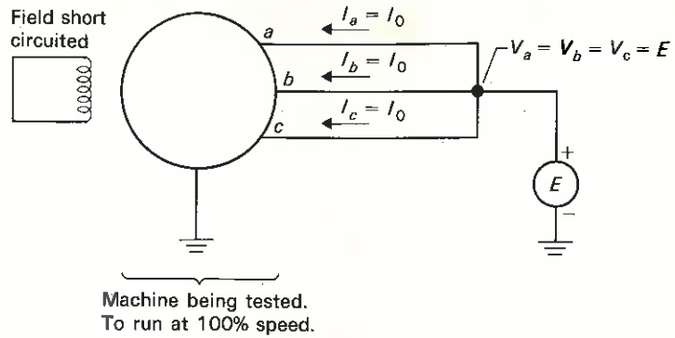

Figure 11-7 Finding generator zero sequence impedance by test.

Caution: As z_- usually is of quite small magnitude (Table 4-1), care should be taken not to overload the armature windings.

As the armature current wave meets the rotor at a relative speed of 200 percent, heavy 120-Hz currents will be induced in the damper winding. The effect, as felt from the stator side, is quite similar to that which created the subtransient reactance (Sec. 4-13-6). (As seen from Table 4-1 x_- and X''_d are therefore of about equal magnitude.)

C. Zero-sequence impedance Figure 11-7 depicts a setup by which the zero-sequence impedance of a synchronous machine can be obtained by *test*. The machine is being run at synchronous speed, and its field is shorted. A single-phase source E impresses zero-sequence voltages upon the three stator windings.

The zero-sequence impedance is obtained from

$$z_0 = \frac{E}{I_a} \tag{11-57}$$

z_0 has a very small value for the following reason. Due to the winding symmetry the three in-phase stator currents will all be of equal magnitude. They therefore create equal fluxes. But the fluxes (compare Fig. 4-1) have such magnetic axes that their vectorial sum vanishes. The reactance which is proportional to the flux-to-current ratio will thus also vanish.†

11-4 SEQUENCE IMPEDANCES OF TRANSMISSION LINES

A transmission line is always terminated in transformers which typically have their HV neutrals grounded, possibly over some grounding impedance. In an unbalanced load or fault situation a return path is therefore provided for a neutral current I_n.

† There will be *some* flux (and reactance) due to leakage fluxes.

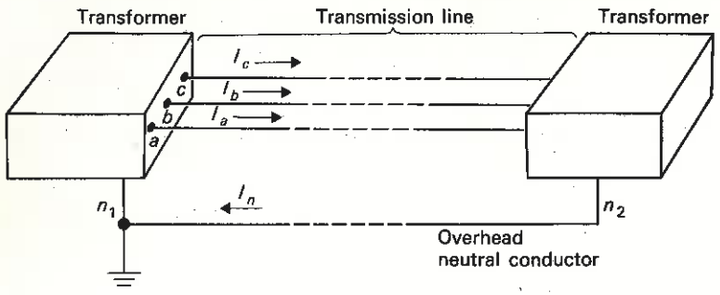

Figure 11-8 In determining zero-sequence impedance of a line it is important to know the return path of neutral current I_n.

11-4-1 Effect of Neutral Current upon Line Equations

Return for a moment to the phase-symmetric transmission line analyzed in Example 6-3. Based upon the assumption of zero neutral current we concluded (compare Eqs. (3-19) and (6-32)) that decoupling exists between the phase currents.

We assume now a fully unbalanced set of line currents including the presence of zero sequence components, i.e., the existence of neutral return current. We assume this current to flow in an overhead "neutral" conductor of radius R_n located at the average† distance D_n from each of the three phase conductors (Fig. 11-8).

In the symmetrically loaded line "ground" potential is everywhere the same and by definition set equal to zero. In the present case the neutrals n_1 and n_2 (Fig. 11-8) have different potentials and we must exercise caution in defining voltage drops.

If we define ΔV_{an_2} to mean the drop measured from terminal marked a to neutral n_2 then the drop equals

$$\Delta V_{an_2} = j\omega \frac{\mu_0}{2\pi}\left[\left(\frac{1}{4} + \ln\frac{1}{R}\right)I_a + \ln\frac{1}{D}I_b + \ln\frac{1}{D}I_c - \ln\frac{1}{D_n}I_n\right] \quad (11\text{-}58)$$

This is the same expression as in Eq. (6-30) with an additional term added representing the voltage induced in the phase conductor by the current in the neutral conductor.

In a practical situation we are more interested in the *total line drop* measured between terminal a and n_1. This drop equals the one in Eq. (11-58) plus the drop along the neutral conductor, the latter equaling

$$\Delta V_n = j\omega \frac{\mu_0}{2\pi}\left[\left(\frac{1}{4} + \ln\frac{1}{R_n}\right)I_n - \ln\frac{1}{D_n}I_a - \ln\frac{1}{D_n}I_b - \ln\frac{1}{D_n}I_c\right] \quad (11\text{-}59)$$

† Achieved by transposition.

By adding Eqs. (11-58) and (11-59) we obtain, after some algebra,

$$\begin{aligned}\Delta V_{an_1} &= \Delta V_{an_2} + \Delta V_n \\ &= j\omega\frac{\mu_0}{2\pi}\left[\left(\frac{1}{2} + \ln\frac{D_n^2}{RR_n}\right)I_a + \left(\frac{1}{4} + \ln\frac{D_n^2}{R_nD}\right)I_b + \left(\frac{1}{4} + \ln\frac{D_n^2}{R_nD}\right)I_c\right]\end{aligned} \quad (11\text{-}60)$$

The line has phase symmetry and therefore similar expressions can be written for ΔV_{bn_1} and ΔV_{cn_1}. In summary we have

$$\begin{bmatrix}\Delta V_{an_1}\\ \Delta V_{bn_1}\\ \Delta V_{cn_1}\end{bmatrix} = \begin{bmatrix} z_1 & z_2 & z_2\\ z_2 & z_1 & z_2\\ z_2 & z_2 & z_1\end{bmatrix}\cdot\begin{bmatrix}I_a\\ I_b\\ I_c\end{bmatrix} \quad (11\text{-}61)$$

For brevity we have introduced the reactive line impedances

$$\begin{aligned} z_1 &\triangleq j\omega\frac{\mu_0}{2\pi}\left(\frac{1}{2} + \ln\frac{D_n^2}{RR_n}\right)\\ z_2 &\triangleq j\omega\frac{\mu_0}{2\pi}\left(\frac{1}{4} + \ln\frac{D_n^2}{R_nD}\right)\end{aligned} \quad (11\text{-}62)$$

11-4-2 Sequence Line Impedances

We write Eqs. (11-61) in compact form

$$\Delta V_p = \mathbf{Z}_p\mathbf{I}_p \quad (11\text{-}63)$$

whereupon we SC transform them

$$\mathbf{T}\Delta\mathbf{V}_s = \mathbf{Z}_p\mathbf{T}\mathbf{I}_s$$

or

$$\Delta\mathbf{V}_s = \mathbf{T}^{-1}\mathbf{Z}_p\mathbf{T}\mathbf{I}_s = \mathbf{Z}_s\mathbf{I}_s \quad (11\text{-}64)$$

We readily confirm that

$$\mathbf{Z}_s \triangleq \mathbf{T}^{-1}\mathbf{Z}_p\mathbf{T} = \begin{bmatrix} z_+ & 0 & 0\\ 0 & z_- & 0\\ 0 & 0 & z_0\end{bmatrix} \quad (11\text{-}65)$$

where

$$z_+ = z_- \triangleq z_1 - z_2 = j\omega\frac{\mu_0}{2\pi}\left(\frac{1}{4} + \ln\frac{D}{R}\right) \quad (11\text{-}66)$$

and

$$z_0 \triangleq z_1 + 2z_2 = j\omega\frac{\mu_0}{2\pi}\left(1 + \ln\frac{D_n^6}{RR_n^3D^2}\right) \quad (11\text{-}67)$$

We make the following observations:

1. The $\mathbf{Z}_s$ matrix is diagonal.
2. The positive sequence reactance, as could be expected, equals the "per-phase" reactance computed in Chap. 6. (Compare Eq. 6-34.)
3. A transmission line, being a *passive* network component, offers the same impedance to positive and negative sequence currents.
4. $|z_0|$ is quite larger than $|z_+|$ and $|z_-|$.

We show this fact in the following numerical example.

Example 11-6 Find the sequence reactances for the phase-symmetric line in Example 6-3, having the conductor data

$$D = 5 \text{ m}$$
$$R = 1.5 \text{ cm}$$
$$D_n = 5 \text{ m}$$
$$R_n = 0.5 \text{ cm}$$
$$f = 60 \text{ Hz}$$

SOLUTION $|z_+| = |z_-|$ was computed in Example 6-3 and was found to equal 0.457 Ω/km. For $|z_0|$ we have

$$|z_0| = 377 \cdot \frac{4\pi \times 10^{-7}}{2\pi}\left(1 + \ln \frac{500^6}{1.5 \times 0.5^3 \times 500^2}\right)$$
$$= 2.08 \ \Omega/\text{km}, \text{ that is, 4.5 times the magnitude of } |z_+|.$$

A final important observation is in order. We were able to derive a formula for z_0 because *the neutral return path was assumed known.* If all or some of the current "vagabonds" through earth (and it usually does) then, at best, we can only derive empiric formulas for z_0. Finding z_0 by measurement is the last resort is such cases.

11-5 SEQUENCE IMPEDANCES OF TRANSFORMERS

11-5-1 Positive- and Negative-Sequence Impedances

The positive-sequence impedance of a transformer equals, of course, the leakage impedance. Since the transformer, like a transmission line, is a *static* device the leakage impedance will *not* change if the phase sequence is altered from *abca*... to *acba*.... As a result, we can conclude that the positive- and negative-sequence impedances are identical, i.e.,

$$z_+ = z_- = Z_L \tag{11-68}$$

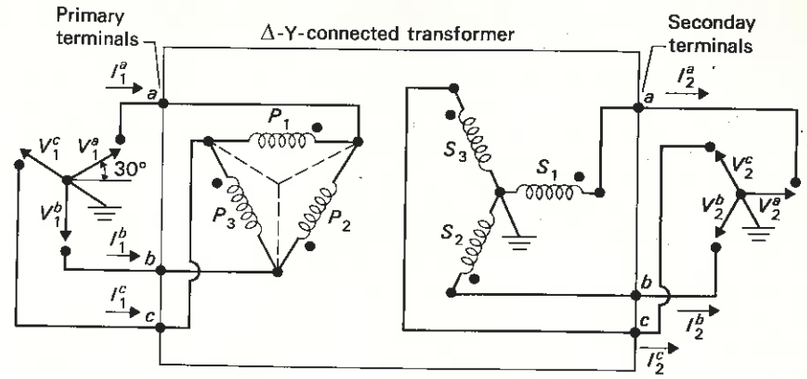

Figure 11-9 Δ-Y-connected transformer energized from a positive-sequence voltage set.

11-5-2 Phaseshift Dependency on Sequence Type

Although the three-phase transformer, *regardless of its connection-type*, offers the same impedance to the positive and negative sequence currents it does affect these sequence components differently in regard to *phase shift*. The phase-shift rule is as follows:

If the transformer imparts a phase shift of α degrees to the positive sequence set of voltages and currents the negative sequence voltages and currents will experience a shift of −α degrees.

The situation is clarified in Figs. 11-9 and 11-10. In the first case (Fig. 11-9) we apply the positive sequence voltage sets V_1^a, V_1^b, and V_1^c to the primary terminals *a*, *b*, and *c* of a Δ-Y-connected transformer. By letting the angular orientation of the six windings coincide with that of their respective voltage

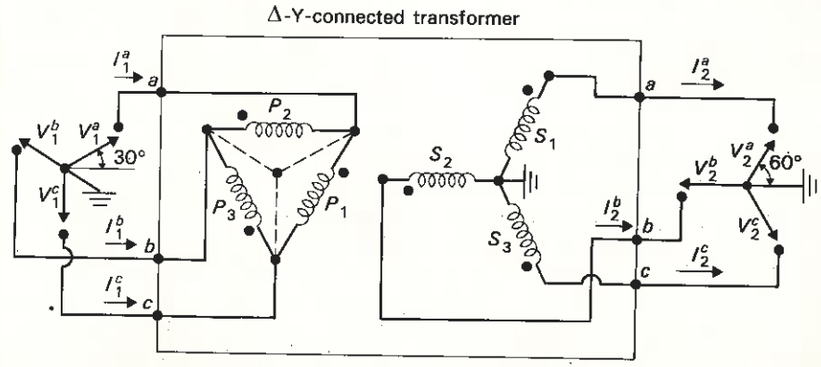

Figure 11-10 The Δ-Y-connected transformer in Fig. 11-9 energized from a negative-sequence voltage set.

phasors† we find by inspection that the secondary voltage set V_2^a, V_2^b, and V_2^c is of *positive sequence* and *lags* the input voltage set by 30°.

In Fig. 11-10 we apply a *negative sequence* voltage set V_1^a, V_1^c, and V_1^b to the *same* set of primary terminals *a*, *b*, and *c*. *Note that we make no internal connection changes in the transformer. We do, however, reorient the windings to account for the angular change in winding voltages.*

By inspection we find this time that the output set of voltages is also of *negative sequence*. In addition the secondary voltages *lead* the primary ones by 30°.

What has been said about voltages also applies to primary and secondary currents as well, as Eq. (5-35) must be satisfied.

Example 11-7 The Δ-Y transformer in Figs. 11-9 and 11-10 serves as a step-up transformer between a 300-MVA, 23-kV generator and a 230-kV grid. A solid short circuit occurs between phases *b* and *c* on the secondary (HV) side. The fault current amounts to 10 kA. Determine the primary currents in all three generator phases. Also find the currents in the transformer primaries.

SOLUTION We solve the problem by two different approaches:

Method A Study the positive and negative sequence currents separately. According to the results in Example 11-2 the sequence current sets for this type of fault are as shown in Fig. 11-3*b*. From Eq. (11-23) we obtain for the *rms* values of the sequence component currents, measured on the HV side,

$$|I_{a+}| = |I_{a-}| = \frac{10}{\sqrt{3}} = 5.774 \text{ kA} \tag{11-69}$$

(No zero sequence current exists.)

The "three-phase transformation ratio" equals $|a| = 23/230 = 0.100$. The sequence current components *measured at the generator terminals* are thus

$$|I_{a+}| = |I_{a-}| = \frac{5.774}{0.1} = 57.74 \text{ kA} \tag{11-70}$$

Due to the transformer phase shift the secondary *positive* sequence currents will be *advanced* by 30° and the *negative* sequence currents *retarded* by 30° as measured at the generator terminals. The current picture in Fig. 11-3*b* thus will change to the one in Fig. 11-11*a*. From the latter diagram we obtain directly

$$\begin{aligned} I_1^b &= I_{b+} + I_{b-} = 115.5 \text{ kA} \\ I_1^a &= I_1^c = I_{c+} + I_{c-} = -57.74 \text{ kA} \end{aligned} \tag{11-71}$$

The phasors I_1^a, I_1^b and I_1^c are shown in Fig. 11-11*b*.

Method B Satisfy the "mmf balance" on all three transformer cores.

After the short circuit the secondary *phase* currents equal

$$I_2^a = 0$$

$$I_2^b = -I_2^c = 10 \text{ kA}$$

† For example, the line voltage $V_1^a - V_1^c$ has a zero phase angle. It is connected across the primary winding P_1. Thus P_1 *and its secondary* S_1 are depicted at zero angle.

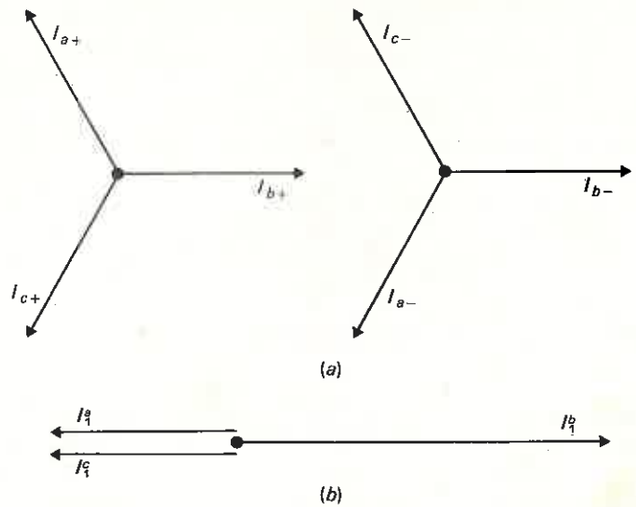

Figure 11-11 Component currents relating to Example 11-7.

According to Figs. 11-9 or 11-10 these three currents also equal the *winding* currents in S_1, S_2, and S_3 respectively. The transformation ratio between the *P* and *S* windings equals $23 : 230/\sqrt{3} = 0.1732$. As the winding S_1 carries zero current the primary winding P_1 must likewise be empty. Thus we have

$$I_1^a = \text{current in } P_2 = -I_2^b/0.1732 = -57.74 \text{ kA}$$

$$I_1^c = \text{current in } P_3 = I_2^c/0.1732 = -57.74 \text{ kA}$$

$$I_1^b = -(I_1^a + I_1^c) = 115.5 \text{ kA}$$

These results agree with those computed by method A.

11-5-3 Zero-sequence Impedance

The zero-sequence impedance of a transformer depends greatly on the winding type (Δ or Y) and also upon whether or not the neutrals are grounded.

Whereas the positive- and negative-sequence per-unit impedances are independent of whether the sequence currents are injected into the primaries or secondaries, the zero-sequence impedance will in general have widely different values, depending upon what terminals we view.

Figure 11-12 depicts the test setup for finding the impedance experimentally. The zero-sequence impedance $z_0 = E/I_0$ may or may not have different values as measured from one side or the other. Let us demonstrate with three important cases.

Case A. Transformer YY-*connected; both neutrals solidly grounded* This case is depicted in Fig. 11-13*a*. The solid grounding of both neutrals guarantees

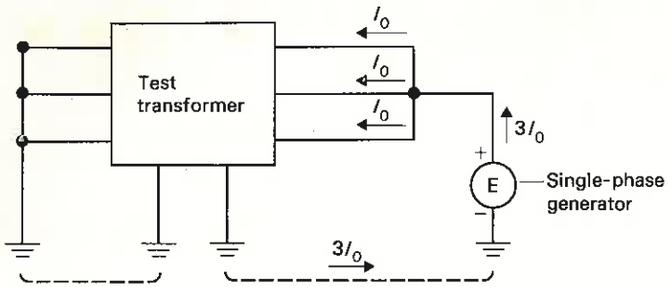

Figure 11-12 Finding the transformer zero-sequence impedance by test.

that the ground currents $3I_0$ and $3I_0/a$ have free circulating paths. Clearly, the current is impeded only by the leakage impedance per phase, and the zero-sequence impedance therefore equals the leakage impedance. Obviously, we measure the same impedance from *both sides* (if expressed in *per*

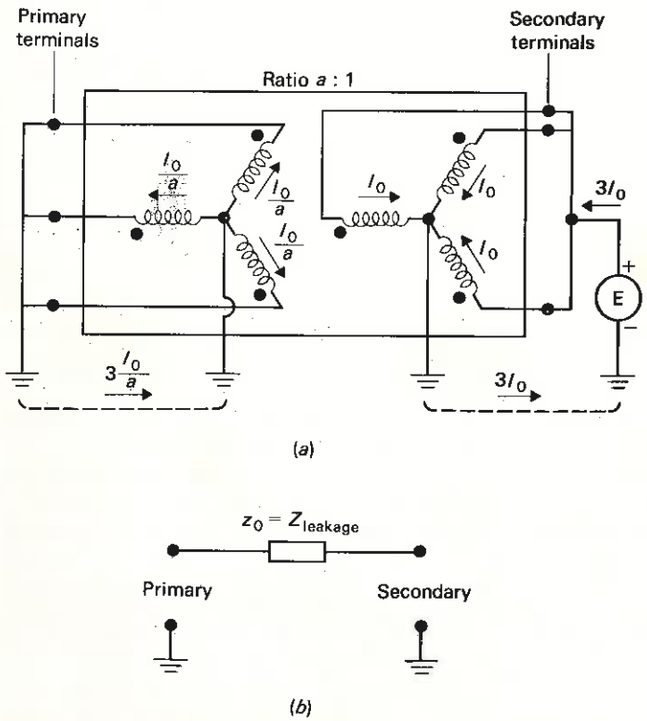

Figure 11-13 Zero-sequence network of Y-Y-connected transformer with both neutrals solidly grounded.

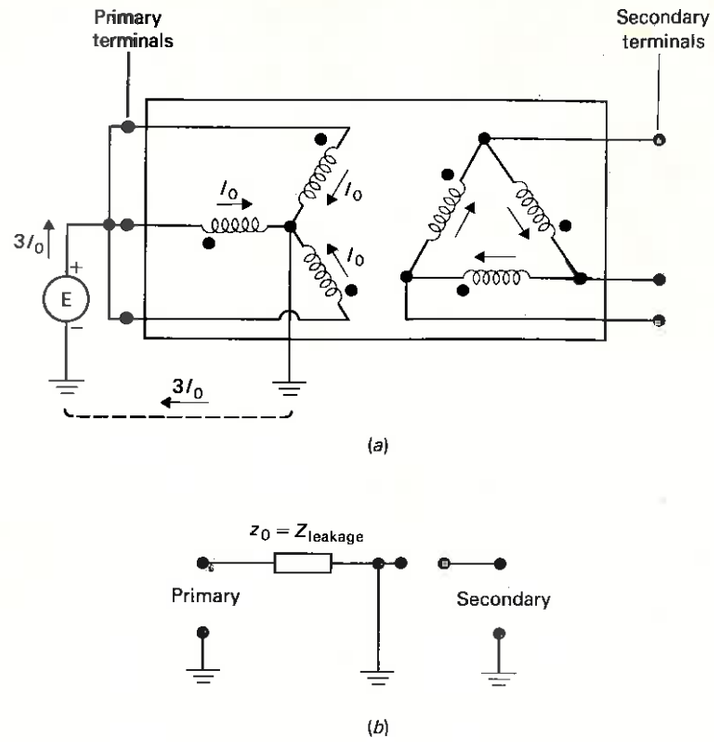

Figure 11-14 Zero-sequence network of Δ-Y-connected transformer with solidly grounded neutral.

unit, of course; the *ohmic* values would be in the ratio a^2). We may represent the zero-sequence network as depicted in Fig. 11-13*b*.

Case B. Transformer YΔ*-connected; neutral solidly grounded* This case, depicted in Fig. 11-14*a* indicates that the zero-sequence impedance measured from the Y side equals the leakage impedance. Note also that as the secondary currents *circulate* in the Δ, *no zero-sequence currents will leave these terminals*. This explains the short circuit to ground in the sequence network in Fig. 11-14*b*. No zero-sequence currents can be injected into the Δ terminals. Thus, in the sequence network, we have an interrupt in the corresponding terminals.

Case C. Transformer YY*-connected; one neutral grounded* This case is shown in Fig. 11-15*a*.

It should be noted that although a path is provided to ground for the zero-sequence currents in the primaries, no such path exists in the secondaries. Consequently, from a zero-sequence point of view, the secondaries will act as if *open-circuited*; i.e., from the primary side we will measure the open-circuit,

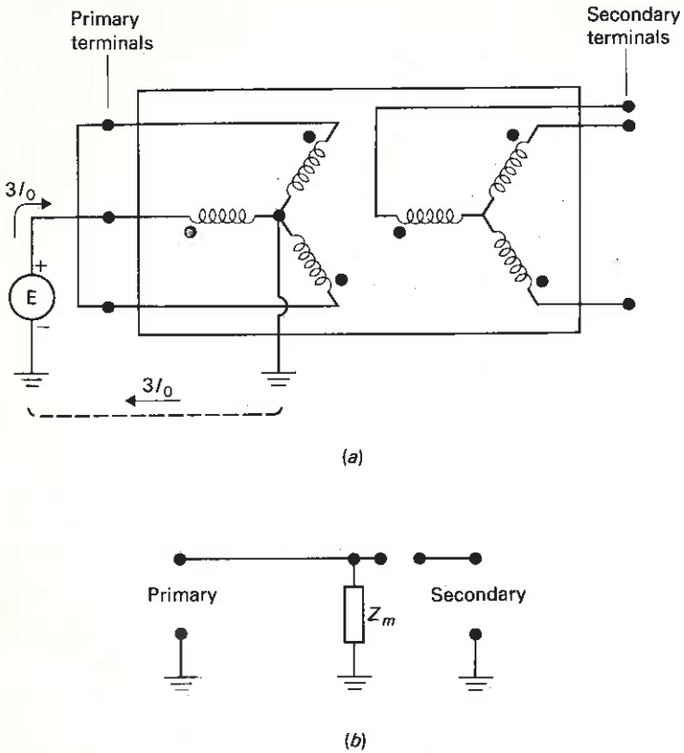

Figure 11-15 Zero-sequence network of Y-Y-connected transformer with one grounded neutral.

or *magnetizing, impedance*. From the secondary side the zero-sequence currents will meet a total interruption. The zero-sequence network will thus appear as shown in Fig. 11-15*b*. It should be noted that, since the magnetizing impedance is very large ($\approx$ 10,000 percent), we can in practice assume infinite impedance from *both* terminals.

The above three cases are the most important from a practical point of view. In determining the zero-sequence networks for *any* three-phase transformer, the following simple rules should be followed:

1. Does the winding type permit zero-sequence currents a path to ground? If not, the sequence network will contain an interruption for the winding in question.
2. Are the zero-sequence currents confined to circulation in a specific winding? If so, provide a short circuit to ground in the sequence network, indicating that the currents are not leaving the terminals.
3. Does the absence of a path to ground mean that the transformer is effectively open circuited for zero-sequence currents? If so, the zero-sequence network must contain the magnetizing impedance in the branch in question.
4. Do the zero-sequence currents injected into a set of terminals flow *freely*? If so, add only the leakage impedance to this branch in question.

Example 11-8 Find the zero-sequence network for the three-winding transformer treated in Example 5-12, assuming that both the primary and secondary neutrals are solidly grounded. The analysis performed in Example 5-5 rendered the equivalent (positive- and negative-sequence) network that was shown in Fig. 5-21*b*.

By direct application of the set of rules given above we obtain the zero-sequence network shown in Fig. 11-16. Note that all leakage impedances are the same as those computed for the positive-sequence network.

11-6 SHORT-CIRCUIT ANALYSIS OF UNBALANCED LOW-ORDER SYSTEMS

We have presented the symmetrical components and developed sequence networks for generators, transformers, and transmission lines. The remaining part of the chapter will be devoted to analysis of systems subject to unbalanced short circuit (or loading). Such studies generally proceed in three steps:

1. Assembly of systems model consisting of three separate sequence networks and their appropriate description.
2. Choice of type and location of fault and the mathematical description of same.
3. Solution of the resulting network equations by means of Thévenin's theorem. Currents and voltages are found not only at the point of fault but throughout the system.

There is a considerable variation of approach for systems of "low" order and for systems that we can term "large scale." For the latter type of system the analysis methods must by necessity be matched to computer use. They must therefore be characterized by a high degree of generality.

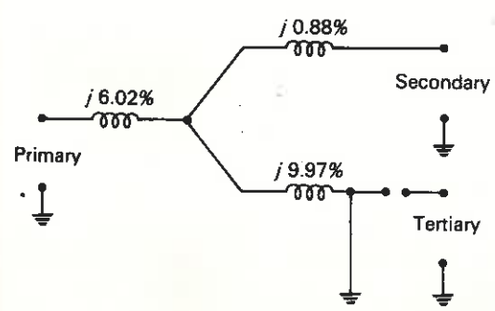

Figure 11-16 Zero-sequence network of Y-Y-Δ-connected three-winding transformer. Both neutrals solidly grounded.

For a low-order system we can take analytical "short cuts" in the form of simple network reduction schemes and in the way the fault is "coupled" to the rest of the network. A low-order system lends itself to textbook use and we begin therefore our analysis by turning again to the two-bus system to which the reader has been earlier introduced.

In the next section we shall develop a more general approach.

11-6-1 The Two-Bus System—Problem Statement

The component data given in Fig. 10-11 still applies.

As in Sec. 10-3-2 we shall assume the fault to occur on bus 1 in Fig. 10-11. We shall be interested in the fault currents *immediately* following the short and shall treat two different fault types:

A. Single-line-to-ground
B. Line-to-line

We shall make use of the Thévenin's theorem and work the problem under the following simplifying assumptions:

1. The prefault bus voltage is 1 pu.
2. The prefault load currents are neglected besides the fault-induced components.
3. All sequence impedances are reactive.
4. Line capacitances are neglected.
5. The faults are solid.

It should be noted that none of the above simplifying assumptions reduces the generality of our approach. However, they simplify considerably our computational efforts and should enhance the clarity of our textbook example.

In addition to the system data presented in Sec. 10-3-2 we add the following:

1. The negative sequence impedance of both generators equals $j0.10$ pu.
2. The zero-sequence impedance of both generators equals $j0.05$ pu. The generator neutrals are solidly grounded.
3. Transformers T_1 and T_2 are connected Y-Y and Δ-Y respectively. In the latter the HV winding is the Y-connected one. All neutrals are solidly grounded.
4. The zero sequence impedance of the line equals $j0.55$ pu.

11-6-2 Sequence Network Assembly and Reduction

We assemble now individually the three sequence networks, whereupon we reduce these networks in such a manner that the fault point, i.e., bus 1, is being preserved after the reduction process.

A. Positive-sequence network The positive-sequence network is identical to the one we used in Chap. 10 and shown in Fig. 10-12. It was reduced to the simple Thévenin equivalent in Fig. 10-12*d* which we thus will make use of in our present case.

B. Negative-sequence network The only parameter that will change from the positive-sequence network is the generator impedance. However, as we here are interested in the currents *immediately* following the fault we shall set $z_+ = jX''_d$. *As $z_- \approx jX''_d$ the positive- and negative-sequence networks are approximately identical as far as impedances are concerned.*† Of course, the negative-sequence network contains no active source.

C. Zero-sequence network This network is radically different from the positive- and negative-sequence ones. Following the rules outlined earlier we assemble the total network as shown in Fig. 11-17*a*. It is reduced in two steps to the one shown in Fig. 11-17*c*.

11-6-3 Single-Line-to-Ground Fault

The stage is now set to select the type of fault or the unbalanced loading we wish to study. The single-line-to-ground fault is the most commonly encountered system disturbance and we choose it as our first example.

A. Sequence network interconnection For this type of fault the sequence components of the fault current are all equal in the faulted phase (Eq. 11-21). As in Example 11-5 we assure equality of I_{a+}, I_{a-}, and I_{a0} by series-connecting the reduced sequence networks with the result shown in Fig. 11-18.

B. Computation of fault current and voltages With the prefault bus voltage of phase a, V_a^0, chosen as phasor reference we obtain from Fig. 11-18 for the sequence currents

$$I_{a+} = I_{a-} = I_{a0} = \frac{1\angle 0^\circ}{j0.144 + j0.144 + j0.136} = 2.358\angle -90^\circ \text{ pu} \quad (11\text{-}72)$$

and for the fault current

$$I^f = 3I_{a+} = 7.08\angle -90^\circ \text{ pu} \quad (11\text{-}73)$$

We then can compute the sequence voltage components

$$\begin{aligned} V_{a+} &= 1\angle 0^\circ - (2.358\angle -90^\circ)j0.144 = 0.660\angle 0^\circ \text{ pu} \\ V_{a-} &= 0 - (2.358\angle -90^\circ)j0.144 = 0.340\angle 180^\circ \text{ pu} \\ V_{a0} &= 0 - (2.358\angle -90^\circ)j0.136 = 0.321\angle 180^\circ \text{ pu} \end{aligned} \quad (11\text{-}74)$$

† It is quite a common industry-practice, even in work with large-scale systems, to set the positive and negative networks, equal.

FAC. DE CIENCIAS EXACTAS Y TECNOLOGIA
BIBLIOTECA

Finally, we compute the phase voltages

$$V_a = 0$$
$$V_b = \alpha^2 V_{a+} + \alpha V_{a-} + V_{a0} = 0.991\underline{/-119.0^\circ} \text{ pu} \qquad (11\text{-}75)$$
$$V_c = \alpha V_{a+} + \alpha^2 V_{a-} + V_{a0} = 0.991\underline{/119.0^\circ} \text{ pu}$$

We note that the short-circuit current in phase a is slightly higher than that resulting from a symmetric fault (Eq. 10-19). This is due to the low zero-sequence generator impedance and the proximity between generator $G1$ and the fault. Note also that although V_a drops to zero, $|V_b|$ and $|V_c|$ remain almost at prefault values.

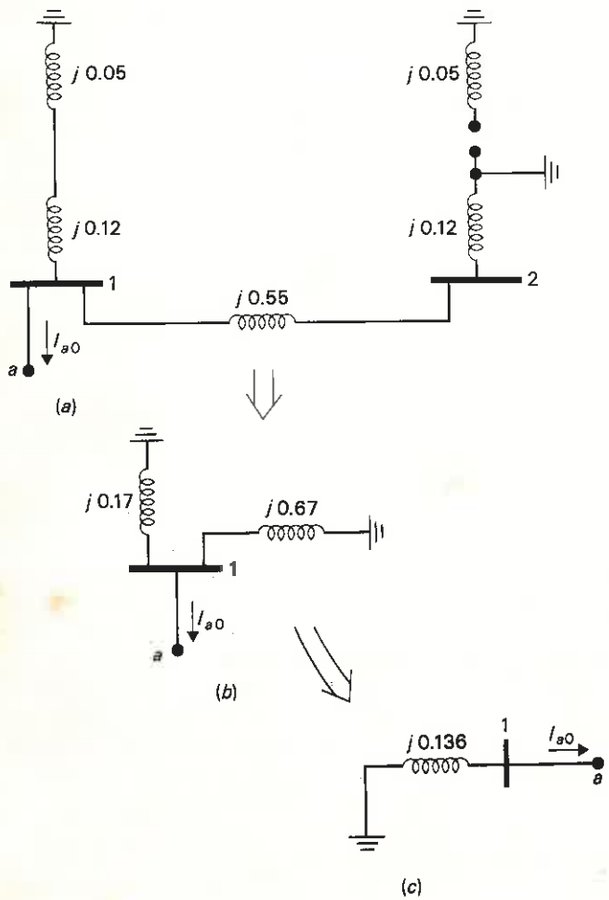

Figure 11-17 Zero sequence network of two-bus example system and its step-by-step reduction.

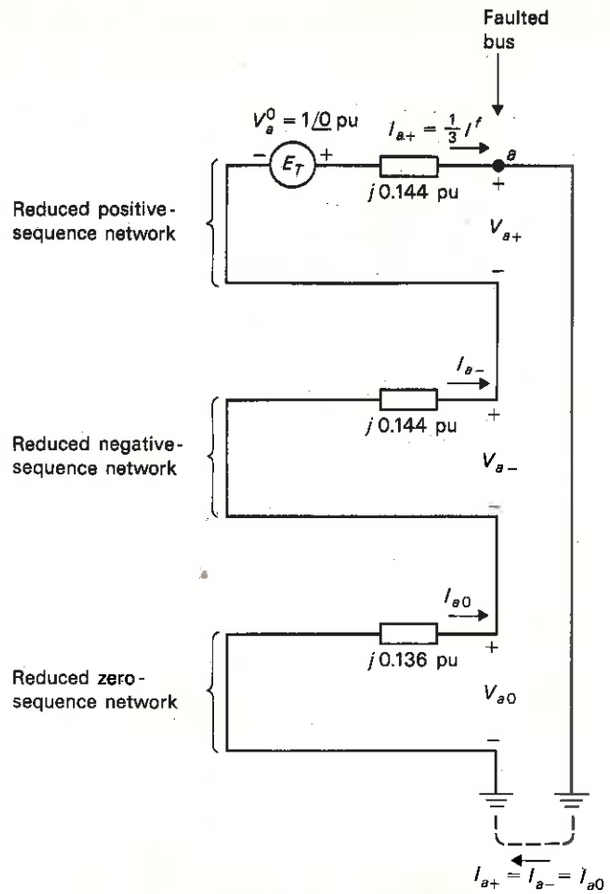

Figure 11-18 Interconnection of the sequence networks to simulate a single-line-to-ground fault at bus 1.

C. Computation of currents in $G1 - T1$ To compute the phase currents in any of the network branches we must first determine what portions of the fault current sequence components will flow in the branch in question.

For example let us compute the phase currents in $G1$ and $T1$. First we note that because of the Y-Y transformer connection (compare Fig. 11-13) all sequence current components have equal magnitudes (expressed in per unit) *and* phase in the $T1$ primaries and secondaries. *Thus, the phase currents in* $G1$ *and* $T1$ *are equal.*

From Fig. 10-12*c* we note that the portions of the positive- and negative-sequence fault currents that will flow in $G1$–$T1$ equal

$$I_{a+} = I_{a-} = \frac{0.42}{0.42 + 0.22}(2.358\underline{/-90^\circ}) = 1.547\underline{/-90^\circ} \text{ pu} \qquad (11\text{-}76)$$

Similarly, Fig. 11-17*b* tells how much zero-sequence current will flow in $T1$–$G1$:

$$I_{a0} = \frac{0.67}{0.67 + 0.17}(2.358\angle{-90^\circ}) = 1.881\angle{-90^\circ} \text{ pu} \tag{11-77}$$

For the $G1$–$T1$ phase currents we then have

$$\begin{bmatrix} I_a \\ I_b \\ I_c \end{bmatrix} = \begin{bmatrix} 1 & 1 & 1 \\ \alpha^2 & \alpha & 1 \\ \alpha & \alpha^2 & 1 \end{bmatrix} \begin{bmatrix} 1.547\angle{-90^\circ} \\ 1.547\angle{-90^\circ} \\ 1.881\angle{-90^\circ} \end{bmatrix} = \begin{bmatrix} 4.98\angle{-90^\circ} \\ 0.33\angle{-90^\circ} \\ 0.33\angle{-90^\circ} \end{bmatrix} \text{pu} \tag{11-78}$$

Note that although the phase currents I_b and I_c are zero *at the fault* they are nonzero in $G1$–$T1$.

The currents in each of the three neutrals of $T1$ and $G1$ equal

$$I_n = 3 \times I_{a0} = 5.643\angle{-90^\circ} \text{ pu} \tag{11-79}$$

D. Computation of currents in line and $T2$ The zero-sequence currents in $T2$ will not reach $G2$. Furthermore the positive- and negative-sequence currents will experience different phase shifts in $T2$. *As a result the phase currents flowing in $T2$ will be different from those in $G2$.*

The phase currents in the $T2$ *secondaries* will equal those in the transmission line. To find these currents we first find their sequence components, using the same technique as above:

$$I_{a+} = I_{a-} = \frac{0.22}{0.22 + 0.42}(2.358\angle{-90^\circ}) = 0.811\angle{-90^\circ} \text{ pu} \tag{11-80}$$

$$I_{a0} = \frac{0.17}{0.17 + 0.67}(2.358\angle{-90^\circ}) = 0.477\angle{-90^\circ} \text{ pu} \tag{11-81}$$

For the actual phase currents we then get

$$\begin{bmatrix} I_a \\ I_b \\ I_c \end{bmatrix} = \begin{bmatrix} 1 & 1 & 1 \\ \alpha^2 & \alpha & 1 \\ \alpha & \alpha^2 & 1 \end{bmatrix} \begin{bmatrix} 0.811\angle{-90^\circ} \\ 0.811\angle{-90^\circ} \\ 0.477\angle{-90^\circ} \end{bmatrix} = \begin{bmatrix} 2.10\angle{-90^\circ} \\ 0.33\angle{+90^\circ} \\ 0.33\angle{+90^\circ} \end{bmatrix} \text{pu} \tag{11-82}$$

The current in the HV neutral of $T2$ equals

$$I_n = 3 \times I_{a0} = 1.43\angle{-90^\circ} \text{ pu} \tag{11-83}$$

Note that the currents in phases b and c are equal, but with opposite phase, to those in $G1$–$T1$. In other words, these currents circulate between the transformers *without reaching the fault.*

E. Computation of currents in $G2$ The currents given in Eq. (11-82) flow in the HV terminals of $T2$ and also in the primary Δ winding. However, they are *not* equal to the currents at the LV terminals of $T2$ and in $G2$.

In the first place the zero-sequence components flowing in the HV winding will not appear outside the LV terminals. Secondly, the positive and negative sequence components that *will* flow at the LV terminals of $T2$ will have experienced different phase shifts.

Assuming that the Δ-Y connected $T2$ has the same internal connection as the transformer in Fig. 11-9 the positive- and negative-sequence currents that we computed under **D** above must be advanced and retarded by 30° respectively. We thus obtain for the phase currents in $G2$

$$\begin{aligned} I_a &= 0.811\angle{-90^\circ + 30^\circ} + 0.811\angle{-90^\circ - 30^\circ} = 1.41\angle{-90^\circ} \text{ pu} \\ I_b &= 0.811\angle{-90^\circ - 120^\circ + 30^\circ} + 0.811\angle{-90^\circ + 120^\circ - 30^\circ} = 0 \text{ pu} \\ I_c &= 0.811\angle{-90^\circ + 120^\circ + 30^\circ} + 0.811\angle{-90^\circ - 120^\circ - 30^\circ} = 1.41\angle{+90^\circ} \end{aligned} \tag{11-84}$$

To complete the analysis we need to find the phase voltages at bus 2 and also at each generator terminal. We reserve this job for the reader (see Prob. 11-10).

11-6-4 Line-to-Line Fault

A. Sequence network interconnection In Example 11-2 we analyzed the composition of the fault currents for this type of fault. We concluded (Eq. 11-23) that

$$I_{a+} = -I_{a-} \tag{11-85}$$

$$I_{a0} = 0 \tag{11-86}$$

As the fault is assumed solid the phases b and c must have equal potential, i.e.,

$$V_b = V_c \tag{11-87}$$

or in terms of sequence components

$$\alpha^2 V_{a+} + \alpha V_{a-} + V_{a0} = \alpha V_{a+} + \alpha^2 V_{a-} + V_{a0} \tag{11-88}$$

The last equation yields

$$V_{a+} = V_{a-} \tag{11-89}$$

Clearly, the three relations (11-85), (11-86), and (11-89) are satisfied if the reduced positive- and negative-sequence networks are interconnected terminal-to-terminal and the zero-sequence network kept open as shown in Fig. 11-19.

B. Computation of fault currents and voltages From the networks in Fig. 11-19 we obtain by inspection for the sequence currents

$$\begin{aligned} I_{a+} &= -I_{a-} = \frac{1\angle{0^\circ}}{j0.144 + j0.144} = 3.472\angle{-90^\circ} \text{ pu} \\ I_{a0} &= 0 \end{aligned} \tag{11-90}$$

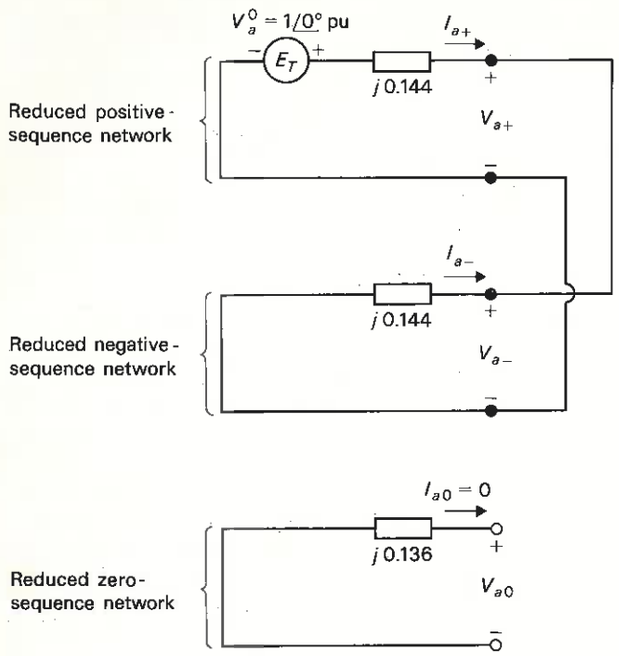

Figure 11-19 Interconnection of the sequence networks to simulate a line-to-line fault at bus 1.

For the phase currents in the fault we thus have

$$I_a = 0$$
$$I_b = \alpha^2(3.472\angle{-90°}) + \alpha(3.472\angle{90°}) = 6.01\angle{-180°} \text{ pu} \tag{11-91}$$
$$I_c = -I_b = 6.01\angle{0°} \text{ pu}$$

From Fig. 11-19 we have for the sequence voltages

$$V_{a+} = V_{a-} = 1\angle{0°} - (3.472\angle{-90°})j0.144 = 0.500\angle{0°} \text{ pu}$$
$$V_{a0} = 0 \tag{11-92}$$

The phase voltages follow from

$$V_a = V_{a+} + V_{a-} + V_{a0} = 0.500\angle{0°} + 0.500\angle{0°} + 0 = 1\angle{0°} \text{ pu} \tag{11-93}$$
$$V_b = V_c = \alpha^2 V_{a+} + \alpha V_{a-} + V_{a0} = 0.500\angle{180°} \text{ pu} \tag{11-94}$$

Note that the voltage of the healthy phase has not changed, whereas the voltages of the faulted phases have dropped to half of their prefault values.

The current and voltage picture at the fault is thus fully known. The current division between $T1$ and $T2$ can then be computed using the same approach as was employed for the single-line-to-ground fault.

The phase currents in $G1$ and $T1$ will be equal but those in $G2$ and $T2$ unequal (due to phase shift). Again, we are asking the reader to work out the details (see Prob. 11-11).

11-7 SHORT-CIRCUIT ANALYSIS OF UNBALANCED LARGE-SCALE SYSTEMS

We presented in Sec. 10-4 a *general* and *systematic* computational approach for the case of a balanced-fault situation. We shall now attempt to do the same for the unbalanced case. In effect, we shall merge the SCT method outlined in this chapter with Thévenin's method as used in Chap. 10. With certain modifications we can actually follow the analysis procedure in Sec. 10-4 step by step. As we encounter dissimilarities, we shall attempt to explain them. To make the comparison with Chap. 10 still more illustrative, we shall apply our analysis methods to the same three-bus example used in Chap. 10.

Since we must distinguish between prefault and postfault variables, phase values of currents and voltages, and their symmetrical components, in addition to keeping track of our regular vectors and matrices, with their respective subscripts, there is a possibility that we may end up in symbol confusion. To avoid this, and also to alert the reader, we shall agree from the outset on certain symbol rules:

Rule 1 Prefault conditions are indicated by the superscript 0.
Rule 2 Postfault or fault conditions are indicated by the superscript f.
Rule 3 Phase values of currents and voltages are indicated collectively by the subscript p, and individually by the subscripts a, b, and c.
Rule 4 Symmetrical components are indicated either collectively by the subscript s or individually by the subscripts $+$, $-$, or 0.
Rule 5 A number subscript always refers to the bus coding.

11-7-1 Problem Statement

We formulate our problem with reference to Fig. 11-20.

The system under study has n buses. It is initially operating in a symmetrical normal state. All prefault bus voltages are assumed known and so are the power flows.

An unbalanced fault occurs at bus q. The nature of the fault is assumed fully known. In the symmetrical fault in Chap. 10 the fault was determined from a knowledge of the fault impedance Z^f. In the present case we shall learn that the fault is fully determined from the knowledge of a fault impedance *matrix* $\mathbf{Z}^f$.

In the postfault state we seek the currents and the bus voltages at the faulted bus. These currents and voltages are indicated in Fig. 11-20. We also compute the bus voltages at all other buses and the currents in all lines, generators, and transformers. Neither the voltages nor currents are, of course, symmetrical.

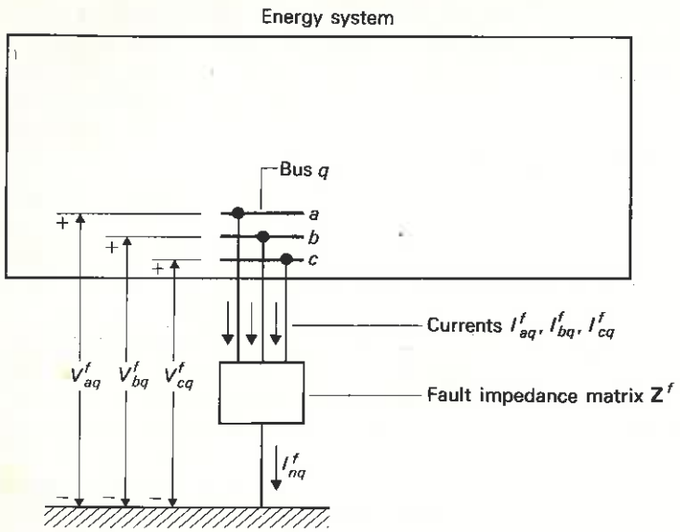

Figure 11-20 n-bus system subject to an unbalanced fault at bus q.

11-7-2 Network Modeling by Means of Sequence Bus Impedance Matrices

In Chap. 10 we learned that the $\mathbf{Z}_{\text{bus}}$ matrix proved to be a very useful network model for the purpose of finding short-circuit currents and voltages in the case of balanced faulting. Presently we shall discover that $\mathbf{Z}_{\text{bus}}$ modeling is equally useful in analysis of unbalanced fault situations.

As the network must be separately modeled for each of the three sequence systems there will be a need to construct three different bus impedance matrices. For both analytical and computational reasons this network data is best assembled into an *SC bus impedance matrix*, $\mathbf{Z}_{\text{s, bus}}$, of dimension $3n \times 3n$.

Example 11-9 Let us exemplify the construction of the SC bus impedance matrix by considering the same three-bus system that we investigated in Example 10-6. The system is depicted in Fig. 10-16 where also the positive-sequence impedances are identified.

The positive-sequence network The positive-sequence network is identical with the network upon which we based our symmetrical short-circuit study in Example 10-6. We had already computed the positive-sequence bus impedance matrix for this network (Eq. (10-38)). We repeat it here for easy reference:

$$\mathbf{Z}_{+\text{bus}} = j\begin{bmatrix} 0.0730 & 0.0386 & 0.0558 \\ 0.0386 & 0.0558 & 0.0472 \\ 0.0558 & 0.0472 & 0.1014 \end{bmatrix} = \begin{bmatrix} Z_{+11} & Z_{+12} & Z_{+13} \\ Z_{+21} & Z_{+22} & Z_{+23} \\ Z_{+31} & Z_{+32} & Z_{+33} \end{bmatrix} \tag{11-95}$$

The negative-sequence network The only changes from the positive-sequence network are found in the generator representations. There are no negative-sequence emf's generated, and the impedance will change from jX''_d to jx_-. Since in most cases x_- and X''_d will have almost equal numerical values, we will for simplicity assume them equal. (This assumption is very common in practice.)

The corresponding negative-sequence bus impedance matrix will thus be identical with that computed for the positive-sequence network, i.e.,

$$\mathbf{Z}_{-\text{bus}} = \mathbf{Z}_{+\text{bus}} \tag{11-96}$$

The zero-sequence network Whereas the positive- and negative-sequence networks are approximately equal from an impedance point of view, the zero-sequence network will be vastly different from both. To obtain this network we must make the following additional assumptions about the system components:

Generators Neutrals solidly grounded. The zero-sequence reactance is 10 percent (based upon ratings).
Transformers Connected ΔY (the generator side is Δ). The neutrals solidly grounded.
Transmission lines The zero-sequence impedance is measured to be $j20$ percent (50-MVA basis) in all three lines.

We can now assemble the zero-sequence network (see Fig. 11-21).
For this network we write down the bus admittance matrix by inspection

$$\mathbf{Y}_{0,\text{bus}} = j\begin{bmatrix} -30 & 5 & 5 \\ 5 & -50 & 5 \\ 5 & 5 & -10 \end{bmatrix} \tag{11-97}$$

We then obtain by inversion the zero sequence bus impedance matrix

$$\mathbf{Z}_{0,\text{bus}} = j\begin{bmatrix} 0.0380 & 0.0060 & 0.0220 \\ 0.0060 & 0.0220 & 0.0140 \\ 0.0220 & 0.0140 & 0.1180 \end{bmatrix} = \begin{bmatrix} Z_{0,11} & Z_{0,12} & Z_{0,13} \\ Z_{0,21} & Z_{0,22} & Z_{0,23} \\ Z_{0,31} & Z_{0,32} & Z_{0,33} \end{bmatrix} \tag{11-98}$$

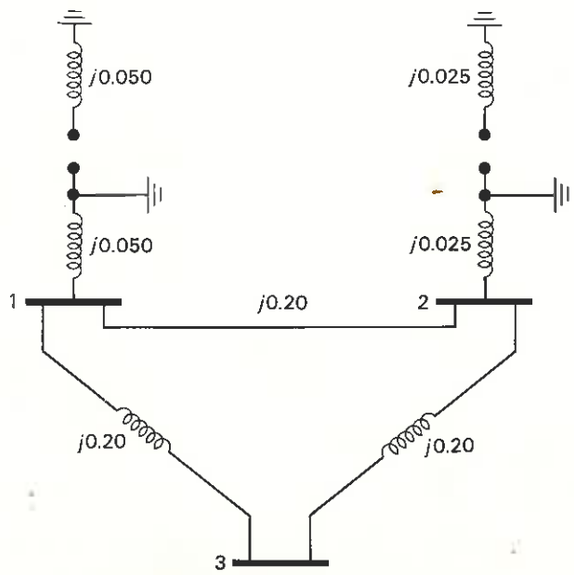

Figure 11-21 Zero-sequence network of three-bus example system.

We construct, finally, the 9 × 9 SC bus impedance matrix:

$$\mathbf{Z}_{s,\,\text{bus}} = \left[\begin{array}{ccc|ccc|ccc}
0.0730 & 0 & 0 & 0.0386 & 0 & 0 & 0.0558 & 0 & 0 \\
0 & 0.0730 & 0 & 0 & 0.0386 & 0 & 0 & 0.0558 & 0 \\
0 & 0 & 0.0380 & 0 & 0 & 0.0060 & 0 & 0 & 0.0220 \\
\hline
0.0386 & 0 & 0 & 0.0558 & 0 & 0 & 0.0472 & 0 & 0 \\
0 & 0.0386 & 0 & 0 & 0.0558 & 0 & 0 & 0.0472 & 0 \\
0 & 0 & 0.0060 & 0 & 0 & 0.0220 & 0 & 0 & 0.0140 \\
\hline
0.0558 & 0 & 0 & 0.0472 & 0 & 0 & 0.1014 & 0 & 0 \\
0 & 0.0558 & 0 & 0 & 0.0472 & 0 & 0 & 0.1014 & 0 \\
0 & 0 & 0.0220 & 0 & 0 & 0.0140 & 0 & 0 & 0.1180
\end{array}\right] \tag{11-99}$$

The SC bus impedance matrix in our example system is obviously constructed by nine submatrices, $\mathbf{Z}_{sij}$ each of dimension 3 × 3. Each 3 × 3 submatrix, $\mathbf{Z}_{sij}$, is *diagonal* with the three diagonal elements equaling z_{+ij}, z_{-ij} and z_{0ij} respectively. For an n-bus system $\mathbf{Z}_{s,\,\text{bus}}$ will consist of n^2 submatrices and be of the form

$$\mathbf{Z}_{s,\,\text{bus}} = \begin{bmatrix} \mathbf{Z}_{s11} & \mathbf{Z}_{s12} & \cdots & \mathbf{Z}_{s1n} \\ \mathbf{Z}_{s21} & \mathbf{Z}_{s22} & \cdots & \mathbf{Z}_{s2n} \\ \cdots & \cdots & \cdots & \cdots \\ \cdots & \cdots & \cdots & \cdots \\ \cdots & \cdots & \cdots & \cdots \\ \mathbf{Z}_{sn1} & \cdots & \cdots & \mathbf{Z}_{snn} \end{bmatrix} \tag{11-100}$$

11-7-3 SC Bus Voltage and Current Vectors

For an n-bus system operated in a balanced mode the n bus voltages and currents can be summarized in n-dimensional vectors $\mathbf{V}_{\text{bus}}$ and $\mathbf{I}_{\text{bus}}$ respectively. In the unsymmetrically faulted (or loaded) case each bus voltage and current can be decomposed into three symmetrical components. The n-bus system will thus be described by $3n$ voltage and current phasors, which can be arranged into $3n$-dimensional *SC bus voltage* and *bus current vectors* defined as follows

$$\mathbf{V}_{s,\,\text{bus}} \triangleq \begin{bmatrix} V_{+1} \\ V_{-1} \\ V_{01} \\ \cdots \\ \vdots \\ \cdots \\ V_{+i} \\ V_{-i} \\ V_{0i} \\ \cdots \\ \vdots \\ \cdots \\ V_{+n} \\ V_{-n} \\ V_{0n} \end{bmatrix} = \begin{bmatrix} \mathbf{V}_{s1} \\ \vdots \\ \mathbf{V}_{si} \\ \vdots \\ \mathbf{V}_{sn} \end{bmatrix} \quad \text{and} \quad \mathbf{I}_{s,\,\text{bus}} \triangleq \begin{bmatrix} I_{+1} \\ I_{-1} \\ I_{01} \\ \cdots \\ \vdots \\ \cdots \\ I_{+i} \\ I_{-i} \\ I_{0i} \\ \cdots \\ \vdots \\ \cdots \\ I_{+n} \\ I_{-n} \\ I_{0n} \end{bmatrix} = \begin{bmatrix} \mathbf{I}_{s1} \\ \vdots \\ \mathbf{I}_{si} \\ \vdots \\ \mathbf{I}_{sn} \end{bmatrix} \tag{11-101}$$

In very compact matrix language the total SC model of the unbalanced n-bus system can thus be written

$$\mathbf{V}_{s,\,\text{bus}} = \mathbf{Z}_{s,\,\text{bus}}\mathbf{I}_{s,\,\text{bus}} \tag{11-102}$$

Equation (11-102) consists of $3n$ *scalar* component equations. Alternatively, we can view the equation as consisting of n *vector* "components," each of dimension 3, the ith component of which reads

$$\mathbf{V}_{si} = \mathbf{Z}_{si1}\mathbf{I}_{s1} + \mathbf{Z}_{si2}\mathbf{I}_{s2} + \cdots + \mathbf{Z}_{sii}\mathbf{I}_{si} + \cdots + \mathbf{Z}_{sin}\mathbf{I}_{sn} \tag{11-103}$$

Much of the analysis to follow is based upon the use of such "3-vectors."

11-7-4 The Fault Matrices $\mathbf{Z}_s^f$ and $\mathbf{Y}_s^f$

In the simple two-bus example system we took account of fault type by appropriate interconnection of the sequence networks at the point of fault (Figs. 11-18 and 11-19). Now we need a more *general* method for describing the unbalanced fault and for incorporating it into our analysis.

The simple *scalar* equation (10-32) sufficed to describe the *balanced* fault in our general fault analysis in Chap. 10. This simple description is no longer possible. We proceed now to show that in the present *unbalanced* fault situation it takes a three-dimensional *vector* equation for a complete fault description.

Consider the *general* unbalanced case depicted in Fig. 11-22. By assigning proper values to the impedances Z_a, Z_b, Z_c, and Z_g, we can obtain any practically important fault case that we wish. For example, by setting

$$Z_a = Z_g = 0$$

and

$$Z_b = Z_c = \infty$$

we in effect create a solid single-line-to-ground short circuit on phase a. By setting

$$Z_a = \infty$$

and

$$Z_b = Z_c = Z_g = 0$$

we obtain a solid line-to-line short circuit with simultaneous ground contact. Other practically important fault configurations can likewise be created.

For the circuit in Fig. 11-22 we have the following relationships between voltages and currents:

$$\begin{aligned} V_{aq}^f &= I_{aq}^f Z_a + (I_{aq}^f + I_{bq}^f + I_{cq}^f)Z_g \\ V_{bq}^f &= I_{bq}^f Z_b + (I_{aq}^f + I_{bq}^f + I_{cq}^f)Z_g \\ V_{cq}^f &= I_{cq}^f Z_c + (I_{aq}^f + I_{bq}^f + I_{cq}^f)Z_g \end{aligned} \tag{11-104}$$

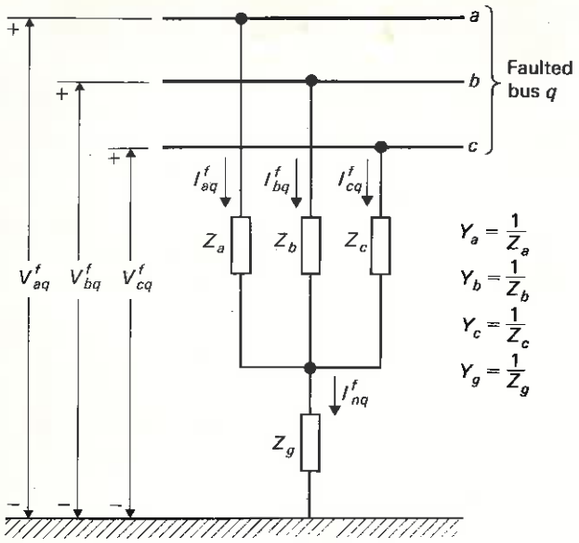

Figure 11-22 By proper choice of the impedances Z_a, Z_b, Z_c, and Z_g all of the most commonly encountered unsymmetrical fault situations can be created.

or in vector form

$$\begin{bmatrix} V^f_{aq} \\ V^f_{bq} \\ V^f_{cq} \end{bmatrix} = \begin{bmatrix} Z_a + Z_g & Z_g & Z_g \\ Z_g & Z_b + Z_g & Z_g \\ Z_g & Z_g & Z_c + Z_g \end{bmatrix} \begin{bmatrix} I^f_{aq} \\ I^f_{bq} \\ I^f_{cq} \end{bmatrix} \tag{11-105}$$

If we here introduce the *fault impedance matrix*

$$\mathbf{Z}^f = \begin{bmatrix} Z_a + Z_g & Z_g & Z_g \\ Z_g & Z_b + Z_g & Z_g \\ Z_g & Z_g & Z_c + Z_g \end{bmatrix} \tag{11-106}$$

Eq. (11-105) can be written in compact form

$$\mathbf{V}^f_{pq} = \mathbf{Z}^f \mathbf{I}^f_{pq} \tag{11-107}$$

This equation must be "matched" to the earlier SC transformed equations. We thus get upon SC transformation

$$\mathbf{T}\mathbf{V}^f_{sq} = \mathbf{Z}^f \mathbf{T}\mathbf{I}^f_{sq}$$

or, upon premultiplying by $\mathbf{T}^{-1}$,

$$\mathbf{V}^f_{sq} = \mathbf{T}^{-1}\mathbf{Z}^f\mathbf{T}\mathbf{I}^f_{sq} \triangleq \mathbf{Z}^f_s \mathbf{I}^f_{sq} \tag{11-108}$$

Upon performing the triple multiplication called for we obtain for the *SC transformed fault* matrix

$$\mathbf{Z}^f_s \triangleq \mathbf{T}^{-1}\mathbf{Z}^f\mathbf{T}$$

$$= \frac{1}{3}\begin{bmatrix} Z_a + Z_b + Z_c & Z_a + \alpha^2 Z_b + \alpha Z_c & Z_a + \alpha Z_b + \alpha^2 Z_c \\ Z_a + \alpha Z_b + \alpha^2 Z_c & Z_a + Z_b + Z_c & Z_a + \alpha^2 Z_b + \alpha Z_c \\ Z_a + \alpha^2 Z_b + \alpha Z_c & Z_a + \alpha Z_b + \alpha^2 Z_c & Z_a + Z_b + Z_c + 9Z_g \end{bmatrix} \tag{11-109}$$

Note that the matrix $\mathbf{Z}^f$ is symmetric but $\mathbf{Z}^f_s$ is not.

When some of the impedances in Fig. 11-22 take on infinite values (and this commonly happens as was exemplified above) some elements of the $\mathbf{Z}^f_s$ matrix become *undefined*. In such cases we must work with its inverse, the SC transformed *fault admittance matrix*, defined from Eq. (11-108):

$$\mathbf{I}^f_{sq} = (\mathbf{Z}^f_s)^{-1}\mathbf{V}^f_{sq} \triangleq \mathbf{Y}^f_s \mathbf{V}^f_{sq} \tag{11-110}$$

Inversion of $\mathbf{Z}^f_s$ yields (after much algebra)

$$\mathbf{Y}^f_s = \frac{1}{Y_a + Y_b + Y_c + Y_g} \times$$

$$\times \begin{bmatrix} \frac{1}{3}Y_g(Y_a + Y_b + Y_c) + (Y_aY_b + Y_bY_c + Y_cY_a) & \frac{1}{3}Y_g(Y_a + \alpha^2 Y_b + \alpha Y_c) - (Y_bY_c + \alpha Y_aY_b + \alpha^2 Y_aY_c) & \frac{1}{3}Y_g(Y_a + \alpha Y_b + \alpha^2 Y_c) \\ \frac{1}{3}Y_g(Y_a + \alpha Y_b + \alpha^2 Y_c) - (Y_bY_c + \alpha^2 Y_aY_b + \alpha Y_aY_c) & \frac{1}{3}Y_g(Y_a + Y_b + Y_c) + (Y_aY_b + Y_bY_c + Y_cY_a) & \frac{1}{3}Y_g(Y_a + \alpha^2 Y_b + \alpha Y_c) \\ \frac{1}{3}Y_g(Y_a + \alpha^2 Y_b + \alpha Y_c) & \frac{1}{3}Y_g(Y_a + \alpha Y_b + \alpha^2 Y_c) & \frac{1}{3}Y_g(Y_a + Y_b + Y_c) \end{bmatrix} \tag{11-111}$$

The admittances $Y_a \cdots Y_g$ are defined in Fig. 11-22.

Example 11-10 Find $\mathbf{Z}^f_s$ and $\mathbf{Y}^f_s$ for the single-line-to-ground fault in Fig. 11-1.

SOLUTION We create this fault by setting

(1) $Z_b = Z_c = \infty \quad (\therefore\ Y_b = Y_c = 0)$

(2) $Z_g = 0 \quad (\therefore\ Y_g = \infty)$

(3) $Z_a = Z^{f\sim} \quad (\therefore\ Y_a = \frac{1}{Z^f} \triangleq Y^f)$

Since $Z_b = Z_c = \infty$ all the nine elements of $\mathbf{Z}^f_s$ become infinite and the impedance matrix is thus undefined. Equation (11-108) thus becomes useless.

Since $Y_g = \infty$ all nine elements of $\mathbf{Y}^f_s$ will be of the type ∞/∞. However, it is easy to find the limit values of these indeterminate expressions. Letting $Y_g \to \infty$ yields

$$\mathbf{Y}^f_s = \frac{1}{3}\begin{bmatrix} Y_a + Y_b + Y_c & Y_a + \alpha^2 Y_b + \alpha Y_c & Y_a + \alpha Y_b + \alpha^2 Y_c \\ Y_a + \alpha Y_b + \alpha^2 Y_c & Y_a + Y_b + Y_c & Y_a + \alpha^2 Y_b + \alpha Y_c \\ Y_a + \alpha^2 Y_b + \alpha Y_c & Y_a + \alpha Y_b + \alpha^2 Y_c & Y_a + Y_b + Y_c \end{bmatrix}$$

Upon substitution of $Y_a = Y^f$ and $Y_b = Y_c = 0$, $\mathbf{Y}^f_s$ simplifies to

$$\mathbf{Y}^f_s = \frac{Y^f}{3}\begin{bmatrix} 1 & 1 & 1 \\ 1 & 1 & 1 \\ 1 & 1 & 1 \end{bmatrix} \tag{11-112}$$

11-7-5 Short-circuit Formulas

We are now prepared to develop a set of general formulas from which we can compute short-circuit currents and voltages in the fault and throughout the system. The formulas will correspond to the set (10-34) to (10-36) in the symmetrical case.

The unbalanced fault was assumed to occur on a system which is in a *prefault balanced* steady state. Thus, all prefault bus voltages contain *only positive sequence components*, i.e., we can write

$$\mathbf{V}^0_{s,\,\text{bus}} = \begin{bmatrix} V^0_1 \\ 0 \\ 0 \\ \hline V^0_2 \\ 0 \\ 0 \\ \hline \vdots \\ \hline V^0_n \\ 0 \\ 0 \end{bmatrix} \tag{11-113}$$

At this point we invoke the Thévenin's theorem that gives us (compare Eq. (10-31)) the postfault bus voltages from the formula

$$\mathbf{V}^f_{s,\,\text{bus}} = \mathbf{V}^0_{s,\,\text{bus}} + \mathbf{Z}_{s,\,\text{bus}}\mathbf{I}^f_{s,\,\text{bus}} \tag{11-114}$$

In this equation the fault current vector $\mathbf{I}^f_{s,\,\text{bus}}$ has as its components the fault currents injected at the various buses. Since fault current is being pumped into the system *only at bus q* in the amount $-\mathbf{I}^f_{sq}$, we can write the fault current vector in the form

$$\mathbf{I}^f_{s,\,\text{bus}} = \begin{bmatrix} \mathbf{0} \\ \mathbf{0} \\ \vdots \\ -\mathbf{I}^f_{sq} \\ \vdots \\ \mathbf{0} \end{bmatrix} \leftarrow q\text{th component} \tag{11-115}$$

The vector equations (11-114) and (11-115) correspond to Eqs. (10-31) and (10-29) in the balanced case. The basic difference between our present vector equations and those in Chap. 10 is the dimensionality. The present vector equations have $3n$ components. We can group them, as we have done, into n "components" of three scalars each, each such "three-group" representing the three symmetrical components of voltage or current at each bus. For example, in Eq. (11-115), the qth component refers to the three-group at bus q.

It should be noted that at this stage we do *not* know the fault current $\mathbf{I}^f_{sq}$, and consequently, Eq. (11-114) cannot provide *directly* the postfault bus voltages, although $\mathbf{V}^0_{s,\,\text{bus}}$ and $\mathbf{Z}_{s,\,\text{bus}}$ *both are known*. We can, however, find $\mathbf{I}^f_{sq}$ in the following manner.

Write Eq. (11-114) in component form. We do *not* write out the $3n$ scalar components, but rather the n vector "components," i.e.,

$$\begin{aligned} \mathbf{V}^f_{s1} &= \mathbf{V}^0_{s1} - \mathbf{Z}_{s1q}\mathbf{I}^f_{sq} \\ &\cdots\cdots\cdots \\ \mathbf{V}^f_{sq} &= \mathbf{V}^0_{sq} - \mathbf{Z}_{sqq}\mathbf{I}^f_{sq} \\ &\cdots\cdots\cdots \\ \mathbf{V}^f_{sn} &= \mathbf{V}^0_{sn} - \mathbf{Z}_{snq}\mathbf{I}^f_{sq} \end{aligned} \tag{11-116}$$

This set of n *vector* equations corresponds to the set of n *scalar* equations (10-33). Between the qth equation (11-116) and Eq. (11-108), we can now eliminate the postfault bus voltage $\mathbf{V}^f_{sq}$. We get

$$\mathbf{Z}^f_s\mathbf{I}^f_{sq} = \mathbf{V}^0_{sq} - \mathbf{Z}_{sqq}\mathbf{I}^f_{sq} \tag{11-117}$$

In this three-dimensional vector equation *everything* is known except $\mathbf{I}^f_{sq}$, and we therefore solve for this unknown.

We obtain

$$\mathbf{I}^f_{sq} = (\mathbf{Z}^f_s + \mathbf{Z}_{sqq})^{-1}\mathbf{V}^0_{sq} \tag{11-118}$$

This three-dimensional vector equation corresponds to the scalar equation (10-34).

Since now the fault currents *are* known, we can substitute $\mathbf{I}^f_{sq}$ back into Eq. (11-116) and obtain the postfault bus voltages. Substitution renders

$$\mathbf{V}^f_{si} = \mathbf{V}^0_{si} - \mathbf{Z}_{siq}(\mathbf{Z}^f_s + \mathbf{Z}_{sqq})^{-1}\mathbf{V}^0_{sq} \qquad \text{for } i \neq q \tag{11-119}$$

For the faulted bus itself, we get

$$\mathbf{V}^f_{sq} = \mathbf{Z}^f_s(\mathbf{Z}^f_s + \mathbf{Z}_{sqq})^{-1}\mathbf{V}^0_{sq} \tag{11-120}$$

The vector equations (11-119) and (11-120) correspond to the scalar equations (10-35)

This, in principle, completes our analysis. With the fault current and all postfault bus voltages known, we can compute the short-circuit currents in all lines.

The following comments are in order concerning the use of the above set of formulas:

1. The formulas are completely general. Note also that the fault has been placed at the likewise general bus q.
2. As a result of the above generality, once the SC bus impedance matrix $\mathbf{Z}_{s,\,\text{bus}}$ has been computed and placed in computer memory, we can with equal ease extend our short-circuit analysis to *any* faulted bus and *any* unbalanced type of fault.
3. All formulas involve three-dimensional vectors and 3×3 matrices. The matrices $\mathbf{Z}_{sij}$ are diagonal, but the matrix $\mathbf{Z}^f_s$ is not. In any case, all the involved matrix operations are easily programmed on a digital computer.

4. The prefault bus voltages V_i^0 are either obtained from a load flow analysis or, as we pointed out in Chap. 10, are usually set equal to 1.0 pu; i.e.,

$$\mathbf{V}_{si}^0 \approx \begin{bmatrix} 1 \\ 0 \\ 0 \end{bmatrix} \qquad \text{for } i = 1, \ldots, n \tag{11-121}$$

5. All formulas give us the postfault currents and voltages *in terms of symmetrical components*. Since, of course, the actual phase currents and voltages are of interest in the final analysis, we must complete each short-circuit analysis with an *indirect* SC transformation, converting all SC components into phase values, using Eqs. (11-8) and (11-19).
6. The bus impedance matrices $\mathbf{Z}_{+\text{bus}}$, $\mathbf{Z}_{-\text{bus}}$ and $\mathbf{Z}_{0\text{bus}}$ can be obtained either by inversion of the corresponding bus admittance matrices or by using the $\mathbf{Z}_{\text{bus}}$ *building algorithms* discussed in Chap. 10.
7. All the foregoing equations were derived, based on the existence of the fault impedance matrix $\mathbf{Z}_s^f$. Example 11-10 demonstrated that in some cases $\mathbf{Z}_s^f$ *is not defined*, but the admittance matrix $\mathbf{Y}_s^f$ is. In such a case we must develop a new set of equations, making use of $\mathbf{Y}_s^f$ instead of $\mathbf{Z}_s^f$. This is simply done by eliminating $\mathbf{I}_{sq}^f$ instead of $\mathbf{V}_{sq}^f$ in deriving Eq. (11-120). The above analysis thus changes as follows: Instead of Eq. (11-117) we get

$$\mathbf{V}_{sq}^f = \mathbf{V}_{sq}^0 - \mathbf{Z}_{sqq}\mathbf{Y}_s^f\mathbf{V}_{sq}^f \tag{11-122}$$

From this equation we can solve for the unknown postfault voltage vector at bus q,

$$\mathbf{V}_{sq}^f = (\mathbf{U} + \mathbf{Z}_{sqq}\mathbf{Y}_s^f)^{-1}\mathbf{V}_{sq}^0 \tag{11-123}$$

where $\mathbf{U}$ is the identity matrix. (Eq. (A-28).)

Equation (11-110) will next give us the fault current.

$$\mathbf{I}_{sq}^f = \mathbf{Y}_s^f\mathbf{V}_{sq}^f = \mathbf{Y}_s^f(\mathbf{U} + \mathbf{Z}_{sqq}\mathbf{Y}_s^f)^{-1}\mathbf{V}_{sq}^0 \tag{11-124}$$

The postfault voltages at the buses, other than the faulted one, are obtained upon substitution of Eq. (11-124) into Eq. (11-116). We get

$$\mathbf{V}_{si}^f = \mathbf{V}_{si}^0 - \mathbf{Z}_{siq}\mathbf{I}_{sq}^f = \mathbf{V}_{si}^0 - \mathbf{Z}_{siq}\mathbf{Y}_s^f(\mathbf{U} + \mathbf{Z}_{sqq}\mathbf{Y}_s^f)^{-1}\mathbf{V}_{sq}^0 \qquad i \neq q \tag{11-125}$$

For the case of *nondefined* $\mathbf{Z}_s^f$, the general equations (11-118) to (11-120) must therefore be replaced by Eqs. (11-123) to (11-125).

Example 11-9 (cont.) We now make use of our analysis results to finish the three-bus example that we started earlier. We had assembled the $\mathbf{Z}_{s,\text{bus}}$ matrix for the system in question. It is given in Eq. (11-99).

We shall find the postfault voltages and currents throughout the system caused by a single-line-to-ground short circuit on bus 3, by making use of the $\mathbf{Y}_s^f$ matrix given by Eq. (11-112).

We start our computations by first computing the voltage of the faulted bus, using Eq. (11-123).

By substitution of the various matrices and the vector $\mathbf{V}_{sq}^0$, we get

$$\mathbf{V}_{sq}^f = \left\{ \begin{bmatrix} 1 & 0 & 0 \\ 0 & 1 & 0 \\ 0 & 0 & 1 \end{bmatrix} + \begin{bmatrix} z_{+qq} & 0 & 0 \\ 0 & z_{-qq} & 0 \\ 0 & 0 & z_{0qq} \end{bmatrix} \frac{Y^f}{3} \begin{bmatrix} 1 & 1 & 1 \\ 1 & 1 & 1 \\ 1 & 1 & 1 \end{bmatrix} \right\}^{-1} \begin{bmatrix} V_q^0 \\ 0 \\ 0 \end{bmatrix} \tag{11-126}$$

By performing the matrix operations called for, this vector equation simplifies to

$$\mathbf{V}_{sq}^f = \frac{V_q^0}{1 + (Y^f/3)(z_{+qq} + z_{-qq} + z_{0qq})} \begin{bmatrix} 1 + \dfrac{Y^f}{3}(z_{-qq} + z_{0qq}) \\ -z_{-qq}\dfrac{Y^f}{3} \\ -z_{0qq}\dfrac{Y^f}{3} \end{bmatrix} \tag{11-127}$$

For the short-circuit at the faulted bus, we use Eq. (11-124)

$$\mathbf{I}_{sq}^f = \mathbf{Y}_s^f\mathbf{V}_{sq}^f = V_q^0 \frac{Y^f/3}{1 + (Y^f/3)(z_{+qq} + z_{-qq} + z_{0qq})} \begin{bmatrix} 1 \\ 1 \\ 1 \end{bmatrix} \tag{11-128}$$

Finally, the postfault voltages at the buses other than the faulted one are obtained from Eq. (11-125)

$$\mathbf{V}_{si}^f = \mathbf{V}_{si}^0 - \mathbf{Z}_{siq}\mathbf{I}_{sq}^f = \begin{bmatrix} V_i^0 \\ 0 \\ 0 \end{bmatrix} - \begin{bmatrix} z_{+iq} & 0 & 0 \\ 0 & z_{-iq} & 0 \\ 0 & 0 & z_{0iq} \end{bmatrix} \mathbf{I}_{sq}^f$$

Upon substitution of the expression for $\mathbf{I}_{sq}^f$, we obtain

$$\mathbf{V}_{si}^f = \begin{bmatrix} V_i^0 \\ 0 \\ 0 \end{bmatrix} - V_q^0 \frac{Y^f/3}{1 + (Y^f/3)(z_{+qq} + z_{-qq} + z_{0qq})} \begin{bmatrix} z_{+iq} \\ z_{-iq} \\ z_{0iq} \end{bmatrix} \qquad \text{for } i \neq q \tag{11-129}$$

Equations (11-127) to (11-129) simplify considerably if we assume that the short circuit is *solid*, that is $Y^f = \infty$. A further simplification is obtained if we make the reasonable assumption that all prefault voltages, V_i^0, equal 1 pu. Upon making use of these two assumptions, the above formulas reduce to the following simple ones:

$$\mathbf{V}_{sq}^f = \frac{1}{z_{+qq} + z_{-qq} + z_{0qq}} \begin{bmatrix} z_{-qq} + z_{0qq} \\ -z_{-qq} \\ -z_{0qq} \end{bmatrix} \tag{11-130}$$

$$\mathbf{I}_{sq}^f = \frac{1}{z_{+qq} + z_{-qq} + z_{0qq}} \begin{bmatrix} 1 \\ 1 \\ 1 \end{bmatrix} \tag{11-131}$$

$$\mathbf{V}_{si}^f = \begin{bmatrix} 1 \\ 0 \\ 0 \end{bmatrix} - \frac{1}{z_{+qq} + z_{-qq} + z_{0qq}} \begin{bmatrix} z_{+iq} \\ z_{-iq} \\ z_{0iq} \end{bmatrix} \qquad \text{for } i \neq q \tag{11-132}$$

It should be noted that these formulas are very general, in the sense that they are applicable for a short circuit (of the single-line-to-ground variety) on *any bus*.

We will now substitute the numerical values that apply to our three-bus system. Since the short circuit occurs on bus 3, we have $q = 3$. From Eq. (11-99)

$$\mathbf{Z}_{sqq} = \mathbf{Z}_{s33} = \begin{bmatrix} z_{+33} & 0 & 0 \\ 0 & z_{-33} & 0 \\ 0 & 0 & z_{033} \end{bmatrix} = \begin{bmatrix} 0.1014 & 0 & 0 \\ 0 & 0.1014 & 0 \\ 0 & 0 & 0.1180 \end{bmatrix} \text{pu}$$

From Eqs. (11-130) and (11-131) we therefore get

$$\mathbf{V}^f_{s3} = \frac{1}{j(0.1014 + 0.1014 + 0.1180)} \begin{bmatrix} j(0.1014 + 0.1180) \\ -j0.1014 \\ -j0.1180 \end{bmatrix} = \begin{bmatrix} 0.685 \\ -0.317 \\ -0.369 \end{bmatrix} \text{pu} \qquad (11\text{-}133)$$

and

$$\mathbf{I}^f_{sq} = \mathbf{I}^f_{s3} = \frac{1}{j(0.1014 + 0.1014 + 0.1180)} \begin{bmatrix} 1 \\ 1 \\ 1 \end{bmatrix} = -j \begin{bmatrix} 3.12 \\ 3.12 \\ 3.12 \end{bmatrix} \text{pu} \qquad (11\text{-}134)$$

To compute the postfault voltages on buses 1 and 2, we need to know the impedance matrices $\mathbf{Z}_{s13}$ and $\mathbf{Z}_{s23}$. From Eq. (11-99) we have

$$\mathbf{Z}_{s13} = \begin{bmatrix} z_{+13} & 0 & 0 \\ 0 & z_{-13} & 0 \\ 0 & 0 & z_{013} \end{bmatrix} = j \begin{bmatrix} 0.0558 & 0 & 0 \\ 0 & 0.0558 & 0 \\ 0 & 0 & 0.0220 \end{bmatrix} \text{pu}$$

$$\mathbf{Z}_{s23} = \begin{bmatrix} z_{+23} & 0 & 0 \\ 0 & z_{-23} & 0 \\ 0 & 0 & z_{023} \end{bmatrix} = j \begin{bmatrix} 0.0472 & 0 & 0 \\ 0 & 0.0472 & 0 \\ 0 & 0 & 0.0140 \end{bmatrix} \text{pu}$$

From Eq. (11-132) we now get

$$\mathbf{V}^f_{s1} = \begin{bmatrix} 1 \\ 0 \\ 0 \end{bmatrix} - \frac{1}{j(0.1014 + 0.1014 + 0.1180)} \begin{bmatrix} j0.0558 \\ j0.0558 \\ j0.0220 \end{bmatrix} = \begin{bmatrix} 0.826 \\ -0.174 \\ -0.069 \end{bmatrix} \text{pu} \qquad (11\text{-}135)$$

$$\mathbf{V}^f_{s2} = \begin{bmatrix} 1 \\ 0 \\ 0 \end{bmatrix} - \frac{1}{j(0.1014 + 0.1014 + 0.1180)} \begin{bmatrix} j0.0472 \\ j0.0472 \\ j0.0140 \end{bmatrix} + \begin{bmatrix} 0.853 \\ -0.147 \\ -0.044 \end{bmatrix} \text{pu} \qquad (11\text{-}136)$$

We note the following facts about these numerical values:

1. The fault current contains the three sequence components in equal proportions.
2. The bus voltages contain more of the positive-sequence and less of the negative- and zero-sequence components the farther from the fault the buses are located.

Since we now know all postfault bus voltages, we can readily compute all postfault line currents. As an example, let us compute the current in the line connecting buses 1 and 3. We remember that the line had the sequence impedances

$$\mathbf{Z}_{s1\to3} = \begin{bmatrix} j0.10 & 0 & 0 \\ 0 & j0.10 & 0 \\ 0 & 0 & j0.20 \end{bmatrix} \text{pu}$$

or in admittance form

$$\mathbf{Y}_{s1\to3} = \begin{bmatrix} -j10 & 0 & 0 \\ 0 & -j10 & 0 \\ 0 & 0 & -j5 \end{bmatrix} \text{pu}$$

We then compute the line sequence currents

$$\mathbf{I}^f_{s1\to3} = \begin{bmatrix} -j10 & 0 & 0 \\ 0 & -j10 & 0 \\ 0 & 0 & -j5 \end{bmatrix} \left\{ \begin{bmatrix} 0.826 \\ -0.174 \\ -0.069 \end{bmatrix} - \begin{bmatrix} 0.685 \\ -0.317 \\ -0.369 \end{bmatrix} \right\} = -j \begin{bmatrix} 1.42 \\ 1.42 \\ 1.50 \end{bmatrix} \text{pu} \qquad (11\text{-}137)$$

It must be noted that all the above voltages and currents are obtained in SC form. Since we are more interested in knowing them in actual phase values we must make them all subject to an *indirect* SC transformation by the matrix T. We get for the phase voltages at bus 3

$$\mathbf{V}^f_{p3} = \begin{bmatrix} V^f_{a3} \\ V^f_{b3} \\ V^f_{c3} \end{bmatrix} = \mathbf{T}\mathbf{V}^f_{s3} = \begin{bmatrix} 0 \\ -0.553 - j0.868 \\ -0.553 + j0.868 \end{bmatrix} \text{pu} \qquad (11\text{-}138)$$

or, in rms values,

$$\begin{bmatrix} V^f_{a3} \\ V^f_{b3} \\ V^f_{c3} \end{bmatrix} = \begin{bmatrix} 0 \\ 1.03 \\ 1.03 \end{bmatrix} \text{pu}$$

For the phase currents in the fault

$$\mathbf{I}^f_{p3} = \begin{bmatrix} I^f_{a3} \\ I^f_{b3} \\ I^f_{c3} \end{bmatrix} = \mathbf{T}\mathbf{I}^f_{s3} = -j \begin{bmatrix} 9.36 \\ 0 \\ 0 \end{bmatrix} \text{pu} \qquad (11\text{-}139)$$

For the phase voltages of buses 1 and 2

$$\mathbf{V}^f_{p1} = \begin{bmatrix} V^f_{a1} \\ V^f_{b1} \\ V^f_{c1} \end{bmatrix} = \mathbf{T}\mathbf{V}^f_{s1} = \begin{bmatrix} 0.583 \\ -0.395 - j0.866 \\ -0.395 + j0.866 \end{bmatrix} \text{pu} \qquad (11\text{-}140)$$

$$\mathbf{V}^f_{p2} = \begin{bmatrix} V^f_{a2} \\ V^f_{b2} \\ V^f_{c2} \end{bmatrix} = \mathbf{T}\mathbf{V}^f_{s2} = \begin{bmatrix} 0.662 \\ -0.400 - j0.865 \\ -0.400 + j0.865 \end{bmatrix} \text{pu} \qquad (11\text{-}141)$$

or, in rms values,

$$\begin{bmatrix} |V^f_{a1}| \\ |V^f_{b1}| \\ |V^f_{c1}| \end{bmatrix} = \begin{bmatrix} 0.583 \\ 0.952 \\ 0.952 \end{bmatrix} \text{pu} \quad \text{and} \quad \begin{bmatrix} |V^f_{a2}| \\ |V^f_{b2}| \\ |V^f_{c2}| \end{bmatrix} = \begin{bmatrix} 0.662 \\ 0.955 \\ 0.955 \end{bmatrix} \text{pu} \quad \text{respectively}$$

For the line currents in the line connecting buses 1 and 3

$$\mathbf{I}^f_{p1\to3} = \mathbf{T}\mathbf{I}_{s1\to3} = -j \begin{bmatrix} 4.34 \\ 0.08 \\ 0.08 \end{bmatrix} \text{pu} \qquad (11\text{-}142)$$

We make these observations in regard to the above numerical values:

1. The fault current 9.36 pu in the short-circuited phase almost equals the value obtained for a solid symmetrical fault on the same bus, 9.86 pu (Chap. 10).
2. As the voltage on the faulted phase drops to zero, the voltages of the two healthy phases jump to 103 percent.
3. Although zero currents flow in phases b and c at the fault, the same phases of the lines leading to the faulted bus carry a slight current. (Compare Eq. 11-78.)

11-8 SUMMARY

In this chapter we have outlined analysis procedures which have proved useful in handling unbalanced fault calculations. The symmetrical component transformation (SCT) occupies a central position. The basic idea behind this transformation is the decomposition of the unbalanced network into three symmetrical component systems. The characteristics of generators, transformers, and transmission lines are such that the three component systems are decoupled from each other. We therefore are permitted to treat them separately.

A sequence network is assembled for each component system. These networks are generally of different structure. The computer assembly methods developed in Chap. 10 may be applied to each sequence network, and the entire network data can be concentrated in a single matrix, the SC admittance matrix.

General formulas have been derived by means of which we can compute the currents and voltages in a general n-bus system, subject to a completely general unbalanced load or fault situation. We demonstrated their use by finding the short-circuit currents, following a single-phase-to-ground fault in a three-bus system.

PROBLEMS

***11-1** Figure 11-2 reveals how the phase currents may be obtained *graphically* by vectorial addition of the sequence components.

Show how the sequence components may be obtained *graphically* from the phase currents.

***11-2** A generator supplying an unbalanced load measures the following phase-to-ground voltages:

$$V_a = 18.0\angle 0^\circ \text{ kV}$$

$$V_b = 13.3\angle -132^\circ \text{ kV}$$

$$V_c = 12.0\angle +110^\circ \text{ kV}$$

Find the symmetrical components of the set of phase voltages.

***11-3** The generator in the previous exercise supplies the following set of phase currents:

$$I_a = 200\angle -10^\circ \text{ A}$$

$$I_b = 350\angle -140^\circ \text{ A}$$

$$I_c = 400\angle +100^\circ \text{ A}$$

Find the megawatts supplied by the generator using formula (11-27) *and* (11-30).

11-4 The generator in Prob. 11-3 is grounded via a 10-Ω reactor. Compute the voltage of the neutral relative to ground if the current load is as indicated.

11-5 Consider the generator subjected to a single-line-to-ground terminal fault as analyzed in Example 11-5. Assume the following data:

$$x_+ = x_- = 0.12 \text{ pu (based on rating)}$$

$$x_0 = 0.06 \text{ pu}$$

One adds a grounding reactor designed to limit the fault current to 5 pu. Compute the fault voltages (relative to ground) of the two healthy phases.

***11-6** Consider the single generator in Example 11-5. Its neutral is solidly grounded. A solid line-to-line fault occurs between phases b and c *with simultaneous solid ground contact.* Phase a remains healthy.

(*a*) How would you interconnect the sequence networks to account for this fault?

(*b*) Find formulas for I_{a+}, I_{a-}, I_{a0} *and* V_{a+}, V_{a-}, V_{a0}.

(*c*) Find formulas for I_b, I_c, and V_a.

(*d*) Find numerical values for I_b, I_c, and V_a using the impedance data given in Prob. 11-5. It is assumed that the fault occurs from a symmetrical prefault voltage level of 100 percent.

***11-7** Consider the three-phase *transposed* line in Example 6-4 having its phase conductors placed in a horizontal plane with a phase distance $D = 3$ m. Its positive- (and negative-) sequence reactance was found to equal 0.466 ohms per kilometer and phase. Two ground wires of 8 mm diameter are strung 3 m apart and 3 m above the phase conductors. If these wires are assumed to carry the total neutral return current in a fault situation what will be the zero-sequence reactance of this line per kilometer and phase?

11-8 A Y-Δ-connected transformer has the following three-phase ratings:

300 MVA, 60 Hz
24/240 kV

Its leakage reactance equals 12 percent.

If its HV neutral is solidly grounded the zero-sequence reactance, according to Fig. 11-14 will equal 0.12 pu. What will be its value if the neutral is grounded via a 3-Ω reactor?

11-9 Consider a Y-Y$_z$connected transformer with the three-phase ratings:

300 MVA, 60 Hz
24/240 kV

Its leakage reactance equals 12 percent.

Find zero sequence reactance with

(*a*) Both neutrals solidly grounded

(*b*) The LV neutral solidly grounded but the HV neutral grounded via 3-Ω reactors

(*c*) The HV neutral solidly grounded but the LV neutral grounded via 3-Ω reactors

(*d*) Both neutrals grounded via 3-Ω reactors

***11-10** Consider the two-bus example analyzed in text, subjected to a single-line-to-ground fault on bus 1. Complete the computations by finding

(*a*) The three phase voltages of bus 2

(*b*) The three phase voltages at *both* generator terminals (All voltages relative to ground.)

***11-11** Consider again the two-bus text example, this time subject to a line-to-line fault at bus 1 between phases b and c. Complete the calculations by finding:

(*a*) Fault currents (all phases) in $G1$–$T1$

(*b*) Fault currents (all phases) in $T2$

(*c*) Fault currents (all phases) in $G2$

(*d*) All three phase voltages at bus 2

(*e*) All three phase voltages of $G1$ and $G2$.

11-12 The two-bus text example is subject at bus 1 to a solid line-to-line fault between phases b and c with simultaneous solid ground contact.

(*a*) Interconnect the three sequence networks in an appropriate manner and find all sequence currents and voltages at the faulted bus. (Compare Prob. 11-6.)

(*b*) Find all phase voltages and currents at the fault.

(*c*) Find *phase* currents in $G1$, $T1$, $G2$, and $T2$.

(*d*) Find phase voltages at bus 2.

11-13 In Example 11-9 we used *general* formulas to analyze the three-bus example system for a solid single-line-to-ground fault.

Use instead *simple* network reduction techniques (of the type we employed for the two-bus system) to find the fault current. Compare your answer with that obtained in the text.

***11-14** Consider the two-bus example system analyzed in the text, subject to a single-line-to-ground fault.

Now, find the $\mathbf{Z}_{bus}$ matrices for this system and then analyze the above fault using the *general* formulas derived in Sec. 11-7

(*a*) for the fault occurring at bus 1;

(*b*) for the fault occurring at bus 2.

Your analysis should include currents and voltages *throughout* the system. Compare your answers with those found in text.

11-15 Same as above problem but the fault is now of *solid line-to-line* variety.

REFERENCES

1. C. L. Fortescue; "Method of Symmetrical Coordinates Applied to the Solution of Polyphase Networks," *Trans. AIEE*, vol. 37, 1918, pp. 1027–1140.
2. Paul M. Anderson: *Analysis of Faulted Power Systems*, Iowa State Press, Ames, Iowa, 1973.
3. C. F. Wagner and R. D. Evans: *Symmetrical Components*, McGraw-Hill Book Company, New York, 1933.
4. C. A. Gross: *Power System Analysis*, John Wiley & Sons, New York, 1979.
5. G. W. Stagg and A. H. El-Abiad: *Computer Methods in Power System Analysis*," McGraw-Hill Book Company, New York, 1968.

CHAPTER

TWELVE

EMERGENCY CONTROL

Scenario Place: New York City
Date: July 13, 1977

2000 hours. On this hot and muggy night the city electrical load is peaking around 6000 megawatts, about half of which is being imported via overhead tie-lines and underground cables. The utility is operating in the *normal* state. An intense electrical storm is moving across the area.

2037 hours. A severe lightning bolt hits a transmission tower carrying two 345-kV lines causing permanent tripping of both. The network loses a load-carrying capacity of about 1000 megawatts, which load is instantaneously shifting over to remaining lines. The system is now in the *alert* state of operation.

2055 hours. The city generation has been raised by 550 megawatts to take the strain off the tie-lines, all of which are still operating below their thermal limits. System still in alert state.

2056 hours. A second lightning stroke cripples a third 345-kV line. Within a fraction of a second a fourth line trips due to the ensuing power transients. Remaining lines are now pushed above their thermal limits. City load is being carried but system now is in *emergency* state. Every serviceable generator is running.

2119 hours. Due to thermal expansion the conductors of one 345-kV line sag deep enough to cause shortcircuit via small tree. The line trips causing further overload of the few remaining ties, which now, one by one, break open. The system is now in *extremis* state.

2129 hours. The last tie with the outside world trips. The system now finds itself with a deficiency of 1700 megawatts resulting in a rapid loss of frequency. Underfrequency relays automatically initiate preset load shedding of section upon section of the city.

The loss of frequency cannot be halted and the generators are tripped automatically and manually to avoid catastrophic machine damage.

2136 hours. New York City goes totally black.

12-1 CONCEPTS OF RELIABILITY, SECURITY, AND TRANSIENT STABILITY

As the above real-life example demonstrates, power system emergencies can build slowly over minutes and even hours. They can also strike suddenly and cripple the system within seconds. As power systems are exposed to the capricious forces of nature it is impossible to design them completely failure safe.

Reliability and *security* are two separate concepts by means of which one attempts to measure the robustness of a power system against disturbances.

"Reliability" is a probabilistic index exemplified by *loss-of-load probability* (LOLP) defined as the long-term average number of days on which daily peak load exceeds the available generating capacity. Determining the "reliability" of a system thus is reduced to a mathematical problem of computing the probability for generated power to reach the load in a given system.[1]

In the above-defined sense "reliability" will not change with time and its achievement becomes a system planning problem. "Security," by contrast, is an operational problem that will change with operational conditions. It depends not only upon the *reserve capacity* available in a given situation but also upon the contingent probability of disturbances. By "reserve" is meant not only unused generators but also numbers of parallel lines, for example.

Whereas "reliability" can be given a precise mathematical definition in terms of probabilities it is much more difficult to attach numerical indices to "security." A very typical feature of power-system "security" is its cumulative deterioration resulting from sequences of events, as exemplified in the 1977 New York blackout. For this reason one often talks about robustness against one, two, or several *contingencies*.

Transient stability is a third more limited concept often used in assessing system robustness. A system is said to be "transient stable" if all its generators are kept operating in a parallel synchronous mode.

12-2 PREVENTIVE AND EMERGENCY CONTROL

The state transition diagram in Fig. 7-1 provides further clarification of the meaning of the above concepts.[2]

In its *normal* state the system is deemed "secure." In this state both *equality* and *inequality constraints* are satisfied.

"Equality" (symbol E in Fig. 7-1) means that the total system generation equals total system load. "Inequality" (symbol I) refers to currents and voltages being kept within rated limits.

Following a first contingency the system enters the *alert* state. The security level now falls below some threshold and the system is deemed "insecure." However, both equality and inequality constraints are still observed.

A second contingency may cause overload of some component thus negating the inequality constraint (symbol $\bar{I}$). The system thus enters the *emergency* state. Note that in this state the equality constraint is still observed.

When the generation no longer can track the load, system disintegration begins and the *extremis* state is reached. At this point, events usually follow in rapid sequence.

If a system reaches the alert state *preventive controls* are taken to restore the normal state. Such control actions may consist of start-up of reserve generation or putting in service other reserve equipment.

If such actions prove inadequate or if additional contingencies push the system into the emergency state then more "heroic" measures, collectively termed *emergency controls*, would be initiated, load shedding being the most common.

These control actions may be initiated from the central *energy control center*, either automatically or by operator intervention. If speed of action is of extreme importance the control actions are implemented through local means.

12-3 PROTECTIVE RELAYING

When abnormal system conditions occur three basic objectives must always be met:

1. All endangered equipment must be protected from damage.
2. The faulted component(s) must be isolated and, if not damaged, reenergized as rapidly as possible.
3. Service interruption should be minimized.

A great portion of the fault protection job in a power system is performed automatically by *protective relays* that base their operation upon continuous measurement of system variables like current, voltage, frequency, etc.

12-3-1 "Instrument" Transformers

The relays sense and measure the currents and voltages in the HV circuits *indirectly* via *current* and *potential transformers*, CT's and PT's.

In addition to transforming the current and voltage to suitable levels these *instrument transformers* serve to isolate the control circuits from the HV circuits (compare Fig. 5-33).

The *open-circuit* secondary voltage V_2 of a PT follows from

$$V_2 = \frac{N_2}{N_1} V_1 = \frac{1}{a} V_1 \tag{12-1}$$

where $a \gg 1$.

The *short-circuit* secondary current I_2 of a CT equals

$$I_2 = \frac{N_1}{N_2} I_1 = a I_1 \tag{12-2}$$

where $a \ll 1$.

Secondary relay loading, referred to as *burden* and measured in VA, upsets the simple proportionalities of Eqs. (12-1) and (12-2), and in practice voltampere limits are imposed.

12-3-2 Relays

The *relays* constitute the "brains" in all protective schemes. They are the "silent sentinels" that continuously monitor and/or compute various electrical variables. When the latter fall outside a certain threshold value the relay initiates control action, for example, by energizing the trip coil of a circuit breaker.

In its simplest form the relay may consist of an electromagnetic plunger which, when the coil current reaches a certain value, will move and close a contact. A more sophisticated relay consists of a small computer that may compute the impedance between a bus and the unknown fault point of a line.

The two overriding relay requirements are *reliability* and *selectivity*. Relays may be called upon to do their assigned duty after long periods of idleness. Malfunctioning relays have been partly responsible for some of the most spectacular blackouts. "Selectivity" is the ability to function only for the intended fault situation. A relay must never be triggered by normal power flows, expected switching transients, transformer inrush currents, and the like.

Relays are available in a vast number of designs.[3] The most important types and operating functions are:

1. *Overcurrent* relay. Main function is protection against short circuits. If the relay is designed to operate only for current flows in a certain direction then the relay is *directional*.
2. *Impedance* (*distance*) relay. Used for selective switching of faulted lines.
3. *Under-* and *overvoltage* relays.
4. *Underfrequency* relays. Used for initiating load shedding.

12-3-3 Unit Protection

The overall protection of a power system is subdivided into component subsystems—so-called *unit protection*. Generators, lines, transformers, buses, motors, etc., thus have their own typical protective schemes. For example a turbogenerator unit would be typically protected for:

1. Armature and field overload
2. Armature and field shorts and grounds
3. Loss of excitation
4. Over- and undervoltage
5. Loss of synchronism
6. Armature and field unbalance

Most of the above protective functions require very special relays and circuits. Certain protective functions, however, can be handled by circuits that will be essentially identical whatever the protected unit may be.

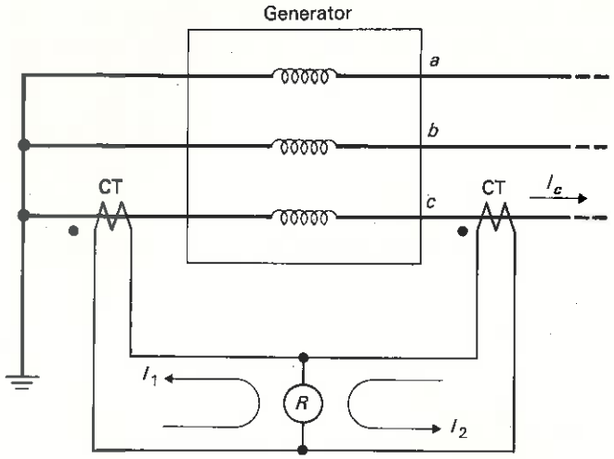

Figure 12-1 Differential current relay.

Consider for example the *differential current* protection shown in Fig. 12-1 (only one phase shown). This circuit is often used for detection of shorts. If phase c is fault-free the primary currents in the two identical CT's are the same. Thus the secondary currents I_1 and I_2 will also be identical, resulting in zero current through the relay R. Should a short circuit occur either between the phase winding and ground or between phase windings the CT primary currents will be unequal and the resulting secondary current imbalance immediately be felt by the relay which would initiate instantaneous deenergizing of the generator.

Differential current relays are used for transformers, buses, lines, and cables. In the latter cases there will be a large physical distance between the two CT's. "Pilot wires," or an equivalent data link† must then be provided ("pilot relays").

Figure 12-2 shows how fault protection is accomplished for a generator-transformer, bus, and two feeder lines. Note that the protective zones *overlap*.

12-3-4 Backup Protection

There is the ever-present chance that relays and/or circuit breakers will malfunction. The cost for failure of disconnecting a severe fault can be of catastrophic proportions. To avoid this possibility one typically will arrange for backup protection. Figure 12-3 depicts one of the most common arrangements.

The circuit breakers A and B should clear a fault on line $L2$. The breakers are operated from *distance relays* which sense the approximate distance to the fault. This is typically accomplished by measuring the *impedance* to the fault.

† Telephone or microwave are often used. So-called *carrier* link using the power line itself with a superimposed high-frequency signal (100–200 kHz) cannot be used for line protection.

Should the relays indicate that the fault lies within, say, 90 percent of the length of $L2$, then they would initiate *instantaneous* tripping. For faults beyond 90 percent the relays have built-in time lags in two steps. In this way breakers A and B serve as backup in the case of failure of the line breakers on $L1$ and $L3$.

12-3-5 Sequence Filters

We noted in Chap. 11 that *solid* faults of the unbalanced type give rise to substantial short-circuit currents. Overcurrent protection of the type discussed

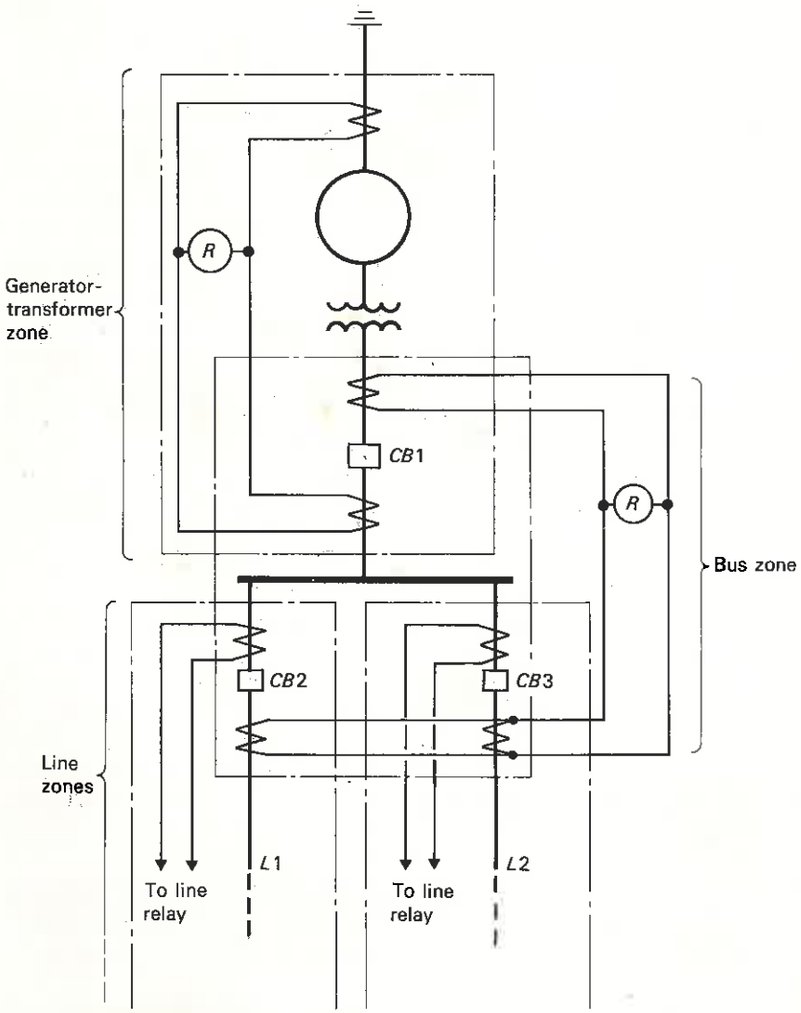

Figure 12-2 Overlapping protection zones.

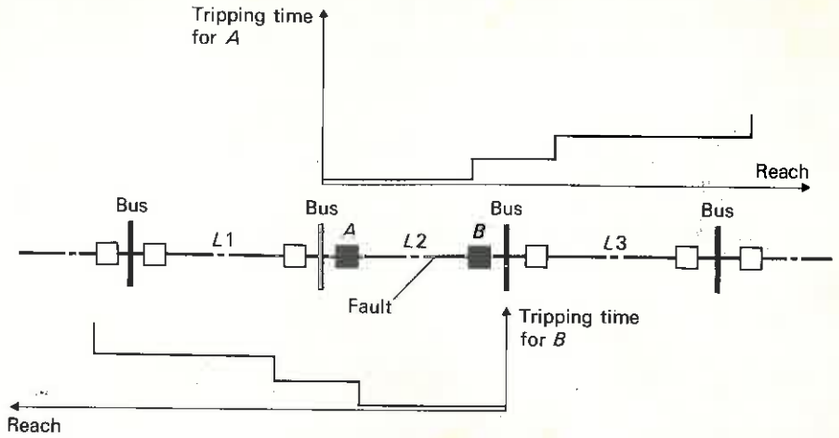

Figure 12-3 Distance relays providing backup protection.

above *if applied in all three phases* will thus protect for balanced and unbalanced faults alike. However, if the fault impedance is large or if the unbalance is caused by loading, the currents may be too small to activate the overcurrent relays.

However, even relatively small negative- and zero-sequence currents will cause excessive heating in generator rotors† and it is important therefore to be able to detect such imbalances. *Sequence filters* are often used for this purpose. They are of both voltage and current type. Figure 12-4 depicts the latter. If the three identical CT's 1, 2 and 3 have a turns ratio a the secondary current I_1 will take on the value:

$$I_1 = a(I_a + I_b + I_c) \tag{12-3}$$

Thus, the voltage across terminals 5 and 6 will be of magnitude

$$|V_{56}| = R|I_1| = aR|I_a + I_b + I_c| \tag{12-4}$$

Positive- and negative-sequence current components I_+ and I_- are characterized by three-phase symmetry and will thus yield zero I_1 and V_{56}. Should zero-sequence components be present then, according to Eq. (11-25), the voltage V_{56} will be of magnitude

$$|V_{56}| = 3aR|I_{a0}| \tag{12-5}$$

A voltage sensitive relay connected across 5-6 will thus "see" the zero-sequence current but be "blind" for the positive- and negative-sequence components.

† By currents induced in the structural parts.

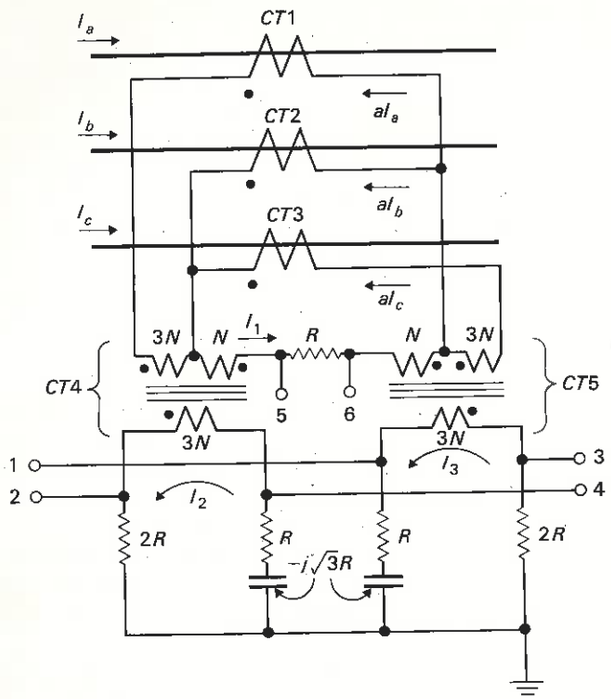

Figure 12-4 Sequence component filter.

The voltages across terminals 1-2 and 3-4 equal, respectively,

$$V_{12} = V_1 - V_2 = (R - j\sqrt{3}R)I_3 - 2RI_2 \tag{12-6}$$

$$V_{34} = V_3 - V_4 = -2RI_3 + (R - j\sqrt{3}R)I_2 \tag{12-7}$$

By expressing I_2 and I_3 in terms of I_a, I_b, and I_c one can prove (and this is left as an exercise for the reader) that

$$|V_{12}| \sim |I_{a+}| \tag{12-8}$$

$$|V_{34}| \sim |I_{a-}| \tag{12-9}$$

Voltage relays connected across 1-2 and 3-4 will thus be sensitive to positive- and negative-sequence currents, respectively.

12-3-6 Line Reclosure

Lightning strikes initiate the majority of faults on the transmission level but in most of these instances the line insulation sustains no permanent damage. Following the dissipation of the electric charges to ground, and deenergizing of the

line, the insulation returns to normal. In case of subtransmission and distribution lines small tree branches and animals are the most common causes of line faults. By letting the arc burn for a few moments the shorted object will ionize.

In all of these cases where the line insulation is "self-healing" the line can be rapidly reenergized. This procedure is referred to as *reclosure* and is performed automatically on command from timer-equipped relays. Typically, the line will be disconnected for a period of not longer than one second.

Reclosure, if delayed too long, will cause a shock to the system that may not be tolerated by its generators. This can be demonstrated by considering the two-area system discussed in Chap. 9. Assume that power flows in direction $1 \rightarrow 2$ on the connecting tie-line. The prefault voltage phasors V_1^0 and V_2^0, separated by the power angle δ^0, are depicted in Fig. 12-5.

Assume a fault to occur which results in the tripping of the tie-line. In the postfault state, area 1 thus finds itself with a power surplus, and area 2 with an equal power deficiency. Area 1 generators will thus experience an acceleration whereas those in area 2 will decelerate.† The two voltages would therefore move apart as indicated by the dashed phasors in Fig. 12-5.

The voltage phasor difference $V_1 - V_2$ represents the voltage drop, jIX_l, across the line reactance X_l. The length of this phasor is thus a measure of the line current. If the two voltages are permitted to move too far apart the line current following reclosure—the so-called "returning current"—can be very high. The accompanying "returning power" will likewise be of large magnitude. This suddenly returning power surge would be accompanied by an equally large

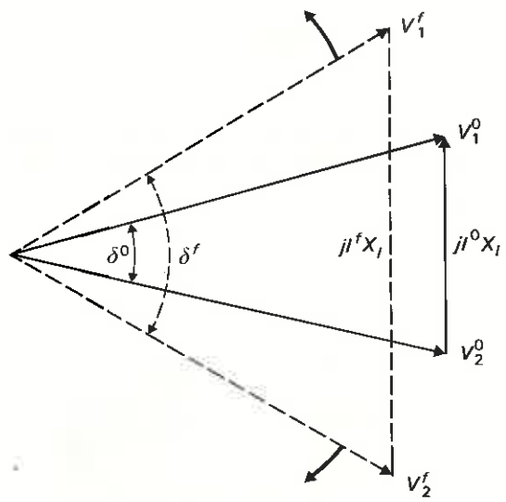

Figure 12-5 A tie-line trip causes an accelerated separation of end-point voltage phasors.

† Compare what would happen in the train analog in Fig. 9-15 if the tie-spring would break.

torque in the synchronous generators in both areas. This torque jolt may give rise to two separate phenomena:

1. If the generator is of turbo type with long shaft and several turbine sections the turbine generator may be excited into *subharmonic resonance* (Sec. 9-5-1). The frequency of such oscillations would lie in the range 20–50 Hz and the oscillations could last maybe for 5–10 seconds. Although the angular amplitudes would be small (less than 1°) the torque amplitudes could be large enough to threaten the integrity of the shaft.†
2. As the returning power would flow in direction $1 \rightarrow 2$ and be larger than the prefault tie-line power it would tend to decelerate the generators in area 1 and accelerate those in area 2. Immediately before reclosure the power angle δ is growing at an accelerated rate. Following the reclosure, due to its momentum, δ will continue to grow but at a decelerating rate. Two end results are possible:
   (*a*) The power angle will reach a maximum and then start to decrease, eventually reaching its prefault value after a few damped swings.
   (*b*) The gained momentum would be too large and although the power-angle growth would decelerate for a few moments the angle would grow beyond $\pi - \delta^0$, thus making the tie-line power too small for resynchronization. This would cause a further accelerating surge in δ resulting in eventual "splitting" of the two-area system.

   In the first case (*a*) the system is said to be *transient stable.*
   In the second case (*b*) the system is said to be *transient unstable.*

12-4 TRANSIENT STABILITY ANALYSIS

As exemplified in the above two-area system faults that cause major structural network changes may result in generator rotor swings leading to breakup of the "synchronizing glue" of a power system.

12-4-1 Mechanical Analog

We can obtain a feel for the general nature of the problem by considering the mechanical analog in Fig. 12-6.

A number of masses, representing the generators in the electric system, are suspended from a "network" consisting of elastic strings, the latter representing the electric transmission lines. The system is in a static steady state, with each

† Actually this becomes such a serious problem for large turbo units that reclosure sometimes cannot be used. (This was the reason why the first lightning strike in the 1977 New York blackout resulted in *permanent* line outage.) Reference 4 contains an excellent presentation of this problem.

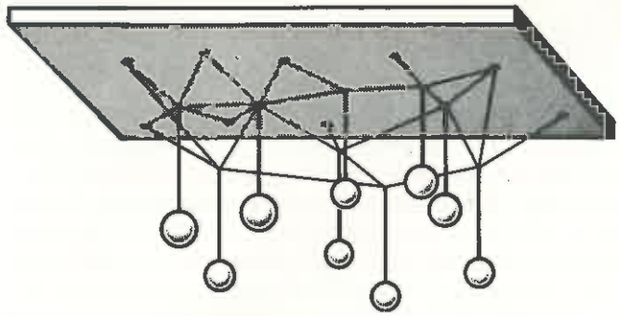

Figure 12-6 Mechanical analog of power-system transient stability.

string loaded below its break point (corresponding to the fact that each transmission line is operated below its static stability limit).

At this point one of the strings is suddenly cut (corresponding to a sudden loss of an electric line). As a result the masses will experience transient coupled motions, and the forces in the strings will fluctuate. The sudden disturbance may cause one of two end effects:

1. The system will settle down to a new equilibrium state, characterized by a new set of string forces (i.e., line powers in the electric case).
2. Due to the transient forces, one additional string will break, causing a still weaker network, resulting in an ensuing chain reaction of broken strings and eventual total system collapse.

If the system has the inherent strength to survive the disturbance and settle in a new steady state, we refer to it as "transient stable for the fault in question." *It should be noted, of course, that the system may be transient stable following the loss of one particular link but unstable following another or others.*

The events that follow upon the loss of a transmission line in a power system are quite similar to the transients in the above system. In detail, the analog has, of course, many discrepancies.

Depending upon the nature and *duration* of the fault, the ensuing mechanical rotor transients may be over in a few seconds or they may continue and grow in severity over the next seconds, or even minutes, ending, eventually, in total system collapse or recovery.

If we were to investigate the system in Fig. 12-6 as to its transient stability, we would proceed as follows:

1. Determine the initial prefault state.
2. Initiate the fault.
3. Compute the postfault transient motion of the masses and resulting forces in the strings.
4. If these forces do not exceed the break points of the strings, the system would be judged stable for the fault in question.

A transient stability study of an electric energy system proceeds along similar lines. Following the disturbance, the rotor angular positions will experience transient deviations. Since the fault is assumed to be of *major* proportions, these swings will be of *large-scale* magnitude, not the small-scale perturbations that we discussed in Chap. 9. If it can be ascertained by analysis that *all* the individual rotor angles will settle down to new postfault steady-state values, corresponding to a new stable synchronous equilibrium state, then we conclude that the system is indeed transient stable.

The key issue is, obviously, the accuracy with which we can predict the postfault rotor swings. This accuracy is intimately connected with the accuracy of the dynamic models that we use.

12-4-2 Basic Model Assumptions

Our models will be based upon these assumptions:

1. All faults will be *symmetrical*. Not only do symmetrical faults represent the most severe contingencies but they also yield the least complicated analysis.
2. In our earlier study of the load-frequency dynamics (Chap. 9), we made the assumption that all generators belonging to a specific "control area" were controlled in unison and also performed their dynamics in *unison*. This coherency assumption does not apply in the present case. We can expect to find certain generators which perform fast swings and others that swing slowly. Consequently, we must now treat the generators *individually*. Only if it can be ascertained with great certainty that some groups of generators (for example, those in some relatively remote power station) are coherent, should we attempt "lumping." The individual power-angle dynamics of each generator follows from the second-order differential "swing equation" (9-85).
3. Due to the high machine inertias, the individual rotor velocity deviations (as measured relative to a 60-Hz synchronous reference) are *very small* compared with the synchronous velocity $\omega = 2\pi f$ rad/s. For all practical purposes we can therefore consider the static portion (lines and transformers) of the electric network to be in a 60-Hz steady state. As we assume three-phase symmetry, all voltages, currents and powers can therefore be computed from the *algebraic* power-flow equations we derived in Chap. 7. Assumptions 2 and 3 have the following consequence: The individual generators will be described by *differential* equations, the "swing equations," which are mutually *coupled* via *algebraic* equations; the "power-flow equations" describing the lines and transformers.

12-4-3 The Single-Generator Case

In a large-scale system with many generators the overall transient stability model can reach formidable complexity. The single generator operating onto an infinite bus (Fig. 4-13) affords us an opportunity to illustrate some of the basic features of transient stability analysis with a minimum of analytical effort.

We shall assume that the generator operates in steady-state when a severe fault occurs on the feeder line causing its instantaneous tripping. At this moment, $t = 0$, we enter the *postfault period* I. The line remains open for a period of T seconds whereupon it recloses. At this moment we enter the *postfault period* II.

We set out to analyze the rotor dynamics of the generator following the line fault. Specifically, we shall make use of the machine data of the 15-MVA hydrogenerator that we earlier analyzed in Examples 4-3, 4-13, and 9-10.

We shall make repeated use of the generator swing equation (9-85) in which the turbine and generator powers P_T and P_G respectively play a dominant role. For these powers we make these simplifying but realistic assumptions:

1. P_T will remain unchanged at its prefault value $P_T^0 = P_G^0$. This assumption means that we neglect the effects of the ALFC loop.
2. In the prefault *steady state* P_G is computed from formula (4-22). Following the onset of the fault the *transient* power formula (4-77) applies. We shall assume that the "emf behind the transient reactance" E' remains unchanged throughout the fault.† This means that we neglect the effects of the AVR loop.

In a more accurate simulation study we would include the dynamics of both the ALFC and AVR loops (Sec. 12-5-1).

We derived earlier both steady-state and transient power formulas (Eqs. 4-30 and 4-83) for our 15-MVA hydrogenerator. We restate them here for easy reference:

$$P_G = 1.341 \sin \delta_N + 0.108 \sin 2\delta_N \qquad \text{pu MW} \tag{12-10}$$

$$P'_G = 2.398 \sin \delta_N - 0.478 \sin 2\delta_N \qquad \text{pu MW} \tag{12-11}$$

In the prefault steady state the generator delivers 10 MW, or 0.667 pu. This corresponds (see Example 4-3) to a prefault power angle δ_N^0 of 0.449 electrical radians‡ (= 25.7°). In Fig. 12-7 the steady-state and transient generator powers are plotted versus the power angle δ_N (graphs A and B respectively).

Postfault period I With the line suddenly open circuited the generator output P_G drops to zero. As the turbine power P_T remains unchanged at its prefault value $P_T = P_G^0$ the swing equation will read

$$P_{\text{acc}} = P_T = P_G^0 = \frac{H}{\pi f^0} \ddot{\delta}_N \tag{12-12}$$

where P_{acc} is the *accelerating power*.

† This assumption is not nearly as valid as that of the constancy of P_T. It is made here to accommodate fairly simple analysis.

‡ The reader is reminded that the swing equation (9-85) yields the rotor angle in *electrical radians*.

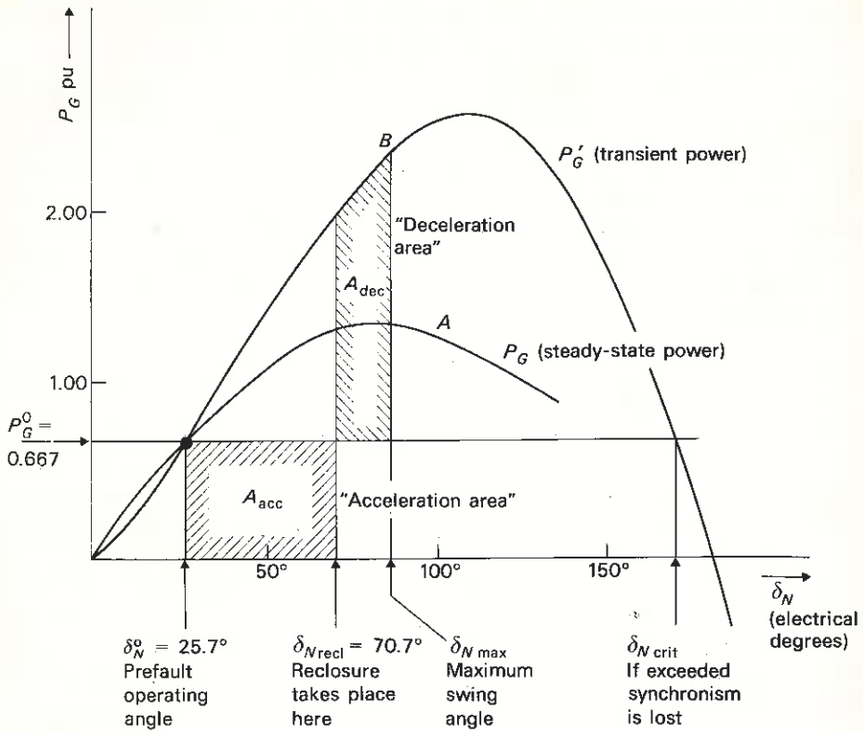

Figure 12-7 The "equal-area" criterion.

As P_{acc} is constant and positive, Eq. (12-12) simply states that the generator rotor is subject to a *constant, positive* angular acceleration of magnitude

$$\ddot{\delta}_N = \frac{\pi f^0 P_{acc}}{H} \qquad \text{rad/s}^2 \tag{12-13}$$

By integrating twice we obtain

$$\delta_N = \delta_N^0 + \frac{\pi f^0 P_{acc}}{2H} t^2 \qquad \text{rad} \tag{12-14}$$

The power angle will increase parabolically with time as depicted in Fig. 12-8. If we use the numerical data for our 15-MVA example generator and if the line is kept open for an interval of $T = 0.250$ s, the rotor angle at the moment of reclosure is computed as follows:

$$\delta_{N\,recl} = 0.449 + \frac{\pi \times 60 \times 0.667}{2 \times 5}(0.250)^2 = 1.235 \text{ rad} \qquad \text{(or 70.7 el. deg.)}$$

This angle has been identified in Fig. 12-7.

Postfault period II Upon reclosure the generator power jumps from zero to the "transient" value given by graph *B* in Fig. 12-7. The swing equation in postfault period II thus reads

$$P_{acc} = P_T - P_G' = \frac{H}{\pi f^0}\ddot{\delta}_N \tag{12-15}$$

As the magnitude of P_G' is far in excess of the turbine power, P_{acc} will now turn negative, resulting in rotor *deceleration*. The velocity $\dot{\delta}_N$ will decrease, reach zero, and then turn negative. If we view the situation in the time domain (Fig. 12-8) δ_N will behave as shown by the dashed graph I.

If the reclosure takes place too late, the rotor will have attained too high a speed, and the torque reversal will only slow down the rotor, although not enough to stop it before it reaches the critical angle $\delta_{N\,crit}$ identified in Fig. 12-7. If the rotor swings beyond this angle, the power difference $P_T - P_G$ will again turn positive, the deceleration will change to acceleration, and now we lose the rotor for good. This case is exemplified by graph II in Fig. 12-8.

12-4-4 The "Equal Area" Stability Criterion

There clearly exists a maximum value T_{max} for the duration of the deenergized state of the line beyond which the generator synchronism will irretrievably be lost. How to determine T_{max}?

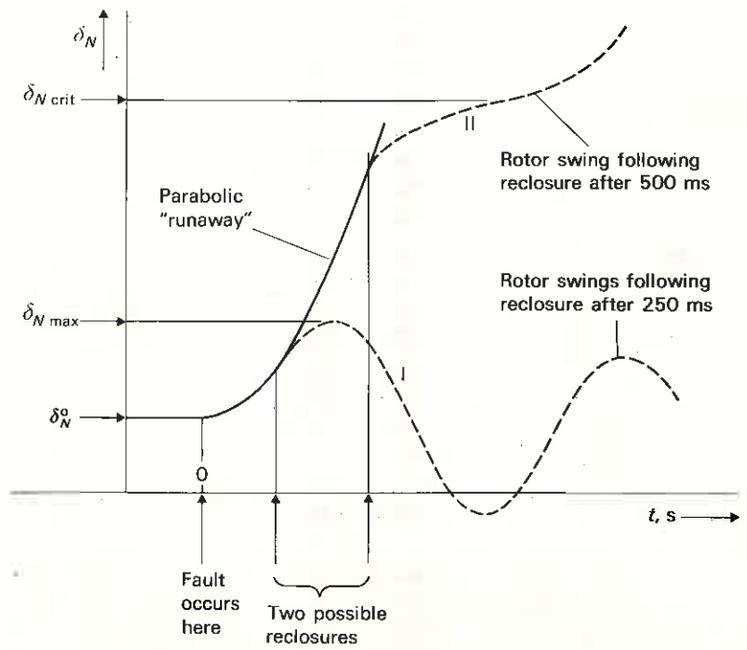

Figure 12-8 "Swing curves" following generation trip and subsequent reclosure.

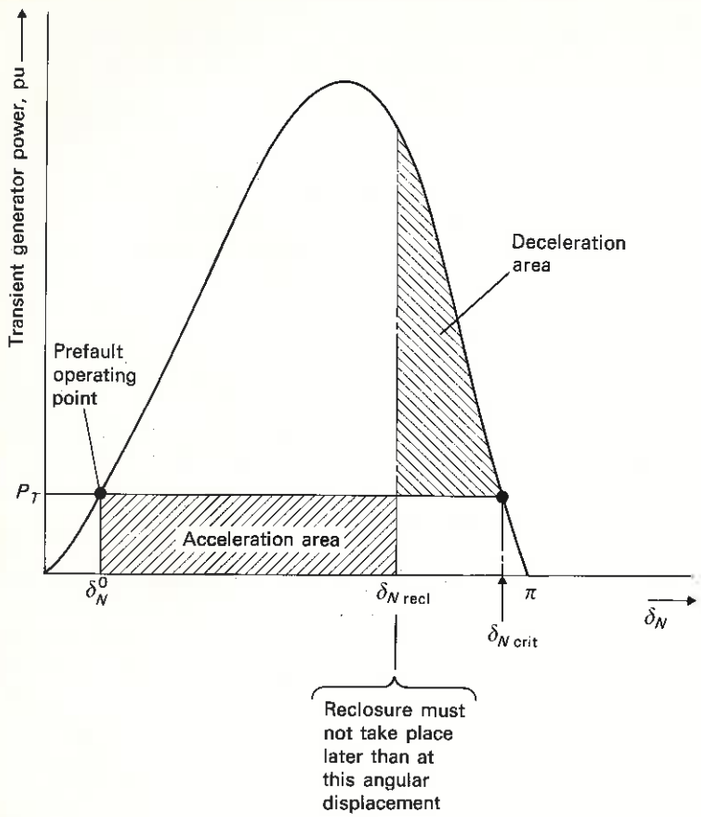

Figure 12-9 Determination of maximum deenergized interval for maintaining transient stability.

If we attempt to integrate the nonlinear differential equation (12-15) we find that, in contrast to the *linear* equation (12-12), it does *not* integrate into any simple analytic function of t. (Later we will discuss how to obtain *numerical* solutions.)

However, it is possible to determine the requirements for stability without actually obtaining *explicit* solutions for the swing equation. To prove this we first rewrite the angular acceleration as follows:

$$\ddot{\delta}_N = \frac{d\dot{\delta}_N}{dt} = \frac{d\dot{\delta}_N}{dt}\frac{d\delta_N}{d\delta_N} = \dot{\delta}_N \frac{d\dot{\delta}_N}{d\delta_N} \tag{12-16}$$

The swing equation can thus be written in the form:

$$\dot{\delta}_N \, d\dot{\delta}_N = \frac{\pi f^0}{H} P_{\text{acc}} \, d\delta_N \tag{12-17}$$

Upon integrating this equation once we obtain

$$\tfrac{1}{2}[\dot{\delta}_N^2(t) - \dot{\delta}_N^2(0)] = \frac{\pi f^0}{H}\int_{\delta_N^{(0)}}^{\delta_N^{(t)}} P_{\text{acc}} \, d\delta_N \tag{12-18}$$

The right-hand-side integral equals the shaded areas in Fig. 12-7. During the postfault period I, P_{acc} is constant and we accumulate the rectangular "acceleration area" marked A_{acc}. In the postfault period II, P_{acc} turns negative. The integral then equals the negative of the "deceleration area" marked A_{dec}. Thus, we can write Eq. (12-18)

$$\tfrac{1}{2}[\dot{\delta}_N^2(t) - \dot{\delta}_N^2(0)] = \frac{\pi f^0}{H}(A_{\text{acc}} - A_{\text{dec}}) \tag{12-19}$$

For the system to be "transient stable" the velocity gained in postfault period I must be reduced to zero in the postfault period II. The left-hand side of Eq. (12-19) represents the *net velocity increase* during *both* periods. *To make this equal to zero we must thus require*

$$A_{\text{acc}} = A_{\text{dec}} \tag{12-20}$$

The turnaround point of the rotor ($\delta_{N\,\text{max}}$) thus is characterized by equal acceleration and deceleration areas, as indicated in Fig. 12-7. If we delay the reclosure too long we will accumulate too large an acceleration area with no time left to accumulate an equal sized deceleration area. The limit case is shown in Fig. 12-9.

Example 12-1 Use the *equal-area criterion* just described to find T_{max} for our 15-MVA hydrogenerator.

SOLUTION The angle $\delta_{N\,\text{crit}}$ is found from the equation

$$P'_G = 2.398 \sin \delta_N - 0.478 \sin 2\delta_N = 0.667 \text{ pu} \tag{12-21}$$

which yields†

$$\delta_N = \delta_{N\,\text{crit}} = 2.940 \text{ rad } (= 168.5°)$$

The "acceleration area" equals

$$A_{\text{acc}} = (\delta_{N\,\text{recl}} - 0.449)0.667 = 0.667\,\delta_{N\,\text{recl}} - 0.299 \tag{12-22}$$

The "deceleration area" equals

$$A_{\text{dec}} = \int_{\delta_{N\,\text{recl}}}^{2.940} (2.398 \sin \delta_N - 0.478 \sin 2\delta_N)\, d\delta_N$$
$$= 2.570 + 2.398 \cos \delta_{N\,\text{recl}} - 0.239 \cos 2\delta_{N\,\text{recl}} \tag{12-23}$$

Equation (12-20) thus reads in this case

$$0.667\,\delta_{N\,\text{recl}} - 2.398 \cos \delta_{N\,\text{recl}} + 0.239 \cos 2\delta_{N\,\text{recl}} - 2.869 = 0 \tag{12-24}$$

† Of course it also yields $\delta_N^0 = 25.7°$ (= 0.449 rad).

By solving this equation we obtain

$$\delta_{N\,\mathrm{rect}} = 2.221 \text{ rad } (=127.2°)$$

Finally, by substitution into Eq. (12-14) we have

$$2.221 = 0.449 + \frac{\pi \times 60 \times 0.667}{2 \times 5} T_{\max}^2 \tag{12-25}$$

which equation yields

$$T_{\max} = 0.375 \text{ s}$$

12-4-5 Coherent Area Dynamics

Consider for a moment the dynamic system in Fig. 12-6. Assume that some of the masses are interconnected with fairly stiff strings. These masses will have a tendency to swing in unison—or *coherently*. For example, if all masses can be divided into two coherent groups which are interconnected with relatively weak strings the overall dynamics of the multimass system approximates closely that of a two-mass system. This simpler "equivalent" or "aggregated" system can then serve as an approximate model in stability studies.

This is the situation that on occasion occurs in power systems. Figure 12-10 depicts† two regional networks interconnected by relatively long tie-lines. Area 1 has a generating capacity of 20 GW but a load demand of only 18 GW. Area 2 has 20 GW of generation but a load demand of 22 GW. By interconnecting the two areas with one or several tie-lines, area 1 will be able to export on a continuing basis its 2-GW surplus power to area 2.

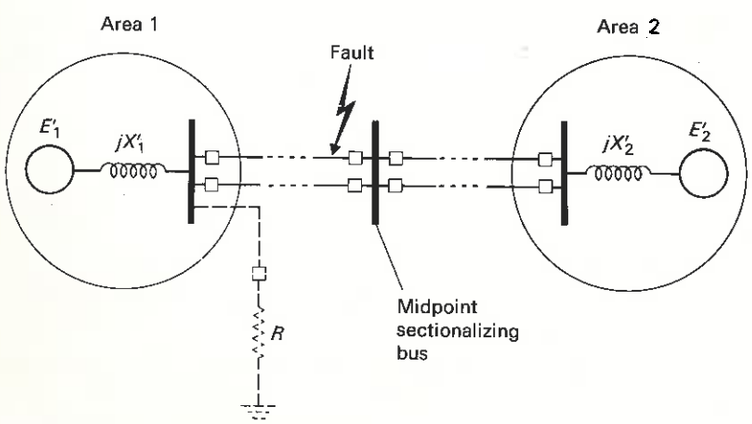

Figure 12-10 Sectionalized double line.

† Disregard for the time being the dashed portion of the network.

Assume that a fault occurs that results in total or partial loss of the ties causing a sudden total or partial interruption of the power flow. As a consequence area 1 generators will experience an acceleration, those in area 2 a deceleration. (Compare also Fig. 12-5.)

As the tie-line power constitutes only a few percent of total area capacity, these accelerations will be far less than that experienced by our 15-MVA example generator upon the sudden loss of 67 percent of its rated power. The power swings that will ensue, referred to as *interarea oscillations*, will thus be much slower than those depicted in Fig. 12-8.

Example 12-2 Assume that the two areas have identical capacity (20 GW) and also identical per-unit inertia, $H = 5$ s. The two 400-mile long parallel lines have a per-phase reactance of 200 ohms each. The addition of the midpoint bus makes it possible to *sectionalize* the tie into four 200-mile sections. The two lines are operating at 500 kV in both ends. Find the maximum megawatt flow on these lines if the transmission must remain intact following a sudden loss of any one of the four line sections.

SOLUTION The total line reactance of the two parallel lines equals 100 ohms per phase. According to formula (3-52) the *static* transmission capacity thus equals

$$P_{\max} = \frac{500^2}{100} = 2.50 \text{ GW}$$

If one line section is lost the remaining line reactance would increase to $100 + 50 = 150$ ohms per phase. The *static* capacity would thus be reduced by 0.83 GW to the new lower value

$$P_{\max} = \frac{500^2}{150} = 1.67 \text{ GW}$$

(If the line had not been sectionalized the same fault would have crippled one full line with a resulting *static* capacity loss of 1.25 GW.)

Clearly, we cannot transmit the full 1.67 MW because this would require a line power-angle of 90° and *zero margin* for emergencies. We now proceed to study what margin we in reality must choose in view of the ensuing power swings. We shall use the "equal area" criterion in our analysis which will be based upon the following assumptions:

1. A three-phase solid fault occurs on one line section close to the midpoint bus (see Fig. 12-10). The fault clears in very short time (≈ 3 cycles) but the faulted section is permanently lost.
2. The two areas are dynamically coherent. The generators of each area can thus be lumped into *one* 20-GW equivalent generator. This one generator is represented with a "Thévenin equivalent" consisting of an emf E' behind a transient reactance X'. For the two areas we have

$$\begin{aligned} E'_1 &= |E'_1| \angle \delta_1 \\ E'_2 &= |E'_2| \angle \delta_2 \end{aligned} \tag{12-26}$$

From a detailed knowledge of each area network it has been found that

$$|E'_1| = |E'_2| = \frac{525}{\sqrt{3}} \text{ kV/phase}$$

and

$$X'_1 = X'_2 = X' = 25 \ \Omega\text{/phase}$$

The angular positions of phasors E'_1 and E'_2 define rotor positions of the equivalent generators. Thus we define the power angle

$$\delta \triangleq \angle E'_1 - \angle E'_2 = \delta_1 - \delta_2 \tag{12-27}$$

With all four line sections intact the total reactance between E'_1 and E'_2 equals

$$X_{tot} = 25 + 100 + 25 = 150\ \Omega/\text{phase} \tag{12-28}$$

With only three line sections operating the total reactance increases to

$$X_{tot} = 25 + 100 + 50 + 25 = 200\ \Omega/\text{phase} \tag{12-29}$$

The transient powers in prefault and postfault line configurations are thus:

$$\text{Prefault:} \quad P'_G = \frac{525^2}{150} \sin\delta = 1.84 \sin\delta \quad \text{GW} \tag{12-30}$$

$$\text{Postfault:} \quad P'_G = \frac{525^2}{200} \sin\delta = 1.38 \sin\delta \quad \text{GW} \tag{12-31}$$

These powers are shown in Fig. 12-11 (graphs A and B).

Let us assume that the prefault tie-line power equals the as yet unknown value P^0 corresponding to the likewise unknown prefault power angle δ^0. P^0 and δ^0 are identified in Fig. 12-11.

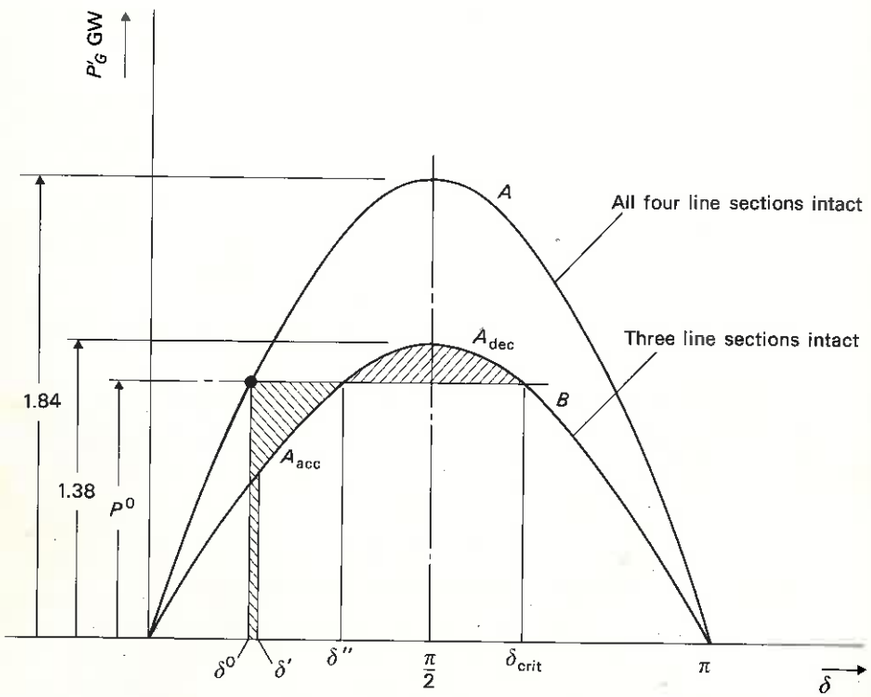

Figure 12-11 "Equal-area" criterion applied to partial loss of transmission capacity.

As the solid short hits, the tie-line power drops to zero where it remains during the three cycles it takes to clear the fault. During this period the power angle δ experiences its largest acceleration. At the end of this period the power angle has increased to the new value δ'. As the fault clears the voltages bounce back and the tie-line power flow resumes but at the lower level due to the lost line section.

The angular acceleration is still positive and will remain so until δ has grown to the value δ''. Further increase in δ causes the generated power to exceed turbine power resulting in an angular deceleration.

If the prefault power level P^0 is chosen sufficiently low the system will now accumulate a "deceleration area," A_{dec}, equal with the "acceleration area," A_{acc}, in which case the system remains synchronized.

As we compute A_{acc} and A_{dec} we neglect for simplicity the small part of A_{acc} accumulated during the brief short circuit. We thus set $\delta' \approx \delta^0$ and obtain

$$\begin{aligned} A_{acc} &\cong \int_{\delta^0}^{\delta''} (P^0 - 1.38 \sin\delta)\, d\delta \\ &= P^0(\delta'' - \delta^0) + 1.38(\cos\delta'' - \cos\delta^0) \end{aligned} \tag{12-32}$$

$$\begin{aligned} A_{dec} &= 2\int_{\delta''}^{\pi/2} (1.38 \sin\delta - P^0)\, d\delta \\ &= 2.76 \cos\delta'' - 2P^0\left(\frac{\pi}{2} - \delta''\right) \end{aligned} \tag{12-33}$$

The "equal-area" criterion thus reads

$$P^0(\pi - \delta^0 - \delta'') - 1.38 \cos\delta^0 - 1.38 \cos\delta'' = 0 \tag{12-34}$$

The two unknown angles δ^0 and δ'' are related (see Fig. 12-11) to P^0 through the two equations:

$$\begin{aligned} \delta^0 &= \sin^{-1}\left(\frac{P^0}{1.84}\right) \\ \delta'' &= \sin^{-1}\left(\frac{P^0}{1.38}\right) \end{aligned} \tag{12-35}$$

Upon substitution of Eqs. (12-35) into (12-34) we obtain an equation in the single unknown P^0.

Trial-and-error solution of Eq. (12-34) yields

$$P^0 = 1.27 \text{ GW}$$

Note that this value amounts to only 51 percent of the prefault *static capacity* of 2.50 GW. *The example therefore reveals that we must operate transmission lines well below their static capacity to ensure that the transmission holds up under the strain of faults.*

12-4-6 Stability Enhancement Methods

Example 12-2 clearly demonstrates that the need for dynamic stability margins in effect means that we are unable to fully utilize the static capacity of transmission lines. This is uneconomical and it becomes important therefore to explore what possibilities exist in a given system to enhance or augment its transient stability.

Fast switching Speedy fault removal is a primary requirement for achieving transient stability. During the duration of a short circuit the voltages are badly depressed. This results in severe reductions in generator outputs and a correspondingly high accelerating power P_{acc}.

It must be realized that the time required for fault removal is the sum of the relay response time plus the breaker operating time. It is possible today to achieve fault isolation in less than two cycles.

The transient stability is also improved by reducing the time interval between line removal and reclosure. However, for the reclosure to be successful the line must remain deenergized for a certain minimum time in order for the line insulation fully to recover. This time varies with the severity of fault and is not known a priori. If the first reclosure fails one may make a second and possibly a third attempt.

Increased inertia Added inertia in the form of separate flywheels slows down the transient angular motions, enabling us to work with larger reclosure times. This is an expensive remedy.

Fast valving The turbine power P_T is the cause of the rotor acceleration following the tripping of the line. If this power somehow could be momentarily reduced, the acceleration and thus the subsequent angular swings could be minimized.

The total turbine power is the sum of the powers of the high-, intermediate-, and low-pressure sections of the turbine (compare App. D). Between the HP and IP sections the steam is led through a "reheater." Bypass paths also exist. It is possible to achieve through sudden closure and subsequent slower opening of certain steam valves (so-called *fast valving*) very substantial and fast reductions in the turbine power. These power dips may last for periods of the order of one second each, and if made to coincide with the fault-induced dips in the generator power we can obviously improve the power balance during these critical moments.[5]

Braking resistors Consider for a moment the system in Fig. 12-10. Assume that it has been determined that tripping and subsequent reclosure will clear most of the occurring line faults. In the majority of cases the loss of power transmitting capacity is thus only of temporary nature.

In such a situation stability can be greatly enhanced by a *braking resistor*, so called because it is designed to reduce the acceleration of the generator rotors following a fault. The resistor (shown dashed in Fig. 12-10) is inserted immediately following the fault and disconnected at the moment of reclosure.

For example, assume that the line tripping causes an instantaneous line power loss of 1000 MW. The line remains open for exactly one second before reclosure takes place. If the braking resistor is designed to absorb exactly 1000 MW for a period of one second then, clearly, *the generators of area 1 will not experience any accelerating power*, and will ride through the fault as if nothing had happened.

A typical application of a braking resistor is a 1400-MW unit installed in the Pacific Northwest. It is intended for use if one of the tie-lines to Southern California is faulted. The resistor is strung on three towers (one per phase) with approximately 15,000 feet of $\frac{1}{2}$-inch stainless steel wire.[7]

Load shedding Insertion of a braking resistor can be used to reduce angular accelerations when a fault causes a momentary power surplus in an area. Removal of load, *load shedding*, can similarly prove useful when the fault has created a power deficiency in an area.

We talk about *fast* load shedding when used in the first instants after the fault for the purposes of improving the transient stability. The term *load skipping* is used for a switching strategy consisting of sudden fast load removal and a subsequent load pickup. The period of disconnect may vary from a fraction of to a few seconds. *Slow* load shedding is a means of control employed in the later phases of an emergency when *sustained* power deficiencies cause a deterioration of frequency (Sec. 12-6). The load is now disconnected in predetermined sections and amounts and kept disconnected for minutes and possibly hours until generating capacity has been restored.

Series capacitors Switched series capacitors can improve substantially the transient stability of a system. We exemplify this by considering the case treated in Example 12-2. We shall add a capacitor C in the midpoint switching station as indicated in Fig. 12-12*a*. Under normal operation the capacitor is shorted out by the circuit breaker marked CB.

Let us assume that the reactance of the capacitor equals 50 ohms per phase. When a fault occurs on one of the four line sections the breaker CB is opened at the same instant as the line breaker opens, thus inserting the capacitor in series with the three remaining line sections. The total reactance between the emf's E'_1 and E'_2 thus will equal

$$X_{tot} = 25 + 100 - 50 + 50 + 25 = 150\ \Omega/\text{phase}$$

The postfault transient power thus will equal

$$P'_G = \frac{525^2}{150} \sin \delta = 1.84 \sin \delta \tag{12-36}$$

The capacitor has thus increased the postfault transient power to the same level as existed in the prefault state (compare Eq. (12-30)).

In Fig. 12-12*b* are shown the "acceleration" and "deceleration" areas in the subsequent angular swings. They should be compared with those in Fig. 12-11. It is quite clear that we can now operate at a substantially higher prefault power level than before.

When the first swing of the δ angle is completed the capacitor can be disconnected from the circuit by closing CB. Like a braking resistor it is used only for very short periods and needs only to have short time ratings which is an economic advantage.

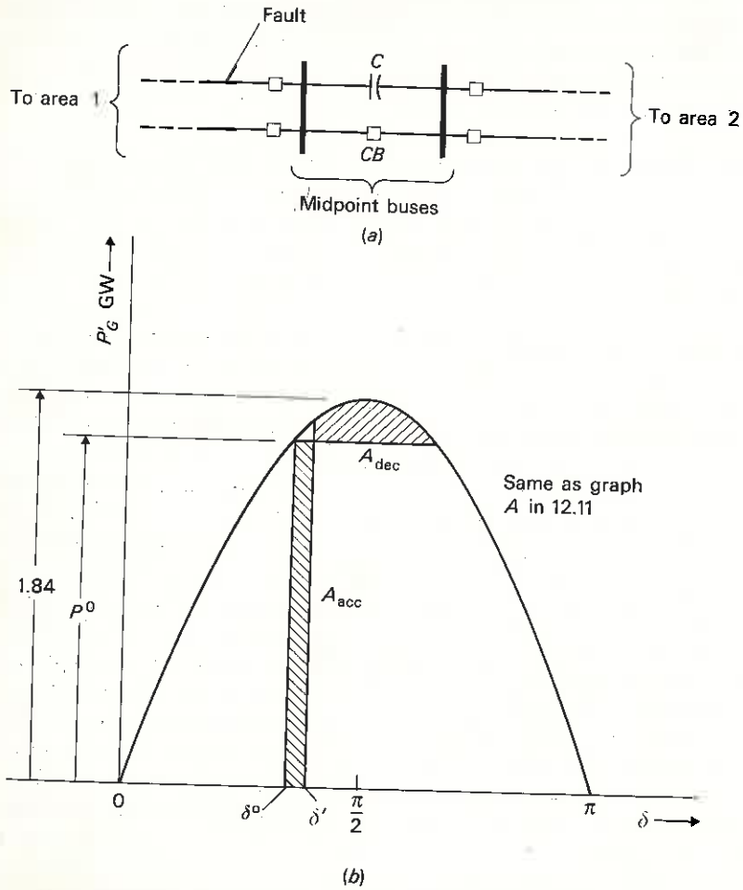

Figure 12-12 Stability enhancement by means of series capacitor injection.

12-5 TRANSIENT ANALYSIS OF LARGE-SCALE SYSTEMS

The single-generator case provided valuable insight into the electromechanical mechanism that determines transient stability in a power system. We also learned that the single-generator model can be applied to large-scale systems when "coherency" is present, thus extending its usefulness beyond purely "academic" cases. In large-scale systems when coherency is not obviously present each generator must be modeled individually causing the overall dynamic model to become extensive. If, in addition, the dynamic effects of the AVR and ALFC loops must be accounted for the dynamic model can get extremely complex.

In the single-generator case the "equal area" stability criterion provided a

means for obtaining numerical answers without actually having to integrate the swing equations. One is thus led to inquire whether a similar stability criterion exists in the more general n-generator case.

A number of such criteria have been proposed,[8] most of them based upon so-called Lyapunov functions. Although these criteria are of considerable theoretical interest the assumptions upon which they are derived make their usefulness questionable. It is probably safe to state in 1982 that numerical integration of the swing equations provides the only practical means of obtaining useful stability information in large-scale systems. A typical large-scale transient stability study proceeds as follows:

Step 1 Develop a static power-flow model of the study system based on $\mathbf{Y}_{bus}$.

Step 2 Perform a power-flow computation based upon the above model. This computation yields information about the *prefault* angular positions δ_i^0 and megawatt outputs P_{Gi}^0 of all n generator units. The angular positions are all measured relative to the prefault reference bus voltage V_1^0.

Step 3 Construct the dynamic model of each turbine-generator. The second-order swing equation (Eq. 9-85) constitutes the essential portion of the dynamic model; in fact if we can neglect the effect of the ALFC and AVR loops the swing equation is *the* model.

Step 4 Select a fault contingency for which the transient stability must be investigated. Apply the fault at $t = 0$.

Step 5 Integrate the swing equations. As these integrations are performed on a digital computer the solutions are obtained at *discrete* time instants $t^{(1)}$, $t^{(2)}$, ... This first integration thus yields the angular positions $\delta_i(t^{(1)})$.

Note: As the fault causes power imbalances throughout the network, *all* generators will participate in the dynamics. This means that the reference phasor V_1 will also change its angular position relative to its prefault value. As we *must*† use a constant angular reference we will continue to use the *prefault* phasor V_1^0 even in the *postfault* state.

Step 6 Plot the angular positions $\delta_i(t^{(1)})$.

Step 7 Perform a power-flow computation to find the new generation values $P_{Gi}(t^{(1)})$ corresponding to the angular rotor positions $\delta_i(t^{(1)})$.

Note: Since the fault changed the network structure this power flow must be based on a different $\mathbf{Y}_{bus}$ than that used in step 2.

Steps 5 to 7 are repeated and in each computation cycle we thus compute and plot the angular positions $\delta_i(t^{(2)})$, $\delta_i(t^{(3)})$, etc.

The computations must continue until the plots ("swing curves") reveal a definite trend as to stability or instability.

We comment now briefly on some important aspects of the above computations.

† Newton's law of acceleration upon which the swing equation is based holds true only in an "inertial" reference frame.

12-5-1 Constructing the Dynamic Generator Model

We restate the swing equation (9-85)

$$P_T - P_G = \frac{H}{\pi f^0}(\ddot{\delta} + D\dot{\delta}) \tag{12-37}$$

Note that we have added a damping term $D\dot{\delta}$. This damping (Sec. 9-5-3) is relatively insignificant and in our earlier analysis we neglected it for the sake of simplicity. As we now will make use of a computer, retaining the term represents only slightly added computational load.

Equation (12-37) is of second order. In this form it is not directly suitable for numerical integration. We rewrite it by first introducing the two dynamic *state variables* x_1 and x_2, defined as follows:

$x_1 \triangleq \delta$ rotor angular position in electrical radians

$x_2 \triangleq \dot{\delta}$ rotor angular velocity in electrical radians per second

These state variables constitute the components of the *state vector*

$$\mathbf{x} = \begin{bmatrix} x_1 \\ x_2 \end{bmatrix} \triangleq \begin{bmatrix} \delta \\ \dot{\delta} \end{bmatrix} \tag{12-38}$$

In terms of these state variables the second-order swing equation can be written as two coupled *first-order differential equations*

$$\begin{aligned} \dot{x}_1 &= x_2 \\ \dot{x}_2 &= \frac{\pi f^0}{H}(P_T - P_G) - Dx_2 \end{aligned} \tag{12-39}$$

The turbine power P_T is constant and the generator power P_G is a function of δ $(=x_1)$, and we can therefore write these equations in the following more general form:

$$\begin{aligned} \dot{x}_1 &= f_1(x_1, x_2) \\ \dot{x}_2 &= f_2(x_1, x_2) \end{aligned} \tag{12-40}$$

or more compactly

$$\dot{\mathbf{x}} = \mathbf{f}(\mathbf{x}) \tag{12-41}$$

Up to this point we have tacitly assumed that the ALFC and AVR loops have no influence, that is, P_T and E' are assumed *constants*. A more accurate analysis must take these control loops into account. We look now at these effects separately.

Effect of ALFC loop upon P_T The fault-induced rotor acceleration translates into a frequency increase Δf of magnitude

$$\Delta f = \frac{1}{2\pi}\dot{\delta} = \frac{1}{2\pi}x_2 \qquad \text{Hz} \tag{12-42}$$

Through the actions of the "primary" ALFC loop this frequency increase will result in a change ΔP_T in the turbine torque that can be obtained from the block diagram in Fig. 9-8. This diagram yields:†

$$\begin{aligned} \Delta P_V(s) &= -\frac{1}{1 + sT_H}\frac{\Delta f(s)}{R} \\ \Delta P_T(s) &= \frac{1}{1 + sT_T}\Delta P_V(s) \end{aligned} \tag{12-43}$$

Inverse transformation of these two equations results in the differential equations

$$\begin{aligned} \Delta P_V + T_H\frac{d}{dt}(\Delta P_V) &= -\frac{1}{R}\Delta f \\ \Delta P_T + T_T\frac{d}{dt}(\Delta P_T) &= \Delta P_V \end{aligned} \tag{12-44}$$

We introduce now the two additional state variables

$$\begin{aligned} x_3 &\triangleq \Delta P_V \\ x_4 &\triangleq \Delta P_T \end{aligned} \tag{12-45}$$

in terms of which we can write equations (12-44) in the form

$$\begin{aligned} \dot{x}_3 &= \frac{1}{T_H}\left(-x_3 - \frac{\Delta f}{R}\right) = -\frac{x_3}{T_H} - \frac{x_2}{2\pi R T_H} \\ \dot{x}_4 &= \frac{1}{T_T}(x_3 - x_4) \end{aligned} \tag{12-46}$$

The effect of the primary ALFC loop has been to add two new state variables to the earlier pair defined by Eq. (12-38). The dynamic model (12-41) has thus increased in complexity from second to fourth order.

Effects of AVR loop upon E' As the fault occurs the system voltages experience a sudden and often severe depression. This change is immediately felt by the AVR control loop (Fig. 9-3) that responds with a change in the field voltage v_f, the field current i_f, and finally the emf E'.

We can write the appropriate differential equations for all these changes which necessitates the introduction of at least three more state variables, x_5, x_6, and x_7. Three additional differential equations of the form (12-46) can then be written. (Compare Prob. 12-5.)

† We neglect completely the slow changes in ΔP_{ref}. We also assume the turbine to be of non-reheat type.

In summary, the modeling of the ALFC and AVR loops has increased the dimensionality of the generator dynamic model from two to seven. For a power system containing 50 generator units we thus obtain a dynamic model consisting of at least $50 \times 7 = 350$ first-order coupled differential equations.

12-5-2 Numerical Integration

Two basic computational procedures are required in a study as outlined above:

1. Power-flow computations (steps 2 and 7)
2. Numerical integration (step 5)

Power-flow computations were discussed in Chap. 7. Presently we shall describe numerical integration procedures. The problem is stated as follows: Given the vector differential equation (12-41) which may be of very high dimensionality, also given the initial state $\mathbf{x}^{(0)}$, compute by means of some appropriate algorithm the new states $\mathbf{x}^{(1)}, \mathbf{x}^{(2)}, \ldots, \mathbf{x}^{(\nu)}, \ldots$.

As always in numerical analysis, the accuracy of the method depends upon the quality of the algorithm used. We shall discuss a couple of algorithms, and start, appropriately, with the simplest of them all.

The Euler numerical integration method Preparatory to discussing the digital solution of the *vector* equations (12-41), let us consider the *scalar* case

$$\dot{x} = f(x) \tag{12-47}$$

For $t = t^{(\nu)}$, we can set with some accuracy

$$\dot{x}^{(\nu)} \approx \frac{\Delta x^{(\nu)}}{\Delta t} = f(x^{(\nu)}) \tag{12-48}$$

Using this formula, we would perform the integration in the following steps (Fig. 12-13):

Step 0 For $t = t^{(0)}$ and $x = x^{(0)}$, compute the state increment $\Delta x^{(0)}$

$$\Delta x^{(0)} = f(x^{(0)})\,\Delta t$$

Step 1 For $t^{(1)} = t^{(0)} + \Delta t$, we therefore have the new state

$$x^{(1)} = x^{(0)} + f(x^{(0)})\,\Delta t$$

Step 2 For $t^{(2)} = t^{(1)} + \Delta t$ we similarly obtain

$$x^{(2)} = x^{(1)} + f(x^{(1)})\,\Delta t$$

etc.

Clearly, the computational algorithm is

$$x^{(\nu+1)} = x^{(\nu)} + f(x^{(\nu)})\,\Delta t \qquad \text{for } \nu = 0, 1, \ldots \tag{12-49}$$

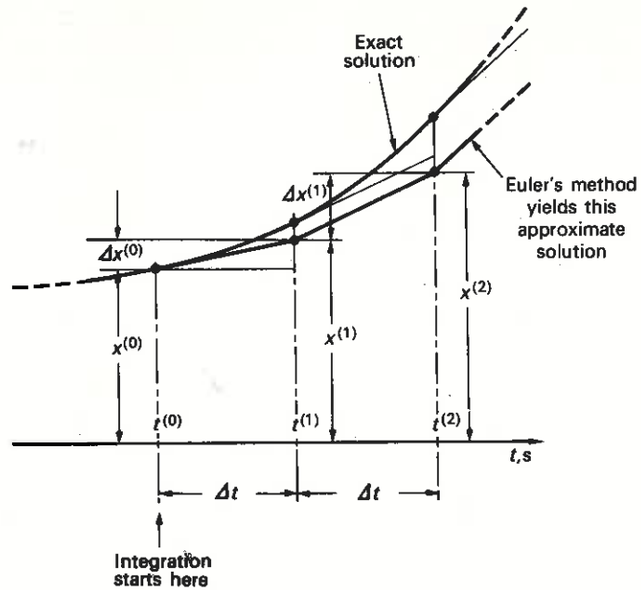

Figure 12-13 Graphical interpretation of Euler's integration method.

We may readily extend this algorithm to the vector case. For the ith component of the $\mathbf{x}$ vector we have

$$x_i^{(\nu+1)} = x_i^{(\nu)} + f_i(x_1^{(\nu)}, x_2^{(\nu)}, \ldots, x_n^{(\nu)})\,\Delta t \qquad \text{for } i = 1, 2, \ldots, n$$

or in vector form

$$\mathbf{x}^{(\nu+1)} = \mathbf{x}^{(\nu)} + \mathbf{f}(\mathbf{x}^{(\nu)})\,\Delta t \tag{12-50}$$

Euler's method is simple, but not particularly accurate. Figure 12-13 shows why. Since the state variables at the end of an interval are computed on the basis of the derivative at the beginning of the interval, an error will be introduced which is the more pronounced the faster the derivative is changing within the interval Δt.

The modified Euler method The accuracy of the Euler method can be improved remarkably by the obvious modification of using an *average* value for the derivative throughout each time interval. The computational algorithm given above will now be modified in accordance with Fig. 12-14. Let us discuss the changes introduced.

The computations proceed as before up to and including block 4. Based upon the *tentative* value of $\mathbf{x}^{(\nu+1)}$ obtained in block 4, we compute in block 5 the derivative at the *end* of interval ν.

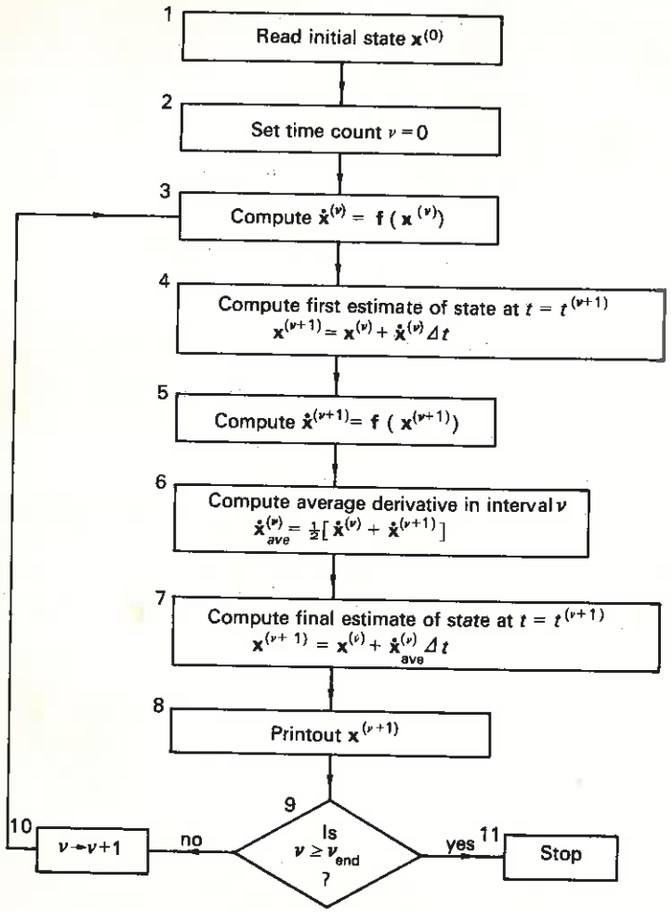

Figure 12-14 Flowchart for Euler modified algorithm.

In the next block 6, we then compute an *average value* for the derivative in interval ν, and based upon this average derivative, we then proceed to recompute an *upgraded* value for $\mathbf{x}^{(\nu+1)}$ in block 7.

Other algorithms There is a large variety of integration algorithms in addition to those detailed above. None of them possess the inherent simplicity of the Euler methods, and all require various amount of computation per time interval. (The reader may consult Ref. 9.)

Example 12-3 We shall perform a numerical transient stability study on the three-bus, two-generator system depicted in Fig. 12-15. The prefault voltage profile is flat with $|V_1^0| = |V_2^0| = |V_3^0| = 1$ pu. (The voltage of bus 3 is controlled by means of the shunt capacitor.)

Load is drawn from buses 1 and 3 in amounts indicated in Fig. 12-15. The real load is divided equally between generators $G1$ and $G2$. All powers, impedances, and inertia constants in this example are given in per unit of 50-MVA base.

Here follow the pertinent component data:

Lines The reactance of each line equals 0.050 pu Ω.

Generators and transformers Total reactance of generator (X'_d) plus transformer (X_L) equals 0.054 pu Ω. Each generator is rated at 600 MVA.

The inertia constants of the generators are:

$$H_1 = 30 \text{ s (or 2.5 s based on rating)}$$

$$H_2 = 300 \text{ s (or 25 s based on rating)}$$

For tutorial purposes we have chosen the inertia of $G2$ ten times larger than that of $G1$ so as to obtain fairly small angular swings in the former machine. The low-inertia machine will therefore, in effect, swing around the high-inertia machine, and we shall find it fairly easy to distinguish between stable and unstable cases.

Fault sequence We shall consider the following sequence of abnormal events:

1. The generator $G1$ is tripped (by opening of CB1) and will remain disconnected from the network for a period of T s. We refer to this as "postfault period I" in the following analysis.
2. When the generator is reconnected to the network after T s, we enter "postfault period II."

During postfault period I the generator $G1$ will obviously experience an acceleration. The generator $G2$, with its relatively high inertia, will remain fairly fixed in angular reference. The two generators are obviously going apart, and the question therefore is whether, upon reclosure,

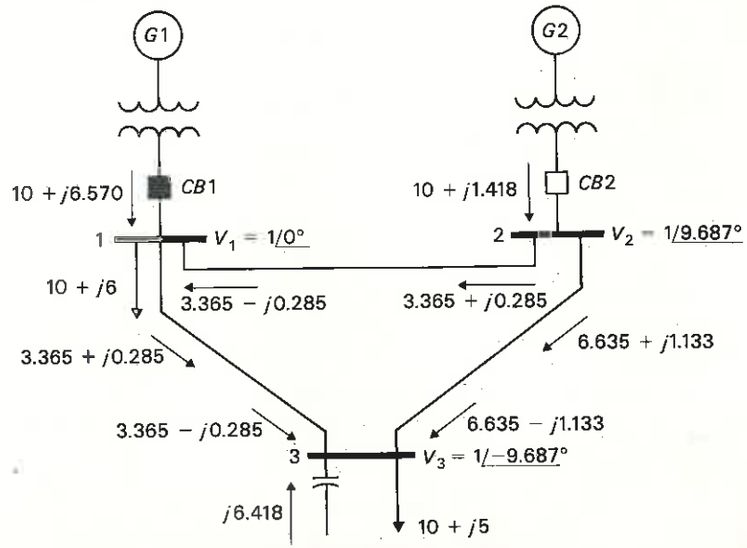

Figure 12-15 A three-bus example system used in Example 12-3.

the system has sufficient synchronizing "glue" to hold them together. Our study will be aimed at finding this out.

Assumptions The subsequent analysis will be based upon the following assumptions:

1. Generator saliency will be neglected, and each transient generator model will therefore consist of an emf E' behind its transient reactance.
2. The emf's behind the transient reactances will retain constant magnitudes throughout the postfault periods. This means that we neglect the effects of the AVR loops.
3. The turbine powers P_{T1} and P_{T2} will be constant throughout the postfault periods (their values being $P_{T1} = P_{T2} = P_G^0 = 10$ pu). This means that we neglect the effects of the ALFC loops.
4. All resistances are neglected.
5. All damping torques are likewise neglected.
6. The bus voltages will undergo major changes during the postfault period. These changes will strongly affect the bus loads (Chap. 3). The nature of the load determines the voltage dependency. We shall assume that bus loads are of "impedance type," i.e., we may represent both by *constant* shunt admittances Y_{D1} and Y_{D3}, which will not change throughout the analysis. The loads will thus vary as the square of the voltage, but the load power factors will be fixed.
7. The frequency will change only slightly, and we will therefore neglect the change of load with frequency.

SOLUTION We shall perform the stability analysis in the following steps:

A. Prefault power flow The stage is set for a power-flow study of the type discussed in Chap. 7. All impedances are given so that the prefault $\mathbf{Y}_{\text{bus}}$ can be found. Bus power and voltage specifications are complete.

We perform such a study and obtain the prefault power flows indicated in Fig. 12-15. Since we will need them in our further analysis, we compute the prefault generator currents I_{G1}^0 and I_{G2}^0 and also the equivalent load admittances Y_{D1} and Y_{D3}

$$I_{G1}^0 = \left(\frac{S_{G1}^0}{V_1^0}\right)^* = 10 - j6.570 \text{ pu kA}$$

$$I_{G2}^0 = \left(\frac{S_{G2}^0}{V_2^0}\right)^* = 10.10 + j0.285 \text{ pu kA}$$

$$Y_{D1} = \frac{(S_{D1}^0)^*}{|V_1^0|^2} = 10 - j6 \text{ pu } \Omega \qquad (12\text{-}51)$$

$$Y_{D3} = \frac{(S_{D3}^0)^*}{|V_3^0|^2} = 10 + j1.418 \text{ pu } \Omega$$

Note that Y_{D3} includes the shunt capacitor at bus 3.

B. Prefault generator emf' and rotor positions From the assumed generator transient model we get

$$(E_1')^0 = V_1^0 + I_{G1}^0 j(X_d' + X_L) = 1.458\underline{/21.73^\circ} \text{ pu kV}$$
$$(E_2')^0 = V_2^0 + I_{G2}^0 j(X_d' + X_L) = 1.205\underline{/36.29^\circ} \text{ pu kV} \qquad (12.52)$$

The magnitudes of these emf's

$$|E_1'|^0 = 1.458 \text{ pu kV}$$
$$|E_2'|^0 = 1.205 \text{ pu kV}$$

will be retained throughout the analysis.

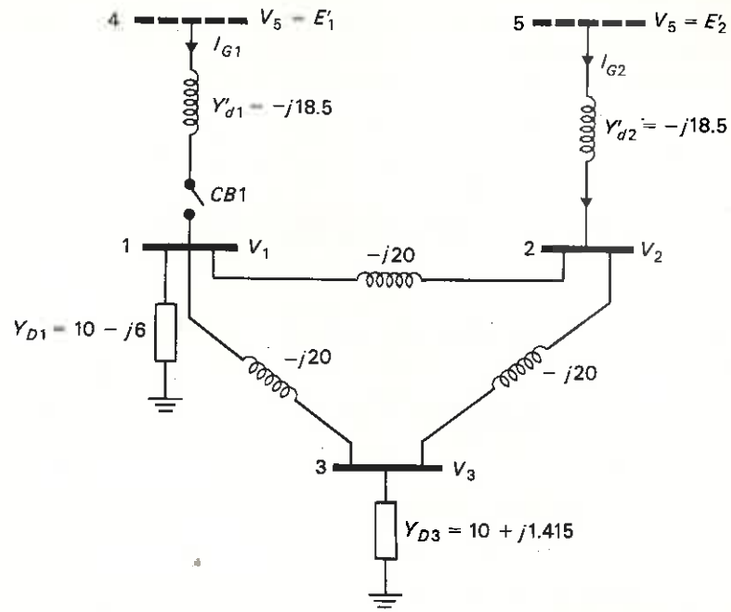

Figure 12-16 Network model for the three-bus system in Fig. 12-15.

As the phasors E_1' and E_2' coincide with the d axes, the initial rotor positions are

$$\delta_1^0 = \underline{/E_1'} = 21.73^\circ = 0.379 \text{ rad}$$
$$\delta_2^0 = \underline{/E_2'} = 36.29^\circ = 0.633 \text{ rad} \qquad (12\text{-}53)$$

Note that V_1^0 has been chosen as reference for the angular positions of *both* generator rotors. In the postfault state, V_1^f will not coincide with V_1^0, but the postfault angles δ_1^f and δ_2^f will still be measured relative to the *prefault synchronous* reference.

At the moment when the fault sets in, the three bus voltages will change instantaneously ("inertialess") to new values. The emf's E_1' and E_2', however, will remain unchanged in both magnitude and phase.† The magnitudes will be constant, for reasons previously explained. The phase angles will remain initially constant because of the rotor inertias, but will immediately start to change due to the torque imbalance resulting from the fault.

C. Network equations (postfault period I) By representing each generator by an emf E' behind its transient reactance X_d', the three-bus system model looks as depicted in Fig. 12-16. Each transformer is modeled with its leakage reactance X_L. Two fictitious buses (coded 4 and 5) have been added, each held at the "bus voltages" $V_4 \triangleq E_1'$ and $V_5 \triangleq E_2'$, respectively.

Note that all network elements have been represented as admittances. The "transient admittances" Y_{d1}' and Y_{d2}' are defined by

$$Y_{d1}' = Y_{d2}' \triangleq \frac{1}{j0.054} = -j18.5 \text{ pu } \mho \qquad (12\text{-}54)$$

† In order not to clutter up our symbols, we will, in the following discussion, delete the postfault superscript f in our symbol notations. No confusion should result.

We had assumed that the bus loads were of "impedance type." They have therefore been represented by the shunt admittances computed earlier in Eq. (12-51).

The bus admittance matrix for the three-bus system can be obtained by inspection

$$\mathbf{Y}_{\text{bus}} = \begin{bmatrix} y_{11} & y_{12} & y_{13} \\ y_{21} & y_{22} & y_{23} \\ y_{31} & y_{32} & y_{33} \end{bmatrix} = \begin{bmatrix} 10 - j46 & j20 & j20 \\ j20 & -j40 & j20 \\ j20 & j20 & 10 - j38.585 \end{bmatrix} \tag{12-55}$$

(Note that this is *not* the same $\mathbf{Y}_{\text{bus}}$ as was used in the prefault load flow study.)

The load currents having been accounted for by the load admittances, the bus currents consist of only the generator currents, and the network equations therefore read

$$\begin{bmatrix} I_{G1} \\ I_{G2} \\ 0 \end{bmatrix} = \begin{bmatrix} y_{11} & y_{12} & y_{13} \\ y_{21} & y_{22} & y_{23} \\ y_{31} & y_{32} & y_{33} \end{bmatrix} \begin{bmatrix} V_1 \\ V_2 \\ V_3 \end{bmatrix} \tag{12-56}$$

Since the onset of the fault is characterized by the disconnection of $G1$, that is, by the opening of $CB1$ in Fig. 12-15, we must have

$$I_{G1} = 0 \tag{12-57}$$

From Fig. 12-16 we realize that I_{G2} must satisfy the relation

$$I_{G2} = Y'_{d2}(E'_2 - V_2) = -j18.5(E'_2 - V_2) \tag{12-58}$$

By substitution of these current values into Eq. (12-56), we obtain the following algebraic network equations *valid in postfault period I*:

$$\begin{aligned} V_1 &= -\frac{1}{y_{11}}(y_{12}V_2 + y_{13}V_3) \\ V_2 &= -\frac{1}{y_{22} + Y'_{d2}}(y_{21}V_1 + y_{23}V_3 - Y'_{d2}E'_2) \\ V_3 &= -\frac{1}{y_{33}}(y_{31}V_1 + y_{32}V_2) \end{aligned} \tag{12-59}$$

These three complex equations suffice to solve for the three complex voltages V_1, V_2, and V_3 *if the emf* E'_2 *is known*. If we use the Gauss-Seidel† iterative method for solving the above equations, the computational algorithm will be

$$\begin{aligned} V_1^{(k+1)} &= -\frac{1}{y_{11}}(y_{12}V_2^{(k)} + y_{13}V_3^{(k)}) \\ V_2^{(k+1)} &= -\frac{1}{y_{22} + Y'_{d2}}(y_{21}V_1^{(k+1)} + y_{23}V_3^{(k)} - Y'_{d2}E'_2) \\ V_3^{(k+1)} &= -\frac{1}{y_{33}}(y_{31}V_1^{(k+1)} + y_{32}V_2^{(k+1)}) \end{aligned} \tag{12-60}$$

(We have used the iteration index k rather than ν so as not to risk confusion with the discrete time index used in the Euler method.)

† Note that Eqs. (12-59) are *linear*. The voltages could therefore be solved by some linear method, e.g., determinants.

D. Swing equations (postfault period I) In analogy with Eq. (12-38), we define the following four-dimensional state vector:

$$\mathbf{x} = \begin{bmatrix} x_1 \\ x_2 \\ x_3 \\ x_4 \end{bmatrix} \triangleq \begin{bmatrix} \delta_1 \\ \dot{\delta}_1 \\ \delta_2 \\ \dot{\delta}_2 \end{bmatrix} \tag{12-61}$$

If we neglect the damping torques, and if we remember that the turbine powers are constant and equal to the prefault value 10 pu, we obtain in analogy with Eq. (12-39) the following swing equations:

$$\begin{aligned} \dot{x}_1 &= x_2 \\ \dot{x}_2 &= 2\pi(10 - P_{G1}) \\ \dot{x}_3 &= x_4 \\ \dot{x}_4 &= 0.2\pi(10 - P_{G2}) \end{aligned} \tag{12-62}$$

In the postfault period I we have

$$\begin{aligned} P_{G1} &= 0 \\ P_{G2} &= \text{Re}\,\{E'_2 I^*_{G2}\} \end{aligned} \tag{12-63}$$

By substitution of Eq. (12-58) into (12-63), we get

$$\begin{aligned} P_{G2} &= \text{Re}\,\{j18.5E'_2(E'^*_2 - V^*_2)\} = \text{Re}\,\{j18.5(|E'_2|^2 - E'_2V^*_2)\} \\ &= \text{Re}\,\{-j18.5E'_2V^*_2\} = \text{Im}\,\{18.5E'_2V^*_2\} \end{aligned} \tag{12-64}$$

Upon substitution of P_{G1} and P_{G2} into Eq. (12-62,), we obtain the following swing equations, *valid in postfault period I*:

$$\begin{aligned} \dot{x}_1 &= x_2 \\ \dot{x}_2 &= 20\pi \\ \dot{x}_3 &= x_4 \\ \dot{x}_4 &= 0.2\pi(10 - \text{Im}\,\{18.5E'_2V^*_2\}) \end{aligned} \tag{12-65}$$

In accordance with Eqs. (12-53), the initial state is

$$\mathbf{x}^{(0)} = \begin{bmatrix} \delta_1^0 \\ \dot{\delta}_1^0 \\ \delta_2^0 \\ \dot{\delta}_2^0 \end{bmatrix} = \begin{bmatrix} 0.379 \\ 0 \\ 0.633 \\ 0 \end{bmatrix} \tag{12-66}$$

E. Postfault system models (postfault period II) Upon reclosure of $CB1$ in Fig. 12-15, we enter the postfault period II. This network change does not affect the bus admittance matrix as given by Eq. (12-56). It will, however, change the value of the bus current at bus 1 from zero to the new value

$$I_{G1} = Y'_{d1}(E'_1 - V_1) = -j18.5(E'_1 - V_1) \tag{12-67}$$

This will change the generator power P_{G1} from zero to the new value

$$P_{G1} = \text{Re}\,\{E'_1 I^*_{G1}\} \tag{12-68}$$

This equation can be written, in analogy with Eq. (12-64), in the form

$$P_{G1} = \text{Im}\,\{18.5E'_1 V_1^*\} \tag{12-69}$$

By substitution of the expression for I_{G1} into Eq. (12-56), the network equations (12-60) change to

$$\begin{aligned} V_1^{(k+1)} &= -\frac{1}{y_{11} + Y'_{d1}}(y_{12}V_2^{(k)} + y_{13}V_3^{(k)} - Y'_{d1}E'_1) \\ V_2^{(k+1)} &= -\frac{1}{y_{22} + Y'_{d2}}(y_{21}V_1^{(k+1)} + y_{23}V_3^{(k)} - Y'_{d2}E'_2) \\ V_3^{(k+1)} &= -\frac{1}{y_{33}}(y_{31}V_1^{(k+1)} + y_{32}V_2^{(k+1)}) \end{aligned} \tag{12-70}$$

Upon substitution of the expression for P_{G1} into Eqs. (12-62), these will read

$$\begin{aligned} \dot{x}_1 &= x_2 \\ \dot{x}_2 &= 2\pi(10 - \text{Im}\,\{18.5E'_1 V_1^*\}) \\ \dot{x}_3 &= x_4 \\ \dot{x}_4 &= 0.2\pi(10 - \text{Im}\,\{18.5E'_2 V_2^*\}) \end{aligned} \tag{12-71}$$

We do not at this time know the initial state $\mathbf{x}^{(0)}$ for period II. The initial state in period II equals the final state in period I, and we have not yet computed the latter.

F. Computational sequence All necessary mathematical models, including algebraic network equations and state differential ("swing") equations, have been assembled at this stage. We need now to settle for a proper sequence in which to solve these equations, using methods that we have discussed earlier. Figure 12-17 shows one possible approach.

The following explanatory remarks should help the reader understand this chart:

1. The computations prescribed in the three first blocks provide us with sufficient data to determine the initial state $\mathbf{x}^{(0)}$, that is, the *prefault* angular rotor positions measured in *electrical* radians relative to our chosen reference. (Note, in particular, the change in block 3 of $\mathbf{Y}_{\text{bus}}$ as was explained in the text.)
2. The postfault period is divided into discrete time intervals $t^{(0)}, t^{(1)}, \ldots$, spaced Δt s apart. A typical interval size may be

$$\Delta t = 0.01 \text{ s}$$

Let us follow the sequence of computations that will take us from $t = t^{(0)}$ to $t = t^{(1)}$.

3. In block 5, distinction is first made between the postfault periods I and II. Assume that we are in period I.
4. Upon arriving at the solution of the *algebraic* network equations in block 7, we will specifically have obtained knowledge of V_2. This permits us to compute the term $E'_2 V_2^*$ in the swing equations as specified in block 8. *Note that E'_2 has not changed from the value we computed in block 3.*
5. Having computed the initial rate of change of the state vector in block 8, we can perform a rough linear extrapolation to $t = t^{(1)}$ in block 9. Upon exit from this block, we therefore have a *rough* idea about the state at $t = t^{(1)}$.
6. Since we thus know the approximate value of $\delta_1(=x_1)$ and $\delta_2(=x_3)$ at $t = t^{(1)}$, we can determine the *rough* value of E'_1 and E'_2 for $t = t^{(1)}$. The magnitudes of these phasors are *constant*, and the phasor tips therefore move along peripheries of circles. This fact (visualized by Fig. 12-18) explains the formula in block 10.

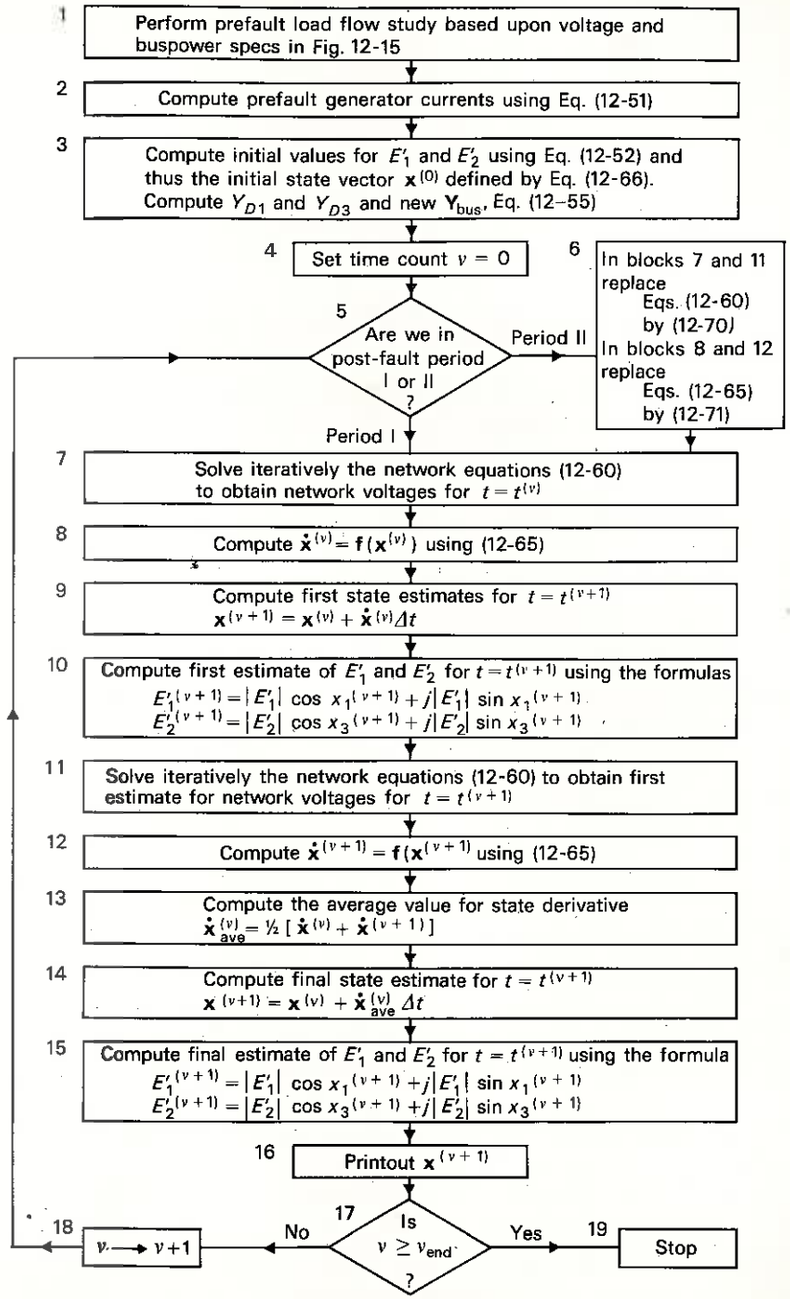

Figure 12-17 Computational flow chart for Example 12-3.

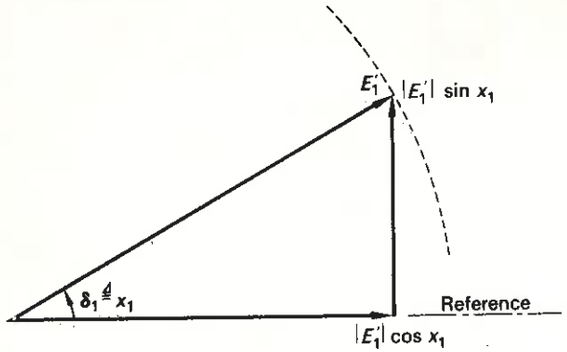

Figure 12-18 The tips of phasors E_1' and E_2' must move on the peripheries of circles.

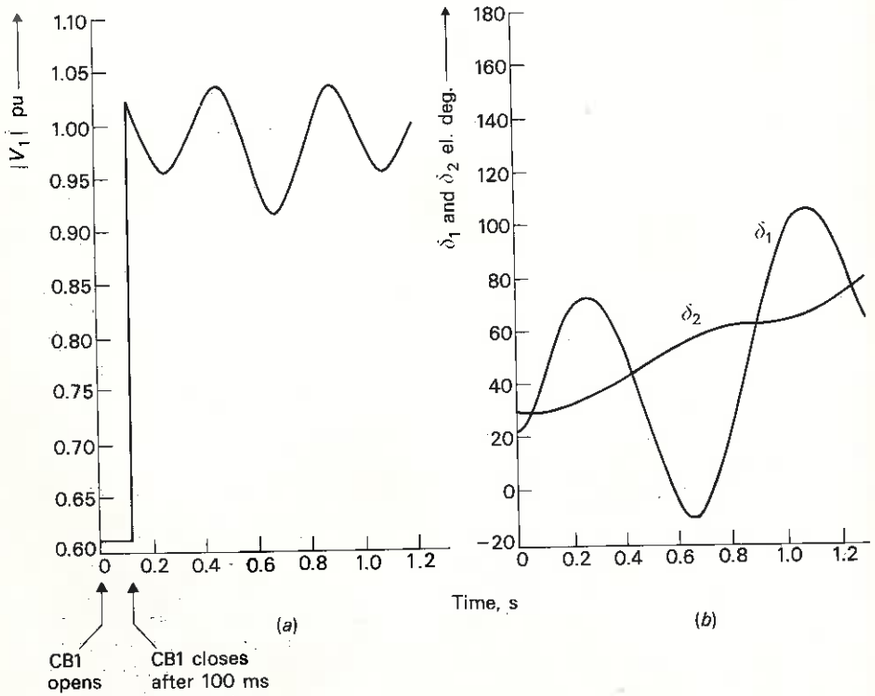

Figure 12-19 A transient stable case corresponding to reclosure after 0.1 s. Graph *a* shows the voltage at bus 1. Graph *b* shows the angular rotor swings of both generators.

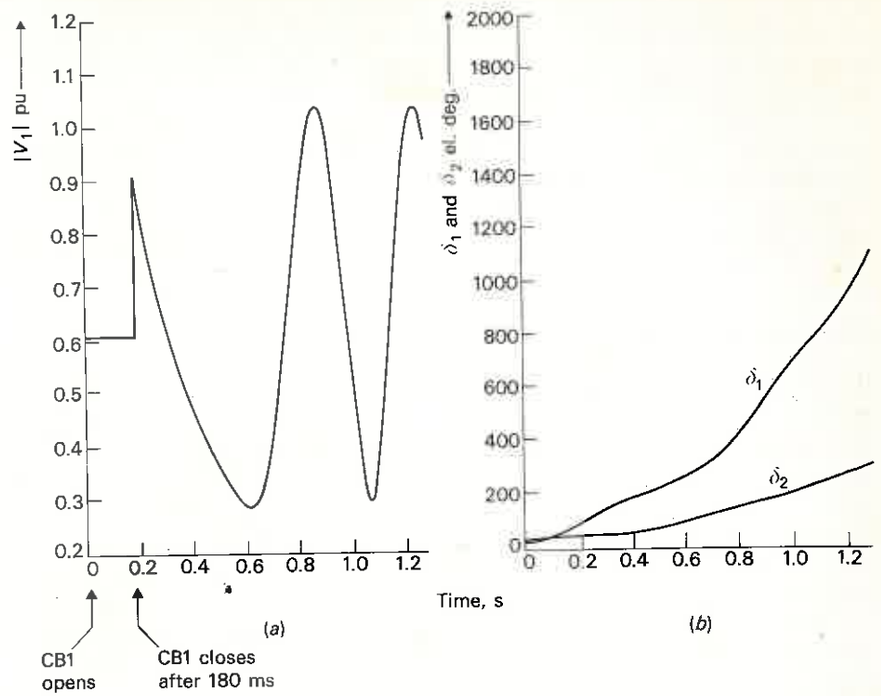

Figure 12-20 A transient unstable case corresponding to reclosure after 0.18 s. Graphs show $|V_1|$, δ_1, and δ_2.

7. Having now a rough idea about E_1' and E_2' for $t = t^{(1)}$, we can again solve the algebraic network equations, and thus obtain the rough voltage state for $t = t^{(1)}$ (block 11).
8. Data are now available to compute the rate of change of the state vector for $t = t^{(1)}$ (block 12).
9. With the knowledge of the derivatives at both ends of the interval, we can compute an average value for the rate of change in the interval (block 13).
10. From a knowledge of the average derivative, we compute an upgraded (and also final) value for the state at $t = t^{(1)}$ (block 14).
11. Finally, we "polish up" the values for the emf's E_1' and E_2' at $t = t^{(1)}$ (block 15).
12. At this stage we print out the result and proceed to the next time interval.

G. Computer results A computer program was developed, based on the flow chart in Fig. 12-17. The program was run for several values of reclosure times T. The results are shown in Figs. 12-19 and 12-20. In Fig. 12-19 we depict the swing curves for a transient stable case corresponding to $T = 0.1$ s. In Fig. 12-20 we have an unstable case corresponding to $T = 0.18$ s.

In both charts we have also included the variations in the bus voltage of bus 1.

We note the following features from these graphs:

1. The onset of the fault results in a 40 percent dip of $|V_1|$, approximately.
2. In the unstable case the voltage undergoes severe swings as the generators "slip poles."
3. Generator 1 performs "livelier" angular rotor swings than generator 2 because of its lower inertia.
4. We have not computed the swing curves beyond about 1 s because our models lose their validity beyond this time. (Compare Sec. 12-6.)
5. The generator rotor positions will not return to their original values even in the stable case. Why?

12-6 LONG-TERM FREQUENCY DYNAMICS

A "transient stable" system will ride through the fault and emerge fully synchronized. A "transient unstable" system will split up into *islands*. However, what the *eventual* outcome of the fault will be cannot be ascertained at this early stage. The "transient stable" system may return to the "normal" state as soon as the rotor swings have subsided. The various islands formed in the "transient unstable" case may be kept individually operating, later to be resynchronized and returned perhaps to its prefault "normal" state, without the loads having been greatly affected by the fault.

The severity of the power imbalance that will be caused by the initial fault will greatly affect the final outcome. The imbalance will cause a change in frequency and, should it persist, the frequency deviations may well assume magnitudes that will cause automatic generator tripping and other major equipment outages.

The frequency behavior will thus become a very important secondary fault symptom. Often it may take minutes, even hours, for the frequency to fully stabilize. By studying these long-term frequency dynamics (LFD) by simulation one can learn of their causes and how best to control them. In this section we comment on some of the aspects of LFD's.

12-6-1 Two Examples

Consider first the "transient unstable" case in Fig. 12-20. The fact that the rotor angles are on a divergent course means that the two generators are running *asynchronously*, i.e., with "slipping poles." The machines cannot be operated in this mode and must therefore be promptly separated. Upon separation the original system consists of two islands, $G1$ running alone and $G2$ still tied to the rest of the three-bus system. Are these two islands viable operating entities?

$G1$ is subject to a severe acceleration from its turbine torque. This machine must be promptly stopped before it reaches destructive speed levels, and its prime mover torque will therefore be reduced to zero as rapidly as possible.

$G2$, in contrast, will be subject to a severe deceleration. With its turbine power still at the prefault level of 10 pu, or 500 MW, it is now called upon to carry the total system load which in the prefault state amounted to 20 pu or 1000 MW. Although the postfault load will certainly be lower† than this, the megawatt output of $G2$ will most likely greatly exceed its turbine input. The power deficiency will be borrowed from the kinetic energy storage resulting in a rapid speed and frequency loss.

To prevent the frequency to reach unpermissibly low values‡ and possible turbine shutdown, we need to establish immediate power balance by *load shedding*. Such actions are typically initiated upon automatic command from underfrequency relays. If performed *fast enough*, in *proper amounts*, and in *right location*, the frequency decline can be halted and the system saved from total collapse.

Consider as a second example the sudden loss of a 1060-MW generator in the peninsular Florida network resulting in the frequency dynamics plotted in Fig. 12-21. The five graphs represent the frequencies as measured in five different generating centers.

Prior to the generator loss about 300 megawatts are imported via the relatively weak north-south ties to Georgia. The 1060-MW power deficiency causes a state-wide *average* frequency drop. Two seconds into the postfault period the tie-line power angles have moved so far apart (compare Fig. 12-5) that the first breakup occurs on a 230-kV tie, followed 300 ms later by all the remaining ties. From this moment on Florida is "islanding," totally separated from the eastern U.S. grid.

The additional loss of the 300-MW import power accelerates the frequency drop. At 4.5 seconds into the postfault period a first load shed is initiated followed one second later by an additional shed. These actions combined with the actions of all the ALFC loops reestablish power balance and the frequency levels off. As the various reserve units are picking up generation the shed loads can be restored and the frequency gradually "lifted" back to 60 Hz. After about 30 minutes the network is resynchronized with the U.S. grid and the system is back to normal. As the load shed involved predetermined *interruptible* industrial load, the system emerged from this emergency with few Floridians even aware of its happening.

12-6-2 Average System Frequency

A look at the five graphs in Fig. 12-21 reveals that already after about one second into the postfault state one can draw the conclusion that the system is "transient stable." The individual generators are still swinging against each other but they are holding together.

† For two reasons:

1. Many large motors would have tripped during the fault due to the violent voltage swings (Fig. 12-20).
2. $G2$ alone cannot uphold the prefault 1 pu voltage level. The lower voltage level results in a lower load (Chap. 3).

‡ A drop of only 1–2 Hz will take a turbogenerator into a speed region where its turbine blades may be subject to severe resonance stresses.

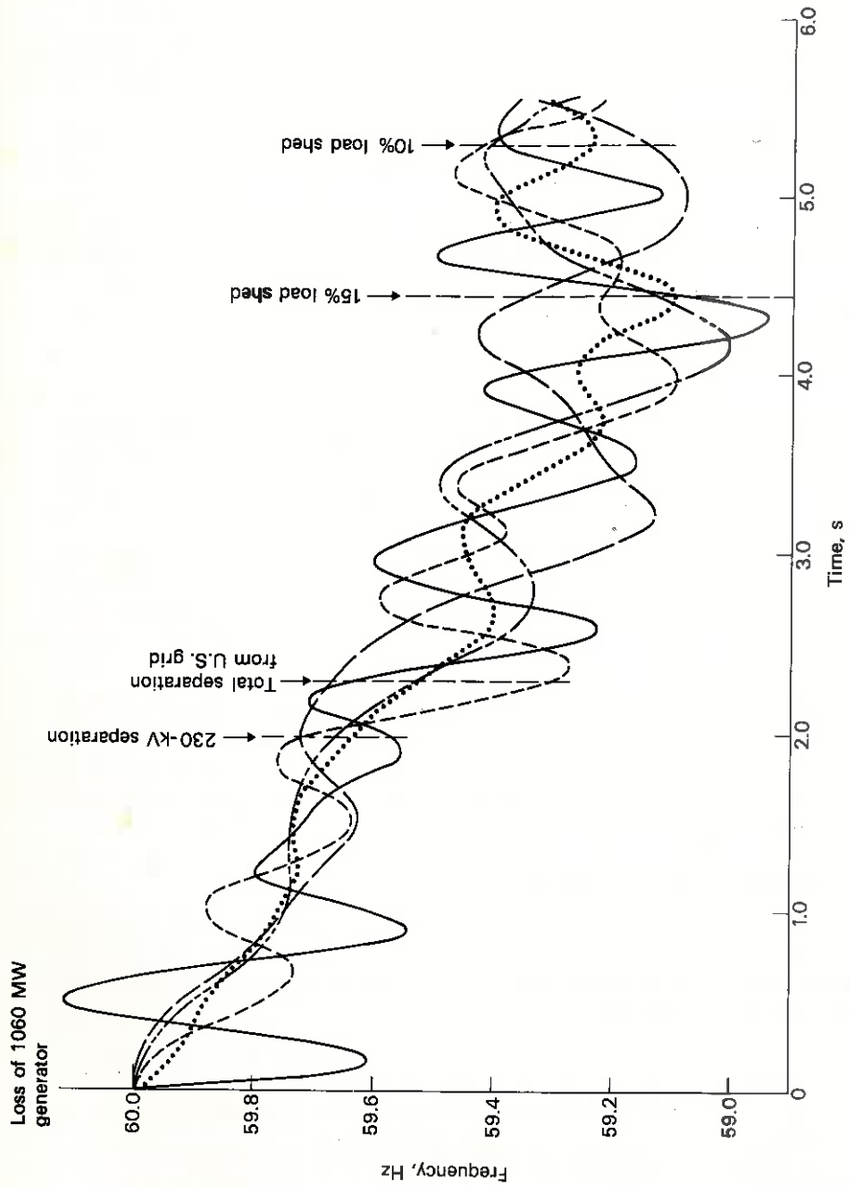

Figure 12-21 Example on frequency fluctuations following loss of generator.

At about this time the interest therefore shifts from *individual angular* excursions to the *collective frequency* behavior of the island.

Consider for a moment the train analog in Fig. 9-15. Assume that the train is subject to some major impact that causes the engines and freight cars to start oscillating against each other. Following the disturbance the oscillations will continue but we now focus our interest instead on the average velocity of the train. How do we define the "average" velocity?

Although the individual masses of the train are subject to wildly fluctuating spring forces these forces cancel each other as we consider the whole train as an aggregate. Therefore, the *center of gravity* of the train will *not* be subject to the internal forces and will consequently be subject to much slower changes and a more regular behavior. As interest shifts to the "collective" or "average" speed of the train we focus our attention to the speed behavior of its center of gravity.

The frequency curves in Fig. 12-21 behave similarly as the individual velocities of the masses of the train.

If we were to plot in this figure an *average area frequency* we would find it to have a *much smoother behavior than the individual rotor frequencies.* The individual generators swing against other area generators with the resulting power surges thus tending to cancel each other. The "center of gravity" in the train analog corresponds to a "center of inertia" in our generator case. As we define an average frequency for the island we do so in terms of the frequency of the inertia center.

12-6-3 Center of Inertia

In principle, a frequency simulation study could be performed by simply extending the integration of the generator swing equations beyond the initial "transient period" and focusing on angular *frequency* rather than angular *excursions.* Let us see how this changes the swing equations.

The rotor *excursion* δ_i of generator i is measured relative to a reference frame rotating at the *constant* radian (electrical) frequency ω^0. Thus the instantaneous radian *frequency* ω_i measured at the generator terminal equals

$$\omega_i = \omega^0 + \dot{\delta}_i \qquad \text{rad/s} \tag{12-72}$$

or, if expressed in hertz,

$$f_i = f^0 + \frac{1}{2\pi}\dot{\delta}_i \qquad \text{Hz} \tag{12-73}$$

From Eq. (12-72) we have for the rotor acceleration

$$\dot{\omega}_i = \ddot{\delta}_i = 2\pi\dot{f}_i \tag{12-74}$$

By substitution of $\ddot{\delta}_i$ into the swing equation (9-85) it assumes the new form

$$P_{\text{acc},\,i} \triangleq P_{Ti} - P_{Gi} = \frac{H_i}{\pi f^0}\dot{\omega}_i = \frac{2H_i}{f^0}\dot{f}_i \qquad \text{for } i = 1, 2, \ldots, n \tag{12-75}$$

The P's and H's must be expressed in per unit of a common base power. Upon solving the individual differential equations (12-75) we would thus obtain the individual generator frequencies f_i.

The numerical solution procedure would be identical to the one described in Sec. 12-5. Upon plotting the f_i's we would obtain frequency plots similar to those in Fig. 12-21.

The problem with this procedure is the need for extending the integration over long time spans (several minutes) *and yet being forced to use the same short integration step* Δt *as was employed in our transient study* ($\Delta t \approx 0.01$ s). The size of Δt is determined by the fast-changing generator power swings P_{Gi}.

Instead of concerning ourselves with the individual generator frequencies we turn now our attention to the overall island. By summing all the n equations (12-75) we obtain

$$P_{\text{acc, tot}} \triangleq \sum_{i=1}^{n} P_{Ti} - \sum_{i=1}^{n} P_{Gi} = \frac{2}{f^0}\sum_{i=1}^{n} H_i \dot{f}_i \tag{12-76}$$

Whereas the individual P_{Gi}'s are characterized by fast fluctuations these cancel each other in the sum $\sum P_{Gi}$. Thus the area accelerating power $P_{\text{acc, tot}}$ can be expected to be a relatively *slow-changing variable.*

At this stage we define the "center of inertia." We remember from mechanics that the position coordinate x_{CG} of the "center of gravity" is defined by

$$m_{\text{tot}} x_{CG} = \sum_{i=1}^{n} m_i x_i \tag{12-77}$$

In an analogous manner we define the angular position coordinate δ_{CI} of the "center of inertia" from the equation

$$H_{\text{tot}}\,\delta_{CI} = \sum_{i=1}^{n} H_i\,\delta_i \tag{12-78}$$

where H_{tot} is the total area inertia

$$H_{\text{tot}} = \sum_{i=1}^{n} H_i \tag{12-79}$$

Defined in this manner the angular position coordinate δ_{CI} indicates the position of an imaginary machine rotor having the total aggregated inertia of all area rotors. From Eq. (12-78) we have

$$H_{\text{tot}}\,\ddot{\delta}_{CI} = H_{\text{tot}}\,\dot{\omega}_{CI} = \sum_{i=1}^{n} H_i\,\dot{\omega}_i \tag{12-80}$$

or if expressed in hertz

$$H_{\text{tot}}\,\dot{f}_{CI} = \sum_{i=1}^{n} H_i\,\dot{f}_i \tag{12-81}$$

By combining Eqs. (12-81) and (12-76) we finally have the differential equation that governs the frequency of the island center of inertia:

$$P_{\text{acc, tot}} = \frac{2}{f^0} H_{\text{tot}}\,\dot{f}_{CI} \tag{12-82}$$

The n individual differential equations (12-75) describing the n individual and *fast-changing* frequencies f_i have been aggregated into *one* differential equation (12-82) describing the *slow-changing* area frequency f_{CI}.

12-6-4 General Comments

It is beyond the scope of this text to present a detailed LTF example study similar to our three-bus transient stability analysis in the previous section. Relatively few such studies have been reported. One EPRI-sponsored computer program (LOTDYS) is available.[10]

We present the following general comments.

1. The size of the integration step Δt recommended in published reports lies in the range 0.1–1.0, s, that is, 1 to 2 powers of ten greater than the step size used in transient stability programs.
2. As an LFD program may have to cover a time span of many minutes the thermal dynamics of power plants will come into play. This greatly complicates the modeling.
3. The LFD simulation follows directly upon the "transient" period resulting from the *initiating event.* As the LFD simulation progresses one or several *consequential events* will occur (for example the tripping of a generator) which are directly related to the frequency level. The LFD program must therefore contain subprograms of the "transient stability" type which can be triggered during the process of simulation.
4. It is humanly impossible to predict a priori all possible fault events that may occur during an LFD study (compare the scenario presented in the beginning of the chapter).
5. Experience shows that proper coordination of load shedding is of utmost importance after the islanding stage has been reached. LFD programs will probably have their greatest usefulness for the purpose of determining the best load-shedding strategy.
6. It has been noted that voltage regulating transformers at load points can be very detrimental. Typically, as the frequency dips so does the voltage level, and this in turn reduces the load thus helping restore power balance. A voltage regulated transformer strives to uphold the voltage thus making it harder to achieve power balance. It would actually be better, *during faults,* if

the voltage were regulated *downward*, which then would act as a "soft" type of load shedding.

7. Present load-shedding strategies (compare Fig. 12-21) call for load cutoff when the frequency *already has dropped* to a certain level. Intuitively it is felt that maybe better results could be achieved with less extensive load drops if the shedding were to take place when the frequency *is about* to drop. This would require more extensive studies involving frequency *rate* relays.

SUMMARY

In this final chapter we have introduced the reader to the basic theory of electromechanical transients in power systems. The electromechanical torques that exist within the synchronous machines tend, under normal operation, to hold the network together in a stable equilibrium state, characterized by torque and power balance within each machine.

As a result of disturbances, which usually take the form of sudden structural network changes, the torque balance is upset within each machine. The individual machines, as a consequence, will be subject to accelerations or decelerations, causing angular rotor swings of such large magnitudes that certain machines may pull out of synchronism.

The differential equations describing the swing dynamics are of nonlinear type and lack, generally, analytical solutions. Numerical solutions can always be found, and we have discussed digital simulation of the swing equations. The differential equations have been expressed in standard "state" form. The advantage of this approach is that we can achieve a great measure of systematization and also make use of the compact vector notation features.

During approximately the first second following a disturbance, the turbine torque and the emf behind the transient reactance remain fairly constant. In this time interval the dynamic state of each generator can be adequately characterized by two state variables. As the voltage and turbine controllers come into play, the dynamics grows more complex, and additional state variables are now required to model the machine behavior adequately.

In all our examples we neglected the damping torques and also the resistances in the network. This procedure has the advantage of rendering results which are on the safe side and thus compensating for uncertain factors in our models.

It should be noted, however, that the computational procedures presented can accommodate with ease both these effects if we wish to do so.

Following the "transient" fault period interest shifts from rotor *angle excursion* to *frequency*. By defining a center of inertia it is possible to describe the area behavior in terms of a single frequency. LFD simulation extends over many minutes and serves the purpose of obtaining best power balance through load shedding, transformer voltage control, emergency generation, and the like.

PROBLEMS

12-1 Using the swing equation (9-85) prove that if the damping is neglected, the speed of the generator, when subject to a constant decelerating power of 1 pu, will be reduced from rated value to zero in $2H$ s. (This gives a good feel for the physical meaning of H.)

12-2 Consider Eqs. (12-13) and (12-15). We can write the two equations in the following forms:

$$\ddot{\delta} = \frac{\pi f^0}{H} P_T^0 \tag{12-83}$$

$$\ddot{\delta} \cong \frac{\pi f^0}{H} (P_T^0 - P_{G,\max} \sin \delta) \tag{12-84}$$

(In the last equation we dropped the saliency term.)

(*a*) Turn your attention now to the mechanical system in Fig. 12-22. Prove that the dynamics of this system is described by an equation of the same form of Eq. (12-84). If you remove the pendulum, the differential equation will be of the form of Eq. (12-83).

(*b*) The system in Fig. 12-22 evidently is a mechanical analog of the single generator operated onto an infinite network.

Assume that the system is in equilibrium at the angle $\delta° = 30°$. Suddenly remove the pendulum and then reattach it T seconds later (which obviously is not an easily performed experiment). Use the "equal area" criterion to find the largest possible T value for which transient stability is preserved.

12-3 Equation (12-83) can be written in state-variable form thus

$$\begin{aligned} \dot{x}_1 &= x_2 \\ \dot{x}_2 &= \frac{\pi f^0}{H} P_T^0 \end{aligned} \tag{12-85}$$

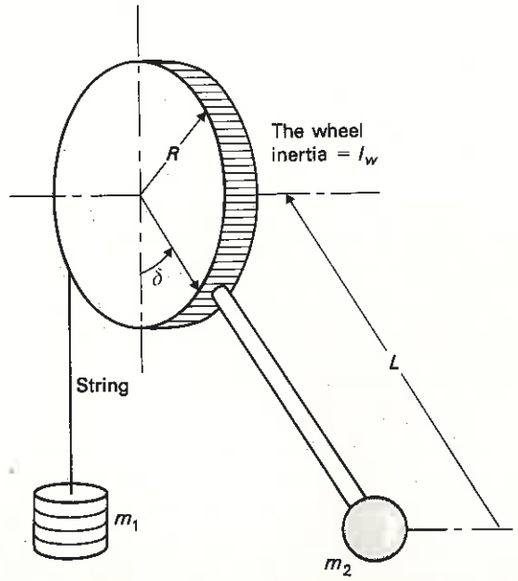

Figure 12-22 Analog of single generator operated onto infinite bus.

By dividing these two equations we have

$$\frac{dx_2}{dx_1} = \frac{\pi f^0 P_T^0}{H} \frac{1}{x_2} \tag{12-86}$$

which equation, after integration, yields

$$x_2^2 = 2\frac{\pi f^0 P_T^0}{H} x_1 + C \tag{12-87}$$

Depending upon the value of the integration constant C, the curves defined by Eq. (12-87) are parabolas, as shown in Fig. 12-23. The $x_2 x_1$ coordinate system is referred to as a *state plane*. The parabolas are called *state trajectories*, and give the relationship between the velocity (x_2) and position (x_1) states before reclosure. Compare also Sec. 9-6-3.

(*a*) Start with Eq. (12-84) and prove that the trajectories *after* reclosure look as shown dashed in Fig. 12-23.

(*b*) Prove that there are two groups of trajectories after reclosure, separated by the so-called *separatrix*. The trajectories inside the separatrix are *stable*; those outside are *unstable*.

(*c*) Find the equation for the separatrix.

(*d*) The generator is in the initial or *equilibrium* state marked 0 in Fig. 12-23. Following the onset of the fault, the generator state traces the boldface trajectory. An early reclosure in state 1 means a switchover onto a stable trajectory T_1. A late reclosure in state 2 results in the unstable trajectory T_2. Correlate these trajectories with the swing curves in Fig. 12-8.

(*e*) Assuming that we had included the damping term $D\dot{\delta}$ in Eq. (12-84), how would this have affected the trajectories in Fig. 12-23?

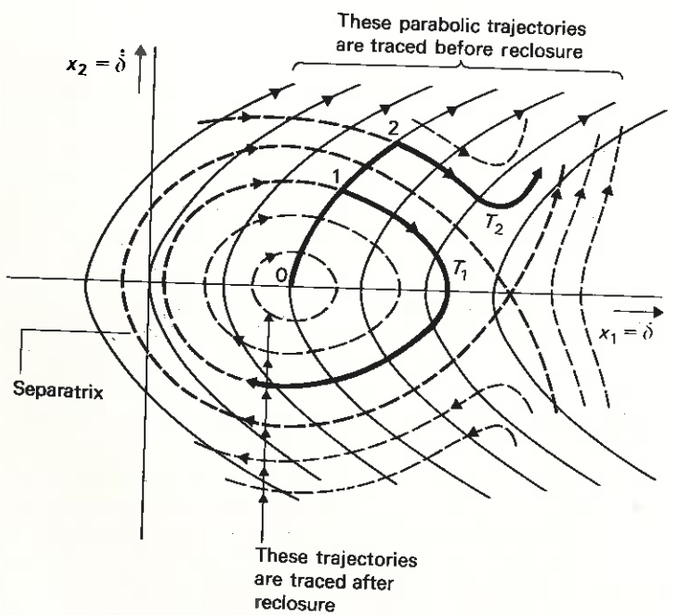

Figure 12-23 State trajectories for Prob. 12-3.

12-4 Consider the two-bus system in Fig. 10-11. Assume the two generators to be identical, each having the data

300 MW, 25 kV, 60 Hz

$X'_d = 0.25$ pu, $H = 5$ s

The two 300-MVA transformers have a reactance of 0.12 pu each. The line reactance is 0.20 pu (on the same base). Initially, the load is 100 MW, cos $\phi = 1$ at bus 1 and 300 MW, cos $\phi = 1$ at bus 2. The load is carried equally by the two generators. Both bus voltages are 1 pu.

A solid three-phase short circuit occurs midline and lasts for one full second whereupon it disappears. Due to a relay malfunction the line remains energized during the short. Is the system transient stable for this situation? Assume constancy of the turbine torques and also the emfs behind the transient reactance.

Treat the following two cases:

Case 1 The loads are assumed of impedance type.

Case 2 Each bus load consists of three components: one component is independent of voltage, one component is proportional to voltage, one component is proportional to voltage square. Initially all three components are equal.

You need a computer for this one.

12-5 In Sect. 12-5-1 we hinted at the fact that taking the AVR loop dynamics into account will add additional state variables to the transient stability study. Research this situation and summarize your findings in a short report.

Note that you cannot use directly the model in Fig. 9-4 as it was derived upon the assumption of *small-scale* variable excursions. As noted from Figs. 12-19 and 12-20 the voltage excursions will be *large*.

REFERENCES

1. R. Billinton, R. J. Ringlee, and A. J. Wood: *Power-System Reliability Calculations*, The MIT Press, Cambridge, Mass., 1973.
2. Lester Fink and Kjell Carlsen: "Operating under Stress and Strain," *IEEE Spectrum*, March 1978, pp. 48–50.
3. A. R. Van C. Warrington: *Protective Relays*, Chapman and Hall, London, 1974.
4. I. M. Canay, H. J. Rohrer, and K. E. Schnirel: "Effect of Disturbances on Torques in Large Turbo Sets," *IEEE Trans.* vol. PAS-99, July–Aug. 1980, pp. 1357–1370.
5. "Description of Discrete Supplementary Controls for Stability," *IEEE Report, IEEE Trans.*, vol. PAS-97, no. 1, Jan.–Feb. 1978, pp. 149–165.
6. W. A. Mittelstadt: "Four Methods of Power System Damping," *IEEE Trans.*, vol. PAS-87, no. 5, May 1968, pp. 1323–1329.
7. M. L. Shelton, P. F. Winkelman, W. A. Mittelstadt, and W. J. Bellerby: "Bonneville Power Administration 1400 MW Braking Resistor," *IEEE Trans. Power Appar. Syst.*, vol. PAS-94, March–April 1975, pp. 602–611.
8. A. A. Fouad: "Stability Theory—Criteria for Transient Stability," Report from conference on System Engineering In Power, Henniker, New Hampshire, Aug. 17–22, 1975.
9. A. H. El-Abiad and G. W. Stagg: *Computer Methods in Power System Analysis*, McGraw-Hill, New York, 1968.
10. "Long-Term Power System Dynamics," EPRI Report no. 90-7, April 1974.
11. O. R. Davidson, D. N. Ewart, and L. K. Kirchmayer: "Long-term Dynamic Response of Power Systems: an Analysis of Major Disturbances," *IEEE Trans.*, vol. PAS-94, May/June 1975, pp. 819–826.
12. J. Zaborszky, K. Whang, and K. Prasad: "Monitoring, Evaluation and Control of Power System Emergencies," DOE Conference on Systems Engineering for Power, Davos, Sept.–Oct. 1979.

APPENDIX

A

ELEMENTS OF VECTOR AND MATRIX ALGEBRA

A-1 VECTORS

We define a vector $\mathbf{x}$ as an ordered set of numbers, the *components* $x_1, x_2, \ldots, x_n$,

$$\mathbf{x} \triangleq \begin{bmatrix} x_1 \\ x_2 \\ \vdots \\ x_n \end{bmatrix} \tag{A-1}$$

The numbers x_i may be real or complex.

n defines the *dimensionality* of the vector.

Although the above column arrangement will be used most commonly, it proves convenient sometimes to use the *row*, or *transposed*, representation

$$\mathbf{x}^T \triangleq [x_1 \quad x_2 \quad \cdots \quad x_n] \tag{A-2}$$

A-1-1 Special Vectors

The *null vector* $\mathbf{0}$ and the *sum vector* $\mathbf{1}$ are defined as follows:

$$\mathbf{0} \triangleq \begin{bmatrix} 0 \\ \vdots \\ 0 \\ 0 \end{bmatrix} \qquad \mathbf{1} \triangleq \begin{bmatrix} 1 \\ 1 \\ \vdots \\ 1 \end{bmatrix}$$

The unit vector $\mathbf{e}_i$ is defined as the vector

$$\mathbf{e}_i \triangleq \begin{bmatrix} 0 \\ \vdots \\ 1 \\ \vdots \\ 0 \end{bmatrix} \leftarrow i\text{th component}$$

A-1-2 Elementary Vector Operations

Two vectors $\mathbf{x}$ and $\mathbf{y}$ are said to be equal if and only if $x_i = y_i$ for $i = 1, 2, \ldots, n$. In such a case, we write

$$\mathbf{x} = \mathbf{y}$$

By the product of a vector $\mathbf{x}$ with the scalar λ, we define a new vector $\lambda\mathbf{x}$, having each component amplified by the same scalar, i.e.,

$$\lambda\mathbf{x} = \mathbf{x}\lambda \triangleq \begin{bmatrix} \lambda x_1 \\ \lambda x_2 \\ \vdots \\ \lambda x_n \end{bmatrix} \tag{A-3}$$

Addition and *subtraction* of two vectors $\mathbf{x}$ and $\mathbf{y}$ result in new vectors

$$\mathbf{x} \pm \mathbf{y} \triangleq \begin{bmatrix} x_1 \pm y_1 \\ x_2 \pm y_2 \\ \vdots \\ x_n \pm y_n \end{bmatrix} \tag{A-4}$$

Clearly, these two last operations make sense only with vectors of the *same* dimensionality.

The following properties apply to the defined operations:

$$\mathbf{x} + \mathbf{y} = \mathbf{y} + \mathbf{x}$$
$$\mathbf{x} + (\mathbf{y} + \mathbf{z}) = (\mathbf{x} + \mathbf{y}) + \mathbf{z}$$
$$\lambda_1(\lambda_2\mathbf{x}) = (\lambda_1\lambda_2)\mathbf{x}$$
$$(\lambda_1 + \lambda_2)\mathbf{x} = \lambda_1\mathbf{x} + \lambda_2\mathbf{x}$$
$$\lambda(\mathbf{x} + \mathbf{y}) = \lambda\mathbf{x} + \lambda\mathbf{y}$$
$$0\mathbf{x} = \mathbf{0}$$

A-1-3 The Inner Vector Product

The so-called *inner*, or *scalar*, multiplication of two vectors $\mathbf{x}$ and $\mathbf{y}$ *of equal dimension* results in a very useful product. This multiplication is defined by

$$\mathbf{x}^T\mathbf{y} \triangleq \sum_{i=1}^{n} x_i y_i \tag{A-5}$$

Our chosen symbol $\mathbf{x}^T\mathbf{y}$ will be explained later in connection with matrix multiplication. In addition to this symbol, one often finds one of the following:

$$\mathbf{x} \cdot \mathbf{y}$$
$$(\mathbf{x}, \mathbf{y})$$
$$\langle \mathbf{x}, \mathbf{y} \rangle$$

(It should be noted that other *useful* vector products exist, for instance, the so-called *cross product* in three-dimensional space. However, for our present objectives, the inner product will suffice.)

Consider the two vectors $\mathbf{x}$ and $\mathbf{y}$ in ordinary two-space, defined by

$$\mathbf{x} = \begin{bmatrix} x_1 \\ x_2 \end{bmatrix} \triangleq \begin{bmatrix} |\mathbf{x}| \cos\alpha \\ |\mathbf{x}| \sin\alpha \end{bmatrix}$$

$$\mathbf{y} = \begin{bmatrix} y_1 \\ y_2 \end{bmatrix} \triangleq \begin{bmatrix} |\mathbf{y}| \cos\beta \\ |\mathbf{y}| \sin\beta \end{bmatrix}$$

and shown in Fig. A-1. $|\mathbf{x}|$ and $|\mathbf{y}|$ represent here the geometric length of each vector.

From the definition of inner product, we have

$$\mathbf{x}^T\mathbf{y} \triangleq x_1y_1 + x_2y_2 = |\mathbf{x}|\,|\mathbf{y}|(\cos\alpha\cos\beta + \sin\alpha\sin\beta)$$
$$= |\mathbf{x}|\,|\mathbf{y}| \cos(\alpha - \beta) = |\mathbf{x}|\,|\mathbf{y}| \cos\theta$$

We also note that

$$\mathbf{x}^T\mathbf{x} = x_1x_1 + x_2x_2 = |\mathbf{x}|^2$$

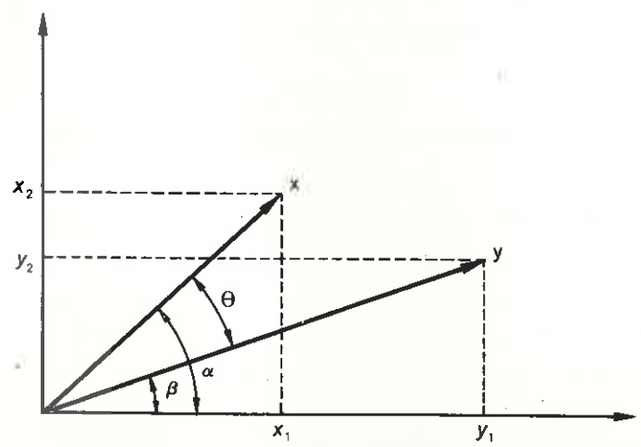

Figure A-1 Two-dimensional vectors.

and

$$\mathbf{y}^T\mathbf{y} = |\mathbf{y}|^2$$

We conclude, therefore, that the inner product between **x** and **y** indicates the *degree of parallelism* between the two vectors, and the inner product of **x** by itself gives information about the length of the vector.

By extending the concepts of *length* $|\mathbf{x}|$ and *angle* θ between vectors to n-dimensional space, we get

$$|\mathbf{x}|^2 \triangleq \mathbf{x}^T\mathbf{x}$$

$$\cos\theta \triangleq \frac{\mathbf{x}^T\mathbf{y}}{|\mathbf{x}|\,|\mathbf{y}|} \tag{A-6}$$

It is not possible to visualize these concepts beyond $n = 3$.

Note that if **x** is *normalized* (i.e., the length $|\mathbf{x}|$ equals unity), then we have

$$|\mathbf{y}|\cos\theta = \mathbf{x}^T\mathbf{y}$$

In words, the inner product gives us the *projection of* **y** *on* **x**.

Two *nonzero* vectors are said to be *orthogonal* if

$$\mathbf{x}^T\mathbf{y} = 0 \tag{A-7}$$

(The scalar product of the "sum vector" and **x** equals

$$\mathbf{1}^T\mathbf{x} = \sum_{i=1}^{n} x_i$$

and this explains the name.)

The following rules for scalar products are easily verified:

$$\begin{aligned} \mathbf{x}^T(\mathbf{y}+\mathbf{z}) &= \mathbf{x}^T\mathbf{y} + \mathbf{x}^T\mathbf{z} \\ (\mathbf{x}+\mathbf{y})^T\mathbf{z} &= \mathbf{x}^T\mathbf{z} + \mathbf{y}^T\mathbf{z} \\ \mathbf{x}^T(\lambda\mathbf{y}) &= \lambda\mathbf{x}^T\mathbf{y} \\ (\lambda\mathbf{x}^T)\mathbf{y} &= \lambda(\mathbf{x}^T\mathbf{y}) \end{aligned} \tag{A-8}$$

Example A-1 In a rectangular three-dimensional coordinate system we have the two vectors

$$\mathbf{x} = \begin{bmatrix}1\\2\\3\end{bmatrix} \quad \text{and} \quad \mathbf{y} = \begin{bmatrix}1\\1\\1\end{bmatrix}$$

Find the angle θ between these vectors. We have

$$|\mathbf{x}| = \sqrt{1+4+9} = \sqrt{14}$$

$$|\mathbf{y}| = \sqrt{1+1+1} = \sqrt{3}$$

$$\mathbf{x}^T\mathbf{y} = 1+2+3 = 6$$

$$\because \quad \cos\theta = \frac{6}{\sqrt{14}\times\sqrt{3}} = 0.926$$

and

$$\theta = 22.2°$$

A-2 MATRICES

An $m \times n$ matrix **A** is defined as a rectangular array of mn numbers

$$\mathbf{A} \triangleq \begin{bmatrix} a_{11} & a_{12} & \cdots & a_{1n} \\ a_{21} & a_{22} & \cdots & a_{2n} \\ \cdots & \cdots & \cdots & \cdots \\ a_{m1} & a_{m2} & \cdots & a_{mn} \end{bmatrix} \triangleq [a_{ij}] \tag{A-9}$$

The mn numbers a_{ij} are referred to as the *matrix elements*.

The integers m and n associated with an $m \times n$ matrix refer to the numbers of rows and columns, respectively.

An $n \times n$ matrix is called a *square matrix*, of *order* n.

An $m \times 1$ matrix is a *column vector* obeying all the rules of the preceding section.

A $1 \times n$ matrix is a *row vector*.

A-2-1 Elementary Matrix Operations

Two matrices **A** and **B** are said to be equal if and only if

$$a_{ij} = b_{ij} \qquad \text{for } i = 1, 2, \ldots, m, \quad j = 1, 2, \ldots, n$$

In such a case, we write

$$\mathbf{A} = \mathbf{B}$$

A matrix is multiplied by a scalar λ if all mn elements are multiplied by λ, that is,

$$\lambda\mathbf{A} = \mathbf{A}\lambda \triangleq \begin{bmatrix} \lambda a_{11} & \cdots & \lambda a_{1n} \\ \cdots & \cdots & \cdots \\ \lambda a_{m1} & \cdots & \lambda a_{mn} \end{bmatrix} \tag{A-10}$$

Addition and *subtraction* of two matrices result in new matrices in accordance with

$$\mathbf{A} \pm \mathbf{B} \triangleq \begin{bmatrix} a_{11} \pm b_{11} & \cdots & a_{1n} \pm b_{1n} \\ \cdots & \cdots & \cdots \\ a_{m1} \pm b_{m1} & \cdots & a_{mn} \pm b_{mn} \end{bmatrix} \tag{A-11}$$

Clearly, these operations apply only to matrices with the same numbers of rows and columns.

Matrix multiplication is defined to facilitate the operations necessary in connection with *linear transformations*. Consider the linear transformation

$$\begin{aligned} y_1 &= a_{11}x_1 + a_{12}x_2 + \cdots + a_{1n}x_n \\ y_2 &= a_{21}x_1 + a_{22}x_2 + \cdots + a_{2n}x_n \\ &\cdots\cdots\cdots\cdots\cdots\cdots \\ y_m &= a_{m1}x_1 + a_{m2}x_2 + \cdots + a_{mn}x_n \end{aligned} \tag{A-12}$$

or

$$y_i = \sum_{j=1}^{n} a_{ij} x_j \qquad \text{for } i = 1, 2, \ldots, m \tag{A-13}$$

We now can consider *formally* the a_{ij}'s as elements in an $m \times n$ matrix **A** and write the above equations in *compact* form:

$$\mathbf{y} = \mathbf{A}\mathbf{x} \tag{A-14}$$

This symbolism will have no meaning, of course, *until we prescribe that the product* **Ax** *will mean an m vector whose ith component will be defined by* (A-13).

This fully defines the *matrix-vector product.* In itself, this new concept would be useful only as a shorthand notation. The full power of the concept of matrix multiplication will be evident only upon definition of a *matrix-matrix product.* Consider for that purpose a new linear transformation

$$\begin{aligned} x_1 &= b_{11} z_1 + b_{12} z_2 + \cdots + b_{1p} z_p \\ x_2 &= b_{21} z_1 + b_{22} z_2 + \cdots + b_{2p} z_p \\ &\cdots\cdots\cdots\cdots\cdots\cdots\cdots\cdots \\ x_n &= b_{n1} z_1 + b_{n2} z_2 + \cdots + b_{np} z_p \end{aligned} \tag{A-15}$$

or

$$x_k = \sum_{r=1}^{p} b_{kr} z_r \qquad \text{for } k = 1, 2, \ldots, n \tag{A-16}$$

Using the accepted shorthand notation, we can also write the last equations

$$\mathbf{x} = \mathbf{B}\mathbf{z} \tag{A-17}$$

where **B** is an $n \times p$ matrix, and **z** a p vector.

By substituting Eq. (A-16) into Eq. (A-13), we can eliminate the x components, and we end up with the following m relations between **y** and **z**:

$$y_i = \sum_{j=1}^{n} a_{ij} \sum_{r=1}^{p} b_{jr} z_r \qquad \text{for } i = 1, 2, \ldots, m \tag{A-18}$$

We rearrange the summation signs in this last expression

$$y_i = \sum_{r=1}^{p} \left(\sum_{j=1}^{n} a_{ij} b_{jr} \right) z_r \qquad \text{for } i = 1, 2, \ldots, m \tag{A-19}$$

and by introduction of the mp new c coefficients, defined by

$$c_{ir} \triangleq \sum_{j=1}^{n} a_{ij} b_{jr} \qquad \text{for } i = 1, 2, \ldots, m, \quad r = 1, 2, \ldots, p \tag{A-20}$$

we can write the m equations (A-19) as

$$y_i = \sum_{r=1}^{p} c_{ir} z_r \qquad \text{for } i = 1, 2, \ldots, m \tag{A-21}$$

Suppose that, instead, we *formally* had eliminated the **x** vector in Eq. (A-14) by using the vector equation (A-17), i.e.,

$$\mathbf{y} = \mathbf{A}\mathbf{B}\mathbf{z} \tag{A-22}$$

Since we can consider Eq. (A-21) a vector equation

$$\mathbf{y} = \mathbf{C}\mathbf{z} \tag{A-23}$$

where the $m \times p$ matrix **C** is defined by Eq. (A-20), it is at this point quite obvious *that we have indeed defined a matrix product*

$$\mathbf{C} \triangleq \mathbf{A}\mathbf{B} \tag{A-24}$$

where the mp equations (A-20) *constitute the rule for multiplication of* **A** *and* **B**.

We note immediately that this product matrix is defined only if the number of columns in **A** equals the number of rows in **B**.

We note also from the definition that, in general,

$$\mathbf{AB} \neq \mathbf{BA}$$

(Indeed, unless p equals m, the product **BA** is not even defined.)

If **AB** and **BA** are both defined and if

$$\mathbf{AB} = \mathbf{BA}$$

then the matrices are said to *commute.*

The associative and distributive laws hold for matrix multiplication (when the appropriate operations are defined); i.e.,

$$\begin{aligned} (\mathbf{AB})\mathbf{C} &= \mathbf{A}(\mathbf{BC}) = \mathbf{ABC} \\ \mathbf{A}(\mathbf{B} + \mathbf{C}) &= \mathbf{AB} + \mathbf{AC} \end{aligned} \tag{A-25}$$

Example A-2 Given the two matrices

$$\mathbf{A} = \begin{bmatrix} 2 & 0 \\ 3 & 1 \\ 1 & 1 \end{bmatrix} \qquad \mathbf{B} = \begin{bmatrix} 1 & 3 & 1 \\ 0 & -1 & 2 \end{bmatrix}$$

Find **AB** and **BA**.

From the definition we have

$$\mathbf{AB} = \begin{bmatrix} 2 & 0 \\ 3 & 1 \\ 1 & 1 \end{bmatrix} \begin{bmatrix} 1 & 3 & 1 \\ 0 & -1 & 2 \end{bmatrix} = \begin{bmatrix} 2 & 6 & 2 \\ 3 & 8 & 5 \\ 1 & 2 & 3 \end{bmatrix}$$

$$\mathbf{BA} = \begin{bmatrix} 1 & 3 & 1 \\ 0 & -1 & 2 \end{bmatrix} \begin{bmatrix} 2 & 0 \\ 3 & 1 \\ 1 & 1 \end{bmatrix} = \begin{bmatrix} 12 & 4 \\ -1 & 1 \end{bmatrix}$$

A-2-2 Special Matrices

The *null matrix* **0** is defined by

$$\mathbf{0} \triangleq \begin{bmatrix} 0 & \cdots & 0 \\ \cdots & \cdots & \cdots \\ 0 & \cdots & 0 \end{bmatrix} \tag{A-26}$$

For a null matrix, we have

$$\begin{aligned} \mathbf{A} + \mathbf{0} &= \mathbf{A} \\ \mathbf{A0} = \mathbf{0A} &= \mathbf{0} \\ \mathbf{A} - \mathbf{A} &= \mathbf{0} \end{aligned} \tag{A-27}$$

Note: In the *scalar* case, we know that the equation $ab = 0$ implies that either a or b or both are zero.

The matrix equation $\mathbf{AB} = \mathbf{0}$ does *not* imply the same thing, as is exemplified by the product

$$\begin{bmatrix} 1 & 4 \\ 0 & 0 \end{bmatrix} \begin{bmatrix} 4 & 0 \\ -1 & 0 \end{bmatrix} = \begin{bmatrix} 0 & 0 \\ 0 & 0 \end{bmatrix}$$

A matrix is referred to as *diagonal* if it is square ($m = n$) and if $a_{ij} = 0$ for $i \neq j$.

A diagonal matrix of special importance is the *identity* or *unit matrix* **U**

$$\mathbf{U} \triangleq \begin{bmatrix} 1 & & & 0 \\ & 1 & & \\ & & \ddots & \\ 0 & & & 1 \end{bmatrix} \tag{A-28}$$

For the **U** matrix, we have

$$\begin{aligned} \mathbf{UA} = \mathbf{AU} &= \mathbf{A} \\ \underbrace{\mathbf{U} \cdots \mathbf{U}}_{n \text{ times}} \triangleq \mathbf{U}^n &= \mathbf{U} \end{aligned} \tag{A-29}$$

The *transpose* $\mathbf{A}^T$ of a matrix **A** is formed by interchanging rows and columns.

Transposition follows the easily confirmed rules

$$\begin{aligned} (\mathbf{A} + \mathbf{B})^T &= \mathbf{A}^T + \mathbf{B}^T \\ (\mathbf{AB})^T &= \mathbf{B}^T\mathbf{A}^T \\ (\mathbf{A}^T)^T &= \mathbf{A} \end{aligned} \tag{A-30}$$

We now can explain better why we earlier denoted the inner vector product of **x** and **y** by the symbol $\mathbf{x}^T\mathbf{y}$.

The reason is, simply, that the two vectors $\mathbf{x}^T$ and **y**, viewed as $1 \times n$ and $n \times 1$ matrices, respectively, can be multiplied, and result in the 1×1 matrix (a scalar) defined by Eq. (A-5).

A matrix is *symmetric* if it satisfies the equation

$$\mathbf{A} = \mathbf{A}^T \tag{A-31}$$

A-2-3 Determinants and Adjugate (Adjoint) Matrices

Consider the $n \times n$ matrix **A**. Now select an element from each row and column of this matrix and form the following product of n elements:

$$a_{1i}a_{2j}a_{3k} \cdots a_{nr}$$

The set of second subscripts $(i, j, k, \ldots, r)$ is a *permutation* of the set of integers $(1, 2, \ldots, n)$. We can form $n!$ different products of the above type. For example, in the case of 3×3 matrix, the six products are

$$\begin{aligned} &a_{11}a_{22}a_{33} \\ &a_{12}a_{23}a_{31} \\ &a_{13}a_{21}a_{32} \\ &a_{11}a_{23}a_{32} \\ &a_{12}a_{21}a_{33} \\ &a_{13}a_{22}a_{31} \end{aligned}$$

We define now the determinant $|\mathbf{A}|$

$$|\mathbf{A}| \triangleq \sum (\pm) a_{1i}a_{2j}a_{3k} \cdots a_{nr} \tag{A-32}$$

The sum has to be extended over the $n!$ different permutations of the second subscripts. Each term will be assigned a sign ($+$ or $-$) in accordance with the following rule: If the permutation is *even*, use the $+$ sign; if *odd*, use the $-$ sign. (A permutation is even or odd depending upon the number of integer interchanges in the set $i, j, k, \ldots, r$. For example, the sequence 132 has one interchange, (3-2), and is therefore odd, whereas the sequence 231 has two, (2-1) and (3-1), and is thus even.)

For example, returning to the example of the 3×3 matrix, we find the determinant, in that case,

$$\begin{aligned} |\mathbf{A}| = a_{11}a_{22}a_{33} + a_{12}a_{23}a_{31} + a_{13}a_{21}a_{32} \\ - a_{11}a_{23}a_{32} - a_{12}a_{21}a_{33} - a_{13}a_{22}a_{31} \end{aligned}$$

The following properties of determinants can be deduced directly from the definition

$$\begin{aligned} |\mathbf{A}| &= |\mathbf{A}^T| \\ |\lambda\mathbf{A}| &= \lambda^n|\mathbf{A}| \qquad n \text{ is the order of } \mathbf{A} \\ |\mathbf{AB}| &= |\mathbf{A}|\,|\mathbf{B}| \end{aligned} \tag{A-33}$$

Another useful property is that an interchange of two columns or rows changes the sign of $|\mathbf{A}|$. We see that this follows directly from the definition when we realize that such an interchange changes all odd permutations to even, and vice versa. As a corollary, it follows that $|\mathbf{A}|$ must equal zero if the matrix has two equal rows or columns.

Any element a_{ij} of $\mathbf{A}$ will appear as a factor in $(n-1)!$ of the $n!$ terms of $|\mathbf{A}|$. Furthermore, *each* of the n elements of *any* particular row or column of $\mathbf{A}$ is a factor in *all* the $n!$ terms of $|\mathbf{A}|$. It is therefore possible to rearrange Eq. (A-32) into either of the following two alternative forms:

$$|\mathbf{A}| = \sum_{j=1}^{n} a_{ij}A_{ij} \qquad \text{or} \qquad \sum_{i=1}^{n} a_{ij}A_{ij} \tag{A-34}$$

where i can be *any* row and j *any* column. The A_{ij}'s, the so-called *cofactors*, will each contain a sum of $(n-1)!$ terms involving those $(n-1)^2$ elements not to be found in row i and column j. By simple reasoning, we find that the rule for computing A_{ij} is

$A_{ij} = (-1)^{i+j}$ times the determinant of the submatrix formed by deleting row i and column j

From Eq. (A-34), we can derive an extremely useful relationship.

Consider the n cofactors $A_{i1}, A_{i2}, \ldots, A_{in}$. They are evidently *completely independent* of the elements of row i. If, therefore, we replace these elements with those in row $k (k \neq i)$ we have, in effect, a matrix with two equal rows and therefore zero determinant. From Eq. (A-34), we thus obtain the relationship

$$\sum_{j=1}^{n} a_{kj}A_{ij} = 0 \qquad \text{for } k \neq i \tag{A-35}$$

By applying the same discussion to a column, we similarly get

$$\sum_{i=1}^{n} a_{ik}A_{ij} = 0 \qquad \text{for } k \neq j \tag{A-36}$$

At this time, we define an $n \times n$ matrix $\mathbf{A}^+$, having as elements the A_{ji}'s (note, *not* the A_{ij}'s) and referred to as the *adjugate*, or *adjoint*, of matrix $\mathbf{A}$, that is,

$$\mathbf{A}^+ \triangleq \begin{bmatrix} A_{11} & A_{21} & \cdots & A_{n1} \\ A_{12} & A_{22} & \cdots & A_{n2} \\ \cdots & \cdots & \cdots & \cdots \\ A_{1n} & A_{2n} & \cdots & A_{nn} \end{bmatrix} \tag{A-37}$$

Equations (A-34) to (A-36) represent a total of $2n^2$ scalar equations. By recalling the definition of a matrix product (A-20), we can summarize them all in the compact matrix formulas

$$\mathbf{A}\mathbf{A}^+ = \mathbf{A}^+\mathbf{A} = |\mathbf{A}|\mathbf{U} \tag{A-38}$$

The reader will easily confirm this statement by simply writing the $2n^2$ scalar equations defined by Eq. (A-38) and noting that they are identical with Eqs. (A-34) to (A-36).

A-2-4 The Matrix Inverse

Consider the linear transformation

$$\mathbf{y} = \mathbf{A}\mathbf{x} \tag{A-39}$$

where $\mathbf{A}$ is a square matrix of order n, having a *nonzero* determinant.

Assume that we desire to solve the x_i's from the n Eqs. (A-39). Intuitively, we feel that the solution should read

$$\mathbf{x} = \mathbf{B}\mathbf{y} \tag{A-40}$$

where $\mathbf{B}$ is one as yet unknown $n \times n$ matrix.

If this solution is substituted back into Eq. (A-39), we obtain

$$\mathbf{y} = \mathbf{A}\mathbf{B}\mathbf{y}$$

On the other hand, if the original $\mathbf{y}$ vector is substituted into the solution equation (A-40), we have

$$\mathbf{x} = \mathbf{B}\mathbf{A}\mathbf{x} \tag{A-41}$$

In either case, if the solution is correct, we evidently must require that the $\mathbf{B}$ matrix satisfy

$$\mathbf{A}\mathbf{B} = \mathbf{B}\mathbf{A} = \mathbf{U} \tag{A-42}$$

A matrix $\mathbf{B}$ possessing this property is called the *inverse of* $\mathbf{A}$ and is designated with the special symbol $\mathbf{B} \triangleq \mathbf{A}^{-1}$.

By comparing Eqs. (A-42) with Eqs. (A-38), we find a matrix that satisfies our requirements, i.e.,

$$\mathbf{A}^{-1} = \frac{1}{|\mathbf{A}|}\mathbf{A}^+ \tag{A-43}$$

It is simple to prove that the inverse is *unique*, so that indeed this $\mathbf{A}^{-1}$ is *the* one.

We can deduce the following properties characterizing the inverse:

$$\begin{aligned} (\mathbf{A}\mathbf{B})^{-1} &= \mathbf{B}^{-1}\mathbf{A}^{-1} \\ (\mathbf{A}^{-1})^T &= (\mathbf{A}^T)^{-1} \\ (\mathbf{A}^{-1})^{-1} &= \mathbf{A} \end{aligned} \tag{A-44}$$

Example A-3 Given the matrix

$$\mathbf{A} = \begin{bmatrix} 1 & 2 \\ 3 & 4 \end{bmatrix}$$

find its inverse.

We first compute the determinant

$$|\mathbf{A}| = 1 \times 4 - 3 \times 2 = -2$$

Then we compute the $n^2 = 4$ cofactors.

$$\begin{bmatrix} A_{11} & A_{12} \\ A_{21} & A_{22} \end{bmatrix} = \begin{bmatrix} 4 & -3 \\ -2 & 1 \end{bmatrix}$$

The adjoint matrix thus equals

$$\mathbf{A}^{+} = \begin{bmatrix} 4 & -2 \\ -3 & 1 \end{bmatrix}$$

From Eq. (A-43) we finally get

$$\mathbf{A}^{-1} = \frac{1}{-2}\begin{bmatrix} 4 & -2 \\ -3 & 1 \end{bmatrix} = \begin{bmatrix} -2 & 1 \\ 1.5 & -0.5 \end{bmatrix}$$

REFERENCES

1. G. Hadley: *Linear Algebra*, Addison-Wesley Publishing Company, Inc., Reading, Mass., 1961.
2. R. Bellman: *Introduction to Matrix Analysis*, McGraw-Hill Book Company, New York, 1960.

APPENDIX

B

TRAVELING CURRENT WAVE IN SYMMETRICALLY LOADED SYNCHRONOUS MACHINE

Study of the air-gap phenomena in a symmetrically operated synchronous machine involves functions that are varying sinusoidally with respect to *both* time t and a tangential space coordinate s. We define two radian frequencies ω and ω_λ in terms of the *period time* T and *wave length* λ depicted in Fig. B-1, that is,

$$\omega \triangleq 2\pi \frac{1}{T} \qquad \text{rad/s}$$

$$\omega_\lambda \triangleq 2\pi \frac{1}{\lambda} \qquad \text{rad/m} \tag{B-1}$$

B-1 STANDING AND TRAVELING WAVES

Consider now the following two sinusoidal functions:

$$f_1(s, t) = f_{\max} \sin \omega t \sin \omega_\lambda s \tag{B-2}$$

$$f_2(s, t) = f_{\max} \sin (\omega_\lambda s - \omega t) \tag{B-3}$$

The two functions have been plotted versus s in Fig. B-2 at two different moments of time, t and $t + \Delta t$ respectively. We note their distinctly different time-space behavior.

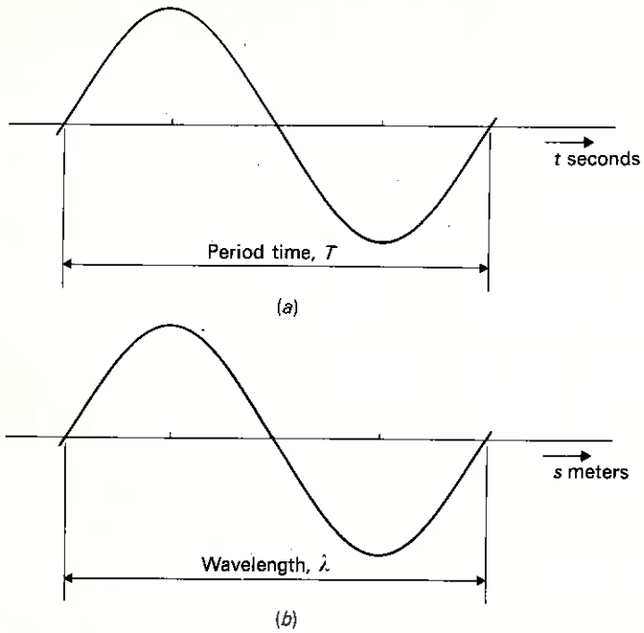

Figure B-1 Definition of "period time" and "wavelength."

The function f_1 has a pulsating amplitude but does not change space position. It is referred to as a *standing wave.*

The function f_2 has a constant amplitude but moves with constant velocity in positive s direction. It is referred to as a *traveling wave.* Its *wave velocity* $v = \Delta s/\Delta t$ is found by noting what increments Δs and Δt will leave the angle $(\omega_\lambda s - \omega t)$ in Eq. (B-3) unchanged. We immediately find

$$v = \frac{\Delta s}{\Delta t} = \frac{\omega}{\omega_\lambda} \qquad \text{m/s} \tag{B-4}$$

For example, if $\omega = 377$ (corresponding to 60 Hz) and $\lambda = 1$ meter we obtain

$$v = \tfrac{377}{1} = 377 \text{ m/s}$$

B-2 APPLICATION TO CURRENT-LOADED ARMATURE WINDING

Figure B-3 depicts a portion of the stator surface of a three-phase generator. In reality the tangential coordinate s is *curved* but is shown here in "straightened-out" version. We have also shown in Fig. B-3*a* two phase belts of the phase a armature winding. There are a total of p such belts belonging to phase a, symmetrically located around the periphery (Sec. 4-2). As the total circumference is

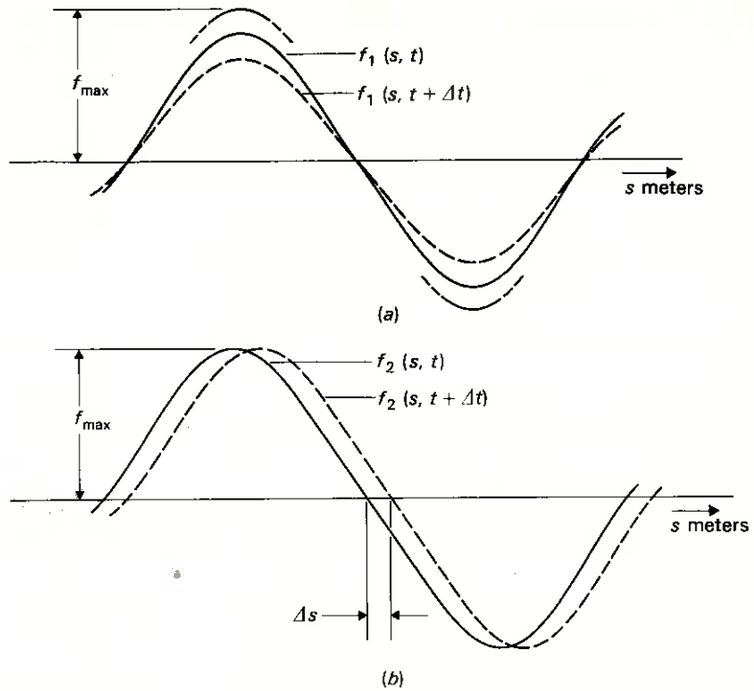

Figure B-2 Different wave types: (*a*) standing wave; (*b*) travelling wave.

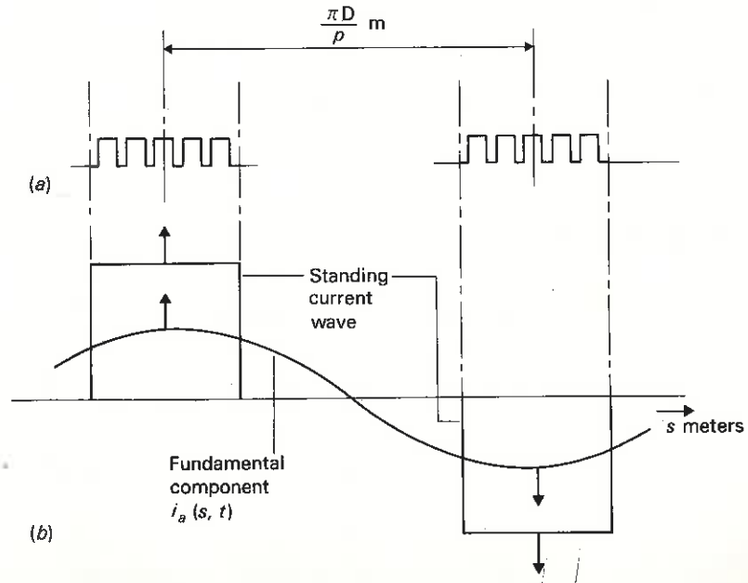

Figure B-3 Contribution to stator current wave by armature current in phase *a*.

πD meters (D = air-gap diameter) each belt center will be separated by $\pi D/p$ meters.

Since the conductors in the phase a winding carry an ac current of radian frequency ω rad/s, a standing current wave will be created that varies sinusoidally with time but nonsinusoidally along the stator periphery. It is shown† in Fig. B-3b at a moment when the phase current is increasing. Note that the wavelength equals

$$\lambda = 2\frac{\pi D}{p} \qquad \text{m} \tag{B-5}$$

From Eq. (B-1) we thus obtain

$$\omega_\lambda = \frac{p}{D} \qquad \text{rad/m} \tag{B-6}$$

The nonsinusoidal wave shown in Fig. B-3b contains a *fundamental* component (shown in the figure) of wavelength λ plus *odd* harmonics of wavelengths $\lambda/3$, $\lambda/5$, ... (not shown).

In the following analysis we include only the fundamental component and, according to Eq. (B-2), we therefore conclude that the contribution to the stator current wave picture from phase a amounts to

$$i_a(s, t) = i_{\max} \sin(\omega t) \sin\left(\frac{p}{D} s\right) \qquad \text{A/m} \tag{B-7}$$

Note that the physical dimension of $i_a(s, t)$ is amperes per meter. We are talking here about a stator "sheet current."

B-3 CONTRIBUTION FROM ALL THREE PHASES

$i_a(s, t)$ represents the contribution only from phase a. The currents in phases b and c create their own standing waves. Now we recall that

1. The three currents possess three-phase symmetry
2. The phase belts b and c are located around the periphery spaced, relative to phase a, by distances of $\lambda/3$ and $2\lambda/3$ respectively.

In view of the above observations we can therefore write the standing-wave contributions from the currents in phases b and c respectively

$$i_b(s, t) = i_{\max} \sin\left(\omega t - \frac{2\pi}{3}\right) \sin\left(\frac{ps}{D} - \frac{2\pi}{3}\right) \qquad \text{A/m} \tag{B-8}$$

$$i_c(s, t) = i_{\max} \sin\left(\omega t - \frac{4\pi}{3}\right) \sin\left(\frac{ps}{D} - \frac{4\pi}{3}\right) \qquad \text{A/m} \tag{B-9}$$

† We have depicted the wave in a "macrosense," i.e., we have neglected the variation due to the individual slots.

B-4 TOTAL EFFECT—A TRAVELING WAVE

The total composite wave is the sum of the phase contributions, i.e.,

$$i_{\text{tot}}(s, t) = i_a(s, t) + i_b(s, t) + i_c(s, t) \qquad \text{A/m} \tag{B-10}$$

In adding the three terms we make use of the following two trigonometric identities:

$$\sin\alpha \sin\beta = \tfrac{1}{2}[\cos(\alpha - \beta) - \cos(\alpha + \beta)] \tag{B-11}$$

and

$$\cos\alpha + \cos\left(\alpha - \frac{2\pi}{3}\right) + \cos\left(\alpha - \frac{4\pi}{3}\right) = 0 \tag{B-12}$$

The end result is very simple:

$$i_{\text{tot}}(s, t) = \frac{3}{2} i_{\max} \cos\left(\frac{ps}{D} - \omega t\right) \qquad \text{A/m} \tag{B-13}$$

In words: *The composite effect of the three standing phase waves is one traveling wave with an amplitude 50 percent higher than the peak value of each standing wave.*

According to Eqs. (B-4) and (B-6) the velocity of the traveling wave equals

$$v = \frac{\omega D}{p} \qquad \text{m/s} \tag{B-14}$$

As the air-gap circumference is πD meters the wave will thus rotate at the rate of

$$\frac{\omega D/p}{\pi D} = \frac{\omega}{p\pi} = \frac{2\pi f}{p\pi} = \frac{2f}{p} \qquad \text{rev/s} \tag{B-15}$$

or

$$\frac{2f}{p} \times 60 = 120\frac{f}{p} \qquad \text{rev/min}$$

According to formula (4-2) *the current wave velocity is thus identical with the rotor speed of the synchronous machine, i.e., the stator current wave and rotor flux wave travel at identical speeds.*

Another very important observation, the proof of which is left to the reader, is the following:

The crest of the traveling current wave will coincide with the center of a specific phase belt at the moment when the current peaks in the phase in question.

B-5 HARMONICS EFFECTS

What happens to the third, fifth, ... space harmonics present in the standing current wave in Fig. B-3? Together with the similar harmonics in phases b and c they will actually give rise to a very complicated traveling wave picture in the

machine. However, the amplitudes of these higher-order waves can be reduced to very insignificant values in several ways:

1. First, the rectangular current wave in Fig. B-3 is not quite accurate. In reality the phase belts of the three phases overlap and will, in addition, not have the abrupt limits shown. This fact obviously will reduce the harmonics amplitudes.
2. By an intelligent choice of "pitch" and "distribution" factors the winding designer can further reduce the harmonics effect.

Normally, the power systems engineer seldom needs to worry about the harmonics effects.

APPENDIX

C

OPTIMUM SEARCH METHODS

C-1 THE UNCONSTRAINED CASE

In engineering one often faces the problem of *optimizing* a *scalar* cost function

$$C = C(x_1, \ldots, x_N) \tag{C-1}$$

The analysis focuses on finding the values of the independent variables x_i that yield minimum or maximum of C. If the x_i's are free to assume *any* values then one talks about an *unconstrained* problem.

C-1-1 Geometrical Interpretation

We can give the problem a simple geometrical interpretation if we consider the two-dimensional case with only two independent variables x_1 and x_2. The cost function C can now be represented by the three-dimensional *cost surface* shown in Fig. C-1. A maximum is assumed to exist for the variable pair $x_{1,\,\mathrm{opt}}$, $x_{2,\,\mathrm{opt}}$. If the cost surface is "sliced" up by horizontal planes and if the resulting intersections are projected onto the x_1-x_2 plane we obtain the *equicost contours*. (Compare the mapmaker's way of representing a three-dimensional hill on a two-dimensional paper).

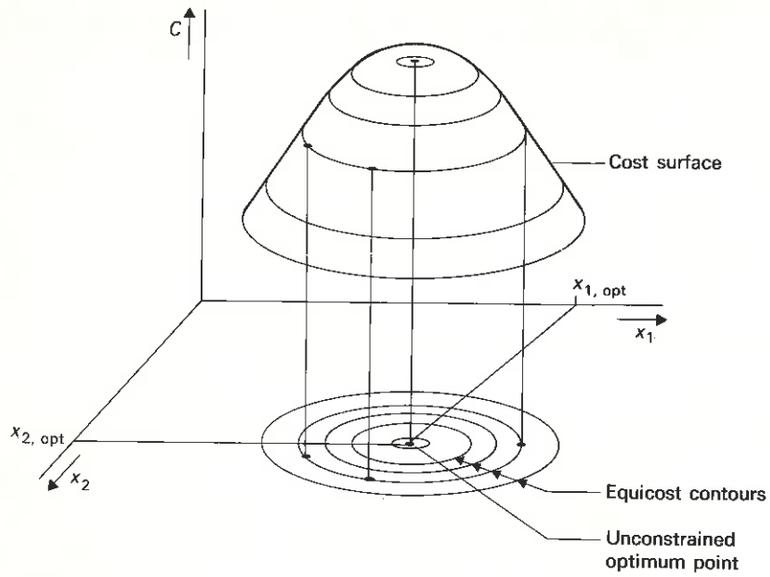

Figure C-1 Cost surface and equicost contours.

C-1-2 Identification of Optimum

How do we find the optimum in the unconstrained case? If we place ourselves on top of the hill in Fig. C-1 and take a *small* step in an *arbitrary* direction *no change will occur in C*. Mathematically, this means that the *total differential*

$$dC = \frac{\partial C}{\partial x_1}\,dx_1 + \frac{\partial C}{\partial x_2}\,dx_2 \tag{C-2}$$

must be zero for *arbitrary* values of dx_1 and dx_2. This condition is only met by requiring that *both* partial derivatives be zero, i.e.,

$$\begin{aligned} \frac{\partial C}{\partial x_1} &= 0 \\ \frac{\partial C}{\partial x_2} &= 0 \end{aligned} \tag{C-3}$$

If we extend this reasoning to the N-dimensional case where the total differential equals

$$dC = \frac{\partial C}{\partial x_1}\,dx_1 + \cdots + \frac{\partial C}{\partial x_N}\,dx_N \tag{C-4}$$

we conclude that we must require that

$$\frac{\partial C}{\partial x_i} = 0 \qquad \text{for } i = 1, \ldots, N \tag{C-5}$$

C now represents a *hypersurface* and a simple geometrical interpretation is no longer possible.

Example C-1 Find the optimum (= minimum) of the cost function

$$C = x_1^2 + 4x_2^2 - 4x_1 + 8 \tag{C-6}$$

SOLUTION For optimality we require

$$\begin{aligned} \frac{\partial C}{\partial x_1} &= 2x_1 - 4 = 0 \\ \frac{\partial C}{\partial x_2} &= 8x_2 = 0 \end{aligned} \tag{C-7}$$

Optimum exists for

$$\begin{bmatrix} x_1 \\ x_2 \end{bmatrix} \triangleq \begin{bmatrix} x_{1,\,opt} \\ x_{2,\,opt} \end{bmatrix} = \begin{bmatrix} 2 \\ 0 \end{bmatrix}$$

The optimal value of C equals

$$C_{min} = C(2, 0) = 4$$

The cost function (C-6) can be written in the form

$$(x_1 - 2)^2 + (2x_2)^2 = (\sqrt{C - 4})^2$$

$\therefore$ for $C > C_{min}$ the equicost contours are ellipses centered in (2, 0).

C-2 THE CONSTRAINED CASE

Assume now that we seek the optimum of C subject to the condition that the equation

$$f(x_1, \ldots, x_N) = 0 \tag{C-8}$$

be satisfied.

This added *constraint equation* results in the loss of one degree of freedom. We see this by differentiating (C-8),

$$\frac{\partial f}{\partial x_1}\,dx_1 + \cdots + \frac{\partial f}{\partial x_N}\,dx_N = 0 \tag{C-9}$$

Clearly we can still choose $N - 1$ of the differentials dx_i arbitrarily, but the remaining one is then fixed by Eq. (C-9).

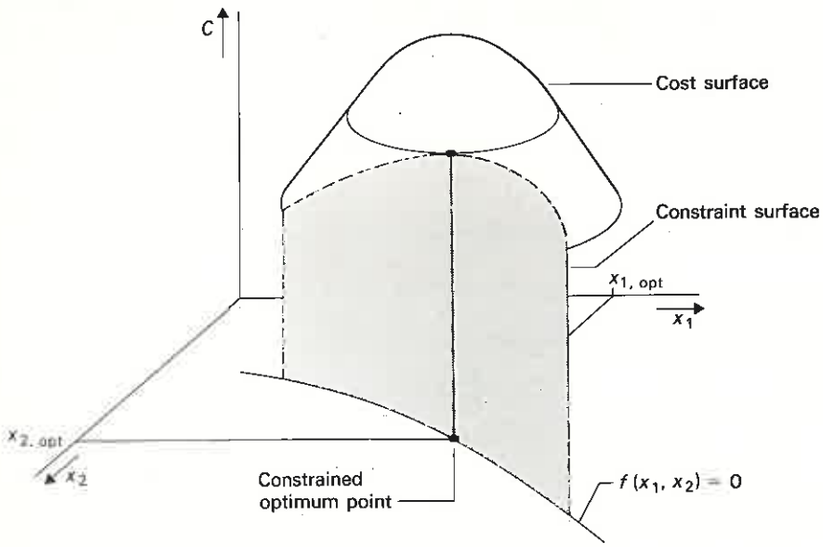

Figure C-2 Intersection of cost surface and constraint surface.

C-2-1 Geometrical Interpretation in Two-Dimensional Case

Equation (C-8) represents a vertical constraint surface in the three-dimensional coordinate system of Fig. C-1. We have added it in Fig. C-2 where we also identify (dashed) the intersection between the constraint surface and the cost surface. *The constrained optimum is the highest† point of this intersection.*

C-2-2 Finding the Constrained Optimum

If we first multiply Eq. (C-9) by a constant λ and then subtract the equation from Eq. (C-4) we obtain, after collecting terms

$$dC = \left(\frac{\partial C}{\partial x_1} - \lambda \frac{\partial f}{\partial x_1}\right) dx_1 + \cdots + \left(\frac{\partial C}{\partial x_N} - \lambda \frac{\partial f}{\partial x_N}\right) dx_N \tag{C-10}$$

Clearly, if all N factors within parentheses are zero then dC will be zero for *any* set of dx_i's. The conditions for an optimum are thus

$$\frac{\partial C}{\partial x_i} - \lambda \frac{\partial f}{\partial x_i} = 0 \qquad \text{for } i = 1, \ldots, N \tag{C-11}$$

These N equations plus the constraint equation (C-8) exactly match the number of unknowns $x_1, \ldots, x_N$ plus λ.

† Lowest, in the case of a minimum.

Example C-2 Find the optimum of C in Example C-1 subject to the linear constraint

$$f(x_1, x_2) = x_1 + 2x_2 - 3 = 0 \tag{C-12}$$

SOLUTION Equations (C-11) read in this case

$$\begin{aligned} 2x_1 - 4 - \lambda \cdot 1 &= 0 \\ 8x_2 - \lambda \cdot 2 &= 0 \end{aligned} \tag{C-13}$$

Equations (C-13) and (C-12) yield the three sought unknowns

$$\begin{aligned} x_1 &= x_{1,\,opt} = 2.5 \\ x_2 &= x_{2,\,opt} = 0.25 \\ \lambda &= 1 \end{aligned}$$

The constrained minimum equals

$$C_{min} = C(2.5, 0.25) = 4.5$$

Note that the unconstrained minimum (Example C-1) is deeper than the constrained one.

C-2-3 Lagrange Cost Function

We form an *augmented* or *Lagrange cost function* C^* defined by

$$C^* \triangleq C - \lambda f \tag{C-14}$$

If we now attempt to find the *unconstrained* optimum of C^* we are led (see Sec. C-1-3) to the N equations

$$\frac{\partial C^*}{\partial x_i} = \frac{\partial C}{\partial x_i} - \lambda \frac{\partial f}{\partial x_i} = 0 \qquad \text{for } i = 1, \ldots, N \tag{C-15}$$

These latter equations are identical to Eqs. (C-11).

The problem of optimizing C subject to the equality constraint $f = 0$ is thus equivalent to seeking the unconstrained optimum of C^*. The constant λ is called a *Lagrange multiplier*.

C-2-4 Several Constraint Equations

Assume we have n constraint equations

$$f_i(x_1, \ldots, x_N) = 0 \qquad i = 1, \ldots, n \tag{C-16}$$

where† $n < N$.

We introduce now n Lagrange multipliers $\lambda_1, \ldots, \lambda_n$ and form the Lagrange cost function

$$C^* \triangleq C - \lambda_1 f_1 - \cdots - \lambda_n f_n \tag{C-17}$$

† If $n = N$ we have zero degrees of freedom. If $n > N$ the problem is *overspecified*.

Optimization of C subject to the n equality constraints is now equivalent with the unconstrained optimization of C^*. (The proof is similar to proof of Eq. (C-11).)

C-3 GRADIENT SEARCH

The above analytical approach works well if

(*a*) the cost surface is smooth so as to ensure the existence of the partial derivatives
(*b*) the resulting set of simultaneous equations (C-5) or (C-11) can be solved analytically

In practice neither of these conditions normally is satisfied. In such cases one can attempt various iterative numerical techniques. Such a "hill-climbing" method is illustrated in Fig. C-3. From an initial starting point one proceeds step by step in the direction of the "C top."

A climber would try to reach a fog-shrouded peak by going in the direction of *steepest ascent. Gradient search* methods are based on this principle.

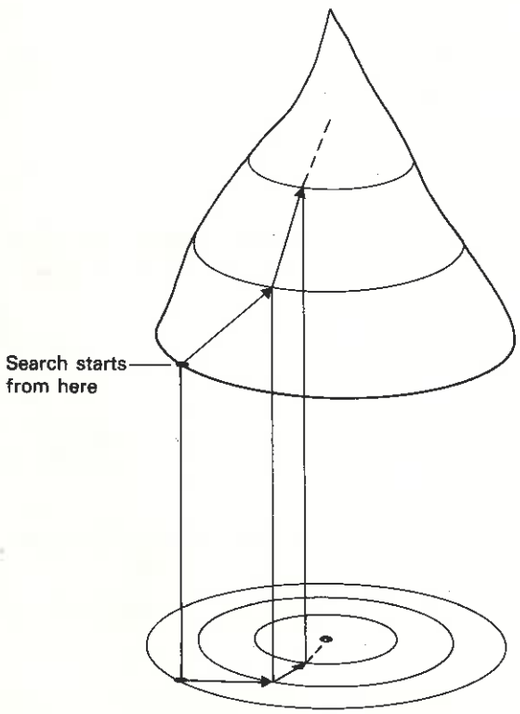

Figure C-3 Geometric interpretation of gradient search process.

C-3-1 Definition of Gradient Vector ∇C

Consider Eq. (C-4). If we introduce the N-dimensional *differential step vector*

$$\mathbf{dx} \triangleq \begin{bmatrix} dx_1 \\ \vdots \\ dx_N \end{bmatrix} \tag{C-18}$$

and *gradient vector*

$$\nabla C \triangleq \begin{bmatrix} \dfrac{\partial C}{\partial x_1} \\ \vdots \\ \dfrac{\partial C}{\partial x_N} \end{bmatrix} \tag{C-19}$$

we can write the total differential dC as the scalar vector product (see App. A, Eq. (A-5))

$$dC = \nabla C^T \cdot \mathbf{dx} \tag{C-20}$$

Since a vector product is maximized if the two vectors are parallel we conclude that the steepest increase in C is obtained *if we move in the direction of the gradient vector.*

C-3-2 Search Algorithm

A gradient search would proceed in the following way:

Step 1 Guess a starting point $\mathbf{x}^{(0)}$
Step 2 Compute the gradient $\nabla C^{(0)}$ and take a step of certain length in the gradient direction to the new point $\mathbf{x}^{(1)}$
Step 3 Repeat the process until a proper stop criterion indicates that we are sufficiently close to the optimum

Example C-3 Start from the point

$$\mathbf{x}^{(0)} = \begin{bmatrix} x_1^{(0)} \\ x_2^{(0)} \end{bmatrix} = \begin{bmatrix} 4 \\ 4 \end{bmatrix}$$

and seek the minimum point of the cost function (C-6).

SOLUTION The gradient vector equals

$$\nabla C = \begin{bmatrix} 2x_1 - 4 \\ 8x_2 \end{bmatrix}$$

We seek the minimum in the following steps:

1. Find the gradient in $\mathbf{x}^{(0)}$

$$\nabla C^{(0)} = \begin{bmatrix} 2 \cdot 4 - 4 \\ 8 \cdot 4 \end{bmatrix} = \begin{bmatrix} 4 \\ 32 \end{bmatrix}$$

2. Normalize $\nabla C^{(0)}$ to unit length

$$\frac{\nabla C^{(0)}}{|\nabla C^{(0)}|} = \frac{1}{\sqrt{4^2 + 32^2}} \begin{bmatrix} 4 \\ 32 \end{bmatrix} = \begin{bmatrix} 0.124 \\ 0.992 \end{bmatrix}$$

3. Choose step size
   Arbitrarily we select $|dx| = 1.5$
4. Take the first step in *negative*† gradient direction to the new point $\mathbf{x}^{(1)}$

$$\mathbf{x}^{(1)} = \begin{bmatrix} 4 \\ 4 \end{bmatrix} - 1.5 \begin{bmatrix} 0.124 \\ 0.992 \end{bmatrix} = \begin{bmatrix} 3.814 \\ 2.512 \end{bmatrix}$$

5. Repeat the process

Figure C-4 illustrates graphically the four first steps in the search. Note the overshoot in the fourth step, due to too large a step size. One would switch to smaller step size as the optimum is approached to achieve faster convergence without overshoot. The cost function C is monitored as the iterations proceed. When the decrease in C would fall below some specified ε the computations would stop.

† Because we are seeking a *minimum*.

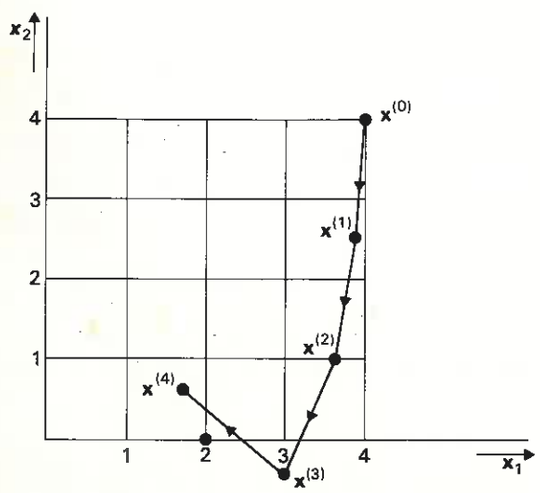

Figure C-4 The gradient search as projected onto the $x_1 - x_2$ plane.

APPENDIX

D

TURBINE MODELING

All mathematical models derived in this appendix are valid only for *small* changes in valve or gate positions.

D-1 STEAM TURBINES

Figure D-1 shows the basic components of a steam turbine system. Water is transformed into steam of high temperature and pressure in the *steam generator*.† A *drum* often serves as a buffer storage before the steam reaches the *control valves*. When expanding in the turbine the steam releases a portion (about one-third) of its energy in mechanical form. The turbine power is directly proportional to the flow (kilograms per second) of the steam.

To increase overall efficiency the turbine is often divided into two or several *stages*. Between the stages the steam is reheated in *reheaters*. From the LP stage the steam exits into the *condenser* in which, upon cooling, steam condenses into water. The *steam cycle* is completed upon pumping the condensed water back into the steam generator.

† In fossil-fired units often called the "boiler."

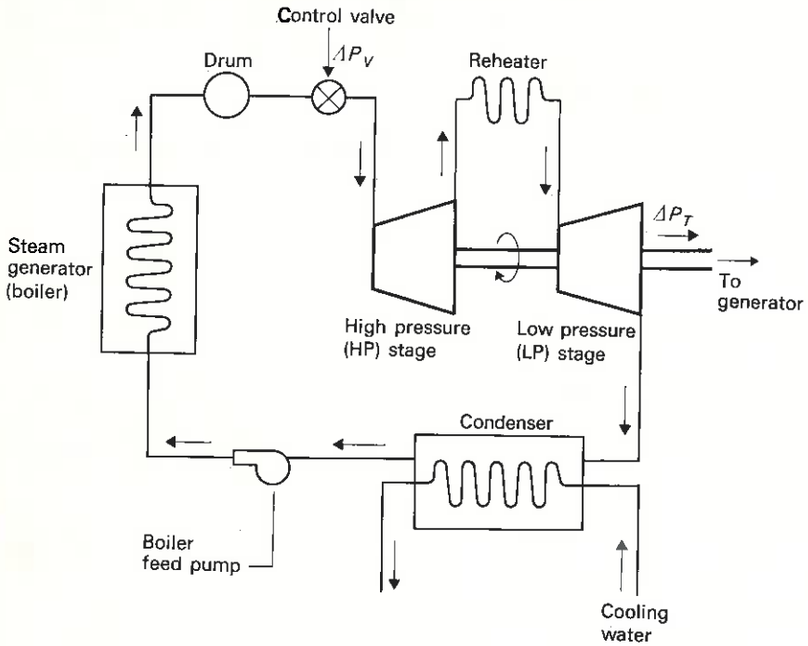

Figure D-1 Schematic diagram of steam cycle in fossil-fired plant.

D-1-1 Nonreheat Turbine

If only one turbine stage is used we talk about a nonreheat turbine. From a response point of view this turbine type is quite simple. Upon opening the control valve the steam flow will not reach the turbine cylinder instantaneously. A delay is experienced in the piping, or *steam chest*. This delay can be modeled as a time constant T_{CH} and this type of turbine will thus have a transfer function of the type

$$G_T(s) = \frac{\Delta P_T}{\Delta P_V} = \frac{1}{1 + sT_{CH}} \tag{D-1}$$

T_{CH} assumes values in the typical range 0.1–0.5 s.

D-1-2 Reheat Type Turbine

Consider the two-stage turbine in Fig. D-1. Assume that the HP and LP stages have the per-unit megawatt ratings α and $1 - \alpha$ respectively.

Upon changing the control valve with the increment ΔP_V the HP turbine contributes the power component

$$\Delta P_{T,HP} = \alpha\, \Delta P_V \frac{1}{1 + sT_{CH}} \quad \text{MW} \tag{D-2}$$

The reheater represents a delay T_{RH} and the LP stage thus contributes

$$\Delta P_{T,LP} = (1 - \alpha)\, \Delta P_V \frac{1}{1 + sT_{CH}} \frac{1}{1 + sT_{RH}} \quad \text{MW} \tag{D-3}$$

The total power is obtained by adding the two components. We thus obtain (after some algebra) the overall turbine transfer function

$$G_T = \frac{\Delta P_{T,HP} + \Delta P_{T,LP}}{\Delta P_V} = \frac{1}{1 + sT_{CH}} \frac{1 + s\alpha T_{RH}}{1 + sT_{RH}} \tag{D-4}$$

T_{RH} assumes values in the typical range 4–10 s making the reheat turbine very slow dynamically.

D-2 HYDROTURBINES

Figure D-2 depicts a socalled Pelton turbine. Depending upon the *water head H* hydroturbines vary considerably in regard to design. However, they all have essentially the same response characteristics which can be expressed by the transfer function

$$G_T = \frac{1 - 2sT_w}{1 + sT_w} \tag{D-5}$$

T_w represents the time required for the water to pass through the penstock in Fig. D-2.

We will not here derive the above transfer function. The reader may find the analytical details in Refs. 1 and 2. Instead we shall discuss the physical meaning

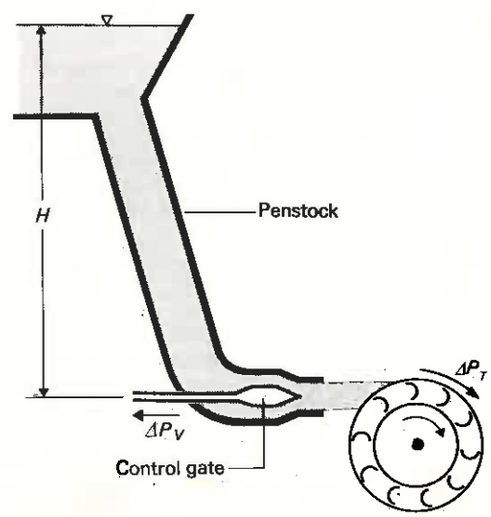

Figure D-2 Torque control of hydroturbine (Pelton type).

N° Reg. 2423
FAC. DE CIENCIAS EXACTAS Y TECNOLOGIA
BIBLIOTECA

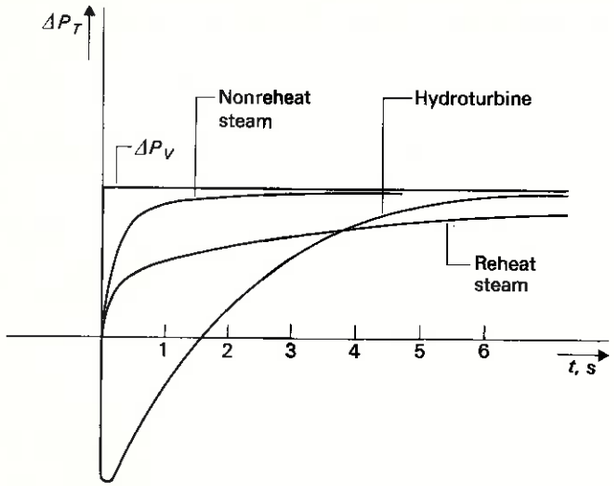

Figure D-3 Step responses for three different turbine types.

of Eq. (D-5). Before we do so we show in Fig. D-3 a comparison of the response features of steam versus hydroturbines. All three graphs represent the response to a *step change* in valve position.

The nonreheat steam turbine gives a fast exponential response. The reheat turbine gives a fast response component due to the *HP* stage and a much slower LP component due to the reheat delay.

The hydroturbine response is characterized by an *initial fast decrease* followed by a slower exponential increase. This type of response is referred to as "nonminimum phase." As the control gate opens up the water pressure experiences an initial dip but recovers and increases as the water in the penstock slowly accelerates to a new and higher velocity.

REFERENCES

1. D. G. Ramey and J. W. Skooglund: "Detailed Hydro Governor Representation for System Stability Studies," Sixth PICA Conference Proceedings, May 1969, pp. 490–501, *IEEE Trans. Power Appar. Syst.*, vol. PAS-89, January 1970, pp. 106–112.
2. R. Oldenburger and J. Donelson: "Dynamic Responses of a Hydro Electric Plant," *AIEE Trans.*, pt. III, vol. 81, October 1962, pp. 403–419.

INDEX

Accelerating power, 459
Acceleration factor, 252
ACSR (aluminum-cable, steel reinforced), 170
Alert state, 220, 448
Algorithm, 242, 390, 474, 521
Alternator, 68
  (*see also* Synchronous machine)
Andersson, P. M., 398, 446
Apparent power, 23–25
Area control error (ACE), 326
Armature winding, 69
  (*See also* Synchronous machine)
Armature reaction, 75
Autoconnected transformers, 150
Automatic load-frequency control:
  area control error, 326
  area frequency response characteristic, 320
  closed-loop model, 316–318
  dynamic response, 321–323
  hydraulic valve actuator, 312
  inertia constant, 317
  of multiarea systems, 329–339
  reset loop, 323–328
  simulation of in stability analysis, 472
  speed governor, 310–312
  static performance, 314–316, 319–321
  tie-line bias, 337–338
  turbine-generator response, 313–314
  of two-area system, 331–338
Automatic generation control, 310
  (*See also* Automatic voltage regulator and Automatic load-frequency control)
Automatic voltage regulator:
  dynamic performance, 306–308
  exciter models, 303–304
  exciter types, 302–303
  generator modeling, 304–306
  loading effects, 309
  simulation of in stability analysis, 473
  stability compensation, 308–309
  static performance, 306
  theory of, 302–310

Backup protection, 451
Base values in per-unit system, 30
  (*See also* Per-unit system)
Baseload, 274–275
Basic insulation level (BIL), 373
Biological field effects in vicinity of transmission lines, 169
Blackout, 3, 221, 447
Braking resistor, 468
Brushless exciter, 302
Bundled conductors, 171, 181, 186, 197
Burden, 450
Bus:
  admittance matrix, 229, 239
  current, 228, 434
  definition of, 8
  impedance matrix, 229, 239, 386, 432
  of load type, 243
  power, 227
  of reference type, 243
  of voltage-control type, 243

Capacitance of transmission lines, 188–199
(*See also* Transmission lines)
Capacitor:
series, for stability control, 469
series, for line compensation, 212
shunt, for line compensation, 61–63, 213, 224
Carpentier, J., 273
Circuit breaker, 8, 373, 374
Coherency, 464
Cohn, N., 338
Contingency, 448
Control area, 319
(*See also* Automatic load-frequency control)
Control valve (or gate), 310
Control vector, 233
Convergence index, 243
Corona, 170
Cost function (*see* Optimum dispatch)
Cost surface, 281, 516
Critical swing angle, 461
Current transformer (*see* Transformer)

Damper winding, 69, 345, 365
(*See also* Synchronous machine)
Decoupled power-flow, 266
Deltaconnected loads, 42
Deltaconnected transformers, 145, 417
Department of Energy (DOE), 9
Differential relays, 451
Direct (*d*-)axis, 69
Direct-axis synchronous reactance, 79
Direct-axis transient reactance, 106
Disconnect switch, 373
Distance relay, 450, 453
Distributed parameter effect, 199
Disturbance variable, 233, 351
Dommel, H., 298
Droop, 312
(*See also* Regulation)
Dy Liacco, T., 219

Earth (*see* Ground)
Economic dispatch control, 328
(*See also* Optimum dispatch)
Eigen frequencies, 341
Eigenvalues, 307, 341
El-Abiad, A. H., 446
Electric Power Research Institute (EPRI) 9
Electric utility industry, 3
Emergency control, 447
Emergency state, 220, 448
EMF behind transient reactance, 109

Energy:
control center, 449
in electric field, 17–18
electromagnetic, 15–17
in magnetic field, 18–19, 173–174
ohmic or dissipative, 19
Equal-area stability criterion, 461, 466
Equipotential surfaces, 190
Euler integration method, 474
Excitation source, 69
(*See also* Automatic voltage regulator)
Extremis state, 220, 447

Fast power-flow, 266
Fast valving, 468
Fault:
analysis, 384, 431
in symmetrical systems, 384
in unbalanced systems, 431
analysis using Thévenin's theorem, 377
computations for *n*-bus system, 384
impedance, 364, 432
impedance matrix, 436
level (*see* Shortcircuit capacity)
line-to-line, 404
matrix, 435
self-healing, 365
single-line-to-ground, 399, 404
symmetric, three-phase, 364, 376–396
Flat voltage start, 249
Floating neutral, 411
Floating voltage base, 137
Flow chart, 253, 254, 294, 295, 476, 483
Fortescue, C. L., 446
Frequency bias parameter, 338
Full matrix, 262

Gauss-Seidel iterative technique, 245–255
Gaussian elimination method, 265
Generation mix, 9, 274
Governor (*see* Speed governor)
Gradient search, 520
Gross, C. A., 398
Ground, 40
Grounding impedance, 399

Harmonic circles, 190
Harmonics, in synchronous machines, 71
High voltage DC (HVDC), 11, 170
Hydraulic valve actuator, 312–313
Hydrogenerator, 71
Hydropower, 9
Hyperbolic functions, 205

Image charge, 193
Impedance of machines, lines and transformers (*see* Reactance)
Impedance matrix (*see* Matrix)
Incremental generation cost, 279
(*See also* Optimum dispatch)
Incremental transmission loss, 288–292
Inductance of machines, lines, and transformers (*see* Reactance)
Inertia constant, 317
Inertia, center of, 489
Infinite network bus, 149, 314, 384
Insulation level, 373
Integration, numerical, 474
Interarea oscillations, 342, 465
Intermachine oscillations, 342
Interrupt capacity, 375
(*See also* Shortcircuit capacity)
Interruptible load, 487
"Islanding', 220, 342, 486
Isochronous control, 324
Iterative computation, 242–245

Jacobian matrix, 257

Kalman, R. E., 350
Kinetic energy, 222–223, 317, 322
Kirchmayer, L., 298

Lagrange multiplier, 279, 519
Lightning arrester, 364
Line (phase-to-phase) voltage, 38
Line-to-line fault (*see* Fault)
Load:
bus, 237
composite, 53
flow (*see* Powerflow)
interruptible, 487
—frequency control (*see* Automatic load-frequency control)
frequency dependency of, 54–55
of impedance type, 23–24
management, 57–58
of motortype 55–57
shedding, 220, 469, 487
voltage dependency of, 54–55
Logarithmic potential, 194
Long-line theory, 199–213
(*See also* Transmission lines)
Long-term frequency dynamics, 486
Loss-of-load probability (LOLP), 448
Lossless line, 209–212, 235
Lumped representation (of continuous line), 372

Magnetic inertia, 101
Magnetizing current (*see* Transformer)
Matrix:
algebra, 497
bus admittance, 229
fault, 435
jacobian, 257
phase impedance, 46, 407
sparse, 262
Megavar-voltage ($Q - |V|$) interaction, 224–226
Megawatt-frequency ($P - f$) interaction, 221–223
Mmf balance, 124, 418
(*See also* Transformer)
Mode of oscillation, 341, 366
(*See also* Natural mode)

Natural mode, 340–342, 343, 345
Negative sequence component, 401
(*See also* Symmetrical components)
Negative sequence reactance:
of generators, 408, 412
of transformers, 416
of lines, 416
(*See also* Reactance)
Neutral, 69
Neutral current, 399
Newton-Raphson method, 255–261
Nonreheat steam turbine, 313, 361
Normal state, 219
Nuclear fission power, 9
Nuclear fusion, 10

One-line diagram, 8
Optimum control index, 353
Optimum dispatch:
computational considerations, 283, 292, 293
computational flow chart, 294–295
constraint relations, 277–279
equality constraints, 278
inequality constraints, 278–279
cost function, 277
equations, 280–282
incremental generation cost, 279–280
incremental transmission loss, 288–292
lossless case, 277
problem formulation, 276
Optimum linear regulator (OLR) designs, 350–358
Optimal ordering (of equations), 265
Optimum search methods, 515
Overcurrent relay, 450

Partitioning of matrices, 267
Peaking units, 274–275
Penalty factor, 353
Per-phase analysis, 44–47
Per-unit system:
  base selection, 30
  change of base, 34
  definitions, 29–30
  in three-phase systems, 47–50
  in transformers, 135–138
Phase sequence, 36, 401
Phase-shift in transformers, 140, 147, 156, 417, 429
Phase symmetry, 44
Phasor, 21, 234
Pilot relay, 451
Pilot valve, 311
Pool operation, 275, 329
Positive sequence component, 401
  (*See also* Symmetrical component)
Potential transformer (*see* Transformer)
Power:
  angle, 60
  apparent, 23–25
  complex, 26–29
  flow (*see* Powerflow)
  fundamental formula, 15
  grid, 4
  mismatch (*see* Powerflow)
  pool, 4, 329
  pullout, 92
  reactive (*see* Reactive power)
  real (*see* Real power)
  single-phase, 20–29
  three-phase, 40
  triangle, 27–28
  in unbalanced systems, 406
  units, 14
Powerflow:
  computational approaches, 241–268
    algorithms, 242
    convergence index, 243
    "decoupled" algorithms, 266
    "fast" algorithms, 266
    Gauss-Seidel method, 245–255
    Gauss elimination method, 265
    iterative techniques, 242–244
    Newton-Raphson method, 255–261
    optimal ordering (of equations), 265
    sparsity-oriented techniques, 263
    storage packing, 264
  control of, 268–270
  definition of problem, 225–226
Powerflow:
  equations
    for 2 bus system, 228–233
    for *n*-bus system, 237–241
  variable classification, 233–234, 237
  variable specification, 234–236
Power system stabilizer, 350
Poynting vector, 16
Prime mover, 69
Propagation constant, 202
Protective relays, 449
Pullout power, 92

Quadrature-axis, 69
Quadrature-axis synchronous reactance, 79

Reactive power:
  control of, 93, 155
  definition of, 22–23
  flow in lines, 63
  generation in capacitors, 23
  generation in synchronous machines, 93
  limits of generators, 99
Reactance:
  of synchronous machines,
    direct-axis synchronous, 79
    direct-axis transient, 105
    negative sequence, 408, 412
    positive sequence, 408, 411
    quadrature-axis synchronous, 79
    table of, 81
    zero sequence, 408, 413
  of transformers,
    leakage, 132
    magnetizing, 130
    negative sequence, 416
    positive sequence, 416
    zero sequence, 419–423
  of transmission lines
    with one conductor per phase, 182
    bundle conductors, 186
    positive sequence, 415
    negative sequence, 415
    zero sequence, 415–416
Real power:
  control of, 90
  definition of, 22–23
  limits on lines, 59–63
  limits in generators, 99
Reclosure, 365, 454
Reference bus, 237
Reflection coefficient (*see* Wave)
Refraction coefficient (*see* Wave)

Regulation:
  speed, 312
  voltage, 34
Reheat steam turbine, 361, 524
Reserve capacity, 274, 448
Restorative state, 221
Restrike, 374
Riccati equation, 356, 357

Saliency effect, 79
Salient poles, 69
Sasson, A. M., 298
Security, 448
Self-excited oscillations, 340, 347–349
Separable function, 277
Separatrix, 494
Sequence:
  filter, 452
  impedance, 408, 412, 415, 416
    (*See also* Reactance)
  network, 409, 424–427, 430
  phase (*see* Phase sequence)
Shortcircuit, 364
  (*See also* Fault)
Short-circuit capacity, 88, 383, 389
Single-line-to-ground fault (*see* Fault)
Single-phase power, 20–29
Slack bus (*see* Reference bus)
Small-signal analysis, 301
Solar power, 9
Sparse matrix, 262
Sparsity-oriented computer programming, 263
Speed changer, 311
Speed governor, 299
Speed voltage, 73–75
  (*See also* Synchronous machine)
Spinning reserve, 220
Stability:
  absence of due to negative damping, 347
  of ALFC loops, 336, 340
  of AVR loops, 308, 360
  enhancement, 467
  frequency, 486
  by means of OLR design, 350
  static limit of generators, 92
  static limit of lines, 59
  transient, 448, 456, 470
Stabilizing transformer, 359
Stagg, G. W., 446
Standing wave, 510
State space, 354
State trajectory, 354–356
State transition diagram, 219–220
State variables, 223, 351
State vector, 223, 351
Static stability limit (of lines), 59–64
Steady-state instability, 340–349
Steam chest, 524
Storage reduction methods, 264
Subharmonic resonance, 342, 456
Subtransients, 113, 381
Surge impedance, 202
Surge impedance loading (SIL), 207–209
Surge phenomena, 364
Swing bus (*see* Reference bus)
Swing curves, 461, 484, 485, 488
Swing equation, 344, 461
Symmetrical component:
  bus currents vectors, 434
  bus voltage vector, 434
  definition of, 401–404
  in fault analysis, 423–443
  in line-to-line faults, 404, 429
  phaseshift of, in transformers, 417
  power, 406
  in single-line-to-ground fault, 404, 425
  transformation, 402–403
  transformation matrix, 403
Symmetrical short circuits (*see* Fault)
Symmetrical three-phase operation, 35
Synchronizing coefficient, 91, 331
Synchronizing power, 344
Synchronous capacitor, 94, 95, 225
Synchronous machine:
  armature reaction, 75–77
  current loading of, 75
  emf generation in, 73–75
  equivalent circuit, 78–79
  operated singly, 85–87
  operating limits, 98–99
  parallel operation of, 43–44, 87–98
  power formulas, 82–84, 110
  pullout power, 92
  reactive power control of, 93–95
  real power control of, 90
  reactances, 79, 81, 408, 412
    (*See also* Reactance)
  saliency, 79
  sequence impedances of, 408, 411–413
    (*See also* Sequence impedance)
  synchronization of, 87–88
  theory of, 68–116
  transients, 99–113
  transient reactance, 105
  traveling waves in, 71, 509
  unbalanced operation of, 406–412

Synchronous machine:
winding design, 69–71
Synchronous reactance, 78
(*See also* Reactance)

Tap changing under load (TCUL), 153
(*See also* Transformer)
Thermal capacity limits, 58–59
Thermal damage, 365
Thévenin's theorem, 377, 385, 424, 438
Three-phase:
current relations, 39
fault-analysis, 376–396
power formula, 40–42
symmetry, 38
theory of symmetrical systems, 35–50
voltage relations, 38
Tie-line, 8, 330
Tie-line bias control, 337
Time error, 324
Tinney, W. F., 273
Torsional oscillations, 341–342
Transformers:
autoconnected, 150–153
core, 118
core losses, 130–131
current (CT), 165, 449
Δ-connected, 145
design, 118–119
dot symbol, 121
equivalent circuit, 126, 127, 131, 141
"ideal," 120–121
impedance transformation in, 128–129
leakage reactance, 131
magnetizing current, 130
n-winding, 120
per-unit analysis of, 135–138
phase-shift, 140, 146
potential (PT), 165, 449
ratings, 135
regulating, 153–162
for controlling voltage magnitude, 155
for controlling voltage phase angle, 156
TCUL, 153
Scott-connected, 166
theory of, 117–167
voltage-per-turn (VPT), 122–123
zig-zag connected, 167
Y-connected, 140
Transients:
in generators, 99–113
switching, 375–376
on transmission lines, 363–373
Transient reactance, 105–106
(*See also* Reactance)
Transient stability, 365, 448, 456
(*See also* Stability)
Transmission capacity, 58–65
Transmission lines:
ACSR (aluminum cable, steel reinforced), 169
biological field effects, 169
capacitance computations, 188–199
bundled lines, 197
image charge, 193
influence of earth, 192–194
logarithmic potentials, 194–195
multiconductor line, 194–199
single-phase line, 188–194
three-phase line, 196–199
design details, 170–171
inductance computations, 173–187
apparent inductance concept, 178
bundled lines, 186
multiconductor lines, 180
single-phase lines, 174–180
three-phase lines, 182
transposed lines, 184
"long-line" theory, 199–213
compensation, 212–213
concept of wavelength, 209
"electrically short and long" lines, 210
equivalent circuit, 204
long-line equations, 202
lossless line, 209–212
surge impedance loading (SIL), 207
traveling waves, 201
power angle of, 60
power capacity of, 58–64
resistance and shunt conductance, 172–173
thermal capacity of, 58
voltage control of, 61–64
Transposition, 44–45, 184, 199
Traveling wave phenomena, 201, 367, 509
(*See also* Wave)
Turbine response, 313, 523
Turbine models, 523
Turbogenerator, 69
(*See also* Synchronous machine)
Two-reaction theory, 79–81
(*See also* Synchronous machine)

Underfrequency relay, 450
Unit protection, 450
Unsymmetrical three-phase systems, 50–52

Vector:
algebra, 497

Vector:
bus current, 239
bus voltage, 237
control, 233
disturbance, 233
state, 233
Voltage:
control bus, 237
distribution level, 6
standard operating (in USA), 5
subtransmission level, 7
transmission level, 7

Wave:
equation, 367
impedance, 202, 368
length, 209–210
phenomena on transmission lines, 364, 367–376
Wave:
reflection, 369–371
refraction, 370

Y_{bus} (*see* bus admittance matrix)

Z_{bus}:
definition, 229, 239
use in short-circuit analysis, 386
building algorithm, 390–396, 440
(*See also* Bus impedance matrix)
Zero sequence component, 401
(*See also* Symmetrical components)
Zero sequence reactance:
of synchronous machine, 413
of transformer, 419–423
of transmission line, 413–415
(*See also* Reactance)
Zone protection, 451–452

F.C. DE CIENCIAS EXACTAS Y TECNOLOGIA
BIBLIOTECA
Modo de Adquisición Compra
Exp. Nº 61.240-81
Edit. ó Librería McGraw-Hill
Fecha 10-5-82 Precio $404.500-

DEVOLUCION
(ESTE LIBRO DEBE SER DEVUELTO INDEFECTIBLEMENTE EN LA FECHA INDICADA)

38.80 8/8/83		

B - CIRC - 88
10.000 - VIII - 73 - 47202 - IMP. U.N.T.

McGraw-Hill
Expte 61240-81
U$S 30.80

217219

UNIVERSIDAD NACIONAL DE TUCUMAN

621.315 Elgerd, Olle I
E41e2 Electric energy systems theory
an introduction
2423

B - CIRC - 87
30.000 - XI - 68 - 35727 - IMP. U.N.T.